LOW AND ZERO SAPS ANTIWEAR ADDITIVES FOR ENGINE OILS

by

Juliane F. L. Benedet

A Thesis submitted to Imperial College London in fulfilment of the degree of Doctor of Philosophy and the Diploma of Imperial College.

November 2012

Tribology Section
Department of Mechanical Engineering
Imperial College of Science, Technology and Medicine
London

PREFACE

This thesis is a description of work carried out in the Tribology Section of the Department of Mechanical Engineering, Imperial College of Science, Technology and Medicine, London, under the supervision of Professor Hugh A. Spikes. Except where acknowledged, this material is original work and no part of it has been submitted for a degree at this or any other university.

ABSTRACT

Almost all modern engine lubricants use the additive zinc dialkyldithiophosphate (ZDDP) to provide antiwear and extreme pressure protection. However existing and proposed emissions regulations include constraints in the concentration of ZDDP or other sulphated ash-, phosphorus- and sulphur- (SAPS) containing additives in engine oils, as well as limits to the permissible phosphorus loss from the oil in running engines. The deleterious effects of SAPS on exhaust aftertreatment systems from ZDDP decomposition has lead to a great interest in identifying alternative low and zero SAPS antiwear additives that can partially of fully replace ZDDP in the next generation of engine oils to extend the life of exhaust after-treatment systems.

The aim of the work described in this thesis is to explore under the same test conditions, the film-forming, friction and wear-reducing properties of a very wide range of low and zero SAPS antiwear additives as possible replacements for ZDDP in engine oils, and, where additive types are effective, to investigate their mechanism of action.

Some of the alternative low and zero SAPS antiwear additives investigated show wear-reducing performance comparable to the ZDDP used as a benchmark in this research. The most promising alternatives to be used as supplements/replacements for ZDDP are suggested and discussed.

One characteristic of ZDDP is that it can form quite thick films on surfaces during rubbing. It is found that many different types of additive can also form thick films, though not generally as thick as ZDDP. However it has been found that there is no significant correlation between the ability of an additive to form a thick boundary film and its ability to control wear. Thick boundary film formation does, however, correlate positively with an increase in friction in contacts operating at intermediate entrainment speeds, so thick film formation should not be taken as a necessary or desirable feature of antiwear additives. It is also found that antiwear additives can give a very wide range of boundary friction coefficient values, depending on the molecular structure of the additive. There thus appears to be scope for optimising the structure of antiwear additives to provide reduced boundary friction.

ACKNOWLEDGEMENTS

I owe my deepest gratitude to my PhD supervisor, Professor Hugh Spikes, for his invaluable support and encouragement throughout this journey.

I am also grateful to Riaz Mufti, Jonathan Green, Gordon Lamb and David Atkinson at Castrol Ltd. for the support and motivation throughout this project.

I would also like to thank all colleagues from the Tribology section of the Mechanical Engineering Department at Imperial College, London, for their help, in special to Tom Reddyhoff and Chrissy Stevens.

Also thanks to Rich Baker, Matt Smeeth, Clive Hamer and John Hutchinson at PCS Instruments, David Scurr at Nottingham University, Mihaela Gorgoi at the Helmholtz-Zentrum Berlin für Materialien und Energie GmbH, Lucia Zuin and Yongfeng Hu at the Canadian Light Source, Maura Crobu at ETH Zurich and Richard Chater at Imperial College London,

And finally, a very special thanks goes to my husband, Ramiro, for his undying support. I could not have done this without you. TAPS.

TABLE OF CONTENTS

PREFACE 2

ABSTRACT 3

ACKNOWLEDGEMENTS 4

TABLE OF CONTENTS 5

LIST OF FIGURES 10

LIST OF TABLES 20

1. INTRODUCTION 22

2. THE IMPACT OF SAPS ON EXHAUST AFTERTREATMENT SYSTEMS 26

2.1 Exhaust Aftertreatment Systems 27

2.1.1 Three-Way Catalyst 28

2.1.2 NOx Storage Catalyst 29

2.1.3 Diesel Oxidation Catalyst 30

2.1.4 Diesel Particulate Filter 31

2.1.5 Selective Catalytic Reduction Catalyst 32

2.2 The Impact of SAPS on Exhaust Aftertreatment Systems 34

2.3 Specifications 35

3. LUBRICATION 37

3.1 Lubrication Regimes 38

3.1.1 Boundary Lubrication 39

3.1.2 Mixed Lubrication 40

3.1.3 Fluid Film Lubrication (Hydrodynamic and Elastohydrodynamic lubrication) 41

3.2 Lubricants 43

3.2.1 Lubricant Formulation Challenges 44

3.3 Wear 45

3.3.1 Archard's Wear Coefficient 47

3.4 Antiwear Additives 48

3.4.1 Zinc Dialkyldithiophosphate (ZDDP) 49

3.4.2 Low and Zero SAPS Antiwear Additives 49

4. EXPERIMENTAL TECHNIQUES 51

4.1 MTM-SLIM Method 52
4.1.1 Description 52
4.1.2 Experimental Procedure 57
4.2 AFM Method 59
4.2.1 Description 59
4.2.2 Experimental Procedure 62
4.3 MTM-Reciprocating Method 63
4.3.1 Description 63
4.3.2 Experimental Procedure 64
4.4 SWLI Method for Measuring Wear 66
4.4.1 SWLI Description 66
4.4.2 Wear Measurement: A Novel Approach 68
4.5 ToF-SIMS Method 79
4.5.1 Description 79
4.5.2 Experimental Procedure 81
4.6 XANES Method 82
4.6.1 Description 82
4.6.2 Experimental Procedure 85
4.7 Test Materials 87

5. FILM-FORMING, FRICTION, MORPHOLOGY AND WEAR-REDUCING PROPERTIES OF ZDDP 90

5.1 Literature Overview of ZDDP 91
5.1.1 Film-forming, Friction and Wear-reducing Properties of ZDDP 92
5.2 Results: Film-forming Properties of ZDDP 94
5.3 Results: Friction Properties of ZDDP-derived Tribofilms 99
5.4 Results: Morphology of ZDDP-derived Tribofilms 100
5.5 Results: Wear-reducing Properties of ZDDP-derived Tribofilms 101
5.6 Discussion of ZDDP Work 104

6. FILM-FORMING, FRICTION, MORPHOLOGY AND WEAR-REDUCING PROPERTIES OF P-CONTAINING ANTIWEAR ADDITIVES 106

6.1 Literature Overview of P-containing Antiwear Additives 107
6.2 Results: Film-forming Properties of P-containing Antiwear Additives 111
6.3 Results: Friction properties of P-containing Antiwear Additive-derived Tribofilm 117
6.4 Results: Morphology of P-containing Antiwear Additive-derived Tribofilms 121

6.5 Results: Wear-reducing Properties of P-containing Antiwear Additive-derived Tribofilms 124
6.6 Discussion of P-containing Antiwear Additives Work 127
7. Film-forming, Friction, Morphology and Wear-reducing Properties of P-S-containing Antiwear Additives 129
7.1 Literature Overview of P-S-containing Antiwear Additives 130
7.2 Results: Film-forming Properties of P-S-containing Antiwear Additives 134
7.3 Results: Friction properties of P-S-containing Antiwear Additive-derived Tribofilm 140
7.4 Results: Morphology of P-S-containing Antiwear Additive-derived Tribofilms 144
7.5 Results: Wear-reducing Properties of P-S-containing Antiwear Additive-derived Tribofilms 147
7.6 Discussion of P-S-containing Antiwear Additives Work 152
8. Film-forming, Friction, Morphology and Wear-reducing Properties of S-containing Antiwear Additives 155
8.1 Literature Overview of S-containing Antiwear Additives 156
8.2 Results: Film-forming Properties of S-containing Antiwear Additives 161
8.3 Results: Friction properties of S-containing Antiwear Additive-derived Tribofilm 167
8.4 Results: Morphology of S-containing Antiwear Additive-derived Tribofilms 169
8.5 Results: Wear-reducing Properties of S-containing Antiwear Additive-derived Tribofilms 172
8.6 Discussion of S-containing Antiwear Additives Work 175
9. Film-forming, Friction, Morphology and Wear-reducing Properties of M-containing Antiwear Additives 177
9.1 Literature Overview of M-containing Antiwear Additives 178
9.2 Results: Film-forming Properties of M-containing Antiwear Additives 182
9.3 Results: Friction properties of M-containing Antiwear Additive-derived Tribofilm 185
9.4 Results: Morphology of M-containing Antiwear Additive-derived Tribofilms 188
9.5 Results: Wear-reducing properties of M-containing Antiwear Additive-derived Tribofilms 190
9.6 Discussion of M-containing Antiwear Additives Work 192
10. Film-forming, Friction, Morphology and Wear-reducing Properties of B-containing Antiwear Additives 194
10.1 Literature Overview of B-containing Antiwear Additives 195
10.2 Results: Film-forming Properties of B-containing Antiwear Additives 200
10.3 Results: Friction properties of B-containing Antiwear Additive-derived Tribofilm 205
10.4 Results: Morphology of B-containing Antiwear Additive-derived Tribofilms 208
10.5 Results: Wear-reducing properties of B-containing Antiwear Additive-derived Tribofilms 210

10.6 Discussion of B-containing Antiwear Additives Work....213

11. FILM-FORMING, FRICTION, MORPHOLOGY AND WEAR-REDUCING PROPERTIES OF N-CONTAINING HETEROCYCLIC ANTIWEAR ADDITIVES....216

11.1 Literature Overview of N-containing Heterocyclic Antiwear Additives....217
11.2 Results: Film-forming Properties of N-containing Heterocyclic Antiwear Additives....220
11.3 Results: Friction properties of N-containing Heterocyclic Antiwear Additive-derived Tribofilm....222
11.4 Results: Morphology of N-containing Heterocyclic Antiwear Additive-derived Tribofilms....224
11.5 Results: Wear-reducing properties of N-containing Heterocyclic Antiwear Additive-derived Tribofilms....225
11.6 Discussion of N-containing Heterocyclic Antiwear Additives Work....227

12. FILM-FORMING, FRICTION, MORPHOLOGY AND WEAR-REDUCING PROPERTIES OF NANOPARTICLE-CONTAINING ANTIWEAR ADDITIVES....228

12.1 Literature Overview of Nanoparticle-containing Antiwear Additives....229
12.2 Results: Film-forming Properties of Nanoparticle-containing Antiwear Additives....238
12.3 Results: Friction properties of Nanoparticle-containing Antiwear Additive-derived Tribofilm....243
12.4 Results: Morphology of Nanoparticle-containing Antiwear Additive-derived Tribofilms....246
12.5 Results: Wear-reducing Properties of Nanoparticle-containing Antiwear Additive-derived Tribofilms249
12.6 Discussion of Nanoparticle-containing Antiwear Additives Work....254

13. SURFACE ANALYSIS OF LOW AND ZERO SAPS ANTIWEAR ADDITIVES-DERIVED TRIBOFILMS....257

13.1 Analysis and Materials....258
13.2 Results: Surface Analysis of ZDDP-derived Tribofilm....261
13.3 Results: Surface Analysis of P-containing Antiwear Additive-derived Tribofilms....263
13.4 Results: Surface Analysis of P-S-containing Antiwear Additive-derived Tribofilms....266
13.5 Results: Surface Analysis of S-containing Antiwear Additive-derived Tribofilms....273
13.6 Results: Surface Analysis of M-containing Antiwear Additive-derived Tribofilms....275
13.7 Results: Surface Analysis of B-containing Antiwear Additive-derived Tribofilms....278
13.8 Results: Surface Analysis of Nanoparticle-containing Antiwear Additive-derived Tribofilms....280
13.9 Summary of Surface Analysis Work....284

14. FILM-FORMING, FRICTION AND WEAR-REDUCING PROPERTIES OF LOW AND ZERO SAPS ANTIWEAR ADDITIVES IN PARTIALLY FORMULATED OILS....286

14.1 Results: Film-forming Properties of Low and Zero SAPS Antiwear Additives in Partially Formulated Oils....287
14.2 Results: Friction Properties of Low and Zero SAPS Antiwear Additives in Partially Formulated Oils 293

14.3 Results: Wear-reducing Properties of Low and Zero SAPS Antiwear Additives in Partially Formulated Oils 295
14.4 Discussion of Low and Zero SAPS Antiwear Additives in Partially Formulated Oils Work 298
15. GENERAL DISCUSSION 302
15.1 Overall Comparison of Film-forming, Friction and Wear-reducing Properties of Low and Zero SAPS Antiwear Additives 303
15.2 Correlations 310
15.3 Most Promising Alternatives 315
16. CONCLUSIONS AND SUGGESTIONS FOR FUTURE WORK 317
16.1 Conclusions 318
16.2 Suggestions for Future Work 320
REFERENCES 322
APPENDIX 348
Stribeck Curves 349
List of Publications 360

LIST OF FIGURES

CHAPTER 2 THE IMPACT OF SAPS ON EXHAUST AFTERTREATMENT SYSTEMS

Figure 2.1: Traffic and smog in Los Angeles, California in the 1950s [3, 4]. 27
Figure 2.2: Ceramic honeycomb "monolith" with varying cell density [8]. 28
Figure 2.3: Schematic diagram of TWC [10]. 29
Figure 2.4: Catalyst conversion efficiency at Rich (λ<1), quasi-Stoichiometric (TWC; λ~1) and Lean (λ>1) driving conditions [11]. 29
Figure 2.5: NOx storage catalyst mechanism under lean and rich operation [13, 14]. 30
Figure 2.6: DPF: exhaust gas flows through the porous filter channels with alternate blocked ends, thus collecting soot [17]. 31
Figure 2.7: CRT: exhaust gas flows through the DOC, which removes HC and CO, while converting NO into NO2. NO2 reacts with the soot trapped in the DPF, regenerating the filter [21]. 32
Figure 2.8: Diesel exhaust aftertreatment system diagram [25]. 33
Figure 2.9: Damaging effect of sulphated ash on DPF [29]. 34

CHAPTER 3 LUBRICATION

Figure 3.1: Stribeck curve: friction coefficient variation with operating parameters (Uη/W) or fluid film thickness (h) [48]. 38
Figure 3.2: Elastohydrodynamic lubrication takes place in gears, rolling elements (*i.e.* ball bearings) and other non-conforming contacts [57]. 42
Figure 3.3:Wear modes: (a) abrasive wear by microcutting of ductile bulk surface; (b) adhesive wear by adhesive shear and transfer; (c) flow wear by accumulated plastic shear flow; (d) fatigue wear by crack initiation and propagation; (e) corrosive wear by shear fracture of ductile tribofilm; (f) corrosive wear by delamination of brittle tribofilm; (g) corrosive wear by accumulated plastic shear flow of soft tribofilm; (h) corrosive wear by shaving of soft tribofilm; and (i) melt wear by local melting and transfer of scattering [61]. 46
Figure 3.4: Molecular structure of ZDDP [65]. 49

CHAPTER 4 EXPERIMENTAL TECHNIQUES

Figure 4.1: Schematic diagram of MTM-SLIM [68]. 52
Figure 4.2: Stribeck curves showing friction coefficient versus entrainment speed at increasing rubbing times for a ZDDP-containing oil at 50% SRR, 31 N and 100 ºC [69]. 53
Figure 4.3: Schematic diagram of film thickness measurement using MTM-SLIM: (a) The ball is loaded against the spacer layer glass disc and (b) an interference image of the rubbed track on the ball is obtained, (c) which enables film growth and thickness evaluation over rubbing time [69, 74]. 56
Figure 4.4: Atomic force microscopy: general components and their functions [78]. 60
Figure 4.5: Typical AFM topography images: (a) two-dimensional (2D) image of ZDDP-derived tribofilm and (b) line profile across the edge of the wear track, spanning rubbed/unrubbed areas. Further topographical representations include: 3D plots, roughness, film thickness, *etc.* 61
Figure 4.6: Reciprocating mechanism diagram showing ball specimen continuously rotating against the reciprocating disc [79]. 63

Figure 4.7: Typical SWLI images: (a) two [69] and (b) three-dimensional profiles of wear tracks after wear testing using MTM-Reciprocating. 66
Figure 4.8: Diagram illustrating the principle of SWLI imaging system [84]. 67
Figure 4.9: Wear scar on the MTM disc after reciprocating test [87]. 68
Figure 4.10: Typical (a) 2D topography image and (b) line profile plot across the wear track on the MTM disc after 4 hours of rubbing in ZDDP-containing oil. These images indicate that the track appears to have worn. 69
Figure 4.11: AFM Topography and line profile plot across the edge of the wear track on the MTM disc after 4 hours of rubbing in ZDDP-containing oil. 69
Figure 4.12: Possible film measured by AFM versus SWLI [89]. 70
Figure 4.13: Molecular structure of EDTA [89]. 70
Figure 4.14: Typical (a) 2D topography and (b) 3D images of the wear track on the MTM disc after part of the tribofilm appears to be removed by EDTA. 71
Figure 4.15: Line profile plot across the wear track before and after removal of the tribofilm with EDTA. 72
Figure 4.16: 2D topography image of wear track after gold deposition. 73
Figure 4.17: Line profile plot showing EDTA/non-EDTA treated regions, tribofilm, EDTA treated region and outside wear track after gold deposition. 73
Figure 4.18: Molecular structure of oxalic acid. 75
Figure 4.19: Typical (a) 2D topography image, (b) 3D image and (c) line profile plot of the wear track on an MTM disc before and after the removal of a non-ZDDP-derived tribofilm with oxalic acid + EDTA. These images reveal the optical artifact in the presence of low and zero SAPS-derived tribofilms; hence the need to remove the film to measure wear depth. 75
Figure 4.20: Typical 2D topography image and line profile plot of the wear track on the MTM disc after the removal of tribofilm. These images exemplify how wear depth measurements are carried out. 76
Figure 4.21: Mean speed versus time of two complete cycles [89]: illustrating disc speed (Ud) variation throughout the cycle. 77
Figure 4.22: Diagram illustrating the removal of secondary ions (*i.e.* positive secondary ions, negative secondary ions and neutral fragments) from the outermost surface of the sample [97]. 79
Figure 4.23: Principle of ToF-SIMS [98]. 80
Figure 4.24: Typical ToF-SIMS chemical map showing the distribution of Fe on the wear track of the MTM disc, spanning rubbed/unrubbed areas. Brighter regions in the image indicate an abundance of element or molecule of interest, while darker regions indicate their absence. The image suggests the formation of a thick protective film inside the wear track and negligible tribofilm outside rubbed area. 81
Figure 4.25: The photoelectric effect [107]. 82
Figure 4.26: Typical sampling depth for XANES analysis of phosphorus and sulphur-containing tribofilms [108]. TEY provides chemical information about the surface/near surface of the film *(i.e.* ≈ 5 nm) at the L-edge; and the bulk of the film *(i.e.* ≈ 50 nm) at the K-edge. FY focuses on the bulk of the film *(i.e.* ≈ 50 nm) at the L-edge; and on the interface steel-protective film through to the substrate (> 5 μm) at the K-edge. 83
Figure 4.27: Typical XANES analysis of sulphur-containing tribofilms [109]: showing S K-edge spectra (TEY) of tribofilms derived from thiophosphate additives (*e.g.* DTP-1, DTP-2, MTP) in the presence of a detergent (*i.e.* DET-1), along with model compounds of varying oxidation states (*i.e.* FeS, FeS_2, Na_2SO_3, $FeSO_4$). A comparison between the tribofilms and model compounds can be established and the chemical nature and oxidation state of elements in the tribofilm can be identified. 84

CHAPTER 5 FILM-FORMING, FRICTION, MORPHOLOGY AND WEAR-REDUCING PROPERTIES OF ZDDP

Figure 5.1:Molecular structure of ZDDP [65]. 91

Figure 5.2: Schematic diagram of ZDDP-derived pad structure and composition [88]. 92
Figure 5.3: Stribeck curves showing friction coefficient *versus* entrainment speed at increasing rubbing times for a ZDDP-containing oil at 50 % SRR, 31 N and 100 ºC [69]. 93
Figure 5.4: MTM-SLIM images showing: a) scuffing on the surface of the ball after 5 minutes of rubbing in base oil without antiwear additive; b) and c) the growth of tribofilm on the ball with increasing rubbing time (*i.e.* zero, 5, 15, 30, 60, 120 minutes). 95
Figure 5.5: MTM-SLIM images showing: a) and b) the growth of tribofilm on the ball with increasing rubbing time (*i.e.* zero, 5, 15, 30, 60, 120 minutes). 96
Figure 5.6: MTM-SLIM images showing: a) to d) the growth of tribofilm on the ball with increasing rubbing time (*i.e.* zero, 5, 15, 30, 60, 120 minutes). 97
Figure 5.7: MTM-SLIM images showing: a) and b) the growth of tribofilm on the ball with increasing rubbing time (*i.e.* zero, 5, 15, 30, 60, 120 minutes). 98
Figure 5.8: Mean film thickness with rubbing time for Primary ZDDP (C). 99
Figure 5.9: Stribeck curve showing friction coefficient *versus* entrainment speed at the beginning and after 2 h of rubbing for Primary ZDDP (C) at 50 % SRR, 30 N and 100 ºC. 100
Figure 5.10: AFM 2D topography image at the centre of the wear track on the MTM-disc (sliding direction in b) shown by the arrow). 101
Figure 5.11: SWLI 2D topography images of the wear track on the disc. 102
Figure 5.12: Wear coefficient (k_1) in the middle (M) and at the ends (E) of the wear track (*i.e.* average of both ends) for tests lasting 4, 8 and 16 hours. 103

CHAPTER 6 FILM-FORMING, FRICTION, MORPHOLOGY AND WEAR-REDUCING PROPERTIES OF P-CONTAINING ANTIWEAR ADDITIVES

Figure 6.1: Molecular structures of main classes of organophosphorus compounds suggested as antiwear additives for engines. 107
Figure 6.2: Molecular structure of TCP. 107
Figure 6.3: Two alternative models for the adsorption and reaction of TCP on iron [159]. 108
Figure 6.4: Tautomerism of dialkyl and diaryl phosphonates. 109
Figure 6.5: Proposed structure of protective film formed by dialkyl and diaryl phosphonates [67]. 110
Figure 6.6: MTM-SLIM images showing: a) scuffing on the surface of the ball after 5 minutes of rubbing in base oil without antiwear additive; b) to g) the growth of tribofilm on the ball with increasing rubbing time (*i.e.* zero, 5, 15, 30, 60, 120 minutes). 113
Figure 6.7: Mean film thickness with rubbing time for P-containing antiwear additives. 114
Figure 6.8: MTM-SLIM images showing: a) to g) the growth of tribofilm on the ball with increasing rubbing time (*i.e.* zero, 5, 15, 30, 60, 120 minutes). 116
Figure 6.9: Stribeck curve showing friction coefficient *versus* entrainment speed at the beginning and after 2 h of rubbing at 50 % SRR, 30 N and 100 ºC. 119
Figure 6.10: Stribeck curve showing friction coefficient *versus* entrainment speed at the beginning and after 2 h of rubbing at 50 % SRR, 30 N and 100 ºC. 120
Figure 6.11: AFM 2D topography image at the centre of the wear track on the MTM-disc (sliding direction in b) to f) shown by the arrow). 122
Figure 6.12: AFM 2D topography image at the centre of the wear track on the MTM-disc (sliding direction in a) and b) shown by the arrow). 123
Figure 6.13: SWLI 2D topography images of the wear track on the disc. 125

Figure 6.14: Wear coefficient (k_1) in the middle (M) and at the ends (E) of the wear track (*i.e.* average of both ends) for tests lasting 4, 8 and 16 hours. 126
Figure 6.15: Wear behaviour of rubbing components over their life span: (i) running-in wear, (ii) steady-state wear and (iii) wear out [176]. 127

CHAPTER 7 FILM-FORMING, FRICTION, MORPHOLOGY AND WEAR-REDUCING PROPERTIES OF P-S-CONTAINING ANTIWEAR ADDITIVES

Figure 7.1: Molecular structure of ashless dithiophosphate [67]. 130
Figure 7.2: Molecular structure of ashless alkyl and aryl thiophosphate and thiophosphite esters [67]. 130
Figure 7.3: Molecular structure of ashless phosphate ester derivatives studied by Schumacher *et al.*, where X^{1-2} = O and/or S; R^1 = alkyl, cycloalkyl, aryl; Z = $-OR^2$, $-N(R^3)_2$; R^2, R^3 = alkyl, cycloalkyl [179]. 131
Figure 7.4: Molecular structure of alkyl amido thiophosphate, where R^2 can be H [67]. 131
Figure 7.5: Molecular structure of alkyl amine dithiophosphate, where $R^{2, 3, 4}$ can be H [67]. 131
Figure 7.6: Synthesis of functionalised dithiophosphates by treating dithiophosphoric acid with methacrylic acid [187]. 132
Figure 7.7: Wear scar width as a function of ZDDP/DDP concentration after 1 hour of reciprocating at 25 Hz, 225 N and 100 ºC [195]. 133
Figure 7.8: MTM-SLIM images showing: a) scuffing on the surface of the ball after 5 minutes of rubbing in base oil without antiwear additive; b) to g) the growth of tribofilm on the ball with increasing rubbing time (*i.e.* zero, 5, 15, 30, 60, 120 minutes). 136
Figure 7.9: Mean film thickness with rubbing time for P-containing antiwear additives. 138
Figure 7.10: MTM-SLIM images showing: a) to g) the growth of tribofilm on the ball with increasing rubbing time (*i.e.* zero, 5, 15, 30, 60, 120 minutes). 139
Figure 7.11: Stribeck curve showing friction coefficient *versus* entrainment speed at the beginning and after 2 h of rubbing at 50 % SRR, 30 N and 100 ºC. 142
Figure 7.12: Stribeck curve showing friction coefficient *versus* entrainment speed at the beginning and after 2 h of rubbing at 50 % SRR, 30 N and 100 ºC. 143
Figure 7.13: AFM 2D topography image at the centre of the wear track on the MTM-disc (sliding direction in b) to f) shown by the arrow). 145
Figure 7.14: AFM 2D topography image at the centre of the wear track on the MTM-disc (sliding direction in a) to c) shown by the arrow). 147
Figure 7.15: Wear coefficient (k_1) in the middle (M) and at the ends (E) of the wear track (*i.e.* average of both ends) for tests lasting 4, 8 and 16 hours. 148
Figure 7.16: SWLI 2D topography images of the wear track on the disc. 150

CHAPTER 8 FILM-FORMING, FRICTION, MORPHOLOGY AND WEAR-REDUCING PROPERTIES OF S-CONTAINING ANTIWEAR ADDITIVES

Figure 8.1: Molecular structures of (a) thiadiazole and (b) dimercaptothiadizole derivatives. 157
Figure 8.2: Molecular structure of 2,5-dialkoxymethylthio-1,3,4-thiadiazole derivatives [215]. 157
Figure 8.3: Molecular structure of (a) 2-mercaptobenzoxazole, (b) 2-mercaptobenzothiazole and (c) 2-mercaptobenzimidazole. 158
Figure 8.4: Molecular structure of (a) bis-(aryl/alkyl) thiuram disulphide, (b) bis-aryl xanthogen and (c) aryl/alkyl dithiocarbamate, where R^1 = naphthyl, ethanol or diethanol; R^2 = phenyl or naphthyl; R^3 = phenyl, naphthyl, ethanol, diethanol or benzyl [227]. 159
Figure 8.5: Molecular structure of (a) S-(1-H-benzimidazole-2-yl)methyl-N,N-dioctyldithiocarbamate and (b) S-ethyl-N,N-dioctyldithiocarbamate [228]. 160

Figure 8.6: Molecular structure of S-(1-H-benzotriazol-1-yl)methyl alkyl xanthate derivatives, where R = ethyl, n-butyl or n-octyl [229]. 160
Figure 8.7: MTM-SLIM images showing: a) scuffing on the surface of the ball after 5 minutes of rubbing in base oil without antiwear additive; b) to g) the growth of tribofilm on the ball with increasing rubbing time (*i.e.* zero, 5, 15, 30, 60, 120 minutes). 164
Figure 8.8: Mean film thickness with rubbing time for S-containing antiwear additives. 166
Figure 8.9: Stribeck curve showing friction coefficient *versus* entrainment speed at the beginning and after 2 h of rubbing at 50 % SRR, 30 N and 100 ºC. 168
Figure 8.10: AFM 2D topography image at the centre of the wear track on the MTM-disc (sliding direction in b) to f) shown by the arrow). 170
Figure 8.11: SWLI 2D topography images of the wear track on the disc. 173
Figure 8.12: Wear coefficient (k_1) in the middle (M) and at the ends (E) of the wear track (*i.e.* average of both ends) for tests lasting 4, 8 and 16 hours. 175

CHAPTER 9 FILM-FORMING, FRICTION, MORPHOLOGY AND WEAR-REDUCING PROPERTIES OF M-CONTAINING ANTIWEAR ADDITIVES

Figure 9.1: Molecular structures of sulphur-free zinc dialkylphosphates studied by Hoshino *et al.* [246]. 179
Figure 9.2: High resolution TEM image of MoS_2 nanoparticle [270] 181
Figure 9.3: Molecular structure of the organomolybdenum additive studied by Yan *et al.* [272]. 182
Figure 9.4: MTM-SLIM images showing: a) scuffing on the surface of the ball after 5 minutes of rubbing in base oil without antiwear additive; b) to g) the growth of tribofilm on the ball with increasing rubbing time (*i.e.* zero, 5, 15, 30, 60, 120 minutes). 184
Figure 9.5: Mean film thickness with rubbing time for M-containing antiwear additives. 185
Figure 9.6: Stribeck curve showing friction coefficient *versus* entrainment speed at the beginning and after 2 h of rubbing at 50 % SRR, 30 N and 100 ºC. 187
Figure 9.7: AFM 2D topography image at the centre of the wear track on the MTM-disc (sliding direction in b) to f) shown by the arrow). 189
Figure 9.8: Wear coefficient (k_1) in the middle (M) and at the ends (E) of the wear track (*i.e.* average of both ends) for tests lasting 4, 8 and 16 hours. 190
Figure 9.9: SWLI 2D topography images of the wear track on the disc. 191

CHAPTER 10 FILM-FORMING, FRICTION, MORPHOLOGY AND WEAR-REDUCING PROPERTIES OF B-CONTAINING ANTIWEAR ADDITIVES

Figure 10.1: Hydrolytic degradation of borated esters, which produce oil-insoluble and abrasive boric acid [293, 294]. 196
Figure 10.2: Molecular structure of amino-ethyl borate ester prepared by Yao *et al.* [293], where R_1, R_2, R_1', R_2' = alkyl substituent groups. 196
Figure 10.3: Evolution of film thickness with rubbing time for boron-containing fully formulated oils, with and without ZDDP [299]. ... 197
Figure 10.4: Topography of the wear scar on the ball after rubbing with base oil alone, 1% ZDDP and 1% DOB-DTP. Images taken using an optical profiler WYKO NT1100 [301]. 198
Figure 10.5: Topography of the wear scar on the ball after rubbing with (a) base oil alone, (b) 1% DBB-EBzDTC, (c) 1% DOB-EBzDTC and (d) 1% DOB-EEDTC. Images taken using an optical profiler WYKO NT1100 [304]. 199
Figure 10.6: Proposed mechanism of film formation by TMB under UHV in gas phase lubrication [305]. 200

Figure 10.7: MTM-SLIM images showing: a) scuffing on the surface of the ball after 5 minutes of rubbing in base oil without antiwear additive; b) to g) the growth of tribofilm on the ball with increasing rubbing time (*i.e.* zero, 5, 15, 30, 60, 120 minutes). 203
Figure 10.8: Mean film thickness with rubbing time for B-containing antiwear additives. 205
Figure 10.9: Stribeck curve showing friction coefficient *versus* entrainment speed at the beginning and after 2 h of rubbing at 50 % SRR, 30 N and 100 ºC. 207
Figure 10.10: AFM 2D topography image at the centre of the wear track on the MTM-disc (sliding direction in b) to f) shown by the arrow). 209
Figure 10.11: Wear coefficient (k_1) in the middle (M) and at the ends (E) of the wear track (*i.e.* average of both ends) for tests lasting 4, 8 and 16 hours. 211
Figure 10.12: SWLI 2D topography images of the wear track on the disc. 212

CHAPTER 11 FILM-FORMING, FRICTION, MORPHOLOGY AND WEAR-REDUCING PROPERTIES OF N-CONTAINING HETEROCYCLIC ANTIWEAR ADDITIVES

Figure 11.1: Molecular structure of some nitrogen-containing heterocyclic compounds, *i.e.* (a) pyridine, (b) quinoline and (c) indole, studied by Rudston *et al.* [309]. 217
Figure 11.2: Molecular structure of nitrogen-containing heterocyclic compounds, *i.e.* (a) indole, (b) indazole and (c) benzotriazole, studied by Ren *et al.* [311]. 218
Figure 11.3: Molecular structure of 8-hydroxyquinoline studied by Wei *et al.* [312, 313]. 218
Figure 11.4: SEM images of rubbed surfaces at different magnifications, *i.e.* 70x and 300x: (a, b) polyurea grease alone, (c, d) zinc dialkyldithiophosphate additive package (T204) and (e, f) novel benzotriazole-containing imidazolium ionic liquid ([BTAMIM][PF_6]). Reciprocating tests were run at 150 ºC for 30 minutes at a load of 30 N, 1 mm stroke length, 25 Hz frequency and 2 % additive in solution [314]. 219
Figure 11.5: MTM-SLIM images showing: a) scuffing on the surface of the ball after 5 minutes of rubbing in base oil without antiwear additive; b) to d) the growth of tribofilm on the ball with increasing rubbing time (*i.e.* zero, 5, 15, 30, 60, 120 minutes). 221
Figure 11.6: Mean film thickness with rubbing time for N-containing heterocyclic antiwear additives. 222
Figure 11.7: Stribeck curve showing friction coefficient *versus* entrainment speed at the beginning and after 2 h of rubbing at 50 % SRR, 30 N and 100 ºC. 223
Figure 11.8: AFM 2D topography image at the centre of the wear track on the MTM-disc (sliding direction in b) to d) shown by the arrow). 224
Figure 11.9: Wear coefficient (k_1) in the middle (M) and at the ends (E) of the wear track (*i.e.* average of both ends) for tests lasting 4, 8 and 16 hours. 225
Figure 11.10: SWLI 2D topography images of the wear track on the disc. 226

CHAPTER 12 FILM-FORMING, FRICTION, MORPHOLOGY AND WEAR-REDUCING PROPERTIES OF NANOPARTICLE-CONTAINING ANTIWEAR ADDITIVES

Figure 12.1: Schematic diagram of overbased calcium alkylsulphonate detergent structure: $CaCO_3$ nanoparticle core stabilised by chemisorbed calcium alkylbenzene sulphonate molecules [333]. 231
Figure 12.2: Topography images of overbased calcium sulphonate detergent-derived tribofilms studied by Topolovec-Miklozic *et al.* [94]. 232

Figure 12.3: Stribeck curves showing friction coefficient *versus* entrainment speed throughout rubbing for the commercially-available overbased calcium sulphonate detergents studied by Topolovec-Miklozic *et al.* [94]. 232
Figure 12.4: Molecular structure of fullerene C_{60}. 233
Figure 12.5: Schematic diagram of fullerene-derived tribofilm suggested by Ginsburg *et al.*: network of fullerene molecules linked by polyolefin chains [356]. 234
Figure 12.6: Wear track on orbiting plate of sliding thrust bearing tester used by Lee *et al.* [357]. Black coloured circles indicating the presence of carbonaceous material formed under rubbing with: a) base oil alone and b) fullerene-containing oil. 235
Figure 12.7: Molecular structure of single- and multi-walled carbon nanotubes [362]. 236
Figure 12.8: High resolution TEM images of IF-WS_2 nanoparticles: a) before rubbing and b) after rubbing, where the arrow indicates the presence of exfoliated sheets [367]. 237
Figure 12.9: SEM images of wear track on SRV test specimens: a) base oil alone, b) IF-MoS_2 and c) trioctylamine-modified IF-WS_2 [369]. 237
Figure 12.10: MTM-SLIM images showing: a) scuffing on the surface of the ball after 5 minutes of rubbing in base oil without antiwear additive; b) to g) the growth of tribofilm on the ball with increasing rubbing time (*i.e.* zero, 5, 15, 30, 60, 120 minutes). 241
Figure 12.11: Mean film thickness with rubbing time for nanoparticle-containing antiwear additives. 243
Figure 12.12: Stribeck curve showing friction coefficient *versus* entrainment speed at the beginning and after 2 h of rubbing at 50 % SRR, 30 N and 100 ºC. 245
Figure 12.13: AFM 2D topography image at the centre of the wear track on the MTM-disc (sliding direction in b) to f) shown by the arrow). 247
Figure 12.14: Wear coefficient (k_1) in the middle (M) and at the ends (E) of the wear track (*i.e.* average of both ends) for tests lasting 4, 8 and 16 hours. 249
Figure 12.15: SWLI 2D topography images of the wear track on the disc. 251

CHAPTER 13 SURFACE ANALYSIS OF LOW AND ZERO SAPS ANTIWEAR ADDITIVES-DERIVED TRIBOFILMS

Figure 13.1: ToF-SIMS chemical maps of tribofilm formed by Primary ZDDP (C), *i.e.* ZDDP1, (outermost surface, 1-2 nm). In this case, the wear track is seen at the top of the images. 262
Figure 13.2: XANES spectra of tribofilm formed by Primary ZDDP (C), corresponding fresh additive and model compounds: (a) phosphorus K-edge FY (bulk through the film-steel interface to the substrate, > 5 μm) and (b) sulphur K-edge FY (bulk through the film-steel interface to the substrate, > 5 μm). 263
Figure 13.3: ToF-SIMS chemical maps of tribofilms formed by: a) Bis(2-ethylhexyl) phosphite, b) Bis(2-ethylhexyl) phosphite + 1% Titanium (IV) isopropoxide and c) Triaryl phosphate (C) (outermost surface, 1-2 nm). In these cases, the tribofilm is seen in the middle of the images. 264
Figure 13.4: XANES spectra of tribofilms formed by Bis(2-ethylhexyl) phosphite, *i.e.* B2EHP, Bis(2-ethylhexyl) phosphite + 1% Titanium (IV) isopropoxide, *i.e.* B2EHP + Ti-IPO, Triaryl phosphate (C), *i.e.* TAP, corresponding fresh additives and model compounds: (a) phosphorus L-edge FY (bulk, ≈ 50 nm) and (b) phosphorus K-edge FY (bulk through the film-steel interface to the substrate, > 5 μm). 265
Figure 13.5: ToF-SIMS chemical maps of tribofilms formed by: a) Ashless dithiophosphate (C) and b) Ashless dithiophosphate (C) + 1 % nCaSu (outermost surface, 1-2 nm). In these cases, the tribofilm is seen in the middle of the images. 267
Figure 13.6: XANES spectra of tribofilms formed by Ashless dithiophosphate (C), *i.e.* ADTP, Ashless dithiophosphate (C) + 1 % Titanium (IV) isopropoxide, *i.e.* ADTP + Ti-IPO, corresponding fresh additives and model compounds: (a) phosphorus L-edge TEY (surface/near surface, ≈ 5 nm) and (b) sulphur L-edge TEY (surface/near surface, ≈ 5 nm). 269

Figure 13.7: XANES spectra of tribofilms formed by Ashless dithiophosphate (C), *i.e.* ADTP, Ashless dithiophosphate (C) + 1 % nCaSu, *i.e.* ADTP + nCaSu, Ashless dithiophosphate (C) + 1 % Titanium (IV) isopropoxide, *i.e.* ADTP + Ti-IPO, corresponding fresh additives and model compounds: (a) phosphorus K-edge FY (bulk through the film-steel interface to the substrate, > 5 µm) and (b) sulphur K-edge FY (bulk through the film-steel interface to the substrate, > 5 µm). 270
Figure 13.8: XANES spectra of tribofilms formed by Triphenyl phosphorothionate (C), *i.e.* TPPT, Alkylated triphenyl phosphorothionate (C), *i.e.* ATPPT, corresponding fresh additives and model compounds: phosphorus L-edge TEY (surface/near surface, ≈ 5 nm). 271
Figure 13.9: XANES spectra of tribofilms formed by Triphenyl phosphorothionate (C), *i.e.* TPPT, Alkylated triphenyl phosphorothionate (C), *i.e.* ATPPT, corresponding fresh additives and model compounds: (a) phosphorus K-edge FY (bulk through the film-steel interface to the substrate, > 5 µm) and (b) sulphur K-edge FY (bulk through the film-steel interface to the substrate, > 5 µm). 272
Figure 13.10: ToF-SIMS chemical map of tribofilm formed by Methylene-bis-dialkyl-dithiocarbamate (C), *i.e.* MBDADTC, (outermost surface, 1-2 nm). In this case, the tribofilm is seen in the middle of the images. 273
Figure 13.11: XANES spectra of tribofilms formed by Dimercaptothiadiazole 2 (C), *i.e.* DMTDA2, Methylene-bis-dialkyl-dithiocarbamate (C), *i.e.* MBDADTC, corresponding fresh additives and model compounds: (a) sulphur L-edge TEY (surface/near surface, ≈ 5 nm) and (b) sulphur K-edge FY (bulk through the film-steel interface to the substrate, > 5 µm). 274
Figure 13.12: ToF-SIMS chemical map of tribofilm formed by Molybdenum dialkyldithiocarbamate (C), *i.e.* MoDTC, (outermost surface, 1-2 nm). In this case, the tribofilm is seen in the middle of the images. 275
Figure 13.13: XANES spectra of tribofilms formed by Zinc diamyl dithiocarbamate (C), *i.e.* ZnDTC, Molybdenum dialkyldithiocarbamate (C), *i.e.* MoDTC, and model compounds: (a) sulphur L-edge TEY (surface/near surface, ≈ 5 nm). 276
Figure 13.14: XANES spectra of tribofilms formed by Zinc diamyl dithiocarbamate (C), *i.e.* ZnDTC, Molybdenum dialkyldithiocarbamate (C), *i.e.* MoDTC, corresponding fresh additives and model compounds: (a) sulphur K-edge TEY (bulk, ≈ 50 nm) and (b) sulphur K-edge FY (bulk through the film-steel interface to the substrate, > 5 µm). 277
Figure 13.15: ToF-SIMS chemical maps of tribofilms formed by: a) Borated polyisobutenyl succinimide (High B) (C), *i.e.* B-PIBS(H), and b) Potassium borate (C), *i.e.* KB, (outermost surface, 1-2 nm). In these cases, the tribofilm is seen in the middle of the images. 278
Figure 13.16: XANES spectra of tribofilms formed by Tris(2-ethylhexyl) borate (C), *i.e.* TEHB, Borated polyisobutenyl succinimide (High B) (C), *i.e.* B-PIBS(H), Potassium borate (C), *i.e.* KB, corresponding fresh additives and model compounds: (a) boron K-edge TEY (surface/near surface, ≈ 6 nm) and (b) boron K-edge FY (bulk through the film-steel interface, ≈ 100 nm). 279
Figure 13.17: ToF-SIMS chemical maps of tribofilms formed by: a) Polyisobutylene succinimide dispersant 1 (C), b) Titanium oxide nanoparticles (C) + 0.1 % PIBS1, c) IF-WS_2 + 0.1 % PIBS1, d) p-Carborane (C) and e) m-Carborane (outermost surface, 1-2 nm). In these cases, the tribofilm is seen in the middle of the images. 281
Figure 13.18: XANES spectra of tribofilms formed by IF-WS_2 + PIBS1, cOBCaSu, aOBCaSu, nCaSu, corresponding fresh additives and model compounds: sulphur K-edge FY (bulk through the film-steel interface to the substrate, > 5 µm). 283

CHAPTER 14 FILM-FORMING, FRICTION AND WEAR-REDUCING PROPERTIES OF LOW AND ZERO SAPS ANTIWEAR ADDITIVES IN PARTIALLY FORMULATED OILS

Figure 14.1: MTM-SLIM images showing: a) scuffing on the surface of the ball after 5 minutes of rubbing in base oil without antiwear additive; b) to g) the growth of tribofilm on the ball with increasing rubbing time (*i.e.* zero, 5, 15, 30, 60, 120 minutes). 290
Figure 14.2: Mean film thickness with rubbing time for low and zero SAPS antiwear additives in partially formulated oils without dispersant. 292
Figure 14.3: Mean film thickness with rubbing time for low and zero SAPS antiwear additives in partially formulated oils with dispersant. 292
Figure 14.4: Stribeck curve showing friction coefficient *versus* entrainment speed at the beginning and after 2 h of rubbing at 50 % SRR, 30 N and 100 ºC. 294

Figure 14.5: Wear coefficient (k_1) in the middle (M) and at the ends (E) of the wear track (*i.e.* average of both ends) for test lasting 16 hours. 296
Figure 14.6: SWLI 2D topography images of the wear track on the disc after 16 h rubbing. 297
Figure 14.7: Mean film thickness after 2 hours of rubbing for low and zero SAPS antiwear additives in partially formulated oils. 298
Figure 14.8: Friction coefficient after 2 hours of rubbing at the low, intermediate and high speed regions, *i.e.* 10, 100 and 1000 mm/s, for low and zero SAPS antiwear additives in partially formulated oils. 299
Figure 14.9: Wear coefficient[1], $k_1 \times 10^{-9}$, after 16 hours of rubbing for low and zero SAPS antiwear additives in partially formulated oils. ([1]This corresponds to the average of wear coefficients taken in the middle and at the edges of the wear track) 299

CHAPTER 15 GENERAL DISCUSSION

Figure 15.1: Mean film thickness after 2 hours of rubbing for ZDDP and low and zero SAPS antiwear additives in base oil alone (*i.e.* whenever possible to measure film thickness using MTM-SLIM). 306
Figure 15.2: Friction coefficient after 2 hours of rubbing at the low speed region, *i.e.* 10 mm/s, for ZDDP and low and zero SAPS antiwear additives in base oil alone. 307
Figure 15.3: Friction coefficient after 2 hours of rubbing at the intermediate speed region, *i.e.* 100 mm/s, for ZDDP and low and zero SAPS antiwear additives in base oil alone. 307
Figure 15.4: Friction coefficient after 2 hours of rubbing at the high speed region, *i.e.* 1000 mm/s, for ZDDP and low and zero SAPS antiwear additives in base oil alone. 308
Figure 15.5: Wear coefficient[1], $k_1 \times 10^{-9}$, after 16 hours of rubbing for ZDDP and low and zero SAPS antiwear additives in base oil alone. ([1]This corresponds to the average of wear coefficients taken in the middle and at the edges of the wear track) 310
Figure 15.6: Mean film thickness *versus* friction coefficient at the low speed region, *i.e.* 10 mm/s, after 2 hours of rubbing for all additives in base oil alone, partially or fully formulated oils (*i.e.* whenever possible to measure film thickness using MTM-SLIM). Legend: red: ZDDP1, orange: phosphorus-containing compounds, light green: phosphorus-sulphur-containing compounds, dark green: sulphur-containing compounds, light blue: metal-containing compounds, dark blue: boron-containing compounds, indigo: nitrogen-containing heterocyclic compounds, magenta: nanoparticle-containing compounds, black: antiwear additives in partially formulated oils. 311
Figure 15.7: Mean film thickness *versus* friction coefficient at the intermediate speed region, *i.e.* 100 mm/s, after 2 hours of rubbing for all additives in base oil alone, partially or fully formulated oils (*i.e.* whenever possible to measure film thickness using MTM-SLIM). Legend: red: ZDDP1, orange: phosphorus-containing compounds, light green: phosphorus-sulphur-containing compounds, dark green: sulphur-containing compounds, light blue: metal-containing compounds, dark blue: boron-containing compounds, indigo: nitrogen-containing heterocyclic compounds, magenta: nanoparticle-containing compounds, black: antiwear additives in partially formulated oils. 312
Figure 15.8: Mean film thickness *versus* friction coefficient at the high speed region, *i.e.* 1000 mm/s, after 2 hours of rubbing for all additives in base oil alone, partially or fully formulated oils (*i.e.* whenever possible to measure film thickness using MTM-SLIM). Legend: red: ZDDP1, orange: phosphorus-containing compounds, light green: phosphorus-sulphur-containing compounds, dark green: sulphur-containing compounds, light blue: metal-containing compounds, dark blue: boron-containing compounds, indigo: nitrogen-containing heterocyclic compounds, magenta: nanoparticle-containing compounds, black: antiwear additives in partially formulated oils. 313

Figure 15.9: Mean film thickness after 2 hours of rubbing *versus* wear coefficient[1], k_1 x 10^{-9}, after 16 hours of rubbing for all additives in base oil alone, partially or fully formulated oils (*i.e.* whenever possible to measure film thickness using MTM-SLIM). Legend: red: ZDDP1, orange: phosphorus-containing compounds, light green: phosphorus-sulphur-containing compounds, dark green: sulphur-containing compounds, light blue: metal-containing compounds, dark blue: boron-containing compounds, indigo: nitrogen-containing heterocyclic compounds, magenta: nanoparticle-containing compounds, black: antiwear additives in partially formulated oils. ([1]This corresponds to the average of wear coefficients taken in the middle and at the edges of the wear track) 314
Figure 15.10: Friction coefficient at the intermediate speed region, *i.e.* 100 mm/s, after 2 hours of rubbing *versus* wear coefficient[1], k_1 x 10^{-9}, after 16 hours of rubbing for all additives in base oil alone, partially or fully formulated oils. Legend: red: ZDDP1, orange: phosphorus-containing compounds, light green: phosphorus-sulphur-containing compounds, dark green: sulphur-containing compounds, light blue: metal-containing compounds, dark blue: boron-containing compounds, indigo: nitrogen-containing heterocyclic compounds, magenta: nanoparticle-containing compounds, black: antiwear additives in partially formulated oils. ([1]This corresponds to the average of wear coefficients taken in the middle and at the edges of the wear track) 315
Figure 15.11: Wear coefficient[1], k_1 x 10^{-9}, after 16 hours of rubbing and MTM-SLIM images taken after 2 hours of rubbing for most promising alternative low and zero SAPS antiwear additives. ([1]This corresponds to the average of wear coefficients taken in the middle and at the edges of the wear track) 316

APPENDIX

Figure A.1: Stribeck curves showing friction coefficient versus entrainment speed at the beginning and after 2 h of rubbing for P-containing antiwear additive solutions at 50% SRR, 30 N and 100 ºC. 349
Figure A.2: Stribeck curves showing friction coefficient versus entrainment speed at the beginning and after 2 h of rubbing for P-S-containing antiwear additive solutions at 50% SRR, 30 N and 100 ºC. 350
Figure A.3: Stribeck curves showing friction coefficient versus entrainment speed at the beginning and after 2 h of rubbing for S-containing antiwear additive solutions at 50% SRR, 30 N and 100 ºC. 352
Figure A.4: Stribeck curves showing friction coefficient versus entrainment speed at the beginning and after 2 h of rubbing for M-containing antiwear additive solutions at 50% SRR, 30 N and 100 ºC. 353
Figure A.5: Stribeck curves showing friction coefficient versus entrainment speed at the beginning and after 2 h of rubbing for B-containing antiwear additive solutions at 50% SRR, 30 N and 100 ºC. 354
Figure A.6: Stribeck curves showing friction coefficient versus entrainment speed at the beginning and after 2 h of rubbing for N-containing heterocyclic antiwear additive solutions at 50% SRR, 30 N and 100 ºC. 355
Figure A.7: Stribeck curves showing friction coefficient versus entrainment speed at the beginning and after 2 h of rubbing for Nanoparticle-containing antiwear additive solutions at 50% SRR, 30 N and 100 ºC. 356
Figure A.8: Stribeck curves showing friction coefficient versus entrainment speed at the beginning and after 2 h of rubbing for low and zero SAPS antiwear additives in partially formulated oils at 50% SRR, 30 N and 100 ºC. 358

LIST OF TABLES

CHAPTER 2 THE IMPACT OF SAPS ON EXHAUST AFTERTREATMENT SYSTEMS

Table 2.1: Permissible levels of SAPS in engine oils 36

CHAPTER 3 LUBRICATION

Table 3.1: API guidelines for gasoline and diesel engines 43
Table 3.2: Main automotive lubricant additive types 44
Table 3.3: Low and zero SAPS antiwear additive types 50

CHAPTER 4 EXPERIMENTAL TECHNIQUES

Table 4.1: MTM-SLIM test conditions 58
Table 4.2: AFM test conditions 62
Table 4.3: MTM-Reciprocating test conditions 65
Table 4.4: ToF-SIMS test conditions 81
Table 4.5: XANES test conditions 85
Table 4.6: Model compounds used in XANES study 86
Table 4.7: Test materials summary 87

CHAPTER 5 FILM-FORMING, FRICTION, MORPHOLOGY AND WEAR-REDUCING PROPERTIES OF ZDDP

Table 5.1: Test materials summary: ZDDP study 94

CHAPTER 6 FILM-FORMING, FRICTION, MORPHOLOGY AND WEAR-REDUCING PROPERTIES OF P-CONTAINING ANTIWEAR ADDITIVES

Table 6.1: Test materials summary: Phosphorus-containing additives study 111

CHAPTER 7 FILM-FORMING, FRICTION, MORPHOLOGY AND WEAR-REDUCING PROPERTIES OF P-S-CONTAINING ANTIWEAR ADDITIVES

Table 7.1: Test materials summary: Phosphorus-sulphur-containing study 134

CHAPTER 8 FILM-FORMING, FRICTION, MORPHOLOGY AND WEAR-REDUCING PROPERTIES OF S-CONTAINING ANTIWEAR ADDITIVES

Table 8.1: Test materials summary: Sulphur-containing additives study 161

CHAPTER 9 FILM-FORMING, FRICTION, MORPHOLOGY AND WEAR-REDUCING PROPERTIES OF M-CONTAINING ANTIWEAR ADDITIVES

Table 9.1: Test materials summary: Metal-containing additives study 182

CHAPTER 10 FILM-FORMING, FRICTION, MORPHOLOGY AND WEAR-REDUCING PROPERTIES OF B-CONTAINING ANTIWEAR ADDITIVES

Table 10.1: Test materials summary: Boron-containing study 201

CHAPTER 11 FILM-FORMING, FRICTION, MORPHOLOGY AND WEAR-REDUCING PROPERTIES OF N-CONTAINING HETEROCYCLIC ANTIWEAR ADDITIVES

Table 11.1: Test materials summary: Nitrogen-containing heterocyclic additives study 220

CHAPTER 12 FILM-FORMING, FRICTION, MORPHOLOGY AND WEAR-REDUCING PROPERTIES OF NANOPARTICLE-CONTAINING ANTIWEAR ADDITIVES

Table 12.1: Test materials summary: Nanoparticle-containing additives study 239

CHAPTER 13 SURFACE ANALYSIS OF LOW AND ZERO SAPS ANTIWEAR ADDITIVES-DERIVED TRIBOFILMS

Table 13.1: Tribofilms studied using ToF-SIMS[1] 259
Table 13.2: Tribofilms studied using XANES[1] 260
Table 13.3: Corresponding additives used as references in XANES analysis 261
Table 13.4: Low and zero SAPS antiwear additives-derived tribofilms: chemical composition 285

CHAPTER 14 FILM-FORMING, FRICTION AND WEAR-REDUCING PROPERTIES OF LOW AND ZERO SAPS ANTIWEAR ADDITIVES IN PARTIALLY FORMULATED OILS

Table 14.1: Test materials summary 288

CHAPTER 15 GENERAL DISCUSSION

Table 15.1: Summary of film thickness, friction coefficient and wear coefficient results for antiwear additives studied in base oil alone 303

1. INTRODUCTION

Vehicle exhaust after-treatment systems to remove noxious emissions such as NOx, CO and soot are now fitted to all new vehicles and they have had a major impact on improving quality of life. Existing and proposed environmental emissions regulations require that these systems must become progressively more effective over the next few years.

One limiting factor in determining the useful life of the catalysts and filters used in exhaust after-treatment systems is contamination by evaporation and combustion products from the engine lubricant. It is believed that sulphated ash (*i.e.* metallic sulphate salts), phosphorus and sulphur, also known as SAPS, due to lubricant oil decomposition can poison the catalysts and block the filters and thus reducing the useful life of exhaust aftertreatment systems.

Due to the deleterious effects that SAPS have on exhaust aftertreatment systems, several Original Equipment Manufacturers (OEMs) have issued guidelines for the physical and chemical composition of engine lubricants, including limitations on the amount of SAPS. This means that the use of zinc dialkyldithiophosphate (ZDDP) and other additive types that contribute to SAPS has been restricted over the years.

ZDDP has been the antiwear additive of choice for lubricating engine oils for more than 60 years. In addition to providing effective antiwear and mild extreme pressure properties, ZDDP also offers good antioxidant and corrosion inhibition performance, proving therefore to be quite versatile and cost effective. Having said that, as emissions regulations become more stringent, lubricants are required to protect the engine while eliminating any impact they may have on the exhaust aftertreatment systems. The deleterious effects of SAPS on exhaust aftertreatment systems from ZDDP decomposition has lead to a great interest in identifying alternative low and zero SAPS antiwear additives that can partially of fully replace ZDDP in the next generation of engine oils to extend the life of exhaust after-treatment systems.

Recently the limits on permissible levels of SAPS have been augmented by restrictions on the extent of phosphorus volatility, as measured by the level of phosphorus retained in the lubricant after an engine test. However this does not change the need to limit and ideally reduce SAPS levels in engine oils.

In addition to contributing to SAPS, ZDDP also has a well documented deleterious effect on engine friction and consequently on fuel economy. It has also been suggested that soot easily abrades the iron phosphate film that initially forms in the presence of ZDDP, exposing reactive iron and thus promotes “corrosion-abrasive” wear, presenting a major drawback for diesel engines. For these reasons there is a great interest in finding alternatives to ZDDP as antiwear additive.

Over the years a wide variety of antiwear additives that do not contain SAPS have been suggested in the literature as alternatives to ZDDP. The proposed replacements lack one or more of the undesirable species, namely sulphur, phosphorus and metal. Unfortunately, although some of them have been quite extensively studied, these studies were carried out under disparate test conditions, so it is not possible to obtain a clear picture of the relative effectiveness of all these low SAPS candidates.

This research aims to measure, under the same test conditions, the film-forming, friction and wear-reducing properties of all of the disparate antiwear additive chemistries that have been suggested as a possible replacements for ZDDP in engine oils, and, where additive types are effective, to investigate their mechanism of action.

This thesis begins with an introduction to the impact of SAPS on exhaust aftertreatment systems in chapter 2, which aims to elucidate the mechanisms by which existing exhaust aftertreatment systems control emissions. It also describes the deleterious effects of SAPS on aftertreatment systems.

Chapter 3 reviews and describes the main lubrication regimes, lubricant additives and wear mechanisms. Archard's wear coefficient is defined and described and the functionality of antiwear additives is briefly reviewed.

Chapter 4 outlines the main experimental techniques and methods employed in this research. The mini traction machine (MTM) was employed to explore the friction, film-forming (MTM-SLIM) and wear-reducing properties (MTM-Reciprocating) of a very wide range of antiwear additive types. A combination of surface analysis techniques was employed to characterize the morphology and chemical composition of tribofilms, *i.e.* atomic force microscopy (AFM), time-of-flight secondary ion mass spectrometry (ToF-SIMS) and X-ray absorption near edge spectroscopy (XANES). Of particular importance is the development by the author of a novel approach to measure wear from antiwear additive-containing oils using scanning white light interferometry (SWLI).

Chapter 5 presents an overview of previous research on ZDDP, with a particular focus on its film-forming, friction and wear-reducing properties. This chapter then describes and discusses the film thickness, friction, surface topography and wear measurements results for ZDDP solutions made in the current study, using the methods outlined in chapter 4. These results provide a benchmark against which to compare all subsequent low SAPS additive performance measurements.

Chapter 6, 7, 8, 9, 10, 11 and 12 present work on the various families of low and zero SAPS antiwear additives, *i.e.* phosphorus, phosphorus-sulphur, sulphur, metal, boron, nitrogen heterocyclic and nanoparticle-based additives. In each chapter, previous research on the family of interest is outlined, then new film-forming, friction, topography and wear measurements are described and discussed.

Chapter 13 presents the chemical characterisation of tribofilms formed by ZDDP and potential low and zero SAPS antiwear additives using the two surface analysis techniques, ToF-SIMS and XANES.

Chapter 14 presents the film-forming, friction and wear measurement results from selected low and zero SAPS antiwear additives in partially formulated oils. The aim is to measure the effectiveness of some low SAPS additives in the presence of other additives. Synergistic and antagonistic effects between low and zero SAPS antiwear additives and other lubricant additive types, *i.e.* detergent and dispersant, are described and discussed.

In chapter 15 the film-forming, friction and wear-reducing properties of the low and zero SAPS antiwear additives studied in this research are summarised and discussed. Correlations between film thickness and friction, film thickness and wear and friction and wear are evaluated and most promising alternatives to ZDDP are presented.

Finally, chapter 16 presents the main findings of this work and makes some suggestions for future research on this field.

2. THE IMPACT OF SAPS ON EXHAUST AFTERTREATMENT SYSTEMS

Vehicle exhaust aftertreatment systems to remove noxious emissions such as NOx, CO, HC and soot are now fitted to all new vehicles and they have had a major impact on improving quality of life over the last 40 years.

Existing and proposed emissions regulations require that these systems must become progressively more effective over the next few years. One limiting factor in determining the useful life of the catalysts and filters used in the exhaust aftertreatment systems is now contamination by evaporation and combustion products from the engine lubricant. In particular sulphated ash, phosphorus and sulphur (SAPS) from lubricant decomposition can poison the catalysts and block the filters.

In this chapter, the mechanism by which existing exhaust aftertreatment systems control emissions is reviewed and the deleterious effects of SAPS on aftertreatment systems are discussed.

2.1 Exhaust Aftertreatment Systems

Vehicle emissions from the internal combustion engine were first proven to be damaging to the environment in the 1950s (Figure 2.1). In addition to producing highly toxic atmospheric pollutant carbon monoxide (CO); it was also found that a photochemical reaction between nitrogen oxides (NOx) and unburned hydrocarbons (HC), from motor vehicle emissions and oxygen present in the atmosphere, react to produce ground-level ozone containing smog which contributes to pollution in urban areas [1, 2].



Figure 2.1: Traffic and smog in Los Angeles, California in the 1950s [3, 4].

The use of autocatalysts was introduced in the 1970s, in order to reduce air pollution and thus comply with ever more stringent emissions regulations. The first mass produced vehicle with built-in “platinum-rhodium-mix” oxidation catalyst, which converts CO and HC to CO_2 and water; was a Volkswagen Rabbit (also known as Golf Mk1) in 1974 [5]. Since then, autocatalyst technology has evolved to maintain reliable performance whilst withstanding the extremely challenging exhaust aftertreatment system (ATS) environment, *e.g.* engine vibration (robustness); temperature fluctuations (thermal durability) and catalyst deactivation by fuel and lubricating oil additives decomposition [6].

The catalytic converter is placed in the exhaust pipe to convert toxic emissions that result from the internal combustion engine into less harmful substances. The exhaust gases flow through the ceramic honeycomb "monolith" channels (Figure 2.2), which are coated with a high surface area alumina-containing layer, also known as "washcoat", on top of which a combination of precious metal-catalysts (platinum, rhodium, palladium), catalytic promoters (cerium dioxide) and surface stabilizers is distributed [1, 5, 7]. The noxious substances removed by the exhaust aftertreatment systems are NOx, CO, HC and soot (in diesel engines).

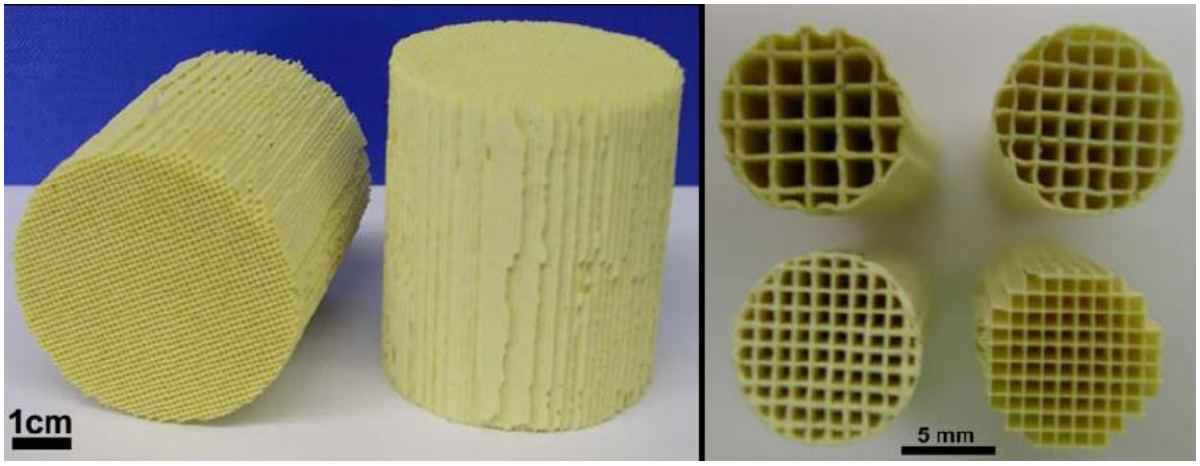


Figure 2.2: Ceramic honeycomb "monolith" with varying cell density [8].

2.1.1 Three-Way Catalyst

Both gasoline and diesel engines benefit from the application of exhaust ATS in order to mitigate pollutants. In gasoline engines, which operate at quasi-stoichiometric air to fuel (A/F) ratio; a "monolithic" three-way catalyst converter (TWC) is used to remove NOx, CO and unburned HC simultaneously (Figure 2.3) [5, 9].

i. Oxidation of CO: $2CO + O_2 \rightarrow 2CO_2$
ii. Oxidation of unburned HC: $HC + O_2 \rightarrow CO_2 + H_2O$
iii. Reduction of NOx: $2CO + 2NO \rightarrow 2CO_2 + N_2$; $HC + NO \rightarrow CO_2 + H_2O + N_2$

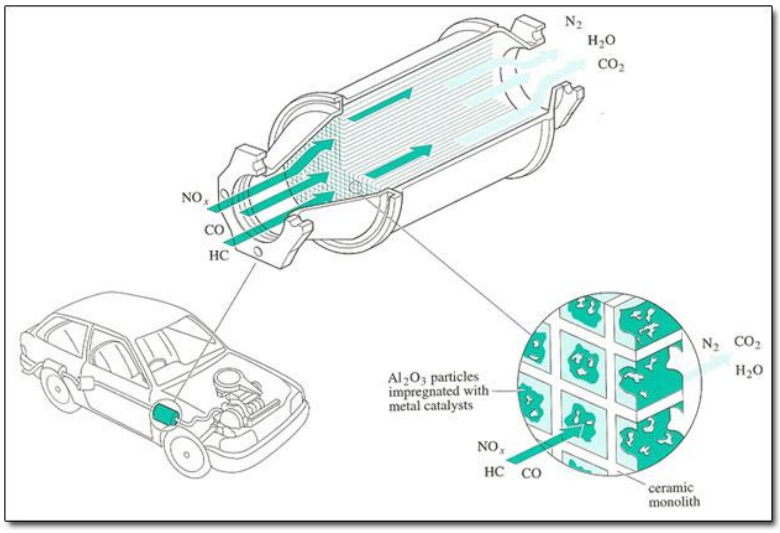


Figure 2.3: Schematic diagram of TWC [10].

2.1.2 NOx Storage Catalyst

For lean burn gasoline engines, common in Japan, where there is excess oxygen in the exhaust gas, the TWC system is ineffective for removing NOx, presumably because the reduction of NOx is inhibited by the lack of CO under these conditions (Figure 2.4).

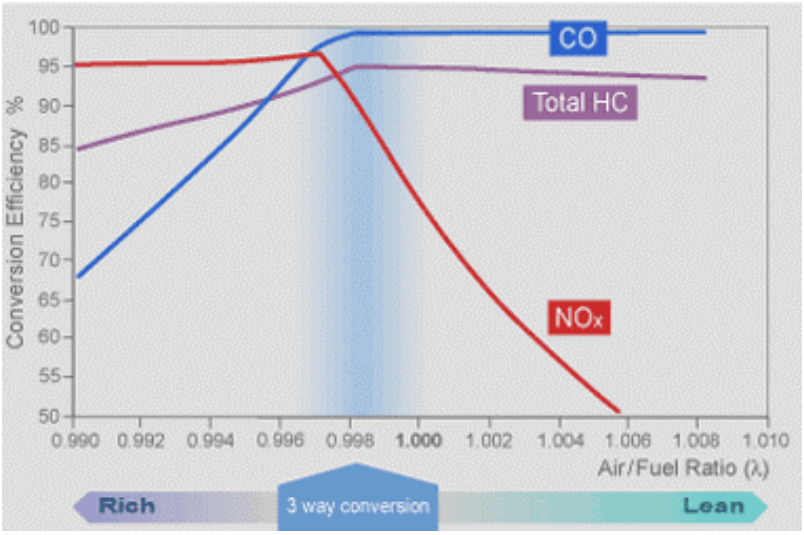


Figure 2.4: Catalyst conversion efficiency at Rich (λ<1), quasi-Stoichiometric (TWC; λ~1) and Lean (λ>1) driving conditions [11].

In this case, a NOx storage catalyst (NSC), also known as NOx storage trap (NST), lean NOx trap (LNT), NOx storage/reduction catalyst (NSRC) or NOx adsorber catalyst (NAC), is employed. This device combines an oxidation catalyst (Pt), a storage component (*e.g.* BaO, $BaCO_3$) and a reducing agent (Rh) in order to adsorb and store NOx as metal nitrate during lean engine operation and reduce it to N_2 during periodic stoichiometric or rich driving conditions (Figure 2.5) [12].

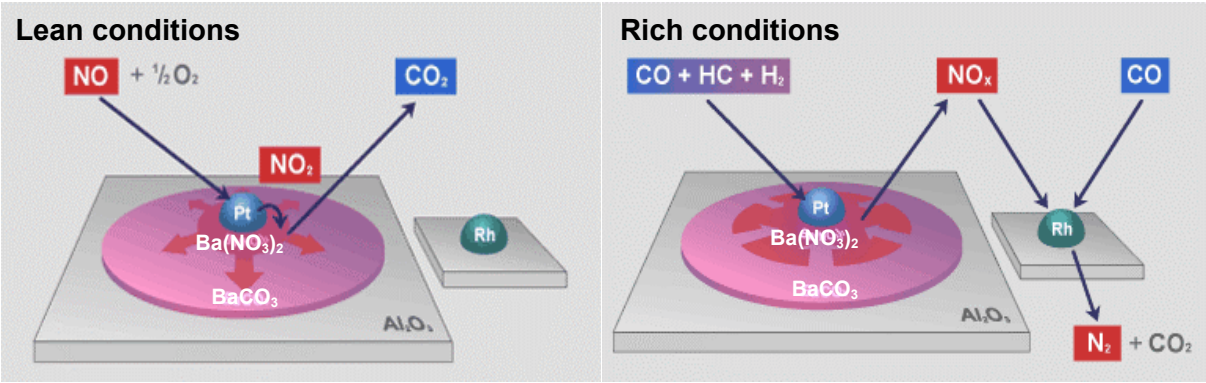


Figure 2.5: NOx storage catalyst mechanism under lean and rich operation [13, 14].

2.1.3 Diesel Oxidation Catalyst

Diesel oxidation catalysts (DOCs), also known as two-way catalysts, were first fitted to diesel vehicles in 1989 by Volkswagen [15]. This Pt/Pd-based oxidation catalyst is used in diesel engines to convert HC and CO emissions into harmless substances [16].

i. Oxidation of CO: $2CO + O_2 \rightarrow 2CO_2$
ii. Oxidation of HC: $HC + O_2 \rightarrow CO_2 + H_2O$

DOCs can also reduce up to 30 % of total particulate matter (PM; or diesel soot) emissions, by oxidation of liquid HC particles (from unburned fuel and lubricating oil), also known as the soluble organic fraction (SOF) of diesel soot [7].

2.1.4 Diesel Particulate Filter

The diesel particulate filter (DPF), a ceramic (*e.g.* cordierite, silicon carbide) monolith-type "wall-flow" filter, retains finely divided soot particles from fuel and lubricant decomposition; as the exhaust gas flows through the porous filter channels walls (Figure 2.6) [7]. Periodic DPF regeneration is required in order to avoid filter blockage and a resulting increase in exhaust back pressure and eventual engine damage.

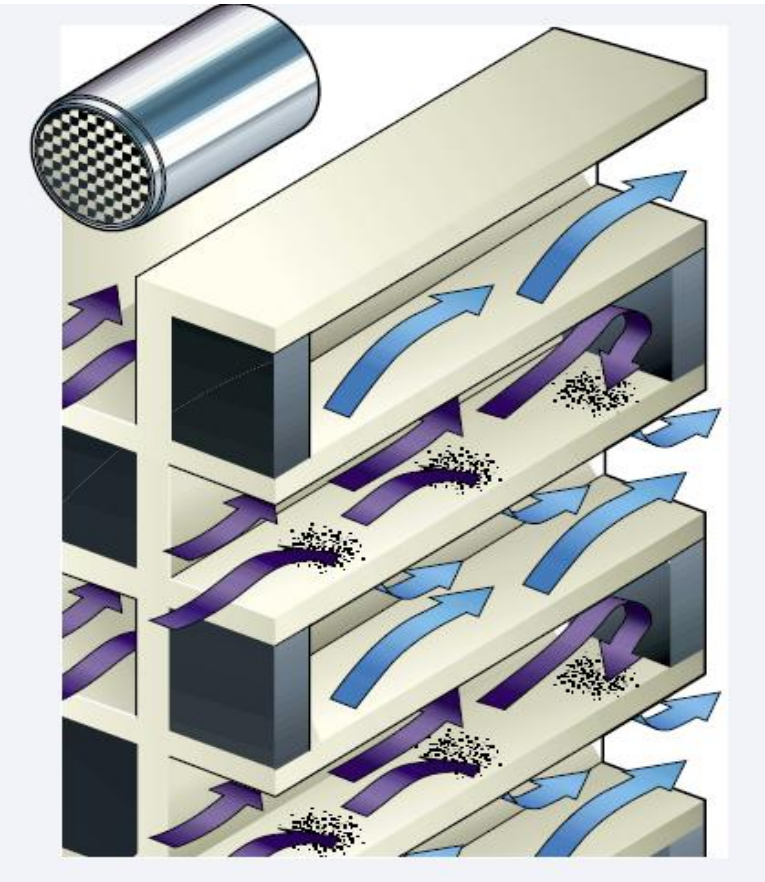


Figure 2.6: DPF: exhaust gas flows through the porous filter channels with alternate blocked ends, thus collecting soot [17].

Active regeneration involves the combustion of soot with oxygen by raising filter temperature to above 600 °C, at which temperature the soot trapped in the filter will rapidly combust, yielding complete regeneration. Passive regeneration is favoured and includes either the use of fuel-borne catalysts (*e.g.* cerium oxide) [18] or catalyst coating the filter [19]; both of which lower the combustion temperature of soot to diesel exhaust temperatures [9]. A continuously regenerating trap (CRT), which employs nitrogen dioxide (NO_2) to regenerate the filter, incorporates a DOC upstream to the DPF. The DOC converts noxious CO and HC (including the SOF of soot) emissions into CO_2 and water, while oxidising NO into NO_2. The NO_2 reaches the DPF, where it reacts with the trapped carbon-containing soot particles at around 250 ºC to form CO_2 and NO, enabling continuous DPF regeneration (Figure 2.7) [16, 20].

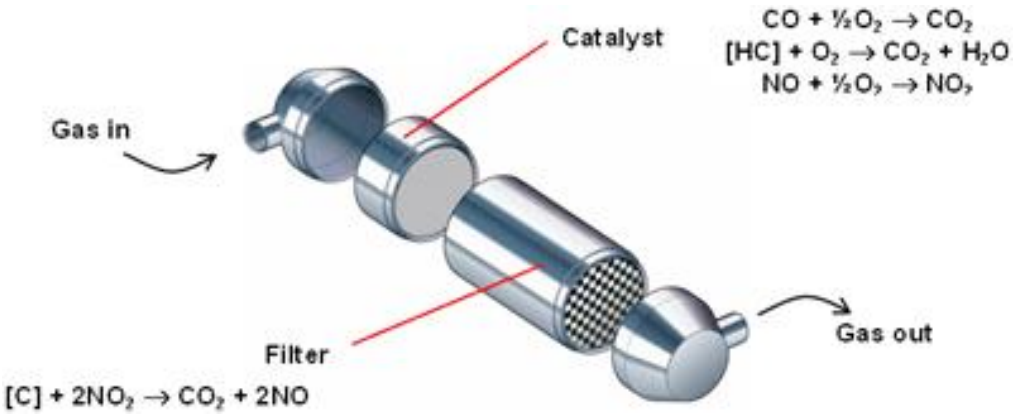


Figure 2.7: CRT: exhaust gas flows through the DOC, which removes HC and CO, while converting NO into NO2. NO2 reacts with the soot trapped in the DPF, regenerating the filter [21].

2.1.5 Selective Catalytic Reduction Catalyst

Extensive research has been carried out to develop effective NOx reducing aftertreatment technologies such as the NOx storage catalyst (NSC), as described in section 2.1.2 of this chapter, and the selective catalytic reduction (SCR) catalyst; both of which are employed under highly oxidising conditions to comply with ever more stringent emissions regulations. SCR catalysts are widely employed in lean burn diesel engines. These devices convert harmful NOx emissions (NO and NO_2) into N_2 using urea, a highly selective reducing agent. In this device an aqueous urea solution, otherwise known as diesel exhaust fluid (DEF), is injected in the exhaust gas stream, where it decomposes at exhaust temperatures to form ammonia and CO_2. NOx is then reduced in the presence of ammonia and excess oxygen to form harmless N_2 and water, while residual ammonia reacts with surplus oxygen to form N_2 and water [22].

i. Hydrolysis of urea to form ammonia:

$$(NH_2)CO(NH_2) \longrightarrow HNCO + NH_3$$

$$HNCO + H_2O \longrightarrow NH_3 + CO_2$$

ii. NOx reduction:

$$4NO + O_2 + 4NH_3 \longrightarrow 4N_2 + 6H_2O$$

$$NO + NO_2 + 2NH_3 \longrightarrow 2N_2 + 3H_2O$$

$$6NO_2 + 8NH_3 \longrightarrow 7N_2 + 12H_2O$$

iii. Excess ammonia removal:

$$4NH_3 + 3O_2 \longrightarrow 2N_2 + 6H_2O$$

The SCR system combines an active reduction catalyst to reduce NOx in the presence of ammonia; and precious metals catalysts (oxidation catalyst, *e.g.* Pt/Pd) to remove excess ammonia. A vanadium-based "washcoat" is used as active reduction catalyst in Europe, whereas in Japan and the USA, a zeolite-based "washcoat" is employed. The latter shows enhanced durability at higher temperatures than the former [23]. It has been suggested that thermal durability is crucial to the performance of SCR catalysts, given that these systems are downstream to the DPF (Figure 2.8), where periodic active regeneration increases exhaust gas temperature [24].

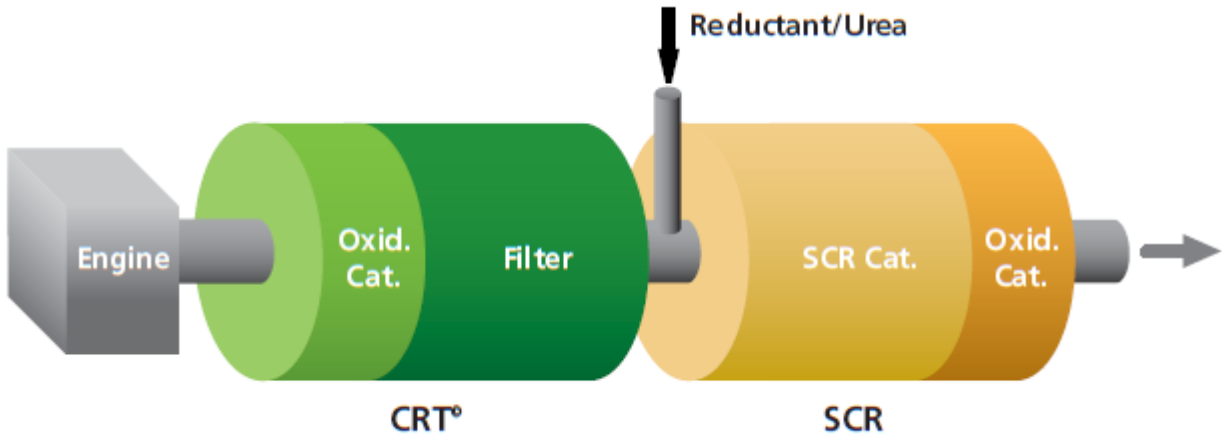


Figure 2.8: Diesel exhaust aftertreatment system diagram [25].

2.2 The Impact of SAPS on Exhaust Aftertreatment Systems

The employment and design of exhaust aftertreatment systems have been strongly influenced by emissions regulations and their challenging levels. It is believed that sulphates, phosphates and metallic ash due to lubricant oil decomposition can reduce catalyst effectiveness, hence degrading the exhaust aftertreatment system. Even though the damage caused by sulphated ash, phosphorus and sulphur (SAPS) can be difficult to quantify; its effects on catalyst performance has been closely observed over the years [26]. The widespread usage of zinc dialkyl dithiophosphate (ZDDP) as antiwear additive contributes to SAPS, which might imply ZDDP's partial or complete replacement in the next generation of engine oils.

Sulphated ash (SA) consists of minuscule solid particles, mainly $CaSO_4$ [27], which derive from ZDDP and Ca and Mg containing detergents [28] present in the lubricant. The non-combustible ash can build up in the filter channels leading to blockage of the DPF (Figure 2.9), increasing exhaust back pressure and thus compromising the performance of the engine.

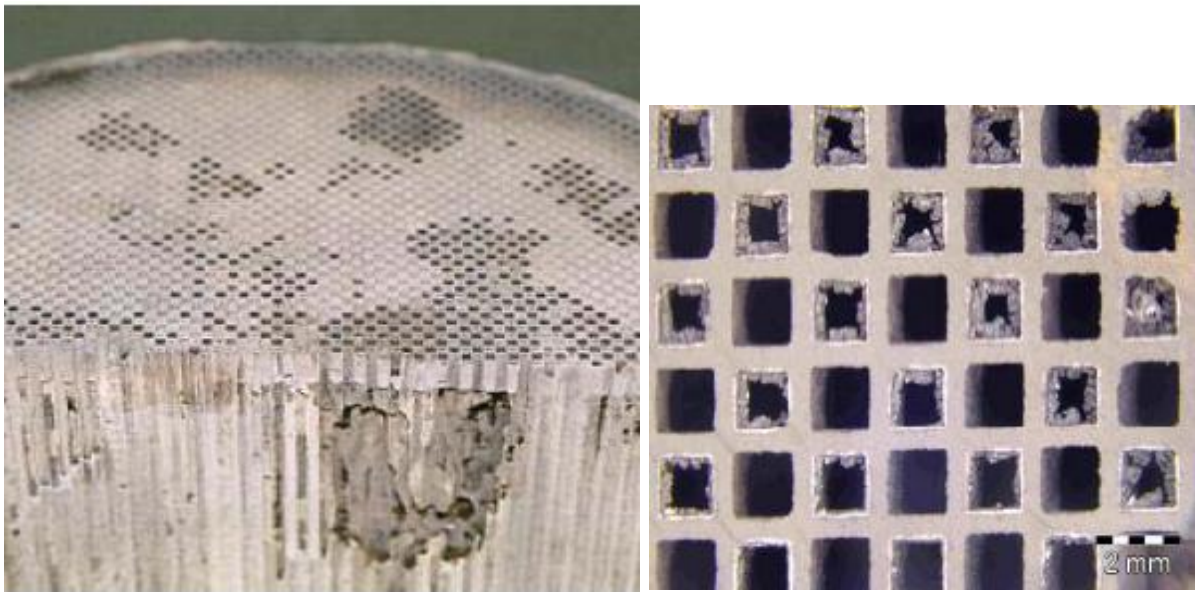


Figure 2.9: Damaging effect of sulphated ash on DPF [29].

It has been suggested that the phosphorus content on the TWC and its deleterious effects on this catalyst's performance is directly proportional to the amount of phosphorus in the lubricant [30, 31]. The phosphorus from phosphorus-containing compounds in the lubricant, such as ZDDP, react to form metal phosphate particulate, *e.g.* calcium phosphate, and phosphorus oxide vapour [32]. The former reduces overall catalyst activity by forming deposits on the "washcoat" on top of which the catalyst is distributed, whereas the latter reacts irreversibly with the catalyst leading to deactivation [33, 34].

Since the introduction of fuels with very low sulphur content (*e.g.* 10 ppm S in Europe), the main sources of sulphur might now be lubricant additives such as ZDDP and detergents (*e.g.* calcium alkyl benzene sulphonate). Sulphur, as sulphur oxides (SOx), *e.g.* SO_2, SO_3, SO_4 [7], builds up on the precious metal containing diesel oxidation catalyst (Pt/Pd), inhibiting catalyst conversion. NOx storage catalysts (NSC) adsorb SOx in the same way as NOx: SO_2 is oxidized to SO_3 on the precious catalyst (Pt); then SO_3 reacts with BaO (storage component) to form $BaSO_4$ [35]. This causes gradual saturation of the barium sites with sulphur and consequent loss of activity towards the adsorption of NOx. Even though catalyst storage capacity can be restored by desulphurisation at high temperatures (above 600 ºC) [36]; the frequency of these regenerations causes an increase in fuel consumption and accelerates "washcoat" degradation.

2.3 Specifications

Due to the abovementioned deleterious effects, several Original Equipment Manufacturers (OEMs) have issued guidelines for the physical and chemical composition of engine lubricants, including limitations on the amount of SAPS. Limiting the amount of SAPS means that the use of ZDDP and other additive types contributing to SAPS formation has been restricted over the years. The evolution of the permissible level of SAPS in engine oils established by the International Lubricant Standardization and Approval Committee (ILSAC) is illustrated in Table 2.1 [37-42].

Table 2.1: Permissible levels of SAPS in engine oils

ILSAC (Model year introduction)	**SA**	**P**	**P Volatility**	**S**
GF-1 (1994)	-	**0.12 % max** (ASTM[3] D4951)	-	-
GF-2 (1997)	**60 mg max** (TEOST[1] 33C, ASTM[3] D6335)	**0.10 % max** (ASTM[3] D4951)	-	-
GF-3 (2002)	**45 mg max** (TEOST[1] MHT[2], ASTM[3] D7097)	**0.10 % max** (ASTM[3] D4951)	-	-
GF-4 (2005)	**35 mg max** (TEOST[1] MHT[2], ASTM[3] D7097)	**0.08 % max** (ASTM[3] D4951)	-	**0.5 % max** (SAE 0W and 5W) **0.7 % max** (SAE 10W) (ASTM[3] D4951, ASTM[3] D2622)
GF-5 (2011)	**35 mg max** (TEOST[1] MHT[2], ASTM[3] D7097) **30 mg max** (TEOST[1] 33C, ASTM[3] D6335)	**0.08 % max** (ASTM[3] D4951)	**79 % min** (ASTM[3] D7320)	**0.5 % max** (SAE 0W-XX and 5W-XX) **0.6 % max** (SAE 10W-30) (ASTM[3] D4951, ASTM[3] D2622)

[1] TEOST: Thermo-oxidation Engine Oil Simulation Test, [2] MHT: Moderately High Temperature, [3] ASTM: American Society for Testing and Materials; SAE: Society of Automotive Engineers.

The latest industry standard, GF-5, reveals a change in direction, where phosphorus content limit remains constant, while phosphorus volatility constraints are introduced. Even though it has been suggested that SAPS entering the exhaust depends strongly on additive volatility, limited research has been published on its effects [43, 44]. Despite this change there is still a continuous need to reduce SAPS. The chapter that follows outlines the role of antiwear additives in lubrication.

3. LUBRICATION

The main purpose of lubrication is to overcome the two main disadvantages of solid-to-solid rubbing contacts: friction and wear. A thin lubricating film separates interacting moving parts, *i.e.* gears, bearings, *etc*; in order to reduce friction and prevent damage to mechanical components due to wear. Therefore, the investigation and understanding of film formation between solid surfaces is essential to the development of lubricants that are capable of meeting friction and wear targets, and hence minimise energy losses, operation costs and downtime.

In this chapter, the main lubrication regimes are reviewed. The main challenges in lubricant formulation, as well as lubricant additives are described. Wear mechanisms are then briefly outlined and Archard's wear coefficient is defined and described. Finally the functionality of antiwear additives is reviewed.

3.1 Lubrication Regimes

The transition between the three well-known liquid lubrication regimes, from boundary to fluid film lubrication (hydrodynamic and elastohydrodynamic lubrication) [45, 46]; is often represented by the Stribeck curve (Figure 3.1). The classical Stribeck curve was first introduced in 1902 to portray the variation of friction in lubricated bearings as a function of speed, lubricant viscosity and load (Uη/W) [47]. This set of values determines hydrodynamic film thickness, so the Stribeck curve represents the change in friction as a fluid film is progressively generated between the rubbing surfaces.

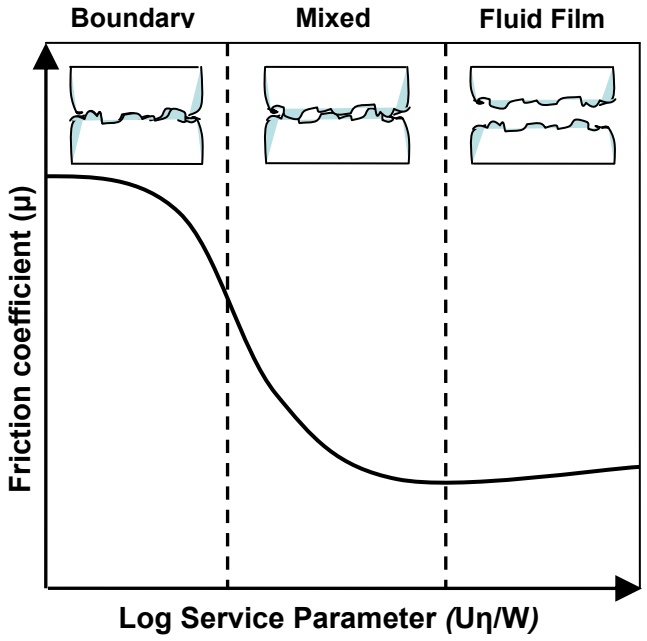


Figure 3.1: Stribeck curve: friction coefficient variation with operating parameters (Uη/W) or fluid film thickness (h) [48].

3.1.1 Boundary Lubrication

The combination of low speed, low viscosity and high load will result in **boundary lubrication**. This regime is characterized by little fluid in the interface and thus the load being almost entirely carried by solid-to-solid contact, resulting in high friction (Figure 3.1). At this stage, the film in the interface, the so-called boundary film is so thin that nearly all the load is borne at the asperities in contact, which begin to experience plastic deformation. The interface is covered with a molecular layer of surface-active additives and their decomposition products, whose specific properties can influence friction and wear characteristics. Such layers are of great importance in practical applications where maintaining long-lasting fluid lubricant films between the surfaces is technically impossible. Antiwear (AW) and extreme pressure (EP) additives in the lubricant formulation prevent seizure and wear caused by direct metal-to-metal contact between moving parts operating in boundary lubrication, *i.e.* bearings, cams and tappet interfaces, piston ring and liner interface, high sliding gears, transmissions, *etc* [49].

3.1.1.1 Tribochemistry

Surface asperity contact in boundary and mixed lubrication regimes can lead to local seizure and consequently damaged machinery. The presence of a low friction protective film prevents wear and failure in rubbing contacts. The understanding of tribochemistry is crucial to the development of lubricating oils, given that tribochemistry controls the chemical reactions that occur between the surfaces in contact and the lubricant in the boundary lubrication regime [50]. The adsorption mechanism in boundary lubrication depends on the reactivity of the additives towards the surfaces and the ability of molecules to react with surfaces can also indicate potential corrosion problems. Therefore in addition to the lubricant, surface composition is a very important aspect in selecting the additive chemistry to protect said surface; which means that not all lubricant formulations perform well on all surfaces. Having said that, to establish the mechanism of boundary film formation remains a great challenge in Tribology, because of the complex nature of the conditions present in boundary lubrication as well as the confined nature of the film.

3.1.2 Mixed Lubrication

As the speed and viscosity increase, the surfaces will begin to separate, and a fluid film begins to form. The load, at this stage, is carried partly by the asperities in contact and partly by the fluid film pressure. Mixed lubrication is the resulting transition stage between boundary lubrication and full fluid film. Although the lubricating film is still very thin, a sharp drop in friction is observed in the Stribeck curve as a result of increasing fluid film thickness and thus decreasing solid-to-solid contact (Figure 3.1) [51].

3.1.2.1 Lambda Ratio (λ)

The lambda ratio or lambda value is the ratio of the minimum fluid film thickness to the composite surface roughness [51]. This parameter, also called specific film thickness, provides a useful measure to illustrate the severity of mixed lubrication [52]. Lambda ratio is given by the following equation:

$$\lambda = \frac{h_0}{R_{qc}} \qquad \text{(Equation 3.1)}$$

where:

λ: lambda ratio;

h_o: minimum lubricant film thickness;

R_{qc}: composite surface roughness of the two surfaces, given by:

$$R_{qc} = \sqrt{{R_{q1}}^2 + {R_{q2}}^2} \qquad \text{(Equation 3.2)}$$

where:

R_{q1}: RMS roughness of first surface;

R_{q2}: RMS roughness of second surface.

For hydrodynamic lubrication, when λ < 1, the system operates under boundary lubrication, where lubricating film thickness is lower than the composite surface roughness, and asperities in contact support the load. When 1 < λ < 3, the system shifts to mixed lubrication, where the surfaces are partially separated by a thin lubricant film, even though asperities conjunction is still experienced. For λ > 4, the system operates in the full film hydrodynamic regime; which is often characterised by low friction, given that there is negligible asperity contact between the surfaces [51]. In high pressure non-conforming contacts, the transition from boundary to mixed lubrication occurs at lower lambda ratio (*ca.* λ < 0.05) because of the in-contact partial flattening of asperities at high pressure [53].

3.1.3 Fluid Film Lubrication (Hydrodynamic and Elastohydrodynamic lubrication)

The surfaces will continue to separate as the speed or viscosity increase until there is a thick fluid film and no contact between the opposing bodies. The friction coefficient will reach its minimum and there is a transition to hydrodynamic lubrication (Figure 3.1). At this stage, the load on the interface is entirely supported by the fluid film pressure and friction resistance to movement is influenced by shearing of viscous fluid. No wear is observed in hydrodynamic lubrication due to the full fluid film and no solid-to-solid contact [54]. According to Cameron, fluid film thickness in well designed, conforming hydrodynamic contacts is given by [55]:

$$h = k\left(\frac{U\eta}{W}\right)^{0.5} \qquad \text{(Equation 3.3)}$$

where:

h: film thickness;

k: contact geometry constant;

U: entrainment speed ($U= (u_1+u_2)/2$); u_1 and u_2: speed of the surfaces;

η: dynamic viscosity (lubricant);

W: load.

Lubricated non-conforming contacts, such as bearings, gears and cams and tappets will experience elastohydrodynamic lubrication (EHD or EHL). The classical description of a non-conforming contact is the ball-on-flat, which is a point contact with extremely high pressure (Figure 3.2). The EHD pressures are high enough to have a significant effect on fluid viscosity, which allows a very thin oil film to form supporting the load, hence separating the contact surfaces [56]. In non-conforming elastohydrodynamic contacts, film thickness is given by Hamrock and Dowson's equation [45]:

$$h = k\frac{(U\eta)^{0.7}\alpha^{0.5}}{W^{0.1}} \qquad \text{(Equation 3.4)}$$

where:

h: film thickness;

k: contact geometry constant (depends on radii and elastic modulus of bodies);

U: entrainment speed ($U= (u_1+u_2)/2$); u_1 and u_2: speed of the surfaces relative to the contact;

η: dynamic viscosity of lubricant;

α: viscosity-pressure coefficient of lubricant;

W: load.



Figure 3.2: Elastohydrodynamic lubrication takes place in gears, rolling elements (*i.e.* ball bearings) and other non-conforming contacts [57].

3.2 Lubricants

Automotive lubricants are a carefully balanced mixture of different components containing base oil and additives. Together, they are expected to contribute not only to the performance and durability of the engine, but also to fuel economy and emissions reduction. Base oils are the predominant component in the majority of lubricants (85% - 95%) and their quality results from the type of crude oil and the refining process used. They are classified in terms of their viscosity, structure (paraffinic, naphthenic and aromatic) and American Petroleum Institute (API) Group Number [58]. Table 3.1, illustrates the API guidelines, in which base oils are classified into five groups, taking into account the content of saturates and sulphur, as well as its viscosity index (VI) and composition [59].

Table 3.1: API guidelines for gasoline and diesel engines

Group	I	II	III	IV	V
Saturates (%)	< 90	≥ 90	≥ 90	-	-
Sulphur (%)	> 0.03	≤ 0.03	≤ 0.03	-	-
VI	80≥ VI <120	80≥ VI < 120	≥ 120	-	-
Composition	-	-	-	Polyalphaolefin (PAO)	All other base oils, not aforementioned.

After the refining process, additive packages are normally blended with the base oil, in order to enhance the latter's inherent qualities and also to impart new properties which are specific to required performance levels. Table 3.2 lists the main lubricant additive types, their functionalities and typical examples. These include additives that improve intrinsic characteristics of the base oil such as viscosity modifiers, for example; whereas other additives work by means of improving stability or boundary lubrication properties, such as antioxidants and friction modifiers, respectively [60].

Table 3.2: Main automotive lubricant additive types		
Additive type	**Functionality**	**Typical additives**
Antioxidants	oxidation inhibitor	hindered phenols amines zinc dialkyldithiophosphate
Antiwear	reduce wear under boundary and mixed lubrication conditions	zinc dialkyldithiophosphate acid phosphates/phosphites
Corrosion inhibitors	protect metal components	zinc dialkyldithiophosphate
Detergents/Dispersants	prevent deposit formation on metal surfaces	M-sulphonates, M-phenates, M-salicylates (*i.e.* M: Ca, Mg) PIB succinimides
Foam inhibitors	foam reduction	High molecular weight silicones
Friction modifiers	modify frictional characteristics	molybdenum dithiocarbamate
Pour-point-depressants (PPD)	improve low temperature stability	polymethacrylates (PMA) alkyl naphthenates
Viscosity Modifiers (VM)	control viscosity-temperature dependence	polymethacrylates (PMA) olefin co-polymers (OCP) polyisoprenes

3.2.1 Lubricant Formulation Challenges

At present, European and US regulations for gasoline and diesel vehicles impose challenging targets concerning both harmful emissions and fuel economy improvement. As a result, lubricant formulations face considerable changes in order to comply with imposed targets. Automotive lubricants are required to have increasingly lower viscosity in order to improve fuel economy. On the downside, low viscosity lubricants give thinner fluid films and thus often increased wear, and consequently further developments in antiwear technology and robust surfaces are required. The growing need for automotive lubricants to have low SAPS and low volatility was fully discussed in the preceding chapter. These requirements imply lower levels of phosphorus- and sulphur-containing additives such as ZDDP, which can increase wear and also reduce extreme pressure properties. They may also require novel antiwear technology including low and zero SAPS and low volatility antiwear additives that are able to deliver effective wear protection [61].

3.3 Wear

Most tribological applications require low friction and wear in order to avoid energy and material losses. A considerable percentage of the power generated in an engine is used in order to overcome the friction between moving bodies. For that reason, it is essential to diminish the resistance offered when bodies in contact move against each other, also known as frictional forces [54]. However wear as well as friction can be controlled by a thin lubricant film between the moving surfaces. In practice, wear can be the result of rolling, sliding, fretting and impact. Wear is a complex process, which more often than not results from a combination of wear mechanisms, *i.e.* abrasive, adhesive, corrosive and fatigue wear (Figure 3.3); whose identification not only enables wear rate prediction, but is also crucial to the development of new materials to comply with increasingly demanding applications [62]. The rate at which the surface is worn is often characterised by whether there is mild or severe wear taking place. Uniformly decreasing wear, which stabilises at very low levels, can be described as running-in wear and is generally desirable. Running-in describes the early stages of machinery operation, in which the system is adjusting to reach a steady-state condition between contact pressure, surface roughness, and the establishment of an effective lubricating film at the interface [61].

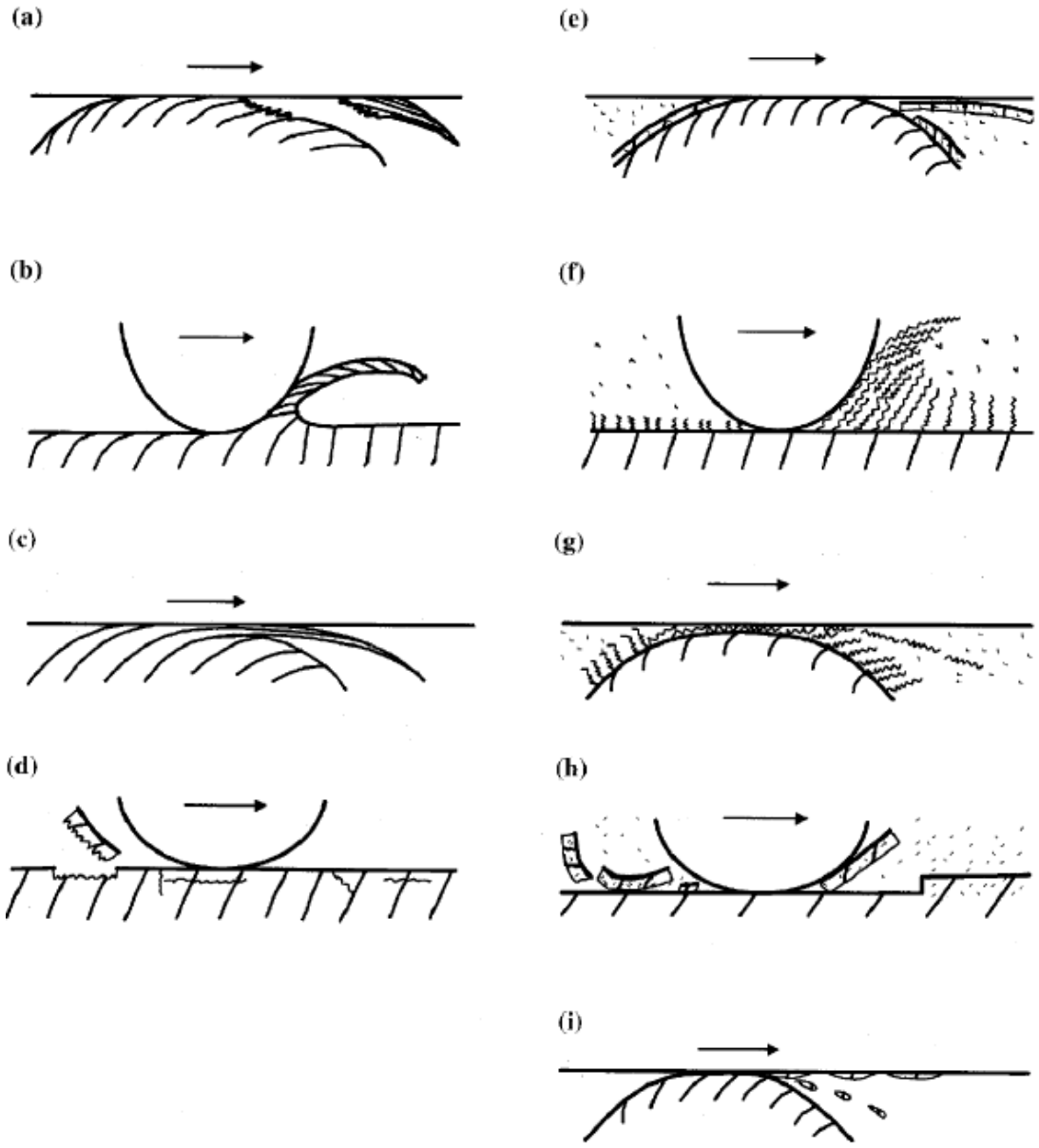


Figure 3.3:Wear modes: (a) abrasive wear by microcutting of ductile bulk surface; (b) adhesive wear by adhesive shear and transfer; (c) flow wear by accumulated plastic shear flow; (d) fatigue wear by crack initiation and propagation; (e) corrosive wear by shear fracture of ductile tribofilm; (f) corrosive wear by delamination of brittle tribofilm; (g) corrosive wear by accumulated plastic shear flow of soft tribofilm; (h) corrosive wear by shaving of soft tribofilm; and (i) melt wear by local melting and transfer of scattering [61].

3.3.1 Archard's Wear Coefficient

Archard's dimensionless wear coefficient (k) is the most widely-accepted wear rate prediction parameter, which is based on the assumption that there is a linear relationship between the total wear volume and sliding distance.

$$V = k\frac{WL}{H} \qquad \text{(Equation 3.5)}$$

so that

$$k = \frac{VH}{WL} \qquad \text{(Equation 3.6)}$$

where:

k: dimensionless Archard's wear coefficient;

V: wear volume;

H: hardness;

W: load;

L: sliding distance.

Archard's wear equation assumes that; (a) wear is proportional to load; (b) wear is proportional to sliding distance and (c) wear is inversely proportional to the hardness of the surface being worn away [61]. In lubricated systems where difficulties are encountered in precisely defining hardness of uppermost layer in the contact; the wear coefficient is defined as k_1:

$$k_1 = \frac{k}{H} \qquad \text{(Equation 3.7)}$$

hence:

$$V = k_1 WL \qquad \text{(Equation 3.8)}$$

where:

V: wear volume;

k_1: wear coefficient;

W: load;

L: sliding distance.

Defining the wear coefficients (k or k_1) is obviously useful to predict and control the extent of surface degradation and material loss. Archard's wear equation has been shown to be valid for cases where mechanical influences are dominant, *i.e.* dry wear. On the other hand, the influence of lubricant chemistry and consequent presence of a boundary lubricating film was not considered when Archard's equation was developed and often these can have a significant effect on wear rate. When automotive engines are running, wear inevitably occurs; which means that design, material selection and lubricant package have to be finely tuned to ensure that wear is kept to a very mild level. According to Stachowiak, wear coefficients of the order of 10^{-9} mm^3/Nm are experienced in the cam and followers in normal running engines. In well lubricated systems, wear coefficient varies between 10^{-8} to 10^{-12} mm^3/Nm; and wear is controlled by boundary films formed mainly from antiwear additives [61].

3.4 Antiwear Additives

Antiwear additives (AW) were introduced to reduce wear in lubricated crankcase components that operate for long periods in boundary or mixed lubrication at high temperatures, and thus with thin lubricating films, *i.e.* cams, gears and pistons [63]. It has been widely suggested that these additives adsorb on or react with metal surfaces to form a thin protective film that prevents metallic asperities from coming directly into contacts and is easily shearable. This film is also known as a tribofilm. Even though both antiwear and extreme pressure additives (EP) create a protective layer that reduces wear, the former perform well under moderate conditions of load, temperature and speed, while the latter interact with the surfaces under extreme conditions [51].

3.4.1 Zinc Dialkyldithiophosphate (ZDDP)

The most extensively used antiwear additive is zinc dialkyl dithiophosphate (ZDDP) (Figure 3.4), which has been in continuous use since the 1940s [64]. Its film formation and wear-reducing properties in engine oils is thoroughly discussed in Chapter 5.

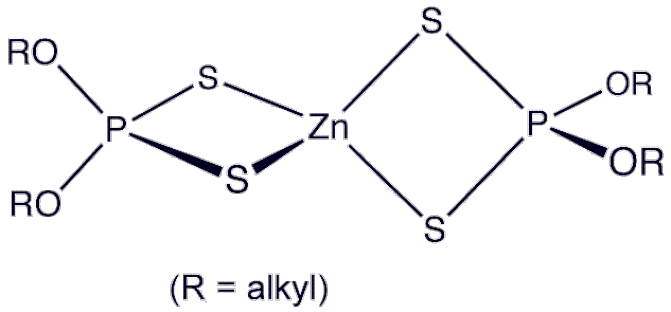


Figure 3.4: Molecular structure of ZDDP [65].

In addition to providing effective antiwear and mild extreme pressure properties, ZDDP also offers good antioxidant and corrosion inhibition performance [66], proving therefore to be quite versatile and cost effective. Having said that, as emissions regulations become more stringent, lubricants are required to protect the engine while eliminating any impact they may have on the exhaust aftertreatment systems (ATS). The deleterious effects of SAPS on ATS from ZDDP decomposition has lead to a great interest in identifying alternative low or even zero SAPS antiwear additives that can partially of fully replace ZDDP in the next generation of engine oils.

3.4.2 Low and Zero SAPS Antiwear Additives

Exhaust aftertreatment system compatibility has been driving the permissible levels of SAPS down over the years, in order to maintain emissions compliance. Table 3.3, represents every conceivable combination of antiwear additive chemistries that has been suggested as a possible replacement for ZDDP in engine oils [67]. The proposed replacements lack one or more of the undesirable species, namely: sulphur, phosphorus and metal; and although some of them have been quite extensively studied, these studies were carried out under disparate conditions; therefore no comparison can be established.

Table 3.3: Low and zero SAPS antiwear additive types			
M	**S**	**P**	**Antiwear additive types**
√	√	√	Zinc dialkyldithiophosphates (ZDDPs)
o	√	√	Thiophosphates, thiophosphonates
√	**o**	√	Metal dialkylphosphates
√	√	**o**	Metal dithiocarbamates
o	**o**	√	Phosphates, phosphonates, amine phosphates, *etc*.
o	√	**o**	Organosulphides, S-containing heterocyclic rings and ashless dithiocarbamates
√	**o**	**o**	Organometallics, *e.g.* Ti-, Sn-containing compounds
√	**o**	**o**	Organoboron compounds
o	**o**	**o**	N-containing heterocyclic compounds
o*	**o**	**o**	Nanocolloids, *e.g.* carbonates, borates, fullerenes* and inorganic fullerenes*

In this thesis, the boundary film-forming, friction and wear properties of the abovementioned additive groups are explored under the same testing conditions. The background of these additives is further reviewed in the following chapters. The chapter that follows describes the main experimental techniques used during this study.

4. EXPERIMENTAL TECHNIQUES

A multi-technique approach was employed to study the tribological characteristics of a wide range of antiwear additives.

In this chapter, the main experimental techniques employed in this study are described, briefly reviewed and discussed. The main technique employed was the mini traction machine (MTM) to explore the friction, film-forming (MTM-SLIM) and wear-reducing properties (MTM-Reciprocating) of a wide range of antiwear additive types.

A combination of surface analysis techniques was employed to characterize the morphology and chemical composition of tribofilms, *i.e.* atomic force microscopy (AFM), time-of-flight secondary ion mass spectrometry (ToF-SIMS) and X-ray absorption near edge spectroscopy (XANES).

Of particular importance is the development of a novel approach to measure wear by the author using scanning white light interferometry (SWLI).

4.1 MTM-SLIM Method

4.1.1 Description

Many practical applications involve mixed rolling/sliding and unidirectional motion, *i.e.* cams and gears. A mini traction machine with spacer layer imaging mapping (MTM-SLIM) (Figure 4.1) is employed in this study to explore the friction and film-forming properties of a wide range of antiwear additive types under mixed rolling/sliding conditions.

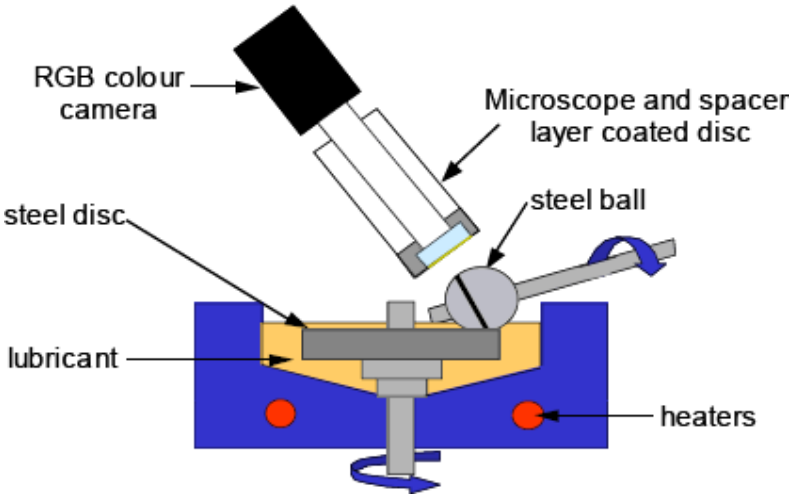


Figure 4.1: Schematic diagram of MTM-SLIM [68].

A rolling/sliding contact is generated between a 19.05 mm diameter steel ball and a 46 mm steel disc. In this ball-on-disc configuration, a ball is loaded against the face of a disc, which is immersed in the lubricant of interest at a controlled temperature. The ball drive-shaft is set up at an angle that minimise spin in the contact, while frictional force between the ball and the disc is measured by a load cell attached to the ball drive-shaft bearing housing. Any combination of entrainment speed and slide-roll ratio can be achieved, as the ball and the disc are driven independently by separate motors. Entrainment speed and SRR are given by equations 4.1 and 4.2, respectively.

$$U = \frac{(u_1 + u_2)}{2} \qquad \text{(Equation 4.1)}$$

where:

U: entrainment speed (m/s);

u_1: speed of the ball (m/s);

u_2: speed of the disc (m/s).

$$SRR = \frac{|u_1 - u_2|}{U} \qquad \text{(Equation 4.2)}$$

where:

SRR: slide-roll ratio (%);

U: entrainment speed (m/s).

In the current work, slide-roll ratio is kept constant and friction is measured over a range of entrainment speeds (also known as mean rolling speed). Because elastohydrodynamic film thickness increases with entrainment speed; the transition from low friction with fluid film lubrication at high speed, through to high friction in mixed and boundary lubrication at low speed, is obtained and illustrated by Stribeck curves (Figure 4.2).

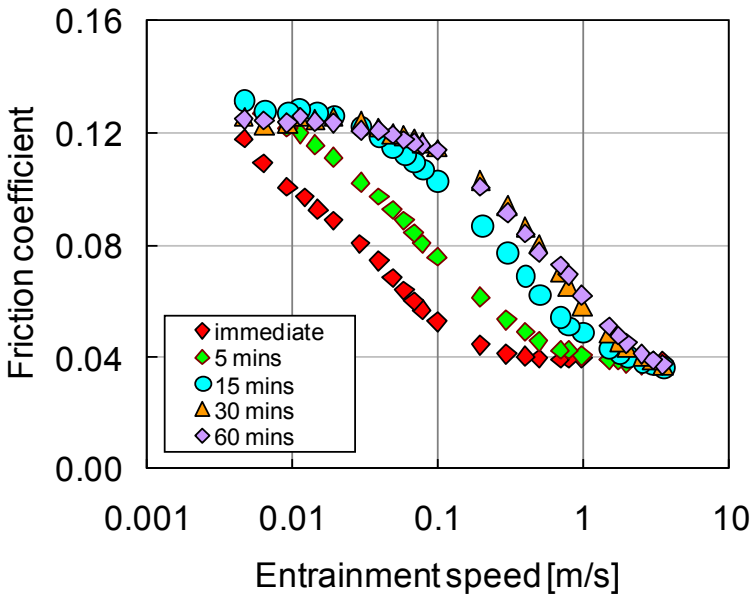


Figure 4.2: Stribeck curves showing friction coefficient versus entrainment speed at increasing rubbing times for a ZDDP-containing oil at 50% SRR, 31 N and 100 ºC [69].

Periodically throughout the test, motion is halted and the ball is loaded upwards against the spacer layer-coated glass disc and an interference image, which represents a map of the reaction film present on the rubbed ball surface, is captured for subsequent analysis to determine the film thickness (Figure 4.3). When the ball is loaded against the glass disc, the lubricant film is squeezed out from the contact between the ball and the glass disc and this enables accurate visualisation of any residual, solid-like reaction film. In order to carry out *in situ* film thickness measurement, the MTM-SLIM relies on an optical attachment, which consists of a spacer layer-coated glass disc, a microscope and a colour camera. The surface of the glass disc is coated with a semi-reflective chromium layer on top of which a transparent silica "spacer layer" is distributed. When white light is shone through the glass disc and into the rubbed track, some of this light bounces off the semi-reflective chromium layer while some passes through the silica spacer layer and the reaction film present on the ball before being reflected back from the ball surface. Because these two beams of light have travelled different distances, when recombined different wavelengths experience either constructive or destructive optical interference, (given by equation 4.3 and 4.4, respectively), depending on the thickness of the reaction film.

Constructive optical interference:

$$h_{film} = \frac{(N - \Phi)\lambda}{2nCos\theta} \qquad \text{(Equation 4.3)}$$

Destructive optical interference:

$$h_{film} = \frac{(N + 1/2 - \Phi)\lambda}{2nCos\theta} \qquad \text{(Equation 4.4)}$$

where:

h_{film}: spatial film thickness of oil film;

N: fringe order, N= 0, 1, 2, 3, …;

Φ: net phase change upon reflection;

λ: wavelength;

n: oil refractive index;

θ: angle of incidence of the beam.

This generates a coloured interference image of the contact that is frame-grabbed using a colour camera, which converts the RGB (red/green/blue) colour of each pixel into a film thickness map of the contact between the rubbed track on the ball and the spacer layer coated glass disc, by means of film thickness/colour calibration [63, 70, 71]. At the beginning of each test the spacer layer film thickness is measured and subtracted from subsequent film thickness measurements in order to determine true film thickness. The steel ball is then loaded against the steel disc and rubbing is resumed under mixed rolling/sliding. The MTM-SLIM is fully computer-programmable, which allows for monitoring film thickness and friction simultaneously via automated test protocols that control ball and disc speed, load, slide-roll ratio and test temperature.

In this study a refractive index of 1.60 was employed for all SLIM measurements in order to convert the measured film thickness into absolute film thickness. The optical properties of tribofilms of zinc phosphate glasses have been investigated and it has been found that their refractive indices vary between 1.50 (zinc methaphosphate) and 1.65 (zinc orthophosphate), so a value of 1.6 is representative of zinc phosphates [72]. Considering the wide range of antiwear additives studied in the current project, the use of a single refractive index value will introduce a systematic error into the calculation of true film thickness values. Fortunately the refractive indices of most transparent materials lie in a relatively narrow range, from about 1.4 to about 1.8, so an assumption of 1.6 means that the error will not exceed about 15%. Fujita *et al.* have noted that this error is less than the experimental scatter from other methods of measuring very thin films [73]. Also, in practice it is usually more important to know whether a tribofilm forms and how its thickness develops with rubbing time than to know its precise thickness, and the former can be deduced by assuming a representative refractive index value.

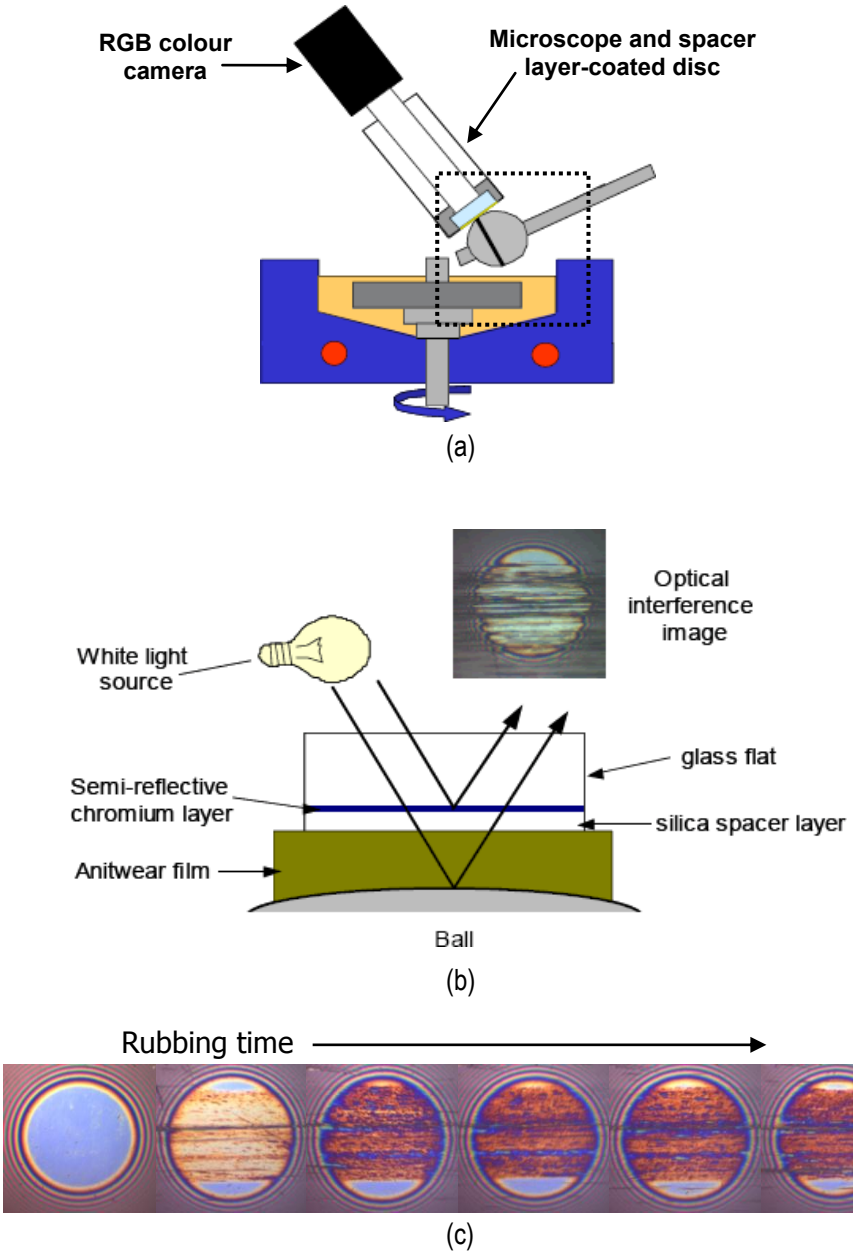


Figure 4.3: Schematic diagram of film thickness measurement using MTM-SLIM: (a) The ball is loaded against the spacer layer glass disc and (b) an interference image of the rubbed track on the ball is obtained, (c) which enables film growth and thickness evaluation over rubbing time [69, 74].

4.1.2 Experimental Procedure

In this research, rolling/sliding experiments were carried out using a highly polished AISI 52100 steel ball and disc at 100 ºC for 2 hours. Friction was measured as a function of entrainment speed at a fixed slide-roll ratio of 50 %. A constant load of 30 N was applied, corresponding to a maximum contact pressure of 0.95 GPa, mean contact pressure of 0.63 GPa and a Hertzian contact diameter of 240 μm. The test assembly was thoroughly cleaned with analytical grade toluene, rinsed with isopropanol and then dried. Each test was performed using fresh ball and disc specimens, which were previously cleaned by consecutive immersion in toluene, isopropanol and acetone in an ultrasonic bath for 10 minutes. At the end of each test, ball and disc were removed from the test rig, rinsed with hexane and wrapped in lens cleaning paper in order to preserve the tribofilms formed on the rubbed tracks, which were then subjected to various surface measurements. Table 4.1 lists the MTM-SLIM test conditions used in this study.

Table 4.1: MTM-SLIM test conditions	
Test apparatus	MTM2 with 3D-SLIM option from PCS Instruments
Temperature	100 ºC
Load	30 N
Maximum Hertzian contact pressure	0.95 GPa
Mean contact pressure	0.63 GPa
Hertzian contact diameter	240 µm
Theoretical film thickness[1] (h_0)	9.06 nm
Lambda ratio[1] (λ)	0.58
Rolling/Sliding	
Entrainment speed	0.1 m/s
Slide-roll ratio (SRR)	50 %
Duration	120 minutes
Stribeck Curve	
Entrainment speed	3.5 m/s to 0.01 m/s
Slide-roll ratio (SRR)	50 %
SLIM	
Load (between ball/glass disc)	20 N
Specimens	
Ball	19.05 mm diameter; AISI 52100 steel; Hardness: 750-770 VPN; Young's Modulus: 210 GPa; R_q[2]: 11 ± 3 nm
Disc	46 mm diameter; AISI 52100 steel; Hardness: 750-770 VPN; Young's Modulus: 210 GPa; R_q[2]: 11 ± 3 nm

[1]Calculated using Hamrock and Dowson's equation, described in Chapter 3 [45].

[2]R_q: RMS roughness of the surface.

4.2 AFM Method

4.2.1 Description

Atomic force microscopy (AFM) is a scanning probe microscopy technique that relies on a mechanical probe to characterise the surfaces at the nanoscale. Because friction and wear depend on the physical and chemical properties of the tribofilms formed on the surfaces in contact [75], since its introduction in 1986 [76], AFM has been extensively employed to characterise the topography and local friction (also known as lateral force microscopy) of tribological surfaces [77]. In this study, AFM is employed to investigate the morphology of boundary films formed on rubbing surfaces from the decomposition of a wide variety of low and zero SAPS antiwear additives, to ultimately establish a relationship between morphology and friction.

AFM scanning modes are classified by the way in which the scanning probe comes into physical contact with the sample surface namely: contact mode, non-contact mode and intermittent contact mode (also known as tapping mode). In contact mode AFM, which was used in the current study, as the tip scans across the sample surface, varying topographic features cause deflection of the tip and cantilever. A laser beam is bounced off of the cantilever and reflected on to a photodetector. The amount of deflection of the cantilever and the force it applies to the sample can be calculated from the change in light falling on the photodetector sectors (Figure 4.4).

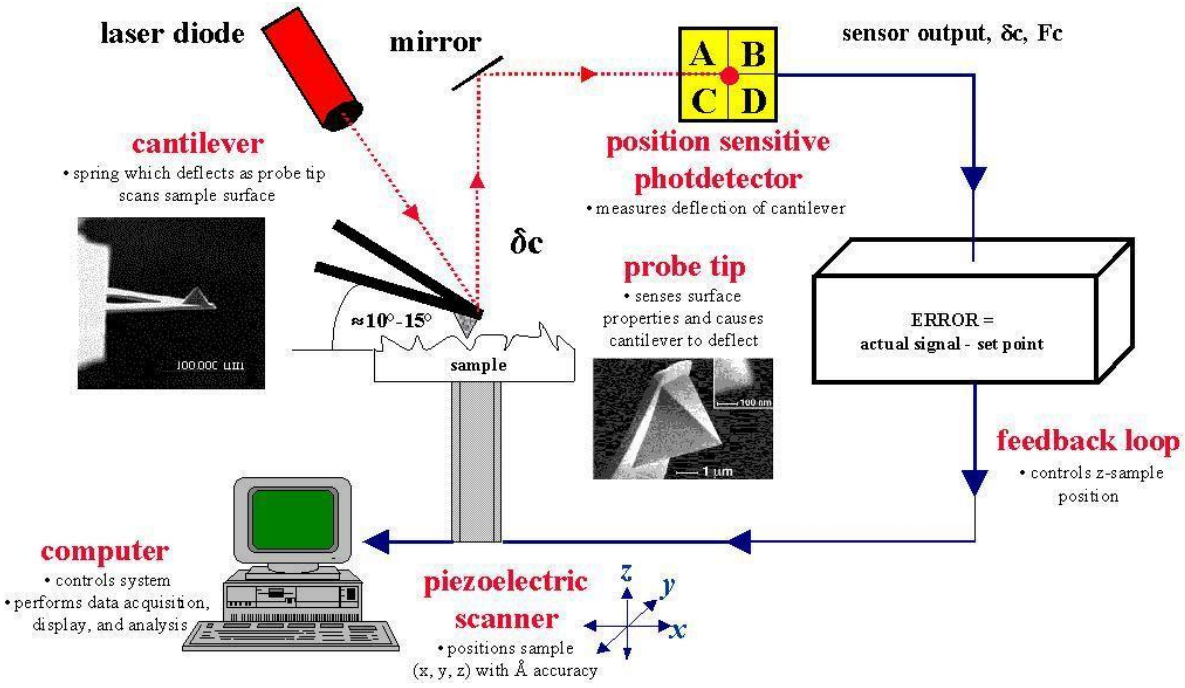
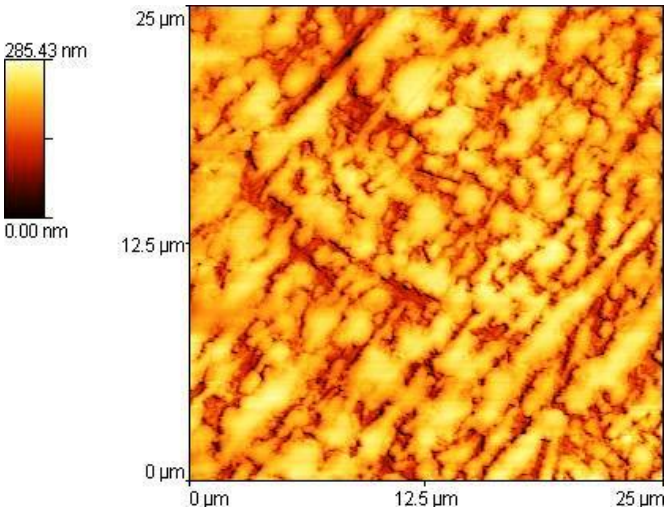


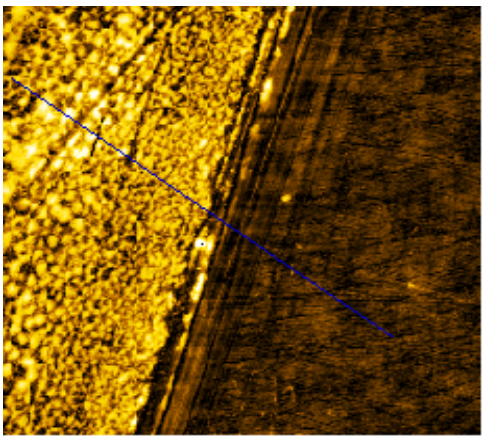
Figure 4.4: Atomic force microscopy: general components and their functions [78].

The resulting change in the detector current signal is used to produce a high resolution topographic representation of the surface (Figure 4.5), hence enabling the morphological characterisation of antiwear additive-derived boundary films. Lateral force, which represents how friction varies spatially, can also be observed by measuring the torsional “twist” of the cantilever, rather than its deflection. It is also possible to monitor force-displacement curves as the tip approaches and retreats from contact. Because the AFM work carried in this project emphasised mainly the topographical and morphological study of tribofilms, lateral force and force displacement curves were not investigated.

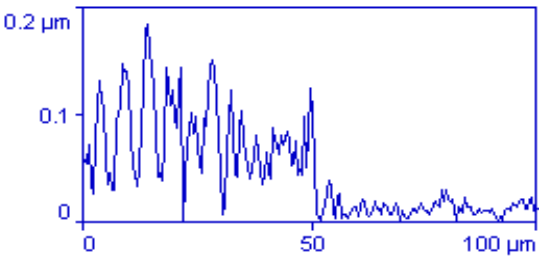
(a)



(b)



Edge of wear track



Line profile across rubbed/unrubbed areas

Figure 4.5: Typical AFM topography images: (a) two-dimensional (2D) image of ZDDP-derived tribofilm and (b) line profile across the edge of the wear track, spanning rubbed/unrubbed areas. Further topographical representations include: 3D plots, roughness, film thickness, *etc*.

4.2.2 Experimental Procedure

In this research, AFM was employed to characterise the morphology of antiwear additive-derived tribofilms. The thin films in question were generated on AISI 52100 steel discs (46 mm diameter), using a mini traction machine (MTM). Two AFMs were employed in this study: a Veeco diCaliber AFM (Imperial College London) and a Veeco Dimension 3100 SPM (University of Nottingham), both using a v-shaped silicon nitride (Si_3N_4) cantilever with a nominal 20 nm radius pyramidal, Si_3N_4 tip, in contact mode. An area of 100 µm x 100 µm in the centre and at the edge of the wear track was scanned and the topography of the tribofilm was evaluated (*e.g.* 2D plot, line profile, roughness, film thickness, *etc*). Additionally, smaller scan sizes (*i.e.* 25 µm x 25 µm, 5 µm x 5 µm) were also used to further characterise the structure of the tribofilms. Upon analysis, the topography images were normalised to a common vertical scale, to enable comparison. Brighter contrast in topography indicates high height while darker contrast indicates low heights. At the end of each test, the disc was removed from the test rig and wrapped in lens cleaning paper in order to preserve the tribofilm for subsequent surface measurements. Table 4.2 lists the AFM test conditions used in this study.

Table 4.2: AFM test conditions

Test apparatus	Veeco diCaliber AFM	Veeco Dimension 3100 SPM
Cantilever	V-shaped Si_3N_4	V-shaped Si_3N_4
Nominal spring constant	0.07 N/m	0.06 N/m
Tip	Pyramidal Si_3N_4	Pyramidal Si_3N_4
Nominal tip radius	20 nm	20 nm
Scan size	100 µm x 100 µm 25 µm x 25 µm	100 µm x 100 µm 25 µm x 25 µm
Scan rate	1.5 Hz	2.0 Hz
Samples/line	256	512

4.3 MTM-Reciprocating Method

4.3.1 Description

To assess the wear performance of proposed low and zero SAPS antiwear additives, an MTM was employed to provide a general method of comparing the mild wear properties of different lubricant compositions. The MTM was fitted with a reciprocating mechanism in which the disc motion is changed into an oscillating movement (Figure 4.6) as opposed to the contra-rotating mode used in the conventional configuration described in section 4.1 of this chapter.

The MTM-Reciprocating configuration offers two main advantages. Firstly, both surfaces are in movement, which simulates dynamic conditions, such as cam and followers that are susceptible to mild wear. Secondly, when using reciprocating motion, the wear on the disc is localised over a relatively small region, thus increasing the wear depth when compared to unidirectional motion, in which wear is distributed around the MTM disc circumference. However, unlike pure sliding (*e.g.* pin-on-disc) where one surface is continuously in contact and thus experiences a very high level of local wear, in the reciprocating MTM, both surfaces move with respect to the contact, therefore the local amount of wear is enough to ensure measurable wear but not so much as to significantly change contact geometry and thus contact pressure.

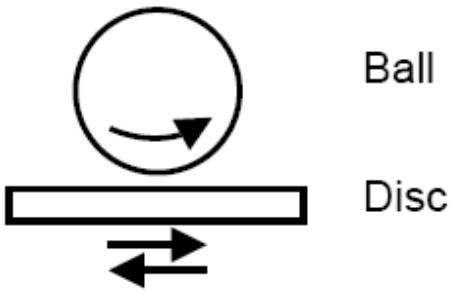


Figure 4.6: Reciprocating mechanism diagram showing ball specimen continuously rotating against the reciprocating disc [79].

4.3.2 Experimental Procedure

In this research, wear experiments were carried out using highly polished AISI 52100 steel ball and disc at 100 ºC in tests lasting 4, 8 and 16 hours. A constant load of 30 N was applied, corresponding to an initial contact pressure of 0.95 GPa, mean contact pressure of 0.63 GPa and a Hertzian contact diameter of 240 μm. In this study, the MTM ball rotated at a fixed unidirectional surface speed of 20 mm/s, while the MTM disc reciprocated at a constant frequency of 10 Hz with a 4 mm stroke length. The test assembly was thoroughly cleaned with analytical grade toluene, rinsed with isopropanol and then dried. Each test was performed using fresh ball and disc specimens, which were previously cleaned by consecutive immersion in toluene, isopropanol and acetone in an ultrasonic bath for 10 minutes. At the end of each test, ball and disc were removed from the test rig, rinsed with hexane and wrapped in lens cleaning paper in order to preserve the tribofilm formed on the rubbed track, which was then subjected to wear depth measurements. The test conditions used in this study, summarised in Table 4.3, are representative of engine conditions (*e.g.* valve train of low emission diesel engines) and they thus produce mild wear in well lubricated systems [80].

Table 4.3: MTM-Reciprocating test conditions	
Test apparatus	MTM-Reciprocating from PCS Instruments
Temperature	100 ºC
Load	30 N
Maximum Hertzian contact pressure	0.95 GPa
Mean contact pressure	0.63 GPa
Hertzian contact diameter	240 µm
Theoretical film thickness[1] (h_0)	9.06 nm
Lambda ratio[1] (λ)	0.58
Test length	4, 8, 16 h
Stroke length	4 mm
Stroke frequency	10 Hz
Ball speed (Ub)	20 mm/s
Disc speed (Ud)	80 mm/s (on average)
Specimens	
Ball	19.05 mm diameter; AISI 52100 steel; Hardness: 750-770 VPN; Young's Modulus: 210 GPa; R_q[2]: 11 ± 3 nm
Disc	46 mm diameter; AISI 52100 steel; Hardness: 750-770 VPN; Young's Modulus: 210 GPa; R_q[2]: 11 ± 3 nm

[1]Calculated using Hamrock and Dowsons' equation, described in Chapter 3 [45].

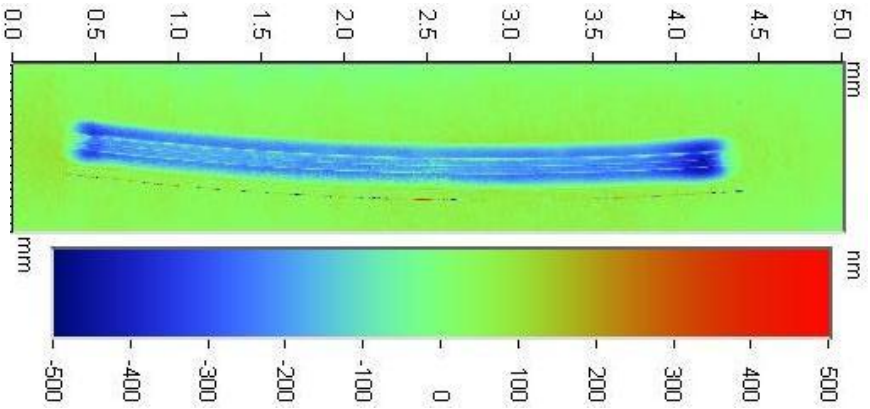
[2]R_q: RMS roughness of the surface.

4.4 SWLI Method for Measuring Wear

4.4.1 SWLI Description

Numerous methods for measuring wear have been developed over time, some specific to certain applications. Useful reviews of test methods for measuring wear are provided by Brown [81], Ruff [82] and Gahlin *et al.* [83]. A scanning white light interferometer (SWLI), also known as coherence scanning interferometer, white-light confocal interferometer and vertical scanning interferometer, produces high quality two and three-dimensional surface maps of the surface under investigation (Figure 4.7). It is a non-contact optical profiler and as such can be used to measure the profile (*e.g.* topography, surface roughness, shape, waviness, *etc.*) of different materials without the risk of damaging the surface.

(a)



(b)

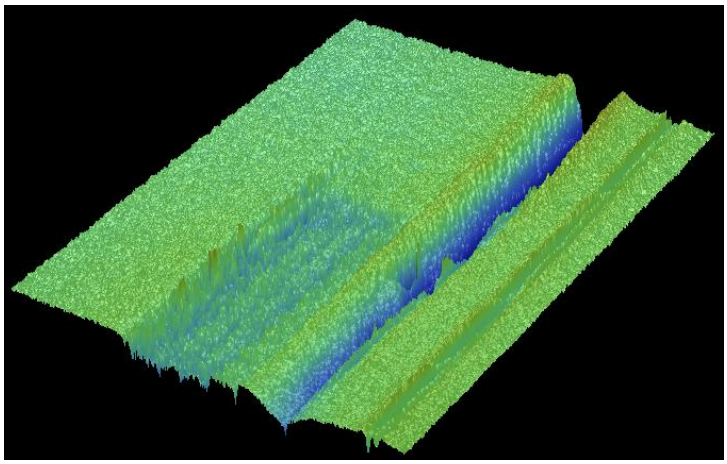


Figure 4.7: Typical SWLI images: (a) two [69] and (b) three-dimensional profiles of wear tracks after wear testing using MTM-Reciprocating.

In SWLI, a white light source filtered through a neutral density filter is passed through an interferometer objective then onto the test surface, which sits on a motorised x,y,z stage (Figure 4.8). The interferometer beam-splitter reflects half of the incidence beam to a reference surface within the interferometer, the two beams reflected from the test surface and the reference surface recombine to form interference fringes. The fringes are observed as alternating dark and light bands that appear on the surface when in focus. At best contrast, the surface is said to have reached its optimum focus. The system measures the degree of fringe modulation to determine the surface profile. During analysis the interferometric objective moves vertically to scan the test surface at different heights. The system begins scanning the test surface just above focus, moves towards peak focus, before finally coming out-of-focus. The camera capture frames of interference data at evenly-spaced intervals as the system moves downwards. The interference signal for each point on the surface is recorded and translated into an image of the test surface [84]. The system includes two measurement options: phase shifting interferometry (PSI) and vertical scanning interferometry (VSI). The PSI mode is limited to fairly smooth, continuous surfaces, whereas the VSI mode allows rough surfaces and steps up to several millimetres high to be measured. In this study, surface analysis by SWLI was carried out using VSI in order to enable wear depth measurement on rubbed surfaces generated during wear studies.

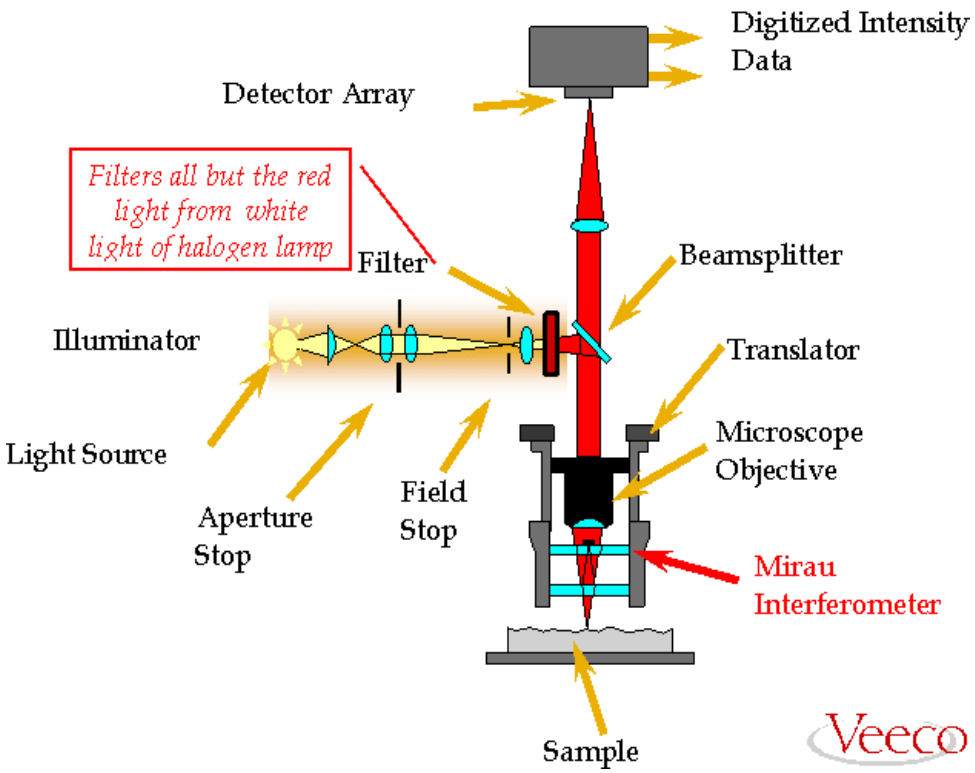


Figure 4.8: Diagram illustrating the principle of SWLI imaging system [84].

4.4.2 Wear Measurement: A Novel Approach

Commercial SWLIs are able to map surface topography to very high resolution and can thus measure very small amounts of wear on rubbed surfaces [85]. These instruments are therefore being increasingly used to study aspects of mild wear, including the wear-reducing properties of antiwear additives in lubricants such as formulated engine oils. However during this project, the author noted that the application of the white light interference microscope to measure the wear of surfaces which had been rubbed in the presence of lubricants containing the antiwear additive zinc dialkyldithiophosphate (ZDDP) produced an apparent, but spurious, wear measurement. The transparent and relatively thick antiwear film generated by ZDDP on rubbed surfaces provided an apparent optical path difference which could be incorrectly interpreted as wear. This finding and its solution has now been published [86].

4.4.2.1 Removal of Tribofilm

In this research, SWLI was employed to measure the wear depth on MTM discs. The wear scars, illustrated in Figure 4.9, were generated on AISI 52100 steel discs (46 mm diameter), using the MTM-Reciprocating configuration discussed in section 4.7 of this chapter. At the end of the test, the MTM disc was removed from the test rig, rinsed with hexane and the rubbed track subjected to various surface measurements as described below. A Veeco WYKO NT9100 [84] was used to image the track and measure wear depth on the discs.

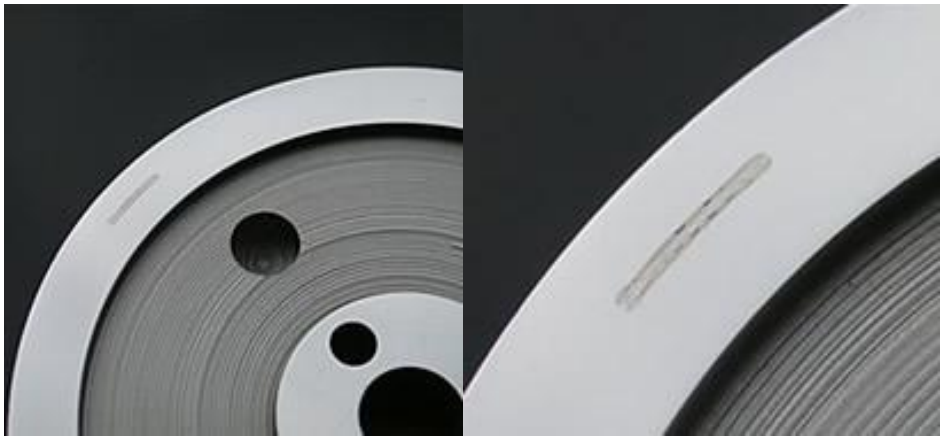


Figure 4.9: Wear scar on the MTM disc after reciprocating test [87].

Figure 4.10 represents a typical topography image of the wear track and line profile plot across the track. For this specific example, it appears that the track contains hollows which are 100 to 300 nm deep, while an average depth of material of *ca.* 50 nm has been removed from the track.

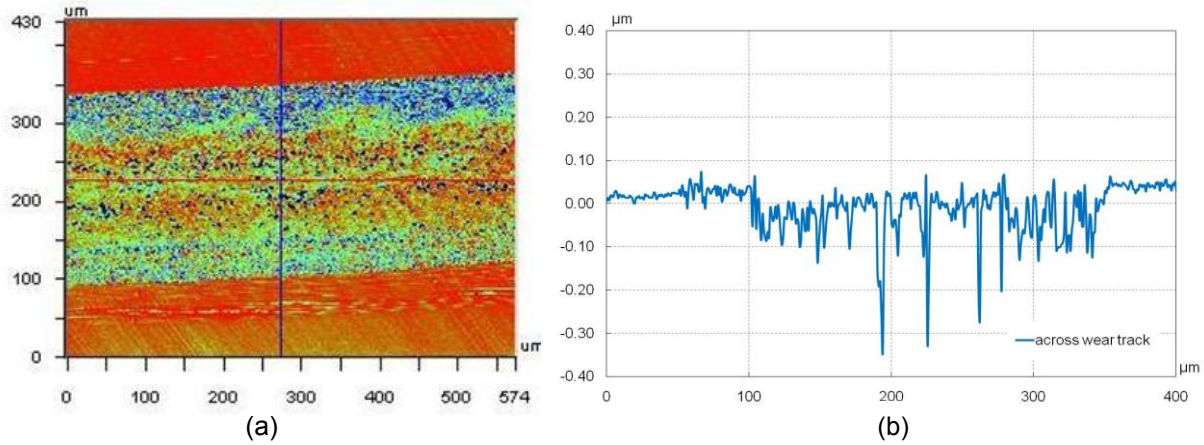


Figure 4.10: Typical (a) 2D topography image and (b) line profile plot across the wear track on the MTM disc after 4 hours of rubbing in ZDDP-containing oil. These images indicate that the track appears to have worn.

Figure 4.11 shows an AFM topographic image and a line profile at the edge of the rubbed track, spanning rubbed and unrubbed areas. The instrument employed was a Veeco Explorer AFM, used in contact mode as described in section 4.2 of this chapter. The film in the rubbed track has the characteristic pad-like structure of ZDDP tribofilms with pads of typically 5 µm diameter separated by deep channels [88]. From the line profile it appears that the film is on average about 100 nm higher than the surrounding, unrubbed surface in the region studied.

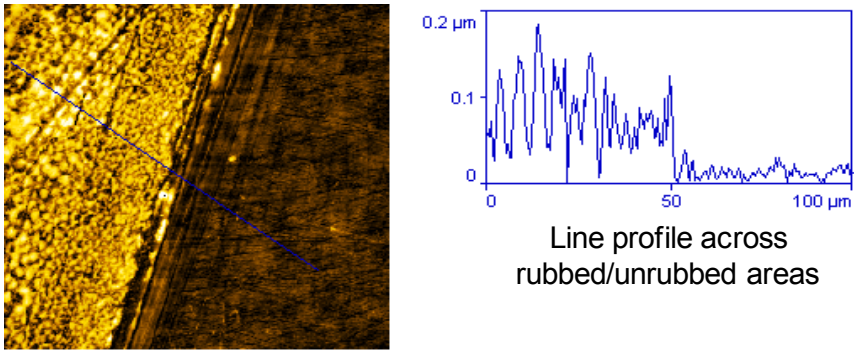


Figure 4.11: AFM Topography and line profile plot across the edge of the wear track on the MTM disc after 4 hours of rubbing in ZDDP-containing oil.

At first sight, the above measurements appear consistent if it is assumed that the AFM maps the topography of the surface of the transparent, solid-like ZDDP-derived antiwear film, while the interference microscope maps the topography of the underlying metal surface, as illustrated schematically in Figure 4.12.

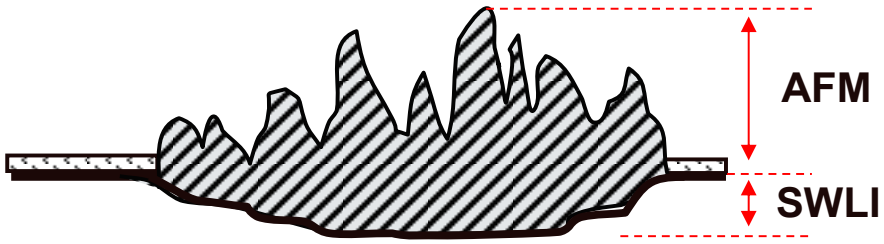


Figure 4.12: Possible film measured by AFM versus SWLI [89].

To validate this assumption, the residual ZDDP-derived tribofilm was removed using ethylenediaminetetraacetic acid (EDTA) solution. EDTA is a highly effective chelating agent and its practical value lies in its ability to form stable, water soluble coordination complexes with many metal cations such as Zn (present in ZDDP-derived tribofilms), Fe (probably present in non-ZDDP-derived and ashless antiwear additives-derived tribofilms), Mg, Ca, *etc.* (Figure 4.13) [90].

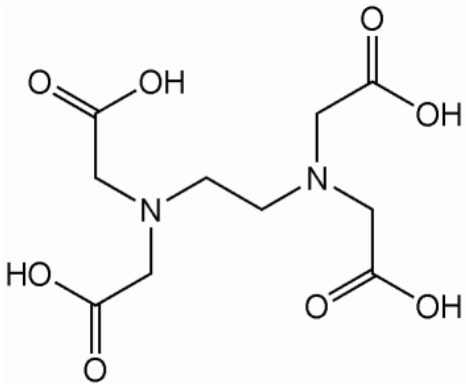
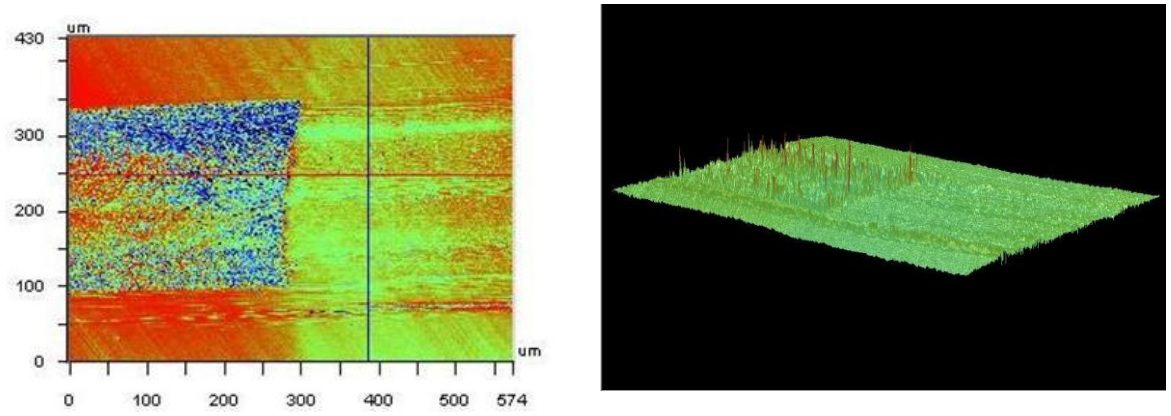


Figure 4.13: Molecular structure of EDTA [89].

A droplet of 0.05 M EDTA solution in distilled water was placed on part of the rubbed track for one minute. The solution was then removed by touching the droplet with a tissue. This method has been shown to effectively remove ZDDP-derived tribofilms, probably by extracting the zinc cations from the zinc phosphate and polyphosphate present in the film [91].

Figure 4.14 shows 2D and 3D SWLI images of the resulting surface. To the right of the image is the region where the EDTA droplet was placed and the ZDDP film removed. The curved border represents the edge of the droplet. By comparing the image inside and outside of the rubbed track it is clear that the tribofilm in the track has been fully removed by EDTA. It can also be seen that the surface outside the wear track in the region treated with EDTA is slightly lower than elsewhere, indicating the presence of a very thin "thermal ZDDP-derived film" outside the rubbed track prior to EDTA treatment.



(a) (b)

Figure 4.14: Typical (a) topography and (b) 3D images of the wear track on the M disc after part of the tribofilm appears to be removed by EDTA.

Figure 4.15 compares line profiles across the EDTA-treated region and the non-treated region, the profiles being taken from positions shown in the images in Figure 4.10 (before removal of tribofilm) and 4.14 (after removal of tribofilm), respectively. When the rubbed surface is treated with EDTA the apparent "wear" largely disappears. This was confirmed by AFM topography measurement of an area spanning both the EDTA and non EDTA-treated regions of the track.

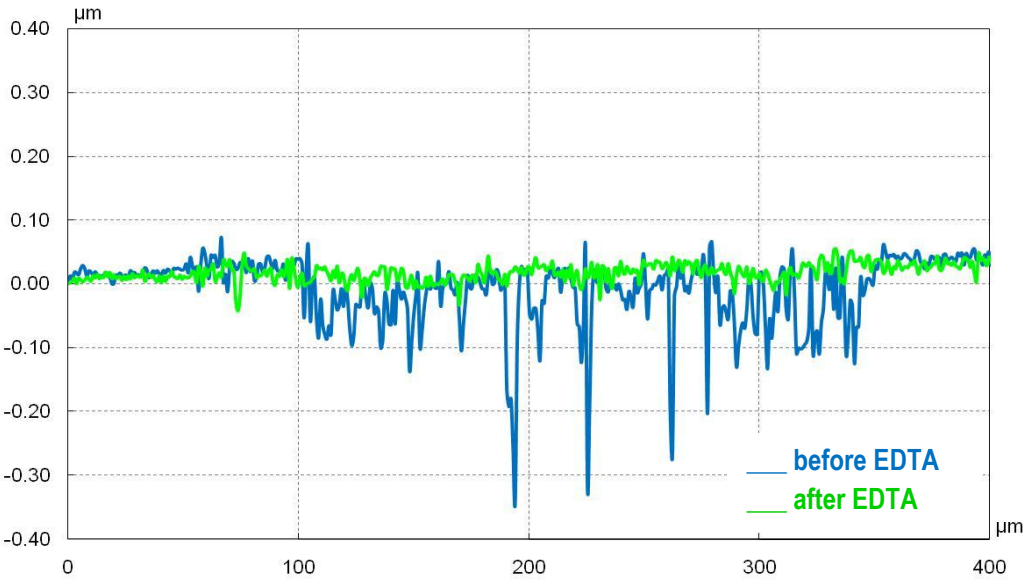


Figure 4.15: Line profile plot across the wear track before and after removal of the tribofilm with EDTA.

After study, the surface shown in Figures 4.14 was coated with a thin layer of gold of *ca.* 25 nm using an EMITECH K575X Turbo Sputter Coating instrument for 2.5 minutes at a current of 30 mAmp. Figure 4.16 shows a SWLI image of the resulting surface. This approach removes the possibility that different parts of the surface might have different reflectivities, which might influence the measurements. The raised area of track due to the presence of the ZDDP tribofilm can be clearly seen in the non EDTA-treated region, together with the absence of any such film (and any measurable wear) in the EDTA-treated region. Figure 4.17 shows line profiles across the track both inside and outside the EDTA-treated regions. It is evident that the tribofilm has been almost fully removed by the EDTA.

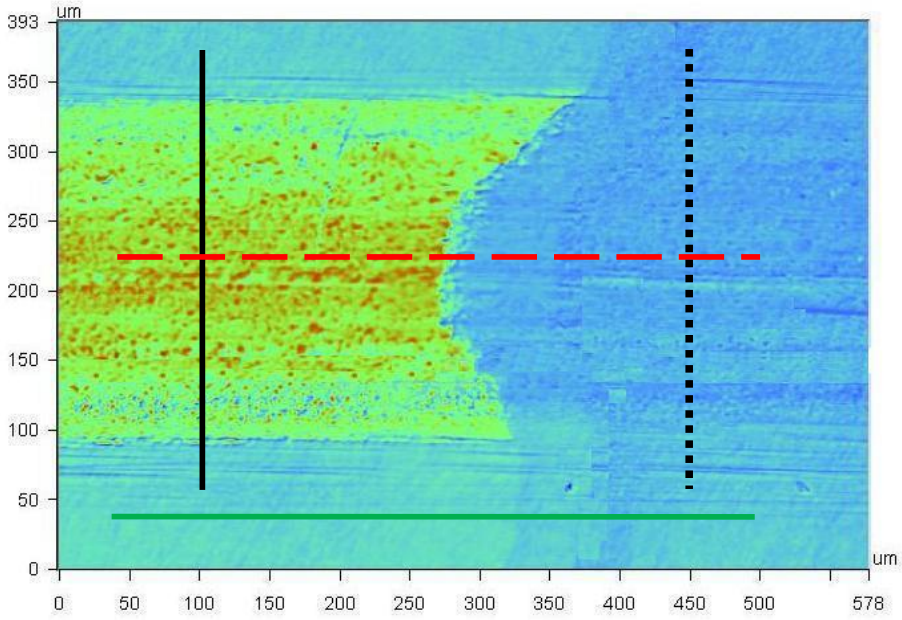


Figure 4.16: 2D topography image of wear track after gold deposition.

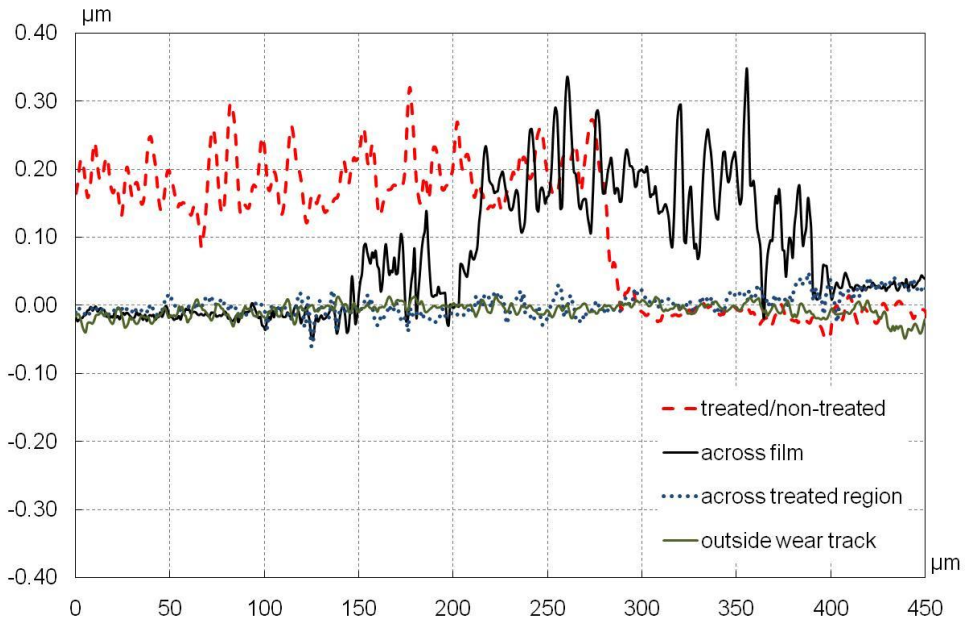


Figure 4.17: Line profile plot showing EDTA/non-EDTA treated regions, tribofilm, EDTA treated region and outside wear track after gold deposition.

From these results it is clear that the application of SWLI to study surfaces that are coated with a thick antiwear film can produce an appearance of material removal even when none exists. This does not originate from a reflectivity change generated by immersion and heating in lubricant since the effect is only present within the rubbed track, even though the region outside the contact should have a very thin "thermal" ZDDP-derived film. The author believes that it is an optical artifact produced by the relatively thick, transparent ZDDP-derived tribofilm. The precise origins of the effect are not clear since the optical properties of the ZDDP-derived tribofilms are not well-characterised. However ZDDP-derived films have a high refractive index of *ca.* 1.6 [88], which results in a very large refractive index difference across the air/film interface. This is likely to produce internal reflection within the film which may contribute to an increase in the apparent path difference between the incident light and the instrument's reference beam, and be misinterpreted as wear. It should be noted that although the artifacts reported here were produced using a Wyko NT9100 [84], similar ones were obtained when the same surfaces were examined by a Zygo NewView 200 [92, 93].

It is interesting to note that a similar effect is not seen when using the spacer layer imaging method (SLIM), which is often used to monitor antiwear film growth in the MTM [91], even though this is also an optical interference method. In this case internal reflection would make the film appear thicker than it actually was. This may be because in SLIM the tribofilm is not adjacent to air but rather to a silica spacer layer, so there is a much smaller refractive index difference across the interface.

These results suggest that SWLI should be used with great caution to measure small levels of wear on rubbed surface that may bear tribofilms. There should be no problem if the film thickness is much less than the wear, *i.e.* if the films are very thin (such as is the case with some antiwear additives and many friction modifiers), or if the wear scar is very deep. But when additives such as ZDDP and overbased detergents are used, which are both known to form thick tribofilms [91, 94], and only mild wear is present, then it is suggested that either the tribofilm be removed before measurement or the interference method be employed in conjunction with some other wear measurement technique.

The same optical artifact was observed in the presence of low and zero SAPS-derived tribofilms. However, it was found that the tribofilms formed by these alternative classes of antiwear additives could not be removed by EDTA alone. Further investigation involving the identification of an alternative sequestering agent revealed that non-ZDDP-derived tribofilms can generally be removed by a combination of oxalic acid (Figure 4.18) and EDTA solutions. Oxalic acid, a dibasic acid and reducing agent, is another chelating agent that forms stable complexes with metal cations, *e.g.* Fe (probably present in non-ZDDP-derived and ashless antiwear additives-derived tribofilms) [37], and it is also well-known for its ability to dissolve iron oxides [95].

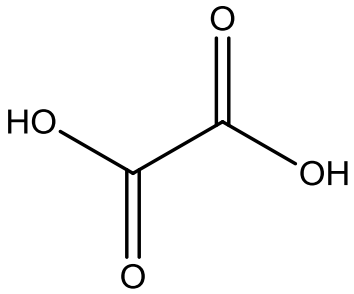
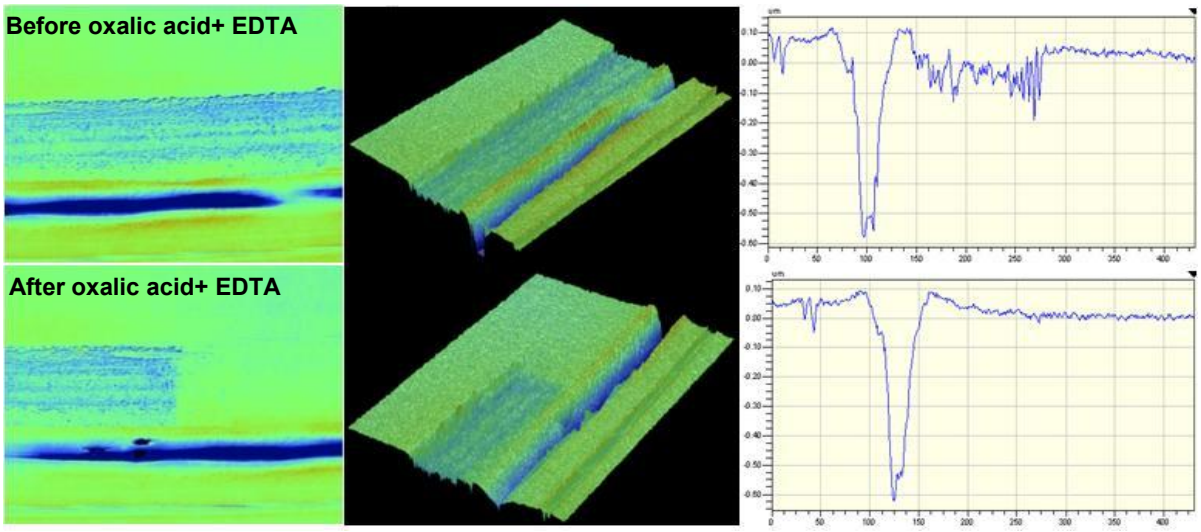


Figure 4.18: Molecular structure of oxalic acid.

For non-ZDDP-derived tribofilms, a droplet of 0.05 M oxalic acid solution in distilled water was placed on the rubbed track for 20 seconds. The solution was then removed by touching the droplet with a tissue. It was found that exposing the surface for longer periods of time caused damage to the surface. Then a droplet of 0.05 M EDTA solution in distilled water was placed on part of the rubbed track for one minute. The solution was then removed by touching the droplet with a tissue. To verify the complete removal of tribofilm, the wear tracks were coated with a thin layer of gold of *ca.* 10 nm using an EMITECH K575X Turbo Sputter Coating instrument for 1 minute at a current of 30 mAmp. Figure 4.19 illustrates that this method was proven effective in removing non-ZDDP-derived tribofilms, probably by extracting the iron cations present in the film.



(a) (b) (c)

Figure 4.19: Typical (a) 2D topography image, (b) 3D image and (c) line profile plot of the wear track on an MTM disc before and after the removal of a non-ZDDP-derived tribofilm with oxalic acid + EDTA. These images reveal the optical artifact in the presence of low and zero SAPS-derived tribofilms; hence the need to remove the film to measure wear depth.

4.4.2.2 Calculating the Wear Coefficient (k_1)

After the tribofilms were removed by EDTA or oxalic acid + EDTA, wear depth measurements were carried out using the SWLI [84]. In this study, the "stitching" data analysis option, available on the WYKO NT9100 Vision software, was used in order to image the entire wear track (≈ 4 mm long). After a topography image was taken, wear depth measurements were taken at both ends and in the middle of the wear track (Figure 4.20).

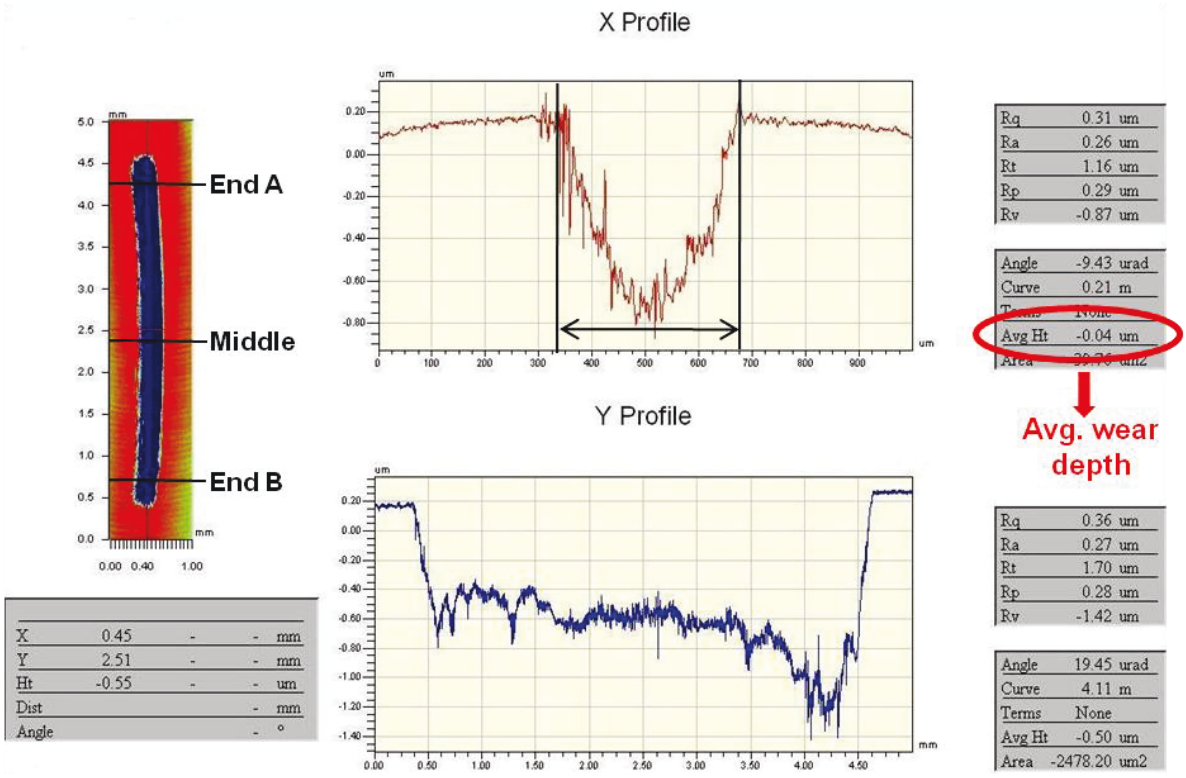


Figure 4.20: Typical 2D topography image and line profile plot of the wear track on the MTM disc after the removal of tribofilm. These images exemplify how wear depth measurements are carried out.

As it was discussed in chapter 3, section 3.3.1, the wear coefficient, calculated using Archard's wear equation, is a very useful parameter to predict and control the extent of surface degradation and material loss. In this study, the wear coefficient, k_1, was calculated using equation 4.5 to compare the wear-reducing properties of low and zero SAPS antiwear additives-derived tribofilms.

Since the speed of the ball is kept constant and the speed of the disc varies throughout the cycle (Figure 4.21), under reciprocating conditions, wear depth measurements were taken in the middle of the wear track, where disc speed is maximum and at the ends of the wear track, where disc speed is minimum because entrainment speed is changing direction.

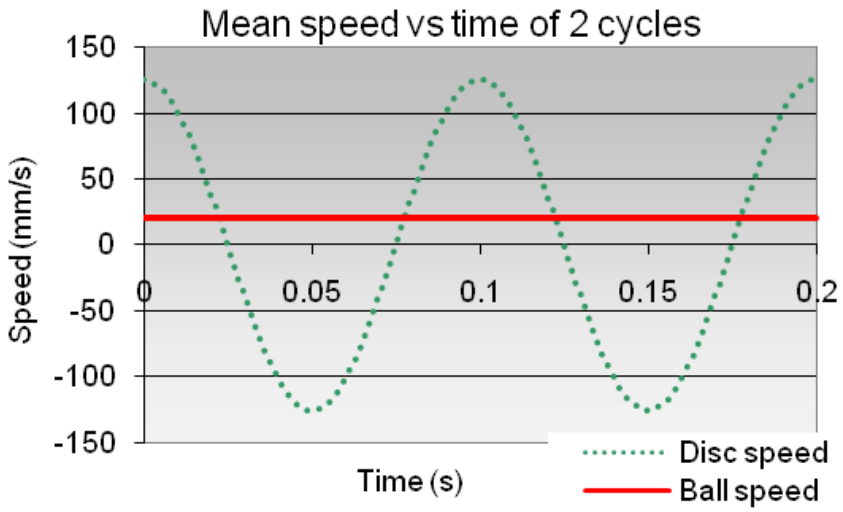


Figure 4.21: Mean speed versus time of two complete cycles [89]: illustrating disc speed (Ud) variation throughout the cycle.

Because of the complex rolling-sliding motion, it is critical to take into account the relationship between the speed of the ball and the speed of the disc (Ub/Ud) when calculating k_1 in this study.

$$V = k_1 \times W \times L$$ (Equation 3.8, Chapter 3, section 3.3.1)

$$V = d \times S$$

$$d = k_1 \times \frac{W}{S} \times L$$

$$p = \frac{W}{S}$$

$$d = k_1 \times p \times L$$

$$L = Us \times f(t)$$

$$L = \left((Ud - Ub) \times \frac{2a}{|Ud|} + (-Ud - Ub) \times \frac{2a}{|Ud|} \right) \times N$$

$$L = \left(\frac{2a}{|Ud|} \times (Ud - Ub - Ud - Ub) \right) \times N$$

$$L = \left(\frac{2a}{|Ud|} \times -2Ub \right) \times N$$

$$L = 4a \times \frac{Ub}{Ud} \times N$$

$$d = k_1 \times p \times 4a \times \frac{Ub}{Ud} \times N$$

$$k_1 = \frac{d}{4a \times p \times N \times \frac{Ub}{Ud}} \qquad \text{(Equation 4.5)}$$

where:

V: wear volume;

k_1: wear coefficient (mm^3/Nm);

W: load;

L: sliding distance;

d: wear depth on the disc (nm; measured by SWLI);

S: area;

p: mean contact pressure (GPa);

Us: sliding speed (mm/s);

f(t): function of time;

Ud: disc speed (mm/s); *e.g.* -Ud: corresponds to ball and disc moving in the opposite direction;

Ub: ball speed (mm/s);

a: semi-contact width (mm);

N: number of cycles (frequency x test length).

4.5 ToF-SIMS Method

4.5.1 Description

Time-of-Flight Secondary Ion Mass Spectrometry (ToF-SIMS) is a surface-sensitive analytical method that uses a focused, pulsed primary ion beam (*e.g.* Caesium, Cs^+; Gallium, Ga^+ and Bismuth, Bi^+) to dislodge chemical species such as ions, molecules and molecular clusters from the very outermost surface of the sample (1-2 nm) [96] (Figure 4.22). In this study, ToF-SIMS is employed to investigate the composition of boundary lubrication tribofilms formed on rubbing surfaces from the decomposition of potential low and zero SAPS antiwear additives.

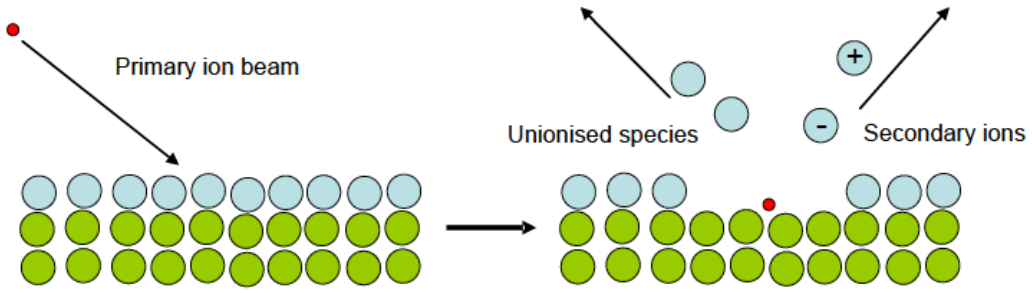


Figure 4.22: Diagram illustrating the removal of secondary ions (*i.e.* positive secondary ions, negative secondary ions and neutral fragments) from the outermost surface of the sample [97].

The chemical species escape from atomic monolayers on the surface (secondary ions) and are then accelerated into a "flight tube" and their mass is determined by measuring the precise time at which they reach the detector (*i.e.* time-of-flight) (Figure 4.23). Three operational modes are available using ToF-SIMS: surface spectroscopy, surface imaging and depth profiling.

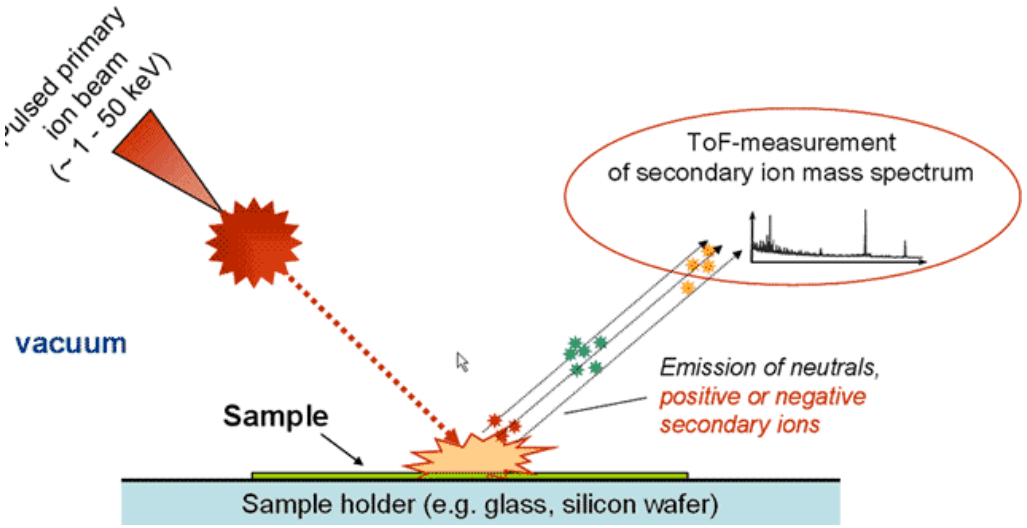


Figure 4.23: Principle of ToF-SIMS [98].

The entire mass spectrum is acquired simultaneously, mass peaks are identified and an image is collected. A chemical map of the surface is generated by collecting a mass spectrum at every pixel as the primary ion beam is rastered across the sample surface. The mass spectrum and the secondary ion images are combined to determine the composition and distribution of selected elements or molecular species on the sample surface [99]. A comprehensive review describing the principle of ToF-SIMS and its capabilities in terms of practical surface chemical analysis is given by Vickerman *et al.* [96].

The ToF-SIMS study carried out in this project focused mainly on obtaining and analysing chemical maps of the surface (*i.e.* surface imaging) (Figure 4.24), rather than spectroscopy or depth profiling to characterise the tribofilms. Surface spectroscopy analysis proved time-consuming, given the number of samples of interest; whereas the topography of tribofilms limits depth profiling resolution, given that tribofilms are not uniformly distributed on the surface (*i.e.* roughness diminishes mass spectroscopy resolution).

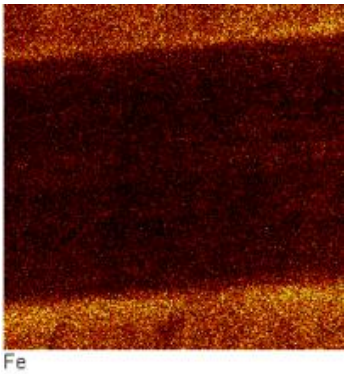


Figure 4.24: Typical ToF-SIMS chemical map showing the distribution of Fe on the wear track of the MTM disc, spanning rubbed/unrubbed areas. Brighter regions in the image indicate an abundance of element or molecule of interest, while darker regions indicate their absence. The image suggests the formation of a thick protective film inside the wear track and negligible tribofilm outside rubbed area.

4.5.2 Experimental Procedure

In this study, ToF-SIMS was used to generate chemical surface maps of antiwear additive-derived tribofilms. The thin films in question were generated on AISI 52100 steel discs (46 mm diameter), using a mini traction machine (MTM). ToF-SIMS experiments were carried out using an ION-TOF IV (University of Nottingham). Surface imaging was obtained using a Bi^+ liquid metal ion gun (LMIG) at a maximum sampling depth of 2 nm. An area of 500 µm x 500 µm spanning rubbed/unrubbed areas or at the edge of the wear track was submitted to analysis and a chemical map for the element or molecule of interest was obtained using the instrument software. Before loading the discs into the ultra high vacuum (UHV) chamber for testing, these were cleaned by immersion in hexane in an ultrasonic bath for 10 minutes. Table 4.4 lists the ToF-SIMS test conditions used in this study.

Table 4.4: ToF-SIMS test conditions	
Test apparatus	ToF-SIMS IV from ION-TOF GmbH of Münster, Germany
Primary ion species	Bi_3^+ (LMIG)
Scan size	500 µm x 500 µm
Image	256 x 256 pixel raster
Sampling depth	2 nm (maximum)
Spatial resolution of 100 nm.	> 100 nm
Mass resolution	> 7000 at m/z = 29
Mass analyser	Reflectron

4.6 XANES Method

4.6.1 Description

It is believed that the characteristics of the tribofilms and their antiwear performance result from the processes by which the additives are adsorbed onto the metal surface during rubbing and subsequently react to form a complex lubricating film. It has been suggested that the tribofilms are not composed by the additives themselves but consist of the decomposition/reaction products of these additives. Thus understanding the chemistry of tribofilms is key to understanding the growth and wear-reducing properties of tribofilms. X-ray absorption near edge spectroscopy (XANES), using synchrotron radiation has been shown to be a powerful technique to investigate the chemical structure of boundary lubrication films generated from engine and transmission oils [100-105]. In XANES, monochromatic X-rays, from synchrotron radiation, excite electrons from a core shell and the emission resulting from the refilling of this shell by an outer electron is observed, either by measuring consequently emitted fluorescent photons (fluorescent yield) or the neutralisation current (total electron yield) ((Figure 4.25). This emission is very dependent on the chemical environment of the atom of interest. A comprehensive review describing the principle, instrumentation and application of XANES is given by Stohr [106].

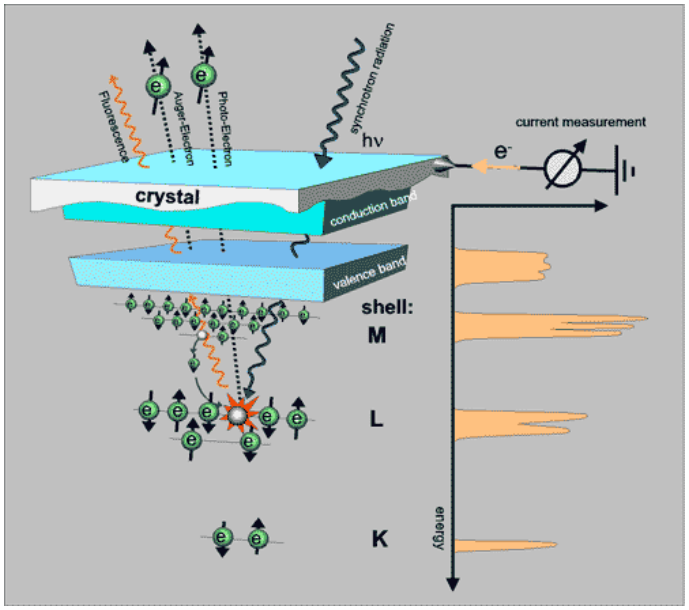


Figure 4.25: The photoelectric effect [107].

In this study, XANES is employed to investigate the local environment and oxidation state of elements in boundary lubrication tribofilms formed on rubbing surfaces from the decomposition of potential low and zero SAPS antiwear additives. Using XANES and combining total electron yield (TEY, outermost surface sensitive) and fluorescence yield (FY, bulk and interface sensitive) detection modes, the complex multilayered composition of tribofilms can be provided simultaneously, from the outermost surface, throughout the bulk and to the interface between the steel and the protective film (Figure 4.26).

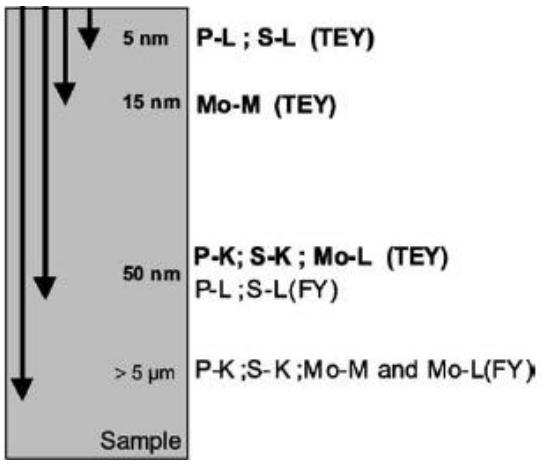


Figure 4.26: Typical sampling depth for XANES analysis of phosphorus and sulphur-containing tribofilms [108]. TEY provides chemical information about the surface/near surface of the film *(i.e.* ≈ 5 nm) at the L-edge; and the bulk of the film *(i.e.* ≈ 50 nm) at the K-edge. FY focuses on the bulk of the film *(i.e.* ≈ 50 nm) at the L-edge; and on the interface steel-protective film through to the substrate (> 5 µm) at the K-edge.

In order to identify the chemical nature and oxidation state of elements in a complex multilayered matrix such as tribofilms, it is essential to compare the XANES spectra of the tribofilms with those of model compounds of known chemical environment (Figure 4.27). The spectra of a wide range of model compounds, spanning the chemistries of interest was obtained. A comprehensive list of model compounds employed in this study is given in Table 4.6.

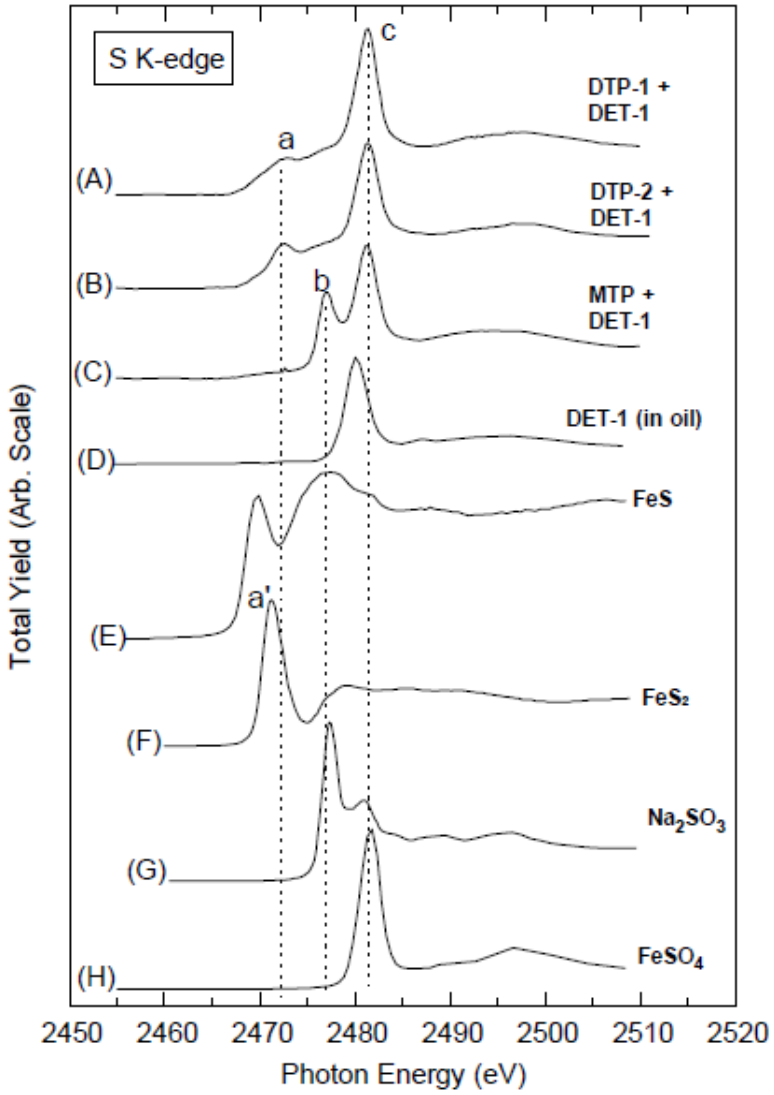


Figure 4.27: Typical XANES analysis of sulphur-containing tribofilms [109]: showing S K-edge spectra (TEY) of tribofilms derived from thiophosphate additives (*e.g.* DTP-1, DTP-2, MTP) in the presence of a detergent (*i.e.* DET-1), along with model compounds of varying oxidation states (*i.e.* FeS, FeS_2, Na_2SO_3, $FeSO_4$). A comparison between the tribofilms and model compounds can be established and the chemical nature and oxidation state of elements in the tribofilm can be identified.

4.6.2 Experimental Procedure

In this study, XANES was employed to investigate the chemical composition of antiwear additive-derived tribofilms. The thin films in question were generated on AISI 52100 steel discs (46 mm diameter), using a mini traction machine (MTM). XANES spectra for the species of interest were obtained at the 1.7 GeV storage ring at Helmholtz-Zentrum Berlin für Materialien und Energie GmbH (HZB, Berlin, Germany; a merger of former Hahn-Meitner-Institut (HMI) and Berliner Elektronenspeicherring-Gesellschaft für Synchrotronstrahlung (BESSY II)) and at the 2.9 GeV storage ring at Canadian Light Source (CLS, Saskatoon, Canada). Measurements were carried out by the author at both sites. To explore the chemical nature and oxidation state of elements at the outermost surface, bulk and interface steel-protective film, the photoadsorption spectra were recorded using TEY and FY modes of detection. The energy ranges were defined in order to include the electron binding energies for the elements of interest in their natural forms, as well as the electron binding energies of the model compounds. At least three scans were digitally combined and a background was removed after normalization. Before loading the discs into the ultra high vacuum (UHV) chamber for testing, these were cleaned by immersion in hexane in an ultrasonic bath for 10 minutes. Table 4.5 summarises XANES test conditions and Table 4.6 lists the extensive range of model compounds employed in this study. Powder and glass-like model compounds were pressed onto the conducting carbon tape mounted on the sample holder and loaded into the UHV chamber for analysis. Due to the volatility of some liquid model compounds, a thin liquid film was prepared by spreading a small drop of liquid on the carbon tape, transferred to the sample holder and subsequently analysed [110].

Table 4.5: XANES test conditions

Synchrotron radiation facility	1.7 GeV storage ring at HZB	2.9 GeV storage ring at CLS	
Beamline	Double crystal monochromator: Si(111); KMC-1	Variable Line Spacing Plane Grating Monochromator (VLS PGM); 11ID-2	Soft X-ray Microcharacterization Beamline; (SXRMB); 06B1-1; XAFS
Energy range	2000-12000 eV	5.5-250 eV	1700-10000 eV
Spot size	500 µm x 500 µm	500 µm x 500 µm	300 µm x 300 µm

Table 4.6: Model compounds used in XANES study		
Model compound name	**Description**	**Supplier**
$Fe(PO_3)_3$	iron metaphosphate glass	Maura Crobu, ETH
$FePO_4$	iron (III) phosphate	Acros Organics
$Fe_4(P_2O_7)_3$	iron (III) pyrophosphate	Sigma-Aldrich
$Fe_{10}P_{18}O_{55}$	iron polyphosphate glass (Fe/P: 0.5)	Maura Crobu, ETH
Zn/P	zinc ultraphosphate glass (Zn/P: 1/3)	Maura Crobu, ETH
ZnP_2O_6	zinc metaphosphate glass	Maura Crobu, ETH
$Zn_2P_2O_7$	zinc pyrophosphate glass	Maura Crobu, ETH
$Zn_4P_6O_{19}$	zinc polyphosphate glass	Maura Crobu, ETH
$Zn_3(PO_4)_2$	zinc phosphate	Sigma-Aldrich
Zn_3P_2	zinc phosphide	Sigma-Aldrich
Amine phosphate	-	-
ZnS	zinc sulphide	Sigma-Aldrich
$ZnSO_4$	zinc sulphate	Sigma-Aldrich
FeS	iron (II) sulphide	Sigma-Aldrich
FeS_2	iron disulphide (pyrite)	Alfa Aesar
Na_2SO_3	sodium sulphite	Sigma-Aldrich
$FeSO_4$	iron (II) sulphate	Sigma-Aldrich
$C_{12}H_{26}S_2$	di-n-hexyl disulphide	Alfa Aesar
$C_4H_6N_2S$	2,5-dimethyl-1,3,4-thiadiazole	Sigma-Aldrich
$C_{21}H_{21}BO_3$	tribenzyl borate	Sigma-Aldrich
BPO_4	boron phosphate	Sigma-Aldrich
B_2O_3	boron oxide	Sigma-Aldrich
$Na_2B_4O_7$	sodium tetraborate	Sigma-Aldrich

4.7 Test Materials

Although the additives used in this study are commercially-available products used without any further purification, their names have been changed for confidentiality reasons. These additives were blended individually, unless otherwise specified, into the Group III base oil (C) (4 cSt at 100 ºC), supplied by Castrol Ltd. Additive concentrations used corresponded to concentrations of 800 ppm phosphorus for P- and P-S-containing antiwear additives, 1000 ppm sulphur for S-containing antiwear additives, 900 ppm M for M-containing antiwear additives (*i.e.* M: Ti, Mn, Zn and Mo), 800 ppm B for B-containing antiwear additives, 1000 ppm N for N-containing heterocyclic antiwear additives and 1000 ppm Nanoparticles for nanoparticle-containing antiwear additives. A comprehensive summary including all materials employed in this study is given in Table 4.7.

Table 4.7: Test materials summary

Abbreviation[1]	**Sample name**
Base oil	
GIII BO	Group III base oil (C)
GI BO	Group I base oil (C)
ZDDP study	
ZDDP1	Primary ZDDP (C)
ZDDP2	Secondary ZDDP (C)
PIBS1	Polyisobutylene succinimide dispersant 1 (C)
PIBS2	Polyisobutylene succinimide dispersant 2 (C)
=	Ethylbenzene
P-containing additives study	
=	Triisopropyl phosphate
=	Triisopropyl phosphite
=	Bis(2-ethylhexyl) phosphate
=	Bis(2-ethylhexyl) phosphite
TAP	Triaryl phosphate (C)
AP	Amine phosphate (C)
nCaSu	Neutral calcium alkylsulphonate (C)
Ti-IPO	Titanium (IV) isopropoxide
P-S-containing additives study	
ADTP	Ashless dithiophosphate (C)
DADTP	Dialkyl dithiophosphate (C)

TPPT	Triphenyl phosphorothionate (C)
ATPPT	Alkylated triphenyl phosphorothionate (C)
BTPPT	Butylated triphenyl phosphorothionate (C)
ATP	Amine thiophosphate (C)
PSN	Phoshporus-sulphur-nitrogen-based (C)
PS	Phosphorus-sulphur-based (C)
nCaSu	Neutral calcium alkylsulphonate (C)
Ti-IPO	Titanium (IV) isopropoxide
S-containing additives study	
=	Di-n-hexyl disulphide
=	Di-n-octadecyl disulphide
=	Dibenzyl disulphide
DA5S	Dialkyl pentasulphide (C)
DAPS	Dialkyl polysulphide (C)
SFAE	Sulphurised fatty acid ester (C)
=	2-Isobutylthiazole
=	2,5-Dimethyl-1,3,4-thiadiazole
=	2-Mercaptobenzoxazole[2]
DMTDA1	Dimercaptothiadiazole 1 (C)
DMTDA2	Dimercaptothiadiazole 2 (C)
DTBTDAT	Dithio-bis-thiadiazolethione (C)[2]
MBTA	Mercaptobenzothiazole (C)
MBDADTC	Methylene-bis-dialkyl-dithiocarbamate (C)
MBDBDTC	Methylene-bis-dibutyl-dithiocarbamate (C)
M-containing additives study	
Ti-IPO	Titanium (IV) isopropoxide
MMT	(Methylcyclopentadienyl)manganese(I)tricarbonyl
ZP	Zinc alkylphosphate (C)
ZnDTC	Zinc diamyl dithiocarbamate (C)
MoDTC	Molybdenum dialkyldithiocarbamate (C)
B-containing additives study	
AB	Amide borate (C)
TEHB	Tris(2-ethylhexyl) borate (C)
HGBB	Hexyleneglycol biborate (C)
DBGBB	Dibutyleneglycol biborate (C)
B-PIBS(H)	Borated polyisobutenyl succinimide (High B) (C)
B-PIBS(L)	Borated polyisobutenyl succinimide (Low B) (C)

KB	Potassium borate (C)
N-containing heterocyclic additives study	
BTA	Benzotriazole (C)
HQ	Hydroxyquinoline (C)
Nanoparticle-containing additives study	
PIBS1	Polyisobutylene succinimide dispersant 1 (C)
TiO_2 NANO	Titanium oxide nanoparticles (C)
=	Fullerene
DWCN	Double walled carbon nanotubes
IF-WS_2	IF-WS_2 (C)
p-CB	p-Carborane (C)
m-CB	m-Carborane (C)
cOBCaSu	Crystalline overbased calcium sulphonate (C)
aOBCaSu	Amorphous overbased calcium sulphonate (C)
nCaSu	Neutral calcium alkylsulphonate (C)
Formulations study	
=	PF[3] without DISP or AW
=	PF[3] + ZDDP
PF[3] + ATPPT	PF[3] + Alkylated triphenyl phosphorothionate (C)
PF[3] + B-PIBS(H)	PF[3] + Borated polyisobutenyl succinimide (High B) (C)
PF[3] + KB	PF[3] + Potassium borate (C)
PF[3] + HQ	PF[3] + Hydroxyquinoline (C)
=	PF[3] + DISP
=	PF[3] + DISP + ZDDP
PF[3]+ DISP + ATPPT	PF[3]+ DISP + Alkylated triphenyl phosphorothionate (C)
PF[3]+ DISP + B-PIBS(H)	PF[3]+ DISP + Borated polyisobutenyl succinimide (High B) (C)
PF[3]+ DISP + KB	PF[3]+ DISP + Potassium borate (C)
PF[3]+ DISP + HQ	PF[3]+ DISP + Hydroxyquinoline (C)
=	FF[4] 250 ppm ZDDP
=	FF[4] 1200 ppm ZDDP

(C): commercially-available.

[1] "=" means abbreviated name is the same as full name

[2] These additives were not submitted to testing because they were not soluble in GIII base oil (C).

[3] PF: partially formulated oil.

[4] FF: fully formulated oil.

5. FILM-FORMING, FRICTION, MORPHOLOGY AND WEAR-REDUCING PROPERTIES OF ZDDP

Although the main concern of the study reported in this thesis is to investigate the film-forming, friction and wear of a wide range of low and zero SAPS antiwear additives, it is important to establish first the behaviour of the antiwear additive ZDDP. This is needed both to provide a benchmark against which to assess the performance of other potential, antiwear additives and also to enable the findings to be related to previous antiwear additive work, which has mainly studied ZDDP.

The chapter first provides an overview of previous research on ZDDP, with a particular focus on the film-forming, friction and wear properties of this additive type. The mechanisms by which ZDDP form films to influence friction and reduce wear are then briefly discussed.

The chapter then describes film thickness, friction, surface topography and wear measurements of ZDDP solutions made in the current study, using the methods outlined in chapter 4.

Some surface analyses of the films formed by ZDDP were also carried out using ToF-SIMS and XANES but these are deferred to chapter 13, where analysis of the films formed by various additives of interest are presented and discussed together.

5.1 Literature Overview of ZDDP

ZDDP has been the main engine oil antiwear and extreme pressure additive choice since the 1940s. In addition to providing effective antiwear and mild extreme pressure properties, ZDDP was initially recognised for its antioxidant and corrosion inhibition performance [111-114]. Its role as antioxidant and corrosion inhibitor, as well as its adsorption and film formation mechanism, friction behaviour and wear-reducing properties in engine oils have been extensively researched. Comprehensive reviews on the history and mechanisms of ZDDP have been given by Spikes [88], Barnes *et al.* [115], Gellman *et al.* [116] and Nicholls *et al.* [117].

The molecular structure of ZDDP is represented in Figure 5.1. There are two main types of ZDDP structure, namely neutral and basic salts. Commercial ZDDPs are usually a mixture of both salts. The molecular structure of ZDDP can be further modified by varying the attached hydrocarbon groups, *i.e.* primary, secondary, aryl. In primary ZDDPs, the OR groups are alkoxy groups with two hydrogen atoms on the carbon attached to the oxygen atom, while in secondary ZDDPs the alkoxy groups have one hydrogen and one carbon atom attached to the carbon bonded to oxygen. In aryl ZDDPs, substituted benzene rings are attached to the oxygen atoms in the ZDDP.

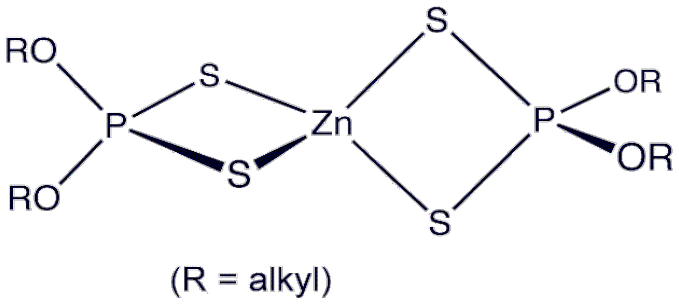


Figure 5.1:Molecular structure of ZDDP [65].

5.1.1 Film-forming, Friction and Wear-reducing Properties of ZDDP

ZDDP tribofilms adsorb rapidly on metal surfaces to form films of monolayer thickness and there is some evidence of a chemical interaction with release of Zn [118, 119]. Unless rubbing occurs, thicker films only form at high temperatures and these are generally called “thermal films”. However when rubbing takes place in thin film conditions where there is asperity contact, thick solid-like films [120] form very rapidly on the surfaces at room temperature [73]. The thickness of these films increases with lubricant temperature to reach values of 50-200 nm [73, 121, 122]. Outside of the rubbing track there is usually negligible film unless the temperatures are high, when a thermal film forms [68, 123].

Morphological studies reveal that the ZDDP-derived tribofilms are initially randomly distributed patches on the rubbed surface, which gradually evolve into a uniformly distributed, pad-like structure [124], separated by deep valleys where practically no film has developed [77]. The tribofilms consists mainly of a glassy phosphate, with a thin superficial layer of zinc polyphosphate (*i.e.* ≈ 10 nm thick) and a pyro- or orthophosphate layer towards the bulk of the film [125, 126]. There is an increase in the proportion of iron towards the interface of the film with the underlying metal surface [126], where a sulphur-rich layer is present. It has been suggested that this layer consists of zinc and iron sulphide [120, 127, 128], though the presence of the latter has been disputed by Martin *et al.* [126]. The ZDDP-derived pad-like structure and its composition are illustrated in Figure 5.2.

In fully formulated oils containing calcium-overbased detergents, it has been suggested that the tribofilm consists of calcium phosphate [129] and calcium carbonate [64]. More recently, Topolovec-Miklozic studied the film formation by mixtures of ZDDP and overbased calcium sulphonate detergent in solution and found that when the surfaces were treated with weak acid to remove CaCO3 after rubbing, this removed discrete patches of the film, leaving others undiminished. This suggests that the surface film consisted of separate CaCO3 and zinc phosphate islands [130].

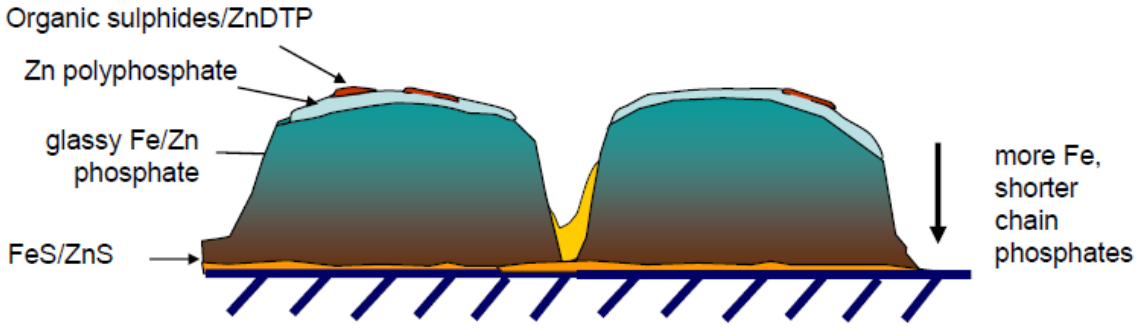


Figure 5.2: Schematic diagram of ZDDP-derived pad structure and composition [88].

The deleterious effect of ZDDP-derived tribofilms on engine friction and consequently on fuel economy were first recognised in the 1980s [131, 132]. Originally it was believed that this effect was due to an increase in boundary friction, but later studies showed that ZDDP-derived tribofilms increased friction primarily in the mixed lubrication regime [133]. The Stribeck curve shown in Figure 5.3, illustrates the typical friction behaviour of ZDDP-derived tribolfims, in which friction coefficient is given as a function of entrainment speed at different stages of rubbing (*i.e.* increasing rubbing time). The Stribeck curve shows that once a protective ZDDP-derived film starts to form on the surface (*i.e.* after 5 minutes of rubbing) the main effect of this film is to shift the entire Stribeck curve to the right, which implies that the contact remains in mixed/boundary lubrication to higher speeds [88].

At first it was proposed that this increase in friction was due to the roughness of the reaction films, given their pad-like structure [123, 134]. However, this effect was also observed on smoother ZDDP films [135, 136], and it was suggested that ZDDP films might inhibit fluid flow through the contact as the result of lubricant slip against the smooth ZDDP pads [137, 138].

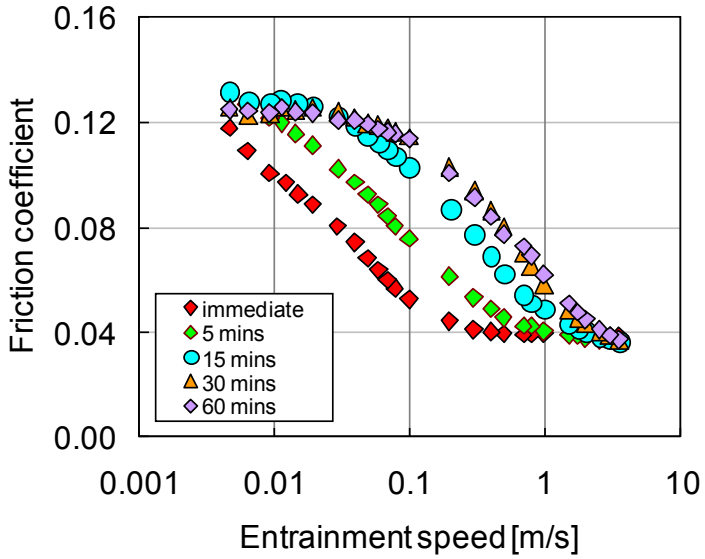


Figure 5.3: Stribeck curves showing friction coefficient *versus* entrainment speed at increasing rubbing times for a ZDDP-containing oil at 50 % SRR, 31 N and 100 ºC [69].

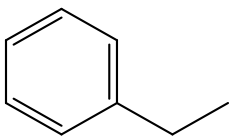
The mechanisms by which ZDDPs prevent wear have been the subject of a great deal of research [88]. Three main mechanisms have been suggested: (i) by forming a mechanically protective barrier between the two surfaces in contact [139], (ii) by removing corrosive peroxides or peroxy-radicals from the lubricant and thus preventing corrosive wear [140, 141] , (iii) by “digesting” hard abrasive iron oxide particles to form soft iron phosphate, hence preventing abrasive wear [142-144].

The most widely-accepted theory is that the ZDDP-derived tribofilm acts as a protective barrier, preventing direct metal-to-metal contact and thus adhesive wear. In general, ZDDP is considered so effective because it reacts very rapidly on the surfaces to form protective films and also because these films contain minimal iron, which means that when the film is worn away and replenished, this does not result in corrosion/abrasion of the substrate [145, 146], unless dispersant or soot particles are present [73]. It has recently been shown that soot easily abrades the soft iron phosphate film that initially forms in the presence of ZDDP, exposing a layer of nascent iron that either reacts with the sulphur in ZDDP to form iron sulphide or with oxygen and ZDDP to form iron phosphate. These films are abraded as rapidly as they form to further expose more reactive iron, giving a "corrosive-abrasive" wear mechanism [48].

5.2 Results: Film-forming Properties of ZDDP

The film-forming properties of ZDDP were studied using MTM-SLIM under mixed rolling/sliding conditions, as described in chapter 4, section 4.1. A primary, *i.e.* ZDDP1 and a secondary ZDDP, *i.e.* ZDDP2 were blended into Group III base oil (C) at a concentration of 800 ppm phosphorus and submitted to rubbing under the same test conditions on the MTM-SLIM. The materials employed in the study described in this chapter are summarised in Table 5.1.

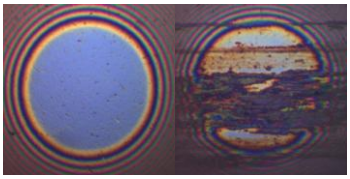
Table 5.1: Test materials summary: ZDDP study

Abreviation[1]	**Sample name**	**Details**
GIII BO	Group III base oil (C)	-
GI BO	Group I base oil (C)	-
ZDDP1	Primary ZDDP (C)	9.5 %P; 20.0 %S; 10.6 %Zn
ZDDP2	Secondary ZDDP (C)	10.0 % P; 21.0 %S; 11.0 %Zn
PIBS1	Polyisobutylene succinimide dispersant 1 (C)	-
PIBS2	Polyisobutylene succinimide dispersant 2 (C)	-
=	Ethylbenzene	*e.g.* 

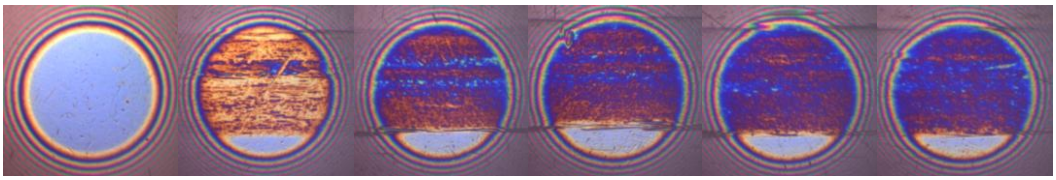
(C): commercially-available.

[1] "=" means abbreviated name is the same as full name

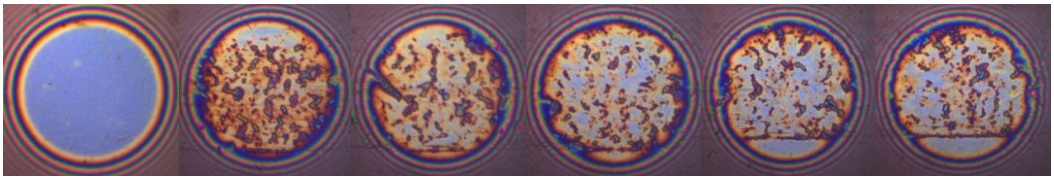
Figure 5.4 shows SLIM results for the base oil and the two ZDDP solutions. With the base oil alone, scuffing occurred after 5 minutes of rubbing, as shown in Figure 5.4[a)] and the test was terminated.



a) Group III base oil (C)



b) Primary ZDDP (C) in GIII BO



c) Secondary ZDDP (C) in GIII BO

0 5 min 15 min 30 min 60 min 120 min

Figure 5.4: MTM-SLIM images showing: a) scuffing on the surface of the ball after 5 minutes of rubbing in base oil without antiwear additive; b) and c) the growth of tribofilm on the ball with increasing rubbing time (*i.e.* zero, 5, 15, 30, 60, 120 minutes).

It can be seen that the Primary ZDDP (C) (Figure 5.4[b]) rapidly forms a thick, solid-like film on the rubbed ball, while the Secondary ZDDP (C) (Figure 5.4[c]) does not form a uniform film, but instead forms randomly-distributed "gummy"-like deposits on the surface. Since secondary ZDDPs have been reported to have similar or even superior performance than primary ZDDPs, these tests were repeated three times and gave the same behaviour in each test. An investigation was therefore carried out to explore the origins of this behaviour.

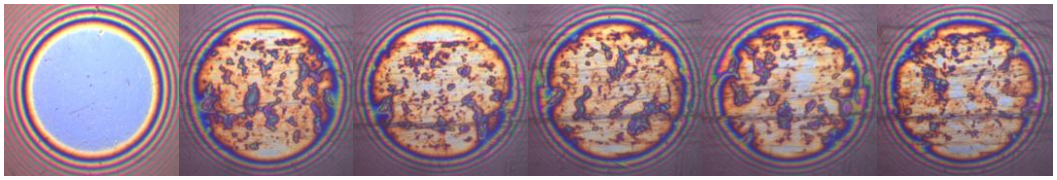
Since the presence of contaminants in Secondary ZDDP (C) might have prevented film formation, a new sample of this additive was supplied, namely "New Sample Secondary ZDDP". Figure 5.5[a] shows that this sample in GIII BO forms similar "gummy"-like deposits to the first sample, indicating that this is a repeatable response of this additive/base oil combination.

A similar type of patchy, "gummy" film was observed by Campen when studying the film-forming properties of glycerol monooleate (GMO) in the same GIII BO [147]. Campen tentatively ascribed this to the formation of insoluble glycerol on the rubbing surfaces. Following this, it is possible that the Secondary ZDDP (C) additive forms low molecular weight alcohols, which are insoluble in the highly non-polar base oil and thus deposit on the surface. According to this hypothesis the GI BO is then sufficiently polar to dissolve these alcohols, while the primary ZDDP has high molecular weight and thus more soluble alcohol groups.

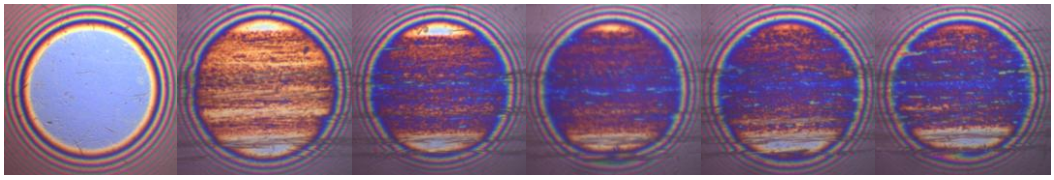
It should be noted that the secondary ZDDP used, *i.e.* ZDDP2, is known to be effective as an antiwear additive in fully-formulated GIII BO, but in this case other additives present will greatly increase the polarity of the blend.

Since the secondary ZDDP, *i.e.* ZDDP2, is an important antiwear additive and its antiwear effectiveness was needed to compare with low SAPS additives it was decided to explore the impact of polarity on ZDPP film formation further.

Initially the New Sample Secondary ZDDP (C) was blended into a GI BO. It can be seen in Figure 5.5[b)] that this blend forms a thick ZDDP-derived tribofilm in GI BO, characteristic of ZDDPs. Since group I base oils contain many more polar species, including aromatics, than group III, this lends support to the significance of polarity on ZDDP film-forming behaviour.



a) New Sample Secondary ZDDP (C) in GIII BO



b) New Sample Secondary ZDDP (C) in GI BO

0 5 min 15 min 30 min 60 min 120 min

Figure 5.5: MTM-SLIM images showing: a) and b) the growth of tribofilm on the ball with increasing rubbing time (*i.e.* zero, 5, 15, 30, 60, 120 minutes).

Tests were then carried out to study the behaviour of Secondary ZDDP (C), *i.e.* the original sample, in a solution of polyisobutylene succinimide dispersant in GIII BO. This additive is polar and will enhance the polarity of its blends. Two polyisobutylene succinimide dispersants with different basicity, *i.e.* PIBS1 and PIBS2, were individually blended at a concentration of 5 % weight, with Secondary ZDDP (C) (800 ppm P) into the GIII BO.

Both of these blends formed thick tribofilms, as shown in Figures 5.6[a)] and 5.6[b)]. The films were not quite as thick as the film formed by Primary ZDDP (C) (Figure 5.4[b)]); probably because of the well documented antagonistic effect that dispersants have on ZDDP-derived tribofilms [73]. As might be expected, similar results were obtained when the secondary ZDDP, *i.e.* ZDDP2, was blended with the dispersants in GI BO (Figure 5.6[c)] and 5.6[d)]).

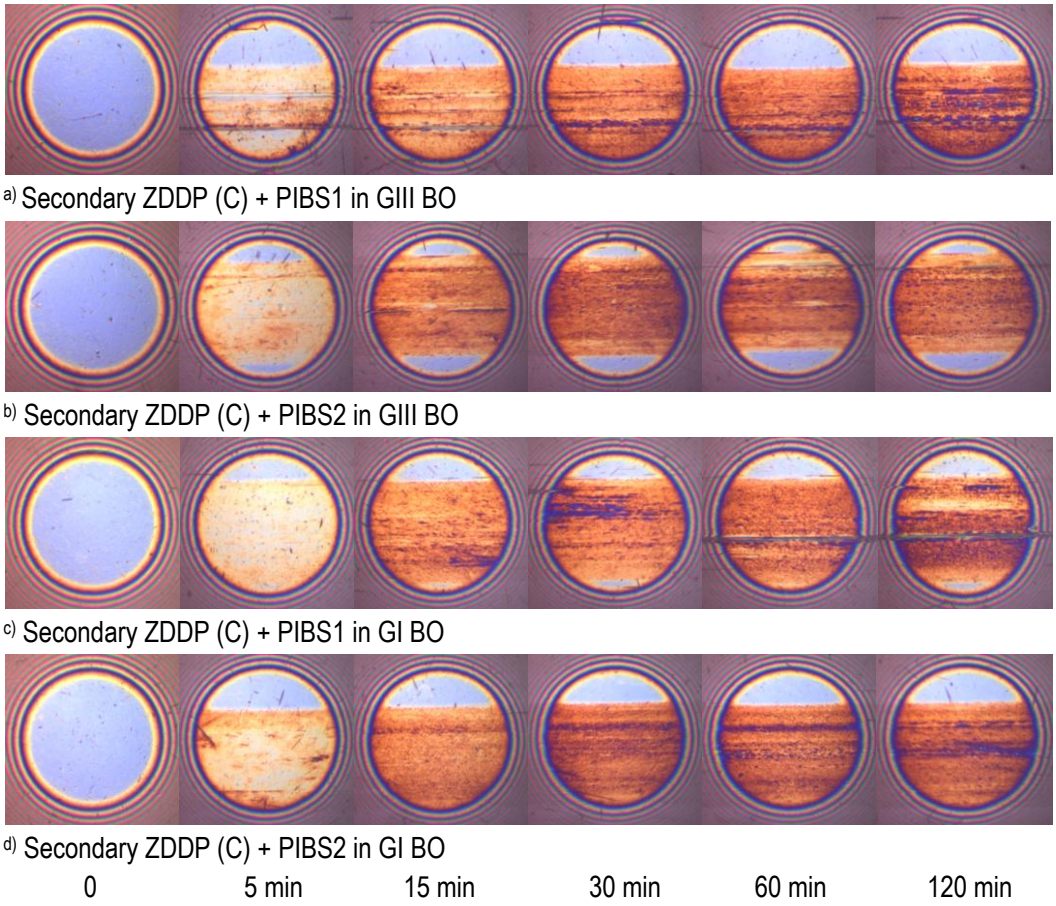


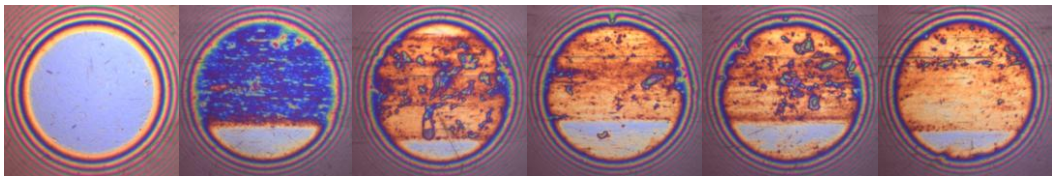
Figure 5.6: MTM-SLIM images showing: a) to d) the growth of tribofilm on the ball with increasing rubbing time (*i.e.* zero, 5, 15, 30, 60, 120 minutes).

To further investigate this solvency effect, ethylbenzene was blended, at a concentration of 5 % weight, with Secondary ZDDP (C) (800 ppm P) into GIII BO. This aromatic hydrocarbon is considerably more polar than alkyl hydrocarbons and will thus increase the overall polarity of the blend. Alkyl benzenes with longer alkyl side-chains are, indeed, added to PAOs for use as lubricants to increase their polarity and thus improve additive solvency and reduce seal swell. They are also present in GI mineral oils. Figure 5.7[a)] shows that this blend rapidly forms a thick tribofilm on the surface, *i.e.* after 5 minutes of rubbing.

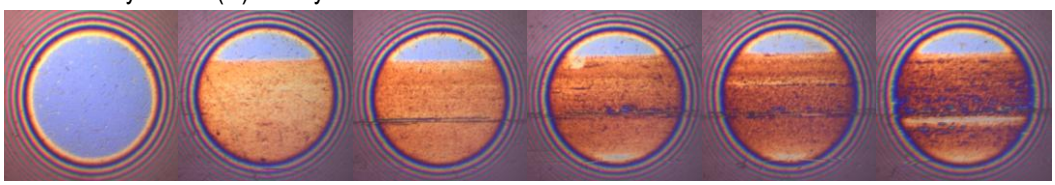
The presence of ethylbenzene seems to adjust the polarity of the base oil improving the solubility of Secondary ZDDP (C), allowing this additive to react with the surface to form a film. However, this film appears to be partially removed over time revealing patches of "gummy"-like deposits on the surface.

Finally a blend of Secondary ZDDP (C) in GIII BO with 5 % weight dispersant and 5% weight ethylbenzene was tested. This forms characteristic ZDDP tribofilm on the surface (Figure 5.7[b)]).

Overall these results suggest that the solubility of Secondary ZDDP (C) in GIII BO is improved by a change in the polarity of the base oil by means of introducing a more polar solvent and/or a dispersant. Since ZDDP was not the main focus of this thesis, no further investigation was carried out.



a) Secondary ZDDP (C) + Ethylbenzene in GIII BO



b) Secondary ZDDP (C) + Ethylbenzene + PIBS1 in GIII BO

0 5 min 15 min 30 min 60 min 120 min

Figure 5.7: MTM-SLIM images showing: a) and b) the growth of tribofilm on the ball with increasing rubbing time (*i.e.* zero, 5, 15, 30, 60, 120 minutes).

Because the Secondary ZDDP (C) did not form a uniform tribofilm in simple solution in GIII BO, its friction, morphology and wear-reducing properties were not further investigated. Thus, Primary ZDDP (C) will be used as the benchmark against which the performance of a wide range of low and zero SAPS antiwear additives will be compared in the rest of this thesis. Figure 5.8 shows the development of mean film thickness with rubbing time for Primary ZDDP (C)-derived tribofilm. It can be seen that this additive reacts rapidly on the surface, developing a thick film (*i.e.* ≈ 80 nm after 5 minutes of rubbing; ≈ 140 nm after 120 minutes of rubbing).

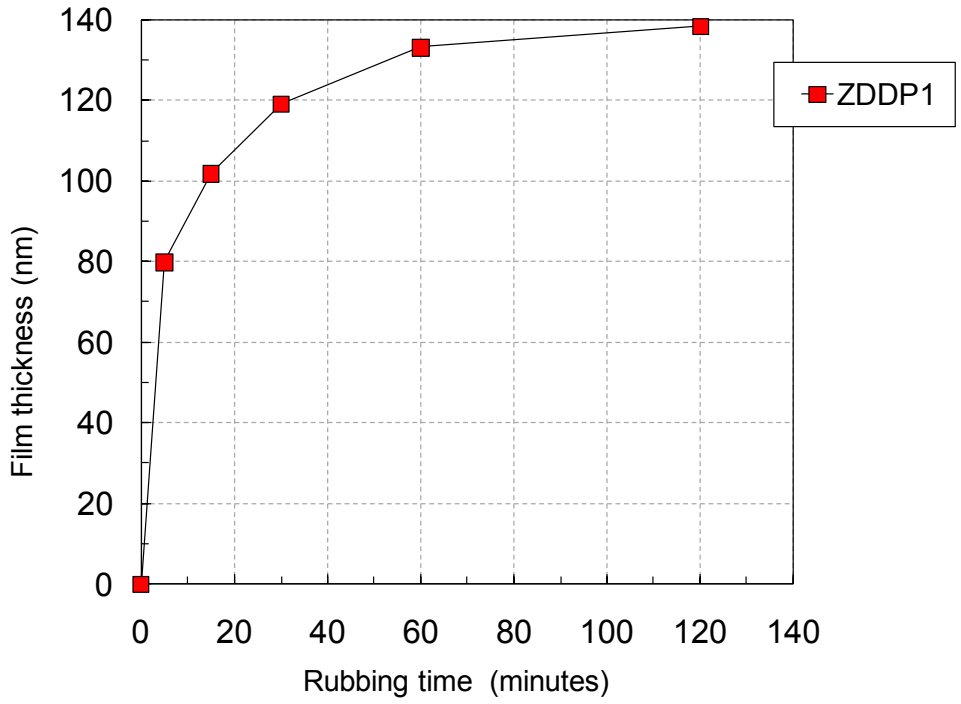


Figure 5.8: Mean film thickness with rubbing time for Primary ZDDP (C).

5.3 Results: Friction Properties of ZDDP-derived Tribofilms

The friction properties of Primary ZDDP (C) were studied using the MTM under mixed rolling/sliding conditions, as described in chapter 4, section 4.1. The Stribeck curve (Figure 5.9) shows the friction coefficient *versus* entrainment speed for this additive at the beginning and after 2 h of rubbing. As discussed in section 5.1.1 of this chapter, there is a significant increase in mixed friction once the protective film forms on the surface, shifting the curve to the right after 2h of rubbing. This increase in mixed friction is probably due to the change in surface texture as a result of the development of a thick solid-like film on the surface (Figure 5.4[b]). It can also be seen that the boundary friction reduces slightly upon formation of a ZDDP film. This suggests that the ZDDP tribofilm-tribofilm interface has a lower shear strength than the steel-steel interface. It has been shown that the boundary friction properties of ZDDP films depends strongly on the length and structure of the alkyl groups present [148].

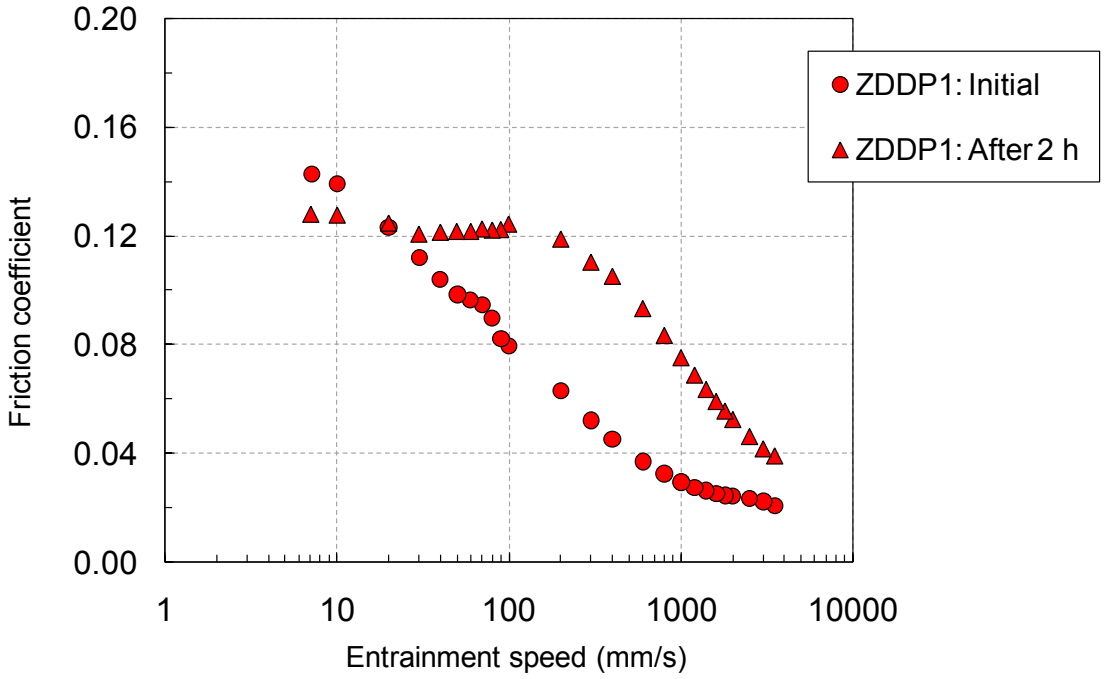
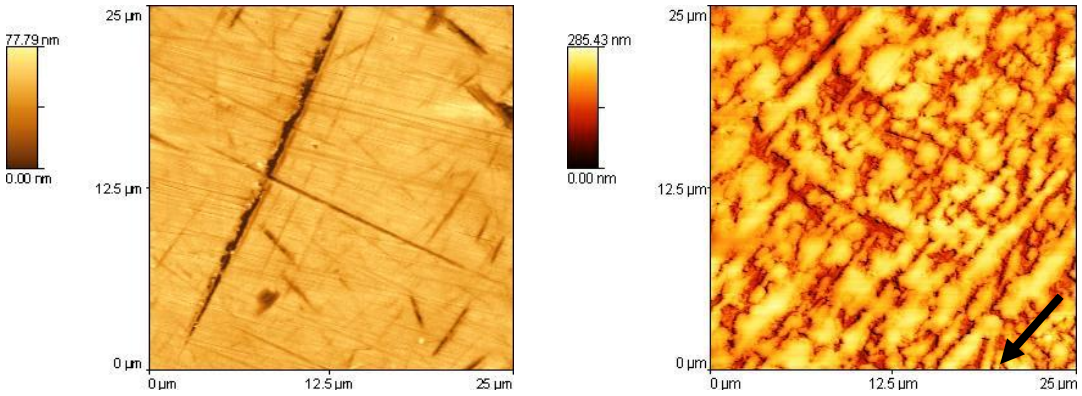


Figure 5.9: Stribeck curve showing friction coefficient *versus* entrainment speed at the beginning and after 2 h of rubbing for Primary ZDDP (C) at 50 % SRR, 30 N and 100 ºC.

5.4 Results: Morphology of ZDDP-derived Tribofilms

The morphology of Primary ZDDP (C) reaction films generated on AISI 52100 steel discs using the MTM was studied by AFM, as described in chapter 4, section 4.2. An area of 25 µm x 25 µm in the centre of the wear track was scanned and the topography of the tribofilm is shown in Figure 5.10[b)]. Figure 5.10[a)] shows the topography of MTM-discs prior to rubbing. It can be seen that the morphology of the tribofilm is strongly oriented along the sliding direction, represented by the arrow. The topography reveals that Primary ZDDP (C) reaction film consists of a pad-like structure separated by deep valleys.



a) MTM-disc before rubbing

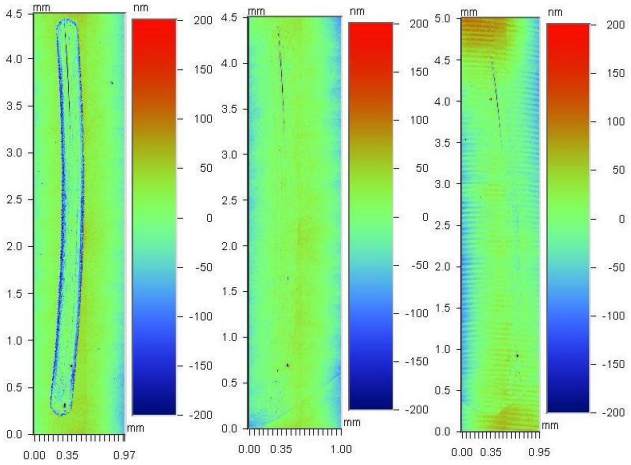
b) Primary ZDDP (C)

Figure 5.10: AFM 2D topography image at the centre of the wear track on the MTM-disc (sliding direction in b) shown by the arrow).

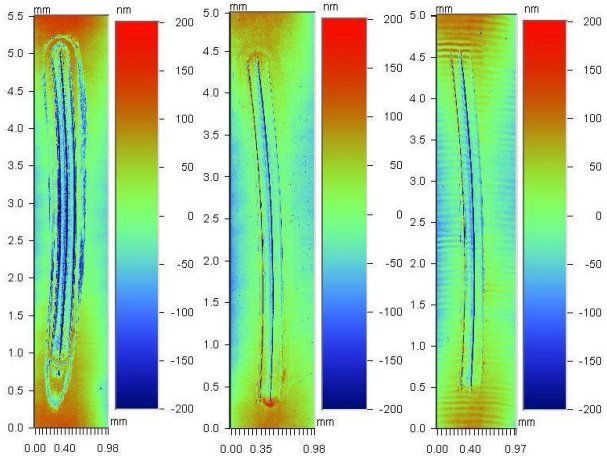
5.5 Results: Wear-reducing Properties of ZDDP-derived Tribofilms

The wear-reducing properties of Primary ZDDP (C) were studied using the method developed by the author, which combines the MTM-Reciprocating rig to generate the wear track on AISI 52100 steel discs with the SWLI to image the track and measure wear depth, as described in chapter 4, sections 4.3 and 4.4.

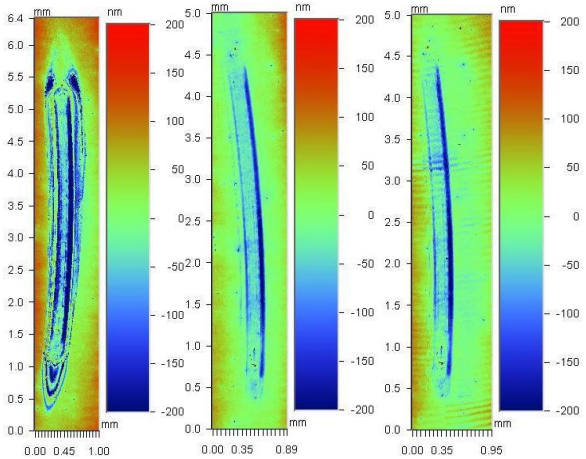
The film removal method to which all samples studied in this project were submitted is illustrated in Figure 5.11, which shows the topography images taken before the wear track was treated with EDTA, after the tribofilm was removed with EDTA, and after a thin layer of gold was deposited on the surface to demonstrate complete removal of tribofilm for tests lasting 4, 8 and 16 hours. This approach removes the possibility that different parts of the surface might have different reflectivities, which might influence the measurements. Chapters that follow show only topography images taken after the tribofilm was removed with EDTA or oxalic acid + EDTA.



4 h: before EDTA, after removal of tribofilm with EDTA and after gold deposition.



8 h: before EDTA, after removal of tribofilm with EDTA and after gold deposition.



16 h: before EDTA, after removal of tribofilm with EDTA and after gold deposition.

Figure 5.11: SWLI 2D topography images of the wear track on the disc.

The topography images reveal no significant increase in the width of the wear track after 16 hours rubbing. Figure 5.12 illustrates the wear coefficient (k_1) calculated using wear depth measurements taken in the middle (M) and at the ends (E) of the wear track (*i.e.* average of both ends) for tests lasting 4, 8 and 16 hours.

The results show no measurable wear after 4 hours of rubbing, while after 8 and 16 h very mild levels of wear can be observed. In addition, it can be seen that in the middle of the wear track, where disc speed is maximum, the displacement of material is slightly more pronounced than at the ends of the wear track, where disc speed is minimum because entrainment speed is changing direction. These tests were repeated twice and gave the same behaviour in each test so the differences in wear rate between 8 and 16 h tests are believed to be significant.

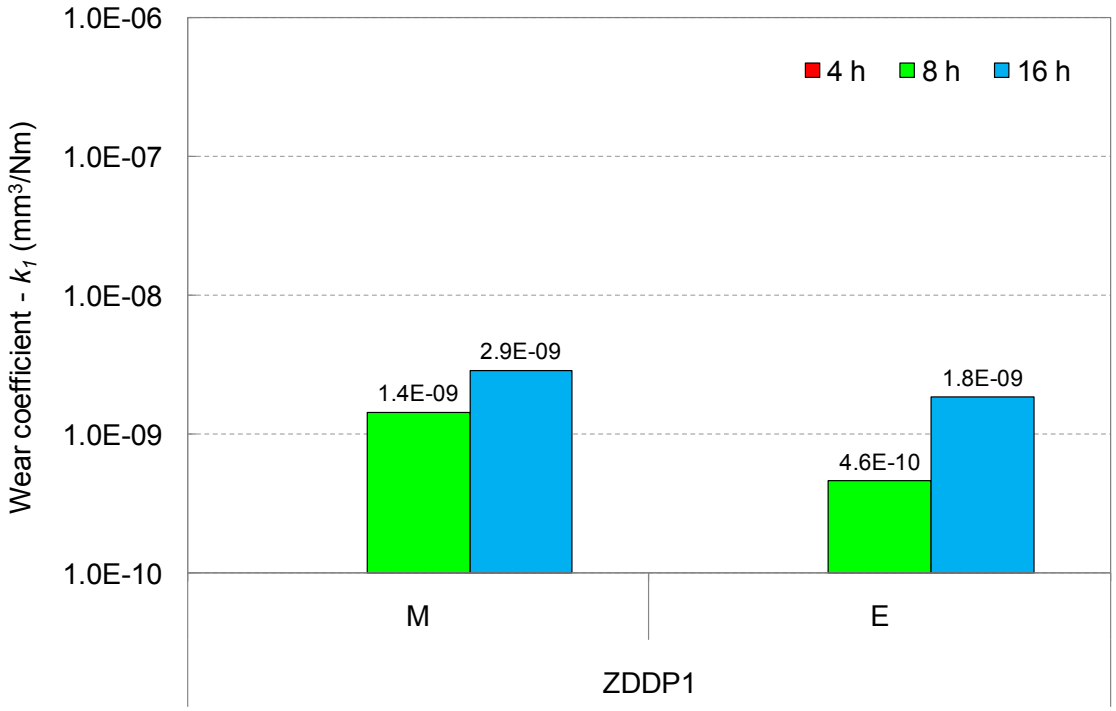


Figure 5.12: Wear coefficient (k_1) in the middle (M) and at the ends (E) of the wear track (*i.e.* average of both ends) for tests lasting 4, 8 and 16 hours.

It is noteworthy that the wear coefficient increases with test duration and is negligible in a short test. This is the opposite of what would be expected if there were significant running-in wear, where higher wear rate at the beginning of the test would be anticipated. This suggests (i) that the ZDDP reacts to form a protective film very quickly and (ii) that wear rate increases as the test proceeds. Two possible reasons for the latter are suggested. One is that wear involves loss of ZDDP film and that this only occurs after extended rubbing, possibly because it involves a fatigue process of the ZDDP pads. The second is that oxidation products that develop during the test promote the removal of the ZDDP film and thus wear. Sheasby *et al.* have shown that hydroperoxides are able to remove ZDDP films [149]. Much further work would be needed to distinguish these possibilities and this was not attempted in the current project.

5.6 Discussion of ZDDP Work

This study has confirmed the characteristic behaviour of ZDDP reported in previous studies in terms of its film-forming, friction and morphological properties. These include (i) the ability of ZDDP to form thick, pad-like films on rubbed steel surfaces, (ii) the increase in mixed friction produced by these films and (iii) the reduction in wear rate produced by ZDDP.

The film-forming study under mixed rolling/sliding conditions using MTM-SLIM, showed that while Primary ZDDP (C) rapidly reacted with the rubbed surface to form a thick reaction film of *ca.* 140 nm, which is typical ZDDP behaviour, the Secondary ZDDP (C) instead formed randomly-distributed “gummy”-like deposits on the surface. Further study showed that this unusual behaviour of Secondary ZDDP (C), is related to the low polarity of the GIII BO, and can be avoided by using a GI BO or adding alkylbenzene or dispersant to the GIII blend. It is hypothesised that GIII BO solubilise organic species in solution, such as short chain, low molecular weight alcohol molecules that might be present as impurities in the commercial Secondary ZDDP (C) and thus inhibit the reaction of ZDDP with the surface. Similar ”gummy”-like deposits have been observed by Campen when studying the film-forming properties of glycerol monooleate (GMO) in the same base oil, which has been ascribed to the formation of insoluble glycerol [147].

Friction behaviour study by MTM showed a significant increase in mixed friction once Primary ZDDP (C) formed a protective film on the surface. This effect is believed to result from the change in surface texture given the pad-like structure of the film formed on the surface, which was confirmed by topography study using AFM.

This study has also shown the wear-reducing properties of Primary ZDDP (C) using a new approach developed by the author. Overall, very mild wear is observed in tests lasting 4, 8 and 16 hours, with wear coefficient (k_1) varying between 10^{-9} to 10^{-10} mm^3/Nm. This is consistent with findings recently reported by Zhang [150], who also observed the same levels of mild wear, with wear coefficient (k_1) of *ca.* 10^{-10} mm^3/Nm for tests lasting 16 h using a different ZDDP at a concentration of 800 ppm P. These results are also consistent with wear coefficients experienced in the cam and followers in normal running engines, *i.e. ca.* 10^{-9} mm^3/Nm, which confirmed ZDDP’s ability to provide very good antiwear performance.

One unexpected observation from the wear measurements is that the calculated wear coefficient appears to increase as the test duration increases, suggesting an increase of wear rate with rubbing time. Two possible explanations for this behaviour have been suggested; that the rate of removal of tribofilm formed by Primary ZDDP (C) is time-dependent, possibly due to fatigue of the film pads, or that oxidation products that accumulate in the blend during testing, such as hydroperoxides, promote ZDDP film removal and thus wear. It will be interesting to see if low SAPS additives show a similar time-dependent wear rate response.

The chapter that follows reviews and describes the film-forming, friction, morphology and wear properties of the P-containing antiwear additives used in this study.

6. FILM-FORMING, FRICTION, MORPHOLOGY AND WEAR-REDUCING PROPERTIES OF P-CONTAINING ANTIWEAR ADDITIVES

This chapter first provides an overview of previous research on phosphorus-only antiwear additives, *i.e.* those containing phosphorus but not sulphur or metals, with a particular focus on the film-forming and wear properties of this additive type.

The chapter then describes film thickness, friction, surface topography and wear measurements carried out on a range of P-containing antiwear additive solutions, using the methods outlined in chapter 4. Additionally, the influence of a separate metal cation on the stabilisation of the protective film was investigated.

Some surface analyses of the films formed by P-containing antiwear additives were also carried out using ToF-SIMS and XANES but these are deferred to chapter 13, where analysis of the films formed by various additives of interest are presented and discussed together.

6.1 Literature Overview of P-containing Antiwear Additives

Ashless phosphorus-containing antiwear additives were first introduced as crankcase and gear lubricants in the 1930s [151]. The main P-containing chemistries proposed as effective antiwear additives are shown in Figure 6.1. The -R substituent groups are usually alkyl, functionalised alkyl, aryl or H, and additionally the -OR groups may be substituted by nitrogen compounds [152, 153]. They are given different suffixes to indicate that there may be two or three different -R groups within the molecule. Comprehensive reviews on the history and mechanisms of P-containing antiwear have been given by Khorramian *et al.* [66], Papay [154] and Spikes [67].

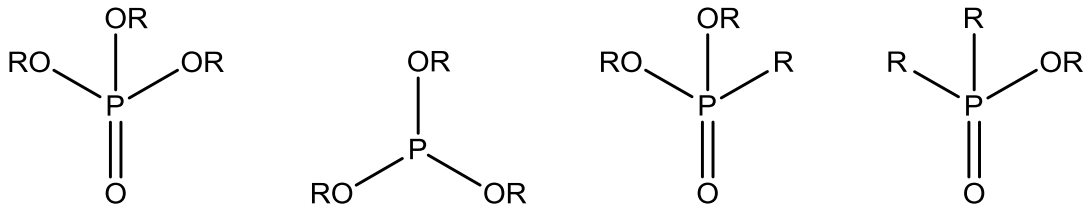


Figure 6.1: Molecular structures of main classes of organophosphorus compounds suggested as antiwear additives for engines.

Tricresyl phosphate (TCP) (Figure 6.2), used in the formulation of gas turbine oils, was one of the first organophosphorus compounds to be extensively studied. Early investigation of the wear-reducing properties of TCP proposed that this additive reacted to form iron phosphide, which led to polishing of the rubbed surfaces [155]. However, later work by Barcroft *et al.* [156], Godfrey [157] and Faut *et al.* [158] suggested that the main component in the protective film formed by TCP during rubbing was iron phosphate.

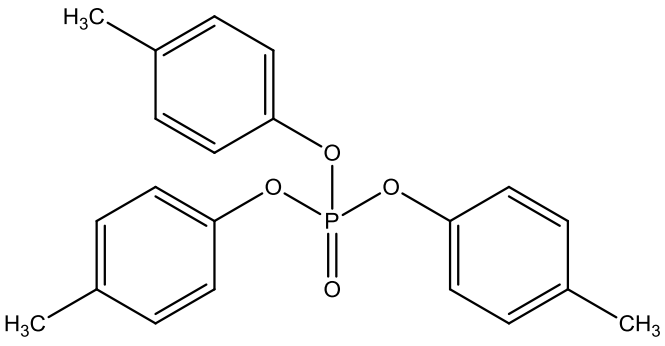


Figure 6.2: Molecular structure of TCP.

Wheeler *et al.* reported that TCP adsorbed reversibly on gold surfaces, while it decomposed on iron surfaces to form an iron phosphate film, which was found to be very stable at high temperatures [159]. Figure 6.3 illustrates the proposed mechanisms by which TCP is adsorbed and reacts with the iron surface.

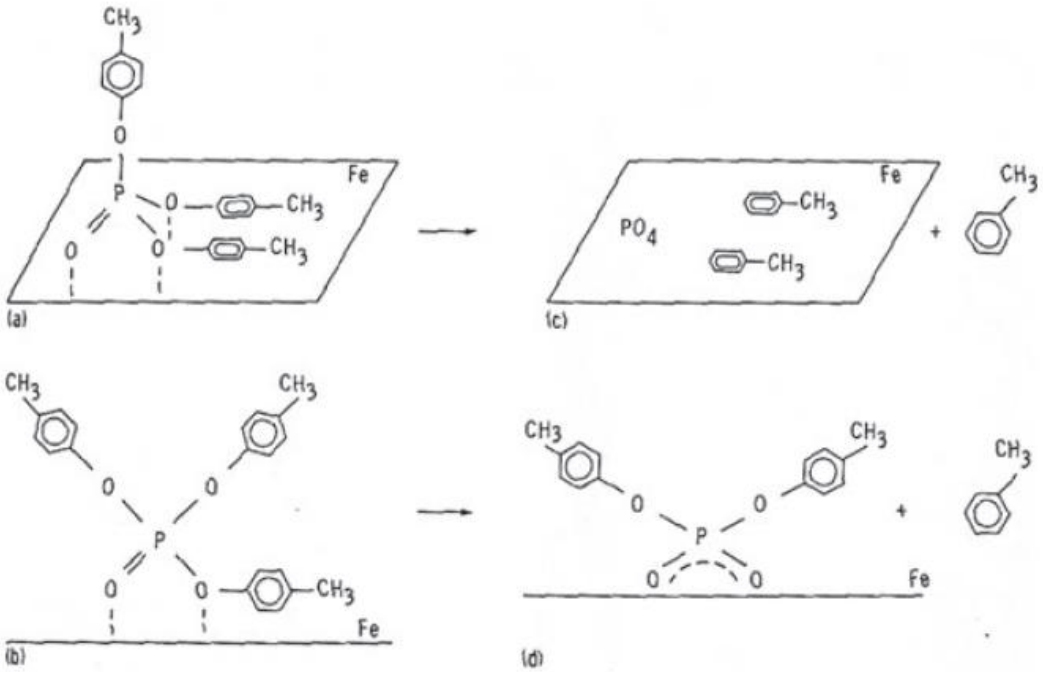


Figure 6.3: Two alternative models for the adsorption and reaction of TCP on iron [159].

Forbes *et al.* investigated the four-ball wear and load-carrying properties of dialkyl phosphoramidates, $(RO)_2P(O)NR^1R^2$ [67, 160]. It was found that their wear-reducing properties were comparable to TCP. They suggested that there was a relationship between the antiwear effectiveness of these nitrogen-containing organophosphorus compounds and the strength of the parent acids formed on its decomposition. Further work by Forbes *et al.* on the load-carrying and antiwear properties of dialkyl phosphates and their amine salts revealed that short-chain esters offered superior load-carrying properties while long-chain esters had better wear-reducing properties [161].

Sakurai *et al.* observed a correlation between the wear-reducing properties of a range of lauryl phosphates and phosphites and their reactivity towards the surface. It was found that acid types (*e.g.* trilauryl phosphate and lauryl acid phosphate) performed better than their neutral counterparts. The antiwear performance of the latter was improved in the presence of sulphur, suggesting increased reactivity towards the iron surface [162]. Subsequent analysis of the protective films by X-ray spectroscopy revealed the presence of basic iron phosphate, *i.e.* $FeFe_4(PO_4)_3(OH)_5$, combined with small quantities of other forms of iron phosphate, *i.e.* $Fe_3(PO_4)_2$ and $Fe(PO_4)$, and traces of iron phosphide on the surface.

Kawamura *et al.* investigated the antiwear properties of trialkyl and aryl phosphates and phosphites [163]. It was found that the phosphates rapidly reacted to form a protective film on the surface, showing superior antiwear properties at lower temperatures. At higher temperatures, however, both additive types gave similar levels of wear protection. The authors attributed this behaviour to differences in adsorptive power. More recently, this hypothesis was revisited by Minami *et al.* [164], who investigated the influence of phosphate ester concentration on wear.

It seems that most phosphate esters reported in the literature appear to protect the surface in broadly the same way, by forming a protective film of iron phosphate on the contact during rubbing. The ability of these additives to reduce wear seems to be affected by their acidity or steric effects, which in turn have an influence on their reactivity towards the surface.

Dialkyl and diaryl phosphites, also called phosphonates, used in the formulation of metalworking fluids and some transmission oils, seem to behave rather differently from the other classes of organophosphorus compounds. It is noteworthy that these compounds are tautomeric and the phosphonate is the predominant species in equilibrium in oil phase (Figure 6.4) [67].

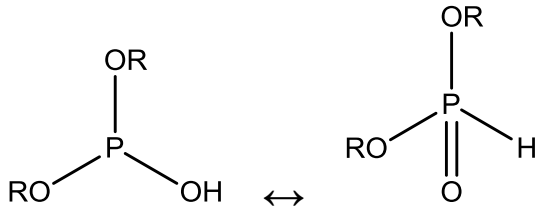


Figure 6.4: Tautomerism of dialkyl and diaryl phosphonates.

Research on this class of P-containing antiwear additives revealed their significant extreme pressure properties [165, 166], good wear-reducing properties [167, 168] and their ability to form relatively thick films on the surface, *i.e.* 60-100 nm [166, 169].

Forbes *et al.* studied the four-ball wear and extreme pressure properties of dialkyl and diaryl phosphonates [170]. It was found that short-chain phosphonates rapidly reacted with the asperities in contact to form phosphoric acid salts (*i.e.* extreme pressure capability), while long-chain phosphonates reacted more slowly to form wear-reducing ester phosphonate films. Comparison between these results and those of phosphate study [161] reveals that short-chain phosphates offer superior wear-reducing properties than corresponding phosphonates, while long-chain phosphonates are somewhat better than corresponding phosphates. Extreme pressure properties of phosphonates are significantly better than the corresponding phosphates, regardless of chain length.

Further work using optical interferometry to study the film-forming properties of a range of dialkyl and diaryl phosphonates showed that these compounds rapidly form thick films, *i.e.* ≈ 100 nm at 75 °C, with film thickness dropping with increasing chain length, under mixed rolling/sliding conditions [171-173]. Subsequent analysis of the reaction films by IR and Mossbauer spectroscopy suggested the formation of an iron alkylphosphate polymer film on the surface (Figure 6.5) for hexyl and octyl phosphonates, with the iron present as low-spin iron (III) [174].

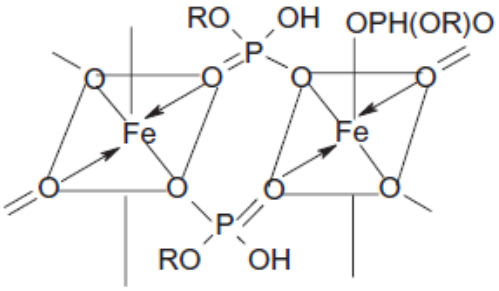


Figure 6.5: Proposed structure of protective film formed by dialkyl and diaryl phosphonates [67].

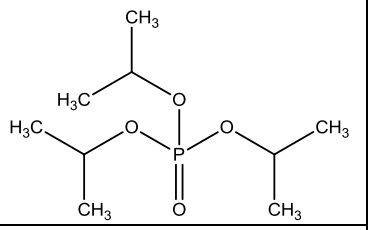
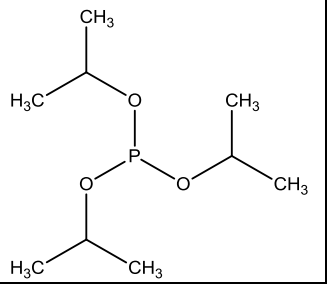
Ashless P-containing antiwear additives have been observed to reduce wear through the formation of a thick phosphate-containing protective film on rubbed surfaces. Although the mechanism by which these additives rapidly react to form a film still remains unclear, their ability to form protective films appears to vary considerably with chain length, structure and nature and reactivity of substituent groups.

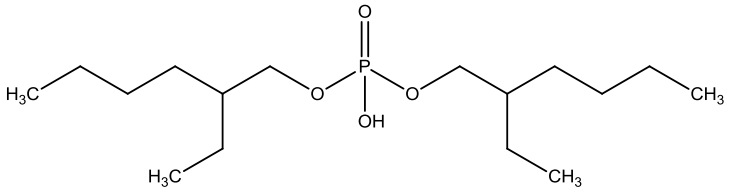
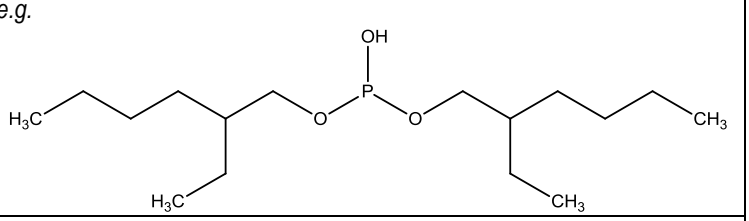
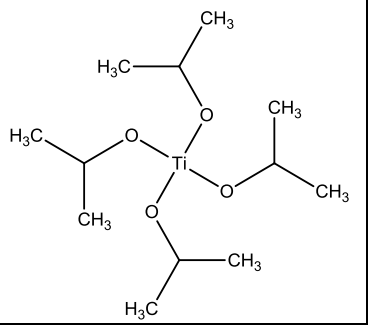
It seems that dialkyl and diaryl phosphonates react more rapidly and show superior wear-reducing properties than most organophosphorus types proposed as antiwear additives. Studies comparing the film-forming properties of ZDDP and ashless thiophosphates indicated the need of a suitable network-forming metal cation to stabilise the phosphate film, such glass stabilisation has been proposed to be the role of Zn in ZDPP [67]. It has been suggested that phosphonates are sufficiently corrosive to provide a supply of Fe cations and thus stabilise the phosphate glass forming a protective film.

6.2 Results: Film-forming Properties of P-containing Antiwear Additives

The film-forming properties of P-containing antiwear additives were studied using MTM-SLIM under mixed rolling/sliding conditions, as described in chapter 4, section 4.1. The additives employed in the study described in this chapter are summarised in Table 6.1. These were blended into Group III base oil (C) at a concentration of 800 ppm phosphorus and submitted to rubbing under the same test conditions on the MTM-SLIM.

Table 6.1: Test materials summary: Phosphorus-containing additives study

Abreviation[1]	**Sample name**	**Details**
GIII BO	Group III base oil (C)	-
ZDDP1	Primary ZDDP (C)	9.5 %P; 20.0 %S; 10.6 %Zn
=	Triisopropyl phosphate	*e.g.* 
=	Triisopropyl phosphite	*e.g.* 

=	Bis(2-ethylhexyl) phosphate	*e.g.* 
=	Bis(2-ethylhexyl) phosphite	*e.g.* 
TAP	Triaryl phosphate (C)	7.3 %P
AP	Amine phosphate (C)	4.8 %P; 2.7 %N
nCaSu	Neutral calcium alkylsulphonate (C)	-
Ti-IPO	Titanium (IV) isopropoxide	*e.g.* 

(C): commercially-available.

[1] "=" means abbreviated name is the same as full name

Figure 6.6 shows the growth of the tribofilm on the MTM-ball with increasing rubbing time (*i.e.* zero, 5, 15, 30, 60, 120 minutes) for the base oil, Primary ZDDP (C) and the P-containing antiwear additive solutions. With the base oil alone, scuffing occurred after 5 minutes of rubbing, as shown in Figure 6.6[a)] and the test was terminated.

It can be seen that Primary ZDDP (C) (Figure 6.6[b)]) rapidly forms a thick solid-like film on the rubbed ball, while the P-containing compounds form thinner (*e.g.* medium-chain organophosphorus compounds: bis(2-ethylhexyl) phosphate and bis(2-ethylhexyl) phosphite) or even negligible tribofilms (*e.g.* Triaryl phosphate (C) and Amine phosphate (C)) when compared to ZDDP.

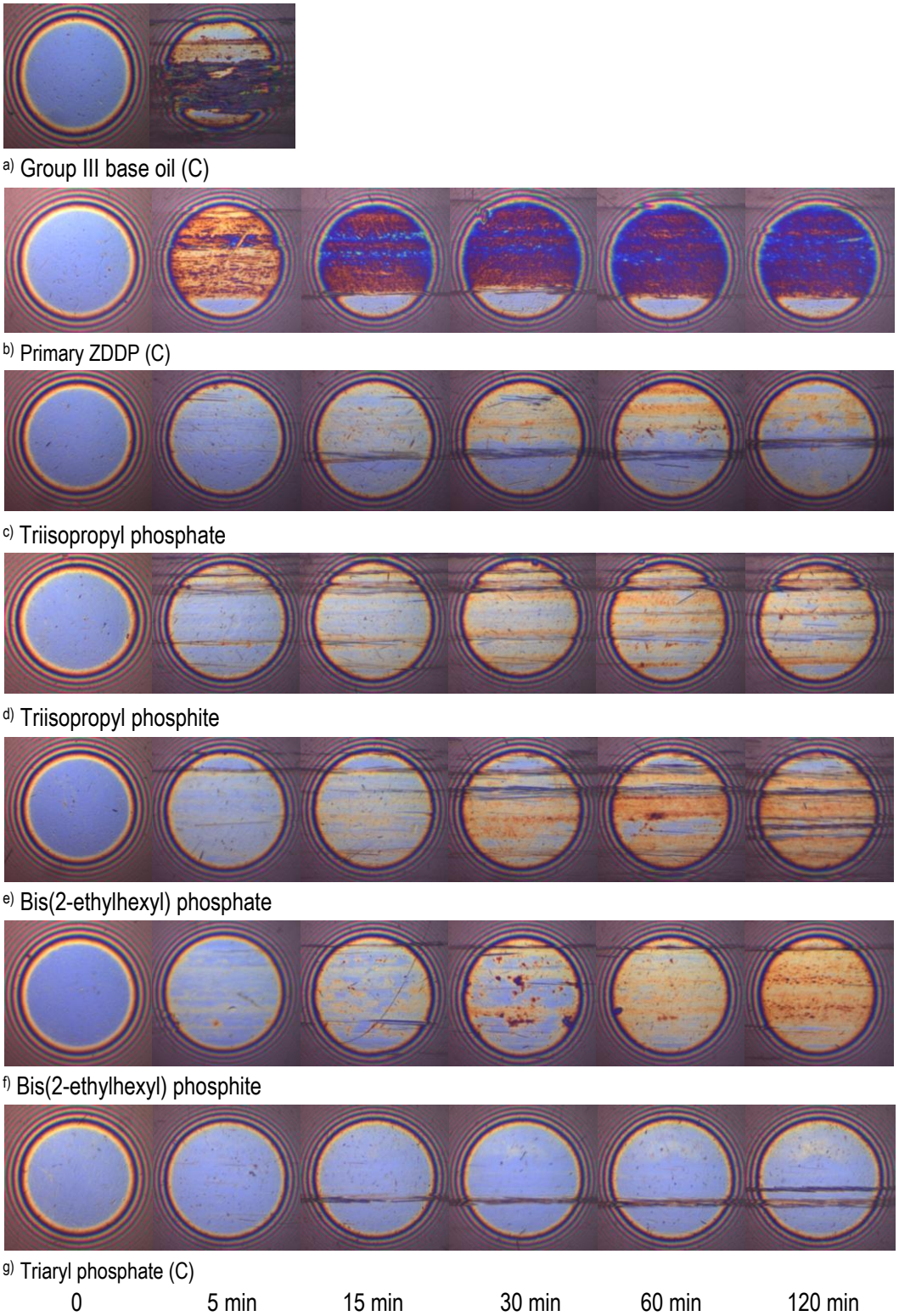
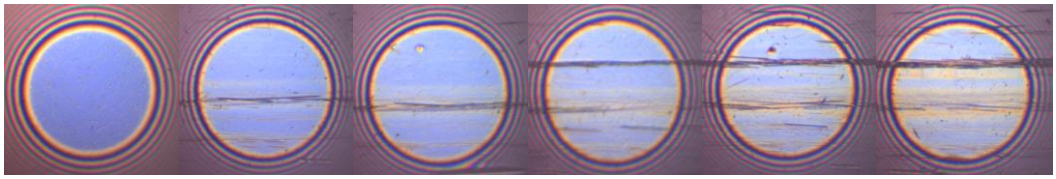


Figure 6.6: MTM-SLIM images showing: a) scuffing on the surface of the ball after 5 minutes of rubbing in base oil without antiwear additive; b) to g) the growth of tribofilm on the ball with increasing rubbing time (*i.e.* zero, 5, 15, 30, 60, 120 minutes).



h) Amine phosphate (C)

0 5 min 15 min 30 min 60 min 120 min

Figure 6.6 (continued): MTM-SLIM images showing: h) the growth of tribofilm on the ball with increasing rubbing time (*i.e.* zero, 5, 15, 30, 60, 120 minutes).

Figure 6.7 compares the development of mean film thickness with rubbing time for Primary ZDDP (C) and P-containing-derived tribofilms. It can be seen that Primary ZDDP (C) reacts rapidly on the surface, developing a thick film (*i.e.* ≈ 140 nm after 120 minutes of rubbing), while the P-containing compounds form thinner (*i.e.* ≈ 80 nm after 120 minutes of rubbing for bis(2-ethylhexyl) phosphate and bis(2-ethylhexyl) phosphite solutions) or even negligible tribofilms (*i.e.* ≈ 30 nm after 120 minutes of rubbing for Triaryl phosphate (C) and Amine phosphate (C) solutions).

Although the isopropyl phosphite shows very rapid film formation, this is not the case for the isopropyl phosphate, suggesting that, unlike ZDDPs, secondary esters (*i.e.* isopropyl) do not react much faster than primary ones (*i.e.* ethylhexyl).

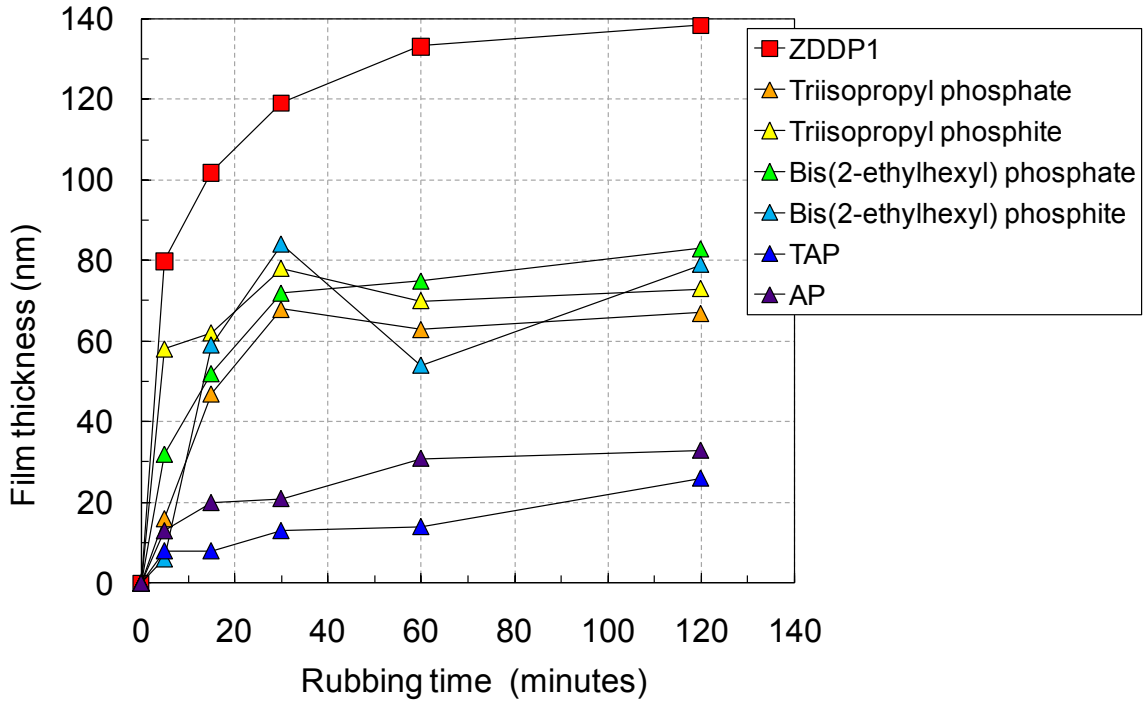
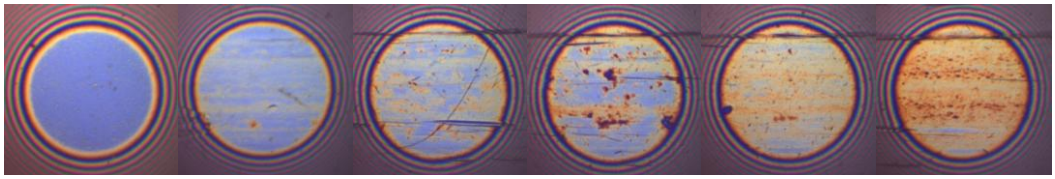


Figure 6.7: Mean film thickness with rubbing time for P-containing antiwear additives.

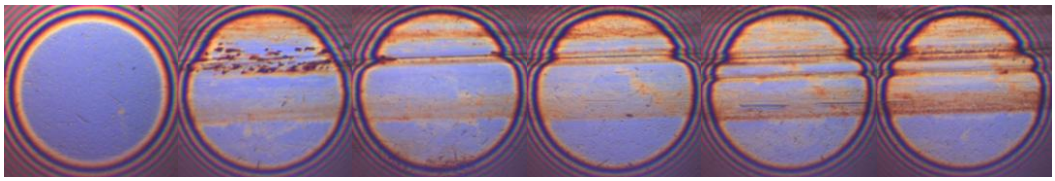
It is likely that these P-containing additives form films less readily than ZDDP because of the absence of Zn cations to stabilise the phosphate film. To explore this, additional tests were carried out to investigate the influence of separate metal cations on the stabilisation of the protective film. Neutral calcium alkylsulphonate (C) and Titanium (IV) isopropoxide were individually blended at a concentration of 1, 5 and 10 % weight with a medium-chain phosphite, *i.e.* bis(2-ethylhexyl) phosphite (800 ppm P), into the GIII BO.

The film-forming properties of Titanium (IV) isopropoxide and Neutral calcium alkylsulphonate (C) in base oil are illustrated in Figure 6.8[b)-c)]. With the Titanium (IV) isopropoxide-only solution, scuffing occurred after 5 minutes of rubbing and the test was terminated. The film formed by the Neutral calcium alkylsulphonate (C)-only solution seems to withstand rubbing, but the change in contact shape might be an indication of wear.

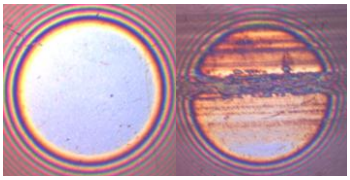
Figure 6.8[g)-i)] shows that Titanium (IV) isopropoxide-phosphite-containing blends rapidly react to form a thick tribofilm on the surface, *i.e.* after 5 minutes of rubbing. The presence of the titanium cation significantly enhances the rate at which the protective film grows, regardless of its concentration in the medium-chain phosphite solution (*i.e.* 1, 5 and 10 % weight). Conversely, it appears that the presence of Neutral calcium alkyl sulphonate (C) hinders film formation and growth at a concentration as low as 1 % weight (Figure 6.8[d)]).



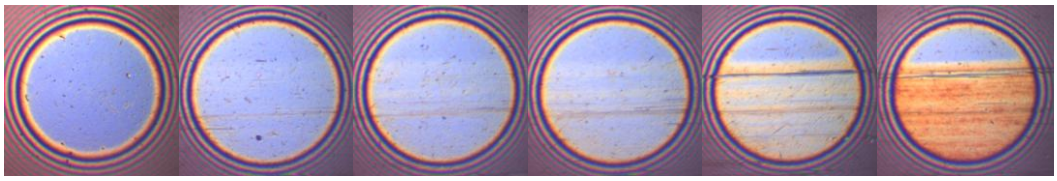
a) Bis(2-ethylhexyl) phosphite



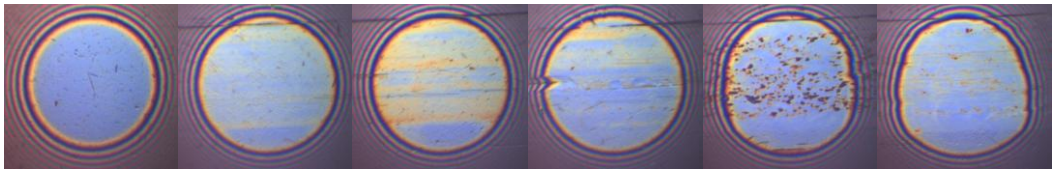
b) Neutral calcium alkylsulphonate (C)



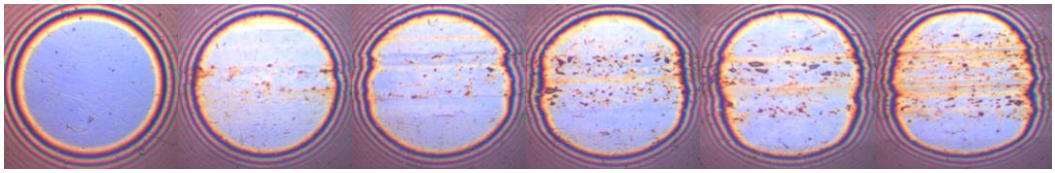
c) Titanium (IV) isopropoxide



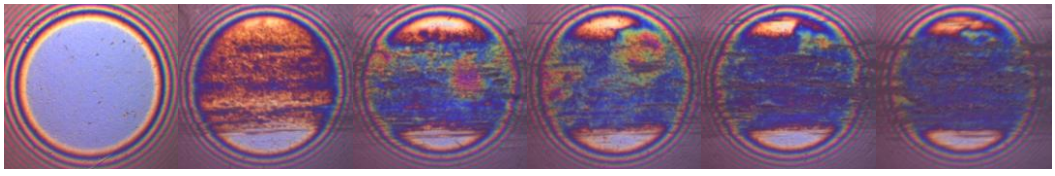
d) Bis(2-ethylhexyl) phosphite + 1 % nCaSu



e) Bis(2-ethylhexyl) phosphite + 5 % nCaSu



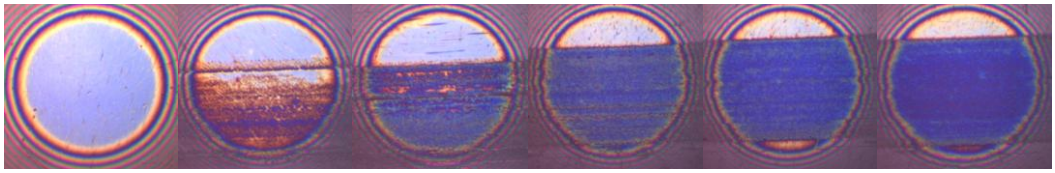
f) Bis(2-ethylhexyl) phosphite + 10 % nCaSu



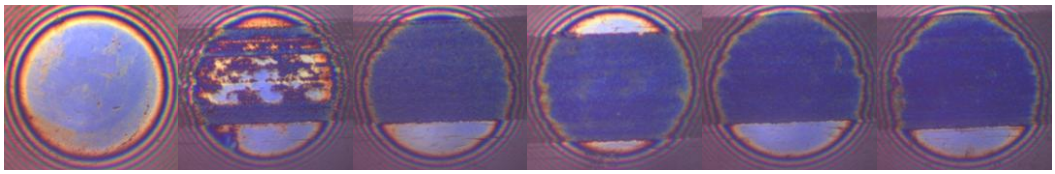
g) Bis(2-ethylhexyl) phosphite + 1 % Ti-IPO

0 5 min 15 min 30 min 60 min 120 min

Figure 6.8: MTM-SLIM images showing: a) to g) the growth of tribofilm on the ball with increasing rubbing time (*i.e.* zero, 5, 15, 30, 60, 120 minutes).



h) Bis(2-ethylhexyl) phosphite + 5 % Ti-IPO



i) Bis(2-ethylhexyl) phosphite + 10 % Ti-IPO

0 5 min 15 min 30 min 60 min 120 min

Figure 6.8 (continued): MTM-SLIM images showing: h) and i) the growth of tribofilm on the ball with increasing rubbing time (*i.e.* zero, 5, 15, 30, 60, 120 minutes).

6.3 Results: Friction properties of P-containing Antiwear Additive-derived Tribofilm

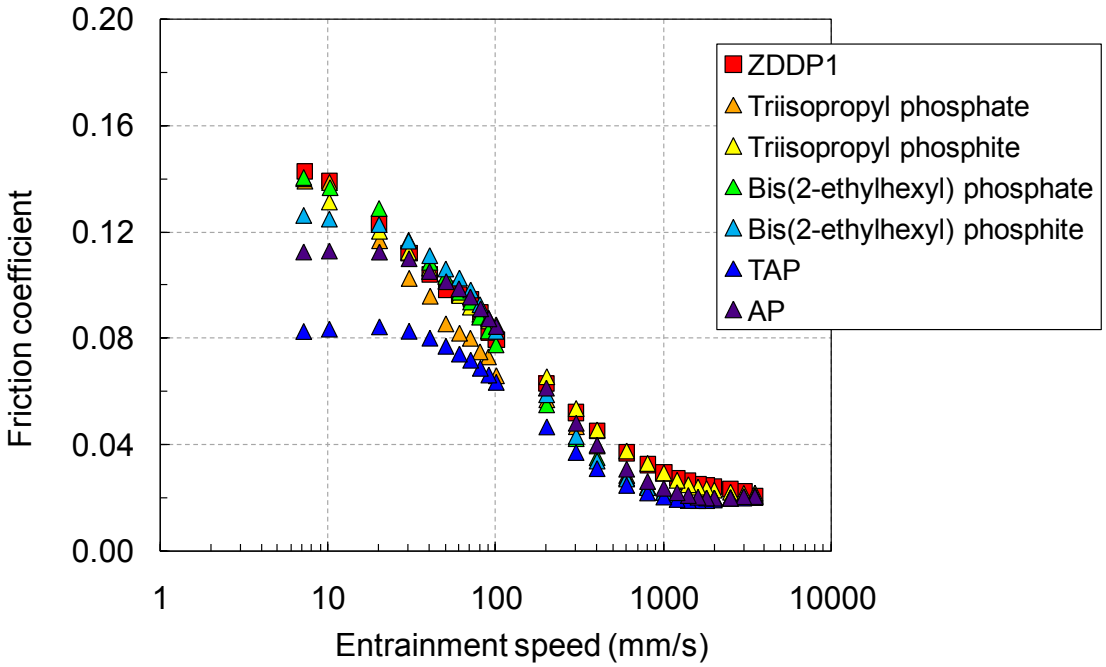
The friction properties of a range of P-containing antiwear additives were studied using the MTM under mixed rolling/sliding conditions, as described in chapter 4, section 4.1. The Stribeck curve (Figure 6.9) shows the friction coefficient *versus* entrainment speed for these additives at the beginning and after 2 h of rubbing.

These friction curves illustrate two different types of behaviour; (i) in some cases shifting of the curves to the right and (ii) changes in low speed boundary friction.

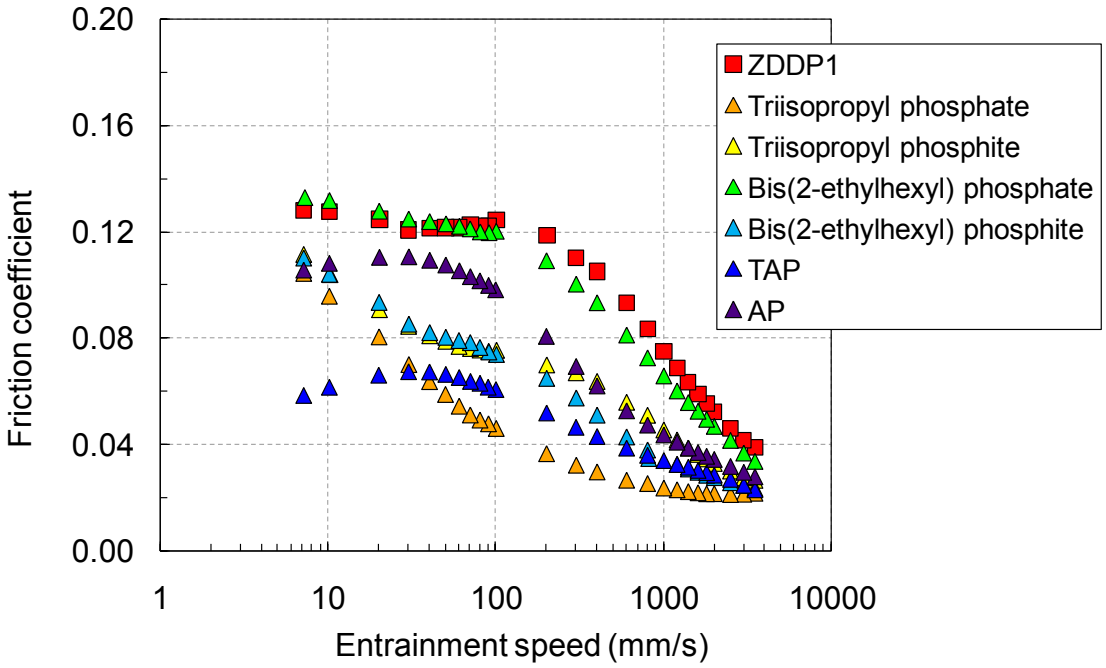
As discussed in section 5.3 of chapter 5, there is a significant increase in mixed friction for Primary ZDDP (C) once the protective film forms on the surface, shifting the curve to the right after 2h of rubbing. This increase in mixed friction is probably due to the change in surface texture as a result of the development of a thick solid-like film on the surface (Figure 6.6[b)]). A slight increase in mixed friction is observed for bis(2-ethylhexyl) phosphate and Amine phosphate (C) solutions. The former can be ascribed to film formation, while the latter is possibly due to scuffing on the surface. Alternatively, the medium-chain phosphite, *i.e.* bis(2-ethylhexyl) phosphite, which appears to form a thick and uniform protective film on the surface (*i.e.* ≈ 80 nm), shows no significant shift in mixed friction throughout the test. This suggests that this additive forms a smooth, low shear strength film on the surface.

The remaining P-containing additives, short-chain trialkyl phosphate and phosphite (*i.e.* triisopropyl phosphate and triisopropyl phosphite) and Triaryl phosphate (C) show a slight decrease in boundary friction after rubbing. The boundary friction should depend on the shear strength of the solid film formed on the rubbed surfaces. This has been shown in previous work on ZDDP and also ZDP and overbased detergents to depend on the linearity and length of the alkyl chains present. In the current work there appears to be little difference between the isopropyl and ethylhexyl esters except that the ethylhexylphosphate gave higher friction. However, Triaryl phosphate (C) gives exceptionally low friction, with friction that increases with sliding speed. This suggests that the alkyl aryl structure is able to impart low boundary friction.

Figure 6.10 shows the influence of Neutral calcium alkylsulphonate (C) and Titanium (IV) isopropoxide on friction for bis(2-ethylhexyl) phosphite solutions. The thick protective films formed in the presence of titanium cation (Figure 6.8[g)-i)]) have a classic effect on friction, shifting the curve to the right after 2h of rubbing. The Neutral calcium alkylsulphonate (C) initially reduces the boundary friction of the films, probably due to the contribution of the alkyl chain structure of the detergent molecule. By contrast, addition of the Titanium (IV) isopropoxide compound resulted in increased boundary friction.

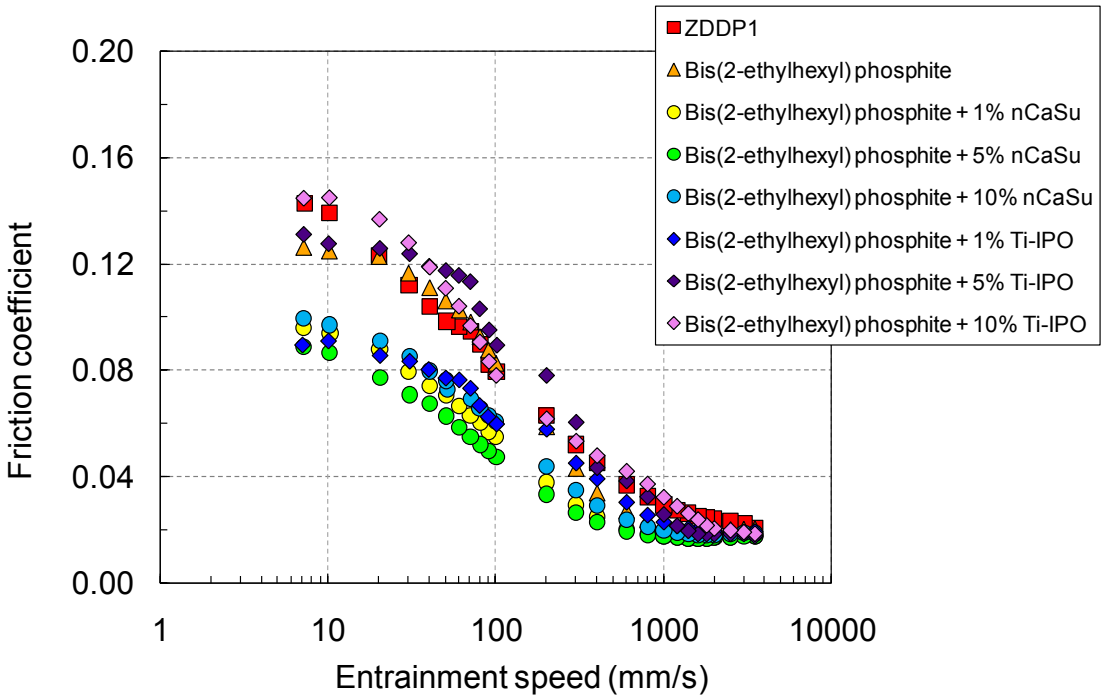


Initial friction, measured at the beginning of the test

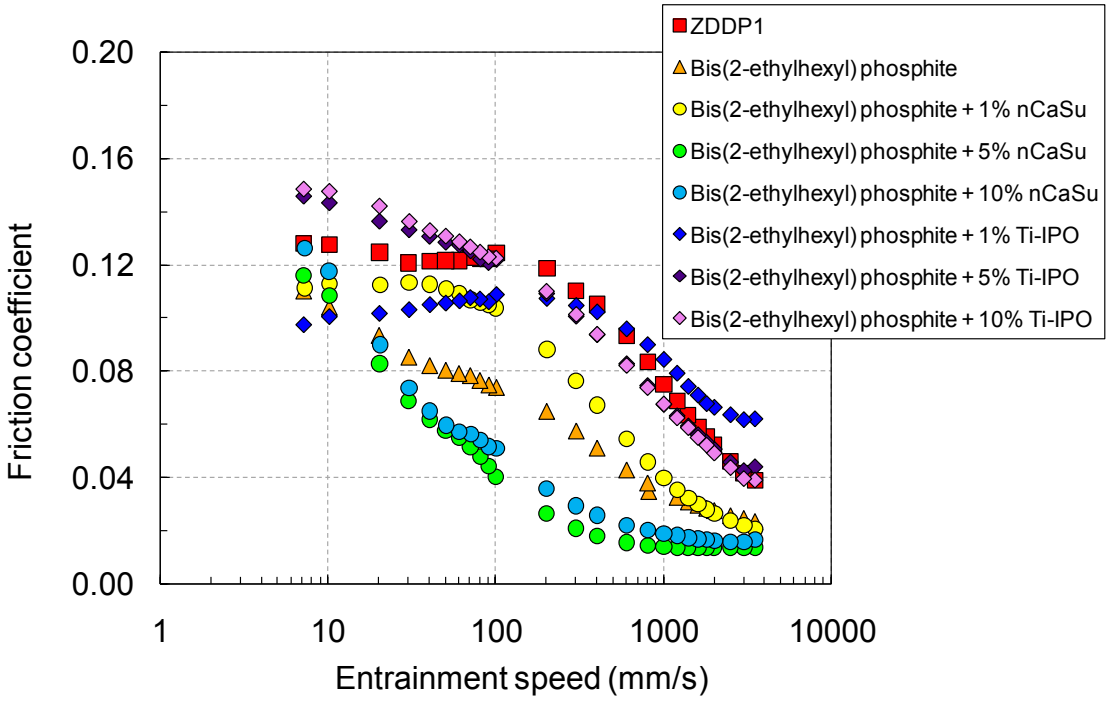


Friction after 2 h of rubbing

Figure 6.9: Stribeck curve showing friction coefficient *versus* entrainment speed at the beginning and after 2 h of rubbing at 50 % SRR, 30 N and 100 ºC.



Initial friction, measured at the beginning of the test



Friction after 2 h of rubbing

Figure 6.10: Stribeck curve showing friction coefficient *versus* entrainment speed at the beginning and after 2 h of rubbing at 50 % SRR, 30 N and 100 ºC.

6.4 Results: Morphology of P-containing Antiwear Additive-derived Tribofilms

The morphology of P-containing antiwear additive reaction films generated on AISI 52100 steel discs using the MTM, was studied by AFM, as described in chapter 4, section 4.2. An area of 25 μm x 25 μm in the centre of the wear track was scanned and the topography of the tribofilms is shown in Figure 6.11. Figure 6.11[a)] shows the topography of MTM-discs prior to rubbing.

It can be seen that the morphology of the tribofilms is strongly oriented along the sliding direction, represented by the arrow. Topography study reveals that P-containing antiwear additive-derived tribofilms consist of discrete pads randomly-distributed along the sliding direction.

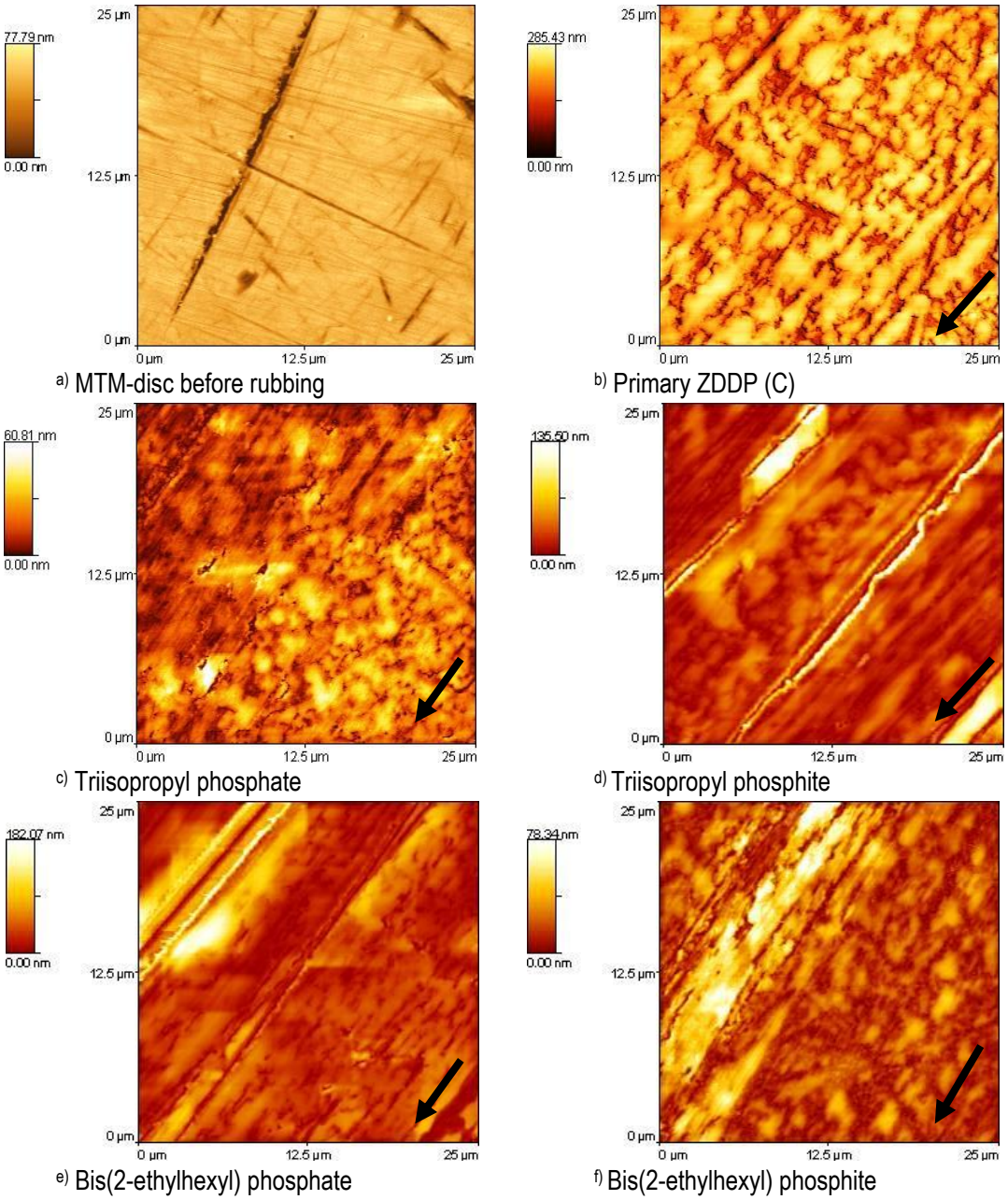
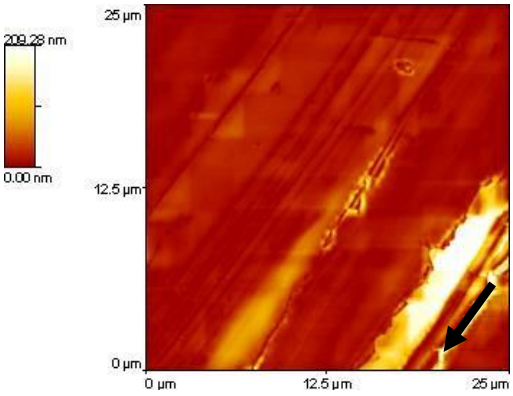
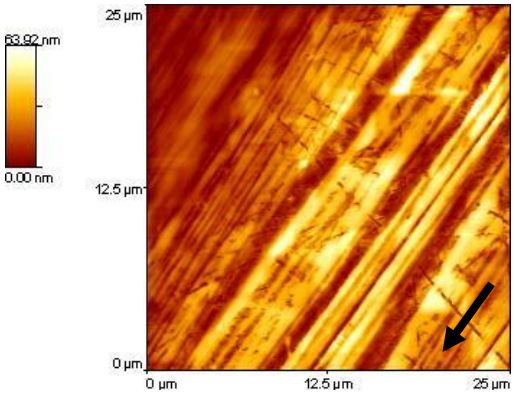


Figure 6.11: AFM 2D topography image at the centre of the wear track on the MTM-disc (sliding direction in b) to f) shown by the arrow).



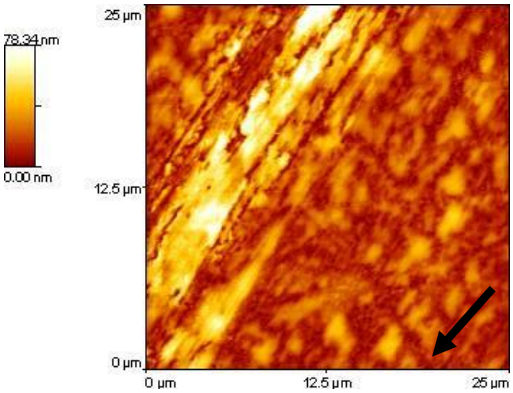
g) Triaryl phosphate (C)



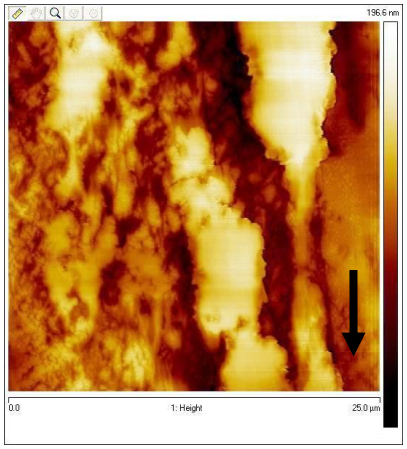
h) Amine phosphate (C)

Figure 6.11 (continued): AFM 2D topography image at the centre of the wear track on the MTM-disc (sliding direction in g) and h) shown by the arrow).

Figure 6.12 shows the morphology of reaction film formed by bis(2-ethylhexyl) phosphite solution in the presence of Titanium (IV) isopropoxide (1 % weight). It appears that the film comprises larger elongated pads separated by deep valleys.



a) Bis(2-ethylhexyl) phosphite



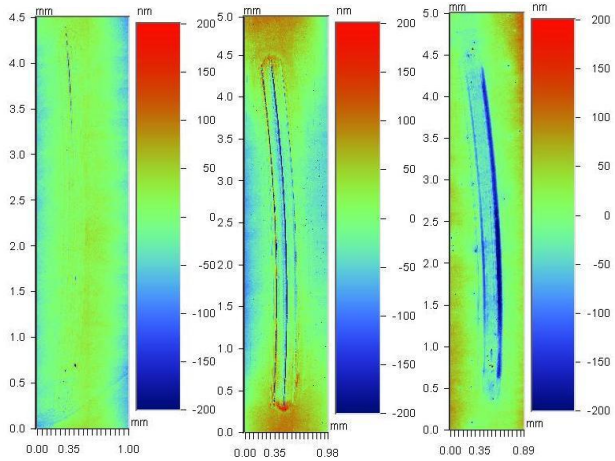
b) Bis(2-ethylhexyl) phosphite + Ti-IPO

Figure 6.12: AFM 2D topography image at the centre of the wear track on the MTM-disc (sliding direction in a) and b) shown by the arrow).

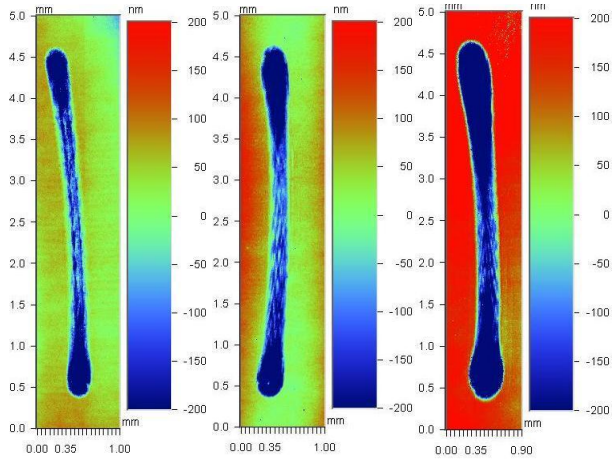
6.5 Results: Wear-reducing Properties of P-containing Antiwear Additive-derived Tribofilms

The wear-reducing properties of two P-containing antiwear additives, bis(2-ethylhexyl) phosphite and Triaryl phosphate (C), were studied using the method developed by the author, which combines the MTM-Reciprocating rig to generate the wear track on AISI 52100 steel discs with the SWLI to image the track and measure wear depth, as described in chapter 4, sections 4.3 and 4.4.

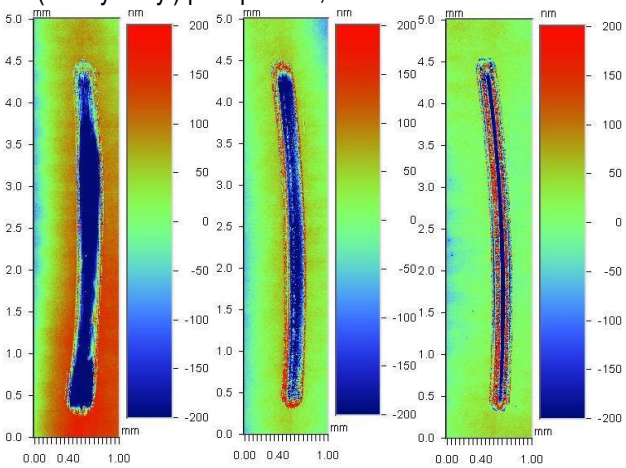
The topography images, shown in Figure 6.13, reveal a slight increase in the width of the wear track with increasing rubbing time for bis(2-ethylhexyl) phosphite and Triaryl phosphate (C) solutions after 16 h of rubbing. The presence of Titanium (IV) isopropoxide (1 % weight) does not appear to have a significant effect on the wear-reducing properties of bis(2-ethylhexyl) phosphite, although it was shown in section 6.2 of this chapter that the rate at which the tribofilm grows is significantly improved by the metal cation, *i.e.* Ti (Figure 6.8[g)-i)]).



Primary ZDDP (C): 4, 8 and 16 hours after EDTA.

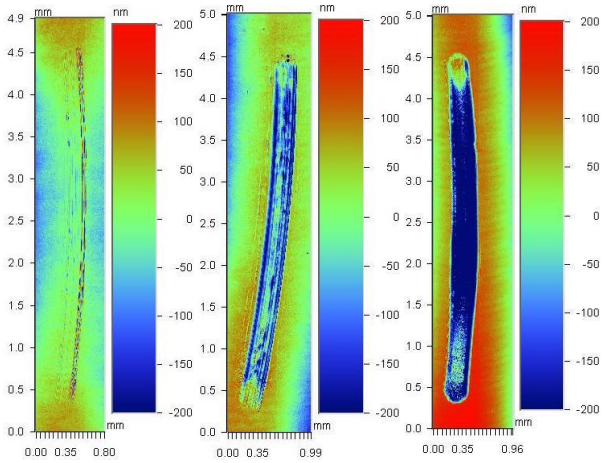


Bis(2-ethylhexyl) phosphite: 4, 8 and 16 hours after EDTA.



Bis(2-ethylhexyl) phosphite + Ti-IPO: 4, 8 and 16 hours after EDTA.

Figure 6.13: SWLI 2D topography images of the wear track on the disc.



Triaryl phosphate (C)

Figure 6.13 (continued): SWLI 2D topography images of the wear track on the disc.

Figure 6.14 illustrates the wear coefficient (k_1) calculated using wear depth measurements taken in the middle (M) and at the ends (E) of the wear track (*i.e.* average of both ends) for tests lasting 4, 8 and 16 hours. The results show that the P-containing antiwear additives investigated in this study are not quite as good as ZDDP. Overall, it appears that there is a decrease in wear rate with increasing rubbing time, probably because of running-in wear.

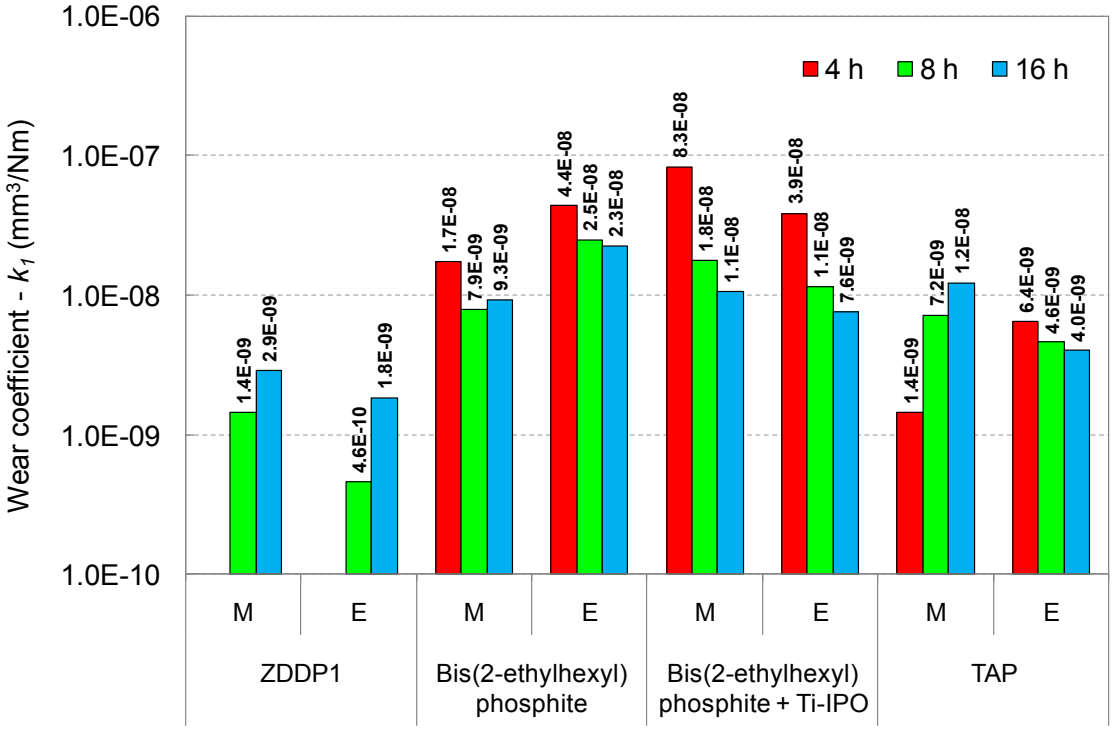


Figure 6.14: Wear coefficient (k_1) in the middle (M) and at the ends (E) of the wear track (*i.e.* average of both ends) for tests lasting 4, 8 and 16 hours.

In the running-in wear period, during which wear depth increases rapidly with time, the wear rate of the rubbing components is greater than during steady-state wear. This is followed by an extended steady-wear rate period during which the displacement of material from the surface is linear with rubbing time. The wear behaviour of rubbing components over their life span is illustrated in Figure 6.15. Throughout the running-in wear process the surface roughness varies and this will result in increased conformity of the rubbing surfaces. Once the steady-state wear regime is reached, surface topography and wear rate stabilize [175].

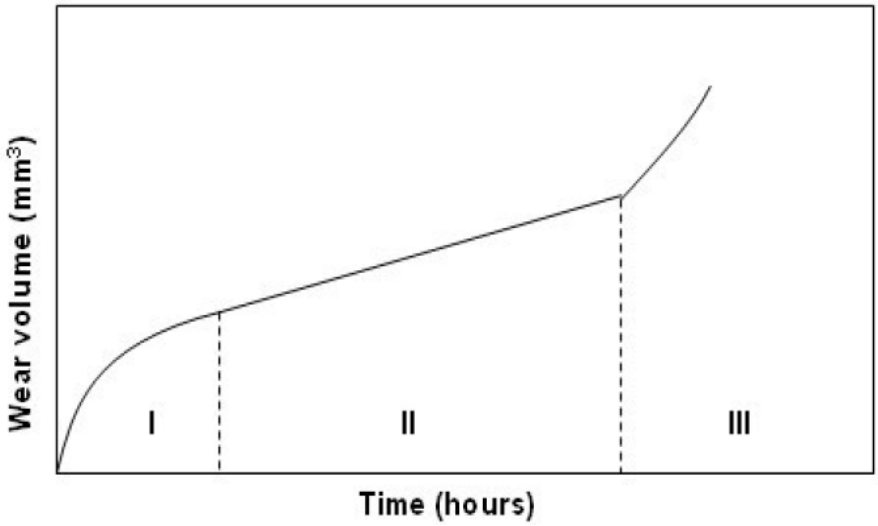


Figure 6.15: Wear behaviour of rubbing components over their life span: (i) running-in wear, (ii) steady-state wear and (iii) wear out [176].

6.6 Discussion of P-containing Antiwear Additives Work

The film-forming study under mixed rolling/sliding conditions using MTM-SLIM, showed that while Primary ZDDP (C) rapidly reacted to form a thick reaction film of *ca.* 140 nm, P-containing compounds form thinner (up to ≈ 80 nm) or even negligible tribofilms on the surface. Further study on the influence of a separate metal cation, *i.e.* Neutral calcium alkylsulphonate (C) and Titanium (IV) isopropoxide, on the film-forming properties of a medium-chain phosphite revealed that Ti-containing blends rapidly reacted to form a thick tribofilm on the surface.

The rate at which the P-containing antiwear additive-derived tribofilms grow seems to be constrained by the amount of nascent iron eventually generated by rubbing. The presence of the titanium cation significantly enhanced film formation, probably because this metal cation enables stabilisation and growth of the protective film; such glass stabilisation has been proposed to be the role of Zn in ZDPP [67]. The same behaviour, however, was not observed in the presence of Neutral calcium alkylsulphonate (C), which appears to hinder film formation and growth. This may originate from various sources, for example; (i) partial neutralisation of the phosphorus acid ester to make it less reactive to iron oxide; (ii) promotion of dissolution of the film as it forms on the surface; (ii) adsorption of the detergent on the oxide surface to reduce its reactivity with the antiwear additive.

Friction behaviour study by MTM showed that there was no significant increase neither in mixed nor in boundary friction for the medium-chain phosphite, bis(2-ethylhexyl) phosphite, which appears to form a thick and uniform protective film. This suggests that this additive forms a smooth, low shear strength film on the surface. Conversely, the thick protective films formed in the presence of titanium cation have a classic effect on friction, shifting the curve to the right after 2h of rubbing. This effect is believed to result from the change in surface texture given the pad-like structure of this film, which was confirmed by topography study using AFM. In terms of boundary friction, the Triaryl phosphate (C) gave very low boundary friction which may indicate that aryl groups are beneficial with respect to friction.

This study has also shown the wear-reducing properties of P-containing antiwear additives using a new approach developed by the author. Overall, very mild wear is observed in tests lasting 4, 8 and 16 hours, with wear coefficient (k_1) varying between 10^{-8} to 10^{-9} mm^3/Nm. However, it appears that the P-containing antiwear additives investigated in this study are not quite as good as ZDDP. In addition, there is a decrease in wear rate with increasing rubbing time, probably because of running-in wear. In the running-in wear period, during which wear depth increases rapidly with time, the wear rate of the rubbing components is greater than during steady-state wear. This is followed by an extended steady-wear rate period during which the displacement of material from the surface is linear with rubbing time.

It was found that the Triaryl phosphate (C) gave the lowest wear of the additives studied, although still not as good as ZDDP. Since this additive does not form a thick boundary film this may suggest that thick boundary film formation is not required for effective wear or friction reduction.

The chapter that follows reviews and describes the film-forming, friction, morphology and wear properties of the P-S-containing antiwear additives used in this study.

7. FILM-FORMING, FRICTION, MORPHOLOGY AND WEAR-REDUCING PROPERTIES OF P-S-CONTAINING ANTIWEAR ADDITIVES

This chapter first provides an overview of previous research on ashless phosphorus-sulphur-containing antiwear additives, *i.e.* mono- and di-thiophosphate and thiophosphite derivatives, with a particular focus on the film-forming and wear properties of this additive type.

The chapter then describes film thickness, friction, surface topography and wear measurements carried out on a range of P-S-containing antiwear additive solutions, using the methods outlined in chapter 4. Additionally, the influence of a separate metal cation on the formation and properties of the boundary films formed was investigated.

Some surface analyses of the films formed by P-S-containing antiwear additives were also carried out using ToF-SIMS and XANES but these are deferred to chapter 13, where analysis of the films formed by various additives of interest are presented and discussed together.

7.1 Literature Overview of P-S-containing Antiwear Additives

Metal-free equivalents of ZDDP, such as dialkyl dithiophosphates (Figure 7.1) and their derivatives have also been extensively studied as potential antiwear additives. This group of additives retain ZDDP's thiophosphate core, while the zinc is replaced by an organic group. The -R' substituent groups are usually alkyl, amine, *e.g.* NHR'', sulphide, *e.g.* SR'', or even more complex species, *e.g.* hydroxyl or carboxylic acid-containing groups. There has been considerable interest in thiophosphate and thiophosphite esters, shown in Figure 7.2, where -X^{1-4} are S or O, and -R^{1-3} are alkyl or aryl groups. A review on the history and mechanisms of P-S-containing antiwear has been given by Spikes [67].

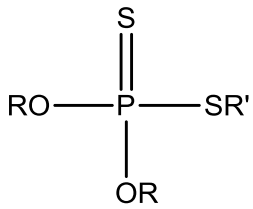


Figure 7.1: Molecular structure of ashless dithiophosphate [67].

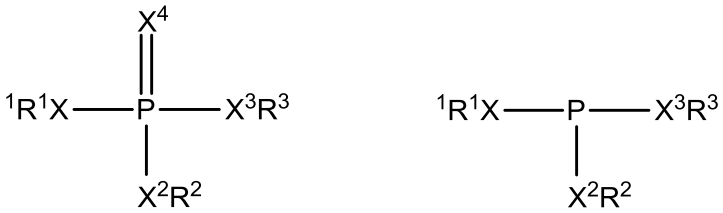


Figure 7.2: Molecular structure of ashless alkyl and aryl thiophosphate and thiophosphite esters [67].

Sanin *et al.* investigated the four-ball wear and load carrying properties of a range of thiophosphates and thiophosphites [177]. The authors reported that short-chain alkyl thiophosphites gave higher initial seizure load and superior wear-reducing properties than longer-chain equivalents. It was also found that increasing the sulphur content in the molecule led to a decrease in the initial seizure load, but lower levels of wear above this load. Sanin *et al.* suggested that the mechanism of action of these additives was a sum of three main processes: (i) initial adsorption of the additive on the surface, (ii) decomposition of the additive due to the high temperatures at the contact and ultimately (iii) chemical reactions between the metal surface and the decomposition products [178].

Schumacher *et al.* studied the influence of alkyl groups and number of S and O atoms on the wear-reducing properties of a range of phosphate esters derivatives (Figure 7.3) [179, 180]. The authors suggested that the key to antiwear efficiency was the thermal stability of the P-S-containing compounds investigated, *i.e.* additives should be thermally stable to avoid decomposition in the bulk, but reactive within the contact. Further surface analysis revealed a correlation between the wear-reducing properties and increasing P content in the phosphate film. This effect was not observed with S content.

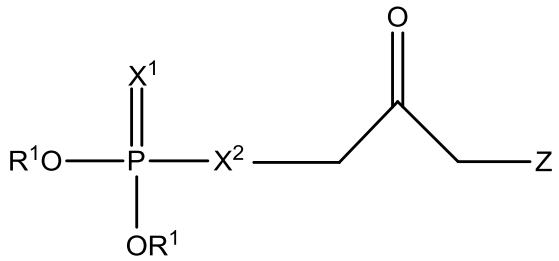


Figure 7.3: Molecular structure of ashless phosphate ester derivatives studied by Schumacher *et al.*, where $X^{1\text{-}2}$ = O and/or S; R^1 = alkyl, cycloalkyl, aryl; Z = -OR^2, -$N(R^3)_2$; R^2, R^3 = alkyl, cycloalkyl [179].

The antiwear properties of thiophosphate and dithiophosphate derivatives such as amido thiophosphates [181-183] (Figure 7.4) and amine dithiophosphates [184, 185] (Figure 7.5), both of which are used in the formulation of some gear oils, were also investigated. It was found that these additives provided excellent wear-reducing properties, with amido compounds better than amines [186]. Further study revealed that amido phosphonates were superior to their phosphate counterparts [182].

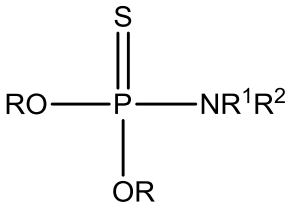


Figure 7.4: Molecular structure of alkyl amido thiophosphate, where R^2 can be H [67].

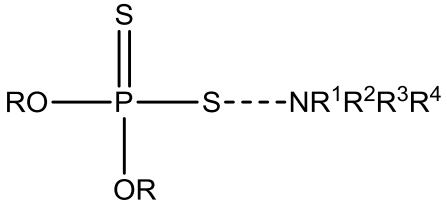


Figure 7.5: Molecular structure of alkyl amine dithiophosphate, where $R^{2,\,3,\,4}$ can be H [67].

Borshchevskii *et al.* studied the antiwear properties of a range of functionalised dithiophosphates prepared by treating dithiophosphoric acid with alkenes (Figure 7.6) [187]. It was found that compounds prepared using functionalised alkenes, *e.g.* methacrylic acid, gave better wear-reducing properties than those prepared using non-functionalised alkenes (*i.e.* simple alkenes C_nH_{2n}). The authors attributed this to the higher nucleophile strength of functionalised alkenes. More recently, Sharma *et al.* ascribed this to the stronger adsorptive power of functionalised dithiophosphate derivatives on steel surfaces [188]. The method illustrated in Figure 7.6 has been used in the synthesis of a wide range of functionalised dithiophosphate-based antiwear, antioxidants and extreme pressure additives [189-193].

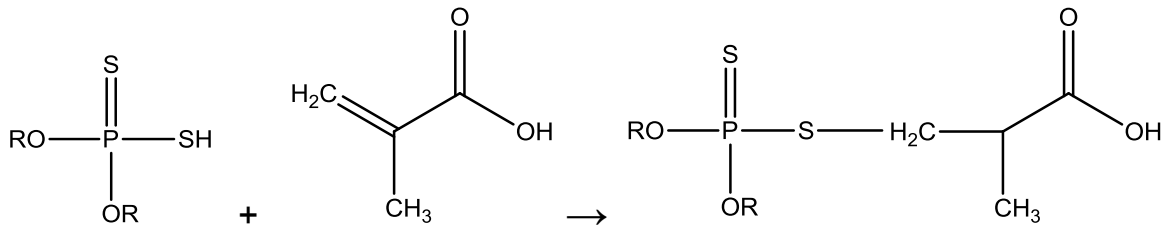


Figure 7.6: Synthesis of functionalised dithiophosphates by treating dithiophosphoric acid with methacrylic acid [187].

Taylor *et al.* used MTM-SLIM to investigate the film-forming properties of tri-n-butyl thiophosphate [194]. It was found that this additive slowly reacted to form a thick protective film on the surface, *i.e.* ≈ 70 nm thick after 3 hours of rubbing at 100 °C [63]. The tribofilm formed by the same thiophosphate was further investigated by Rossi *et al.* using XPS and FTIR analysis. The authors reported the formation of iron polyphosphate and iron sulphate in the contact.

Zhang *et al.* investigated the wear-reducing properties of a functionalised dithiophosphate using a Plint tribometer under reciprocating sliding conditions [195]. It was reported that this compound provided very good wear-reducing properties when combined with small amounts of ZDDP (Figure 7.7). The authors ascribed this to rapid film formation in the presence of ZDDP.

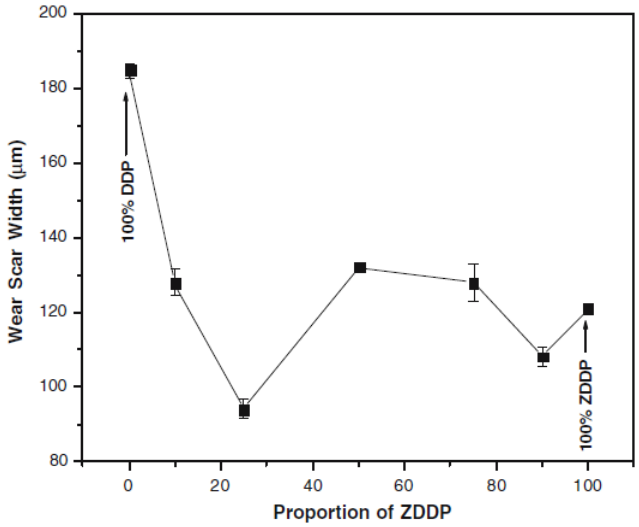


Figure 7.7: Wear scar width as a function of ZDDP/DDP concentration after 1 hour of reciprocating at 25 Hz, 225 N and 100 ºC [195].

Najman *et al.* used XANES to investigate the nature of the protective films formed by two functionalised dialkyldithiophosphates: a carboxylic acid-substituted, *i.e.* -COOH, and an ester-substituted, *i.e.* -COOR; and one trialkyl aryl monothiophosphate [64]. All three additives gradually reacted to form a short-chain Fe(II) polyphosphate film after 5 minutes of rubbing. Further analysis revealed the presence of $FeSO_4$ on the surface after extended periods of rubbing, *i.e.* 6 hours. It was also reported that the carboxylic acid-substituted dithiophosphate reacted more rapidly than the other additives to form a tribofilm, but gave higher initial wear. This was attributed to the mildly corrosive nature of the acidic by-products generated by tribochemical decomposition, which in turn contribute to the removal of Fe cations from the substrate that react to form the polyphosphate film. Subsequent morphological study by AFM revealed that prolonged rubbing had an effect on the topography of the films, with small nodules replacing elongated pad-like structure found initially.

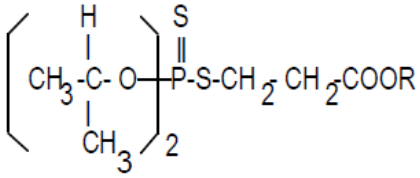
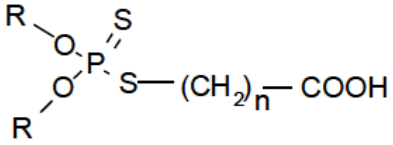
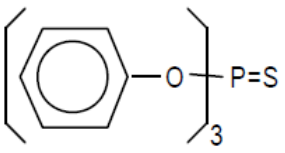
More recently, Kim *et al.* studied the wear-reducing properties of a range of functionalised alkyl and aryl dithiophosphate derivatives under extreme pressure conditions [196]. It was reported that the acid-substituted dialkyldithiophosphate, *i.e.* -COOH, offered better antiwear properties than its neutral counterpart. This additive also showed superior wear-reducing properties to aryl dithiophosphates. Subsequent analysis of the wear debris by transmission electron microscopy (TEM) revealed the presence of nanocrystalline particles of Fe_3O_4 embedded within an amorphous film. The authors suggested that wear was proportional to the amount of oxide particles found embedded in the wear debris.

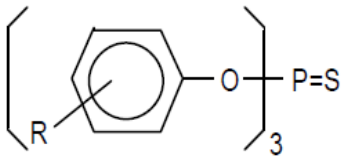
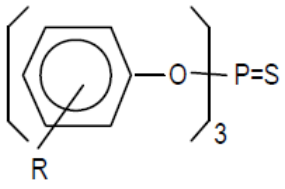
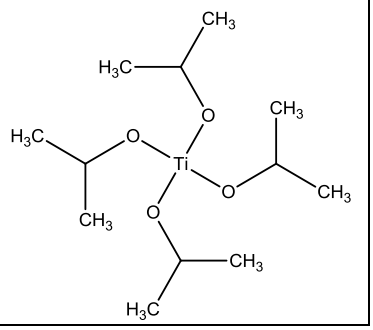
Most ashless thiophosphates have shown comparable antiwear performance to ZDDP. Overall, it appears that this group of additives gradually reacts to form phosphate-containing protective films on rubbed surfaces. The growth of P-S-derived tribofilms seems to be inhibited by the lack of suitable network-forming metal cation, which is ultimately provided by the iron generated by rubbing, but the rate at which the film grows seems to be limited by that [67]. Functionalised thiophosphates appear the best, probably due to their stronger initial adsorption [178, 188].

7.2 Results: Film-forming Properties of P-S-containing Antiwear Additives

The film-forming properties of P-S-containing antiwear additives were studied using MTM-SLIM under mixed rolling/sliding conditions, as described in chapter 4, section 4.1. The additives employed in the study described in this chapter are summarised in Table 7.1. These were blended into Group III base oil (C) at a concentration of 800 ppm phosphorus and submitted to rubbing under the same test conditions on the MTM-SLIM.

Table 7.1: Test materials summary: Phosphorus-sulphur-containing study

Abreviation	Sample name	Details
GIII BO	Group III base oil (C)	-
ZDDP1	Primary ZDDP (C)	9.5 %P; 20.0 %S; 10.6 %Zn
ADTP	Ashless dithiophosphate (C)	9.7 %P; 21.5 %S; *e.g.* 
DADTP	Dialkyl dithiophosphate (C)	9.3 %P; 19.8 %S; *e.g.* 
TPPT	Triphenyl phosphorothionate (C)	8.9 %P; 9.3 %S; *e.g.* 

ATPPT	Alkylated triphenyl phosphorothionate (C)	4.3 %P; 4.4 %S; *e.g.* 
BTPPT	Butylated triphenyl phosphorothionate (C)	7.9 %P; 8.1 %S; *e.g.*  R = H, tert. butyl
ATP	Amine thiophosphate (C)	3.8 %P; 6.2 %S; 3.1 %N
PSN	Phoshporus-sulphur-nitrogen-based (C)	4.2 %P; 9.1 %S; 3.0 %N
PS	Phosphorus-sulphur-based (C)	4.5 %P; 10.0 %S
nCaSu	Neutral calcium alkylsulphonate (C)	-
Ti-IPO	Titanium (IV) isopropoxide	*e.g.* 

(C): commercially-available.

Figure 7.8 shows the growth of the tribofilm on the MTM-ball with increasing rubbing time (*i.e.* zero, 5, 15, 30, 60, 120 minutes) for the base oil, Primary ZDDP (C) and P-S-containing antiwear additive solutions. With the base oil alone, scuffing occurred after 5 minutes of rubbing, as shown in Figure 7.8[a)] and the test was terminated.

It can be seen that Primary ZDDP (C) (Figure 7.8[b)]) rapidly forms a thick solid-like film on the rubbed ball, while some P-S-containing compounds form tribofilms (*e.g.* Ashless dithiophosphate (C) and Alkylated triphenyl phosphorothionate (C)), albeit thinner than some of the P-containing additives studied in chapter 6. It is noteworthy that there is no visible damage to the rubbing contact even when using P-S-compounds that form negligible films on the surface (*e.g.* Triphenyl phosphorothionate (C)). This may suggest that thick boundary film formation is not required for effective wear reduction.

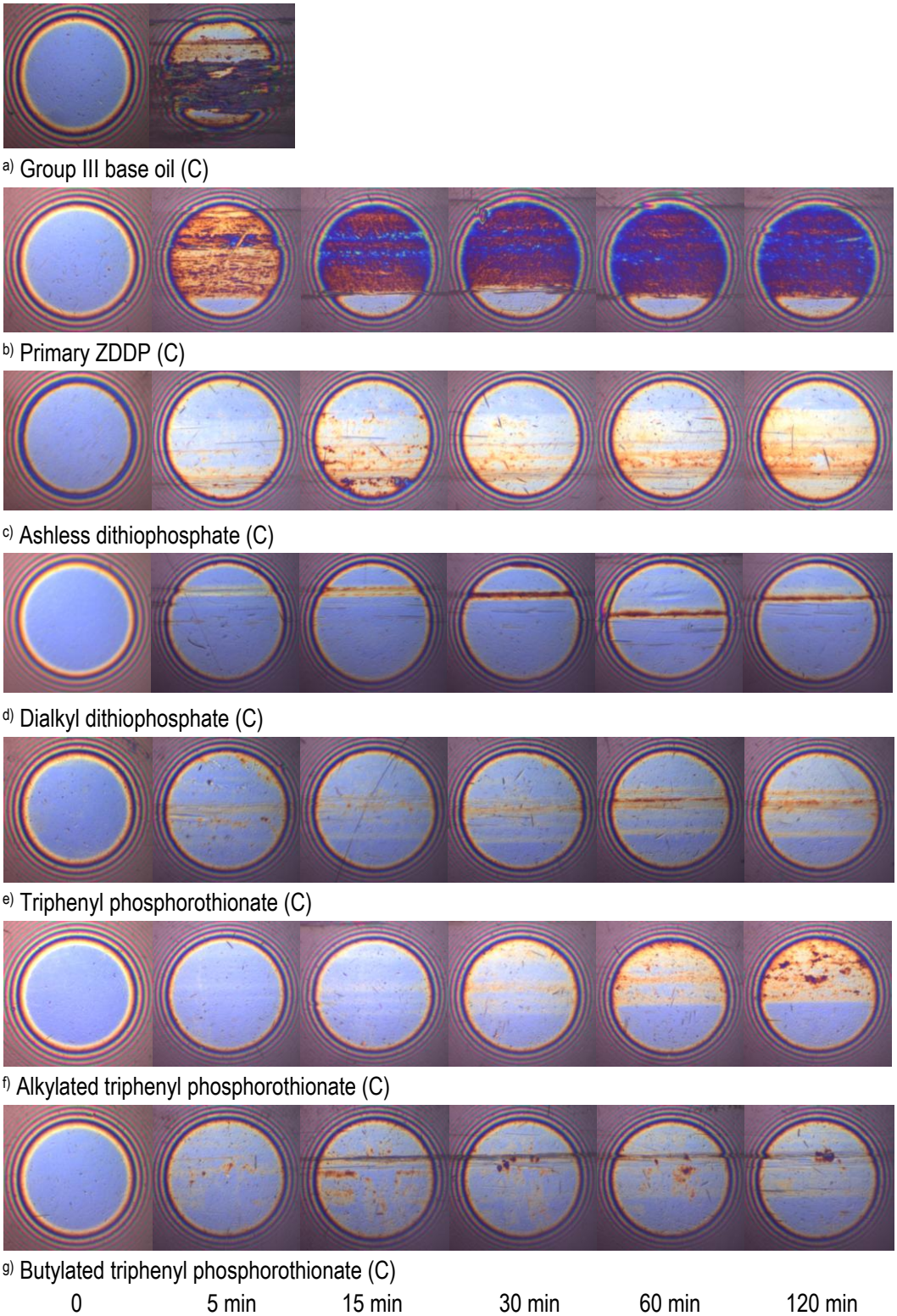
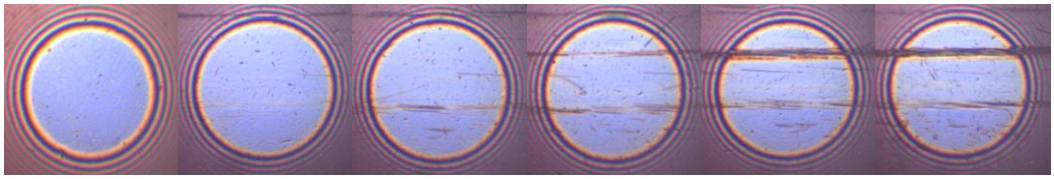
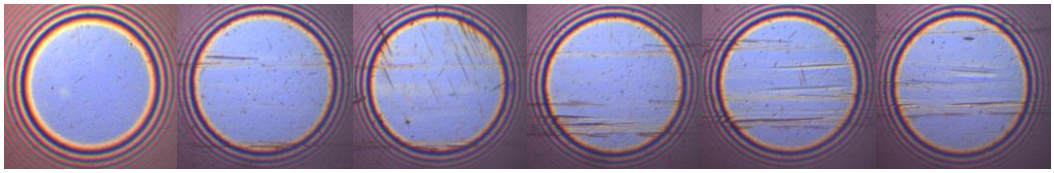


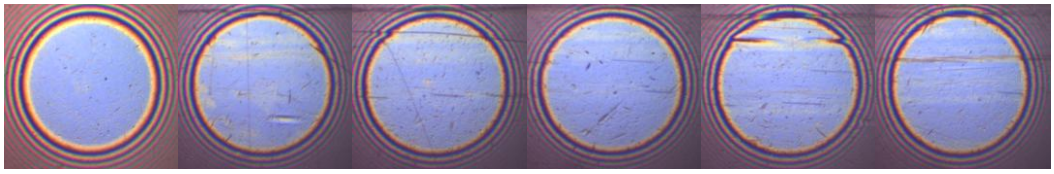
Figure 7.8: MTM-SLIM images showing: a) scuffing on the surface of the ball after 5 minutes of rubbing in base oil without antiwear additive; b) to g) the growth of tribofilm on the ball with increasing rubbing time (*i.e.* zero, 5, 15, 30, 60, 120 minutes).



h) Amine thiophosphate (C)



i) Phoshporus-sulphur-nitrogen-based (C)



j) Phosphorus-sulphur-based (C)

0 5 min 15 min 30 min 60 min 120 min

Figure 7.8 (continued): MTM-SLIM images showing: h) to j) the growth of tribofilm on the ball with increasing rubbing time (*i.e.* zero, 5, 15, 30, 60, 120 minutes).

Figure 7.9 summarises the development of mean film thickness with rubbing time for Primary ZDDP (C) and P-S-containing-derived tribofilms. It can be seen that Primary ZDDP (C) reacts rapidly on the surface, developing a thick film (*i.e.* ≈ 140 nm after 120 minutes of rubbing), while the P-S-containing compounds form thinner (*i.e.* 50-60 nm after 120 minutes of rubbing for Ashless dithiophosphate (C) and Alkylated triphenyl phosphorothionate (C) solutions) or even negligible tribofilms (*i.e.* ≈ 30 nm after 120 minutes of rubbing for Triphenyl phosphorothionate (C) solution).

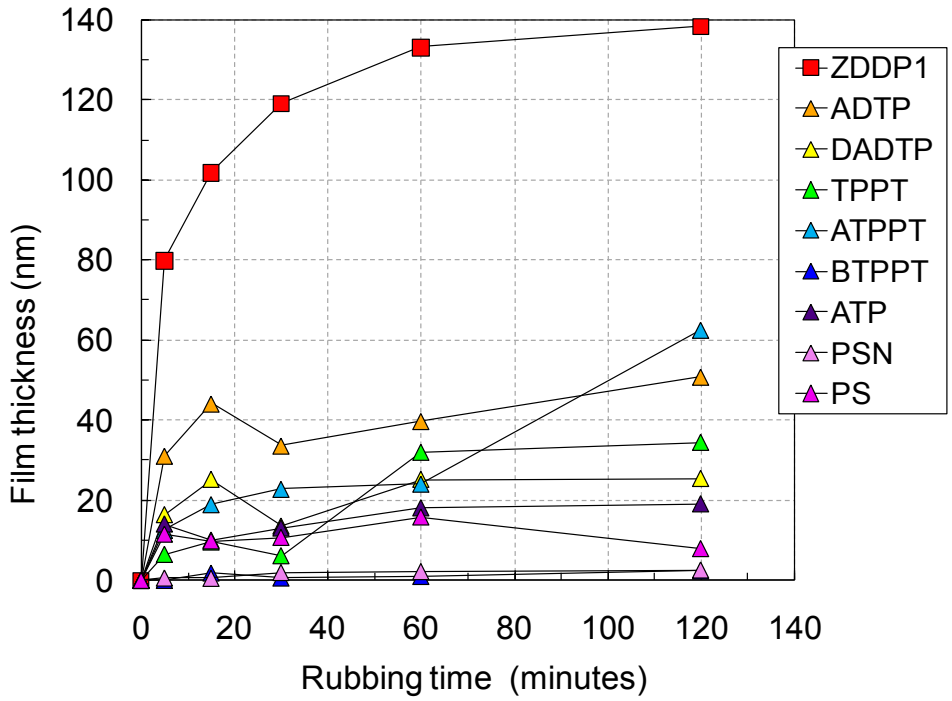


Figure 7.9: Mean film thickness with rubbing time for P-containing antiwear additives.

It has been suggested that P-S-containing additives form films less readily than ZDDP because of the absence of zinc cations to stabilise the phosphate film. To explore this, additional tests were carried out to investigate the influence of separate metal cations on the stabilisation of the protective film. Neutral calcium alkylsulphonate (C) and Titanium (IV) isopropoxide were individually blended at a concentration of 1, 5 and 10 % weight with Ashless dithiophosphate (C), *i.e.* ADTP, (800 ppm P), into GIII BO.

The film-forming properties of Titanium (IV) isopropoxide and Neutral calcium alkylsulphonate (C) in base oil are illustrated in Figure 7.10[b)-c)]. With the titanium-only solution, scuffing occurred after 5 minutes of rubbing and the test was terminated. The Neutral calcium alkylsulphonate (C)-only solution appears to form a film that withstands rubbing, but the change in contact shape may be due to wear.

Figure 7.10[d)-i)] shows that both the Neutral calcium alkylsulphonate (C)- and the Titanium (IV) isopropoxide-containing blends rapidly react to form a thick tribofilm on the surface, *i.e.* after 5 minutes of rubbing. The presence of a separate metal cation significantly enhances the rate at which the protective film grows, regardless of its concentration in the Ashless dithiophosphate (C) solution (*i.e.* 1, 5 and 10 % weight). It can be seen in Figure 7.10[i)] that at 10 % weight of Titanium (IV) isopropoxide the solution is almost saturated and the excess solute starts to evaporate at high temperature, *i.e.* 100 ºC, followed by precipitation on the spacer layer-coated glass disc.

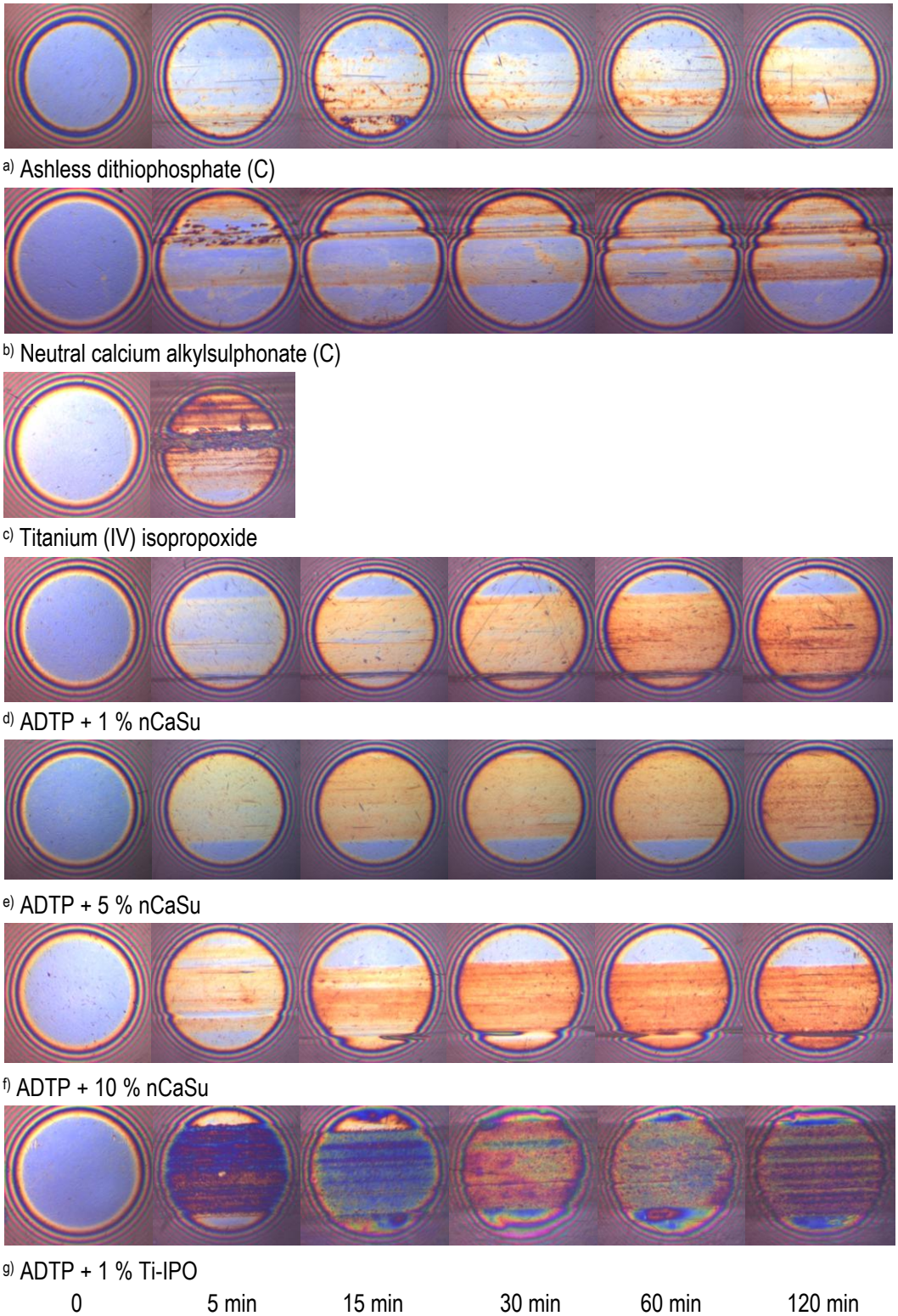
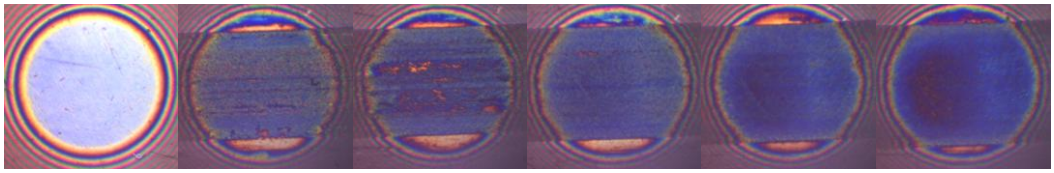
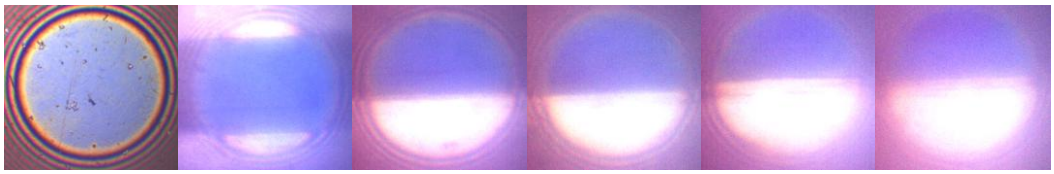


Figure 7.10: MTM-SLIM images showing: a) to g) the growth of tribofilm on the ball with increasing rubbing time (*i.e.* zero, 5, 15, 30, 60, 120 minutes).



h) ADTP + 5 % Ti-IPO



i) ADTP + 10 % Ti-IPO

0 5 min 15 min 30 min 60 min 120 min

Figure 7.10 (continued): MTM-SLIM images showing: h) and i) the growth of tribofilm on the ball with increasing rubbing time (*i.e.* zero, 5, 15, 30, 60, 120 minutes).

7.3 Results: Friction properties of P-S-containing Antiwear Additive-derived Tribofilm

The friction properties of a range of P-S-containing antiwear additives were studied using the MTM under mixed rolling/sliding conditions, as described in chapter 4, section 4.1. The Stribeck curve (Figure 7.11) shows the friction coefficient *versus* entrainment speed for these additives at the beginning and after 2 h of rubbing.

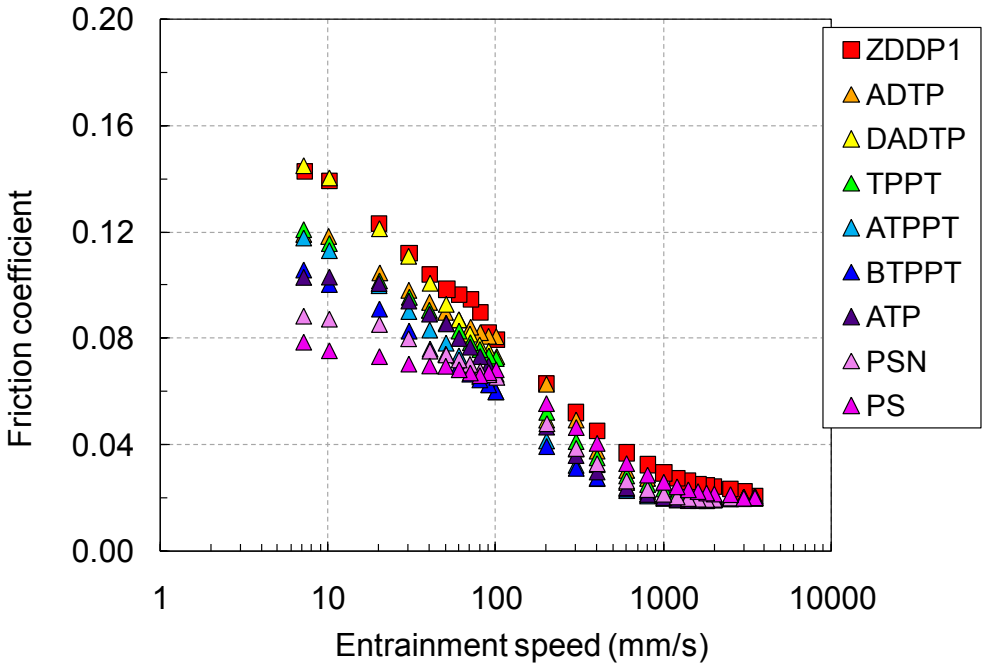
As discussed in section 5.3 of chapter 5, there is a significant increase in mixed friction for Primary ZDDP (C) once the protective film forms on the surface, shifting the curve to the right after 2h of rubbing. This increase in mixed friction is probably due to the change in surface texture as a result of the development of a thick solid-like film on the surface (Figure 7.8[b)]). A very slight increase in mixed friction is also observed for Alkylated triphenyl phosphorothionate (C) and Amine thiophosphate (C) solutions. The former can be ascribed to film formation, while the latter is possibly due to damage to the surface.

The Ashless dithiophosphate (C), which appears to form a thick and uniform protective film on the surface (*i.e.* ≈ 50 nm), shows no significant shift in mixed friction throughout the test. This may be because this additive forms a smooth, low shear strength film on the surface, rather than the rough pad-like structure generated by ZDDP.

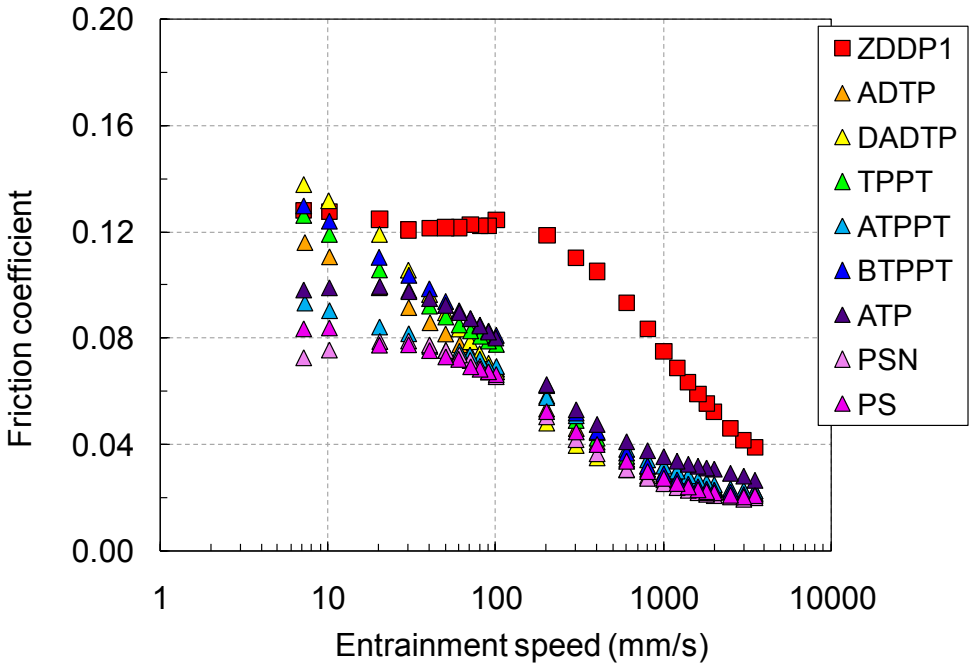
The remaining P-S-containing additives, Dialkyl dithiophosphate (C), Triphenyl phosphorothionate (C), Phoshporus-sulphur-nitrogen-based (C) and Phosphorus-sulphur-based (C) show no significant changes in mixed friction after rubbing, apart from Butylated triphenyl phosphorothionate (C), which does not form a protective film on the surface.

In terms of boundary friction, Phoshporus-sulphur-nitrogen-based (C) and Phosphorus-sulphur-based (C) additives give low friction both immediately and after two hours rubbing. The Alkylated triphenyl phosphorothionate (C), also gives low boundary friction, as did Amine thiophosphate (C).

Figure 7.12 shows the influence of Neutral calcium alkylsulphonate (C) and Titanium (IV) isopropoxide on friction for Ashless dithiophosphate (C) solutions. The thick protective films formed in the presence of a separate metal cation (Figure 7.10[d)-i)]) have the classical effect on mixed friction, shifting the curve to the right after 2h of rubbing. The Neutral calcium alkylsulphonate (C) initially reduces the boundary friction of the films, probably due to the contribution of the alkyl chain structure of the detergent molecule. By contrast, addition of the titanium compound resulted in increased boundary friction. The same behaviour was observed for P-containing solutions (*i.e.* bis(2-ethylhexyl) phosphite) treated with a separate metal cation, as described in chapter 6, section 6.3.

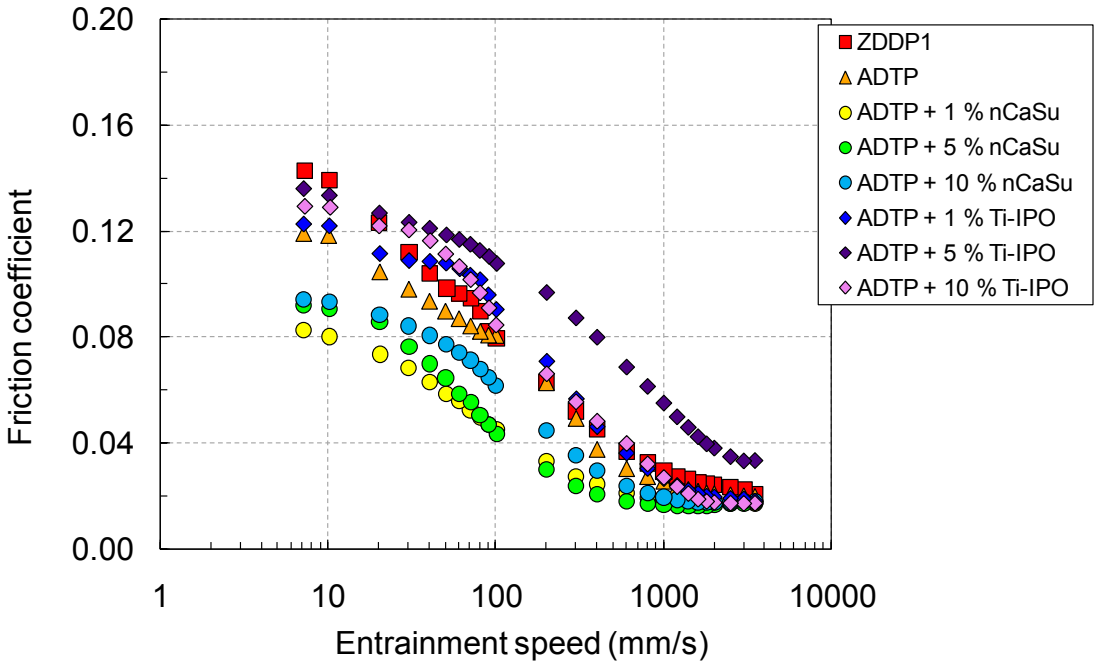


Initial friction, measured at the beginning of the test

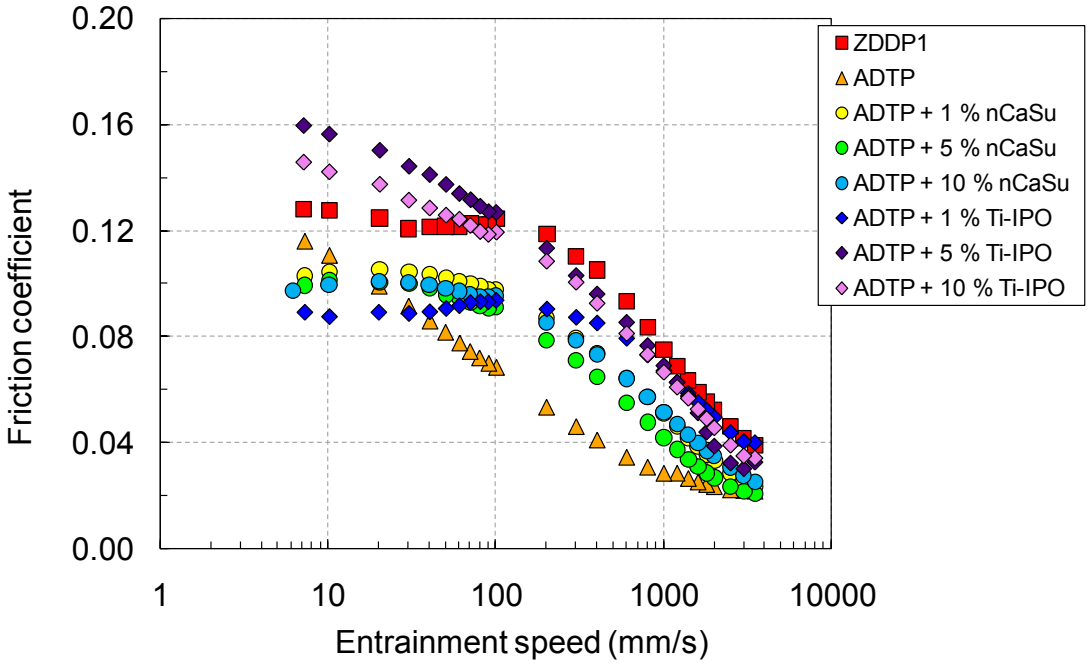


Friction after 2 h of rubbing

Figure 7.11: Stribeck curve showing friction coefficient *versus* entrainment speed at the beginning and after 2 h of rubbing at 50 % SRR, 30 N and 100 ºC.



Initial friction, measured at the beginning of the test



Friction after 2 h of rubbing

Figure 7.12: Stribeck curve showing friction coefficient *versus* entrainment speed at the beginning and after 2 h of rubbing at 50 % SRR, 30 N and 100 ºC.

7.4 Results: Morphology of P-S-containing Antiwear Additive-derived Tribofilms

The morphology of P-S-containing antiwear additive reaction films generated on AISI 52100 steel discs using the MTM, was studied by AFM, as described in chapter 4, section 4.2. An area of 25 µm x 25 µm in the centre of the wear track was scanned and the topography of the tribofilms is shown in Figure 7.13. Figure 7.13[a)] shows the topography of MTM-discs prior to rubbing.

It can be seen that the morphology of the tribofilms is strongly oriented along the sliding direction, represented by the arrow. Topography study reveals that P-S-containing antiwear additive-derived tribofilms consist of discrete pads randomly-distributed along the sliding direction. One exception is Alkylated triphenyl phosphorothionate (C)-derived tribofilm, which comprises rather larger pads.

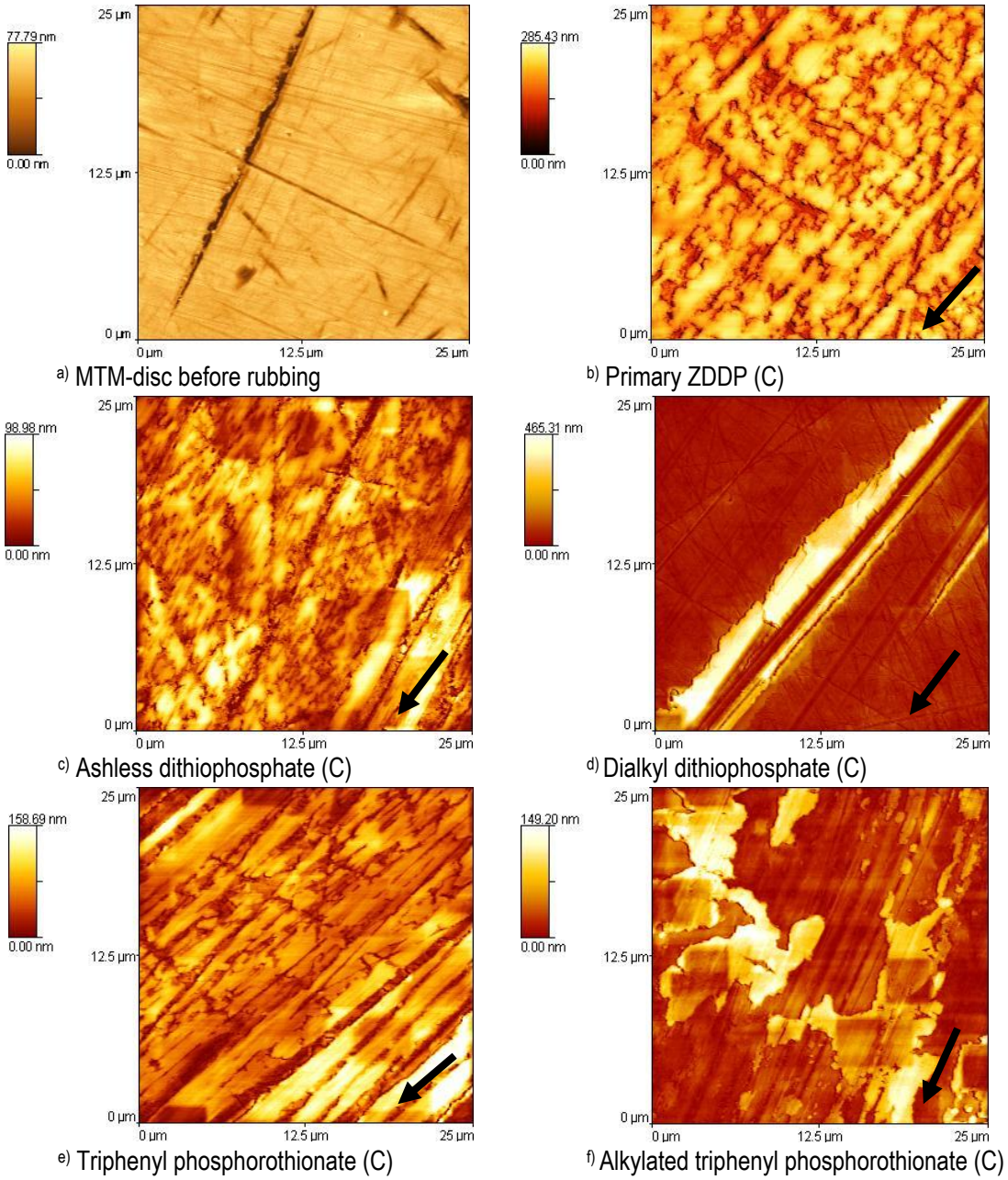


Figure 7.13: AFM 2D topography image at the centre of the wear track on the MTM-disc (sliding direction in b) to f) shown by the arrow).

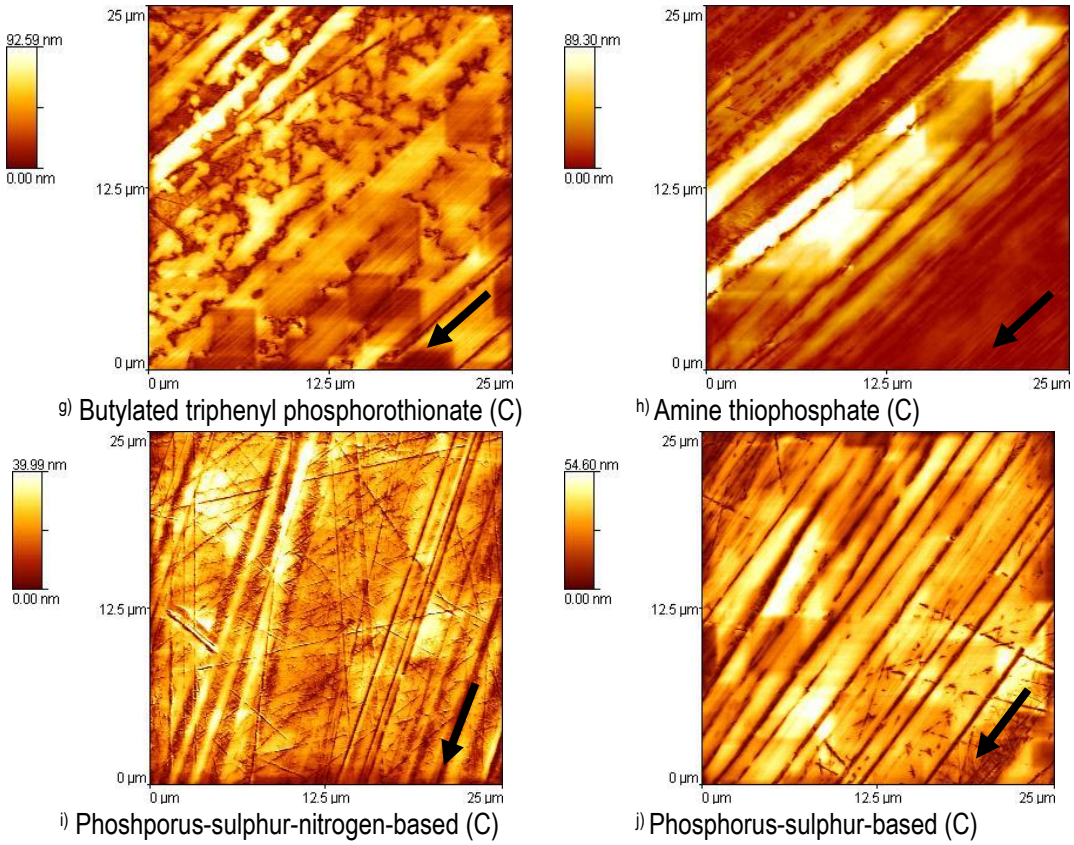


Figure 7.13 (continued): AFM 2D topography image at the centre of the wear track on the MTM-disc (sliding direction in g) to j) shown by the arrow).

Figure 7.14 shows the morphology of reaction films formed by Ashless dithiophosphate (C) solution in the presence of a separate metal cation (1 % weight). It appears that there is a slight increase in pad size in the presence of Neutral calcium alkylsulphonate (C), while the Titanium (IV) isopropoxide-containing tribofilm appears amorphous in nature.

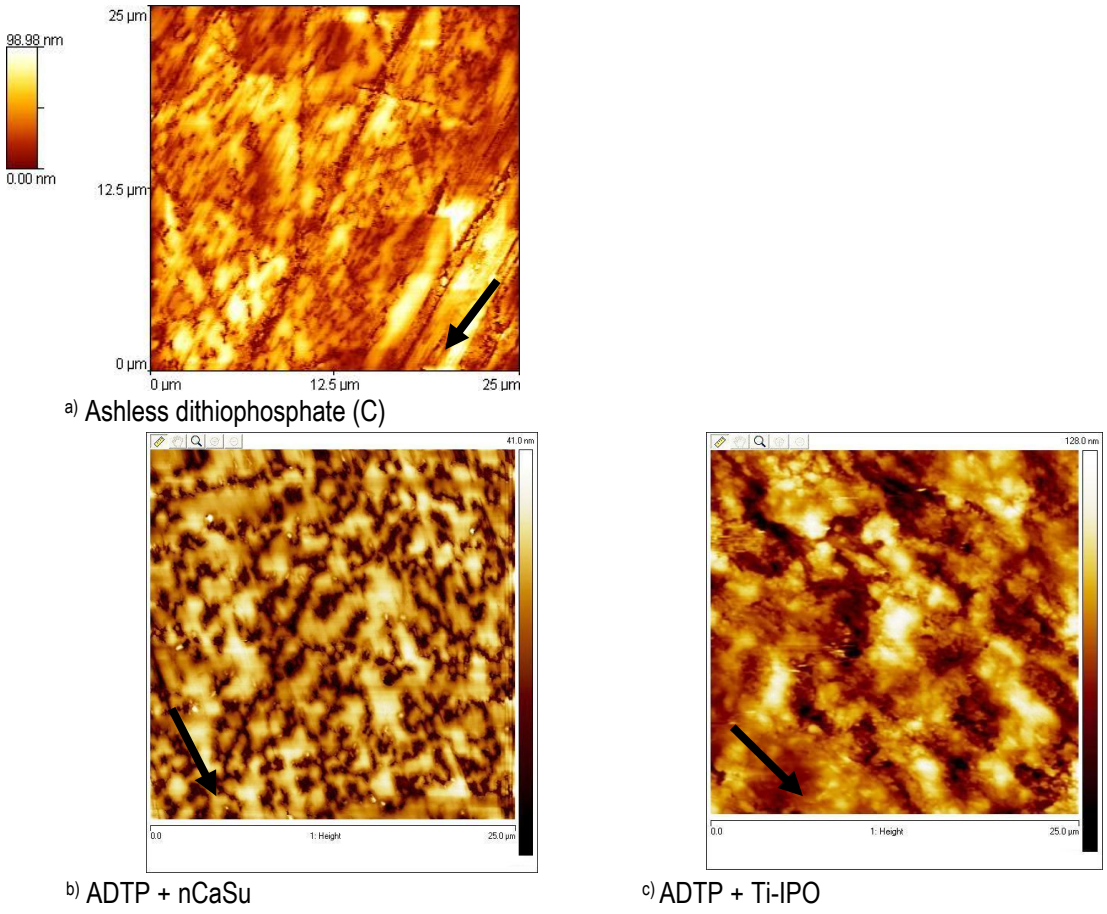


Figure 7.14: AFM 2D topography image at the centre of the wear track on the MTM-disc (sliding direction in a) to c) shown by the arrow).

7.5 Results: Wear-reducing Properties of P-S-containing Antiwear Additive-derived Tribofilms

The wear-reducing properties of three P-S-containing antiwear additives, Ashless dithiophosphate (C), Triphenyl phosphorothionate (C) and Alkylated triphenyl phosphorothionate (C), were studied using the method developed by the author, which combines the MTM-Reciprocating rig to generate the wear track on AISI 52100 steel discs with the SWLI to image the track and measure wear depth, as described in chapter 4, sections 4.3 and 4.4. Results are summarised in Figures 7.15 and 7.16.

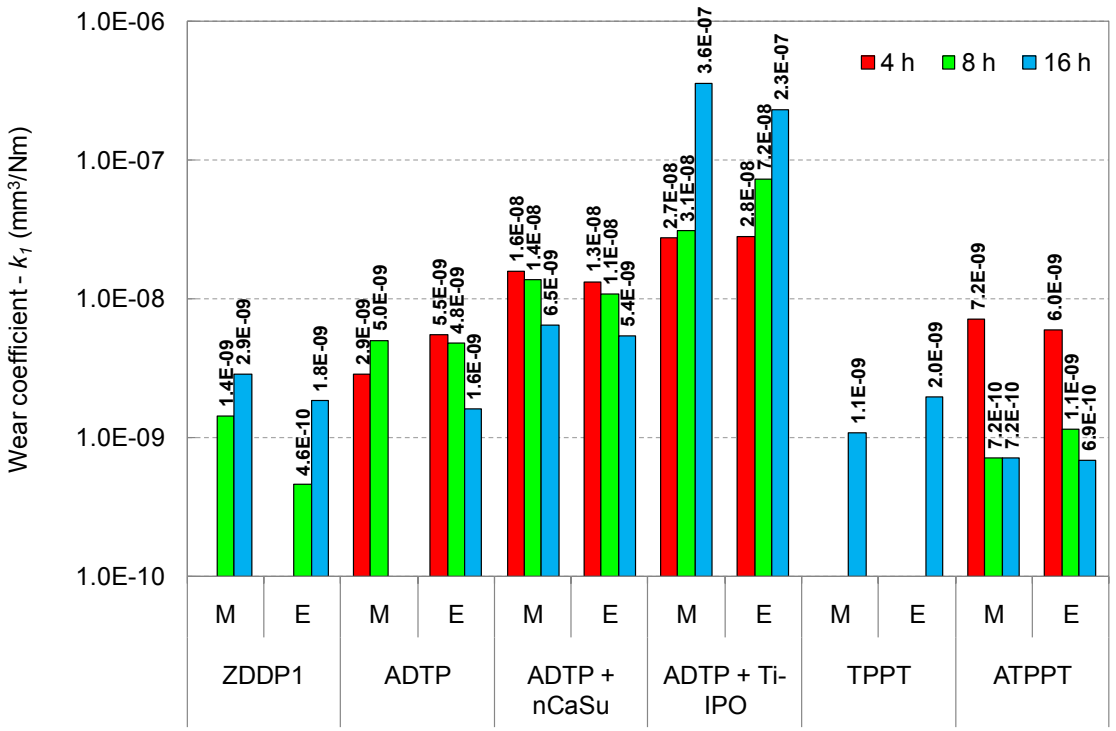
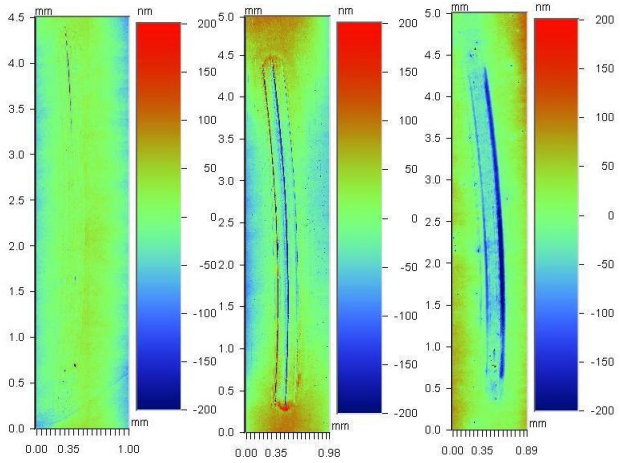


Figure 7.15: Wear coefficient (k_1) in the middle (M) and at the ends (E) of the wear track (*i.e.* average of both ends) for tests lasting 4, 8 and 16 hours.

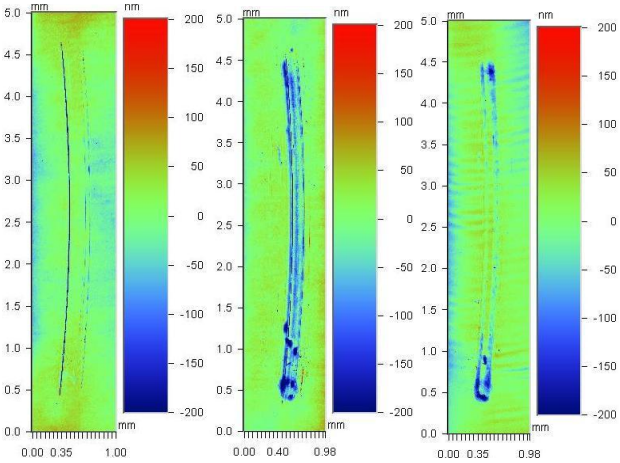
The results show that Ashless dithiophosphate (C), Triphenyl phosphorothionate (C) and Alkylated triphenyl phosphorothionate (C) offer wear-reducing properties, comparable to Primary ZDDP (C). It appears that there is a decrease in wear rate for Alkylated triphenyl phosphorothionate (C) with increasing rubbing time, probably because of the development of a protective film during initial rubbing. Triphenyl phosphorothionate (C), however, shows no measurable wear after 4 and 8 hours of rubbing, while after 16 h only very mild levels of wear can be observed.

The influence of adding separate metal ions on wear was also studied. The topography images, shown in Figure 7.16, reveal a considerable increase in the width of the wear track with increasing rubbing time when Titanium (IV) isopropoxide (1 % weight) solution is added to Ashless dithiophosphate (C). To a lesser extent, the same phenomenon is observed near the ends of the wear track for Ashless dithiophosphate (C) with Neutral calcium alkylsulphonate (C) (1 % weight) after 16 h of rubbing.

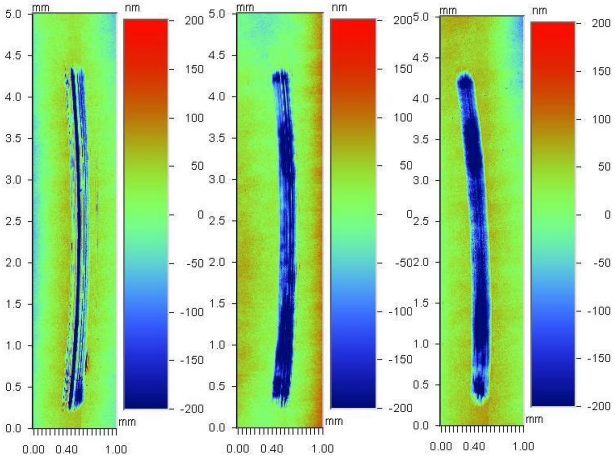
Figure 7.15 also indicates that the addition of Neutral calcium alkylsulphonate (C) and particularly Titanium (IV) isopropoxide increased wear rate significantly. This may be because of excess titanium that might be abrading the tribofilm and thus promoting abrasive wear. Additionally, there is an increase in the wear rate of Ashless dithiophosphate (C) in the presence of Neutral calcium alkylsulphonate (C). This indicates that although the Ca cation accelerates film formation (Figure 7.10[d)-f)]), the film formed does not have the same ability to reduce wear, over extended periods of rubbing, as the film formed by Ashless dithiophosphate (C) alone (Figure 7.10[a)]). It is hypothesised that as reaction occurs in the presence of Ca cation and a film is being formed, there is also removal and replenishment of this film. The latter will involve the continuous removal of Fe from the substrate, which in turn yields mild corrosive wear. Similar behaviour has been reported by Olomolehin *et al.*, who found that sulphonic acid favours film formation, but also yields corrosive wear [197].



Primary ZDDP (C): 4, 8 and 16 hours after EDTA.

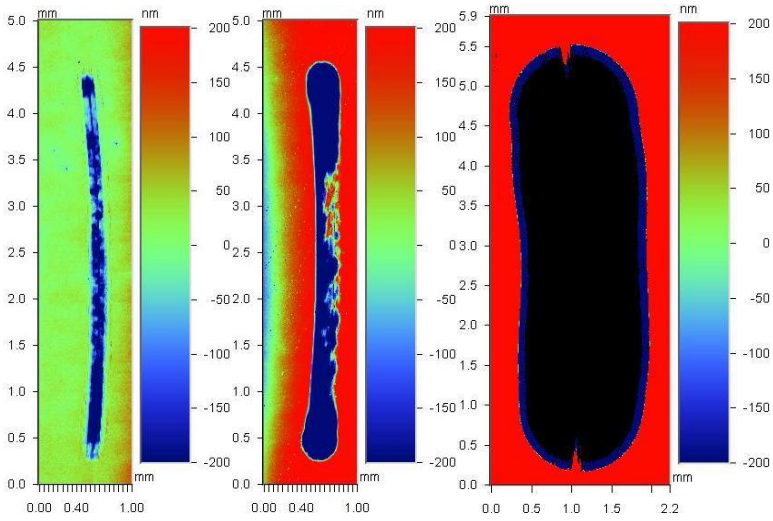


Ashless dithiophosphate (C): 4, 8 and 16 hours after EDTA.

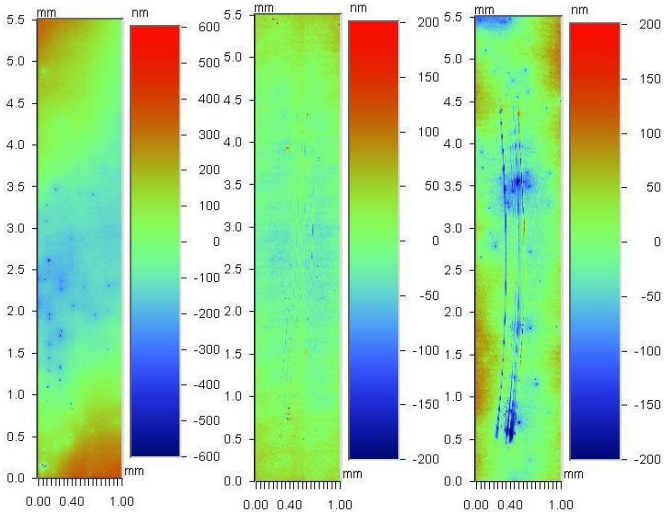


Ashless dithiophosphate (C) + nCaSu: 4, 8 and 16 hours after EDTA.

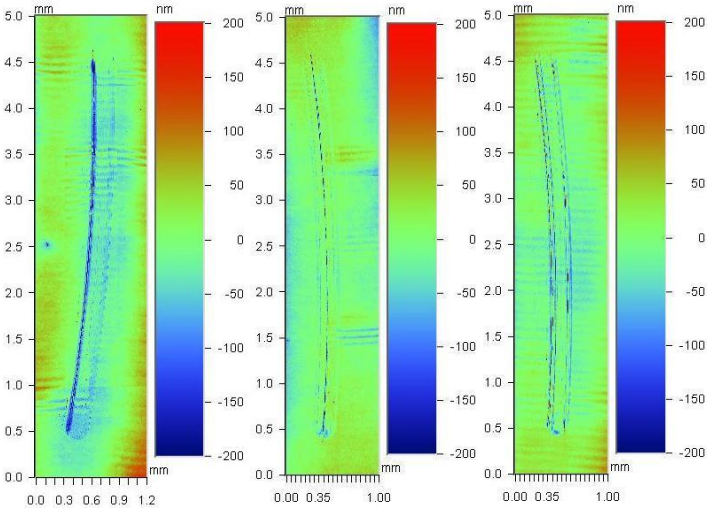
Figure 7.16: SWLI 2D topography images of the wear track on the disc.



Ashless dithiophosphate (C) + Ti-IPO: 4, 8 and 16 hours after EDTA.



Triphenyl phosphorothionate (C): 4, 8 and 16 hours after EDTA.



Alkylated triphenyl phosphorothionate (C): 4, 8 and 16 hours after EDTA.

Figure 7.16 (continued): SWLI 2D topography images of the wear track on the disc.

7.6 Discussion of P-S-containing Antiwear Additives Work

This film-forming study under mixed rolling/sliding conditions using MTM-SLIM shows that P-S-containing compounds form thin (up to ≈ 60 nm) or even negligible tribofilms on the surface. It is noteworthy, however, that there is no visible damage to the rubbing contact even in the presence of P-S-compounds that form negligible films on the surface (*e.g.* Triphenyl phosphorothionate (C)). This indicates that thick boundary film formation is not required for effective wear reduction, which is also confirmed for the three P-S additives for which wear tests were carried out.

A study of the influence of a separate metal cation, *i.e.* Neutral calcium alkylsulphonate (C) and Titanium (IV) isopropoxide, on the film-forming properties of an Ashless dithiophosphate (C) reveals that these blends react rapidly to form thick tribofilms on the surface. This supports the conjecture that the rate at which the P-S-containing antiwear additive-derived tribofilms grow is constrained by the quantity of iron cations generated by rubbing. The presence of a separate metal cation significantly enhances film formation, probably because this cation enables stabilisation and growth of the protective film; such glass stabilisation has been proposed to be the role of Zn in ZDPP [67].

It is seen that the Neutral calcium alkylsulphonate (C) forms a patchy film on rubbed surfaces. Overbased detergents are well known to form thick films, but this was not expected of a neutral calcium alkylsulphonate detergent, which should not have $CaCO_3$ cores. This suggests that even this neutral additive may contain a small amount of residual $CaCO_3$ nanoparticles. Alternatively, it is possible that CO_2 from the atmosphere may be reacting with the calcium alkyl sulphonate molecules to form $CaCO_3$.

The friction behaviour study by MTM shows that there is a slight increase in mixed friction for Alkylated triphenyl phosphorothionate (C) and Amine thiophosphate (C) solutions. The former can be ascribed to its relatively thick film formation, while the latter is possibly due to scuffing on the surface. Alternatively Ashless dithiophosphate (C), which appears to form a thick and uniform protective film on the surface (*i.e.* ≈ 50 nm), shows no significant shift in mixed friction throughout the test. This suggests that this additive forms a smooth, low shear strength film on the surface. By contrast, when a separate metal cation is added to Ashless dithiophosphate (C), the friction curves are shifted to the right after 2h of rubbing. This implies that the thicker films formed from the addition of Ca ions are no longer smooth, so that its texture starts to resemble that of ZDDP films. This was confirmed by topography study using AFM.

Significant differences in the boundary friction of the various P-S-containing antiwear additives was observed, with the Phoshporus-sulphur-nitrogen-based (C) and Phosphorus-sulphur-based (C) giving the lowest friction and low friction also from Alkylated triphenyl phosphorothionate (C) and Amine thiophosphate (C).

Assuming that Alkylated triphenyl phosphorothionate (C), is a pure additive and taking into account its phosphorus content, *i.e.* 4.3 %P, it is estimated that the alkyl chain length of the -R substituent group attached to each phenyl ring (*i.e.* triphenyl) is equal to 9. It is hypothesised that the low boundary friction given by this additive might arise from its relatively long alkyl chain [198, 199]. Unfortunately, not enough information was provided about the other additives (*e.g.* Phoshporus-sulphur-nitrogen-based (C), Phosphorus-sulphur-based (C) and Amine thiophosphate (C)) to explain the origins of low boundary friction further.

This study has also demonstrated the wear-reducing properties of P-S-containing antiwear additives using the reciprocating MTM. It was found that Ashless dithiophosphate (C), Triphenyl phosphorothionate (C) and Alkylated triphenyl phosphorothionate (C) offer wear-reducing properties comparable to Primary ZDDP (C). In addition, there is a decrease in wear rate for Alkylated triphenyl phosphorothionate (C) with increasing rubbing time, probably because of initial film formation. Triphenyl phosphorothionate (C), however, shows immediate wear reduction, with no measurable wear after 4 and 8 hours of rubbing. Since these three additives form thinner boundary films than Primary ZDDP (C) (or even negligible, *e.g.* Triphenyl phosphorothionate (C) ≈ 30 nm) this supports the finding made in the previous chapter, that thick boundary film formation is not a pre-requisite for effective wear or friction reduction.

It is noteworthy that aryl substituted compounds, *i.e.* Triphenyl phosphorothionate (C) and Alkylated triphenyl phosphorothionate (C), offered better wear-reducing properties than alkyl substituted ones, *i.e.* Ashless dithiophosphate (C). These results oppose those published by Kim *et al.* [196], in which the authors reported that acid-substituted dialkyldithiophosphates showed superior wear-reducing properties to its neutral counterparts and aryl dithiophosphates. These discrepancies might me due to the fact that the additives studied by Kim *et al.* were investigated under extreme pressure conditions, and such conditions tend to favour rapidly-reacting additives.

Overall, the presence of a separate metal cation in Ashless dithiophosphate (C) solution seems to promote wear. It is hypothesised that abrasive wear takes place in the presence of Ti, possibly because of excess titanium oxide that might be forming an oxide film, which abrades the tribofilm and thus promotes wear; or because of the formation of a weakly-bound mixed Fe/Ti phosphate film that is rapidly formed and removed. The increase in wear rate observed in the presence of Neutral calcium alkylsulphonate (C) is ascribed to removal and replenishment of the protective film, which involves the continuous removal of Fe from the substrate, which in turn yields mild corrosive wear.

8. FILM-FORMING, FRICTION, MORPHOLOGY AND WEAR-REDUCING PROPERTIES OF S-CONTAINING ANTIWEAR ADDITIVES

This chapter first provides an overview of previous research on sulphur-containing antiwear additives, *i.e.* functionalised organosulphides, S-containing heterocyclic rings and ashless dithiocarbamates, with a particular focus on the film-forming and wear properties of this additive type.

The chapter then describes film thickness, friction, surface topography and wear measurements carried out on a range of S-containing antiwear additive solutions, using the methods outlined in chapter 4.

Some surface analyses of the films formed by S-containing antiwear additives were also carried out using ToF-SIMS and XANES but these are deferred to chapter 13, where analysis of the films formed by various additives of interest are presented and discussed together.

8.1 Literature Overview of S-containing Antiwear Additives

Organosulphur compounds were first introduced as extreme pressure additives for gear lubricants in the 1930s [200]. Since then numerous S-containing compounds have been proposed as antiwear additives for the formulation of crankcase lubricants. These S-containing chemistries are divided into three main classes, namely functionalised organosulphides, S-containing heterocyclic rings and ashless dithiocarbamates. Reviews on the history and mechanisms of S-containing antiwear additives have been given by Papay [154] and Spikes [67].

Allum *et al.* investigated the antiwear and load-carrying properties of a range of organic disulphides. The authors reported that the nature of substituent group attached to S- greatly influences antiwear performance. It was also suggested that the S-S bond in disulphides breaks down to form a wear-reducing iron mercaptide layer [201], while extreme pressure properties were improved by the formation of iron sulphide on the surface [202].

Further work by Forbes *et al.* studying the four-ball wear of a series of ester- and alkoxy-substituted disulphides revealed that the presence of strong polar groups at both ends of the molecule improved antiwear properties, *i.e.* at low concentrations diester-substituted disulphides were superior to dialkyl disulphides, whereas diether-substituted disulphides gave similar levels of wear protection [203]. It was also observed by the authors that high concentrations of ester-substituted disulphides gave corrosive wear. This was ascribed to the strong adsorptive power of polar ester groups, which in turn prevented the sulphur from reacting with the surface and thus prevent wear. Belov *et al.* reported that bis-(alkylpentanoate) monosulphides offered similar wear-reducing properties to ZDDP with better copper compatibility [204]. More recently, Katafuchi *et al.* observed similar behaviour for disulphide equivalents [205].

Baldwin compared the wear-reducing properties of acid- (*i.e.* n-$C_{12}H_{25}S(CH_2)_2COOH$), ester- (*i.e.* n-$C_{12}H_{25}S(CH_2)_2COOCH_3$) and alcohol-substituted monosulphides (*i.e.* n-$C_{12}H_{25}S(CH_2)_3OH$) to those of a long-chain monosulphide (*i.e.* n-$C_{12}H_{25}S(CH_2)_2CH_3$) [206]. It was found that the presence of polar groups increased reactivity towards the surface, suggesting that functionality plays a key role in antiwear effectiveness of organosulphur compounds.

The use of heterocyclic thio-compounds as antiwear additives has been the subject of considerable research [207-211]. Singh *et al.* studied the load-carrying and wear-reducing properties of amine- and pyridine-substituted thiadiazoles (Figure 8.1). The authors reported that both additive types gave good antiwear properties, even at high loads [212, 213]. Surface analysis of the rubbed surfaces revealed the presence of iron oxide and iron sulphide.

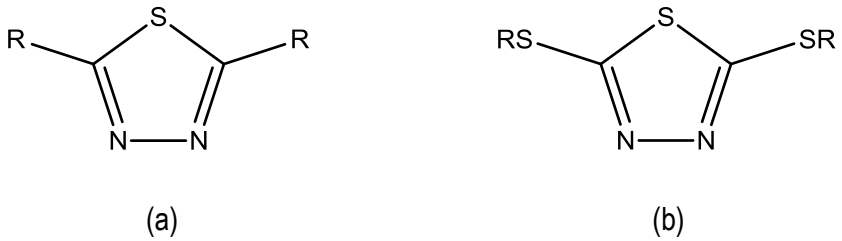


Figure 8.1: Molecular structures of (a) thiadiazole and (b) dimercaptothiadizole derivatives.

Wei *et al.* investigated the influence of substituent groups on the antiwear properties of dimercaptothiadiazole derivatives (Figure 8.2) [214]. It was reported that the OH- functional group, attached to the monosulphide side chain in 10-hydroxy-1-octyl-decylthio-dimercaptothiadiazole (HODDT), significantly increased reactivity towards the surface, whereas the S-S bond improved antiwear and load-carrying properties. Subsequent analysis of the protective layer by XPS and AES revealed the presence of FeS, $FeSO_4$ and polysulphide species.

Gao *et al.* attributed the antiwear and extreme pressure effectiveness of a range of 2,5-dialkoxymethylthio-1,3,4-thiadiazole derivatives (Figure 8.2) to a combination of factors [215]. It was suggested that (i) thiadiazole molecules have an intrinsic ability to coordinate with metal surfaces to form a stable protective layer (*i.e.* polydentate ligands), (ii) additive decomposition yields $ROCH_2S$ and other SH-containing species, which interact with the rubbing surface to form a load-carrying film comprised of FeS and FeSO4 and (iii) the formation of a N-containing resin-like polymer, which adheres to the surface improving lubrication.

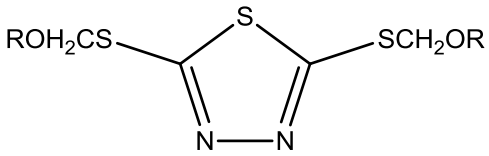
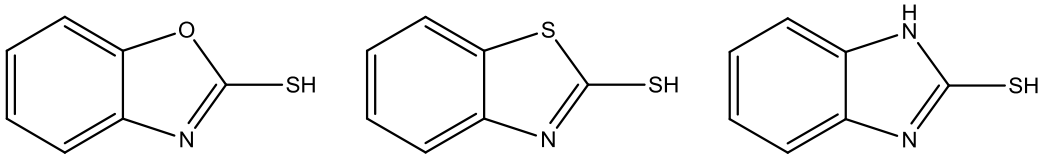


Figure 8.2: Molecular structure of 2,5-dialkoxymethylthio-1,3,4-thiadiazole derivatives [215].

Zhu *et al.* reported that 5-dodecyldithio-3-phenyl-1,3,4-thiadiazole-2-thione and 5-cetyldithio-3-phenyl-1,3,4-thiadiazole-2-thione have a beneficial effect on the friction and wear properties of rapeseed oil, particularly at high loads [216]. The authors ascribed this behaviour to the formation of a protective layer, which consists of sulphate, sulphide, FeO and nitrogen-containing compounds. More recently, Chen *et al.* found that long-chain di-substituted dimercaptothiadiazole derivatives showed superior friction and wear-reducing properties than mono-substituted ones [217].

Zhang *et al.* investigated the effect of molecular structure on the wear-reducing properties of three S-containing heterocyclic compounds, namely 2-mercaptobenzoxazole, 2-mercaptobenzothiazole and 2-mercaptobenzimidazole (Figure 8.3) [218]. It was observed that all three additives reduced wear and friction, with 2-mercaptobenzoxazole superior to 2-mercaptobenzothiazole and 2-mercaptobenzimidazole. The authors credited this behaviour to the superior coordination capacity of the oxygen atoms in 2-mercaptobenzoxazole with the metal surfaces. It was also proposed that the reactivity towards the surface and thus the ability to break down during rubbing to form a tribochemical film on the surface is O- > S- > N-containing molecules.



(a) (b) (c)

Figure 8.3: Molecular structure of (a) 2-mercaptobenzoxazole, (b) 2-mercaptobenzothiazole and (c) 2-mercaptobenzimidazole.

Liang *et al.* studied two 2-mercaptobenzothiazole derivatives (Figure 8.3 (b)) and they found that these additives decompose under rubbing to form a FeS, FeS_2 and $FeSO_4$-rich protective layer on the surface, which is beneficial to wear and friction [219]. Further work by Liang *et al.* revealed that 1-ethylhexyl-ethyl ester-thiomethyl-2-sulphur-benzothiazole (MBES) provided very good wear and load-carrying properties when combined with ZDDP [220]. Li *et al.* reported that a borate ester-containing benzothiazole derivative gave superior friction and load-carrying properties to ZDDP, but its wear-reducing properties were not quite as good as ZDDP's [221].

The wear-reducing properties of ashless dithiocarbamates have also been extensively researched [222-226]. Kumar *et al.* investigated the four-ball wear and load carrying properties of thiuram disulphide, xanthogen and dithiocarbamate derivatives (Figure 8.4) [227]. Although the compounds studied showed good extreme pressure properties, none of them provided antiwear performance comparable to the P-containing compound used as a reference, *i.e.* TCP.

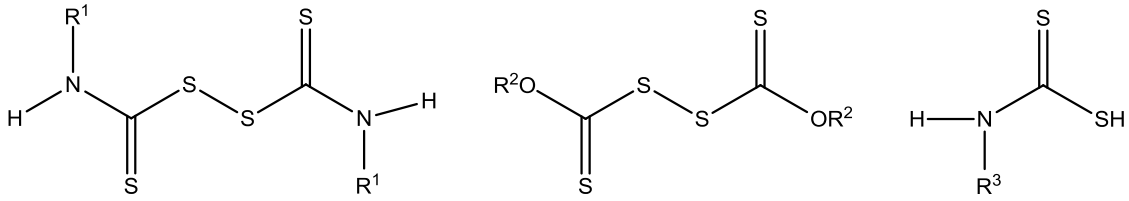


Figure 8.4: Molecular structure of (a) bis-(aryl/alkyl) thiuram disulphide, (b) bis-aryl xanthogen and (c) aryl/alkyl dithiocarbamate, where R^1 = naphthyl, ethanol or diethanol; R^2 = phenyl or naphthyl; R^3 = phenyl, naphthyl, ethanol, diethanol or benzyl [227].

Xu *et al.* studied the influence of substituent groups on the antiwear properties of two dithiocarbamate derivatives, namely S-(1-H-benzimidazole-2-yl)methyl-N,N-dioctyldithiocarbamate and S-ethyl-N,N-dioctyldithiocarbamate (Figure 8.5) [228]. It was found that, the benzimidazole-substituted dithiocarbamate gave antiwear performance comparable to ZDDP at low loads, but considerably better than ZDDP at higher loads. Whereas the ethyl-substituted compound was worse than the base oil alone, at higher loads. The authors ascribed the wear-reducing properties of the benzimidazole-substituted additive to the formation of a stable lubricating film comprised of reaction and adsorption layers. It was proposed that the former consists of FeS and FeS_2, while the latter was formed through bonding the lone electron pair of nitrogen from the benzimidazole group. Subsequent surface analysis revealed that the adsorption layer mainly occurs on the outer surface, preventing the inner reaction layer from being worn out. Furthermore, the poor performance of the ethyl-substituted additive was attributed to its unstable molecular structure, which reacts with the air under rubbing to form corrosive species, such as SO_x^{2-}, -O-SO_2 and NO_3^-, on the surface.

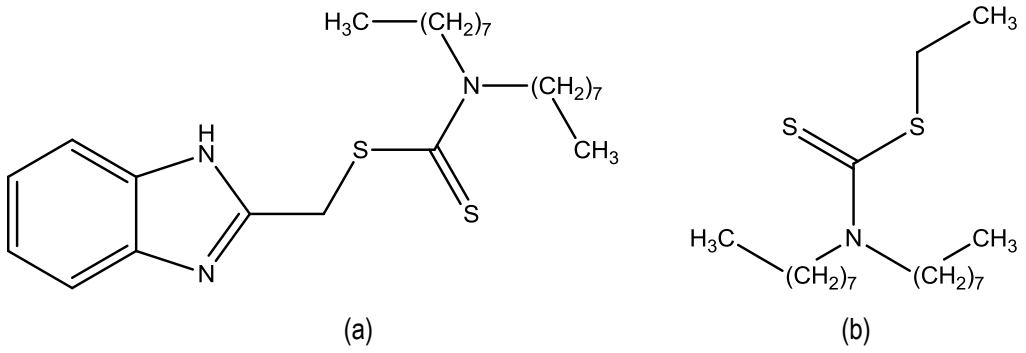


Figure 8.5: Molecular structure of (a) S-(1-H-benzimidazole-2-yl)methyl-N,N-dioctyldithiocarbamate and (b) S-ethyl-N,N-dioctyldithiocarbamate [228].

Ren *et al.* compared the wear-reducing properties of S-(1-H-benzotriazol-1-yl)methyl alkyl xanthate derivatives (Figure 8.6) to those of ZDDP [229]. It was found that the benzotriazole-substituted xanthates show similar antiwear performance to ZDDP. Further analysis by AES and XPS revealed the presence of C, O, FeS, FeO and the benzotriazole group still intact on the surface.

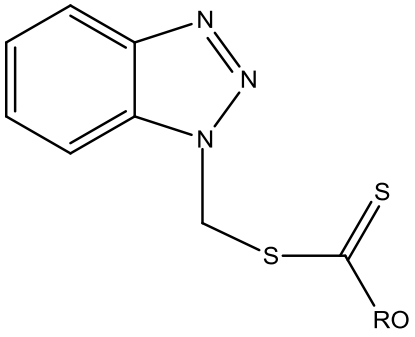


Figure 8.6: Molecular structure of S-(1-H-benzotriazol-1-yl)methyl alkyl xanthate derivatives, where R = ethyl, n-butyl or n-octyl [229].

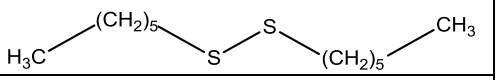
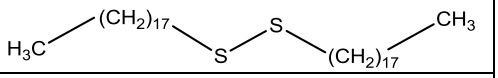
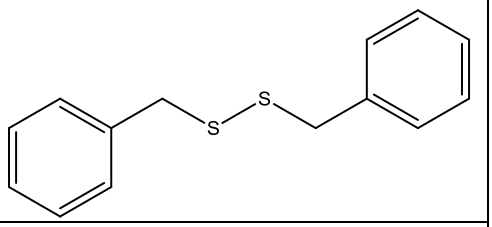
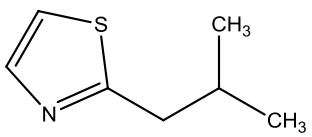
Fan *et al.* investigated the tribological characteristics of two dithiocarbamate derivatives, *i.e.* octyl 2-(dibutylcarbamothioylthio) acetate (DDCO) and S-dodecyl 2-(dibutylcarbamothioylthio) ethanthioate (DDCS) [230]. The authors reported that both additives had a synergistic effect on the friction, load-carrying and wear-reducing properties of ZDDP. Further work by Wu *et al.* on dithiocarbamate derivatives suggested that these additives can give antiwear performance comparable to ZDDP, but only at higher loads [231].

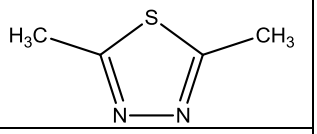
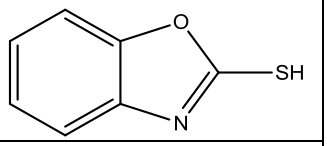
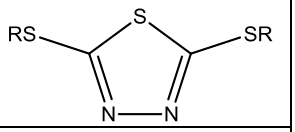
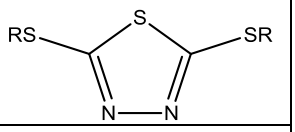
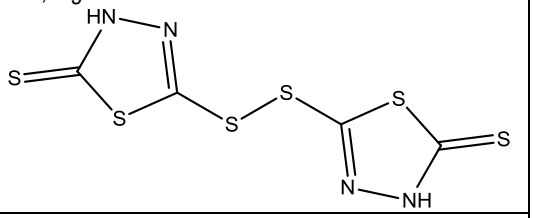
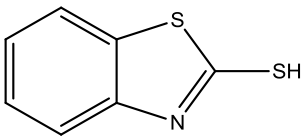
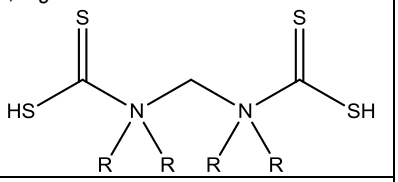
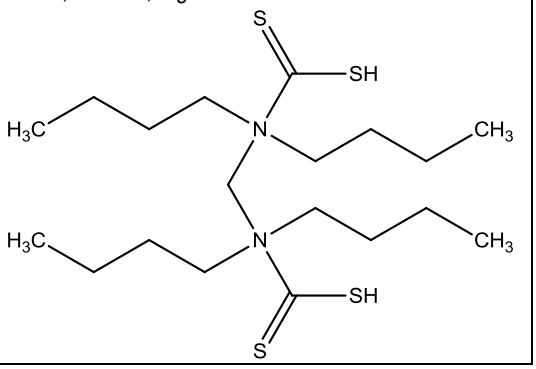
Overall it has been reported that a range of S-containing additives break down to form a sulphide-containing tribofilm on the surface giving good antiwear performance, despite the fact that these compounds are considered fairly corrosive in nature, which is key to their extreme pressure behaviour. It seems as though the S-containing compounds that can provide good wear-reducing properties are usually employed as corrosion inhibitors, *i.e.* heterocyclic thio-compounds.

8.2 Results: Film-forming Properties of S-containing Antiwear Additives

The film-forming properties of S-containing antiwear additives were studied using MTM-SLIM under mixed rolling/sliding conditions, as described in chapter 4, section 4.1. The additives employed in the study described in this chapter are summarised in Table 8.1. These were blended into Group III base oil at a concentration of 1000 ppm sulphur and submitted to rubbing under the same test conditions on the MTM-SLIM.

Table 8.1: Test materials summary: Sulphur-containing additives study

Abreviation[1]	**Sample name**	**Details**
GIII BO	Group III base oil (C)	-
ZDDP1	Primary ZDDP (C)	9.5 %P; 20.0 %S; 10.6 %Zn
=	Di-n-hexyl disulphide	*e.g.* 
=	Di-n-octadecyl disulphide	*e.g.* 
=	Dibenzyl disulphide	*e.g.* 
DA5S	Dialkyl pentasulphide (C)	40.0 %S
DAPS	Dialkyl polysulphide (C)	40.0 %S
SFAE	Sulphurised fatty acid ester (C)	10.0 %S
=	2-Isobutylthiazole	*e.g.* 

=	2,5-Dimethyl-1,3,4-thiadiazole	*e.g.* 
=	2-Mercaptobenzoxazole[2]	*e.g.* 
DMTDA1	Dimercaptothiadiazole 1 (C)	30.0 %S; *e.g.* 
DMTDA2	Dimercaptothiadiazole 2 (C)	31.0 %S; 4.5 %N; *e.g.* 
DTBTDAT	Dithio-bis-thiadiazolethione (C)[2]	66 %S; *e.g.* 
MBTA	Mercaptobenzothiazole (C)	38.3 %S; *e.g.* 
MBDADTC	Methylene-bis-dialkyl-dithiocarbamate (C)	30.0 %S; 6.5 %N; *e.g.* 
MBDBDTC	Methylene-bis-dibutyl-dithiocarbamate (C)	30.2 %S; 6.7 %N; *e.g.* 

(C): commercially-available.

[1] "=" means abbreviated name is the same as full name

[2] These additives were not submitted to testing because they were not soluble in GIII base oil (C).

Figure 8.7 shows the growth of the tribofilm on the MTM-ball with increasing rubbing time (*i.e.* zero, 5, 15, 30, 60, 120 minutes) for the base oil, Primary ZDDP (C) and S-containing antiwear additive solutions. With the base oil alone, scuffing occurred after 5 minutes of rubbing, as shown in Figure 8.7[a)] and the test was terminated.

It can be seen that the Primary ZDDP (C) (Figure 8.7[b)]) rapidly forms a thick solid-like film on the rubbed ball, while the S-containing compounds form thinner (*e.g.* Methylene-bis-dialkyl-dithiocarbamate (C) and Mercaptobenzothiazole (C)) or even negligible tribofilms (*e.g.* both dimercaptothiadiazoles, DMTDA1 and DMTDA2). It appears as though the film formed by 2-isobutylthiazole is removed by rubbing, whereas the change in contact shape observed in the presence of dibenzyl disulphide and Sulphurised fatty acid ester (C) might be due to wear.

The remaining organosulphur compounds do not seem to sufficiently protect the surface and thus scuffing is observed at high sliding. Because of that these additives were not further investigated.

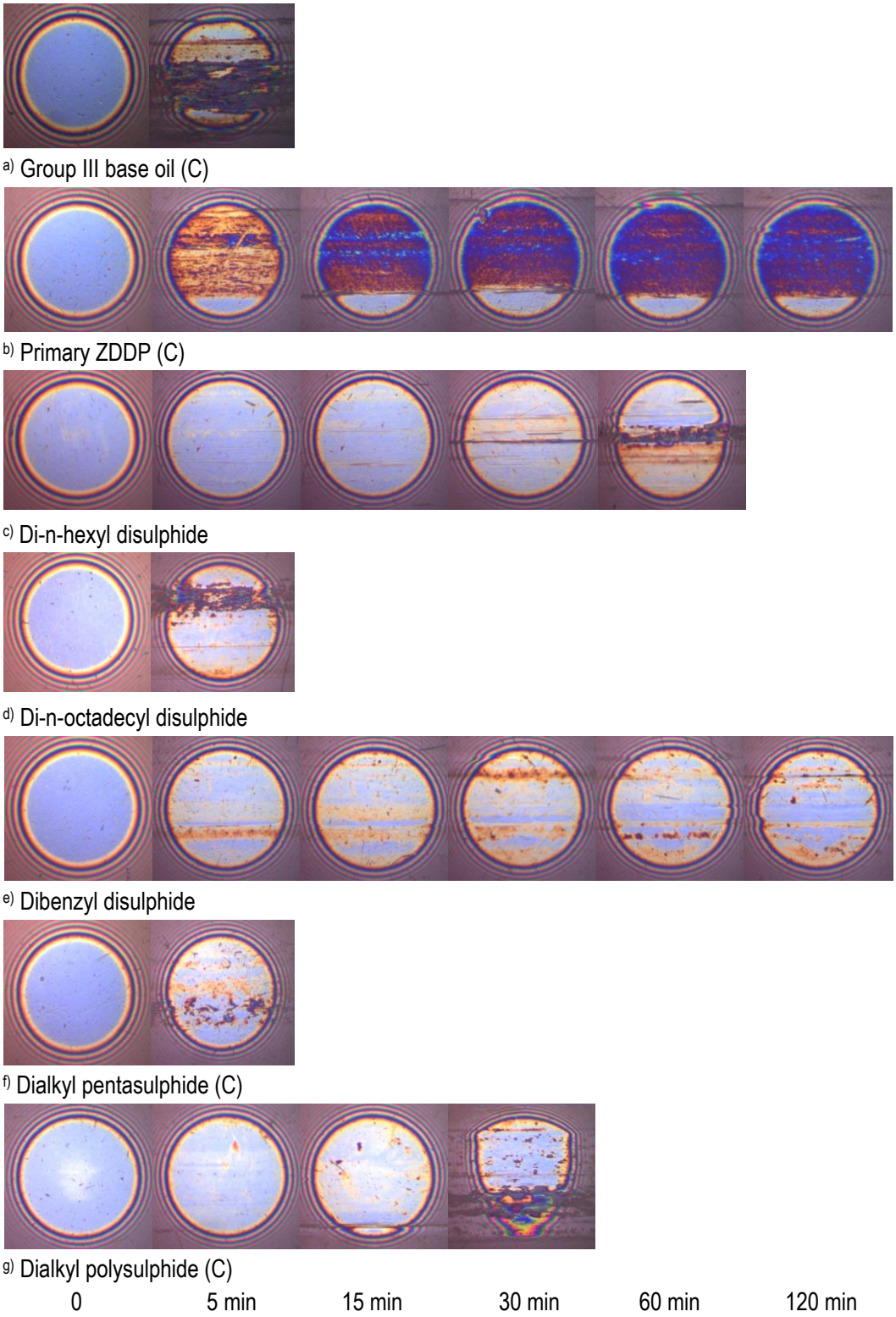
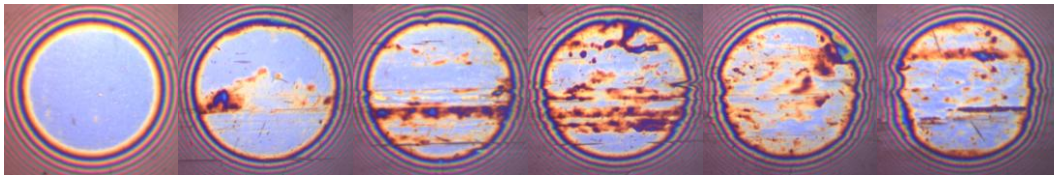
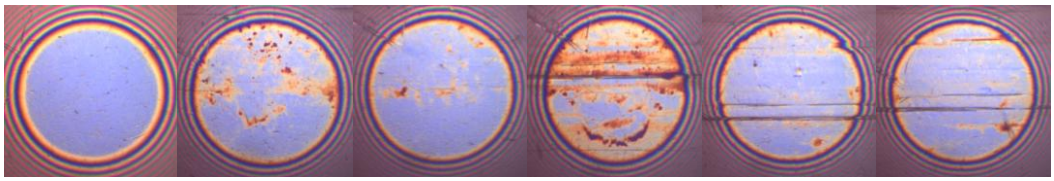


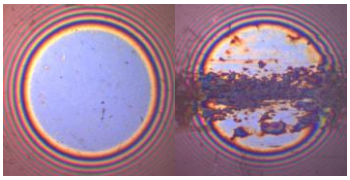
Figure 8.7: MTM-SLIM images showing: a) scuffing on the surface of the ball after 5 minutes of rubbing in base oil without antiwear additive; b) to g) the growth of tribofilm on the ball with increasing rubbing time (*i.e.* zero, 5, 15, 30, 60, 120 minutes).



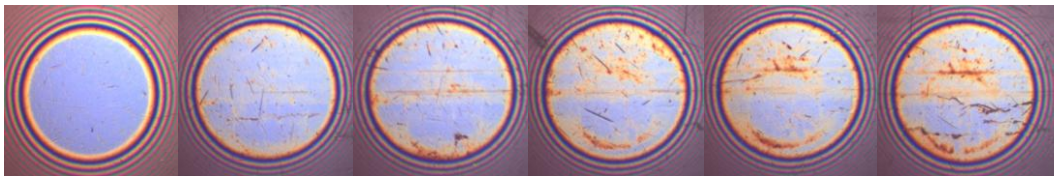
h) Sulphurised fatty acid ester (C)



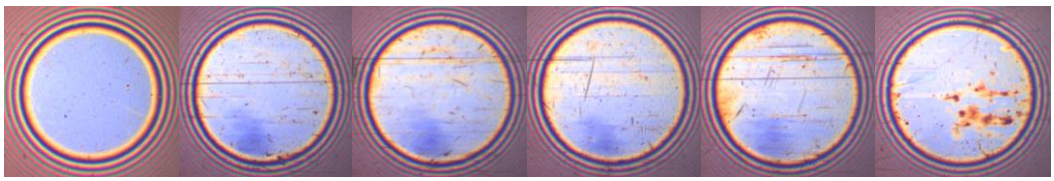
i) 2-Isobutylthiazole



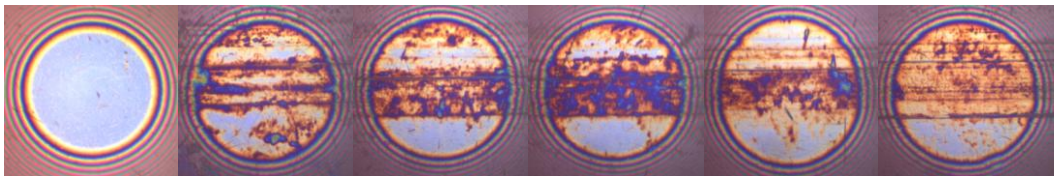
j) 2,5-Dimethyl-1,3,4-thiadiazole



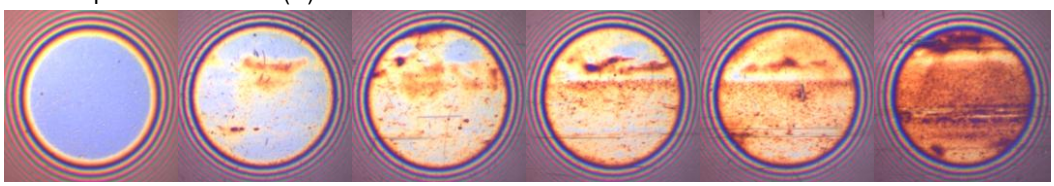
k) Dimercaptothiadiazole 1 (C)



l) Dimercaptothiadiazole 2 (C)



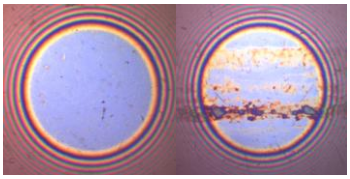
m) Mercaptobenzothiazole (C)



n) Methylene-bis-dialkyl-dithiocarbamate (C)

0 5 min 15 min 30 min 60 min 120 min

Figure 8.7 (continued): MTM-SLIM images showing: h) to n) the growth of tribofilm on the ball with increasing rubbing time (*i.e.* zero, 5, 15, 30, 60, 120 minutes).



o) Methylene-bis-dibutyl-dithiocarbamate (C)

0 5 min 15 min 30 min 60 min 120 min

Figure 8.7 (continued): MTM-SLIM images showing: o) the growth of tribofilm on the ball with increasing rubbing time (*i.e.* zero, 5, 15, 30, 60, 120 minutes).

Figure 8.8 compares the development of mean film thickness with rubbing time for Primary ZDDP (C) and S-containing-derived tribofilms. It can be seen that the primary ZDDP reacts rapidly on the surface, developing a thick film (*i.e.* ≈ 140 nm after 120 minutes of rubbing), while the S-containing compounds form thinner (*i.e.* ≈ 70 nm after 120 minutes of rubbing for Methylene-bis-dialkyl-dithiocarbamate (C)) or even negligible tribofilms (*i.e.* ≈ 20 nm after 120 minutes of rubbing for both dimercaptothiadiazoles, DMTDA1 and DMTDA2).

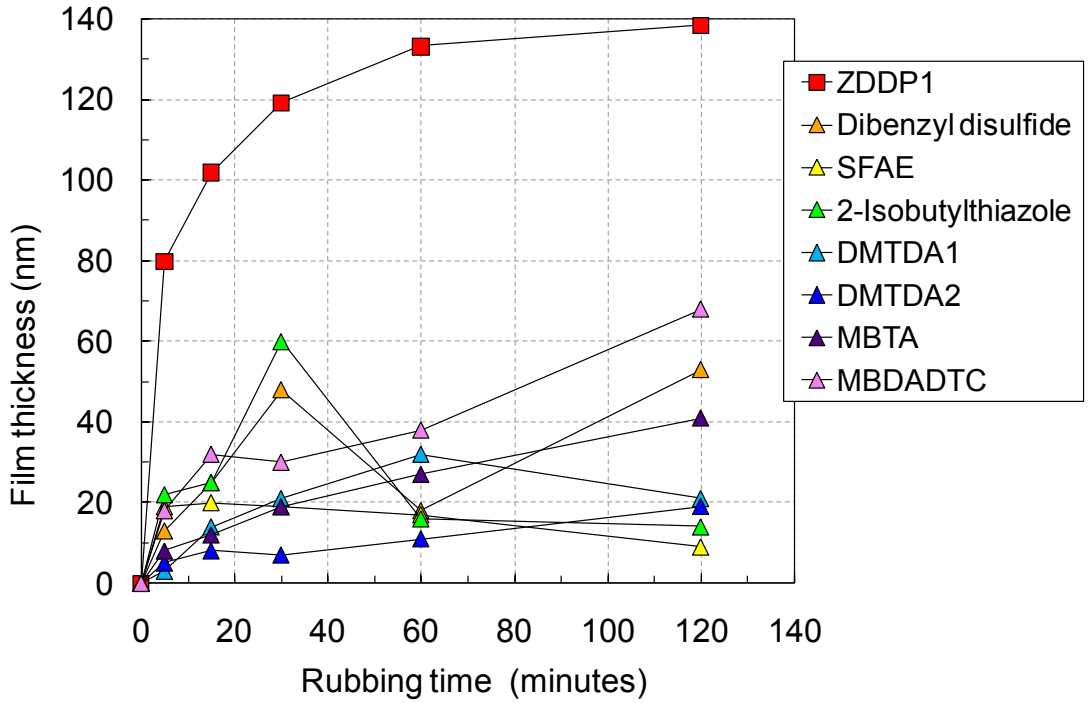


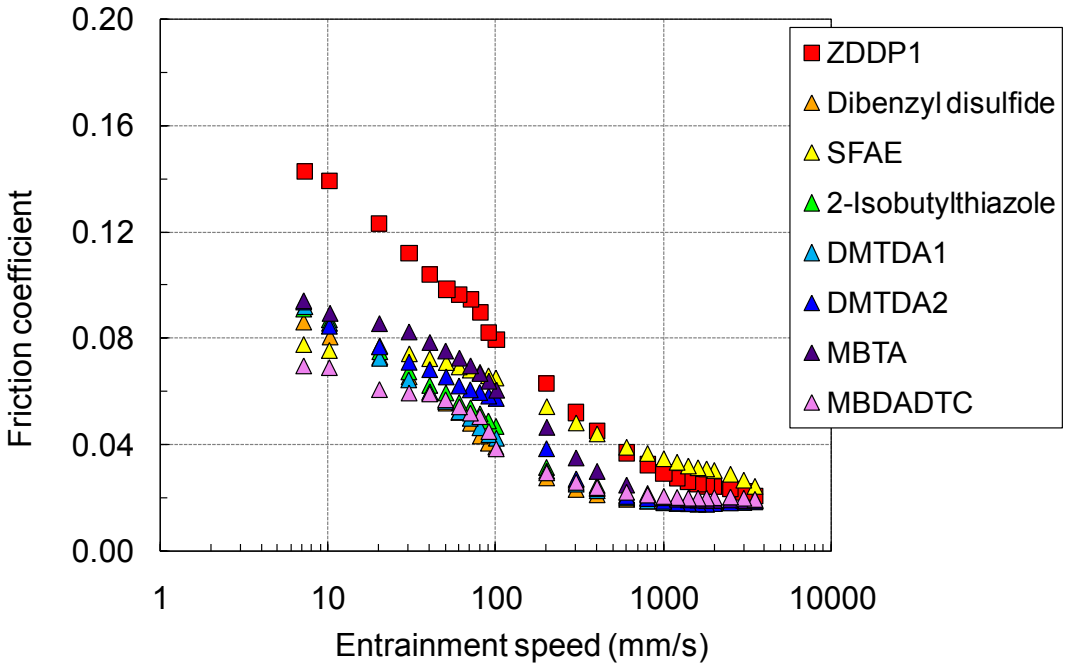
Figure 8.8: Mean film thickness with rubbing time for S-containing antiwear additives.

8.3 Results: Friction properties of S-containing Antiwear Additive-derived Tribofilm

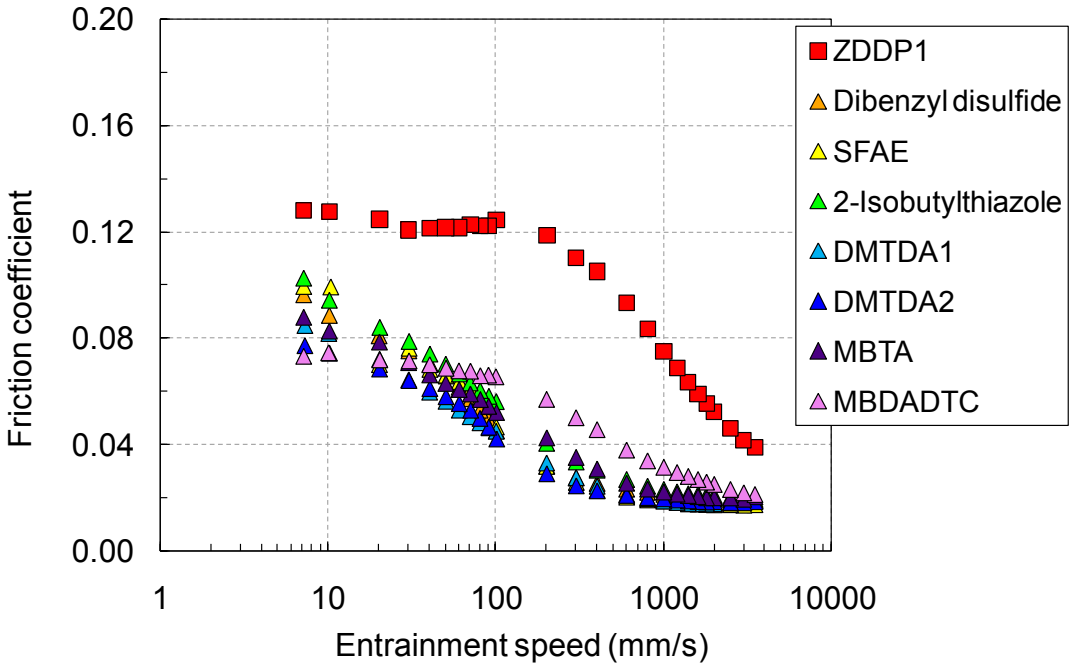
The friction properties of a range of S-containing antiwear additives were studied using the MTM under mixed rolling/sliding conditions, as described in chapter 4, section 4.1. The Stribeck curve (Figure 8.9) shows the friction coefficient *versus* entrainment speed for these additives at the beginning and after 2 h of rubbing.

As discussed in section 5.3 of chapter 5, there is a significant increase in mixed friction for Primary ZDDP (C) once the protective film forms on the surface, shifting the curve to the right after 2h of rubbing. This increase in mixed friction is probably due to the change in surface texture as a result of the development of a thick solid-like film on the surface (Figure 8.7[b)]). A slight increase in mixed friction is observed for Methylene-bis-dialkyl-dithiocarbamate (C) solution, which can be ascribed to film formation. It is noteworthy that the film formed by Mercaptobenzothiazole (C), shows no significant shift in mixed friction throughout the test. This suggests that this additive may form a smooth, low shear strength film on the surface.

Overall very low boundary friction was observed, with no significant variation throughout the test.



Initial friction, measured at the beginning of the test



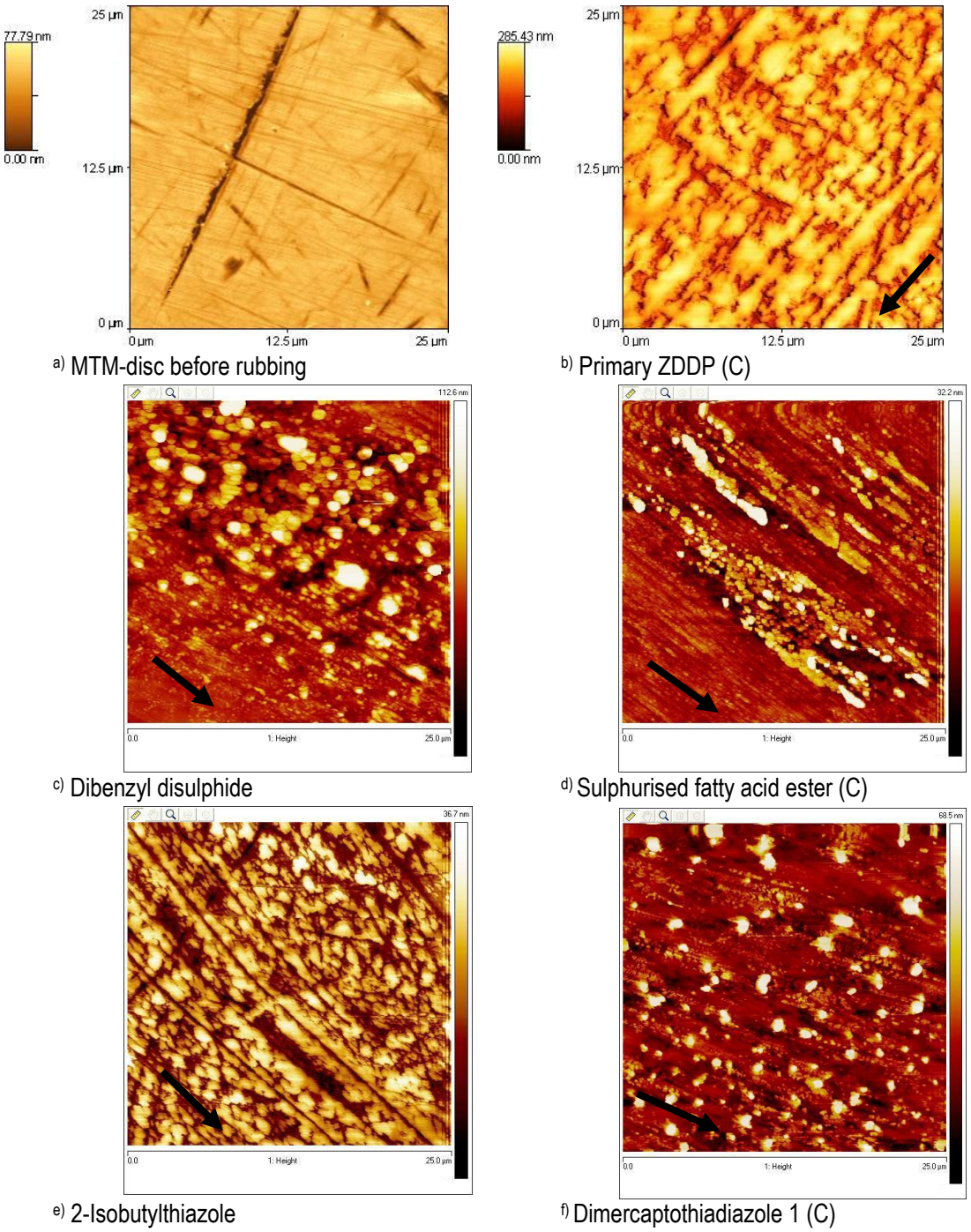
Friction after 2 h of rubbing

Figure 8.9: Stribeck curve showing friction coefficient *versus* entrainment speed at the beginning and after 2 h of rubbing at 50 % SRR, 30 N and 100 ºC.

8.4 Results: Morphology of S-containing Antiwear Additive-derived Tribofilms

The morphology of S-containing antiwear additive reaction films generated on AISI 52100 steel discs using the MTM, was studied by AFM, as described in chapter 4, section 4.2. An area of 25 µm x 25 µm in the centre of the wear track was scanned and the topography of the tribofilms is shown in Figure 8.10. Figure 8.10[a)] shows the topography of MTM-discs prior to rubbing.

It can be seen that the morphology of the tribofilms is strongly oriented along the sliding direction, represented by the arrow. Topography study reveals that some S-containing antiwear additive-derived tribofilms are quite patchy in nature, *i.e.* Dibenzyl disulphide, Sulphurised fatty acid ester (C), Dimercaptothiadiazole 1 (C) and Mercaptobenzothiazole (C). The films formed by 2-Isobutylthiazole and Dimercaptothiadiazole 2 (C) consist of discrete pads randomly-distributed along the sliding direction, similar to ZDDP. Conversely, the film formed by Methylene-bis-dialkyl-dithiocarbamate (C) comprises quite large pads.



a) MTM-disc before rubbing

b) Primary ZDDP (C)

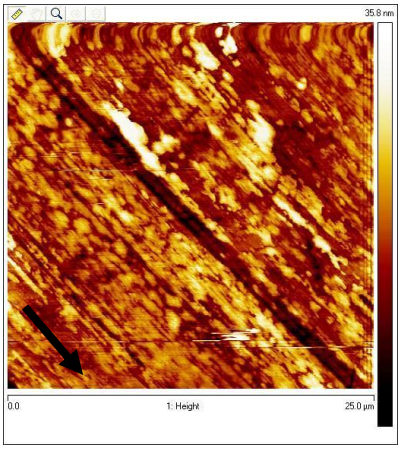
c) Dibenzyl disulphide

d) Sulphurised fatty acid ester (C)

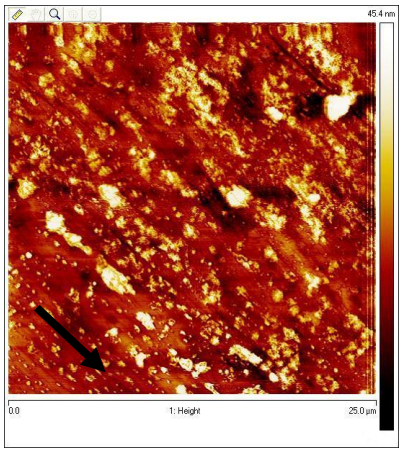
e) 2-Isobutylthiazole

f) Dimercaptothiadiazole 1 (C)

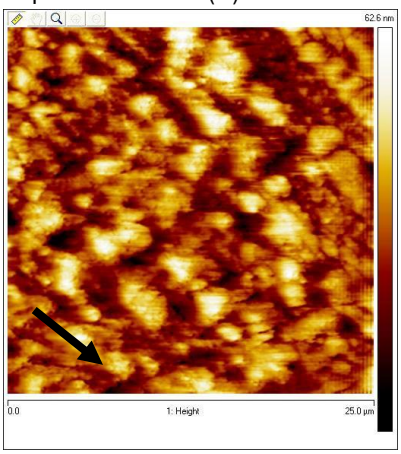
Figure 8.10: AFM 2D topography image at the centre of the wear track on the MTM-disc (sliding direction in b) to f) shown by the arrow).



g) Dimercaptothiadiazole 2 (C)



h) Mercaptobenzothiazole (C)



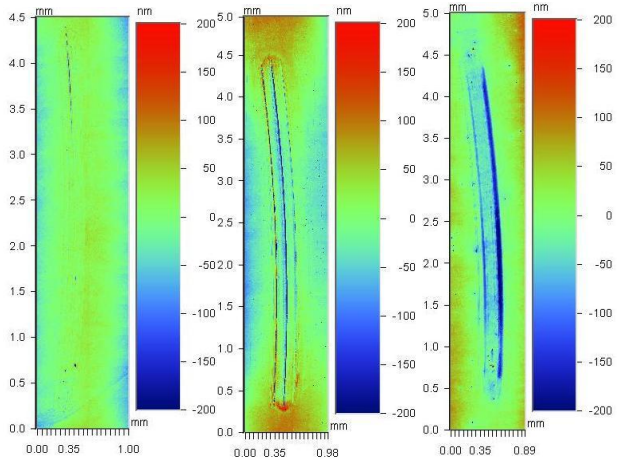
i) Methylene-bis-dialkyl-dithiocarbamate (C)

Figure 8.10 (continued): AFM 2D topography image at the centre of the wear track on the MTM-disc (sliding direction in g) to i) shown by the arrow).

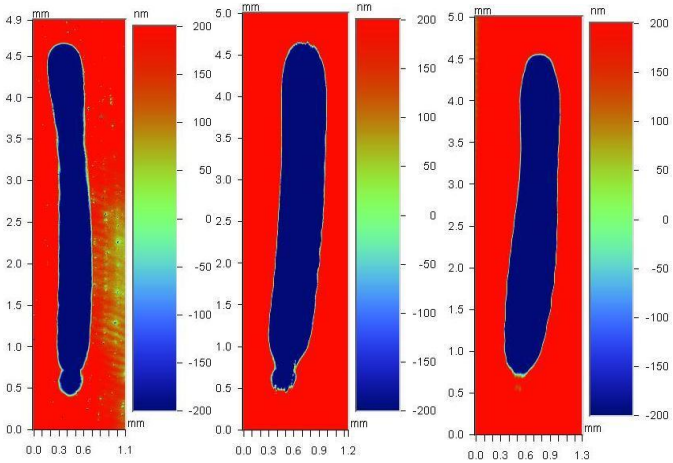
8.5 Results: Wear-reducing Properties of S-containing Antiwear Additive-derived Tribofilms

The wear-reducing properties of three S-containing antiwear additives, Dimercaptothiadiazole 1 (C), Dimercaptothiadiazole 2 (C) and Methylene-bis-dialkyl-dithiocarbamate (C) were studied using the method developed by the author, which combines the MTM-Reciprocating rig to generate the wear track on AISI 52100 steel discs with the SWLI to image the track and measure wear depth, as described in chapter 4, sections 4.3 and 4.4.

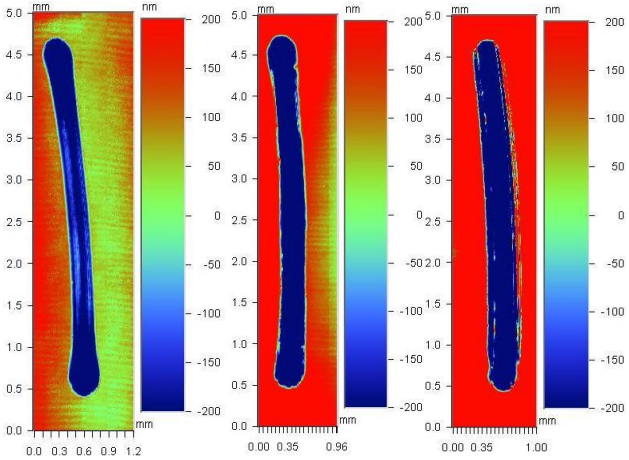
The topography images, shown in Figure 8.11, reveal a considerable increase in the width of the wear track with increasing rubbing time for Methylene-bis-dialkyl-dithiocarbamate (C). The same effect is not observed for the dimercaptothiadiazoles, DMTDA1 and DMTDA2, although these also show relatively high levels of wear (*i.e.* higher than ZDDP).



Primary ZDDP (C): 4, 8 and 16 hours after EDTA.

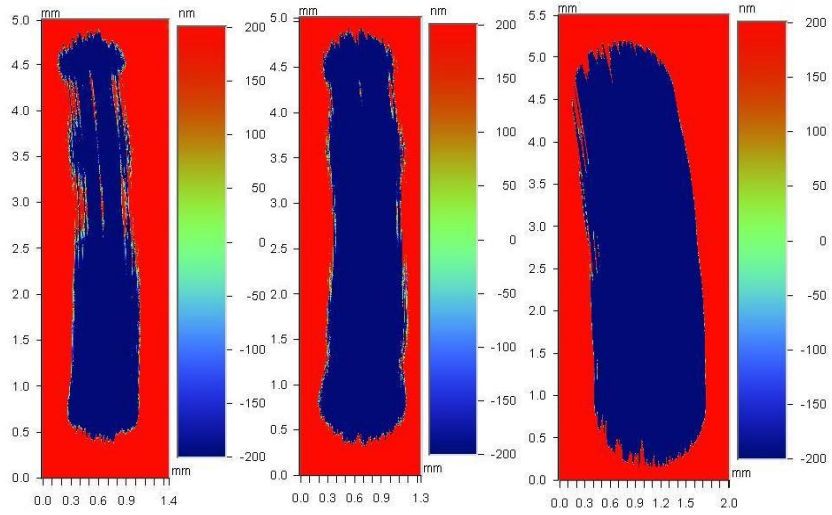


Dimercaptothiadiazole 1 (C): 4, 8 and 16 hours after EDTA.



Dimercaptothiadiazole 2 (C): 4, 8 and 16 hours after EDTA.

Figure 8.11: SWLI 2D topography images of the wear track on the disc.



Methylene-bis-dialkyl-dithiocarbamate (C): 4, 8 and 16 hours after EDTA.

Figure 8.11 (continued): SWLI 2D topography images of the wear track on the disc after 4, 8 and 16 h rubbing.

Figure 7.12 illustrates the wear coefficient (k_1) calculated using wear depth measurements taken in the middle (M) and at the ends (E) of the wear track (*i.e.* average of both ends) for tests lasting 4, 8 and 16 hours. The results show that the S-containing antiwear additives investigated in this study do not perform as well as ZDDP. The wear coefficient results (k_1) vary between 10^{-7} to 10^{-8} mm^3/Nm, which also indicate that these additives are slightly out of mild wear range, *i.e.* 10^{-8} to 10^{-12} mm^3/Nm [61].

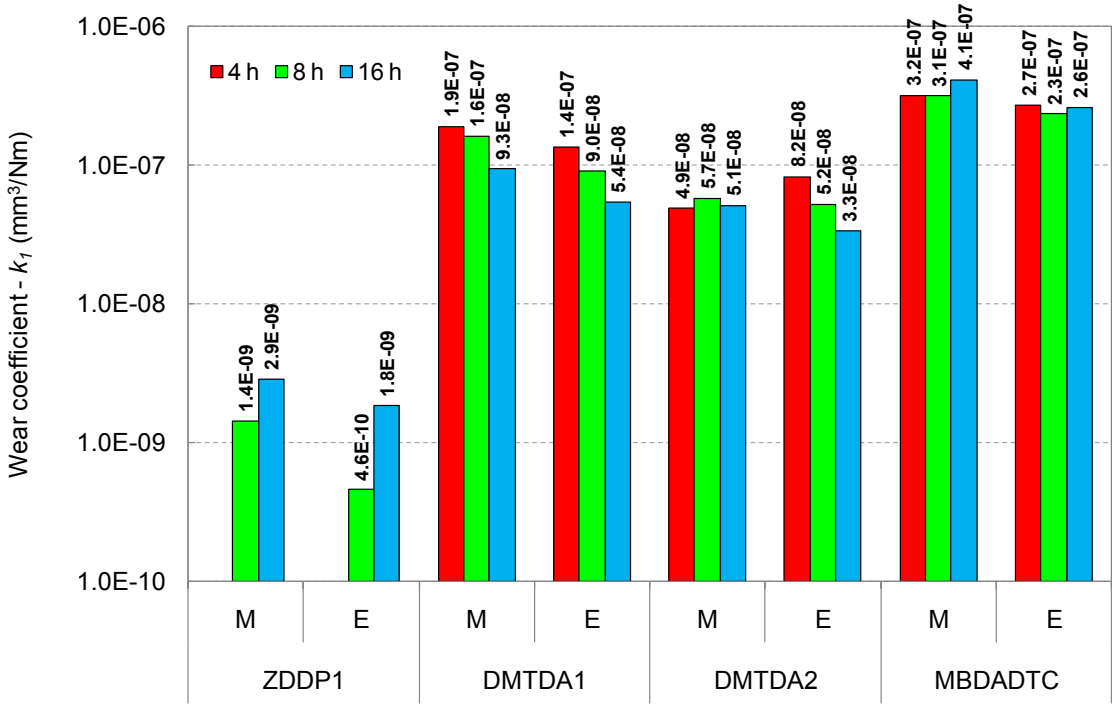


Figure 8.12: Wear coefficient (k_1) in the middle (M) and at the ends (E) of the wear track (*i.e.* average of both ends) for tests lasting 4, 8 and 16 hours.

8.6 Discussion of S-containing Antiwear Additives Work

The film-forming study under mixed rolling/sliding conditions using MTM-SLIM shows that while Primary ZDDP (C) rapidly reacts to form a thick reaction film of *ca.* 140 nm, S-containing compounds form thinner (up to ≈ 70 nm) or even negligible tribofilms on the surface. Apart from Dibenzyl disulphide solution, scuffing was observed in the presence of most sulphides, *i.e.* medium-, long-chain disulphides, penta- and polysulphides. This might be attributed to their high reactivity towards the surface, which yields corrosive wear.

Assuming that both dithiocarbamate additives, *i.e.* Methylene-bis-dialkyl-dithiocarbamate (C) and Methylene-bis-dibutyl-dithiocarbamate (C), are pure additives and taking into account their sulphur content, *i.e.* ≈ 30 %S; it can be estimated that the alkyl chain length of the R substituent group attached to nitrogen is the same for both, *i.e.* butyl. Although it appears that both dithiocarbamate additives are the same compound, *i.e.* methylene-bis-dibutyl-dithiocarbamate, it is noteworthy that their film-forming properties are significantly different, with Methylene-bis-dialkyl-dithiocarbamate (C) forming a thick uniform film on the surface, while scuffing is observed after 5 minutes of rubbing with Methylene-bis-dibutyl-dithiocarbamate (C) solution. The latter might be due to impurities or sub-species which prevent film formation.

Friction behaviour study by MTM shows that there is a slight increase in mixed friction for Methylene-bis-dialkyl-dithiocarbamate (C), which can be ascribed to film formation. Alternatively the film formed by Mercaptobenzothiazole (C), shows no significant shift in mixed friction throughout the test, which is quite surprising given the patchy nature of the protective film. Overall very low boundary friction was observed, with no significant variation throughout the test.

Topography study of the tribofilms formed by S-containing compounds revealed distinct morphological features, such as large pads with Methylene-bis-dialkyl-dithiocarbamate (C); discrete pads similar to ZDDP with Dimercaptothiadiazole 2 (C) and 2-Isobutylthiazole; and patchy films formed by Dimercaptothiadiazole 1 (C) solution.

This study has also demonstrated the wear-reducing properties of S-containing antiwear additives using the reciprocating MTM. It was found that the S-containing antiwear additives investigated in this study do not perform as well as ZDDP. The wear coefficient results (k_1) vary between 10^{-7} to 10^{-8} mm^3/Nm, which also indicate that these additives are slightly out of mild wear range, *i.e.* 10^{-8} to 10^{-12} mm^3/Nm [61].

In addition, there is a considerable increase in the width of the wear track with increasing rubbing time for Methylene-bis-dialkyl-dithiocarbamate (C), which is quite surprising given that this additive formed a relatively thick uniform protective film on the surface. This indicates that thick boundary film formation does not guarantee antiwear effectiveness.

Although both dimercaptothiadiazoles, *i.e.* DMTDA1 and DMTDA2 also show relatively high levels of wear (*i.e.* higher than ZDDP), there is a decrease in wear rate with increasing rubbing time, probably because of running-in wear. The higher levels of wear observed in the presence of organosulphur compounds can be ascribed to their corrosive nature. It is suggested that iron is initially removed from the surface to form FeS film. This film is continuously removed by rubbing and replenished with the removal of additional iron from the surface, which in turn yields corrosive wear.

9. FILM-FORMING, FRICTION, MORPHOLOGY AND WEAR-REDUCING PROPERTIES OF M-CONTAINING ANTIWEAR ADDITIVES

This chapter first provides an overview of previous research on the film-forming and wear properties of metal-containing antiwear additives, such as organometallic compounds, where M = Ti, Pb, Cd, Sn and Fe, metal organophosphates, where M = Zn, metal organothiophosphates, where M= Pb and Cd, and metal dithiocarbamates, M = Zn, Mo, Cu, Ce, Pb, Sb and Bi.

The chapter then describes film thickness, friction, surface topography and wear measurements carried out on a range of metal-containing antiwear additive solutions, using the methods outlined in chapter 4.

Some surface analyses of the films formed by M-containing antiwear additives were also carried out using ToF-SIMS and XANES but these are deferred to chapter 13, where analysis of the films formed by various additives of interest are presented and discussed together.

9.1 Literature Overview of M-containing Antiwear Additives

Metal-containing antiwear additives, such as organotitanate derivatives were first introduced in the formulation of military and commercial turbine engine oils in the 1950s [232]. Soon afterwards the use of S-containing organotitanates as high temperature additives was patented [233]. More recently, the use of titanium-containing chemistries as antiwear additives was revisited by Guevremont *et al.* [234]. It was reported that Ti-containing additives offered good wear-reducing properties, while controlling friction. Further analysis of the wear track by AES, SIMS, XPS and XANES suggested the formation of a Fe/Ti protective film.

Although lead naphthenate is not suitable for the formulation of crankcase lubricants, this additive has been successfully employed as antiwear and extreme pressure additive in spacecraft mechanisms [235, 236]. It has been suggested that this additive is chemisorbed onto the surface to improve wear-reducing properties, while metallic Pb improves extreme pressure properties under high loads. Similar behaviour was observed by Buckley who reported that organocadmium-containing additives also decomposed under rubbing to form free metal [237].

It was also reported that organotin-containing compounds show good wear-reducing properties [238, 239]. Lashki *et al.* ascribed the wear-reducing properties of this class of additives to the strong adsorptive power of the oxygen in the Sn-O bond, which favours reaction with the surface and thus the formation of a protective film [240].

Kajdas *et al.* investigated the four-ball wear of ferrocenyl alcohols and ferrocenyl sulphides. It was reported that ferrocenyl alcohols were superior to ferrocenyl sulphides at low loads [241]. The authors proposed that this class of additives reduced wear by means of a carbonium ion/steel surface interaction.

The use of metal organophosphates as antiwear additives was patented before their thiophosphate equivalents [242, 243]. Nevertheless, it was not until recently that the wear-reducing properties of these additives have been revisited, mainly because of the widespread use of thiophosphates, particularly ZDDP and its multifunctional applications, *i.e.* antiwear, extreme pressure, antioxidant and corrosion inhibitor. Dorinson investigated the antiwear properties of zinc di-n-butylphosphates. The authors reported that this additive gave performance comparable to its ZDDP equivalent [244].

Yagashita *et al.* patented the use of zinc dialkylphosphate derivatives in the formulation of engine oils [245]. This class of additives are quite promising for two reasons: (i) the need to reduce the amount of sulphur in the lubricating oil and (ii) also because they are weaker peroxide-decomposing antioxidants than corresponding dithiophosphates, which in turn limits their consumption by reaction with peroxides and thus reduces the amount of additive required.

More recently, Hoshino *et al.* investigated the influence of alkyl-substituent groups on the film-forming, friction and HFRR (high frequency reciprocating rig) wear properties of a range of sulphur-free zinc dialkylphosphates, also known as ZDPs (Figure 9.1) [246]. Overall, it was observed that zinc dialkylphosphate-derivatives form films slower and thinner than corresponding ZDDPs, regardless of their alkyl chain. This was ascribed to ZDP molecules being more stable than ZDDP molecules, which retard additive decomposition and thus the formation of a protective film on the surface. Comparable antiwear and friction properties were observed between primary ZDPs and ZDDP equivalents, while significant differences were seen between secondary ZDPs and corresponding ZDDPs. The authors suggested that secondary ZDP and ZDDP derivatives do not form stable adsorbed films on the surface because of the steric hindrance of the branched alkyl chains, and thus friction and wear-reducing properties are influenced mainly by the nature of reaction films formed.

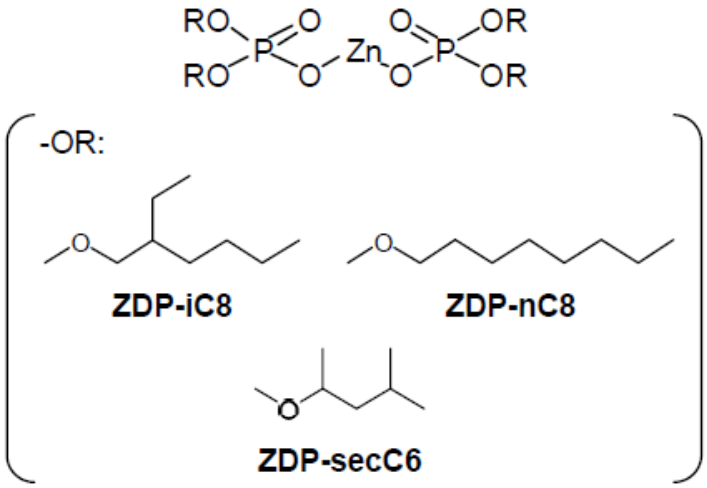


Figure 9.1: Molecular structures of sulphur-free zinc dialkylphosphates studied by Hoshino *et al.* [246].

Research on metal dithiophosphate derivatives based on metals other than zinc, *i.e.* MDDPs, where M = lead and cadmium, revealed that these additives, although damaging to the environment, give antiwear properties comparable to ZDDP [247-253]. It is noteworthy that most metal-containing dialkyldithiophosphate compounds have not been studied in fully formulated oils, and so the effect of nitrogen-based dispersants, which have an antagonistic effect on film formation in the presence of ZDDP [254]; and other engine oil additives, has not been measured. It has also been proposed that MDDPs where M is not zinc may be less damaging to the exhaust aftertreatment systems, due to their lower volatility [67, 255].

The antiwear properties of metal dithiocarbamates, *i.e.* MDTCs, where M = zinc, molybdenum, copper, cerium, lead, antimony and bismuth have also been the subject of considerable research [121, 256-261].

Tuli *et al.* investigated the four-ball wear of metal-containing isoamyl dithiocarbamate derivates. The authors found that heavier metals showed superior antiwear properties to lighter ones, with effectiveness in the order: Pb > Bi > Sb > Zn > Mo [262]. The same method was employed by Verma *et al.* to explore the wear-reducing properties of zinc alkyl and aryl dithiocarbamates [256]. Similar levels of wear protection were reported, with the formation of thick protective films at lower loads and thinner films at higher loads. Taylor *et al.* used MTM-SLIM to investigate the film-forming properties of zinc dithiocarbamate [134]. It was found that this additive formed a thick, *i.e.* ≈ 200 nm, non-uniform deposit inside/outside the wear track. Further HFRR wear study carried out by the author revealed that this additive has no beneficial effect on wear, showing inferior performance than the base stock alone.

Molybdenum dithiocarbamates, also known as MoDTC, were first introduced as antioxidants and extreme pressure additives [162, 263]. Sakurai *et al.* showed that the pyrolysis of MoDTC yielded MoS_2, which gave good wear-reducing and extreme pressure properties in greases [264]. More recently, it was also demonstrated that this group of additives decompose under rubbing to form MoS_2 nanoparticles (Figure 9.2) [265], which have low shear strength because of their layer lattice structure, hence their widespread application as friction modifier additives. Although MoDTC alone is very effective in reducing friction [266], in particular boundary friction [267], the presence of ZDDP improves its friction-reducing properties even further, suggesting a synergistic effect. It was also reported that MoDTC solutions considerably improved the friction and wear characteristics of a series of alloy steels [268, 269].

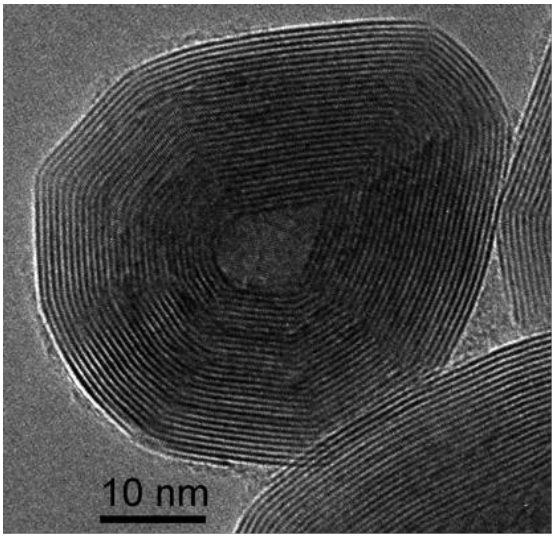


Figure 9.2: High resolution TEM image of MoS_2 nanoparticle [270]

Palacios studied the four-ball wear of antimony dithiocarbamate, *i.e.* SbDTC. It was found that SbDTC gives superior wear-reducing properties to ZnDTC, but not ZDDP. Subsequent analysis of the wear track using energy dispersive X-ray revealed the formation of a thick protective film of *ca.* 200 nm with SbDTC solution [121, 261].

Although it has been reported that some lead dithiocarbamate derivatives, *i.e.* phenyl lead dithiocarbamates and dithiocarbonates (xanthates), decompose to form PbS on the surface and thus give good extreme pressure properties under severe conditions [271], it was also found that this group of additives gives poor wear-reducing properties under mild conditions [260, 271]. The antiwear properties of cerium and copper dithiocarbamates have also been investigated. It was reported that both Ce- and CuDTC offer good wear and extreme pressure properties. Further analysis revealed that the former forms cerium oxides and sulphides, while the latter forms metallic copper on the rubbed surfaces [258, 259].

More recently, Yan *et al.* synthesised and investigated the tribological properties of a phosphorus- and sulphur-free organomolybdenum additive, namely N, N-bis (2-hydroxyethyl)-dodecanamide molybdate (NNDM) (Figure 9.3) [272]. The authors reported that this additive gave superior friction and wear-reducing properties to ZDDP. Subsequent surface analysis of the NNDM-derived tribofilm revealed the presence of long-chain alkylamide and molybdenum and iron oxides.

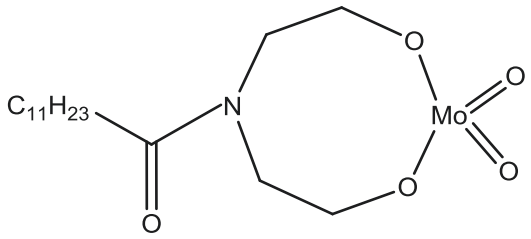


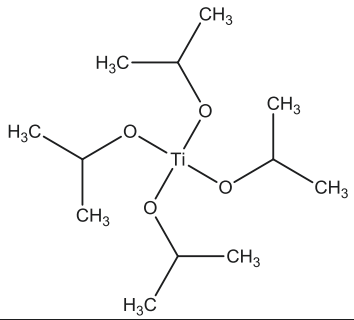
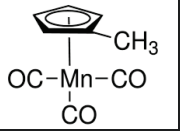
Figure 9.3: Molecular structure of the organomolybdenum additive studied by Yan *et al.* [272].

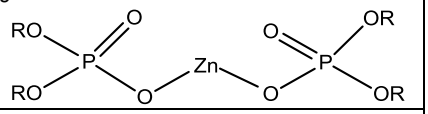
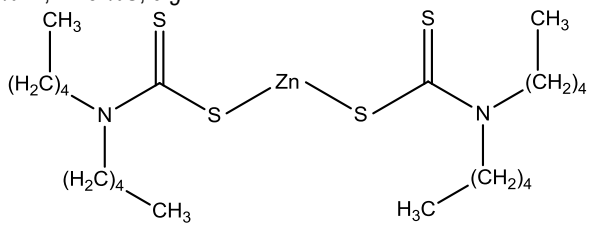
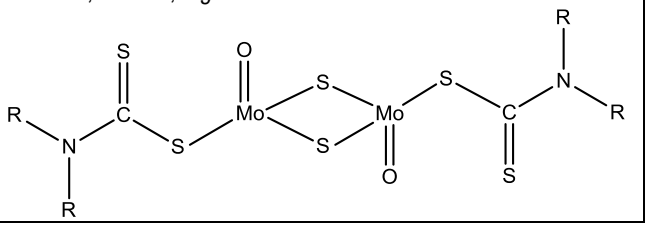
Overall it has been reported that some metal-containing additives give good antiwear, friction and extreme pressure properties, although some are not suitable for the formulation of crankcase lubricants. It appears that the most promising classes are zinc dialkylphosphates, *i.e.* ZDPs, and molybdenum dithiocarbamates, *i.e.* MoDTC, albeit limited results have been published on the wear-reducing properties of the latter.

9.2 Results: Film-forming Properties of M-containing Antiwear Additives

The film-forming properties of M-containing antiwear additives were studied using MTM-SLIM under mixed rolling/sliding conditions, as described in chapter 4, section 4.1. The additives employed in the study described in this chapter are summarised in Table 9.1. These were blended into Group III base oil (C) at a concentration of 900 ppm metal and submitted to rubbing under the same test conditions on the MTM-SLIM.

Table 9.1: Test materials summary: Metal-containing additives study

Abreviation	Sample name	Details
GIII BO	Group III base oil (C)	-
ZDDP1	Primary ZDDP (C)	9.5 %P; 20.0 %S; 10.6 %Zn
Ti-IPO	Titanium (IV) isopropoxide	*e.g.* 
MMT	(Methylcyclopentadienyl) manganese(I)tricarbonyl	*e.g.* 

ZP	Zinc alkylphosphate (C)	11.0 %Zn; 10.4 %P; *e.g.* 
ZnDTC	Zinc diamyl dithiocarbamate (C)	6.3 %Zn; 12.3 %S; *e.g.* 
MoDTC	Molybdenum dialkyldithiocarbamate (C)	4.5 %Mo; 5.0 %S; *e.g.* 

(C): commercially-available.

Figure 9.4 shows the growth of the tribofilm on the MTM-ball with increasing rubbing time (*i.e.* zero, 5, 15, 30, 60, 120 minutes) for the base oil, Primary ZDDP (C) and S-containing antiwear additive solutions. With the base oil alone, scuffing occurred after 5 minutes of rubbing, as shown in Figure 9.4[a)] and the test was terminated.

It can be seen that the Primary ZDDP (C) (Figure 9.4[b)]) rapidly forms a thick solid-like film on the rubbed ball, while some M-containing compounds form thinner (*e.g.* Zinc alkylphosphate (C)) or even negligible tribofilms (*e.g.* Zinc diamyl dithiocarbamate (C) and Molybdenum dialkyldithiocarbamate (C)). It is noteworthy that there is no visible damage to the rubbing contact in the presence of M-containing additives that form negligible films on the surface. Alternatively, it appears as though the film formed by MMT is removed by rubbing and the subsequent change in contact shape might be due to wear.

Titanium (IV) isopropoxide does not seem to adequately protect the surface and thus scuffing is observed after 5 minutes of rubbing. Because of that this additive was not further investigated.

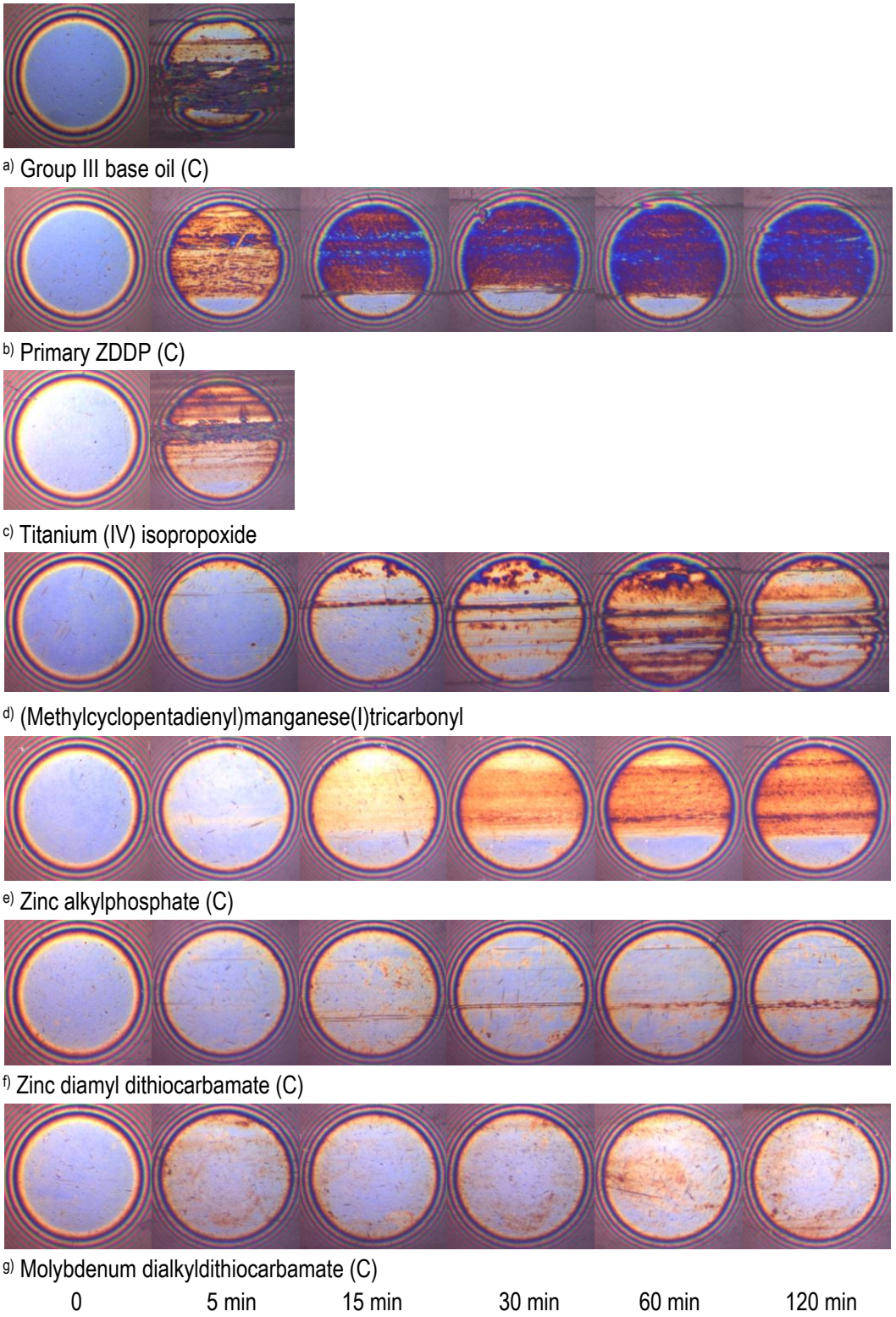


Figure 9.4: MTM-SLIM images showing: a) scuffing on the surface of the ball after 5 minutes of rubbing in base oil without antiwear additive; b) to g) the growth of tribofilm on the ball with increasing rubbing time (*i.e.* zero, 5, 15, 30, 60, 120 minutes).

Figure 9.5 compares the development of mean film thickness with rubbing time for Primary ZDDP (C) and M-containing-derived tribofilms. It can be seen that the Primary ZDDP (C) reacts rapidly on the surface, developing a thick film (*i.e.* ≈ 140 nm after 120 minutes of rubbing), while the M-containing additives form thinner (*i.e.* ≈ 60 nm after 120 minutes of rubbing for Zinc alkylphosphate (C) solution) or even negligible tribofilms (*i.e.* 10-20 nm after 120 minutes of rubbing for Zinc diamyl dithiocarbamate (C) and Molybdenum dialkyldithiocarbamate (C)).

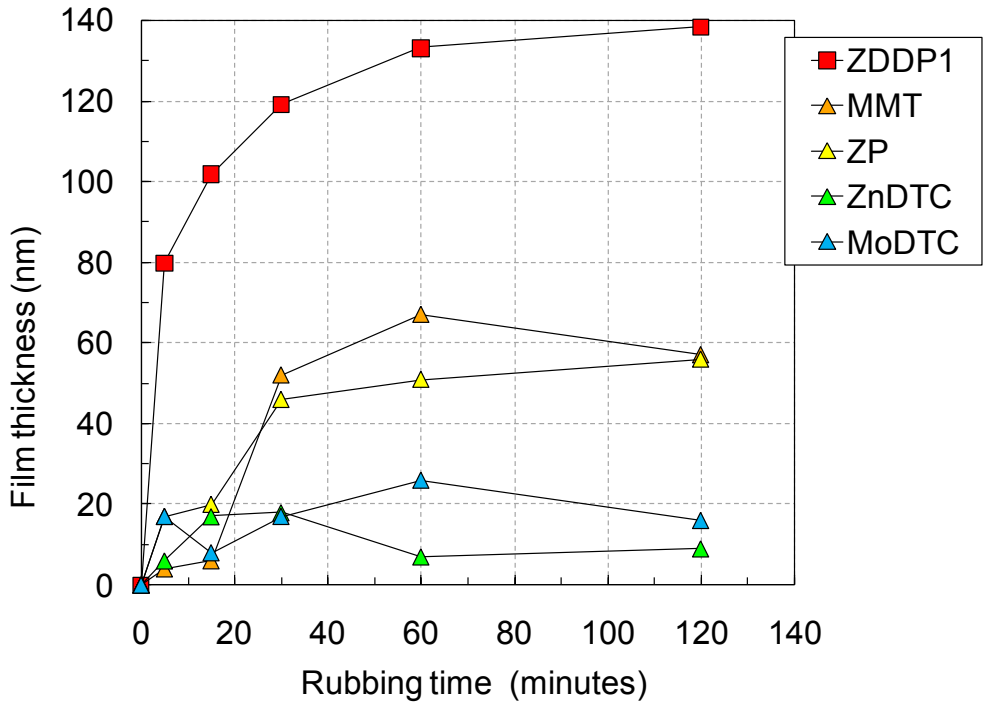


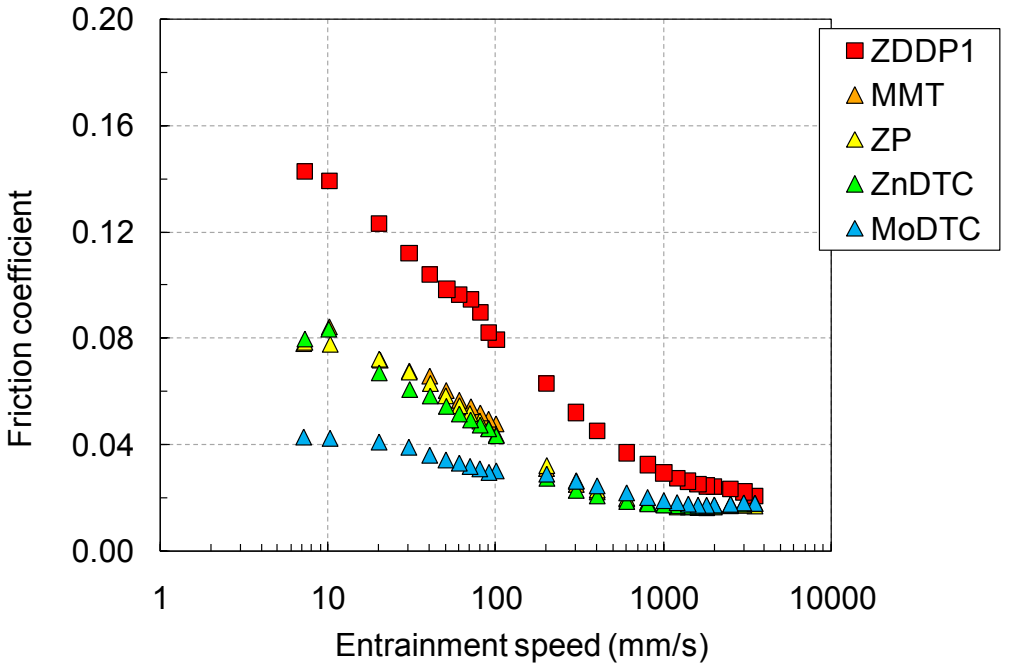
Figure 9.5: Mean film thickness with rubbing time for M-containing antiwear additives.

9.3 Results: Friction properties of M-containing Antiwear Additive-derived Tribofilm

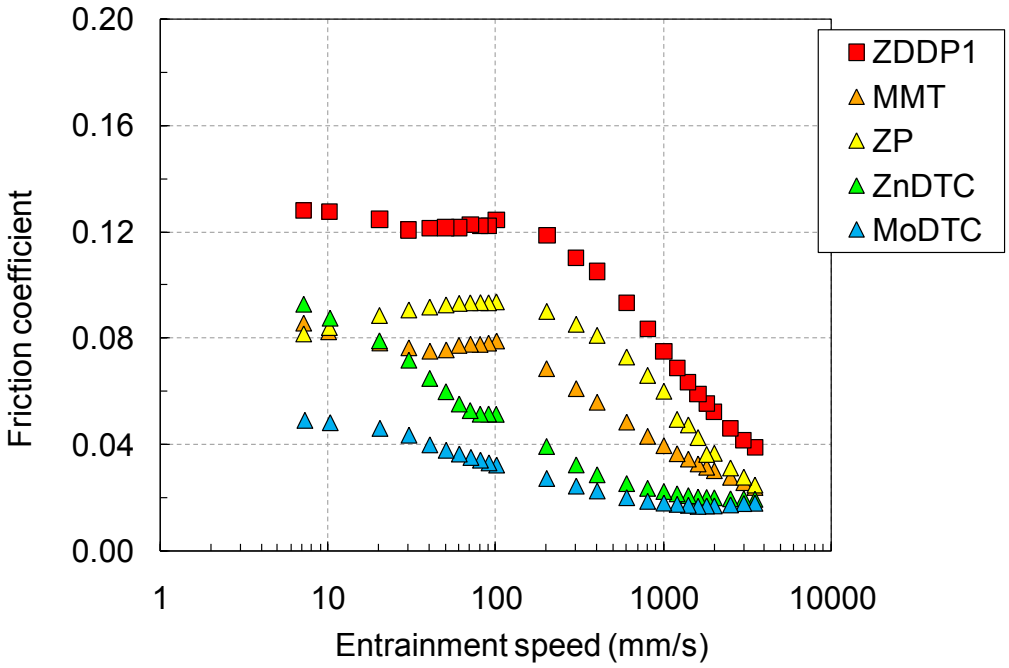
The friction properties of a range of M-containing antiwear additives were studied using the MTM under mixed rolling/sliding conditions, as described in chapter 4, section 4.1. The Stribeck curve (Figure 9.6) shows the friction coefficient *versus* entrainment speed for these additives at the beginning and after 2 h of rubbing.

These friction curves illustrate two different types of behaviour; (i) in some cases shifting of the curves to the right and (ii) changes in low speed boundary friction.

As discussed in section 5.3 of chapter 5, there is a significant increase in mixed friction for Primary ZDDP (C) once the protective film forms on the surface, shifting the curve to the right after 2h of rubbing. This increase in mixed friction is probably due to the change in surface texture as a result of the development of a thick solid-like film on the surface (Figure 9.4[b)]). A significant increase in mixed friction is also observed for Zinc alkylphosphate (C) and MMT solutions. The former can be ascribed to film formation, while the latter is possibly due to film formation or roughening of the surface caused by wear. Zinc diamyl dithiocarbamate (C), *i.e.* ZnDTC, shows a slight increase in mixed friction after two hours of rubbing, while Molybdenum dialkyldithiocarbamate (C), *i.e.* MoDTC, gives very low mixed and boundary friction both immediately and after two hours rubbing. A very slight increase in boundary friction is observed overall, except for ZDDP.



Initial friction, measured at the beginning of the test



Friction after 2 h of rubbing

Figure 9.6: Stribeck curve showing friction coefficient *versus* entrainment speed at the beginning and after 2 h of rubbing at 50 % SRR, 30 N and 100 ºC.

9.4 Results: Morphology of M-containing Antiwear Additive-derived Tribofilms

The morphology of M-containing antiwear additive reaction films generated on AISI 52100 steel discs using the MTM, was studied by AFM, as described in chapter 4, section 4.2. An area of 25 μm x 25 μm in the centre of the wear track was scanned and the topography of the tribofilms is shown in Figure 9.7. Figure 9.7[a)] shows the topography of MTM-discs prior to rubbing.

It can be seen that the morphology of the tribofilms is strongly oriented along the sliding direction, represented by the arrow. Topography study reveals that some M-containing antiwear additive-derived tribofilms consist of discrete pads randomly-distributed along the sliding direction, *i.e.* MMT and Zinc alkylphosphate (C), which are similar to ZDDP. Conversely, the negligible film formed by Zinc diamyl dithiocarbamate (C) comprises elongated pads, whereas no measurable MoS_2 film was observed in the surface rubbed with Molybdenum dialkyldithiocarbamate (C) solution.

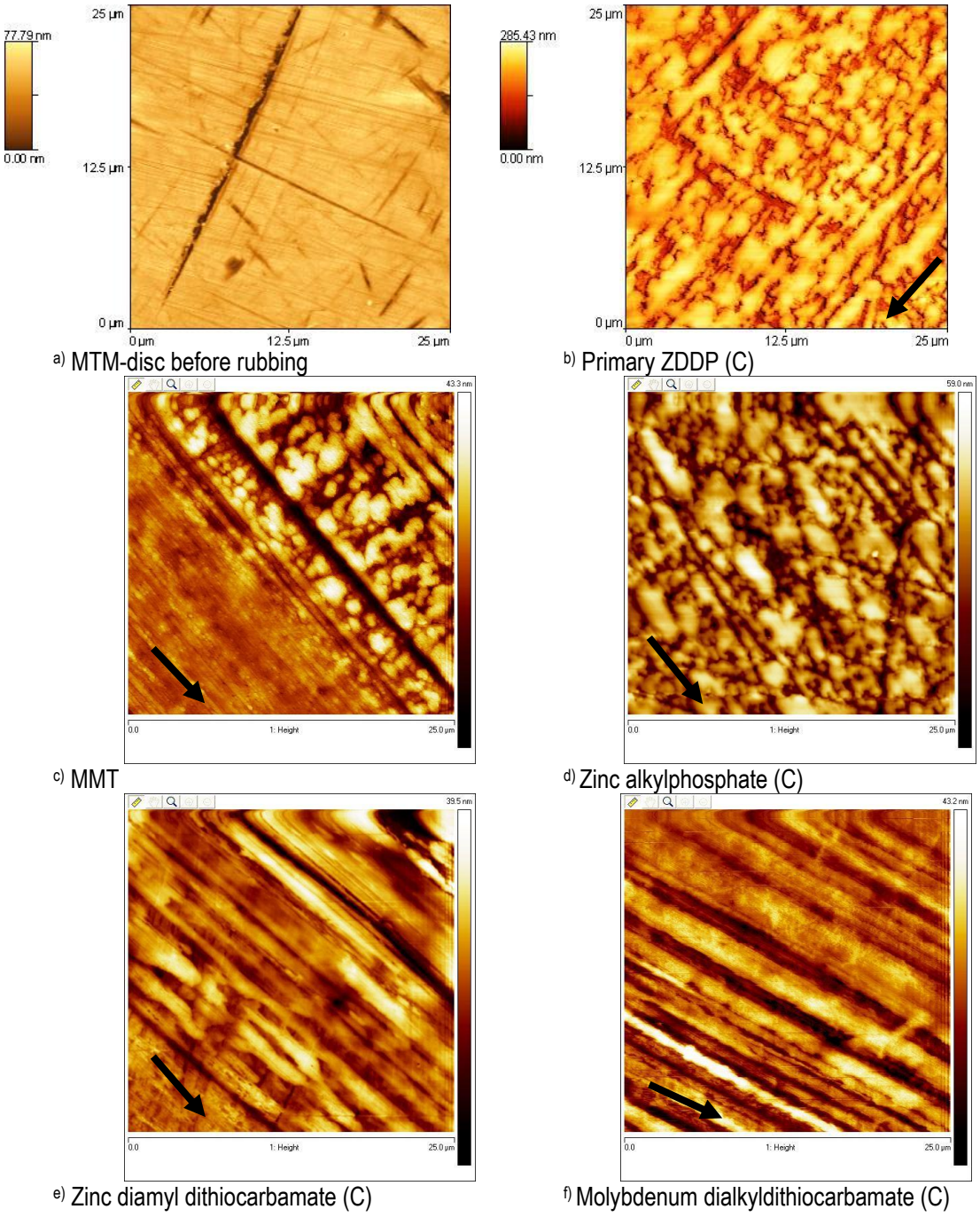


Figure 9.7: AFM 2D topography image at the centre of the wear track on the MTM-disc (sliding direction in b) to f) shown by the arrow).

Due to proprietary restrictions Zinc alkylphosphate (C), *i.e.* ZP, was not submitted to further analyses.

9.5 Results: Wear-reducing properties of M-containing Antiwear Additive-derived Tribofilms

The wear-reducing properties of three M-containing antiwear additives, MMT, Zinc diamyl dithiocarbamate (C) and Molybdenum dialkyldithiocarbamate (C), were studied using the method developed by the author, which combines the MTM-Reciprocating rig to generate the wear track on AISI 52100 steel discs with the SWLI to image the track and measure wear depth, as described in chapter 4, sections 4.3 and 4.4. Results are summarised in Figures 9.8 and 9.8.

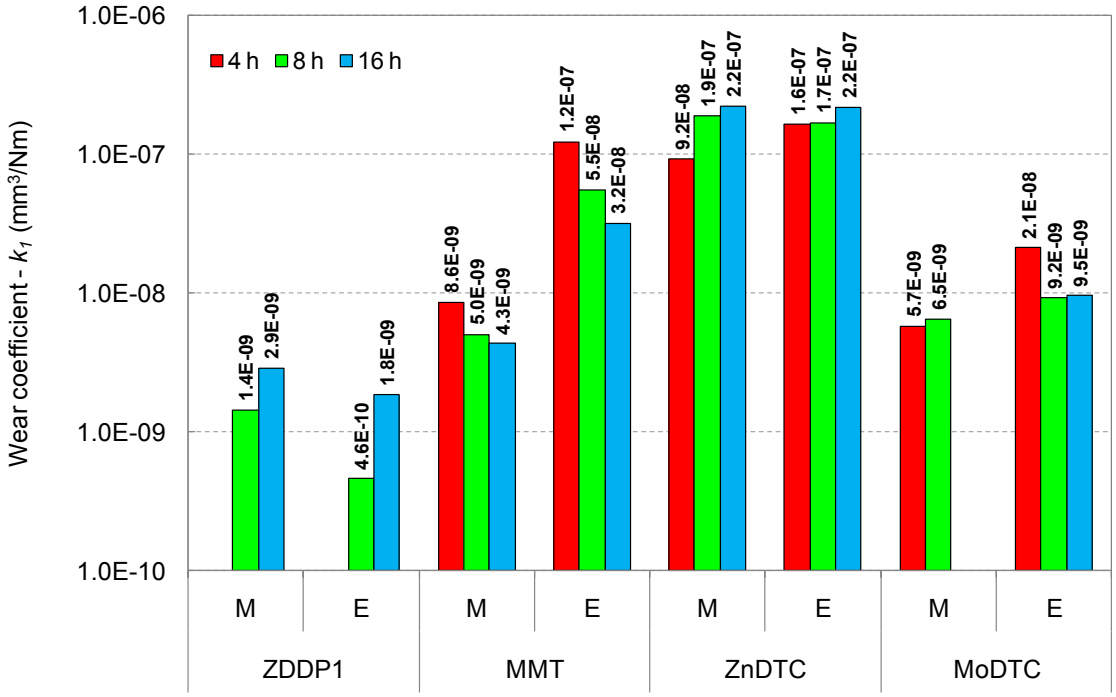
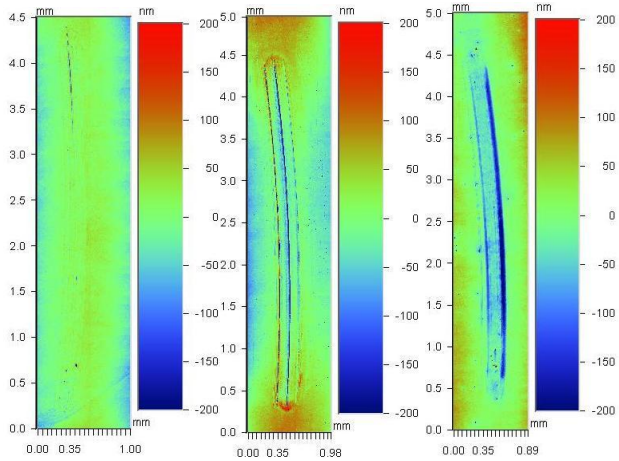
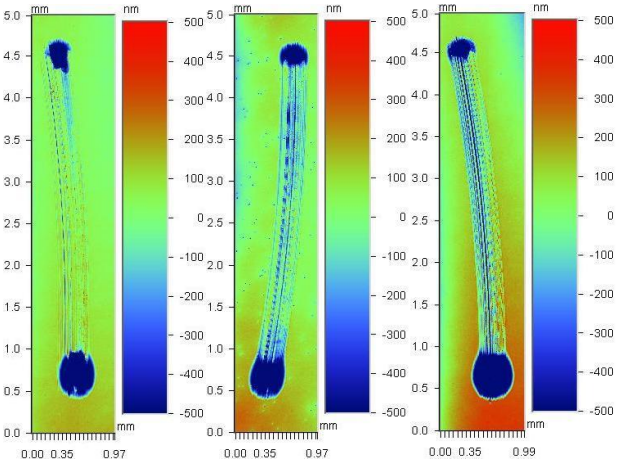


Figure 9.8: Wear coefficient (k_1) in the middle (M) and at the ends (E) of the wear track (*i.e.* average of both ends) for tests lasting 4, 8 and 16 hours.

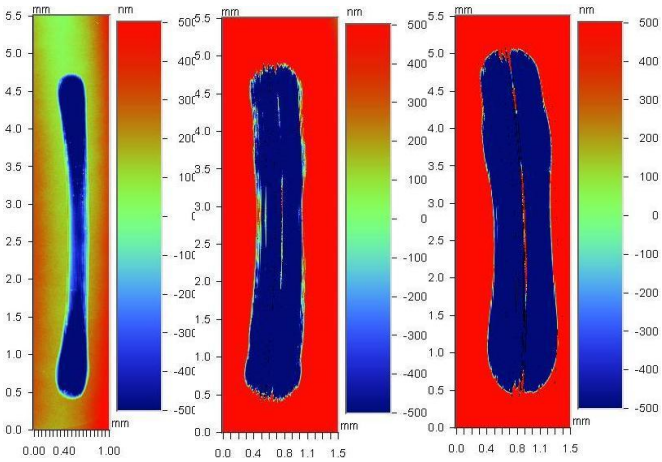
The results show that MoDTC, offer wear-reducing properties, comparable to ZDDP, with no measurable wear after 16 hours of rubbing, probably because of the development of a protective film during initial rubbing. In the presence of MMT, however, displacement of material is slightly more pronounced at the ends of the wear track, where disc speed is minimum because entrainment speed is changing direction; than in the middle of the wear track, where disc speed is maximum. The topography images, shown in Figure 9.9, reveal a considerable increase in the width of the wear track with increasing rubbing time for ZnDTC.



Primary ZDDP (C): 4, 8 and 16 hours after EDTA.

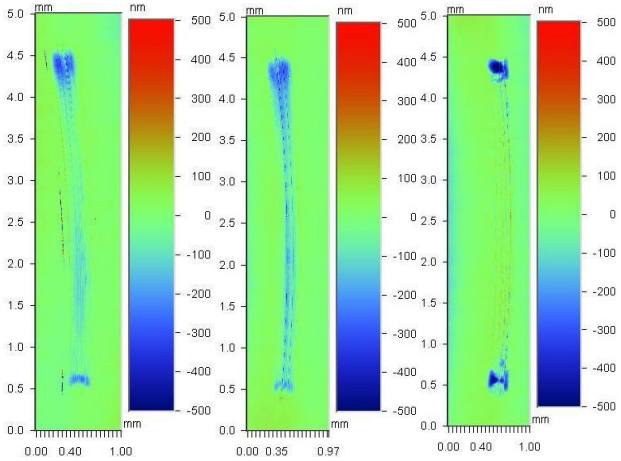


MMT: 4, 8 and 16 hours after EDTA.



Zinc diamyl dithiocarbamate (C): 4, 8 and 16 hours after EDTA.

Figure 9.9: SWLI 2D topography images of the wear track on the disc.



Molybdenum dialkyldithiocarbamate (C): 4, 8 and 16 hours after EDTA.

Figure 9.9 (continued): SWLI 2D topography images of the wear track on the disc.

9.6 Discussion of M-containing Antiwear Additives Work

This film-forming study under mixed rolling/sliding conditions using MTM-SLIM shows that M-containing compounds form thin (up to ≈ 60 nm for Zinc alkylphosphate (C)) or even negligible tribofilms on the surface. It is noteworthy that there is no visible damage to the rubbing contact in the presence of MoDTC, which forms a negligible film *ca.* 20 nm on the surface. This suggests that thick boundary film formation is not always required for effective wear reduction, which is also confirmed by wear testing.

The same behaviour, however, is not observed with ZnDTC, which also forms a negligible film *ca.* 10 nm. These results oppose those published by Taylor *et al.* in terms of film-forming properties, in which the authors reported that ZnDTC formed a very thick, *ca.* 200 nm, irregular deposit on the surface [134]. With regards to wear-reducing properties, however, the results found in this study are consistent with those found by the abovementioned author, who also observed that ZnDTC has no beneficial effect on wear.

Although, it appears that the film formed by MMT is removed by rubbing, which leads to a change in contact shape (Figure 9.4[d]), there is a decrease in wear rate with increasing rubbing time, probably because of initial film formation and stabilisation to protect the surface. Titanium (IV) isopropoxide does not seem to adequately protect the surface and thus scuffing is observed after 5 minutes of rubbing. This might be attributed to abrasive wear caused by excess titanium oxide on the surface.

Friction behaviour study by MTM shows that there is a significant increase in mixed friction for ZP and MMT solutions. The former can be ascribed to film formation, while the latter is possibly due to film formation or roughening of the surface caused by wear. This was confirmed by topography study using AFM, which shows that both ZP- and MMT-derived tribofilms consist of discrete pads randomly-distributed along the sliding direction, similar to ZDDP. In addition, the presence of grooves is observed on the surface rubbed with MMT, which might indicate initial wear.

Alternatively, Molybdenum dialkyldithiocarbamate (C), gives very low mixed and boundary friction both immediately and after two hours rubbing. This low friction behaviour is attributed to the formation of a low shear strength protective layer comprised of MoS_2 nanoparticles, which is characteristic of MoDTC, a well-know and widely used friction modifier additive [266, 267].

This study has also demonstrated the wear-reducing properties of M-containing antiwear additives using the reciprocating MTM. It was found that Molybdenum dialkyldithiocarbamate (C), has a beneficial effect on wear, with no measurable wear after 16 hours of rubbing, probably because of the development of a protective film during initial rubbing. Since this additive forms a negligible protective layer on the surface, this supports the finding made in previous chapters, that thick boundary film formation is not a pre-requisite for effective wear and particularly friction reduction. Unfortunately, the wear-reducing properties of Zinc alkylphosphate (C), *i.e.* ZP, were not evaluated in this study because of proprietary restrictions.

The chapter that follows reviews and describes the film-forming, friction, morphology and wear properties of the B-containing antiwear additives used in this study.

10. FILM-FORMING, FRICTION, MORPHOLOGY AND WEAR-REDUCING PROPERTIES OF B-CONTAINING ANTIWEAR ADDITIVES

This chapter first provides an overview of previous research on soluble organoboron-containing antiwear additives, *e.g.* borate esters and borated dispersants, with a particular focus on the film-forming and wear properties of this additive type.

The chapter then describes film thickness, friction, surface topography and wear measurements carried out on a range of boron-containing antiwear additive solutions, using the methods outlined in chapter 4.

Some surface analyses of the films formed by B-containing antiwear additives were also carried out using ToF-SIMS and XANES but these are deferred to chapter 13, where analysis of the films formed by various additives of interest are presented and discussed together.

10.1 Literature Overview of B-containing Antiwear Additives

Organoboron compounds were first introduced as corrosion inhibitor additives in the 1930s [273] and later as antioxidants in the 1950s [274, 275]. However it was not until the 1960s that this group of additives was found to offer effective wear-reducing properties [276]. Since then two main classes of B-containing antiwear additives have been proposed for the formulation of liquid lubricants: organoboron compounds, which are soluble in oil and insoluble inorganic boron salts, which are dispersed in oil as nanoparticles. Review of the latter is deferred to chapter 12, where the film-forming, friction, morphology and wear properties of nanoparticle-containing antiwear additives are presented and discussed together. Reviews on the history and mechanisms of B-containing antiwear have been given by Choudhary *et al.* [277] and Spikes [67].

Kreuz *et al.* used IAE gear testing to investigate the load-carrying properties of tribenzylborate [278, 279]. The authors reported that the extreme pressure properties were improved by this additive. Subsequent analysis of the surface revealed the presence of a thick, *i.e.* 100-200 nm, solid, amorphous film comprised of boric acid and ferrous oxide species.

Baldwin studied the antiwear properties of a range of soluble organoboron additives with and without sulphur [280]. They found that sulphur-containing organoboron compounds offered better antiwear properties than the ones without sulphur. Therefore, the antiwear effectiveness of the additives studied was ascribed mainly to sulphur rather than boron. Surface analysis by XPS revealed the presence of divalent borate on the surface.

The use of organoboron compounds as lubricant additives was extensively patented throughout the 1980s [281-289]. Liu *et al.* investigated the friction and wear-reducing properties of a range of triborate esters [290, 291]. It was observed that long-chain-substituted triborate esters gave superior friction and wear-reducing properties to shorter-chain equivalents. Chemical analysis by XPS of the protective layer formed on the rubbed surfaces suggested that degradation of the additive under rubbing leads to the loss of the alkyl group, however neither borate oxide nor boric acid were found on the surface.

Liu *et al.* also evaluated the influence of sulphur on the antiwear properties of borate esters [292]. The authors reported that sulphur-free additives showed superior wear-reducing properties to sulphur-containing esters. These results contradict those published by Baldwin [280], possibly because of their disparate conditions, *e.g.* additive structure, purity and composition, boron and sulphur content and concentration in solution, test rig, test conditions, *etc.*

One initial problem noted with borate esters was their susceptibility to hydrolysis by water, as illustrated in Figure 10.1 [293, 294]. It was found that the hydrolytic stability of borate compounds could be improved by the addition of hindered phenol [288] and amine groups [289].

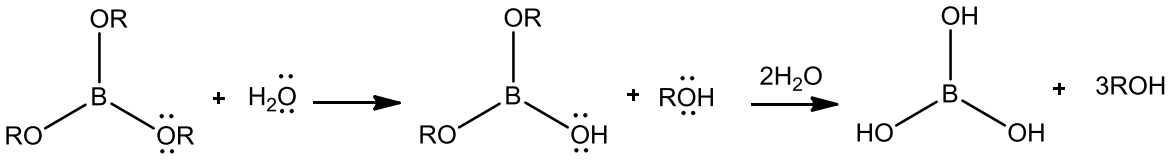


Figure 10.1: Hydrolytic degradation of borated esters, which produce oil-insoluble and abrasive boric acid [293, 294].

Yao *et al.* proposed that the hydrolytic stability of borate esters could be improved by incorporating amino-ethyl species into boron additive molecules, yielding a stable boron-nitrogen five-membered coordination complex, shown in Figure 10.2 [293]. It was also reported that long-chain-substituted borates were more stable to hydrolytic degradation than shorter-chain counterparts, with good antiwear properties overall.

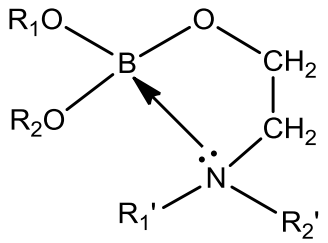


Figure 10.2: Molecular structure of amino-ethyl borate ester prepared by Yao *et al.* [293], where R_1, R_2, R_1', R_2' = alkyl substituent groups.

Further work by Yao *et al.* investigating the four-ball wear of N,N-di-n-butylaminoethyl-di-dodecyl borate showed an improvement of the wear-reducing properties of this additive with an increase of its concentration in oil [295]. Surface analysis of the rubbed surfaces by XPS and XRD revealed the presence of borate ester under low loads and borate ester and boron nitride under higher loads. The authors ascribed the latter to the decomposition of the chemisorbed ester, which in turn enabled the formation of a boron-nitrogen coordination complex.

The antiwear properties of metal-containing organoboron compounds have also been studied [286, 287]. It has been reported by Yao *et al.* that the combination of borate ester with copper and tin oleate salts yields better performance than the borate esters on their own [296, 297]. The authors credited this behaviour to the formation of copper and tin on the rubbed surfaces, rather than to the stabilisation of the borate glass-like film by free network-forming metal cations.

Zhang *et al.* used XANES and XPS to investigate the nature of the protective films formed by borated succinimide dispersant, with and without ZDDP [298]. The authors reported the formation of zinc/amine/ammonium polyphosphates, zinc sulphide, trigonal and tetrahedral borate species on surfaces rubbed with borated dispersant and ZDDP. It was also observed that the borated dispersant did not have a significant effect on the antiwear performance of ZDDP, while the dispersant on its own showed good wear-reducing properties, being superior to non-borated dispersants.

Kapadia *et al.* used MTM-SLIM to investigate the film-forming properties of organoboron-containing fully formulated oils, with and without ZDDP [299]. It was found that the boron, without ZDDP, rapidly reacted to form a thick protective film on the surface, *i.e.* ≈ 185 nm after 1 hour of rubbing at 100 °C (Figure 10.3). The surface was further investigated using SIMS, which suggested the diffusion of boron into the substrate. Unfortunately, this paper does not clarify whether the additive used was a soluble or nanoparticle boron compound.

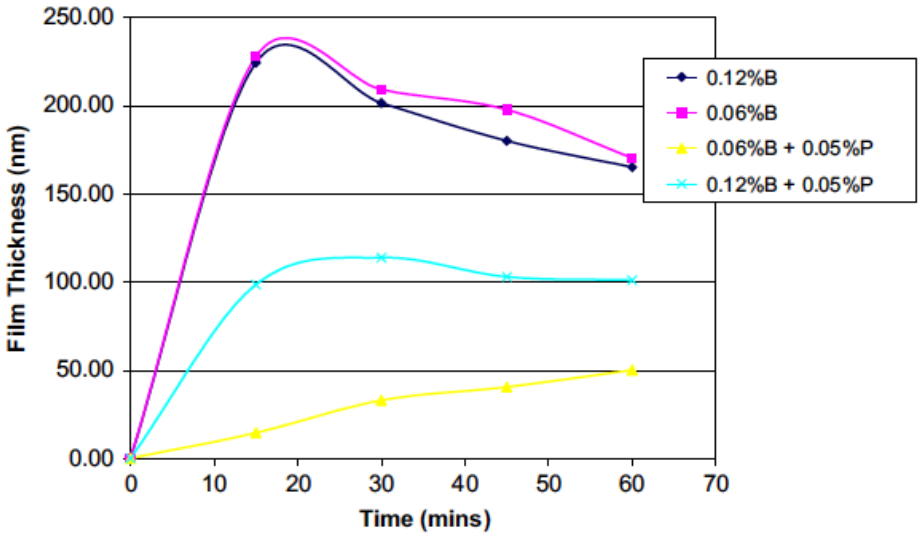


Figure 10.3: Evolution of film thickness with rubbing time for boron-containing fully formulated oils, with and without ZDDP [299].

Shah *et al.* synthesised and investigated the four-ball wear of S-di-n-octoxyboron-O,O'-di-n-octyldithiophosphate (DOB-DTP) [300]. It was found that this additive offered better antiwear properties than ZDDP, as seen in Figure 10.4. The superior performance of the B-P-S compound was credited to its strong coordination capacity with rubbing surfaces, which in turn enabled the formation of a stable protective film on the surface.

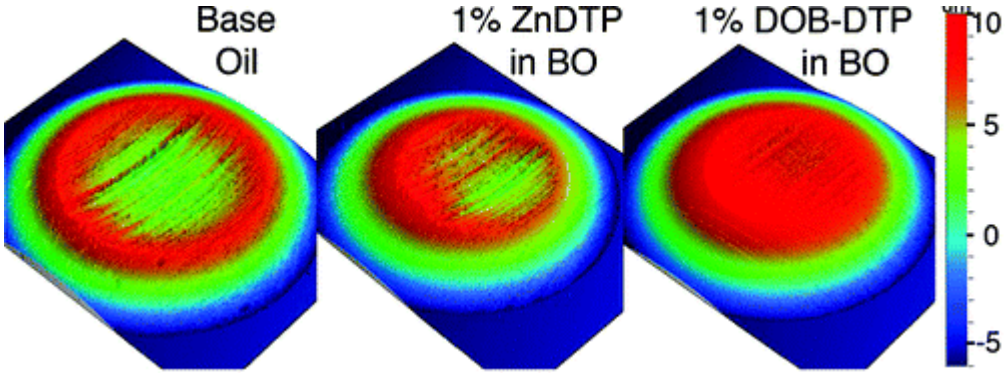


Figure 10.4: Topography of the wear scar on the ball after rubbing with base oil alone, 1% ZDDP and 1% DOB-DTP. Images taken using an optical profiler WYKO NT1100 [301].

More recently, Wang *et al.* also investigated the wear-reducing properties of a boron-thiophosphate derivative (BTP), for use in the formulation of hydraulic fluids [302]. It was reported that the synthesised BTP gave better antiwear and friction properties than its thiophosphate equivalent. Subsequent surface analysis of the tribofilm by XPS revealed the presence of phosphate, sulphide, sulphate, amine and boron oxide, *i.e.* B_2O_3 on the surface.

The combination of organoboron additives with sulphur compounds, such as mercaptobenzothiazole [218] and particularly dithiocarbamate derivatives [303], and their antiwear properties has also been extensively researched. Recently, Shah *et al.* synthesised and characterised the antiwear properties of three alkylborate-dithiocarbamate derivatives, namely S-(di-n-butyl-borate)-ethyl-N,N'-dibenzyldithiocarbamate (DBB-EBzDTC), S-(di-n-octyl-borate)-ethyl-N,N'-dibenzyldithiocarbamate (DOB-EBzDTC) and S-(di-n-octyl-borate)-ethyl-N,N'-di-n-ethyldithiocarbamate (DOB-EEDTC) [304]. The authors found that longer alkyl chains (Figure 10.5 (c)) attached to the boron gave better wear-reducing properties than their shorter-chain equivalents (Figure 10.5 (b)). The same effect was not observed for the alkyl chain attached to the nitrogen of the DTC group, where shorter, linear chains favoured antiwear properties over heterocyclic substituent groups (Figure 10.5 (d)). It should be noted that no attempt was made to chemically remove any antiwear tribofilm prior to surface analysis using WYKO NT1100 in this study.

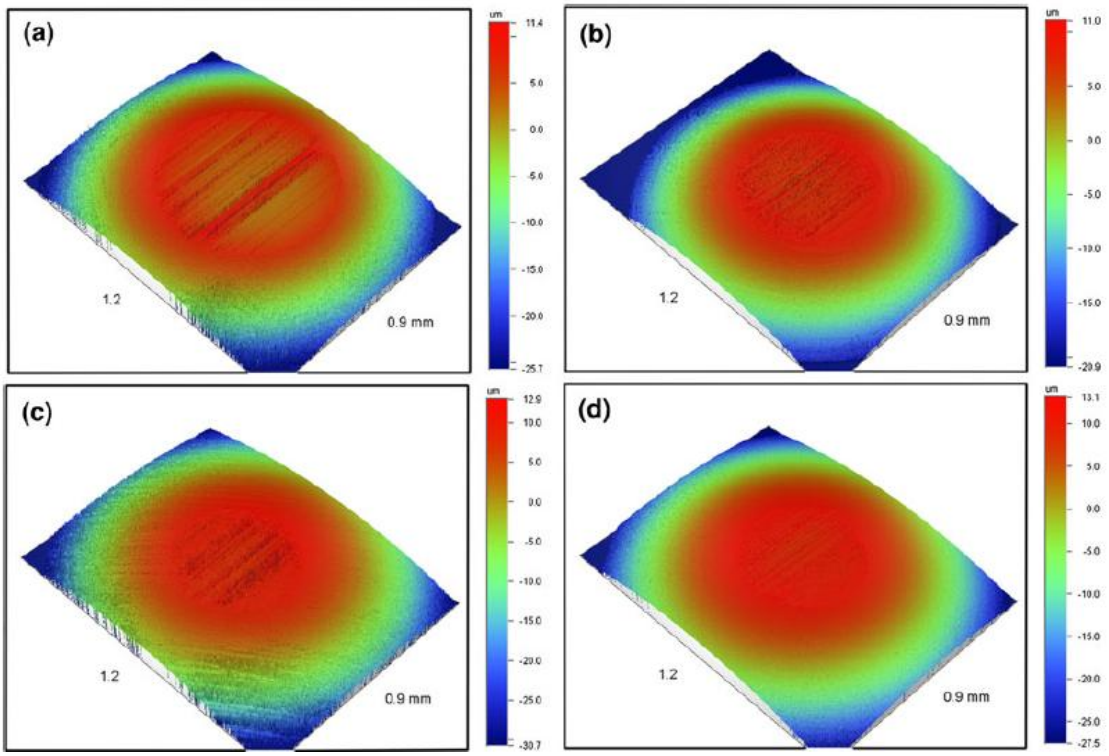


Figure 10.5: Topography of the wear scar on the ball after rubbing with (a) base oil alone, (b) 1% DBB-EBzDTC, (c) 1% DOB-EBzDTC and (d) 1% DOB-EEDTC. Images taken using an optical profiler WYKO NT1100 [304].

Philippon *et al.* proposed a mechanism of action for trimethylborate (TMB) (Figure 10.6) using the hard and soft acid base principle (HSAB), which takes into account the preferential reaction between chemical species [305]. The authors hypothesised that TMB decomposes under rubbing to form methyl, *i.e.* CH_3^+ and borate, *i.e.* BO_3^{3-}, a borderline base, which then reacts with Fe^{3+}, a hard, borderline acid. This results in the formation of a borate glass that partially digests the abrasive iron oxide particles generated by rubbing and thus prevents abrasive wear.

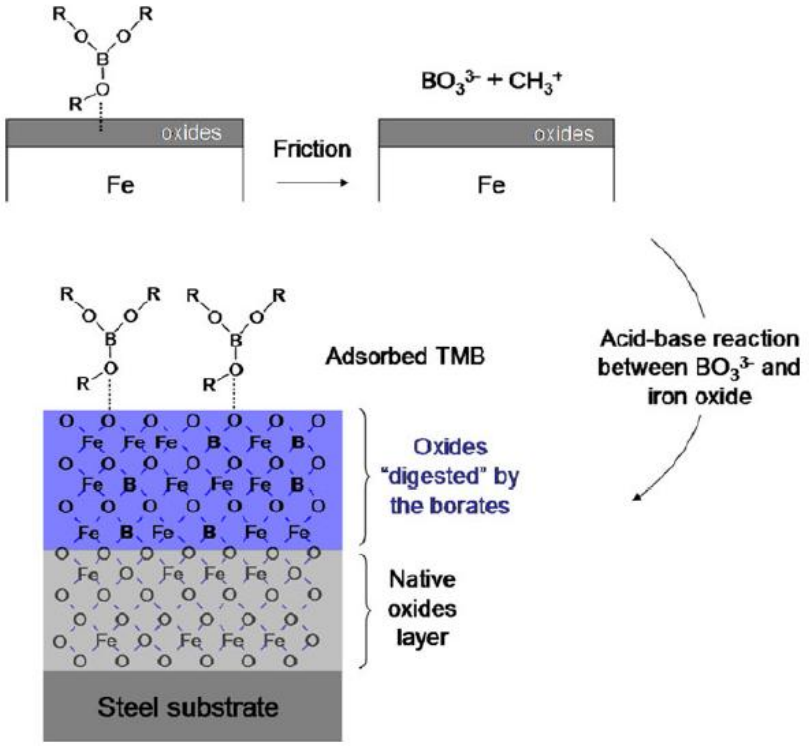
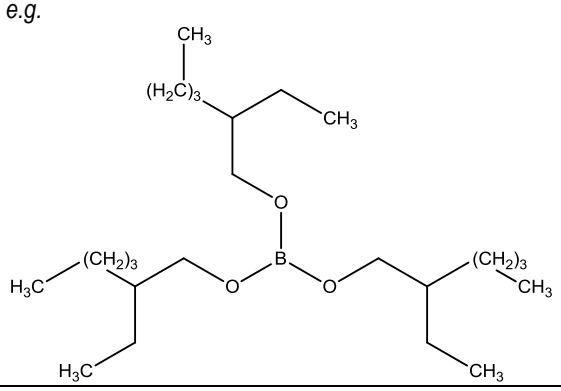
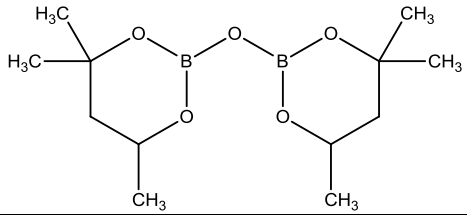
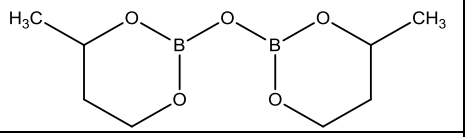


Figure 10.6: Proposed mechanism of film formation by TMB under UHV in gas phase lubrication [305].

Most soluble B-containing additives can give good antiwear performance, with the formation of thick protective films, similar to ZDDP, during rubbing. It is particularly noteworthy, that this group of additives appears to be more effective than phosphate and thiophosphate esters. Moreover, because this group of additives appears to be environmentally- and hardware-friendly, as well as formulation-compatible, *i.e.* soluble in oil; there is a growing interest in the development and tribological characterisation of organoboron-containing additives for lubricants.

10.2 Results: Film-forming Properties of B-containing Antiwear Additives

The film-forming properties of B-containing antiwear additives were studied using MTM-SLIM under mixed rolling/sliding conditions, as described in chapter 4, section 4.1. The additives employed in the study are summarised in Table 10.1. These were blended into Group III base oil (C) at a concentration of 800 ppm boron and submitted to rubbing under the same test conditions on the MTM-SLIM.

Table 10.1: Test materials summary: Boron-containing study		
Abreviation	**Sample name**	**Details**
GIII BO	Group III base oil (C)	-
ZDDP1	Primary ZDDP (C)	9.5 %P; 20.0 %S; 10.6 %Zn
AB	Amide borate (C)	-
TEHB	Tris(2-ethylhexyl) borate (C)	*e.g.* 
HGBB	Hexyleneglycol biborate (C)	*e.g.* 
DBGBB	Dibutyleneglycol biborate (C)	*e.g.* 
B-PIBS(H)	Borated polyisobutenyl succinimide (High B) (C)	-
B-PIBS(L)	Borated polyisobutenyl succinimide (Low B) (C)[1]	-
KB	Potassium borate (C)	-

(C): commercially-available.

[1] Castrol Ltd. requested the characterisation of Borated polyisobutenyl succinimide (Low B) (C) in terms of its film-forming and friction properties (only) for internal comparison with Borated polyisobutenyl succinimide (High B) (C) and because of that the former was not used in other tests.

Figure 10.7 shows the growth of the tribofilm on the MTM-ball with increasing rubbing time (*i.e.* zero, 5, 15, 30, 60, 120 minutes) for the base oil, Primary ZDDP (C) and B-containing antiwear additive solutions. With the base oil alone, scuffing occurred after 5 minutes of rubbing, as shown in Figure 10.7[a)] and the test was terminated.

It can be seen that Primary ZDDP (C) (Figure 10.7[b)]) rapidly forms a thick solid-like film on the rubbed ball, while the B-containing compounds form thinner tribofilms (*e.g.* Borated polyisobutenyl succinimide (High B) (C) and Potassium borate (C)) on the surface. Some boron-containing additives, *i.e.* Borated polyisobutenyl succinimide (Low B) (C) and Tris(2-ethylhexyl) borate (C) form negligible tribofilms on the surface. It is noteworthy, that there is no visible damage to the rubbing contact in the presence of Tris(2-ethylhexyl) borate (C), even though this formed a negligible tribofilm on the surface. A disturbance in contact shape is observed for Amide borate (C), which has formed a negligible film on the surface, Dibutyleneglycol biborate (C), which has formed a thick film on the surface, and Hexyleneglycol biborate (C). It appears as though the films formed by Dibutyleneglycol biborate (C) and Hexyleneglycol biborate (C) do not protect the surface adequately during rubbing and thus disturbances probably due to wear are observed on the surface, *e.g.* change in contact shape, roughening of the surface, *etc*.

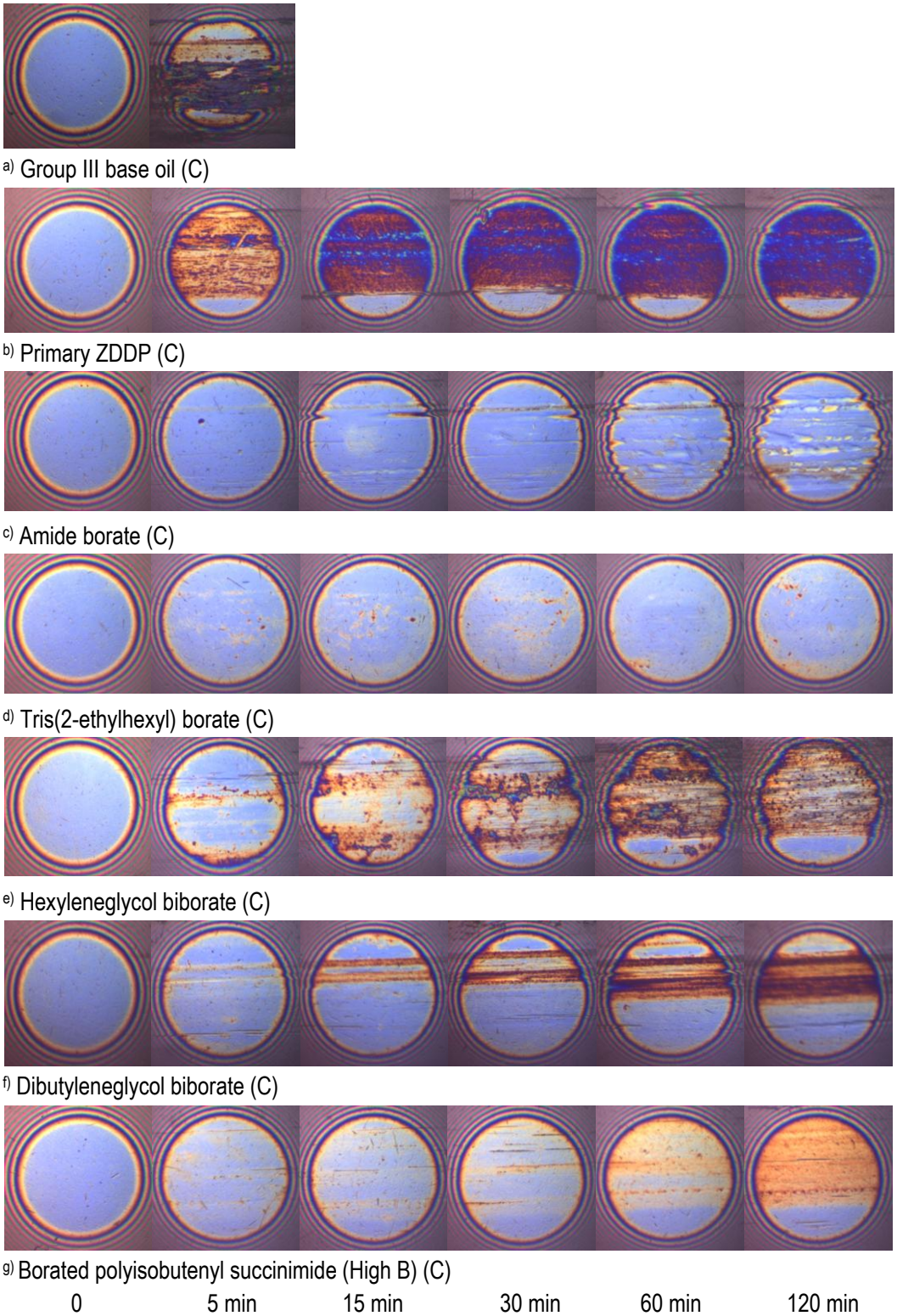
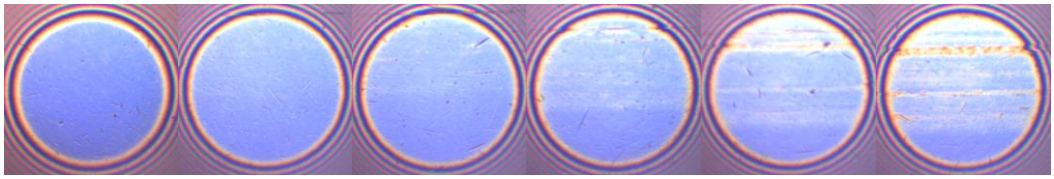
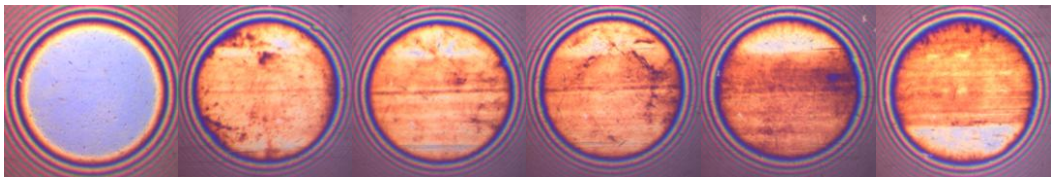


Figure 10.7: MTM-SLIM images showing: a) scuffing on the surface of the ball after 5 minutes of rubbing in base oil without antiwear additive; b) to g) the growth of tribofilm on the ball with increasing rubbing time (*i.e.* zero, 5, 15, 30, 60, 120 minutes).



h) Borated polyisobutenyl succinimide (Low B) (C)



i) Potassium borate (C)

0 5 min 15 min 30 min 60 min 120 min

Figure 10.7 (continued): MTM-SLIM images showing: h) and i) the growth of tribofilm on the ball with increasing rubbing time (*i.e.* zero, 5, 15, 30, 60, 120 minutes).

Figure 10.8 compares the development of mean film thickness with rubbing time for Primary ZDDP (C) and B-containing-derived tribofilms. It can be seen that Primary ZDDP (C) reacts rapidly on the surface, developing a thick film (*i.e.* ≈ 140 nm after 120 minutes of rubbing), while the B-containing compounds form thinner (*i.e.* 50-55 nm after 120 minutes of rubbing for Potassium borate (C) and Borated polyisobutenyl succinimide (High B) (C) solutions) or even negligible tribofilms (*i.e.* ≈ 25 nm after 120 minutes of rubbing for Borated polyisobutenyl succinimide (Low B) (C) and ≈ 10 nm after 120 minutes of rubbing for Tris(2-ethylhexyl) borate (C) solutions).

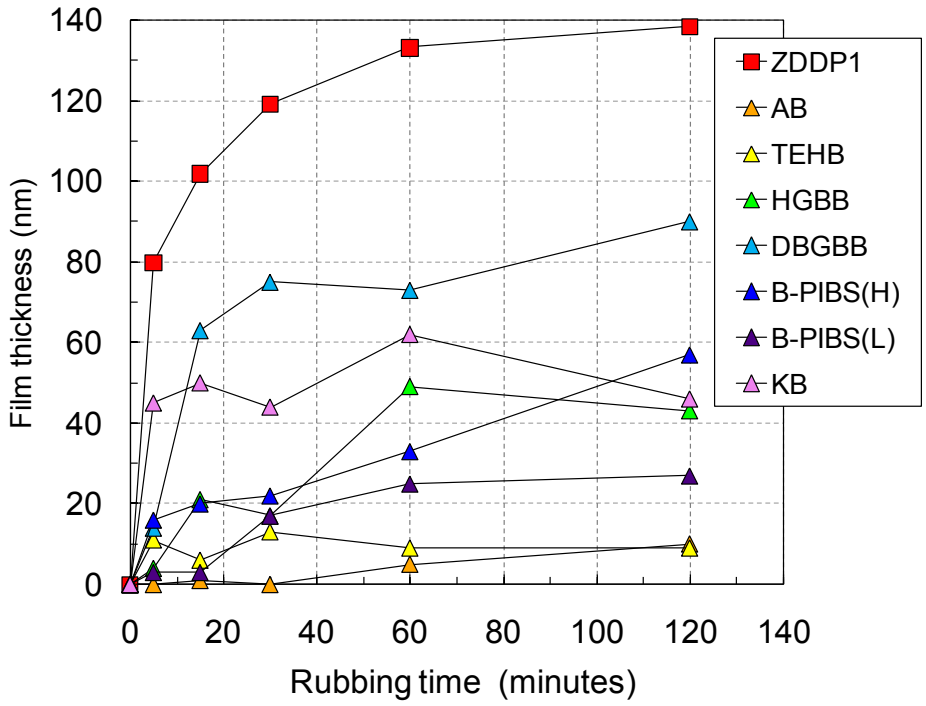


Figure 10.8: Mean film thickness with rubbing time for B-containing antiwear additives.

10.3 Results: Friction properties of B-containing Antiwear Additive-derived Tribofilm

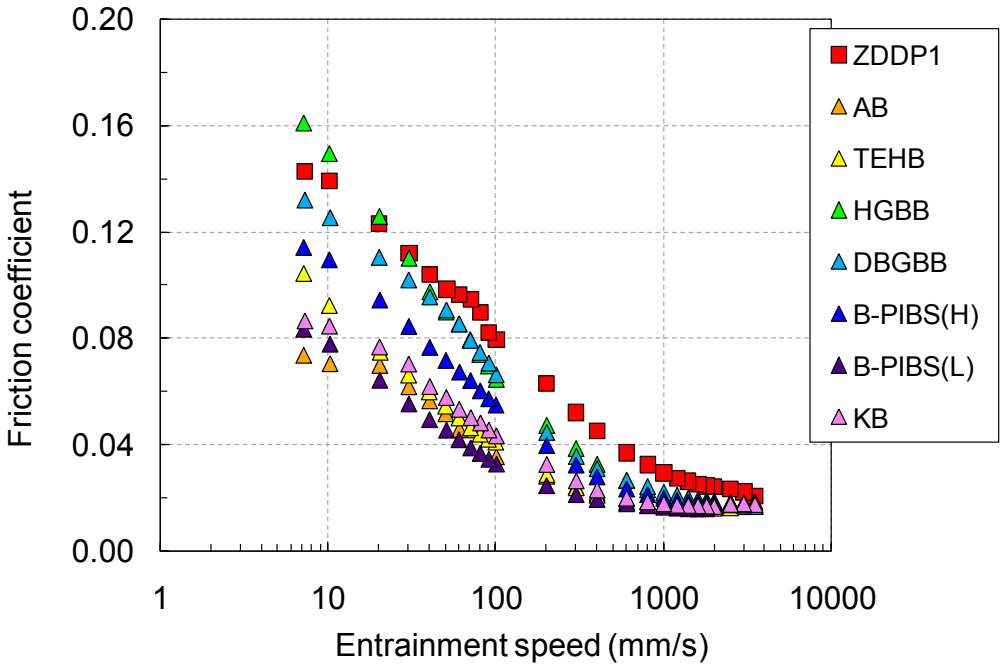
The friction properties of a range of B-containing antiwear additives were studied using the MTM under mixed rolling/sliding conditions, as described in chapter 4, section 4.1. The Stribeck curves (Figure 10.9) show the friction coefficient *versus* entrainment speed for these additives at the beginning and after 2 h of rubbing.

These friction curves illustrate two different types of behaviour; (i) in some cases shifting of the curves to the right and (ii) changes in low speed boundary friction.

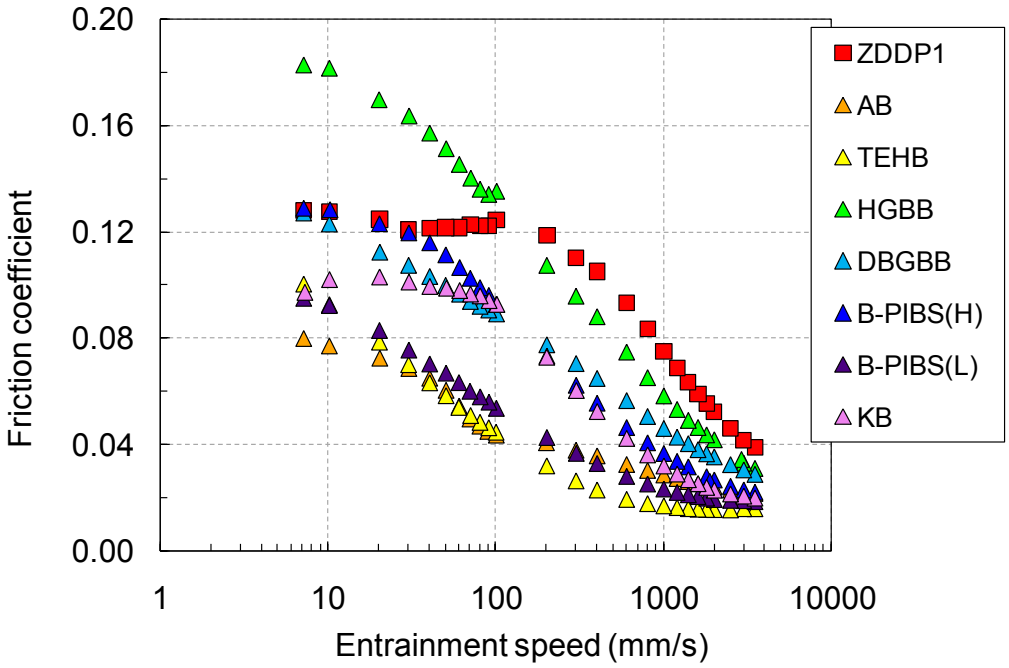
As discussed in section 5.3 of chapter 5, there is a significant increase in mixed friction for Primary ZDDP (C) once the protective film forms on the surface, shifting the curve to the right after 2h of rubbing. This increase in mixed friction is probably due to the change in surface texture as a result of the development of a thick solid-like film on the surface (Figure 10.7[b)]). An increase in mixed friction, which can also be credited to film formation, is observed for Potassium borate (C), Borated polyisobutenyl succinimide (High B) (C) and Borated polyisobutenyl succinimide (Low B) (C) solutions; while Amide borate (C) and Tris(2-ethylhexyl) borate (C), both of which formed negligible films on the surface, show no significant changes in mixed friction after rubbing.

The increase in mixed friction for Dibutyleneglycol biborate (C) is probably due either to film formation or roughening of the surface caused by wear, while the overall high friction observed for Hexyleneglycol biborate (C) is probably due to the extreme roughening observed on the surface, possibly due to wear.

In terms of boundary friction, Amide borate (C) gives low initial boundary friction which may indicate the presence of long alkyl chain groups attached to the molecule. Alternatively there is a slight increase in boundary friction for Borated polyisobutenyl succinimide (High B) (C) and Borated polyisobutenyl succinimide (Low B) (C), while Potassium borate (C) shows classical boundary friction behaviour observed when long chain surfactants are present, of friction that increases with speed in the slow speed region. This may reflect the nature of the dispersant present.



Initial friction, measured at the beginning of the test



Friction after 2 h of rubbing

Figure 10.9: Stribeck curve showing friction coefficient *versus* entrainment speed at the beginning and after 2 h of rubbing at 50 % SRR, 30 N and 100 ºC.

10.4 Results: Morphology of B-containing Antiwear Additive-derived Tribofilms

The morphology of B-containing antiwear additive reaction films generated on AISI 52100 steel discs using the MTM, was studied by AFM, as described in chapter 4, section 4.2. An area of 25 µm x 25 µm in the centre of the wear track was scanned and the topography of the tribofilms is shown in Figure 10.10. Figure 10.10[a)] shows the topography of MTM-discs prior to rubbing.

It can be seen that the morphology of the tribofilms is strongly oriented along the sliding direction, represented by the arrow. Topography measurement reveals that some B-containing antiwear additive-derived tribofilms consist of discrete pads randomly-distributed along the sliding direction, *i.e.* Tris(2-ethylhexyl) borate (C) and Dibutyleneglycol biborate (C). Hexyleneglycol biborate (C) seems to form a patchy film on the surface and the presence of rough debris can also be observed.

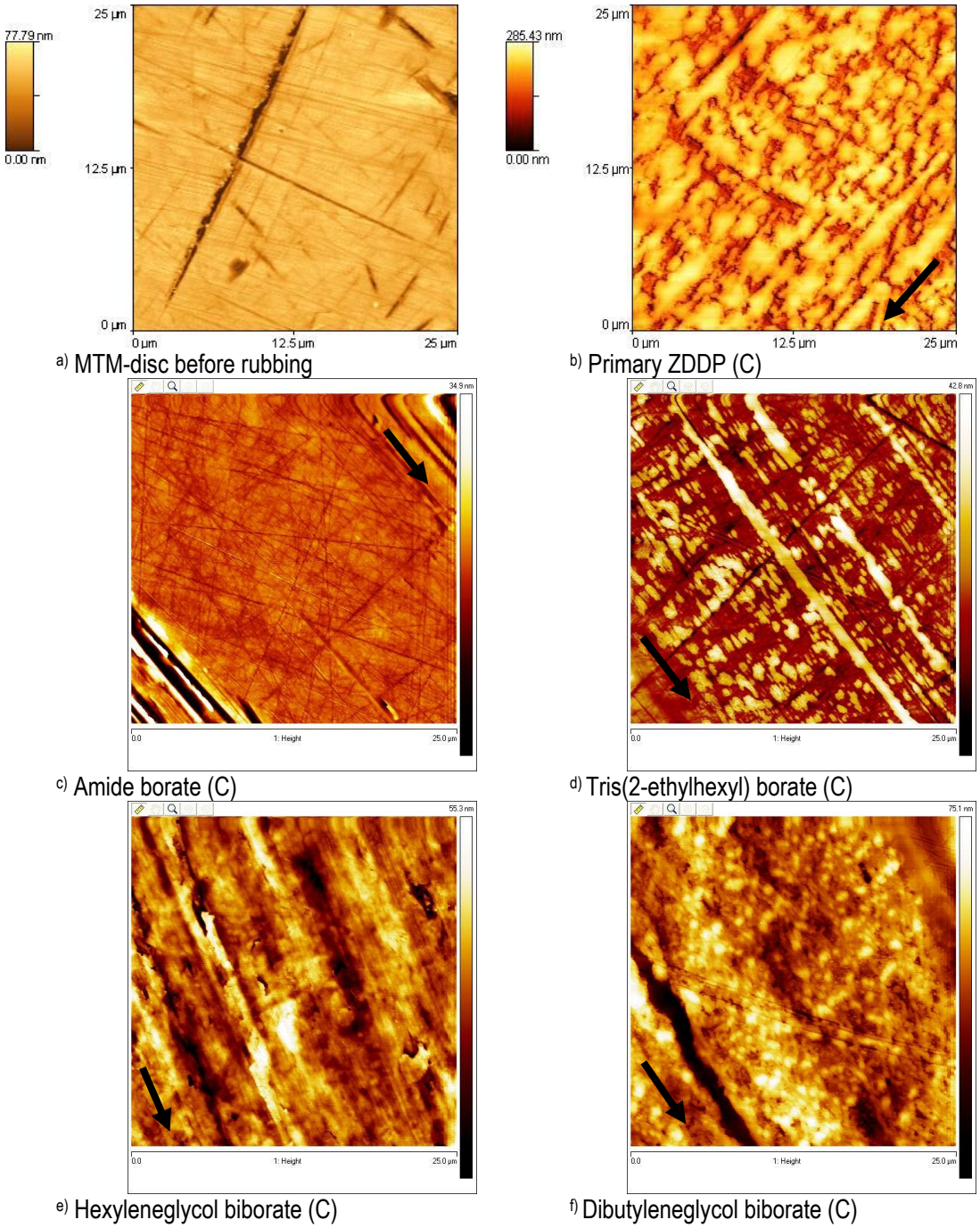
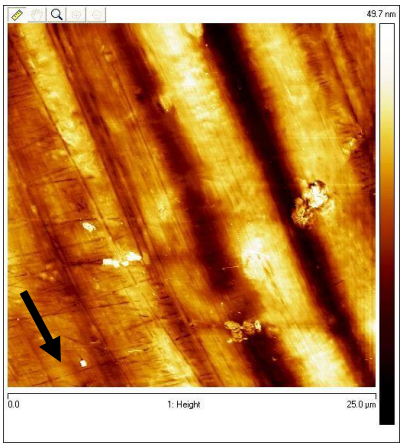
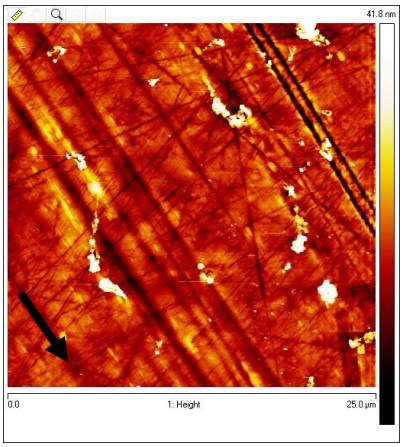


Figure 10.10: AFM 2D topography image at the centre of the wear track on the MTM-disc (sliding direction in b) to f) shown by the arrow).



g) Borated polyisobutenyl succinimide (High B) (C)



h) Potassium borate (C)

Figure 10.10 (continued): AFM 2D topography image at the centre of the wear track on the MTM-disc (sliding direction in g) to h) shown by the arrow).

10.5 Results: Wear-reducing properties of B-containing Antiwear Additive-derived Tribofilms

The wear-reducing properties of four B-containing antiwear additives, Tris(2-ethylhexyl) borate (C), Dibutyleneglycol biborate (C), Borated polyisobutenyl succinimide (High B) (C) and Potassium borate (C), were studied using the method developed by the author, which combines the MTM-Reciprocating rig to generate the wear track on AISI 52100 steel discs with SWLI to image the track and measure wear depth, as described in chapter 4, sections 4.3 and 4.4. Results are summarised in Figures 10.11 and 10.12.

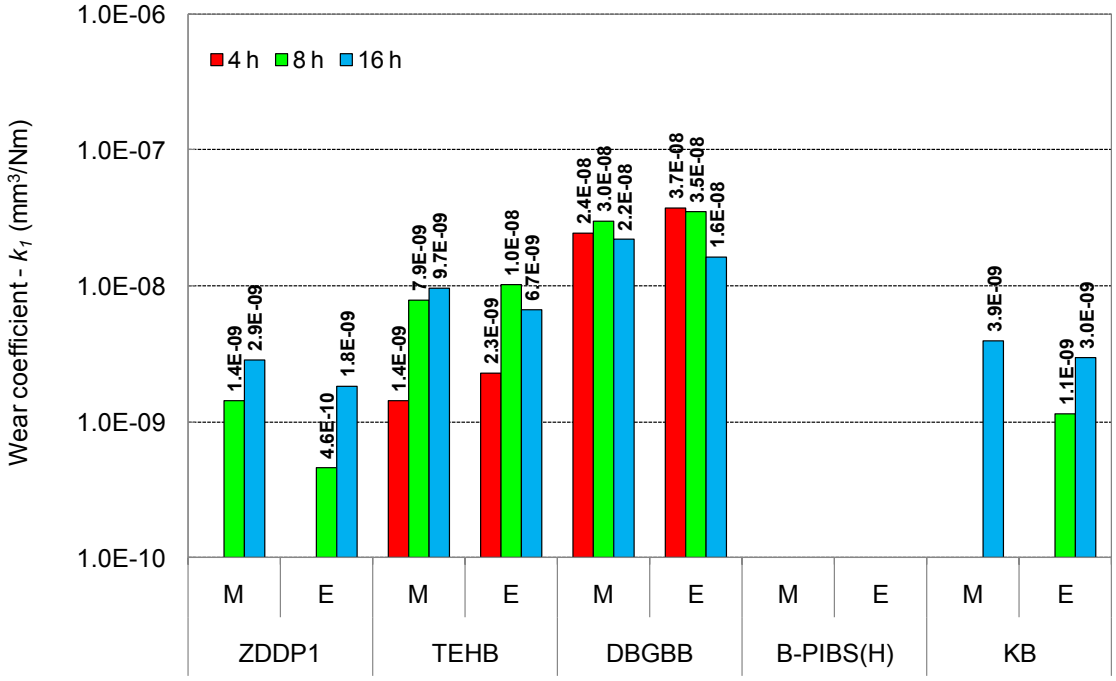
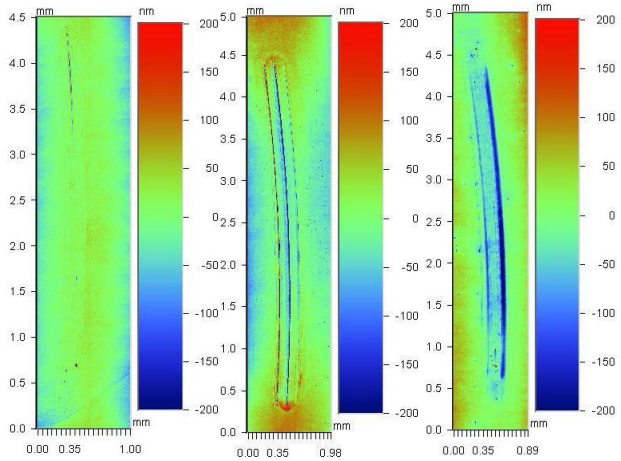
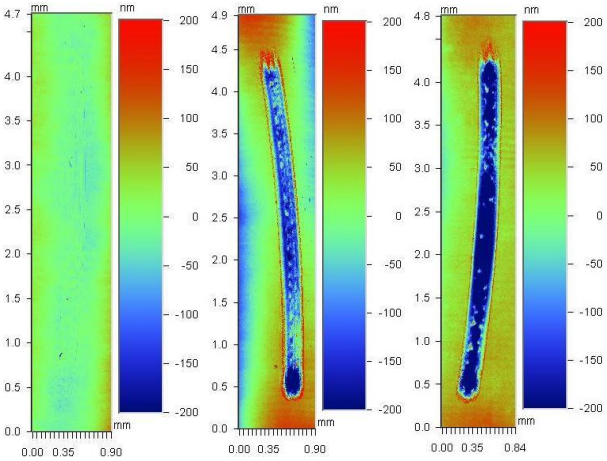


Figure 10.11: Wear coefficient (k_1) in the middle (M) and at the ends (E) of the wear track (*i.e.* average of both ends) for tests lasting 4, 8 and 16 hours.

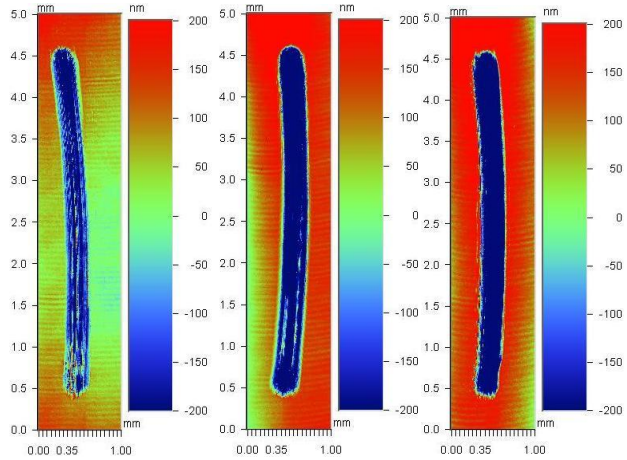
The results show that there is an increase in wear rate for Tris(2-ethylhexyl) borate (C), while higher levels of wear are observed for Dibutyleneglycol biborate (C). Borated polyisobutenyl succinimide (High B) (C) shows no measurable wear after 4, 8 and 16 hours of rubbing. It also appears that Potassium borate (C) offers wear-reducing properties comparable to ZDDP, with no measurable wear after 4 hours of rubbing and very mild wear at the ends of the wear track, where disc speed is minimum because entrainment speed is changing direction, after 8 hours of rubbing. Mild, localised displacement of material from the surface is observed, however, after 16 hours of rubbing, probably due to the removal of tribofilm by rubbing. The topography images, shown in Figure 10.12, reveal an increase in the width in the middle of the wear track with increasing rubbing time for Tris(2-ethylhexyl) borate (C).



Primary ZDDP (C): 4, 8 and 16 hours after EDTA.

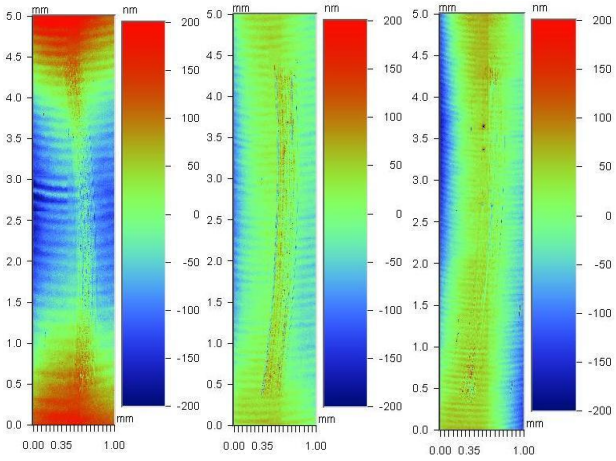


Tris(2-ethylhexyl) borate (C): 4, 8 and 16 hours after EDTA.

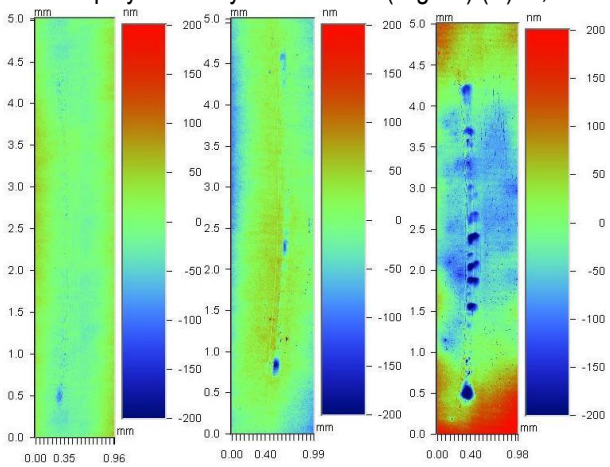


Dibutyleneglycol biborate (C): 4, 8 and 16 hours after EDTA.

Figure 10.12: SWLI 2D topography images of the wear track on the disc.



Borated polyisobutenyl succinimide (High B) (C): 4, 8 and 16 hours after EDTA.



Potassium borate (C): 4, 8 and 16 hours after EDTA.

Figure 10.12 (continued): SWLI 2D topography images of the wear track on the disc.

10.6 Discussion of B-containing Antiwear Additives Work

This film-forming study under mixed rolling/sliding conditions using MTM-SLIM shows that B-containing compounds form thin (50-55 nm for Potassium borate (C) and Borated polyisobutenyl succinimide (High B) (C) additives) or even negligible tribofilms on the rubbed surfaces. It is noteworthy that there is no visible damage to the rubbing contact in the presence of Tris(2-ethylhexyl) borate (C), which forms a negligible film *ca.* 10 nm on the surface. However surface damage is observed with Amide borate (C), which also forms a negligible film of thickness *ca.* 10 nm.

It appears that the film formed by Dibutyleneglycol biborate (C), does not protect the surface adequately during rubbing and thus disturbances probably caused by wear are observed on the surface, *e.g.* change in contact shape, roughening of the surface, *etc*. In the presence of Hexyleneglycol biborate (C), extreme roughening is observed on the surface, possibly because of the removal of FeO during rubbing, which promotes abrasive wear. The presence of rough debris can be observed by AFM on the surface rubbed with this additive.

Interestingly, the film formed by Borated polyisobutenyl succinimide (High B) (C) is much thicker than the film formed by the Borated polyisobutenyl succinimide (Low B) (C). This is quite surprising, since the boron concentration was adjusted to 800 ppm of boron for both additives. This indicates that there is a difference in the molecular structure/composition of the two additives rather than simply just a difference in concentration of the active molecules in the additives. It is possible that overboration of the Borated polyisobutenyl succinimide (High B) (C) compound might result in free residual boric oxide, B_2O_3, nanoparticles, which might be contributing to the formation of a thick film on the surface.

Friction measurements by MTM show that there is an increase in mixed friction for Potassium borate (C) and Borated polyisobutenyl succinimide (High B) (C), which can be attributed to film formation. By contrast, Amide borate (C) and Tris(2-ethylhexyl) borate (C), both of which formed negligible films on the surface, show no significant changes in mixed friction after rubbing. The increase in mixed friction for Dibutyleneglycol biborate (C) is possibly due to film formation or roughening of the surface caused by wear, while the overall high friction observed for Hexyleneglycol biborate (C) is probably due to extreme roughening of the surface, possibly due to wear. This was confirmed by topography study using AFM, which shows the presence of rough debris on the surface.

In terms of boundary friction, the Amide borate (C) gave low initial boundary friction which may indicate the presence of long alkyl chain groups attached to the molecule. The presence of such groups has been found beneficial with respect to friction [94]. Alternatively there is a slight increase in boundary friction for Borated polyisobutenyl succinimide (High B) (C) and Borated polyisobutenyl succinimide (Low B) (C), while Potassium borate (C) shows a classical boundary friction behaviour observed when long chain surfactants are present.

This study has also demonstrated the wear-reducing properties of organoboron antiwear additives using the reciprocating MTM. It was found that Potassium borate (C) offers wear-reducing properties comparable to ZDDP, while Borated polyisobutenyl succinimide (High B) (C) gave performance superior to ZDDP.

There has always been a question whether organoboron-derived tribofilms are as good as phosphate films to prevent wear and, based on the abovementioned findings, it can be said that some soluble organoboron compounds are at least as good as phosphate and thiophosphate additives.

It was requested by Castrol that the Potassium borate (C), presumably a nanoparticle-based dispersion, be studied with and compared to soluble organoboron compounds, and although particle size distribution was not provided for this sample, it is hypothesised that this additive consists of a reaction product of KOH and H_3BO_3, which is dehydrated and then stabilised with a dispersant. The preparation of a similar product is described by Harrison *et al.* [306]. The authors showed that an analogous potassium borate dispersion, where 90 % of the particles are < 0.6 μm diameter, effectively inhibited wear and fatigue in gears at high temperatures. The results found in the study described in this chapter are consistent with those found by these authors.

11. FILM-FORMING, FRICTION, MORPHOLOGY AND WEAR-REDUCING PROPERTIES OF N-CONTAINING HETEROCYCLIC ANTIWEAR ADDITIVES

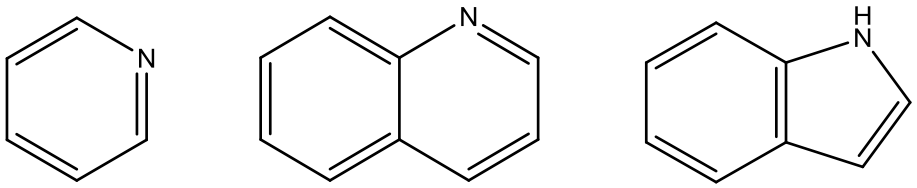
This chapter first provides an overview of previous research on the film-forming and wear properties of nitrogen-containing heterocyclic antiwear additives, such as quinoline, pyridine, indole, indazole, benzotriazole and hydroxyquinoline derivatives.

The chapter then describes film thickness, friction, surface topography and wear measurements carried out on a range of N-containing heterocyclic antiwear additive solutions, using the methods outlined in chapter 4.

11.1 Literature Overview of N-containing Heterocyclic Antiwear Additives

Nitrogen-containing heterocyclic compounds, such as quinoline and benzotriazole derivatives, bond very strongly to rubbing surfaces to form protective films [307, 308]. This group of additives are well known copper corrosion inhibitors used in the formulation of aqueous and oil based lubricating fluids. However they have also been proposed as possible antiwear additives for ferrous surfaces. A review on the history and mechanisms of N-containing heterocyclic antiwear additives was given by Spikes [67].

Rudston *et al.* investigated the wear of a range of sulphur-, oxygen- and nitrogen-containing compounds using a four-ball tester [309]. The authors reported that nitrogen-containing heterocyclic compounds, *i.e.* pyridine, quinoline and indole (Figure 11.1), showed good wear-reducing properties. Their beneficial contribution to wear reduction was attributed to the strong coordination capacity of basic nitrogen compounds to nascent iron, generated by rubbing. It was also observed that basic nitrogen compounds, comprised of a lone electron pair, *e.g.* quinoline, were superior to non-basic compounds, *e.g.* indole.

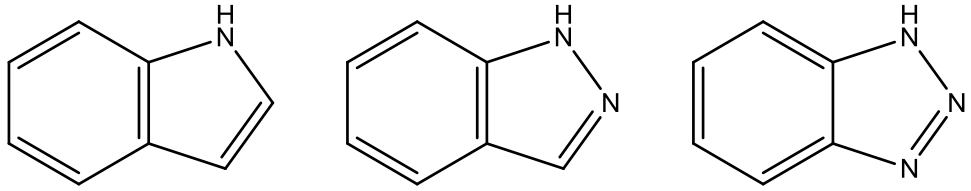


(a) (b) (c)

Figure 11.1: Molecular structure of some nitrogen-containing heterocyclic compounds, *i.e.* (a) pyridine, (b) quinoline and (c) indole, studied by Rudston *et al.* [309].

Miller investigated the effect of the position of alkyl substituent groups on the antiwear properties of pyridine and quinoline derivatives [310]. Although, it was found that both alkyl-substituted pyridines and quinolines were effective in reducing wear, it was also observed that the antiwear effectiveness of this group of additives was strongly influenced by the size and, particularly, the position of substituent alkyl groups relative to the nitrogen atom on the ring, *i.e.* ortho-substituted pyridines showed inferior antiwear activity to para-substituted ones. This was ascribed to the steric hindrance caused by alkyl substituent groups adjacent to nitrogen.

Ren *et al.* studied the influence of number of N atoms on the wear-reducing properties of N-containing heterocyclic compounds, namely indole, indazole and benzotriazole (Figure 11.2) [311]. The authors reported that antiwear effectiveness increased with the number of nitrogen atoms in the molecule, *i.e.* benzotriazole > indazole > indole. This behaviour was credited to the increase in coordinating capacity, and thus reactivity towards the surface, with the increase in basic nitrogen atoms. Further surface analysis by XPS revealed the presence of benzotriazole still intact on the surface, which indicated the formation of an adsorbed rather than a reaction film on the surface.



(a) (b) (c)

Figure 11.2: Molecular structure of nitrogen-containing heterocyclic compounds, *i.e.* (a) indole, (b) indazole and (c) benzotriazole, studied by Ren *et al.* [311].

Wei *et al.* investigated the wear-reducing properties of a series of oxygen- and sulphur-substituted N-containing heterocyclic additives [312, 313]. The authors reported that oxygen-substituted compounds, *e.g.* 8-hydroxyquinoline (Figure 11.3) showed very good antiwear properties. These results are consistent with those published by Miller who also observed that methoxyquinoline derivatives are beneficial to wear [310]. Subsequent surface analysis by SIMS and FT-IR suggested that 8-hydroxyquinoline decomposes under rubbing to form a polymer-like protective film, rich in nitrogen, on the rubbed surfaces. Interestingly sulphur-substituted compounds, *e.g.* benzothiazole derivatives, gave better wear-reducing properties under reciprocating conditions. This was ascribed to sulphur being more effective under severe, extreme pressure conditions.

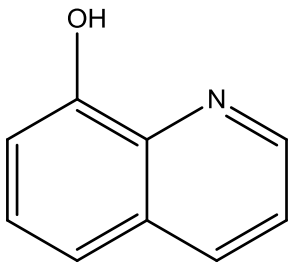


Figure 11.3: Molecular structure of 8-hydroxyquinoline studied by Wei *et al.* [312, 313].

More recently, Cai *et al.* prepared and evaluated the friction and wear-reducing properties of novel benzotriazole-containing imidazolium ionic liquids in PEG and polyurea grease under reciprocating conditions [314]. The authors reported that the benzotriazole-containing compounds showed superior antiwear properties to ZDDP, as well as lower friction at the same concentration (Figure 11.4).

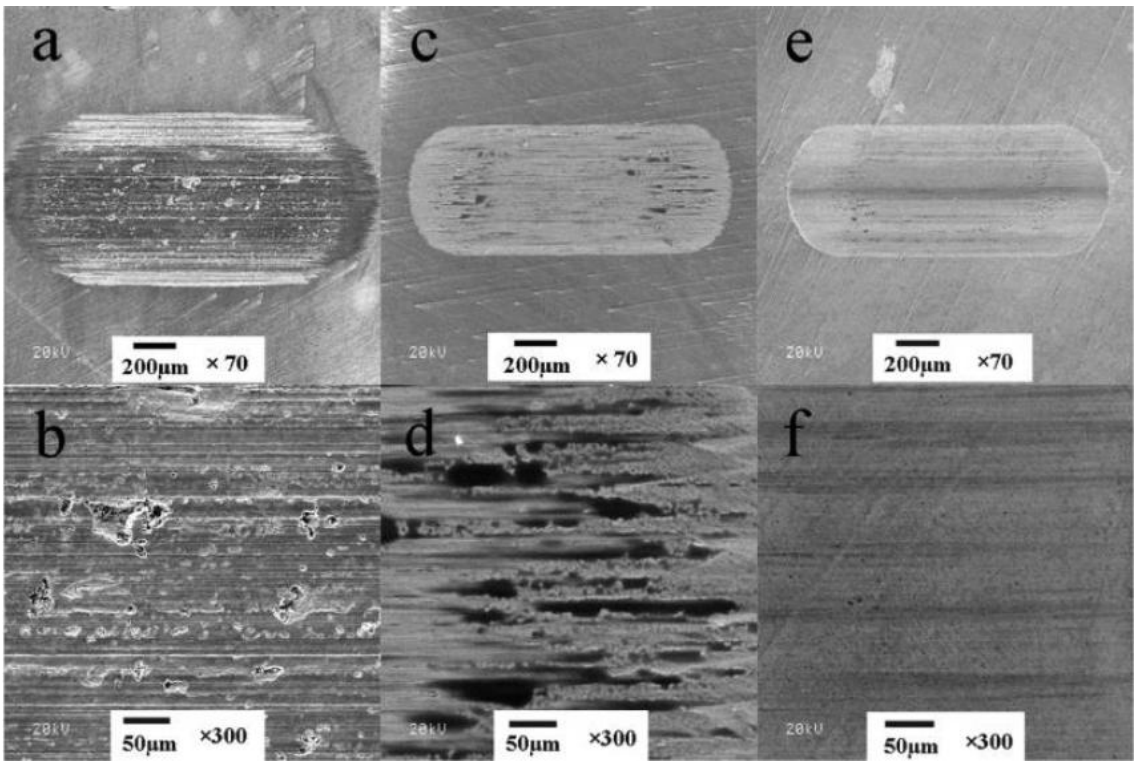


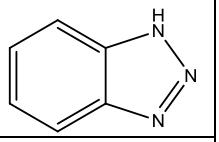
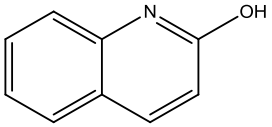
Figure 11.4: SEM images of rubbed surfaces at different magnifications, *i.e.* 70x and 300x: (a, b) polyurea grease alone, (c, d) zinc dialkyldithiophosphate additive package (T204) and (e, f) novel benzotriazole-containing imidazolium ionic liquid ([BTAMIM][PF_6]). Reciprocating tests were run at 150 ºC for 30 minutes at a load of 30 N, 1 mm stroke length, 25 Hz frequency and 2 % additive in solution [314].

It appears that there has been limited research on the antiwear properties of N-containing heterocyclic additives, but is clear that some of this group of additives can give good wear-reducing properties, *e.g.* benzotriazole and hydroxyquinoline derivatives, with the formation of polymer-like protective films on rubbed surfaces.

11.2 Results: Film-forming Properties of N-containing Heterocyclic Antiwear Additives

The film-forming properties of two N-containing heterocyclic antiwear additives were studied using MTM-SLIM under mixed rolling/sliding conditions, as described in chapter 4, section 4.1. The additives employed in this study are summarised in Table 11.1. These were blended into Group III base oil (C) at a concentration of 1000 ppm nitrogen and submitted to rubbing under the same test conditions on the MTM-SLIM.

Table 11.1: Test materials summary: Nitrogen-containing heterocyclic additives study

Abreviation	Sample name	Details
GIII BO	Group III base oil (C)	-
ZDDP1	Primary ZDDP (C)	9.5 %P; 20.0 %S; 10.6 %Zn
BTA	Benzotriazole (C)	14.5 %N; *e.g.* 
HQ	Hydroxyquinoline (C)	8.1 %N; *e.g.* 

(C): commercially-available.

Figure 11.5 shows the growth of the tribofilm on the MTM-ball with increasing rubbing time (*i.e.* zero, 5, 15, 30, 60, 120 minutes) for the base oil, Primary ZDDP (C) and S-containing antiwear additive solutions. With the base oil alone, scuffing occurred after 5 minutes of rubbing, as shown in Figure 11.5[a)] and the test was terminated.

It can be seen that the Primary ZDDP (C) (Figure 11.5[b)]) rapidly forms a thick solid-like film on the rubbed ball, while the N-containing heterocyclic compounds form thinner tribofilms. It appears as though the N-containing additives studied rapidly form relatively thick films, which are then removed by rubbing with the subsequent appearance of a localised groove with Benzotriazole (C), and change in contact shape with Hydroxyquinoline (C), both of which might be due to wear.

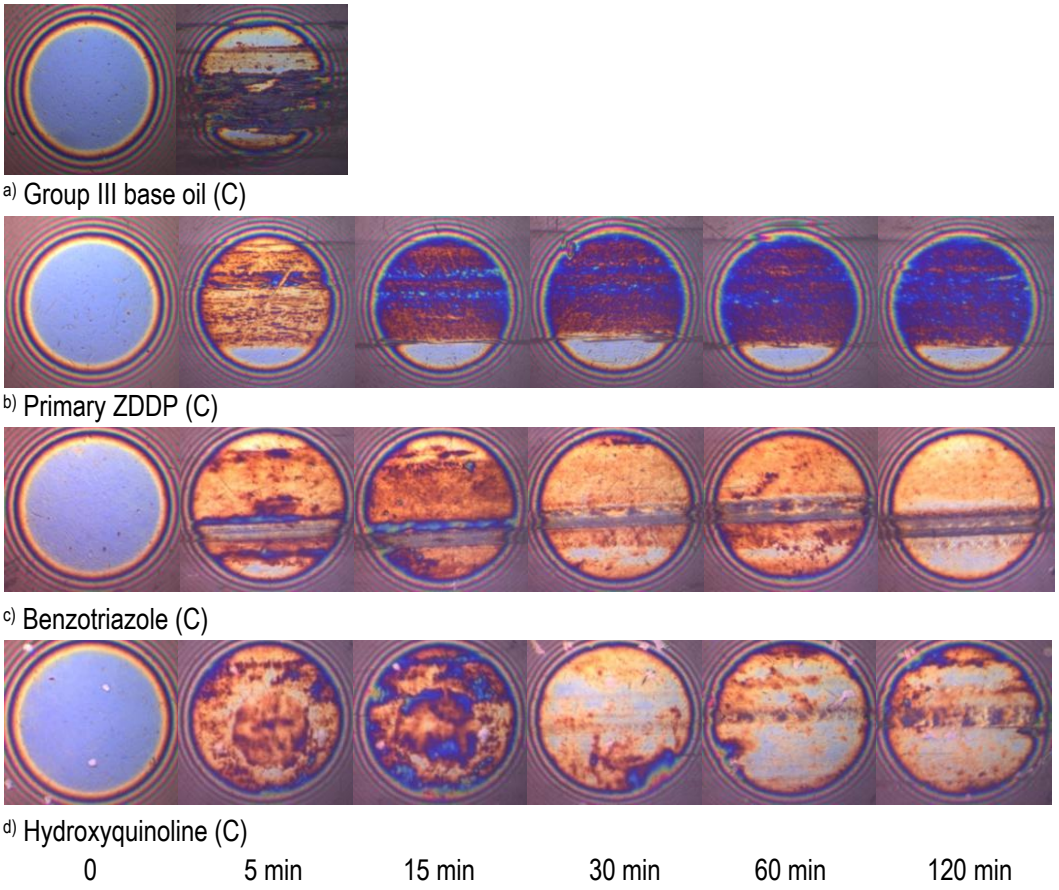


Figure 11.5: MTM-SLIM images showing: a) scuffing on the surface of the ball after 5 minutes of rubbing in base oil without antiwear additive; b) to d) the growth of tribofilm on the ball with increasing rubbing time (*i.e.* zero, 5, 15, 30, 60, 120 minutes).

Figure 11.6 compares the development of mean film thickness with rubbing time for Primary ZDDP (C) and N-containing heterocyclic-derived tribofilms. It can be seen that the Primary ZDDP (C) reacts rapidly on the surface, developing a thick film (*i.e.* ≈ 140 nm after 120 minutes of rubbing), while the N-containing compounds form thinner (*i.e.* ≈ 55 nm after 120 minutes of rubbing for Benzotriazole (C) solution and ≈ 60 nm after 120 minutes of rubbing for Hydroxyquinoline (C) solution).

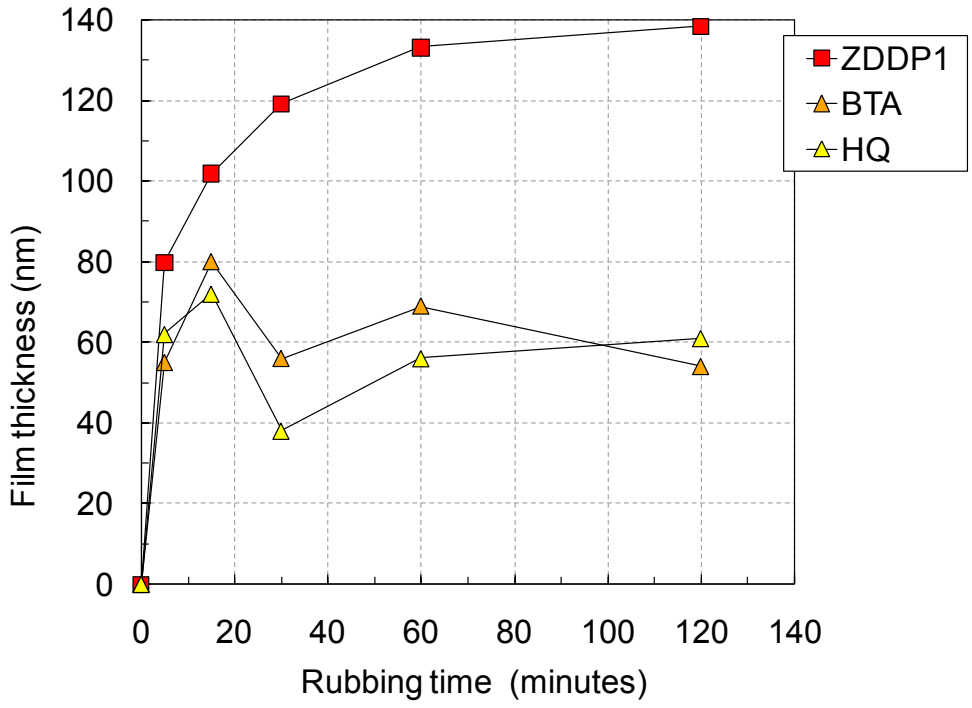


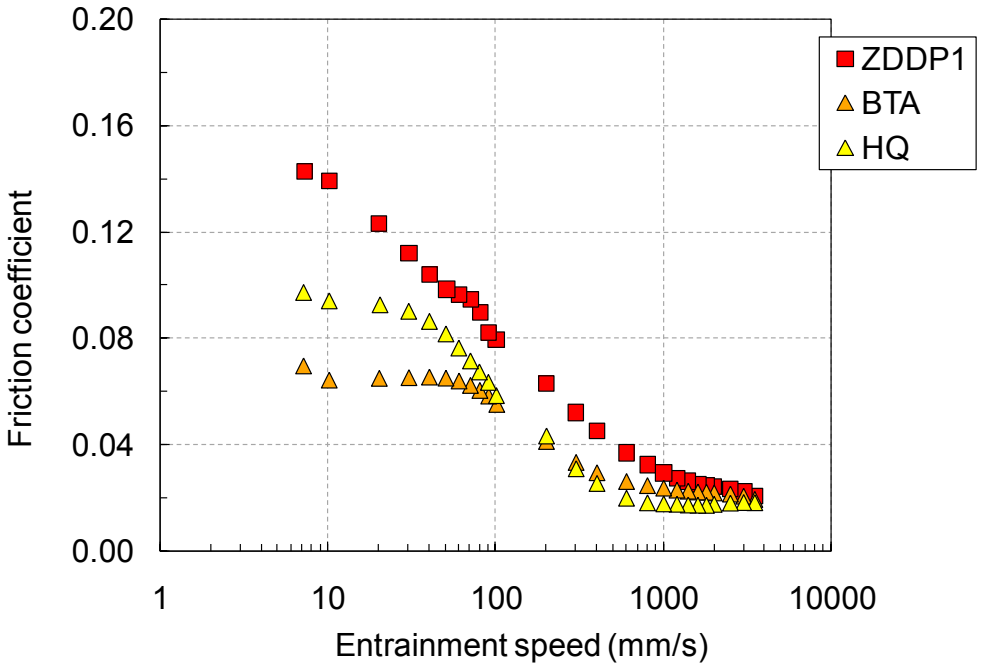
Figure 11.6: Mean film thickness with rubbing time for N-containing heterocyclic antiwear additives.

11.3 Results: Friction properties of N-containing Heterocyclic Antiwear Additive-derived Tribofilm

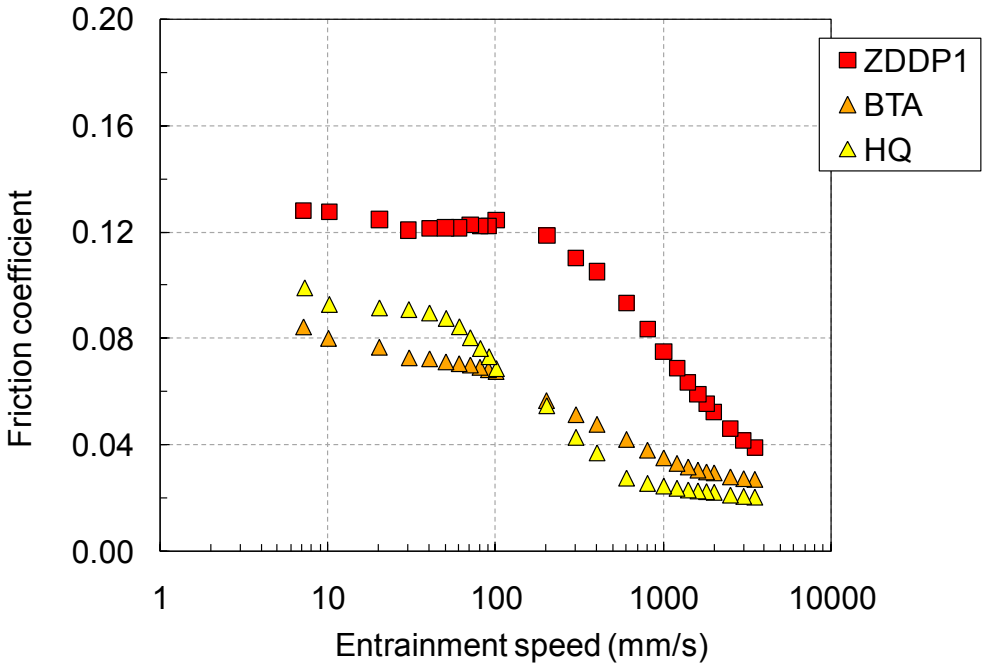
The friction properties of two N-containing heterocyclic antiwear additives were studied using the MTM under mixed rolling/sliding conditions, as described in chapter 4, section 4.1. The Stribeck curve (Figure 11.7) shows the friction coefficient *versus* entrainment speed for these additives at the beginning and after 2 h of rubbing.

The two N-containing heterocyclic additives show a very slight increase in mixed friction, which is considerably less than seen with ZDDP. This is most clearly seen in the individual additive friction curves in Appendix A, Figure A6. This increase may be due to a roughening of the surfaces due either to wear or film formation.

In terms of boundary friction, the Benzotriazole (C) gives low initial boundary friction, with a very slight increase observed after 2 hours of rubbing, but it remains quite low. Hydroxyquinoline (C) gives boundary friction coefficient *ca.* 0.10, which does not change significantly during rubbing.



Initial friction, measured at the beginning of the test.



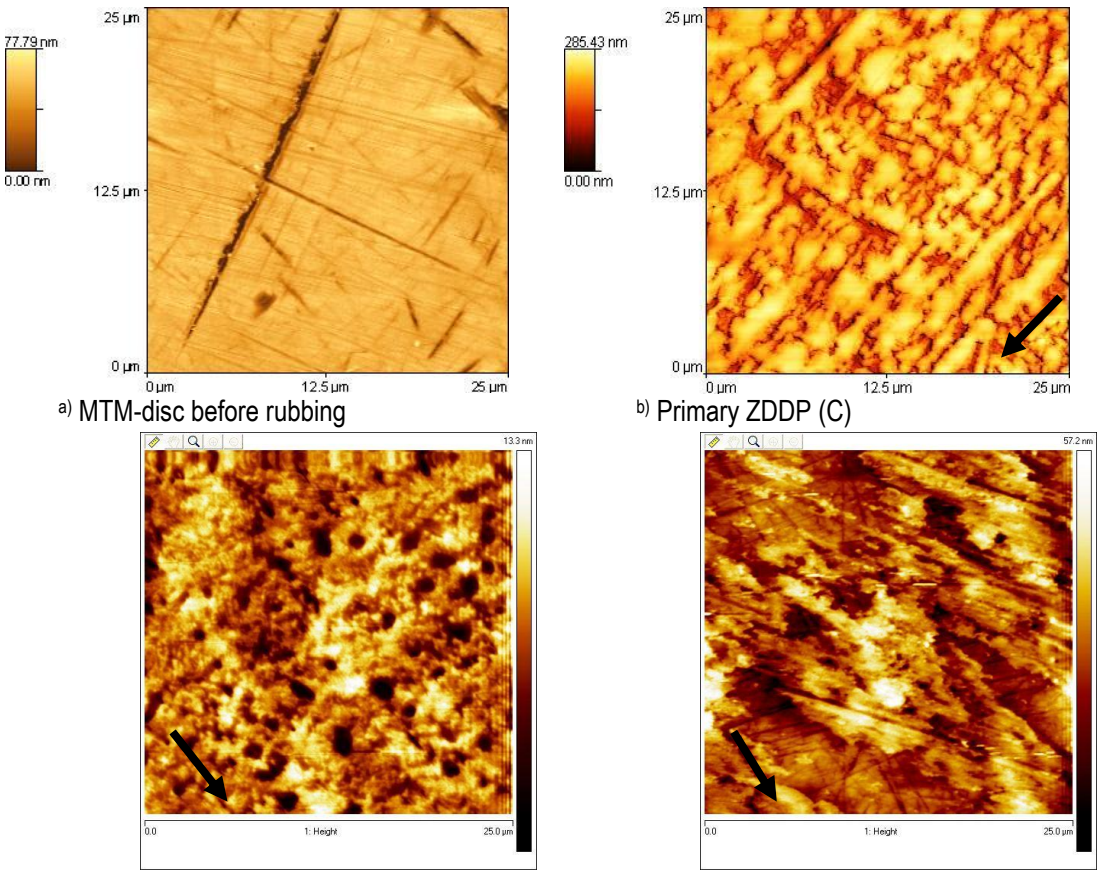
Friction after 2 h of rubbing.

Figure 11.7: Stribeck curve showing friction coefficient *versus* entrainment speed at the beginning and after 2 h of rubbing at 50 % SRR, 30 N and 100 ºC.

11.4 Results: Morphology of N-containing Heterocyclic Antiwear Additive-derived Tribofilms

The morphology of N-containing heterocyclic antiwear additive reaction films generated on AISI 52100 steel discs using the MTM, was studied by AFM, as described in chapter 4, section 4.2. An area of 25 µm x 25 µm in the centre of the wear track was scanned and the topography of the tribofilms is shown in Figure 11.8. Figure 11.8a) shows the topography of MTM-discs prior to rubbing.

It can be seen that the morphology of the tribofilms is strongly oriented along the sliding direction, shown by the arrow. Topography study reveals that Benzotriazole (C), seems to form a smooth film, while Hydroxyquinoline (C), forms a patchy deposit-like film on the surface.



a) MTM-disc before rubbing

b) Primary ZDDP (C)

c) Benzotriazole (C)

d) Hydroxyquinoline (C)

Figure 11.8: AFM 2D topography image at the centre of the wear track on the MTM-disc (sliding direction in b) to d) shown by the arrow).

11.5 Results: Wear-reducing properties of N-containing Heterocyclic Antiwear Additive-derived Tribofilms

The wear-reducing properties of Benzotriazole (C) and Hydroxyquinoline (C), were studied using the method developed by the author, which combines the MTM-Reciprocating rig to generate the wear track on AISI 52100 steel discs with SWLI to image the track and measure wear depth, as described in chapter 4, sections 4.3 and 4.4. Results are summarised in Figures 11.9 and 11.10.

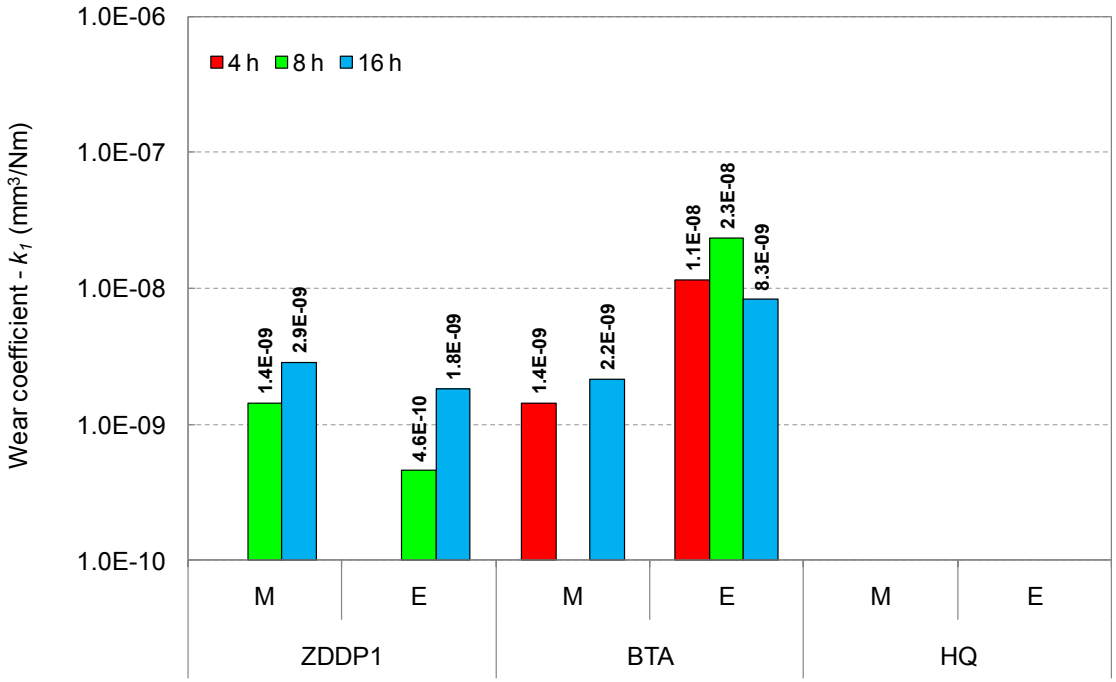
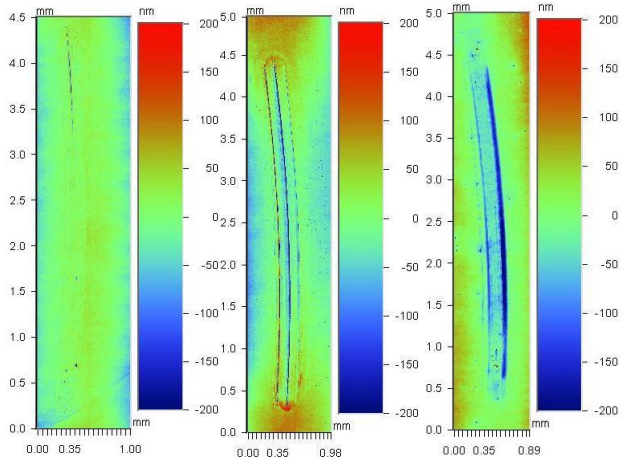
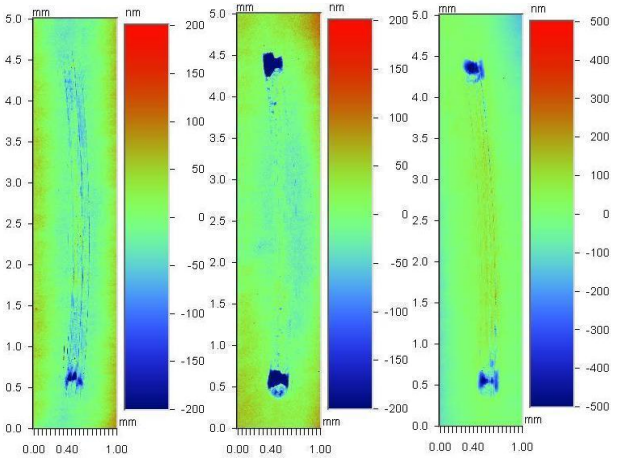


Figure 11.9: Wear coefficient (k_1) in the middle (M) and at the ends (E) of the wear track (*i.e.* average of both ends) for tests lasting 4, 8 and 16 hours.

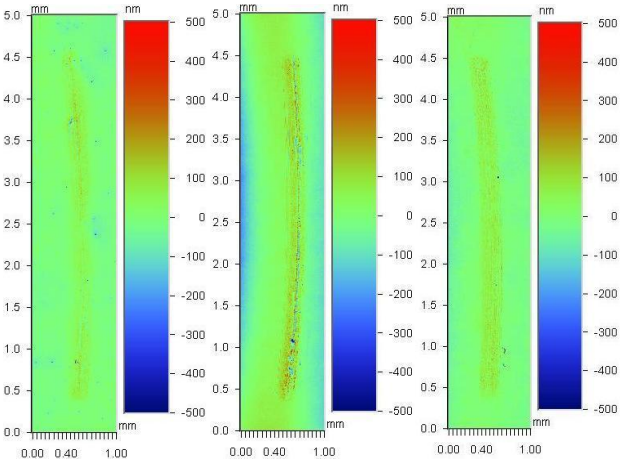
The results show that Benzotriazole (C) and Hydroxyquinoline (C) offer wear-reducing properties, comparable to ZDDP. The former shows very mild wear only at the ends of the wear track (Figure 11.10), where disc speed is minimum because entrainment speed is changing direction, while the latter shows no measurable wear after 4, 8 and 16 hours of rubbing.



Primary ZDDP (C): 4, 8 and 16 hours after EDTA.



Benzotriazole (C): 4, 8 and 16 hours after EDTA.



Hydroxyquinoline (C): 4, 8 and 16 hours after EDTA.

Figure 11.10: SWLI 2D topography images of the wear track on the disc.

11.6 Discussion of N-containing Heterocyclic Antiwear Additives Work

This film-forming study under mixed rolling/sliding conditions using MTM-SLIM shows that N-containing heterocyclic compounds form quite thick films on the surface after 120 minutes of rubbing, *i.e.* ≈ 55 nm with Benzotriazole (C), and ≈ 60 nm with Hydroxyquinoline (C). It appears as though the N-containing additives studied rapidly form films *ca.* 80 nm thick, which are then partially removed by rubbing with the subsequent appearance of a localised grove with Benzotriazole (C) and change in contact shape with Hydroxyquinoline (C), both of which might be due to slight wear.

The formation of thick films indicates that these molecules adsorb onto the surface to form a multilayered deposit-like protective film, as suggested by Ren *et al.* [311] and Wei *et al.* [312, 313]. This is consistent with topography study using AFM, which shows that Benzotriazole (C) forms a smooth film, while Hydroxyquinoline (C) forms a patchy deposit-like film on the surface. Rapid film formation can be ascribed to the strong coordination capacity of nitrogen with the iron generated by rubbing, as proposed by Ren *et al.* [311].

The friction measurements using MTM show that there is a very slight increase in mixed friction for both N-containing solutions, probably due either to film formation or roughening of the surface, which might be caused by the formation of a groove with Benzotriazole (C) or the disturbances in contact shape with Hydroxyquinoline (C). Nevertheless, even if roughening of the surface due to wear contributes to friction, both additives show much lower mixed friction than ZDDP, which indicate they form smooth, low shear strength films on the surface. In terms of boundary friction, Benzotriazole(C) gave low initial boundary friction, with a very slight increase observed after 2 hours of rubbing. Hydroxyquinoline (C) gives boundary friction coefficient *ca.* 0.10, which does not change significantly during rubbing. This friction behaviour indicates that nitrogen heterocyclic additives, *i.e.* benzotriazole and hydroxyquinoline derivatives, are beneficial with respect to boundary friction.

This study has also demonstrated the wear-reducing properties of N-containing heterocyclic additives using the reciprocating MTM. It was found that Benzotriazole(C) offers wear-reducing properties comparable to ZDDP, while Hydroxyquinoline (C) gave performance superior to ZDDP, with no measurable wear after 4, 8 and 16 hours of rubbing.

The results found in this work are consistent with those found by Fodor [315], who also observed the formation of thick, adsorbed multimolecular protective layers on rubbing surfaces, which are beneficial to friction and wear.

12. FILM-FORMING, FRICTION, MORPHOLOGY AND WEAR-REDUCING PROPERTIES OF NANOPARTICLE-CONTAINING ANTIWEAR ADDITIVES

This chapter first provides an overview of previous literature on the film-forming and wear properties of nanoparticle-containing antiwear additives. This includes nanoparticles based on unreactive metals, metallic oxides, carbonates, borates, fullerenes, carbon nanotubes and inorganic fullerenes.

The chapter then describes film thickness, friction, surface topography and wear measurements carried out on a range of nanoparticle-containing solutions, using the methods outlined in chapter 4.

Some surface analyses of the films formed by nanoparticle additives were also carried out using ToF-SIMS and XANES but these are deferred to chapter 13, where analysis of the films formed by various additives of interest are presented and discussed together.

12.1 Literature Overview of Nanoparticle-containing Antiwear Additives

Nanoparticles, *i.e.* solid particles of diameter less than 100 nm have been used in lubricants for many years in the form of overbased detergents. Used engine oils from diesel engines and direct injection gasoline engines also contain nanoparticles in the form of engine soot. In addition to these, however, there has been strong recent interest in the use of nanoparticle additives specifically to reduce friction and/or wear.

Species considered as potential nanoparticulate antiwear additives include: unreactive metals, metallic oxides, carbonates and borates, *e.g.* overbased detergents, fullerenes, carbon nanotubes and inorganic fullerenes. Most of these require a surfactant to stabilise the nanoparticles in the lubricant and in assessing the impact of nanoparticle additives on friction and wear it is important to test the surfactant solution alone, in parallel with tests on the particulate suspension. Reviews on the history, performance and mechanisms of nanoparticle-containing antiwear additives were given by Chinas-Castillo [316], Bakunin *et al.* [317] and Spikes [67].

There has been considerable interest in the use of metal and metal oxide nanoparticles. Zhou *et al.* studied the antiwear and extreme pressure properties of dialkyl dithiophosphate-coated Cu nanoparticles *ca.* 8 nm diameter, *i.e.* DDP-Cu [318]. The authors found that the performance of DDP-Cu was superior to ZDDP and that it formed a deposited Cu nanoparticles protective layer on rubbed surfaces. Qiu *et al.* observed similar behaviour for Ni nanoparticles *ca.* 10 nm diameter [319]. Chinas-Castillo *et al.* investigated the film-forming properties of Ag and Au nanoparticle dispersions under rolling/sliding [320, 321]. It was found that these additives formed a monolayer-thick film that reduced boundary friction but was easily removed at high speeds.

Li *et al.* investigated the antiwear properties of a range of dialkyl dithiophosphate-coated nanoparticles, including those of Cu, Ag, LaF_3 *ca.* 5, 4 and 8 nm diameter, respectively [322]. The authors also compared the four-ball wear of these additives with that of organic acid-coated TiO_2 nanoparticles *ca.* 2 nm diameter and with ZDDP. It was found that the nanoparticle dispersions offered comparable load-carrying and superior wear-reducing properties to ZDDP, particularly Cu nanoparticles. This behaviour was attributed to the formation of a deposited protective layer of nanoparticles on the rubbing contact, identified by SEM, EDS and XPS, which carried part of the load and thus separated the surfaces.

Metallic oxide nanoparticle dispersions, such as those of Ti [323, 324] and Fe(III) [325] oxides were found to offer good friction and wear-reducing properties, with the formation of a deposited film on the rubbed surface. It was also reported that nitrogen-containing $La(OH)_3$ nanoparticles *ca.* 30 nm diameter, showed antiwear properties comparable to ZDDP. Surface analysis of the rubbed surfaces revealed that the protective film comprises a chemisorbed La_2O_3 layer covered by a nitrogen-rich deposited outer-layer [326]. Battez *et al.* investigated the contribution of dispersing agents to the wear-reducing properties of ZnO nanoparticles *ca.* 20 nm diameter [327]. They observed that, although the dispersants employed to stabilise the nanoparticles showed good antiwear properties, the ZnO nanoparticles had a deleterious effect on wear. Wu *et al.* reported an improvement on the friction and wear-reducing properties of fully formulated oils treated with CuO and TiO_2 nanoparticle dispersions [328].

Gu *et al.* studied the friction, load-carrying and antiwear properties of surfactant-modified CeO_2 and TiO_2 nanoparticles *ca.* 10 and 15 nm diameter, respectively [329]. The authors found that the combination of both additives, *i.e.* CeO_2:TiO_2 = 1:3, yielded better performance than either additive on its own. Zhang *et al.* observed that stearic acid-modified TiO_2 nanoparticles *ca.* 10 nm diameter exhibited good friction and wear-reducing properties [330]. Subsequent surface analysis by XPS revealed the presence of TiO_2 deposits and a chemisorbed stearic acid protective layer on the surface. Ogasenova *et al.* compared the antiwear properties of organotitanates, *i.e.* titanium 2-ethylhexanoate and titanium oleate, to those of TiO_2 nanoparticles, *ca.* 1-10 nm diameter, modified with tetra(2-ethylhexyl)thiuram disulphide (TDS) and di(2ethylhexyl)thiophosphonodisulphide (TPDS) [331]. It was reported that the thiocarbamic-modified, *i.e.* TDS, and the thiophosphoric-modified, *i.e.* TPDS, TiO_2 nanoparticles offered superior wear-reducing properties to titanium carboxylates, with TPDS-modified one better than TDS-modified TiO_2 nanoparticles.

While unreactive metal and metal oxide nanoparticle dispersions seem to form thin, easily displaced protective layers, it has been demonstrated that metal carbonate and borate dispersions, both of which are used in overbased detergents, are capable of forming thick, relatively strongly held tribofilms on rubbed surfaces.

Overbased detergents usually consist of $CaCO_3$ or $MgCO_3$ nanoparticles, of diameter in the range 5-500 nm [332], stabilised by chemisorbed detergent molecules [333], *e.g.* alkylsulphonate, alkylsalicylate, alkylphenate (Figure 12.1). These additives are widely used in the formulation of crankcase lubricants both to neutralise acidic combustion by-products and to prevent deposit build up. In addition to these, several researchers have shown that overbased detergents have a beneficial effect on wear and scuffing [94, 334, 335].

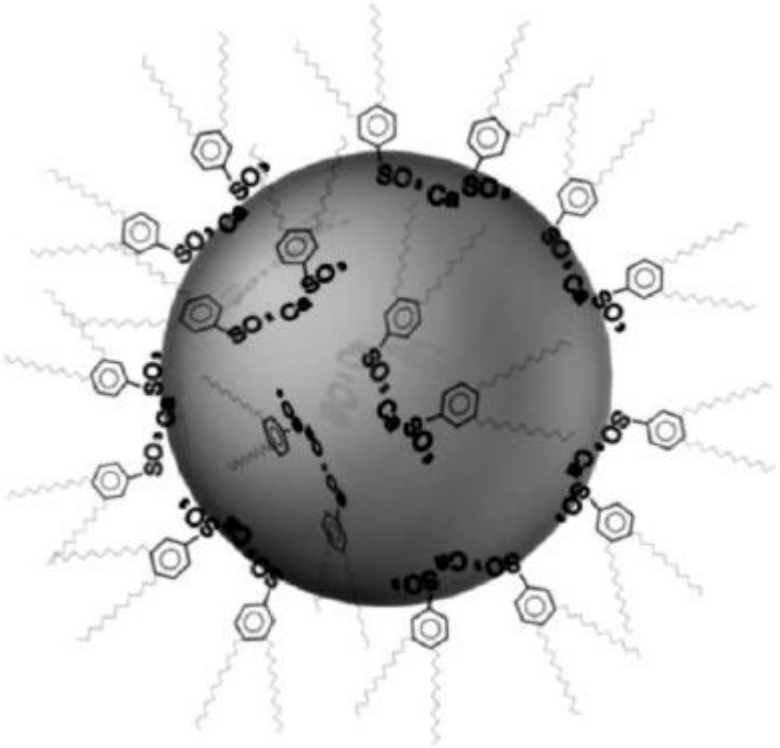


Figure 12.1: Schematic diagram of overbased calcium alkylsulphonate detergent structure: $CaCO_3$ nanoparticle core stabilised by chemisorbed calcium alkylbenzene sulphonate molecules [333].

Topolovec-Miklozic *et al.* investigated the film-forming, friction and morphological properties of a series of commercially-available, overbased calcium sulphonate detergents [94]. It was found that these additives formed thick, solid-like $CaCO_3$ protective films on rubbed surfaces, *i.e.* ≈ 100-150 nm thick during 2 hours of rubbing at 100 °C. Subsequent morphological study of the tribofilm by AFM revealed that the film consists of a pad-like structure separated by deep valleys (Figure 12.2), quite similar to ZDDP. The authors also observed an overall increase in mixed friction for all additives studied after 2 hours of rubbing and considerable differences in boundary friction behaviour (Figure 12.3). The former was ascribed to the pad-like structure of the protective films, which inhibits fluid entrainment and thus the formation of an EHD film; while the latter was credited to the structural effect of the different alkyl chains attached to the detergent molecules.

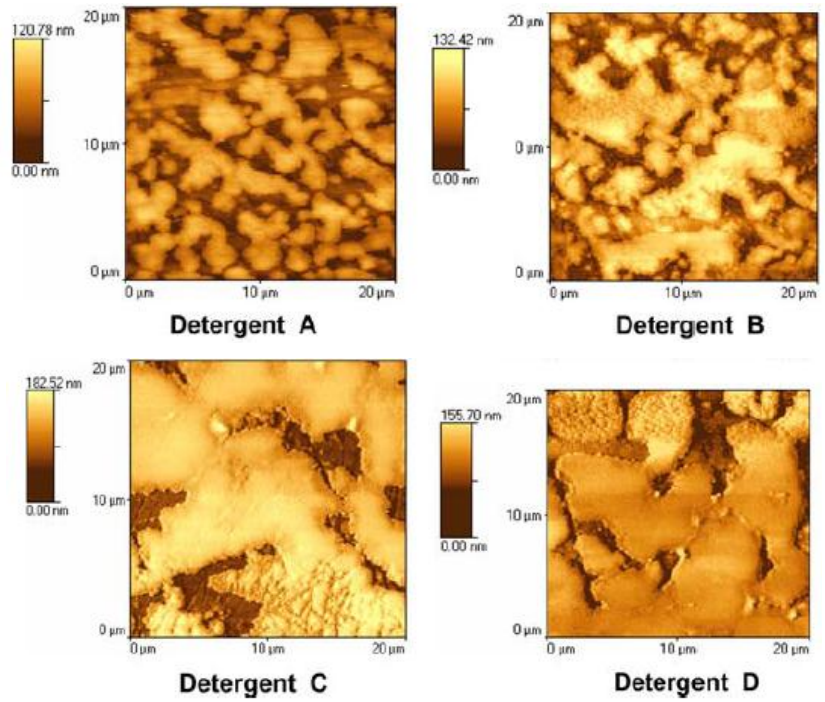


Figure 12.2: Topography images of overbased calcium sulphonate detergent-derived tribofilms studied by Topolovec-Miklozic *et al.* [94].

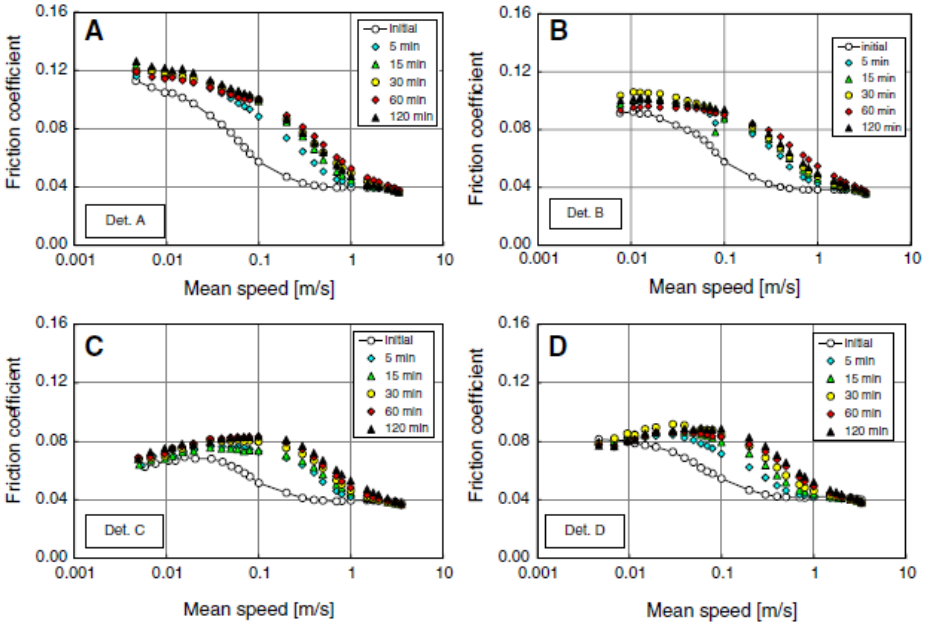


Figure 12.3: Stribeck curves showing friction coefficient *versus* entrainment speed throughout rubbing for the commercially-available overbased calcium sulphonate detergents studied by Topolovec-Miklozic *et al.* [94].

Borate salt dispersions were first introduced as antiwear and extreme pressure additives for lubricating oils in the 1970s [336]. Since then several borate salts have been proposed as antiwear additives, namely sodium [337-339], potassium [340-342], calcium [343], titanium [344], zinc [345], lanthanum [346], aluminium [347], strontium [348] and magnesium [349] borates.

Liu *et al.* studied the contribution of dispersing agents to the wear-reducing properties of sodium metaborate *ca.* < 5 μm diameter [338]. The authors observed that the succinimide dispersant had a synergistic effect on the antiwear properties of $NaBO_2$, while the sulphonate dispersants, *i.e.* those of Na and Ca, had no beneficial effect on wear. Normand *et al.* investigated the antiwear properties of overbased calcium carbonate and calcium borate, both of which were stabilised by salicylate detergent molecules [343]. It was found that the calcium borate gave superior wear performance to calcium carbonate dispersions. Surface analysis revealed that the calcium borate-derived tribofilm consisted of a thin, amorphous Ca/Fe borate glass-like film, which, according to the authors, partially digested the abrasive iron oxide particles generated by rubbing and thus prevented abrasive wear. Hu *et al.* observed that titanium borate nanoparticles, *ca.* 10-70 nm diameter, gave higher initial wear and friction than the base oil alone; however, a significant improvement, in both friction and wear, was observed over time [344]. Similar wear-reducing behaviour was observed with aluminium borate nanoparticles, *ca.* 10-70 nm diameter [347].

Fullerene, *i.e.* C_{60} (Figure 12.4), and analogous carbon nanotube dispersions have also shown good friction and wear-reducing properties as additives in liquid lubricants [350-354]. Gupta *et al.* compared the friction and wear properties of fullerene nanoparticles, *ca.* 1-6 μm diameter, to those of graphite, *ca.* 1-1.5 μm diameter, and MoS_2, *ca.* 0.8 μm diameter, both of which are also solid nanoparticle additives used in the formulation of oils and greases to improve friction and wear [355]. It was reported that the fullerene nanoparticle dispersion gave performance comparable to graphite and MoS_2, which was ascribed to the formation of a transfer film on rubbed surfaces.

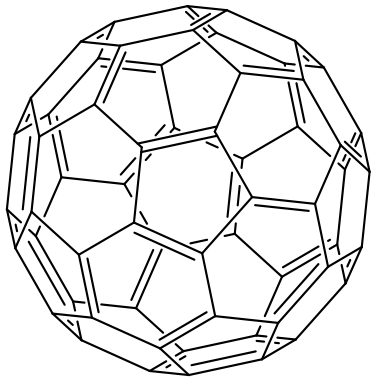


Figure 12.4: Molecular structure of fullerene C_{60}.

Ginzburg *et al.* used SEM, XRD, TEM and mass spectroscopy to investigate the nature of the protective films formed by fullerenes [356]. The authors hypothesised that fullerene rapidly forms a polymer-like protective film on the surface, which consists of a network of fullerene molecules with attached polyolefin chains (Figure 12.5). The superior performance of this group of nanoparticle additives was attributed to a combination between the wear-reducing behaviour of fullerene and the beneficial effect of polyolefin chains on friction.

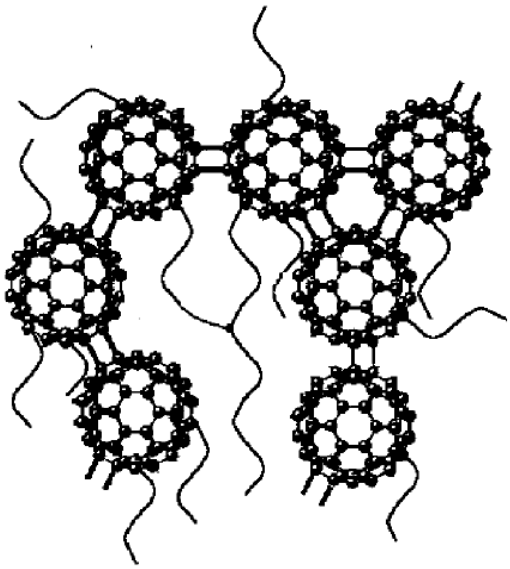


Figure 12.5: Schematic diagram of fullerene-derived tribofilm suggested by Ginsburg *et al.*: network of fullerene molecules linked by polyolefin chains [356].

Lee *et al.* reported that fullerene nanoparticle dispersions improved the friction and wear properties of sliding thrust bearings, while reducing oil degradation and thus the formation of carbonaceous material on rubbing surfaces (Figure 12.6) [357]. Ku *et al.* investigated the effect of base oil viscosity on the wear-reducing properties of fullerene nanoparticles, *ca.* 10 nm diameter [358]. It was reported that fullerene was beneficial to the friction and wear properties of low viscosity oils by separating rubbing surfaces and thus reducing local metal-to-metal contact. The same effect was, however, not observed when high viscosity oils were employed.

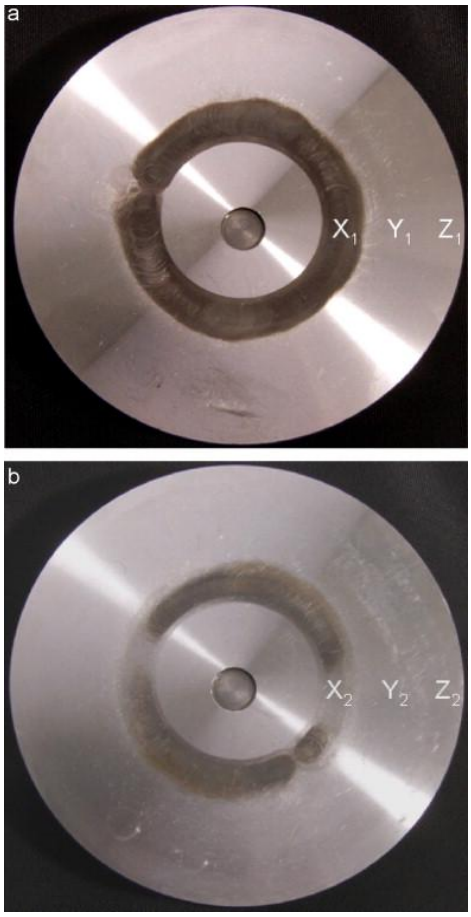


Figure 12.6: Wear track on orbiting plate of sliding thrust bearing tester used by Lee *et al.* [357]. Black coloured circles indicating the presence of carbonaceous material formed under rubbing with: a) base oil alone and b) fullerene-containing oil.

Carbon nanotubes (CN), also known as single-walled carbon nanotubes (SWCN), double-walled carbon nanotubes (DWCN) and multi-walled carbon nanotubes (MWCN) (Figure 12.7) have also been studied. Chen *et al.* compared the friction and wear-reducing properties of stearic acid-modified, multi-walled carbon nanotubes to those of non-modified, multi-walled carbon nanotubes [359]. It was found that fatty acid-modified nanotubes showed superior performance to non-modified ones. The authors credited this behaviour to the contribution of dispersing agents to friction and wear. Peng *et al.* observed similar behaviour for sodium dodecyl sulphate-modified multi-walled carbon nanotubes in water-based lubricants. Surface analysis of the rubbed track by SEM revealed the formation of an amorphous lamella-type carbon structure on the surface by crushing of nanotubes during rubbing [360]. Choo *et al.* reported that multi-walled carbon nanotubes, *ca.* 50-80 nm outer-diameter, showed much lower friction than organic friction modifiers and comparable friction reduction to MoS_2, with even better friction performance in fully-formulated oils, due to synergistic effect with other additives [361].

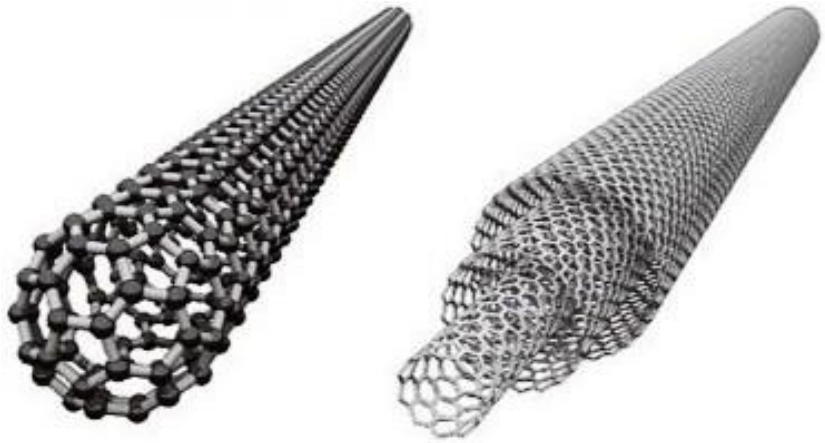


Figure 12.7: Molecular structure of single- and multi-walled carbon nanotubes [362].

Hwang *et al.* investigated the effect of morphology on the wear-reducing properties of a wide range of nanoparticle dispersions, *i.e.* graphite, *ca.* 55 nm diameter, carbon black, *ca.* 54 nm diameter, graphite nanofibre, *ca.* 140 nm diameter and 25 µm long, and carbon nanotubes, *ca.* 20 nm diameter and 40 µm long [363]. The authors reported that nanoparticles that are spherical in nature, *i.e.* graphite and carbon black, were more effective in reducing friction and wear than nanoparticles that are fibrous in nature, *i.e.* graphite nanofibre and carbon nanotubes. The behaviour of the latter was ascribed to agglomeration of fibrous nanoparticles, which led to an increase in surface roughness and thus inhibiting of oil flow into the contact.

Inorganic fullerenes (IFs) are lamellar inorganic compounds, mostly spherical in shape and built up of several concentric layers in a similar manner to fullerene and carbon nanotubes [67, 364]. A series of fullerene-like structures has been identified, including those of V, Ti, Ni, Cs, Ga, In and Sb; however, only IF-MoS_2 and IF-WS_2 have been considered in tribological applications [365]. Jolly-Pottuz *et al.* investigated the friction and wear properties of IF-WS_2 nanoparticles *ca.* 140 nm diameter, stabilised in base oil using an ultrasonic bath. The authors reported an improvement in the friction and wear-reducing properties with increasing rubbing contact pressure. This was ascribed to exfoliation of the outer-layers of IF-nanoparticles at higher pressures (Figure 12.8), which yields a low shear strength layer-lattice protective film on rubbed surfaces [366, 367]. The beneficial effect of IF-MoS_2 nanoparticles on friction and wear was also ascribed to the exfoliation of IF-MoS_2 nanoparticles by Huang *et al.* [368].

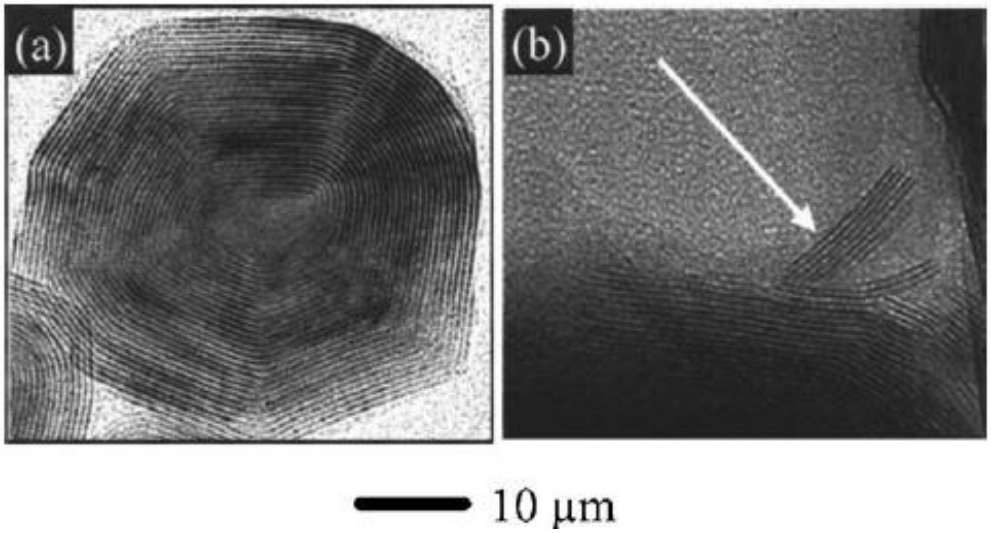


Figure 12.8: High resolution TEM images of IF-WS_2 nanoparticles: a) before rubbing and b) after rubbing, where the arrow indicates the presence of exfoliated sheets [367].

Wu *et al.* compared the friction and wear properties of trioctylamine-modified IF-WS_2 nanoparticles, *ca.* 200 nm diameter, with those of a commercial colloidal IF-MoS_2 dispersion [369]. It was found that surface-modified IF-WS_2 gave superior friction and wear-reducing properties to commercial IF-MoS_2 (Figure 12.9). The performance of the former was credited to the presence of long alkyl chains, from trioctylamine, attached to the IF-WS_2 nanoparticle surface, which in turn protects the IF-WS_2 nanoparticles from chemical and mechanical degradation.

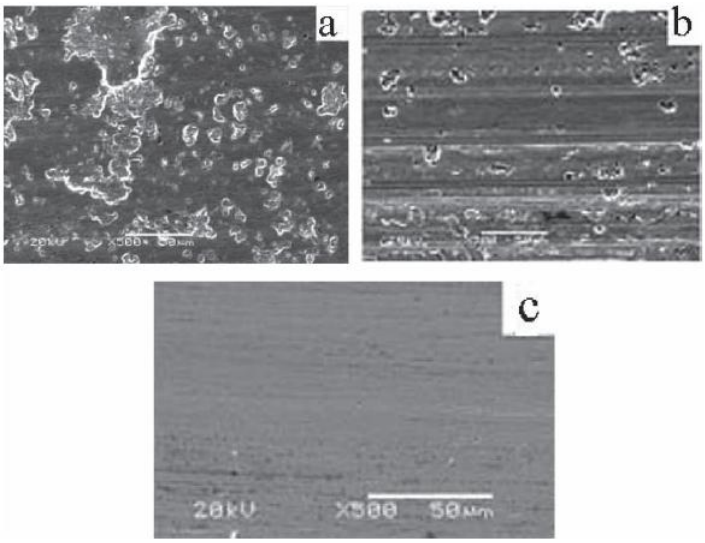


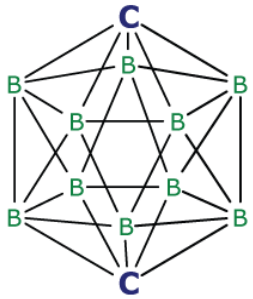
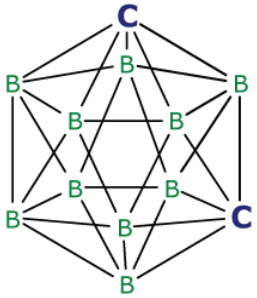
Figure 12.9: SEM images of wear track on SRV test specimens: a) base oil alone, b) IF-MoS_2 and c) trioctylamine-modified IF-WS_2 [369].

Overall it has been reported that some nanoparticle-containing additives give good friction, extreme pressure and wear-reducing properties. Metal and metal oxide nanoparticles seem to form loosely held monolayer-thickness films, while metal carbonates and borates form thick, protective films, with borates superior to carbonates. It appears that fullerenes form a polymer-like film, which is beneficial to wear and particularly friction, while IF nanoparticles appear to be crushed to form a low shear strength layer-lattice film, which adhere to the contact under rubbing to protect the surface.

It has been suggested that a number of factors contributes to the effectiveness of this group of additives [67]: (i) enough nanoparticles need to enter the rubbing contact and overcome deflection round the sides by oil flow [370, 371], (ii) they need to react or adhere to the surface, forming a protective film, and (iii) the film formed needs to be tenacious enough to withstand rubbing conditions, *e.g.* high load.

12.2 Results: Film-forming Properties of Nanoparticle-containing Antiwear Additives

The film-forming properties of nanoparticle-containing antiwear additives were studied using MTM-SLIM under mixed rolling/sliding conditions, as described in chapter 4, section 4.1. The additives employed in this study are summarised in Table 12.1. These were blended into Group III base oil (C) at a concentration of 1000 ppm nanoparticles, and submitted to rubbing under the same test conditions on the MTM-SLIM. Some of these dispersions were stabilised with Polyisobutylene succinimide dispersant 1 (C) at a concentration of 0.1 % in weight, *i.e.* Titanium oxide nanoparticles (C), Fullerene, Double walled carbon nanotubes and IF-WS_2.

Table 12.1: Test materials summary: Nanoparticle-containing additives study		
Abreviation[1]	**Sample name**	**Details**
GIII BO	Group III base oil (C)	-
ZDDP1	Primary ZDDP (C)	9.5 %P; 20.0 %S; 10.6 %Zn
PIBS1	Polyisobutylene succinimide dispersant 1 (C)	-
TiO_2 NANO	Titanium oxide nanoparticles (C)[2]	-
=	Fullerene[2]	-
DWCN	Double walled carbon nanotubes[2]	-
IF-WS_2	IF-WS_2 (C)[2]	-
p-CB	p-Carborane (C)	*e.g.* 
m-CB	m-Carborane (C)	*e.g.* 
cOBCaSu	Crystalline overbased calcium sulphonate (C)	-
aOBCaSu	Amorphous overbased calcium sulphonate (C)	-
nCaSu	Neutral calcium alkylsulphonate (C)	-

(C): commercially-available.

[1] "=" means abbreviated name is the same as full name

[2] Nanoparticle-containing dispersions treated with 0.1 % weight Polyisobutylene succinimide dispersant 1 (C).

Figure 12.10 shows the growth of the tribofilm on the MTM-ball with increasing rubbing time (*i.e.* zero, 5, 15, 30, 60, 120 minutes) for the base oil, Primary ZDDP (C) and nanoparticle-containing fluids. With the base oil alone, scuffing occurred after 5 minutes of rubbing, as shown in Figure 12.10[a)] and the test was terminated. TiO_2 NANO, Fullerene, DWCN and IF-WS_2 dispersions required the use of a dispersing agent, *i.e.* PIBS1, to stabilise the nanoparticles in oil and, because of that, the contribution of the dispersant alone to film-forming, friction, morphology and wear-reducing properties was also investigated.

Apart from crystalline overbased, *i.e.* cOBCaSu, amorphous overbased, *i.e.* aOBCaSu, and neutral calcium sulphonate, *i.e* nCaSu, derived tribofilms, the films formed by the remaining nanoparticle additives are noticeably different from typical tribofilms, such as those formed by ZDDP. The protective film formed by ZDDP is transparent; whereas it appears that the protective films formed by some nanoparticle dispersions are not, *e.g.* PIBS1-, TiO_2 NANO + PIBS1-, Fullerene + PIBS1-, DWCN + PIBS1-, p-CB- and m-CB-derived protective layers. Because of this, a film can be observed on the rubbed track outside the area of contact between the ball and the spacer-layer coated glass disc, where the interference image is obtained, as well as inside it. The protective layer formed by some of these additives appears to be changing the reflective properties of the surface and thus changing the light path. The layer is presumably so thick and reflective that it scatters light instead of reflecting it. This indicates that film thickness measured using MTM-SLIM is not true film thickness, and thus film thickness cannot be measured using this method.

Disturbances in contact shape, probably due to wear, are observed for several additives. Polyisobutylene succinimide dispersant 1 (C), *i.e.* PIBS1 (Figure 12.10[c)]), forms a rough, amorphous deposited layer on the ball surface and a distorted interference image at the front and rear, indicative of wear. Similar distortion is seen for TiO_2 NANO + PIBS1 (Figure 12.10[d)]) and IF-WS_2 + PIBS1 (Figure 12.10[g)]), which form negligible protective layers, Fullerene + PIBS1 (Figure 12.10[e)]) and DWCN + PIBS1 (Figure 12.10[f)]), which form thick protective layers, and p-Carborane (C) (Figure 12.10[h)]) and m-Carborane (C) (Figure 12.10[i)]), both of which initially form a typical reaction film, *i.e.* similar to ZDDP, but much thinner, which is then replaced by a highly reflective protective layer, *i.e.* similar to that formed by PIBS1, Fullerene + PIBS1, DWCN + PIBS1. Changes in contact shape indicative of wear are also observed for Amorphous overbased calcium sulphonate (C), *i.e.* aOBCaSu, (Figure 12.10[k)]) and Neutral calcium alkylsulphonate (C), *i.e.* nCaSu (Figure 12.10[l)]).

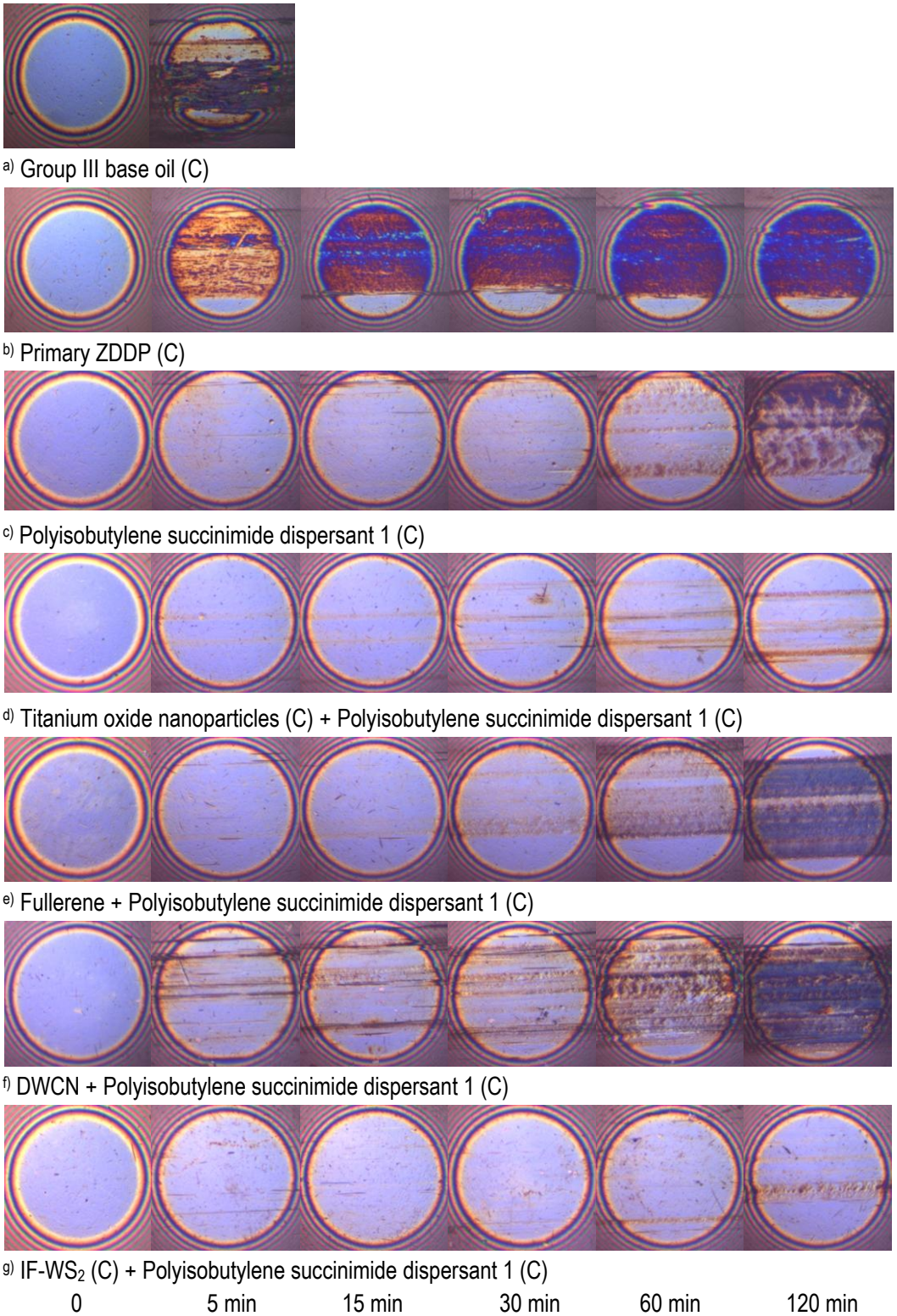


Figure 12.10: MTM-SLIM images showing: a) scuffing on the surface of the ball after 5 minutes of rubbing in base oil without antiwear additive; b) to g) the growth of tribofilm on the ball with increasing rubbing time (*i.e.* zero, 5, 15, 30, 60, 120 minutes).

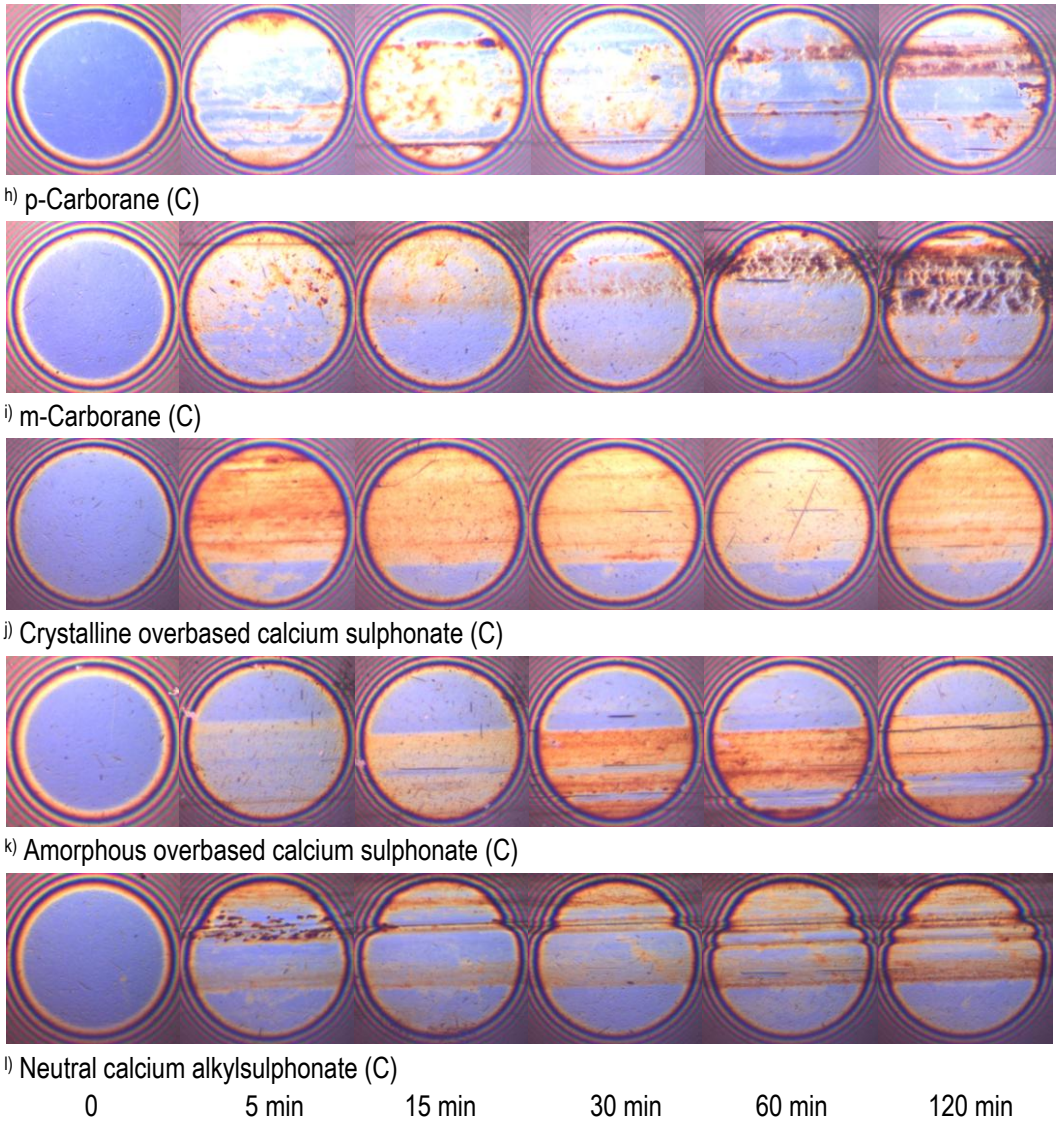


Figure 12.10 (continued): MTM-SLIM images showing: h) to l) the growth of tribofilm on the ball with increasing rubbing time (*i.e.* zero, 5, 15, 30, 60, 120 minutes).

Figure 12.11 compares the development of mean film thickness with rubbing time for Primary ZDDP (C) and those nanoparticle dispersions that have formed typical tribofilms on rubbed surfaces, *i.e.* Crystalline overbased calcium sulphonate (C), Amorphous overbased calcium sulphonate (C) and Neutral calcium alkylsulphonate (C) detergent. It can be seen that the detergents form thinner tribofilms than ZDDP, *i.e.* ≈ 55 nm after 120 minutes of rubbing for Amorphous overbased calcium sulphonate (C) and Neutral calcium alkylsulphonate (C) dispersions and ≈ 40 nm after 120 minutes of rubbing for Crystalline overbased calcium sulphonate (C) dispersion.

Crystalline overbased calcium sulphonate (C) rapidly forms a thick film on the surface, *ca.* 60 nm, which appears to be slightly removed and then replenished during rubbing to yield a uniform but thinner protective film after 2 hours of rubbing, *ca.* 40 nm.

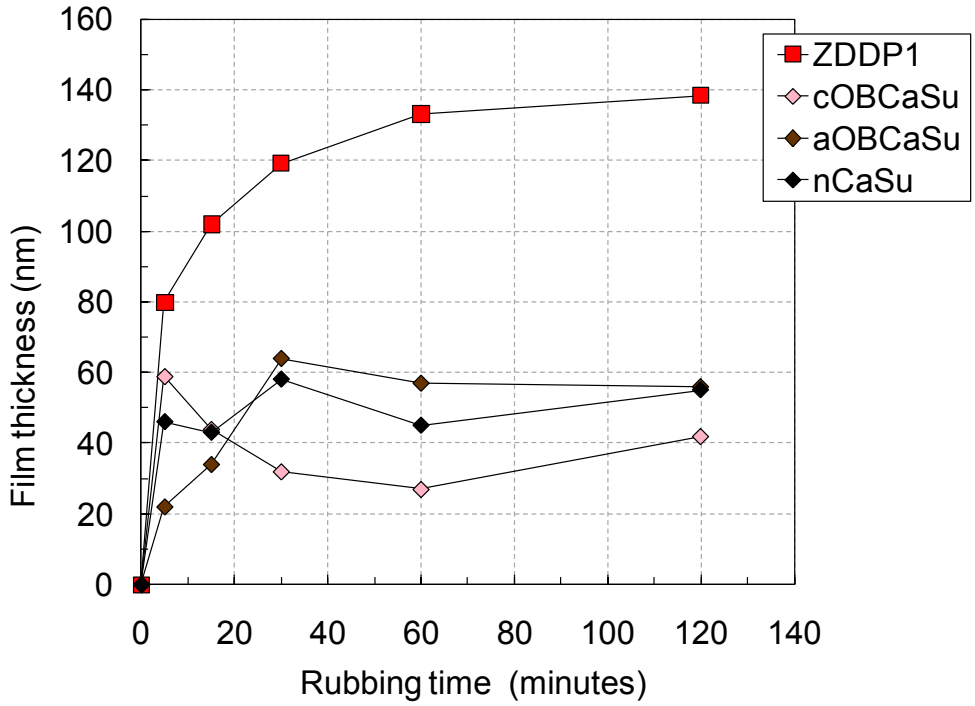


Figure 12.11: Mean film thickness with rubbing time for nanoparticle-containing antiwear additives.

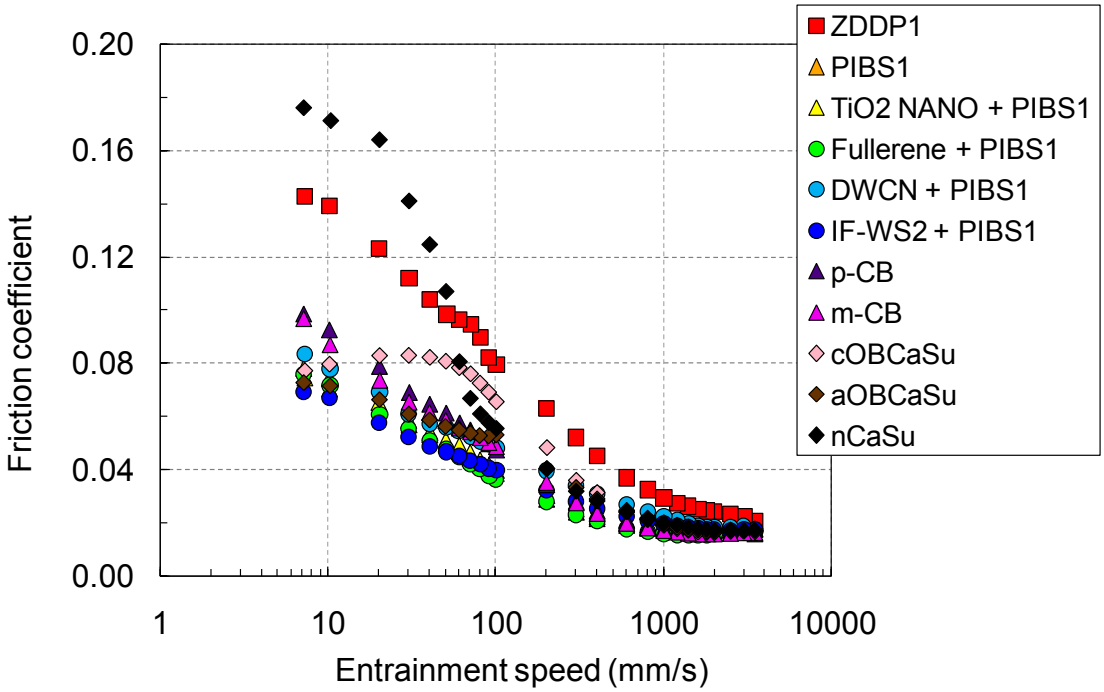
12.3 Results: Friction properties of Nanoparticle-containing Antiwear Additive-derived Tribofilm

The friction properties of a range of nanoparticle-containing dispersions were studied using the MTM under mixed rolling/sliding conditions, as described in chapter 4, section 4.1. The Stribeck curves (Figure 12.12) show the friction coefficient *versus* entrainment speed for these additives at the beginning and after 2 h of rubbing.

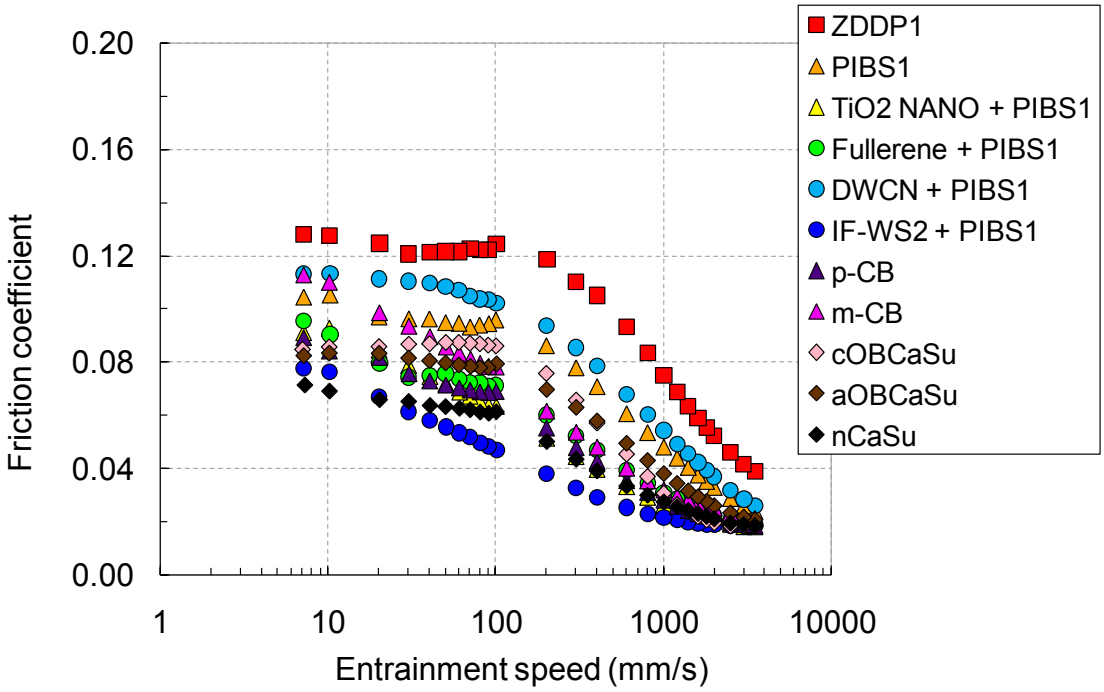
These friction curves illustrate two different types of behaviour; (i) in some cases shifting of the curves to the right and (ii) changes in low speed boundary friction.

An increase in mixed friction can be ascribed to changes in surface texture caused, either by the development of a thick protective layer, *e.g.* PIBS1, Fullerene + PIBS1 and DWCN + PIBS1, or by roughening of the surface due to wear. Conversely, nanoparticle dispersions that formed negligible tribofilms show only a slight increase in mixed friction, *e.g.* TiO_2 NANO + PIBS1 and IF-WS_2 + PIBS1.

In terms of boundary friction, there is a slight increase for all nanoparticle dispersions, except for Neutral calcium alkylsulphonate (C), which gave high initial boundary friction. Crystalline overbased calcium sulphonate (C) shows classical boundary friction behaviour observed when long, linear chain surfactants are present, of friction that increases with speed in the slow speed region.



Initial friction, measured at the beginning of the test



Friction after 2 h of rubbing

Figure 12.12: Stribeck curve showing friction coefficient *versus* entrainment speed at the beginning and after 2 h of rubbing at 50 % SRR, 30 N and 100 ºC.

12.4 Results: Morphology of Nanoparticle-containing Antiwear Additive-derived Tribofilms

The morphology of nanoparticle-containing additive-derived films generated on AISI 52100 steel discs using the MTM was studied by AFM, as described in chapter 4, section 4.2. An area of 25 μm x 25 μm in the centre of the wear track was scanned and the topography of the tribofilms is shown in Figure 12.13. Figure 12.13[a)] shows the topography of an MTM-disc prior to rubbing.

Topography measurements reveal that most nanoparticle-derived protective films consist of discrete pads randomly-distributed along the sliding direction, *i.e.* Fullerene + PIBS1, DWCN + PIBS1, IF-WS_2 + PIBS1, p-CB and m-CB.

Crystalline overbased calcium sulphonate (C) and Amorphous overbased calcium sulphonate (C) comprise quite large pads, while Neutral calcium alkylsulphonate (C) forms a patchy transfer film on the surface. No measurable film was observed using AFM, however, on the surface rubbed with TiO_2 NANO + PIBS1, although PIBS1 alone formed a patchy film on rubbed surfaces. These results are consistent with the MTM-SLIM results (Figure 12.10[d)]).

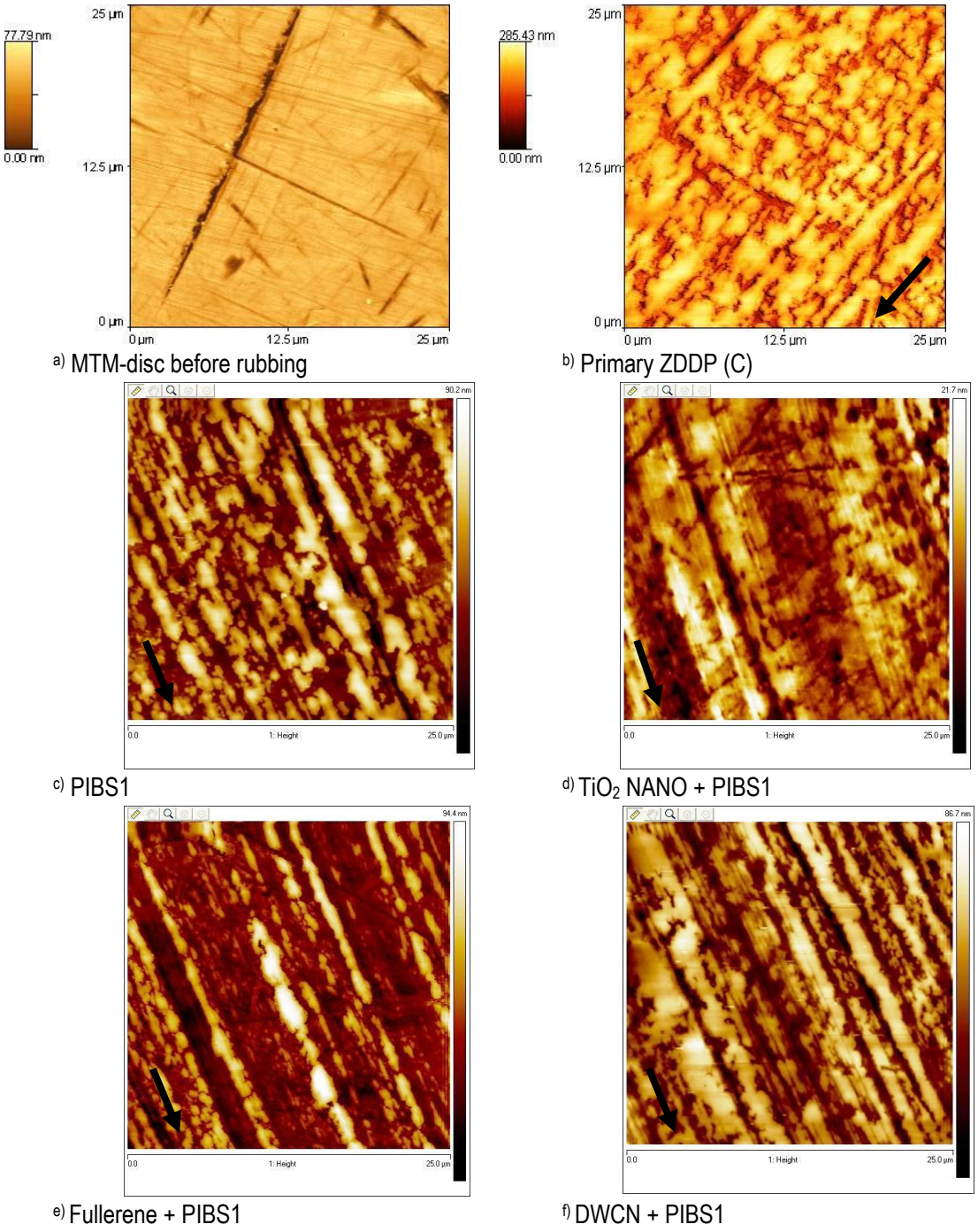
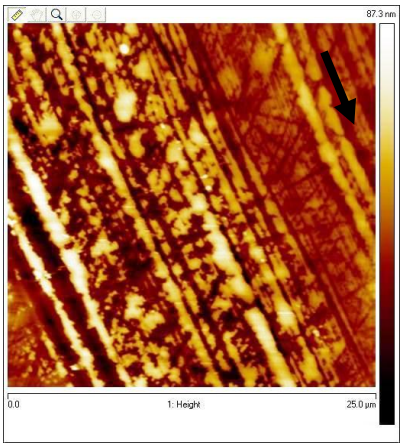
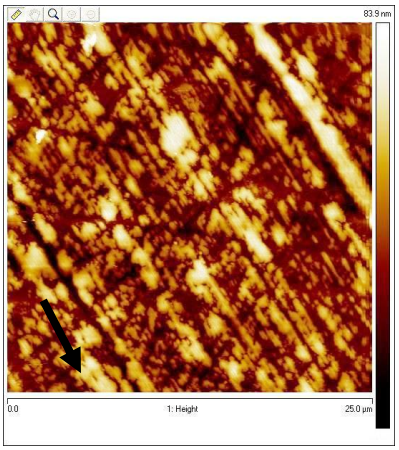


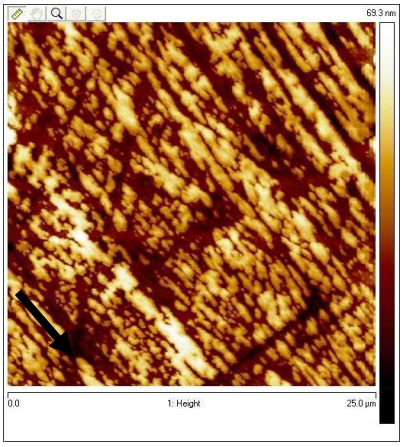
Figure 12.13: AFM 2D topography image at the centre of the wear track on the MTM-disc (sliding direction in b) to f) shown by the arrow).



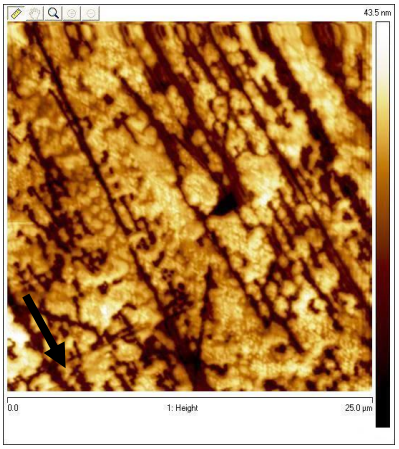
g) IF-WS_2 + PIBS1



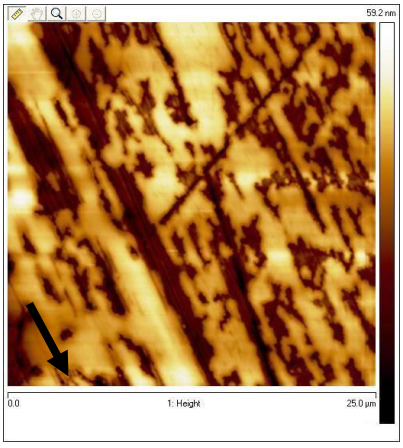
h) p-CB



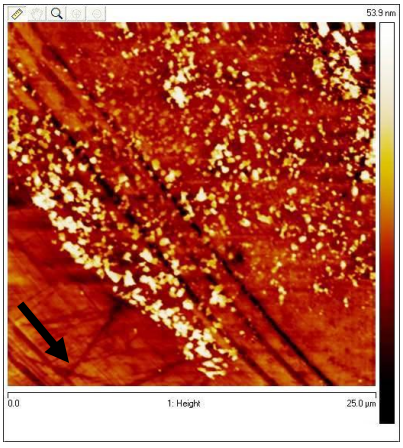
i) m-CB



j) cOBCaSu



k) aOBCaSu



l) nCaSu

Figure 12.13 (continued): AFM 2D topography image at the centre of the wear track on the MTM-disc (sliding direction in g) to l) shown by the arrow).

12.5 Results: Wear-reducing Properties of Nanoparticle-containing Antiwear Additive-derived Tribofilms

The wear-reducing properties of nanoparticle-containing additives were studied using the method developed by the author, which combines the MTM-Reciprocating rig to generate the wear track on AISI 52100 steel discs with SWLI to image the track and measure wear depth, as described in chapter 4, sections 4.3 and 4.4. Results are summarised in Figures 12.14 and 12.15.

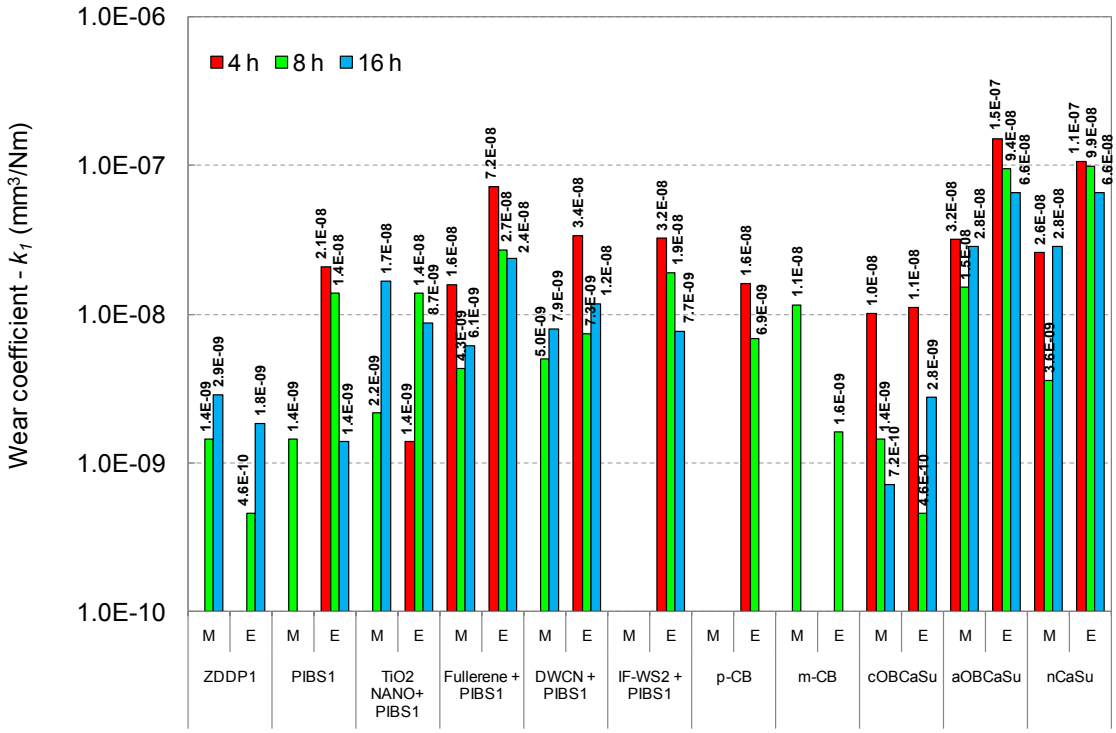
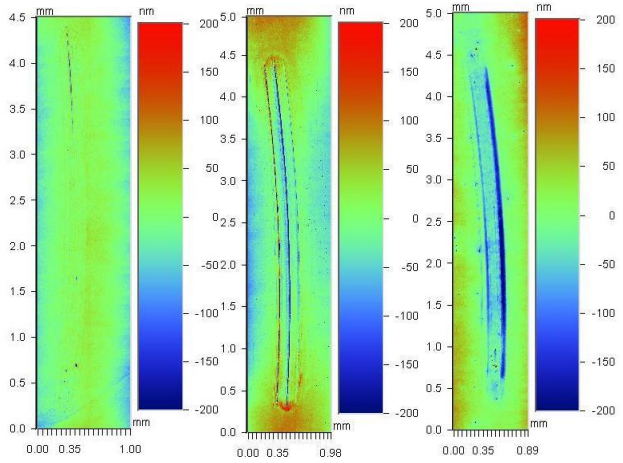


Figure 12.14: Wear coefficient (k_1) in the middle (M) and at the ends (E) of the wear track (*i.e.* average of both ends) for tests lasting 4, 8 and 16 hours.

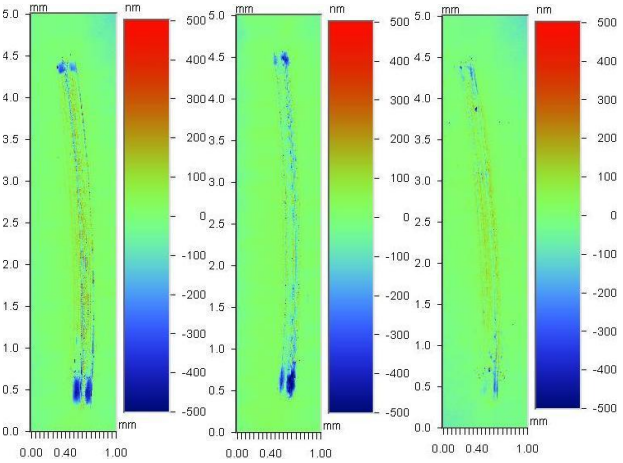
The wear coefficient results show that nanoparticle-containing antiwear additives are not as effective as ZDDP. It is noteworthy that the dispersant alone, PIBS1, shows better performance than when combined with the nanoparticle-containing additives used in this study, except when combined with IF-WS_2.

It can be seen in Figure 12.15 that IF-WS_2 + PIBS1 shows mild measurable wear only at the edges of the wear track, where disc speed is minimum because entrainment speed is changing direction, which might indicate that nanoparticles are being swept around the edges of the contact at low speeds, but once they enter the rubbing contact they adhere to the surface, forming a protective layer able to withstand rubbing at higher speeds, *i.e.* no measurable wear in the middle of the wear track, where disc speed is maximum.

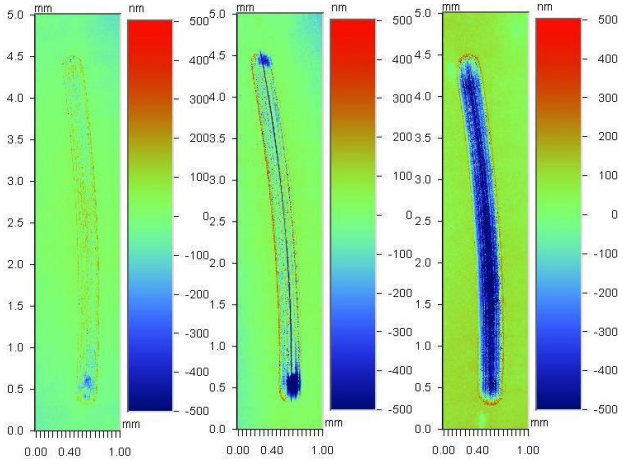
It appears that p-Carborane (C) and m-Carborane (C) show a decrease in wear rate with increasing rubbing time, *i.e.* no measurable wear after 16 h of rubbing, probably because of the development of a protective film during initial rubbing, while Crystalline overbased calcium sulphonate (C) (Figure 12.15), shows comparable wear-reducing properties to ZDDP.



Primary ZDDP (C): 4, 8 and 16 hours after EDTA.

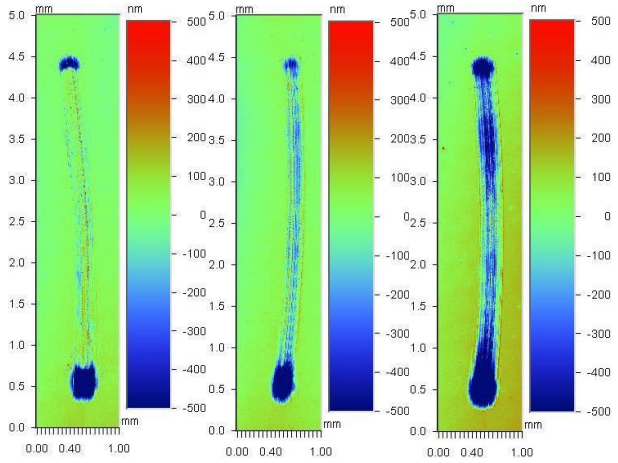


Polyisobutylene succinimide dispersant 1 (C): 4, 8 and 16 hours after EDTA.

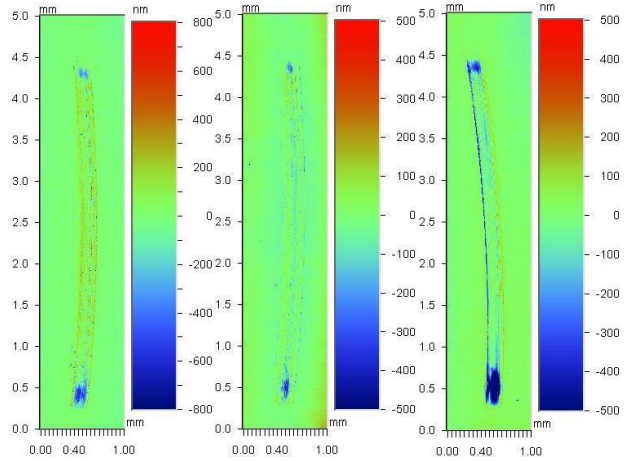


TiO_2 NANO + PIBS1: 4, 8 and 16 hours after EDTA.

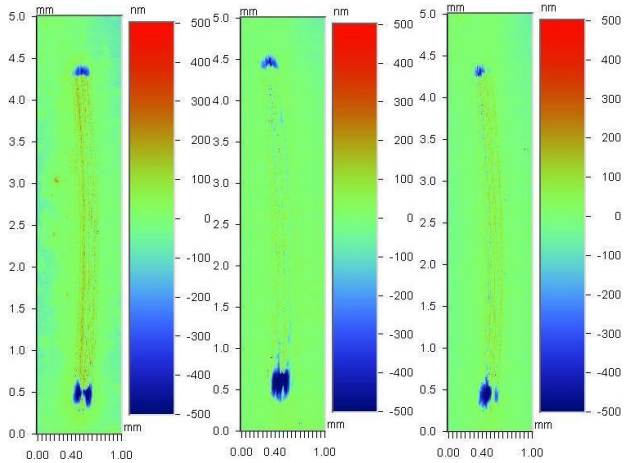
Figure 12.15: SWLI 2D topography images of the wear track on the disc.



Fullerene + PIBS1: 4, 8 and 16 hours after EDTA.

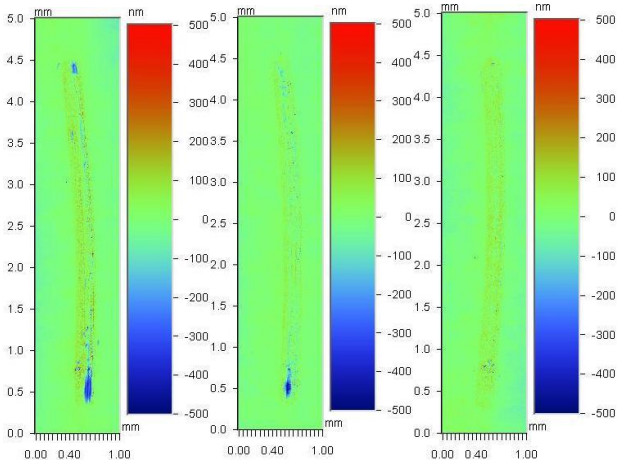


DWCN + PIBS1: 4, 8 and 16 hours after EDTA.

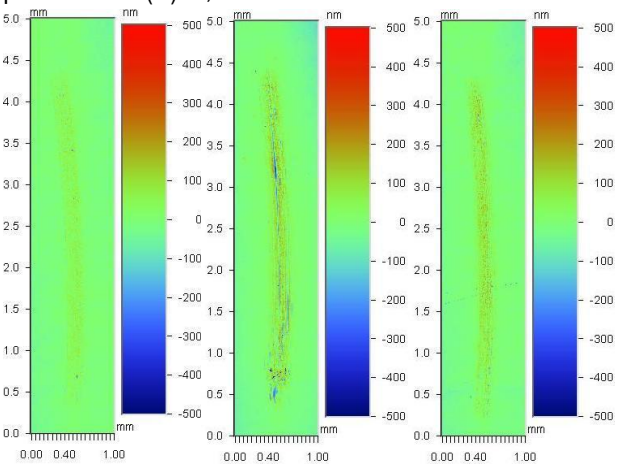


IF-WS_2 + PIBS1: 4, 8 and 16 hours after EDTA.

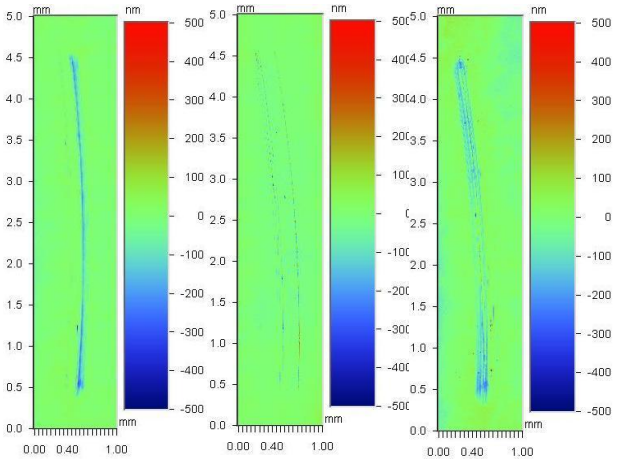
Figure 12.15 (continued): SWLI 2D topography images of the wear track on the disc.



p-Carborane (C): 4, 8 and 16 hours after EDTA.

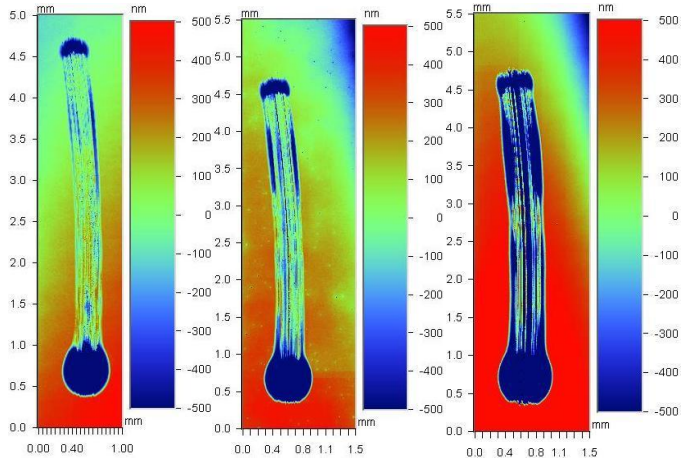


m-Carborane (C): 4, 8 and 16 hours after EDTA.

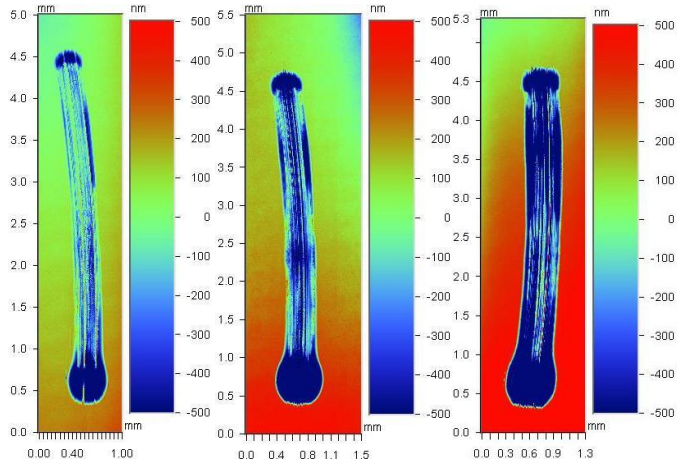


Crystalline overbased calcium sulphonate (C): 4, 8 and 16 hours after EDTA.

Figure 12.15 (continued): SWLI 2D topography images of the wear track on the disc.



Amorphous overbased calcium sulphonate (C): 4, 8 and 16 hours after EDTA



Neutral calcium alkylsulphonate (C): 4, 8 and 16 hours after EDTA.

Figure 12.15 (continued): SWLI 2D topography images of the wear track on the disc after 4, 8 and 16 h rubbing.

12.6 Discussion of Nanoparticle-containing Antiwear Additives Work

The film-forming study under mixed rolling/sliding conditions using MTM-SLIM shows that apart from Crystalline overbased calcium sulphonate (C), Amorphous overbased calcium sulphonate (C) and Neutral calcium alkylsulphonate (C) derived tribofilms, the films formed by the remaining nanoparticle-containing solutions are noticeably different from typical tribofilms, such as those formed by ZDDP.

The protective film formed by ZDDP is transparent; whereas it appears that the protective films formed by some nanoparticle dispersions are not, *e.g.* Fullerene + PIBS1-, DWCN + PIBS1-, p-Carborane (C)- and m-Carborane (C)-derived protective layers. Because of this, a film can be observed on the rubbed track outside the area of contact between the ball and the spacer-layer coated glass disc, where the interference image is obtained, as well as inside the contact. The protective layer formed by some of these additives appears to be changing the reflective properties of the surface and thus changing the light path. The layer is presumably so thick and reflective that it scatters light instead of reflecting it, probably due to its high reflectivity index, *i.e.* like diamonds. This indicates that film thickness measured using MTM-SLIM is not true film thickness, and thus film thickness could not be measured using this method. It was also noted that the PIBS1 dispersant also gave such a film even in the absence of nanoparticles. This may represent decomposition of the dispersant during rubbing to form small carbonaceous particles.

Changes in contact shape, probably caused by wear, are observed for several additive-containing fluids. These include, Amorphous overbased calcium sulphonate (C), Neutral calcium alkylsulphonate (C), Polyisobutylene succinimide dispersant 1 (C), TiO_2 + PIBS1, IF-WS_2 + PIBS1, Fullerene + PIBS1, DWCN + PIBS1, p-Carborane (C) and m-Carborane (C). Although, film thickness could not be measured by MTM-SLIM, it is clear that some of these additives formed thick films on rubbed surfaces, as was confirmed by topography study using AFM.

Although it has been shown by Lee *et al.*, that fullerene reduces oil degradation [357], it is possible that the highly reflective protective films formed by some of the nanoparticle-containing additives consist of a deposited nanoparticle-derived layer and carbonaceous deposits, due to base oil and dispersant degradation, which might be contributing to the formation of a thick film on the surface.

Study of friction behaviour shows that the increase in mixed friction can be ascribed to changes in surface texture caused, either by the development of a thick protective layer, *e.g.* PIBS1, Fullerene + PIBS1 and DWCN + PIBS1, or by roughening of the surface due to wear. Conversely, nanoparticle dispersions that formed negligible tribofilms show only a slight increase in mixed friction, *e.g.* TiO_2 NANO + PIBS1 and IF-WS_2 + PIBS1.

In terms of boundary friction, there is a slight increase for all nanoparticle dispersions, except for Neutral calcium alkylsulphonate (C), which gave high initial boundary friction probably because of the nature of the alkyl chain length of groups attached to the molecule. Amorphous overbased calcium sulphonate (C) shows classical boundary friction behaviour observed when long linear chain surfactants are present, of friction that increases with speed in the slow speed region.

This study has also demonstrated the wear-reducing properties of nanoparticle-containing antiwear additives using the reciprocating MTM. It was found that this group of additives are not as effective as ZDDP. It is noteworthy that the dispersant alone, PIBS1, shows better performance than when combined with the nanoparticle-containing additives used in this study, except when combined with IF-WS_2. This is consistent with findings published by Battez *et al.* [327], who found that the dispersant employed to stabilise the nanoparticles showed better wear-reducing properties alone than when combined with the nanoparticles.

The IF-WS_2 + PIBS1 dispersion shows mild measurable wear only at the edges of the wear track, where disc speed is minimum because entrainment speed is changing direction, which might indicate that nanoparticles are being swept around the edges of the contact at low speeds, but once they enter the rubbing contact they adhere to the surface, forming a protective layer able to withstand rubbing at higher speeds, *i.e.* no measurable wear in the middle of the wear track, where disc speed is maximum.

It appears that p-Carborane (C) and m-Carborane (C) show a decrease in wear rate with increasing rubbing time, *i.e.* no measurable wear after 16 h of rubbing, probably because of the development of a protective film during initial rubbing, while Crystalline overbased calcium sulphonate (C), shows comparable wear-reducing properties to ZDDP.

The Crystalline overbased calcium sulphonate (C) additive rapidly forms a thick film on the surface, *ca.* 60 nm, which appears to be slightly removed and then replenished during rubbing to yield a uniform but, thinner protective film after 2 hours of rubbing, *ca.* 40 nm. It has been suggested by Costello that crystalline calcium sulphonates are more stable than amorphous calcium sulphonate detergents, because the latter forms either a calcite-deposited film or calcite-containing wear debris [332], which might give abrasive wear. Hence, the superior performance of the crystalline overbased detergent over the amorphous overbased and neutral calcium sulphonate detergents might be ascribed to its higher stability under rubbing conditions.

The chapter that follows presents the surface analysis of films formed by various additives of interest.

13. SURFACE ANALYSIS OF LOW AND ZERO SAPS ANTIWEAR ADDITIVES-DERIVED TRIBOFILMS

It is believed that the characteristics of the tribofilms and their antiwear performance result from the processes by which these additives are adsorbed onto the metal surface during rubbing and subsequently react to form a complex lubricating film. It has been suggested that most antiwear tribofilms are not composed by the additives themselves but consist of the decomposition/reaction products of these additives. Thus, by better understanding the chemistry of tribofilms one might be able to identify which chemical species improve film formation, growth and longevity, as well as, its wear-reducing properties.

This chapter presents results of the chemical characterisation of tribofilms formed by ZDDP and potential low and zero SAPS antiwear additives using the two surface analysis techniques, ToF-SIMS and XANES.

13.1 Analysis and Materials

The chemical nature of antiwear additives-derived tribofilms generated on AISI 52100 steel discs from the MTM after two hours rubbing, was studied using ToF-SIMS and XANES, as described in chapter 4, sections 4.5 and 4.6.

ToF-SIMS was employed to obtain chemical maps based on the distribution of positive and negative ions present on the outermost surface, *i.e.* maximum sampling depth of 2 nm. An area of 500 μm x 500 μm spanning rubbed/unrubbed areas or at the edge of the wear track was submitted to analysis and a chemical map was obtained. Brighter regions in the image indicate an abundance of element, molecule or ion of interest, while darker regions indicate their absence.

XANES photoadsorption spectra were recorded using TEY and FY modes of detection. TEY detection mode provides chemical information about the surface/near surface of the film *(i.e.* ≈ 5 nm) at the L-edge; and the bulk of the film *(i.e.* ≈ 50 nm) at the K-edge. FY focuses on the bulk of the film *(i.e.* ≈ 50 nm) at the L-edge; and on the bulk of the film through the film-steel interface to the substrate (*i.e.* > 5 μm) at the K-edge.

The tribofilms studied in this chapter are summarised in Table 13.1 and 13.2. Model compounds of various nature and oxidation states used in XANES analysis to help identify chemical species by qualitative comparison were presented in chapter 4, Table 4.6. Fresh samples of corresponding antiwear additives were also used for reference as listed in Table13.3.

Table 13.1: Tribofilms studied using ToF-SIMS[1]	
Abreviation	**Sample name**
ZDDP1	Primary ZDDP (C) tribofilm
B2EHP	Bis(2-ethylhexyl) phosphite tribofilm
B2EHP + Ti-IPO	Bis(2-ethylhexyl) phosphite + 1 % Titanium (IV) isopropoxide tribofilm
TAP	Triaryl phosphate (C) tribofilm
ADTP	Ashless dithiophosphate (C) tribofilm
ADTP + nCaSu	Ashless dithiophosphate (C) + 1 % Neutral calcium alkylsulphonate (C)
ADTP + Ti-IPO	Ashless dithiophosphate (C) + 1 % Titanium (IV) isopropoxide tribofilm
TPPT	Triphenyl phosphorothionate (C) tribofilm
ATPPT	Alkylated triphenyl phosphorothionate (C) tribofilm
MBDADTC	Methylene-bis-dialkyl-dithiocarbamate (C)
MoDTC	Molybdenum dialkyldithiocarbamate (C) tribofilm
B-PIBS(H)	Borated polyisobutenyl succinimide (High B) (C) tribofilm
KB	Potassium borate (C) tribofilm
PIBS1	Polyisobutylene succinimide dispersant 1 (C) tribofilm
TiO_2 NANO + PIBS1	Titanium oxide nanoparticles (C) + 0.1 % PIBS1 tribofilm
IF-WS_2 + PIBS1	IF-WS_2 (C) + 0.1 % PIBS1 tribofilm
p-CB	p-Carborane (C) tribofilm
m-CB	m-Carborane (C) tribofilm
cOBCaSu	Crystalline overbased calcium sulphonate (C) tribofilm
aOBCaSu	Amorphous overbased calcium sulphonate (C) tribofilm
nCaSu	Neutral calcium alkylsulphonate (C) tribofilm

(C): commercially-available.

[1] The concentration of nitrogen in the tribofilms formed by nitrogen-containing heterocyclic antiwear additives, *i.e.* Benzotriazole (C) and Hydroxyquinoline (C), was below the detection limit for the instrument, so these tribofilms could not be studied using ToF-SIMS.

Table 13.2: Tribofilms studied using XANES[1]	
Abreviation	**Sample name**
ZDDP1 (TF)	Primary ZDDP (C) tribofilm
B2EHP (TF)	Bis(2-ethylhexyl) phosphite tribofilm
B2EHP + Ti-IPO (TF)	Bis(2-ethylhexyl) phosphite + 1 % Titanium (IV) isopropoxide tribofilm
TAP (TF)	Triaryl phosphate (C) tribofilm
ADTP (TF)	Ashless dithiophosphate (C) tribofilm
ADTP + nCaSu (TF)	Ashless dithiophosphate (C) + 1 % Neutral calcium alkylsulphonate (C) tribofilm
ADTP + Ti-IPO (TF)	Ashless dithiophosphate (C) + 1 % Titanium (IV) isopropoxide tribofilm
TPPT (TF)	Triphenyl phosphorothionate (C) tribofilm
ATPPT (TF)	Alkylated triphenyl phosphorothionate (C) tribofilm
DMTDA2 (TF)	Dimercaptothiadiazole 2 (C) tribofilm
MBDADTC (TF)	Methylene-bis-dialkyl-dithiocarbamate (C) tribofilm
ZnDTC (TF)	Zinc diamyl dithiocarbamate (C) tribofilm
MoDTC (TF)	Molybdenum dialkyldithiocarbamate (C) tribofilm
TEHB (TF)	Tris(2-ethylhexyl) borate (C) tribofilm
B-PIBS(H) (TF)	Borated polyisobutenyl succinimide (High B) (C) tribofilm
KB (TF)	Potassium borate (C) tribofilm
IF-WS_2 + PIBS1 (TF)	IF-WS_2 (C) + 0.1 % PIBS1 tribofilm
cOBCaSu (TF)	Crystalline overbased calcium sulphonate (C) tribofilm
aOBCaSu (TF)	Amorphous overbased calcium sulphonate (C) tribofilm
nCaSu (TF)	Neutral calcium alkylsulphonate (C) tribofilm

(C): commercially-available; (TF): tribofilm.

[1] The concentration of nitrogen in the tribofilms formed by nitrogen-containing heterocyclic antiwear additives, *i.e.* Benzotriazole (C) and Hydroxyquinoline (C), and of boron in the tribofilms formed by some nanoparticle-containing antiwear additives, *i.e.* p-Carborane (C) and m-Carborane (C), were below the detection limit for the instrument, so these tribofilms could not be studied using XANES.

Table 13.3: Corresponding additives used as references in XANES analysis	
Abreviation	**Sample name**
ZDDP1 (ad)	Primary ZDDP (C)
B2EHP (ad)	Bis(2-ethylhexyl) phosphite
TAP (ad)	Triaryl phosphate (C)
ADTP (ad)	Ashless dithiophosphate (C)
TPPT (ad)	Triphenyl phosphorothionate (C)
ATPPT (ad)	Alkylated triphenyl phosphorothionate (C)
DMTDA2 (ad)	Dimercaptothiadiazole 2 (C)
MBDADTC (ad)	Methylene-bis-dialkyl-dithiocarbamate (C)
ZnDTC (ad)	Zinc diamyl dithiocarbamate (C)
MoDTC (ad)	Molybdenum dialkyldithiocarbamate (C)
TEHB (ad)	Tris(2-ethylhexyl) borate (C)
B-PIBS(H) (ad)	Borated polyisobutenyl succinimide (High B) (C)
KB (ad)	Potassium borate (C)
IF-WS_2 (ad)	IF-WS_2 (C)
cOBCaSu (ad)	Crystalline overbased calcium sulphonate (C)
aOBCaSu (ad)	Amorphous overbased calcium sulphonate (C)
nCaSu (ad)	Neutral calcium alkylsulphonate (C)

(C): commercially-available; (ad): fresh additive.

13.2 Results: Surface Analysis of ZDDP-derived Tribofilm

ToF-SIMS chemical maps (Figure 13.1) show that the outer layer of ZDDP1-derived tribofilms consist mainly of phosphorus species, *i.e.* PO_2^-, PO_3^- and PO_4^-, with some sulphur also present. Zn-containing species appear mainly in the wear track, indicating that there is negligible tribofilm formation outside the rubbed area. No Fe-containing species were detected inside the wear track.

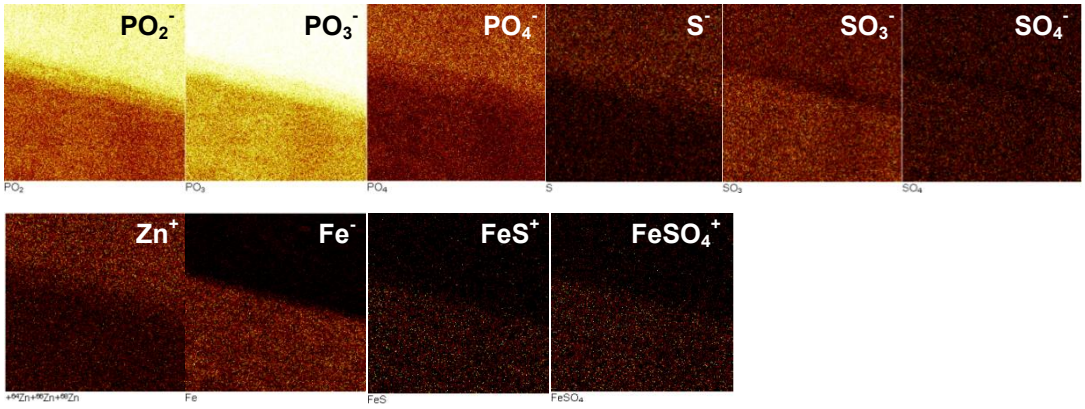
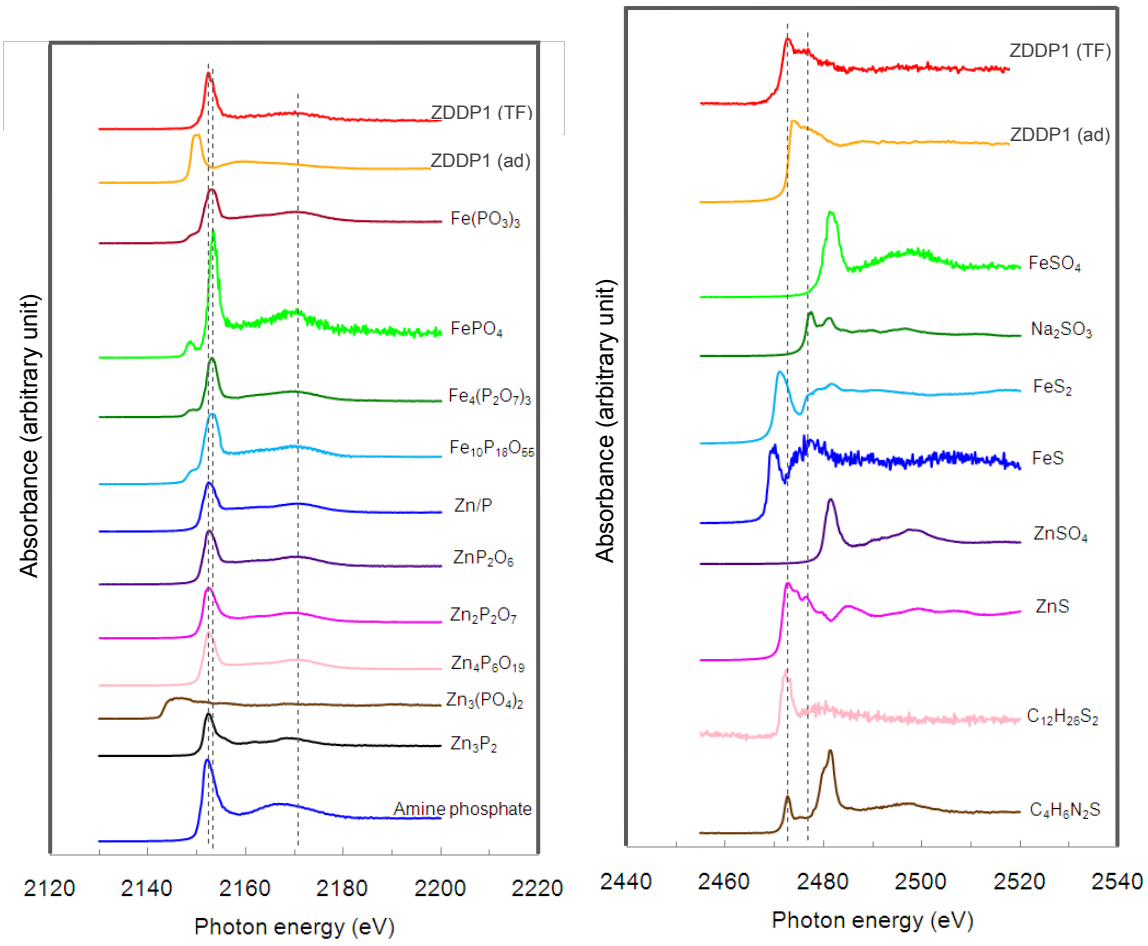


Figure 13.1: ToF-SIMS chemical maps of tribofilm formed by Primary ZDDP (C), *i.e.* ZDDP1, (outermost surface, 1-2 nm). In this case, the wear track is seen at the top of the images.

The XANES spectra (Figure 13.2), shows that the bulk of the tribofilm through the interface between film and steel comprises a mixture of Zn phosphates and polyphosphates of varying chain lengths, *i.e.* Zn/P, ZnP_2O_6, $Zn_2P_2O_7$, $Zn_4P_6O_{19}$, Zn_3P_2, with some Fe-containing species also present, *i.e.* $Fe(PO_3)_3$, $FePO_4$, $Fe_4(P_2O_7)_3$, $Fe_{10}P_{18}O_{55}$. The presence of ZnS and FeS, as well as some organic sulphide and disulphide was also detected at the bulk/interface. These results are consistent with those published by Martin *et al.* [126], Yamaguchi *et al.* [372], Zhang *et al.* [101] and Nicholls *et al.* [105].

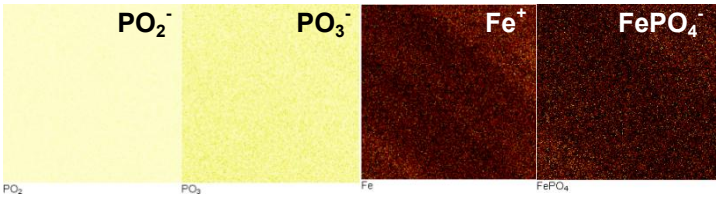


(a) (b)

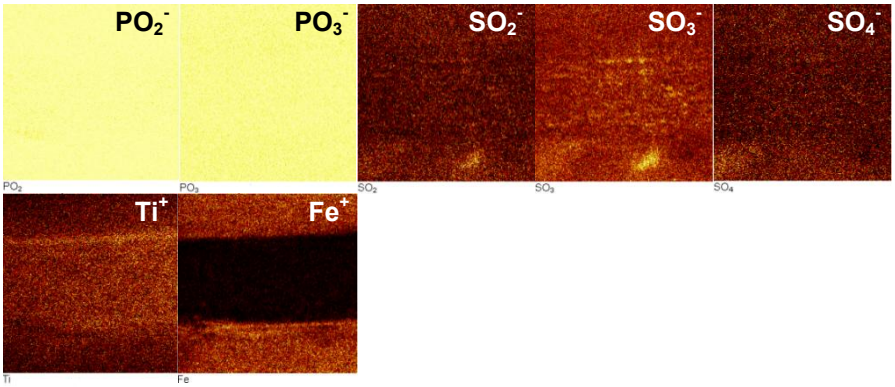
Figure 13.2: XANES spectra of tribofilm formed by Primary ZDDP (C), corresponding fresh additive and model compounds: (a) phosphorus K-edge FY (bulk through the film-steel interface to the substrate, > 5 µm) and (b) sulphur K-edge FY (bulk through the film-steel interface to the substrate, > 5 µm).

13.3 Results: Surface Analysis of P-containing Antiwear Additive-derived Tribofilms

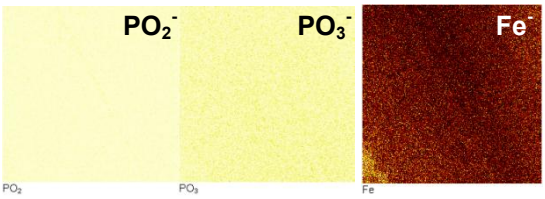
Figure 13.3 shows that the outer layer of the films formed by Bis(2-ethylhexyl) phosphite and Triaryl phosphate (C) consists mainly of phosphorus species, *i.e.* PO_2-, PO_3-, with no $FePO_4$ being detected on the surface rubbed in the presence of medium-chain phosphite (Figures 13.3a)). Interestingly, there seems to be almost as much PO_2^- and PO_3^- outside as inside the rubbed track, which is not surprising given the maximum sampling depth of ToF-SIMS, *i.e.* ≈ 2 nm. The Fe is completely obscured in the presence of Ti-containing reaction film formed by Bis(2-ethylhexyl) phosphite + 1 % titanium (IV) isopropoxide (Figures 13.3[b)]). This is consistent with results shown in chapter 6, Figure 6.8[g)].



a) Bis(2-ethylhexyl) phosphite



b) Bis(2-ethylhexyl) phosphite + 1% Titanium (IV) isopropoxide



c) Triaryl phosphate (C)

Figure 13.3: ToF-SIMS chemical maps of tribofilms formed by: a) Bis(2-ethylhexyl) phosphite, b) Bis(2-ethylhexyl) phosphite + 1% Titanium (IV) isopropoxide and c) Triaryl phosphate (C) (outermost surface, 1-2 nm). In these cases, the tribofilm is seen in the middle of the images.

Figure 13.4 (a) and (b) show the chemical composition of the bulk and the interface film-steel, respectively. The bulk of the tribofilm formed by Bis(2-ethylhexyl) phosphite comprises phosphite, probably from additive decomposition, phosphate and Fe polyphosphate, *i.e.* $Fe_{10}P_{18}O_{55}$. The interface consists of a mixture of Fe-P-containing species, *i.e.* $Fe(PO_3)_3$, $FePO_4$, $Fe_4(P_2O_7)_3$, $Fe_{10}P_{18}O_{55}$. These results are consistent with those published by Najman *et al.* [373]. There seems to be no significant change in the composition of the bulk of this film in the presence of titanium (IV) isopropoxide, albeit ToF-SIMS chemical maps revealed the presence of Ti^+ on the outermost surface of the film, *i.e.* 1-2 nm (Figure 13.3[b)]).

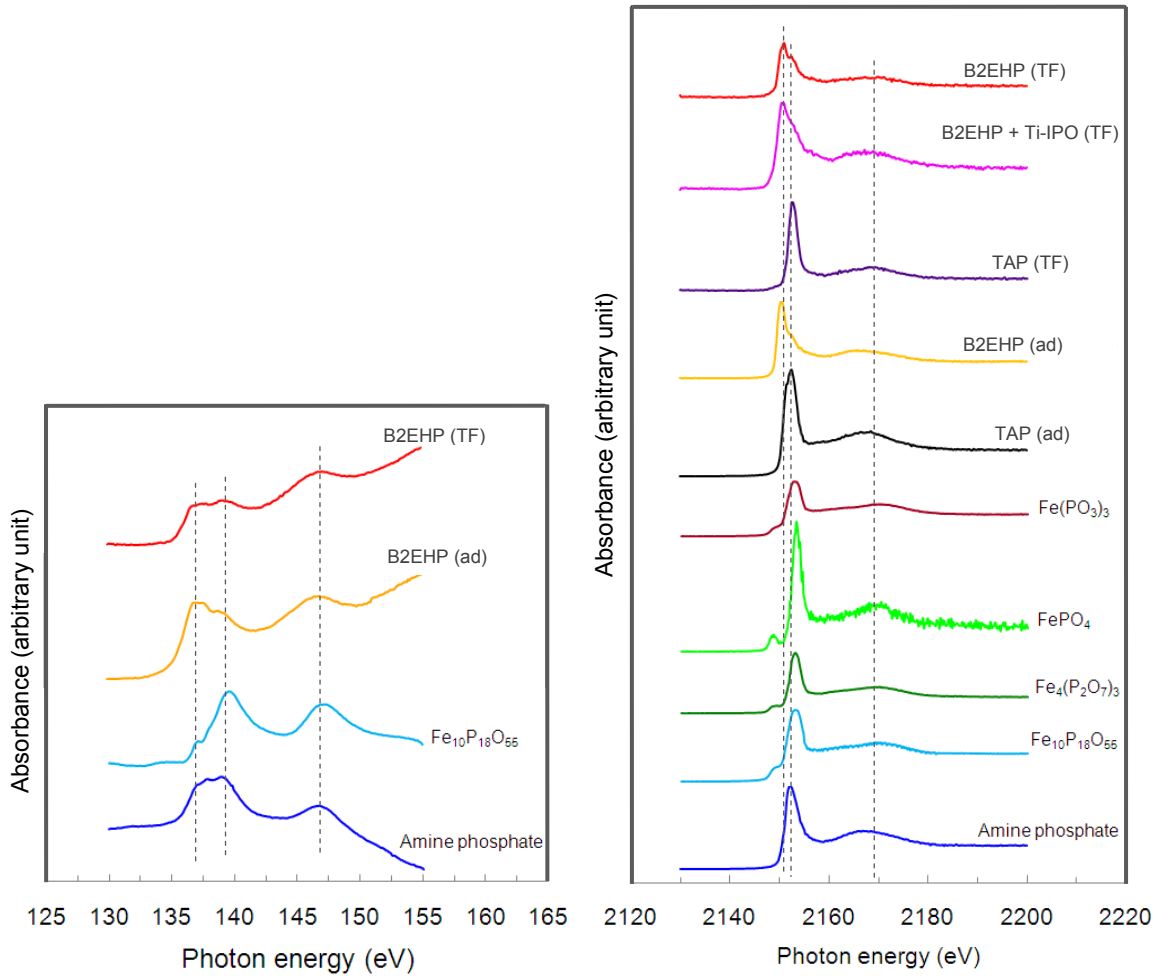


Figure 13.4: XANES spectra of tribofilms formed by Bis(2-ethylhexyl) phosphite, *i.e.* B2EHP, Bis(2-ethylhexyl) phosphite + 1% Titanium (IV) isopropoxide, *i.e.* B2EHP + Ti-IPO, Triaryl phosphate (C), *i.e.* TAP, corresponding fresh additives and model compounds: (a) phosphorus L-edge FY (bulk, ≈ 50 nm) and (b) phosphorus K-edge FY (bulk through the film-steel interface to the substrate, > 5 µm).

13.4 Results: Surface Analysis of P-S-containing Antiwear Additive-derived Tribofilms

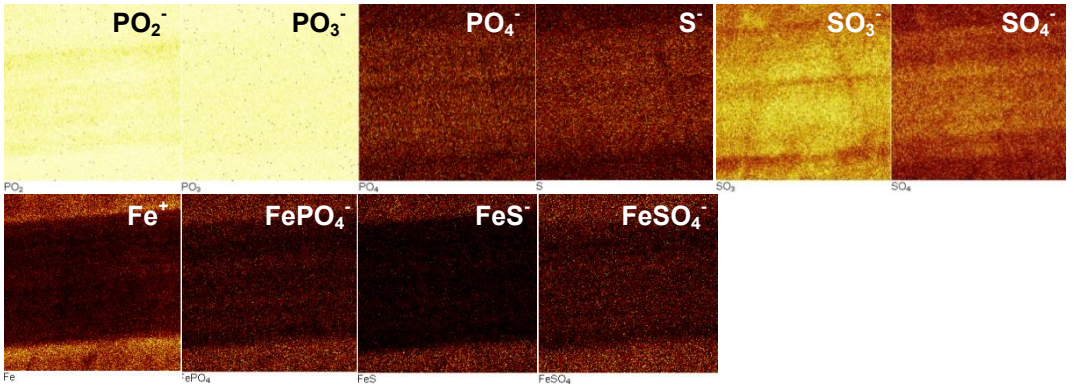
The surface of the tribofilms formed by P-S-containing antiwear additives consists primarily of PO_2^-, PO_3^- and SO_3^-, as can be seen in Figure 13.5. The Fe is obscured by the tribofilm in most cases, except for the Triphenyl phosphorothionate (C)-derived tribofilm, *i.e.* TPPT (TF), (Figure 13.5[d)]) and the Alkylated triphenyl phosphorothionate (C)-derived tribofilm, *i.e.* ATPPT (TF) (Figure 13.5[e)]), both of which appear to incorporate Fe into the film. Some of the phosphorus and sulphur species seem spread evenly inside and outside the rubbed track, and although in most cases higher concentration of these species can be seen inside the track, these results suggest the formation of very thin films outside the rubbed area.

The outer layer of the reaction films formed by Ashless dithiophosphate (C), *i.e.* ADTP (TF), in the presence of separate metal cations, *i.e.* Neutral calcium alkylsulphonate (C) and the Titanium (IV) isopropoxide was also analysed. The chemical maps show the presence of Ca species, *i.e.* Ca^+ and $CaOH^+$ (Figure 13.5[b)]) and Ti species (Figure 13.5[c)]) on the surface, which indicate that these cations have been incorporated into the tribofilm formed by Ashless dithiophosphate (C), *i.e.* ADTP (TF) under rubbing. This is consistent with results shown in chapter 7, Figure 7.10[d)] and 7.10[e)].

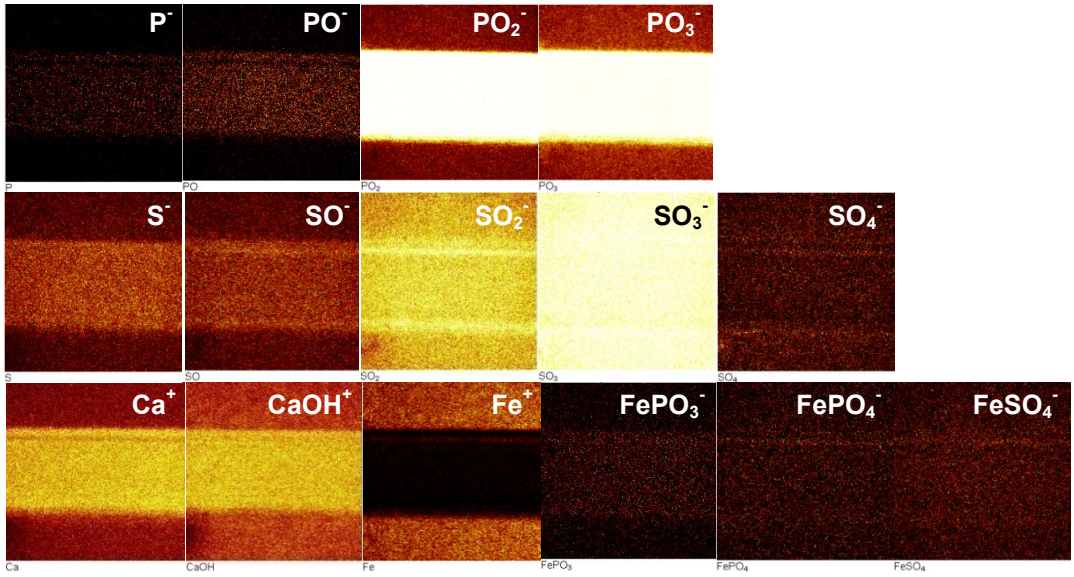
XANES spectra of the surface/near surface, *i.e.* ≈ 5 nm, seen in Figures 13.6 and 13.8, show the presence of phosphate, Fe polyphosphate, *i.e.* $Fe_{10}P_{18}O_{55}$, sulphite and $FeSO_4$. This is consistent with chemical maps obtained using ToF-SIMS (Figure 13.5).

The composition of the bulk of the tribofilm through the interface film-steel, illustrated in Figures 13.7 and 13.9, comprises a mixture of Fe-P- and Fe-S-containing species, *i.e.* $Fe(PO_3)_3$, $FePO_4$, $Fe_4(P_2O_7)_3$, $Fe_{10}P_{18}O_{55}$, $FeSO_4$,, sulphite, FeS_2, organic sulphide and disulphide.

These results are consistent with those published by Zhang *et al.* [101], Najman *et al.* [100, 109, 374], Nicholls *et al.* [105] and Kim *et al.* [375].

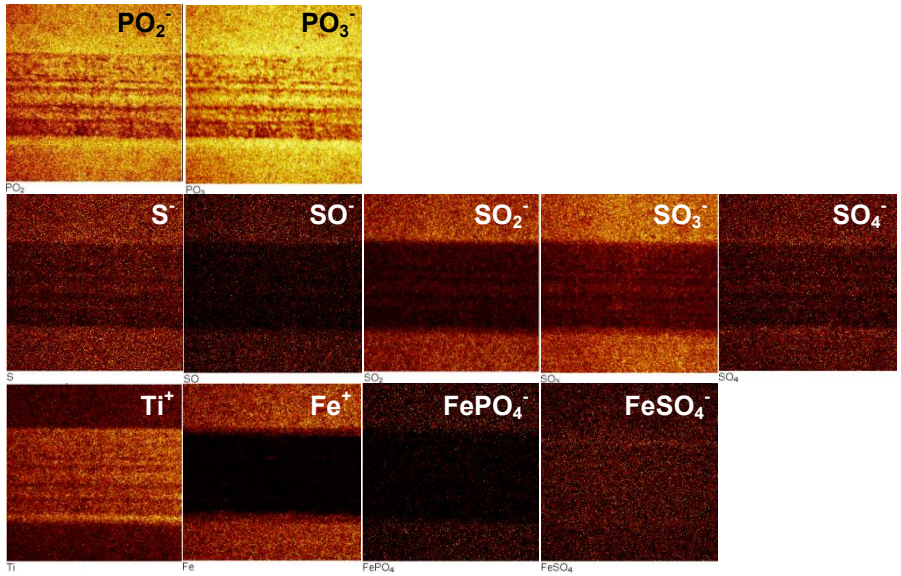


a) Ashless dithiophosphate (C)

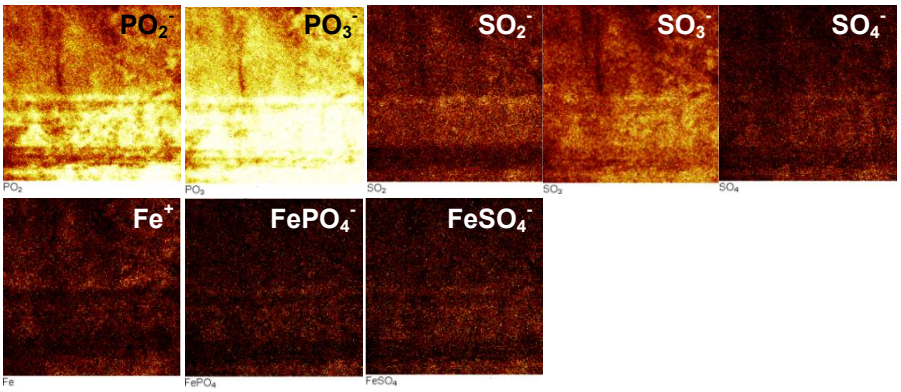


b) Ashless dithiophosphate (C) + 1 % nCaSu

Figure 13.5: ToF-SIMS chemical maps of tribofilms formed by: a) Ashless dithiophosphate (C) and b) Ashless dithiophosphate (C) + 1 % nCaSu (outermost surface, 1-2 nm). In these cases, the tribofilm is seen in the middle of the images.

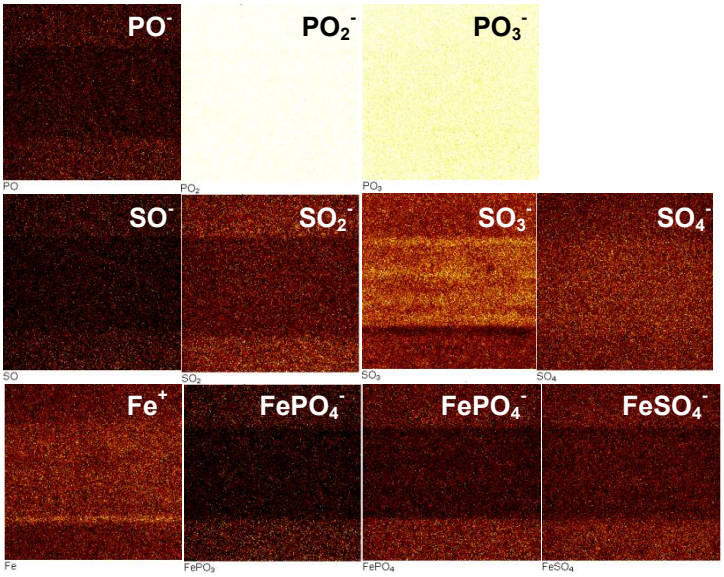


c) Ashless dithiophosphate (C) + 1% Titanium (IV) isopropoxide



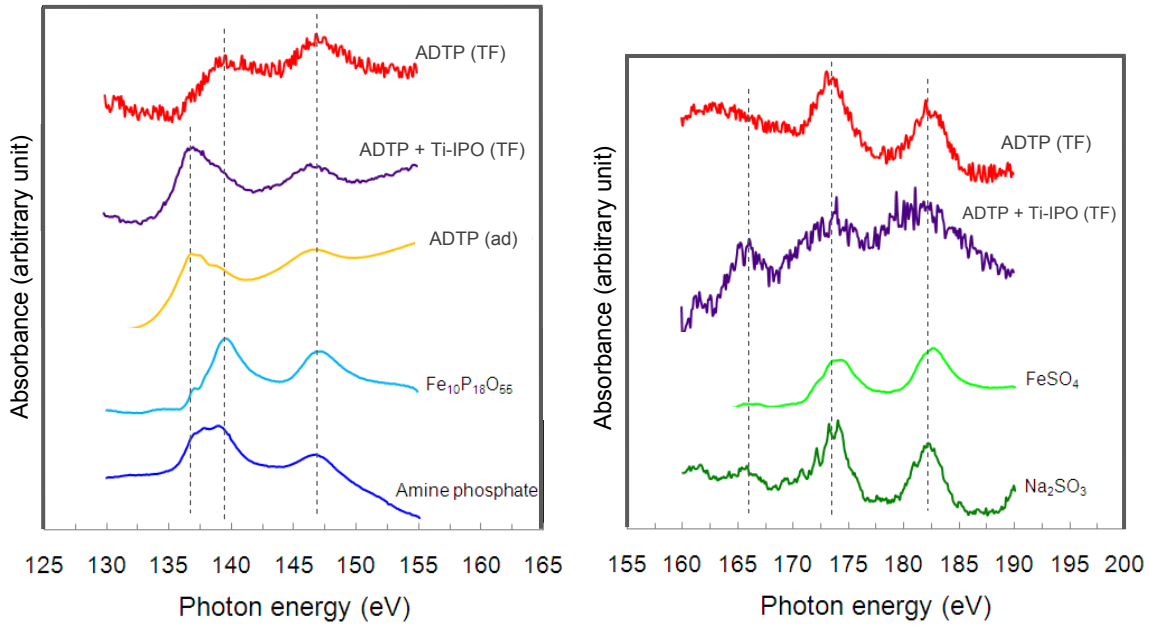
d) Triphenyl phosphorothionate (C)

Figure 13.5 (continued): ToF-SIMS chemical maps of tribofilms formed by: c) Ashless dithiophosphate (C) + Titanium (IV) isopropoxide and d) Triphenyl phosphorothionate (C) (outermost surface, 1-2 nm). The tribofilm is seen in the middle of the images for Ashless dithiophosphate (C) + 1% Titanium (IV) isopropoxide and at the bottom of the images for Triphenyl phosphorothionate (C).



e) Alkylated triphenyl phosphorothionate (C)

Figure 13.5 (continued): ToF-SIMS chemical maps of tribofilms formed by: e) Alkylated triphenyl phosphorothionate (C) (outermost surface, 1-2 nm). In this case, the tribofilm is seen in the middle of the images.



(a) (b)

Figure 13.6: XANES spectra of tribofilms formed by Ashless dithiophosphate (C), *i.e.* ADTP, Ashless dithiophosphate (C) + 1 % Titanium (IV) isopropoxide, *i.e.* ADTP + Ti-IPO, corresponding fresh additives and model compounds: (a) phosphorus L-edge TEY (surface/near surface, ≈ 5 nm) and (b) sulphur L-edge TEY (surface/near surface, ≈ 5 nm).

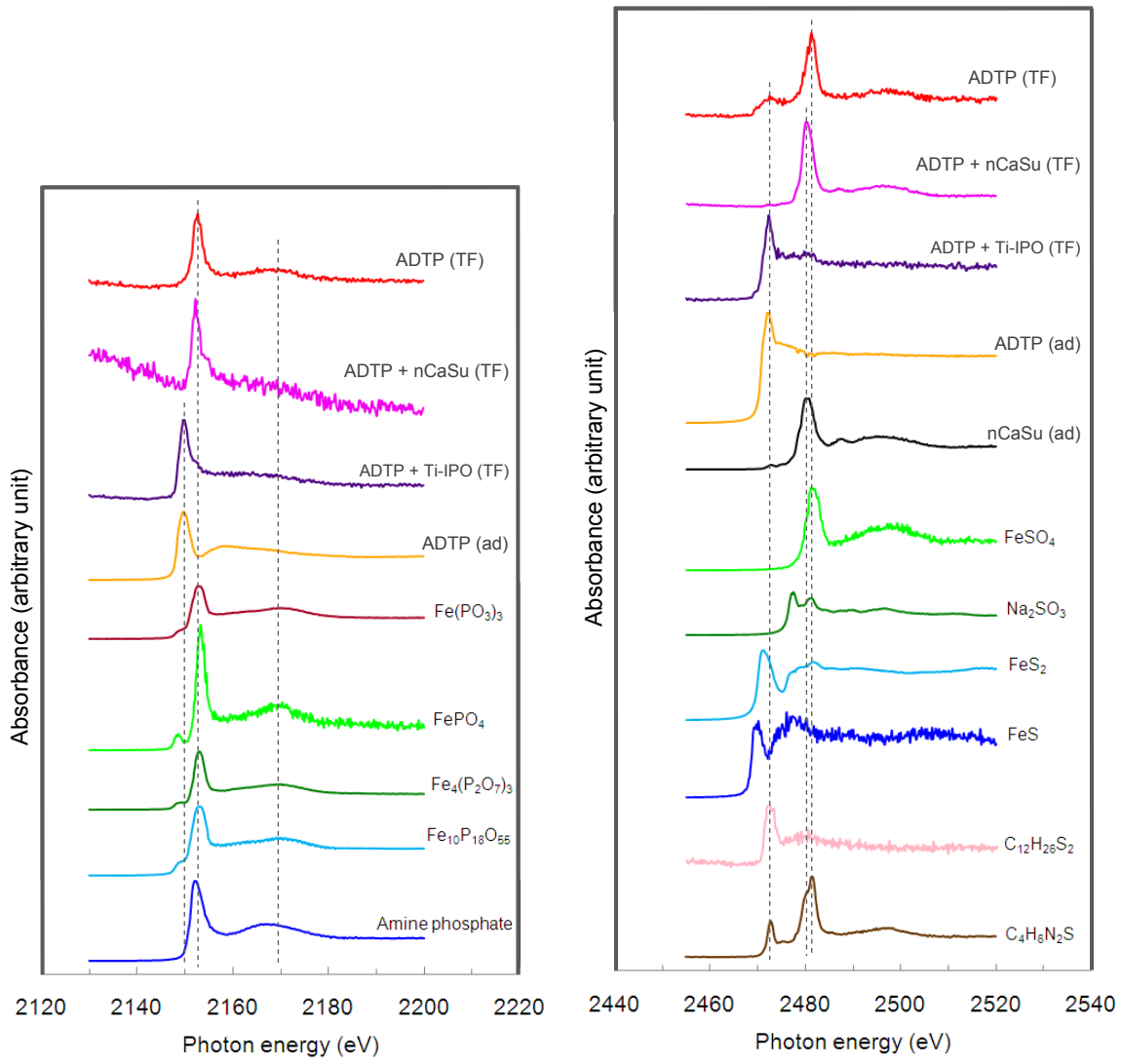


Figure 13.7: XANES spectra of tribofilms formed by Ashless dithiophosphate (C), *i.e.* ADTP, Ashless dithiophosphate (C) + 1 % nCaSu, *i.e.* ADTP + nCaSu, Ashless dithiophosphate (C) + 1 % Titanium (IV) isopropoxide, *i.e.* ADTP + Ti-IPO, corresponding fresh additives and model compounds: (a) phosphorus K-edge FY (bulk through the film-steel interface to the substrate, > 5 µm) and (b) sulphur K-edge FY (bulk through the film-steel interface to the substrate, > 5 µm).

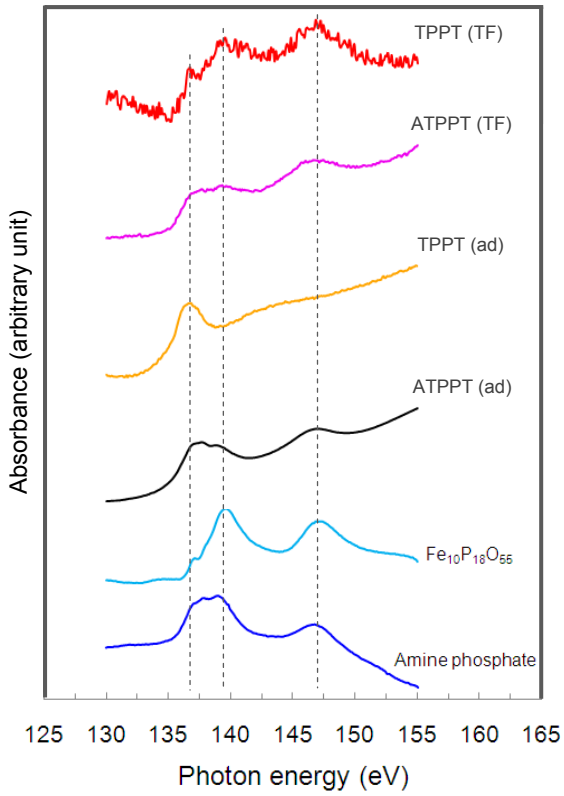


Figure 13.8: XANES spectra of tribofilms formed by Triphenyl phosphorothionate (C), *i.e.* TPPT, Alkylated triphenyl phosphorothionate (C), *i.e.* ATPPT, corresponding fresh additives and model compounds: phosphorus L-edge TEY (surface/near surface, ≈ 5 nm).

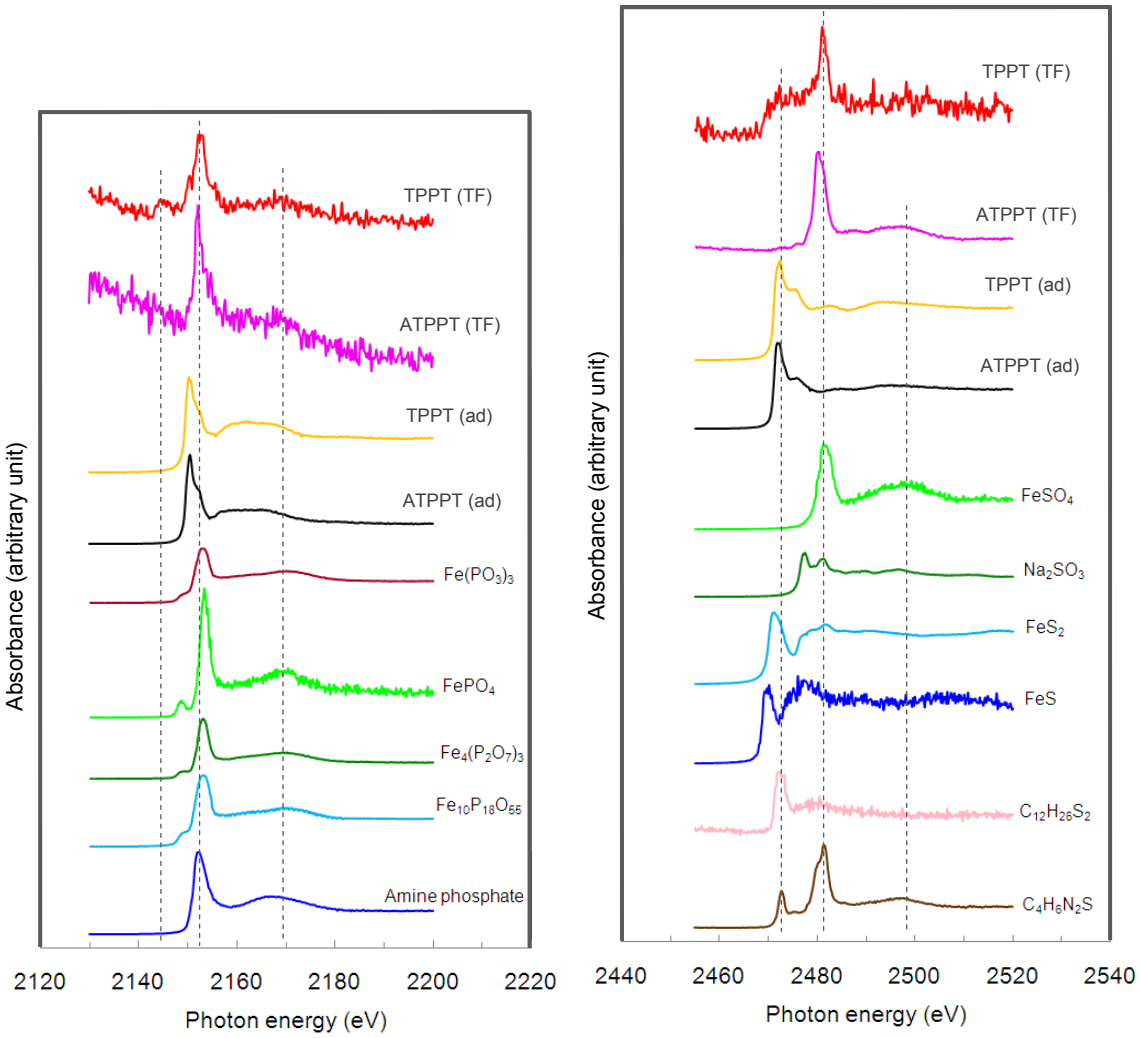


Figure 13.9: XANES spectra of tribofilms formed by Triphenyl phosphorothionate (C), *i.e.* TPPT, Alkylated triphenyl phosphorothionate (C), *i.e.* ATPPT, corresponding fresh additives and model compounds: (a) phosphorus K-edge FY (bulk through the film-steel interface to the substrate, > 5 µm) and (b) sulphur K-edge FY (bulk through the film-steel interface to the substrate, > 5 µm).

13.5 Results: Surface Analysis of S-containing Antiwear Additive-derived Tribofilms

The tribofilms formed by Dimercaptothiadiazole 2 (C), *i.e.* DMTDA2, and Methylene-bis-dialkyl-dithiocarbamate (C), *i.e.* MBDADTC, comprise $FeSO_4$ and sulphite at the surface/near surface, as can be seen on Figures 13.10 and 13.11 (a). The bulk of the tribofilm through the interface between film and steel consists mainly of FeS_2, with some FeS, sulphite, organic sulphide and disulphide (Figure 13.11 (b)). It can be seen in Figure 13.10 that the Fe is completely obscured by the Methylene-bis-dialkyl-dithiocarbamate (C)-derived tribofilm, which is consistent with the results shown in chapter 8, Figure 8.7[n)].

These results are consistent with those published by Najman *et al.* [100], Fan *et al.* [230] and Li *et al.* [376].

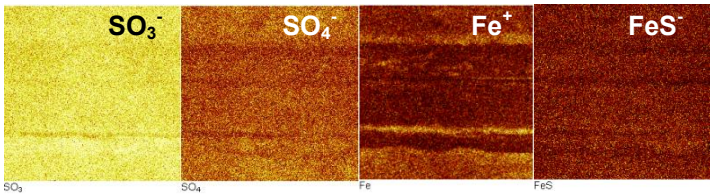


Figure 13.10: ToF-SIMS chemical map of tribofilm formed by Methylene-bis-dialkyl-dithiocarbamate (C), *i.e.* MBDADTC, (outermost surface, 1-2 nm). In this case, the tribofilm is seen in the middle of the images.

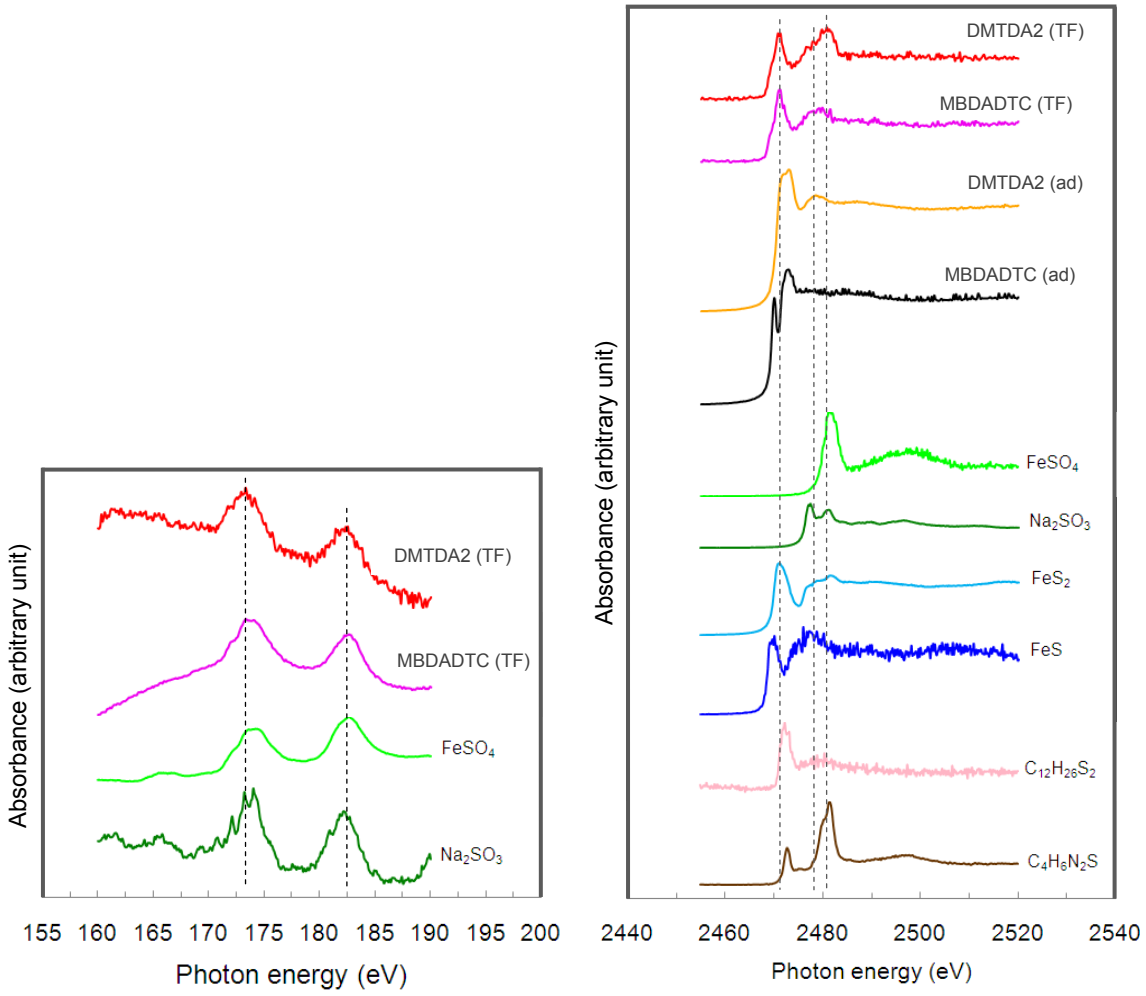


Figure 13.11: XANES spectra of tribofilms formed by Dimercaptothiadiazole 2 (C), *i.e.* DMTDA2, Methylene-bis-dialkyl-dithiocarbamate (C), *i.e.* MBDADTC, corresponding fresh additives and model compounds: (a) sulphur L-edge TEY (surface/near surface, ≈ 5 nm) and (b) sulphur K-edge FY (bulk through the film-steel interface to the substrate, > 5 µm).

13.6 Results: Surface Analysis of M-containing Antiwear Additive-derived Tribofilms

Figure 13.12 shows that the outer layer of the film formed by Molybdenum dialkyldithiocarbamate (C), *i.e.* MoDTC, consists mainly of molybdenum oxides, *i.e.* MoO_3^-, with some iron oxide and sulphur species also present. This is consistent with the XANES spectra seen in Figure 13.13, which shows the presence of sulphites and $FeSO_4$ on the surface/near surface of this film, *i.e.* ≈ 5 nm. The bulk of this film comprises mainly $FeSO_4$ (Figure 13.14 (a)), while some FeS, FeS_2, organic sulphide and disulphide can be found through the bulk to the interface between film and steel (Figure 13.14 (b)).

The weak peak at ≈ 2470.5 eV in the bulk and interface can be attributed to MoS_2, as observed by De Barros *et al.* [108], who also showed that a molybdenum dithiocarbamate additive alone, decomposes under rubbing to form MoS_2 and MoO_3. It was suggested, however, that the decomposition of MoDTC alone favours the formation of MoO_3, with higher concentrations of MoS_2 being observed under rubbing only in the presence of ZDDP. This was attributed to a synergistic effect seen in the presence of MoDTC and ZDDP.

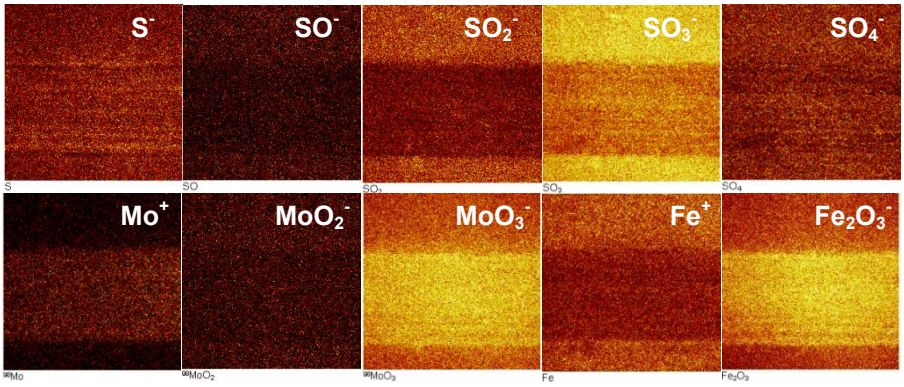


Figure 13.12: ToF-SIMS chemical map of tribofilm formed by Molybdenum dialkyldithiocarbamate (C), *i.e.* MoDTC, (outermost surface, 1-2 nm). In this case, the tribofilm is seen in the middle of the images.

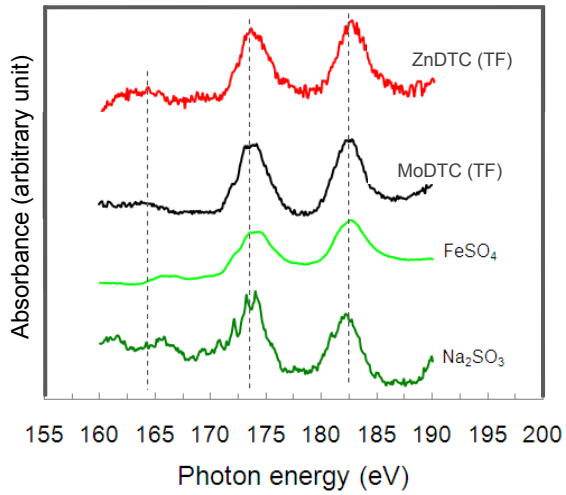


Figure 13.13: XANES spectra of tribofilms formed by Zinc diamyl dithiocarbamate (C), *i.e.* ZnDTC, Molybdenum dialkyldithiocarbamate (C), *i.e.* MoDTC, and model compounds: (a) sulphur L-edge TEY (surface/near surface, ≈ 5 nm).

The tribofilm formed by Zinc diamyl dithiocarbamate (C), *i.e.* ZnDTC, comprises sulphite and $FeSO_4$ at the surface/near surface (Figure 13.13), ZnS, with some $FeSO_4$ in the bulk (Figure 13.14 (a)) and a mixture of ZnS, FeS, with some FeS_2 and organic disulphide through the bulk to the interface film-steel (Figure 13.14 (b)).

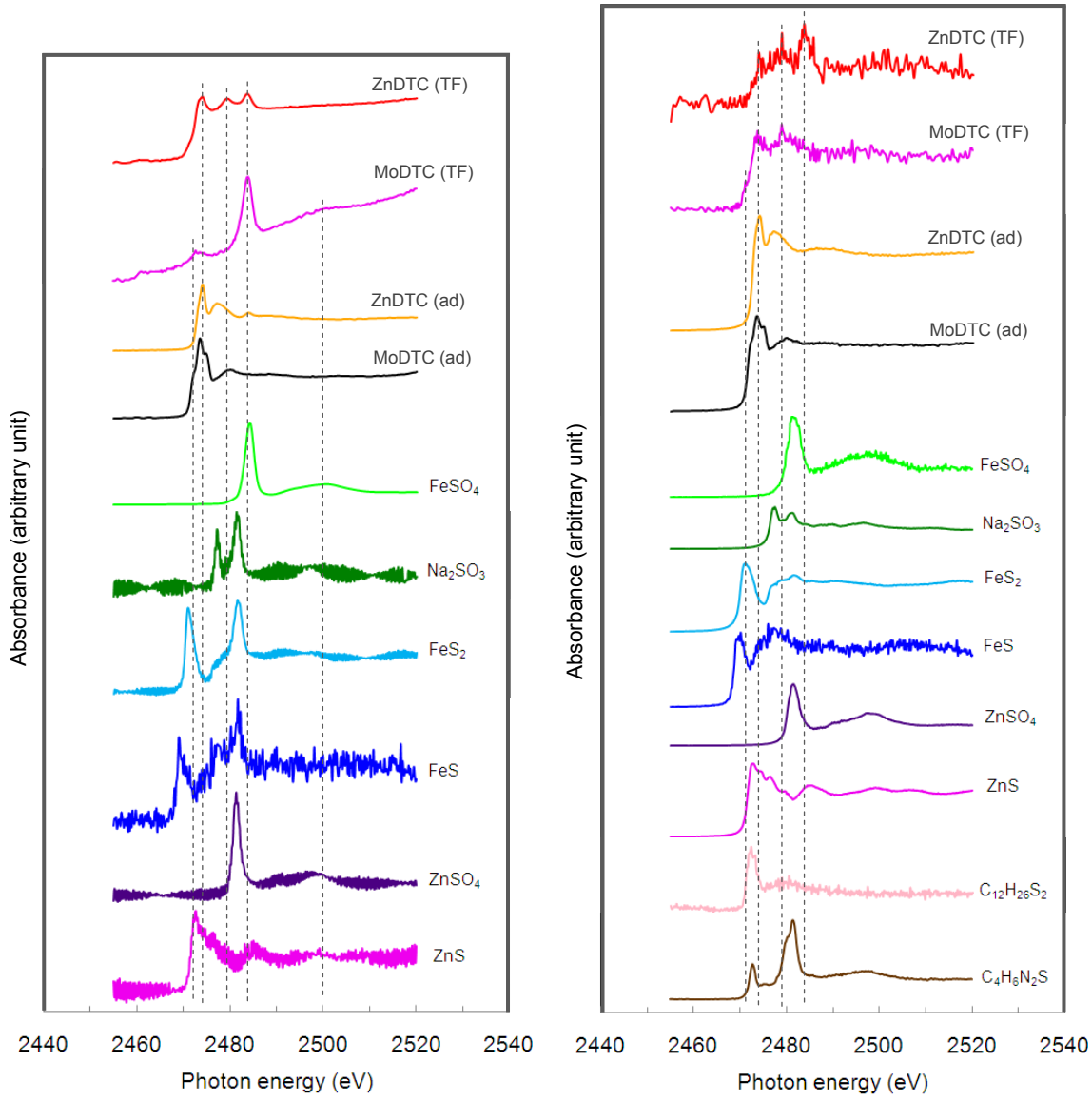
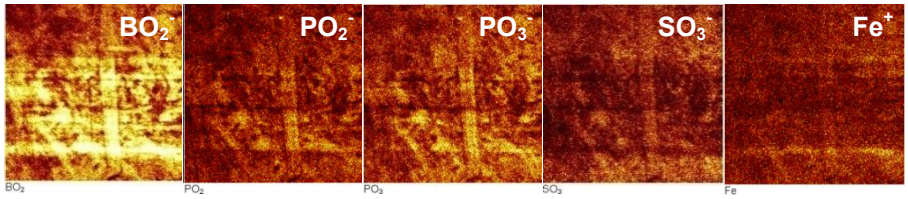


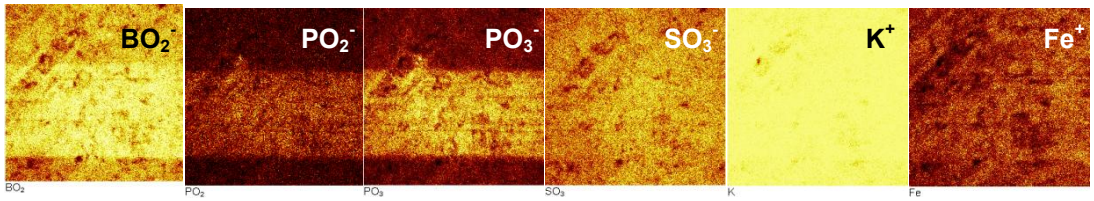
Figure 13.14: XANES spectra of tribofilms formed by Zinc diamyl dithiocarbamate (C), *i.e.* ZnDTC, Molybdenum dialkyldithiocarbamate (C), *i.e.* MoDTC, corresponding fresh additives and model compounds: (a) sulphur K-edge TEY (bulk, ≈ 50 nm) and (b) sulphur K-edge FY (bulk through the film-steel interface to the substrate, > 5 µm).

13.7 Results: Surface Analysis of B-containing Antiwear Additive-derived Tribofilms

The outermost layer of tribofilms, *i.e.* 1-2 nm, formed by B-containing antiwear additives consists mainly of boron species, *i.e.* BO_2^-, with some phosphorus and sulphur also present, as can be seen in Figure 13.15. The potassium from the Potassium borate (C), *i.e.* KB, appears adsorbed all over the steel surface, which indicates the formation of a very thin film outside the rubbed area.



a) Borated polyisobutenyl succinimide (High B) (C)



b) Potassium borate (C)

Figure 13.15: ToF-SIMS chemical maps of tribofilms formed by: a) Borated polyisobutenyl succinimide (High B) (C), *i.e.* B-PIBS(H), and b) Potassium borate (C), *i.e.* KB, (outermost surface, 1-2 nm). In these cases, the tribofilm is seen in the middle of the images.

XANES sampling depth at the boron K-edge has been studied by Kasrai *et al.* [377, 378], who determined that TEY samples near surface, *i.e.* ≈ 6 nm, while FY probes the bulk through to the interface between the film and steel, depending on film thickness, *i.e.* ≈ 100 nm. Although the signal from the tribofilms was relatively weak, hence the noisy spectra seen in Figure 13.16, it appears that be tribofilms formed by the boron additives studied in this work have undergone partial conversion from trigonal coordination, *i.e.* B_2O_3, to tetrahedral coordination, *i.e.* BPO_4, as previously reported by Marezio *et al.* [379] and Varlot *et al.* [380].

It can also be hypothesised that the tribofilms comprise a mixture of trigonal and tetrahedral boron, from the similarities between these tribofilms and $Na_2B_4O_7$, which comprises 50 % trigonal and 50 % tetrahedral boron [381].

These results are consistent with those published by Zhang *et al.* [298, 382].

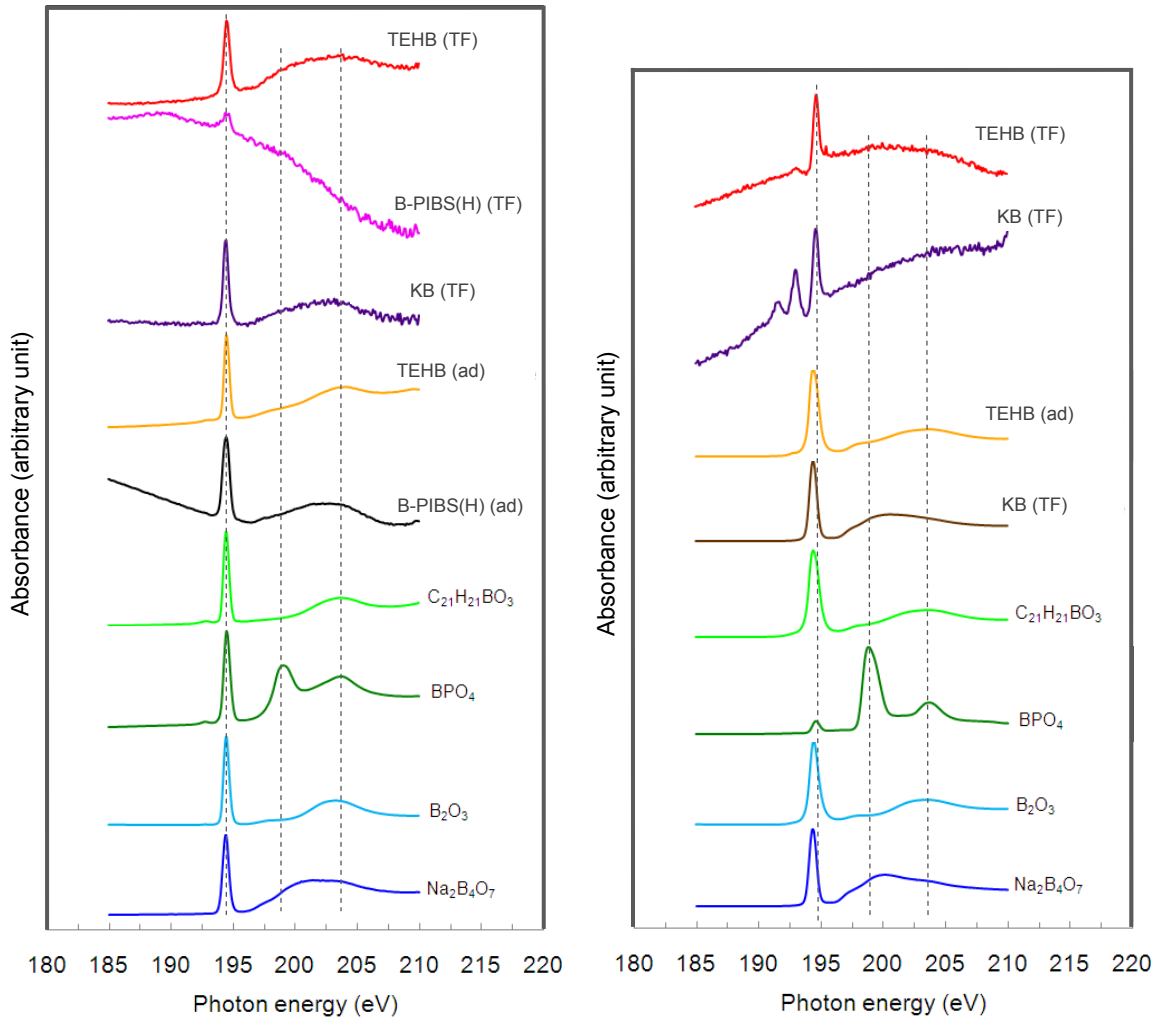


Figure 13.16: XANES spectra of tribofilms formed by Tris(2-ethylhexyl) borate (C), *i.e.* TEHB, Borated polyisobutenyl succinimide (High B) (C), *i.e.* B-PIBS(H), Potassium borate (C), *i.e.* KB, corresponding fresh additives and model compounds: (a) boron K-edge TEY (surface/near surface, ≈ 6 nm) and (b) boron K-edge FY (bulk through the film-steel interface, ≈ 100 nm).

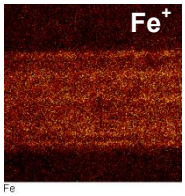
13.8 Results: Surface Analysis of Nanoparticle-containing Antiwear Additive-derived Tribofilms

Figure 13.17[a)] shows that Fe is incorporated into the film formed by the Polyisobutylene succinimide dispersant 1 (C), *i.e.* PIBS1, which was shown to be relatively thick in chapter 12, Figure 12.10[c)] and 12.13[c)].

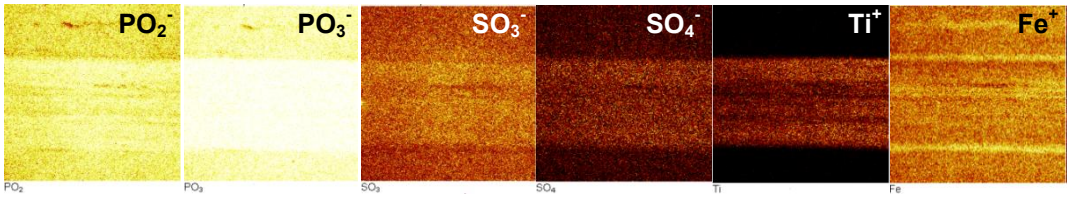
Interestingly, the film formed by Titanium oxide nanoparticles (C) + 0.1 % PIBS1 tribofilm, *i.e.* TiO_2 NANO + PIBS1, although very thin as can be seen in chapter 12, Figure 12.10[d)] and 12.13[d)], comprises a considerable amount of titanium, with some phosphorus and sulphur species also present in the surface. Slightly higher concentration of Fe can be seen delineating the edges of the wear track in Figure 13.17[b)], probably due to wear. This is consistent with the SLIM images shown in chapter 12, Figure 12.10[d)]. The IF-WS_2 + 0.1 % PIBS1-derived tribofilm, *i.e.* IF-WS_2 + PIBS1, shown in Figure 13.17[c)], also relatively thin, as seen in chapter 12, Figure 12.10[g)], consists mainly of sulphur species, with some Fe being incorporated into the film.

The p-Carborane (C) and m-Carborane (C) additives appear to form boron-iron rich films (Figures 13.17[d)] and 13.17[e)], respectively), with a substantial amount of Fe being incorporated into the protective layer.

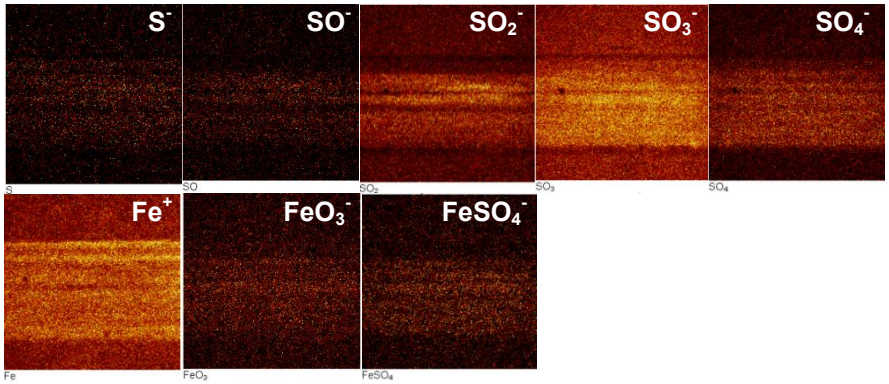
The outer layer of tribofilms formed by Crystalline overbased calcium sulphonate (C), *i.e.* cOBCaSu and Amorphous overbased calcium sulphonate (C), *i.e.* aOBCaSu, seen in Figure 13.17[f)] and 13.17[g)], consist mainly of calcium species, *i.e.* Ca^+ and $CaOH^+$, which completely obscure the Fe, with high concentration of sulphur species seen outside the wear track, probably due to sulphonate being adsorbed onto the surface. In addition to calcium species, the film formed by Neutral calcium alkylsulphonate (C), *i.e.* nCaSu, also contains some sulphur species, *i.e.* SO_2^- and SO_3^- (Figure 13.17[h)]), probably due to oxidation of sulphonate under rubbing. The bulk of these tribofilms through to the film-steel interface comprises FeS, FeS_2 and $FeSO_4$ (Figure 13.18). These results are consistent with those published by Kasrai *et al.* [383] and Costello *et al.* [384].



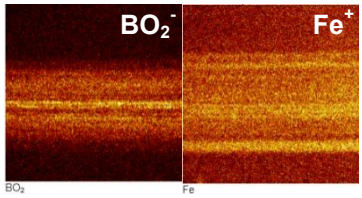
a) Polyisobutylene succinimide dispersant 1 (C)



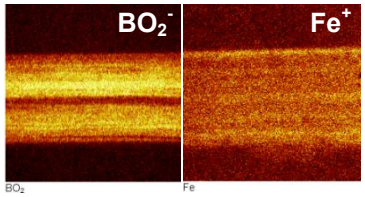
b) Titanium oxide nanoparticles (C) + 0.1 % PIBS1



c) IF-WS_2 + 0.1 % PIBS1

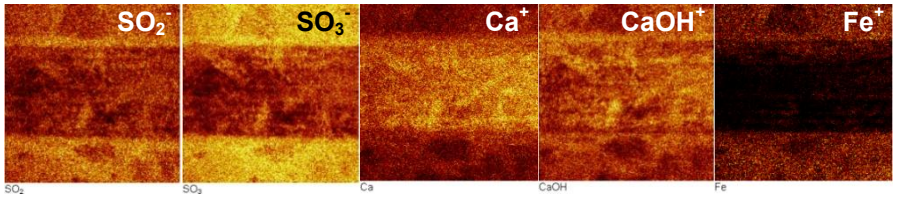


d) p-Carborane (C)

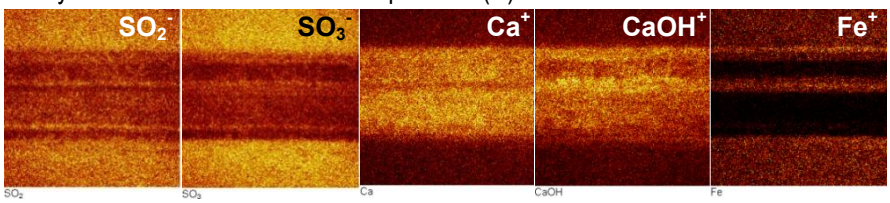


e) m-Carborane (C)

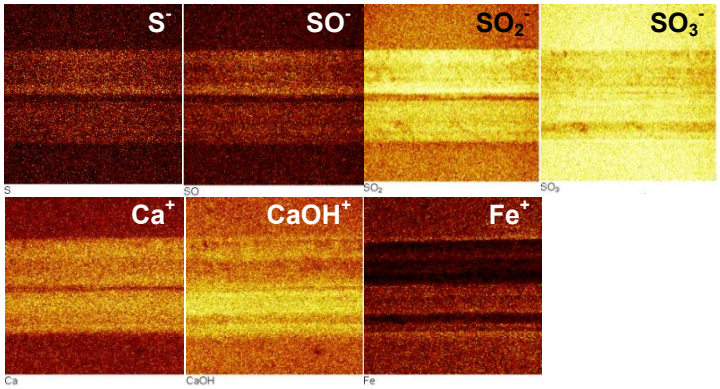
Figure 13.17: ToF-SIMS chemical maps of tribofilms formed by: a) Polyisobutylene succinimide dispersant 1 (C), b) Titanium oxide nanoparticles (C) + 0.1 % PIBS1, c) IF-WS_2 + 0.1 % PIBS1, d) p-Carborane (C) and e) m-Carborane (outermost surface, 1-2 nm). In these cases, the tribofilm is seen in the middle of the images.



f) Crystalline overbased calcium sulphonate (C)



g) Amorphous overbased calcium sulphonate (C)



h) Neutral calcium alkylsulphonate (C)

Figure 13.17 (continued): ToF-SIMS chemical maps of tribofilms formed by: f) Crystalline overbased calcium sulphonate (C), g) Amorphous overbased calcium sulphonate (C) and h) Neutral calcium alkylsulphonate (C) (outermost surface, 1-2 nm). In these cases, the tribofilm is seen in the middle of the images.

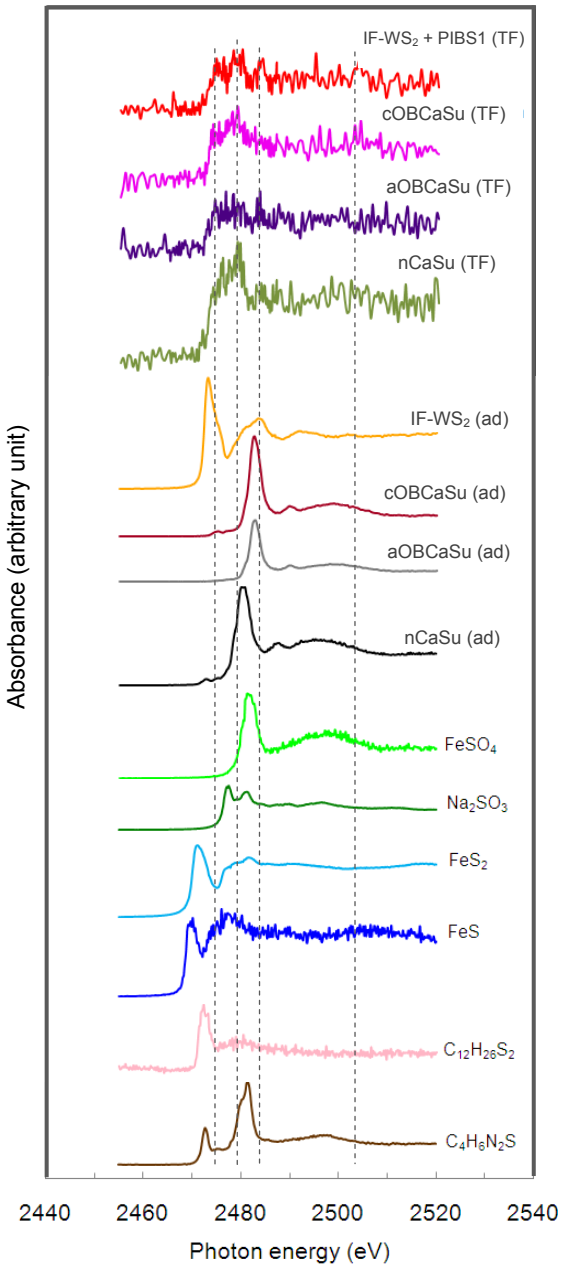


Figure 13.18: XANES spectra of tribofilms formed by IF-WS_2 + PIBS1, cOBCaSu, aOBCaSu, nCaSu, corresponding fresh additives and model compounds: sulphur K-edge FY (bulk through the film-steel interface to the substrate, > 5 µm).

13.9 Summary of Surface Analysis Work

This chemical nature study of antiwear additives-derived tribofilms has demonstrated that the tribofilms formed by these additives are not composed by the additives themselves, but consist of the decomposition products of these additives. More importantly, it has been shown that most commercially-available antiwear additives undergo reaction/decomposition under rubbing to form complex multilayered-type protective films.

Phosphorus and phosphorus-sulphur antiwear additives form analogous films to ZDDP, with Fe being the predominant cation stabilising the phosphate/polyphosphate glass instead of Zn. Metal cations are readily incorporated into the tribofilms formed by these additives, producing thicker tribofilms, but for the metals studied, this has a detrimental effect on wear, as it was shown in chapter 6, Figure 6.14 and chapter 7, Figure 7.15.

In general, the sulphur from sulphur- and metal-containing antiwear additives seems to react strongly with the metal surface producing FeS and FeS_2, which then oxidise to produce $FeSO_4$. In addition to Fe-S species, the metal containing antiwear additives studied in this work, *i.e.* ZnDTC and MoDTC, also decompose under rubbing to form sulphides, *i.e.* ZnS, MoS_2 and oxides *i.e.* MoO_3, Fe_2O_3.

Boron antiwear additives form a mixture of trigonal and tetrahedral boron rich-film, which was shown in chapter 10 Figure 10.11, to be very effective in reducing wear.

It is noteworthy that some of the nanoparticle-containing antiwear additives seem to undergo decomposition under rubbing, which indicates the presence of a chemisorbed/deposit-like film on the surface.

The composition of tribofilms formed by ZDDP and low and zero SAPS antiwear additives is summarised in Table 13.4.

Table 13.4: Low and zero SAPS antiwear additives-derived tribofilms: chemical composition

Composition	Surface/near surface	Bulk/Interface
ZDDP	PO_2^-, PO_3^-, PO_4^-, S^-, Zn^+	Zn/P, ZnP_2O_6, $Zn_2P_2O_7$, $Zn_4P_6O_{19}$, Zn_3P_2, $Fe(PO_3)_3$, $FePO_4$, $Fe_4(P_2O_7)_3$, $Fe_{10}P_{18}O_{55}$, ZnS, FeS, organic sulphide and disulphide
Phosphorus	PO_2^-, PO_3^- Phosphorus + Ti-IPO: PO_2^-, PO_3^-, Ti^+	Bulk: $Fe_{10}P_{18}O_{55}$ Interface: $Fe(PO_3)_3$, $FePO_4$, $Fe_4(P_2O_7)_3$, $Fe_{10}P_{18}O_{55}$
Phosphorus-Sulphur	Surface: PO_2^-, PO_3^-, SO_3^- Fe^+: TPPT and ATPPT tribofilms only ADTP + nCaSu: PO_2^-, PO_3^-, SO_3^-, Ca^+, $CaOH^+$ ADTP + Ti-IPO: Ti^+ Near surface: $Fe_{10}P_{18}O_{55}$, $FeSO_4$, sulphite	$Fe(PO_3)_3$, $FePO_4$, $Fe_4(P_2O_7)_3$, $Fe_{10}P_{18}O_{55}$, $FeSO_4$,, sulphite, FeS_2, organic sulphide and disulphide
Sulphur	SO_3^-, $FeSO_4$	FeS_2, FeS, sulphite, organic sulphide and disulphide
Metal	ZnDTC, near surface: $FeSO_4$, sulphite MoDTC, surface: MoO_3^-, $Fe_2O_3^-$, SO_3^- MoDTC, near surface: $FeSO_4$, sulphite	ZnDTC, bulk: ZnS, $FeSO_4$ ZnDTC, interface: ZnS, FeS, FeS_2, organic disulphide MoDTC, bulk: $FeSO_4$, MoS_2 MoDTC, interface: FeS, FeS_2, organic sulphide and disulphide, MoS_2
Boron	BO_2^- Potassium borate (C): K^+	Mixture of trigonal and tetrahedral boron
Nanoparticles	PIBS1: Fe^+ TiO_2 NANO + PIBS1: Ti^+ IF-WS_2 + PIBS1: SO_2^-, SO_3^-, SO_4^-, Fe^+ p-CB and m-CB: BO_2^-, Fe^+ cOBCaSu and aOBCaSu: Ca^+, CaOH+ nCaSu: SO_2^-, SO_3^-, Ca^+, $CaOH^+$	cOBCaSu, aOBCaSu and nCaSu: FeS, FeS_2, $FeSO_4$

14. FILM-FORMING, FRICTION AND WEAR-REDUCING PROPERTIES OF LOW AND ZERO SAPS ANTIWEAR ADDITIVES IN PARTIALLY FORMULATED OILS

This chapter presents the film-forming, friction and wear-reducing properties of selected low and zero SAPS antiwear additives in partially formulated oils with and without dispersant. Synergistic and antagonistic effects between low and zero SAPS antiwear additives and other lubricant additive types, *i.e.* detergent and dispersant, are also presented and discussed.

Reference oils of varying ZDDP concentration are also studied in this chapter in order to establish a correlation between the methods used by the author and future engine test outcomes.

14.1 Results: Film-forming Properties of Low and Zero SAPS Antiwear Additives in Partially Formulated Oils

The film-forming properties of low and zero SAPS antiwear additives in partially formulated oils were studied using MTM-SLIM under mixed rolling/sliding conditions, as described in chapter 4, section 4.1. Low and zero SAPS antiwear additives, *i.e.* Alkylated triphenyl phosphorothionate (C), Borated polyisobutenyl succinimide (High B) (C), Potassium borate (C) and Hydroxyquinoline (C), were blended into partially formulated oils at a concentration of 800 ppm B for B-containing antiwear additives, 800 ppm phosphorus for P-S-containing antiwear additives and 1000 ppm N for N-containing heterocyclic antiwear additives, and submitted to rubbing under the same test conditions on the MTM-SLIM.

Four partially formulated oils and two fully formulated oils were supplied by Castrol for this study, as described in Table 14.1. The partially formulated oils comprise one blend without dispersant or antiwear additive, *i.e.* PF without DISP or AW (to which the abovementioned low and zero SAPS antiwear additives were added to, *i.e.* PF + ATPPT, PF + B-PIBS(H), PF + KB, PF + HQ), one blend without dispersant but with 780 ppm ZDDP, *i.e.* PF + ZDDP and one blend with dispersant but without antiwear additive, *i.e.* PF + DISP (to which the abovementioned low and zero SAPS antiwear additives were added to, *i.e.* PF + DISP + ATPPT, PF + DISP + B-PIBS(H), PF + DISP + KB, PF + DISP + HQ). The two fully formulated oils, *i.e.* FF 250 ppm ZDDP and FF 1200 ppm ZDDP are included in the wear-reducing properties study only, section 14.3 of this chapter, as benchmark for comparison between the mild wear measurement method developed by the author and future engine test outcomes.

The Primary ZDDP (C) blend (800 ppm P), *i.e.* ZDDP1, used as a reference in previous chapters is included in the results described in this chapter for comparison purposes. However, it should be noted that this is probably not the same ZDDP used in the partially or fully formulated oils supplied by Castrol.

Table 14.1: Test materials summary

Code name	Sample name	Sample description
GIII BO	Group III base oil (C)	-
ZDDP1	Primary ZDDP (C)	9.5 %P; 20.0 %S; 10.6 %Zn
PF without DISP or AW	PF without DISP or AW	Partially formulated oil without dispersant, without antiwear additive
PF + ZDDP	PF + ZDDP	Partially formulated oil without dispersant, with ZDDP (780 ppm)
PF + ATPPT	PF + Alkylated triphenyl phosphorothionate (C)	Partially formulated oil without dispersant, with Alkylated triphenyl phosphorothionate (C) (800 ppm P)
PF + B-PIBS(H)	PF + Borated polyisobutenyl succinimide (High B) (C)	Partially formulated oil without dispersant, with Borated polyisobutenyl succinimide (High B) (C) (800 ppm B)
PF + KB	PF + Potassium borate (C)	Partially formulated oil without dispersant, with Potassium borate (C) (800 ppm B)
PF + HQ[1]	PF + Hydroxyquinoline (C)[1]	Partially formulated oil without dispersant, with Hydroxyquinoline (C)[1] (1000 ppm N)
PF + DISP	PF + DISP	Partially formulated oil with dispersant, without antiwear
PF + DISP + ZDDP	PF + DISP + ZDDP	Partially formulated oil with dispersant, with ZDDP (780 ppm)
PF+ DISP + ATPPT	PF+ DISP + Alkylated triphenyl phosphorothionate (C)	Partially formulated oil with dispersant, with Alkylated triphenyl phosphorothionate (C) (800 ppm P)
PF+ DISP + B-PIBS(H)	PF+ DISP + Borated polyisobutenyl succinimide (High B) (C)	Partially formulated oil with dispersant, with Borated polyisobutenyl succinimide (High B) (C) (800 ppm B)
PF+ DISP + KB	PF+ DISP + Potassium borate (C)	Partially formulated oil with dispersant, with Potassium borate (C) (800 ppm B)
PF+ DISP + HQ[1]	PF+ DISP + Hydroxyquinoline (C)[1]	Partially formulated oil with dispersant, with Hydroxyquinoline (C)[1] (1000 ppm N)
FF 250 ppm ZDDP	FF 250 ppm ZDDP	Fully formulated oil 250 ppm ZDDP
FF 1200 ppm ZDDP	FF 1200 ppm ZDDP	Fully formulated oil 1200 ppm ZDDP

(C): commercially-available.

[1] Hydroxyquinoline was not soluble in the partially formulated oils, with or without dispersant, employed in this study and because of that this additive was not tested.

Figure 14.1 shows the growth of the tribofilm on the MTM-ball with increasing rubbing time (*i.e.* zero, 5, 15, 30, 60, 120 minutes) for base oil alone, Primary ZDDP (C) in group III base oil (C) and selected low and zero SAPS antiwear additives in partially formulated oils with and without dispersant. With the base oil alone, scuffing occurred after 5 minutes of rubbing, as shown in Figure 14.1[a)] and the test was terminated.

It is noteworthy that Alkylated triphenyl phosphorothionate (C) and Borated polyisobutenyl succinimide (High B) (C) react much faster to form films in partially formulated oils than in base oil alone, as it was shown in chapter 7, Figure 7.9 and chapter 10, Figure 10.7, respectively. This indicates that these compounds have a synergistic effect with other additives present in the partially formulated oils studied.

The films formed in the absence of ZDDP or other antiwear additives by the PF without DISP or AW blend and PF + DISP blend are presumably due to the beneficial effect of the detergent, which is present in all partially formulated oils studied. The boundary film-forming properties of overbased detergents was demonstrated in chapter 12, Figure 12.10[j)-l)]. Interestingly, it appears that the presence of dispersant, *i.e.* PF + DISP blend, hinders the growth of the tribofilm formed by the detergent when no dispersant is present, *i.e.* PF without DISP or AW blend, as can be seen in Figures 14.1[h)] and 14.1[c)], respectively.

The presence of the dispersant seems to inhibit the growth of the protective films formed by Alkylated triphenyl phosphorothionate (C) and Potassium borate (C), as can be seen without dispersant, *i.e.* PF + ATPPT and PF + KB, in Figures 14.1[e)] and 14.1[g)], respectively, and with dispersant, *i.e.* PF + DISP + ATPPT and PF + DISP + KB, in Figures 14.1[j)] and 14.1[l)], respectively. This indicates an antagonistic effect of the dispersant on the film-forming properties of these additives. The growth of the tribofilms formed by Borated polyisobutenyl succinimide (High B) (C)-containing formulations, *i.e.* PF + B-PIBS(H) and PF + DISP + B-PIBS(H), are not affected by the dispersant, as shown in Figures 14.1[f)] and 14.1[k)].

Interestingly, the well documented antagonistic effect of dispersants on the film-forming properties of ZDDP is not clear from this work, as there is no significant difference between ZDDP-containing formulations with, *i.e.* PF + DISP + ZDDP, and without dispersant, *i.e.* PF + ZDDP, in the rate at which the film grows, as can be seen in Figure 14.1[i)] and 14.1[d)], respectively.

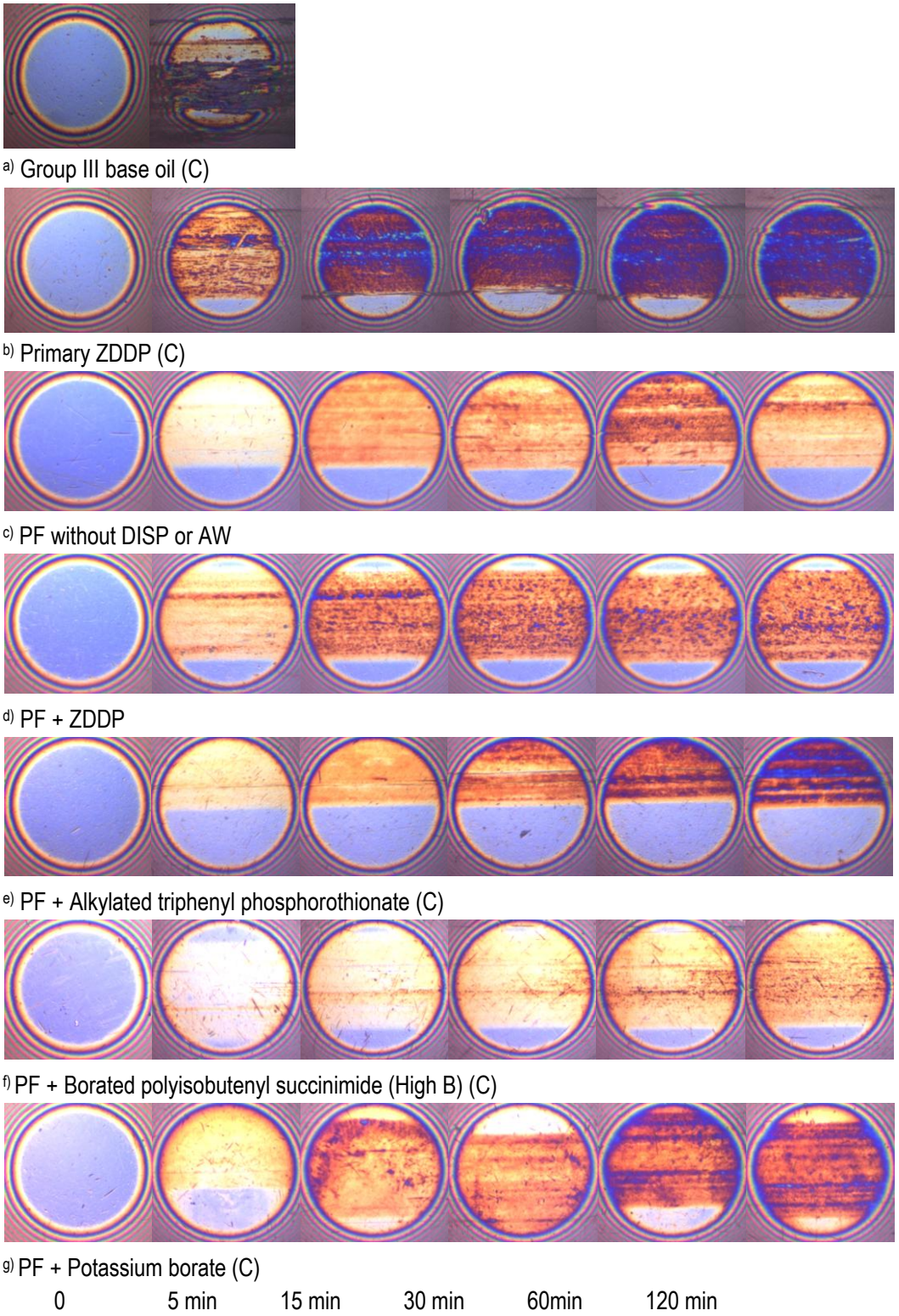


Figure 14.1: MTM-SLIM images showing: a) scuffing on the surface of the ball after 5 minutes of rubbing in base oil without antiwear additive; b) to g) the growth of tribofilm on the ball with increasing rubbing time (*i.e.* zero, 5, 15, 30, 60, 120 minutes).

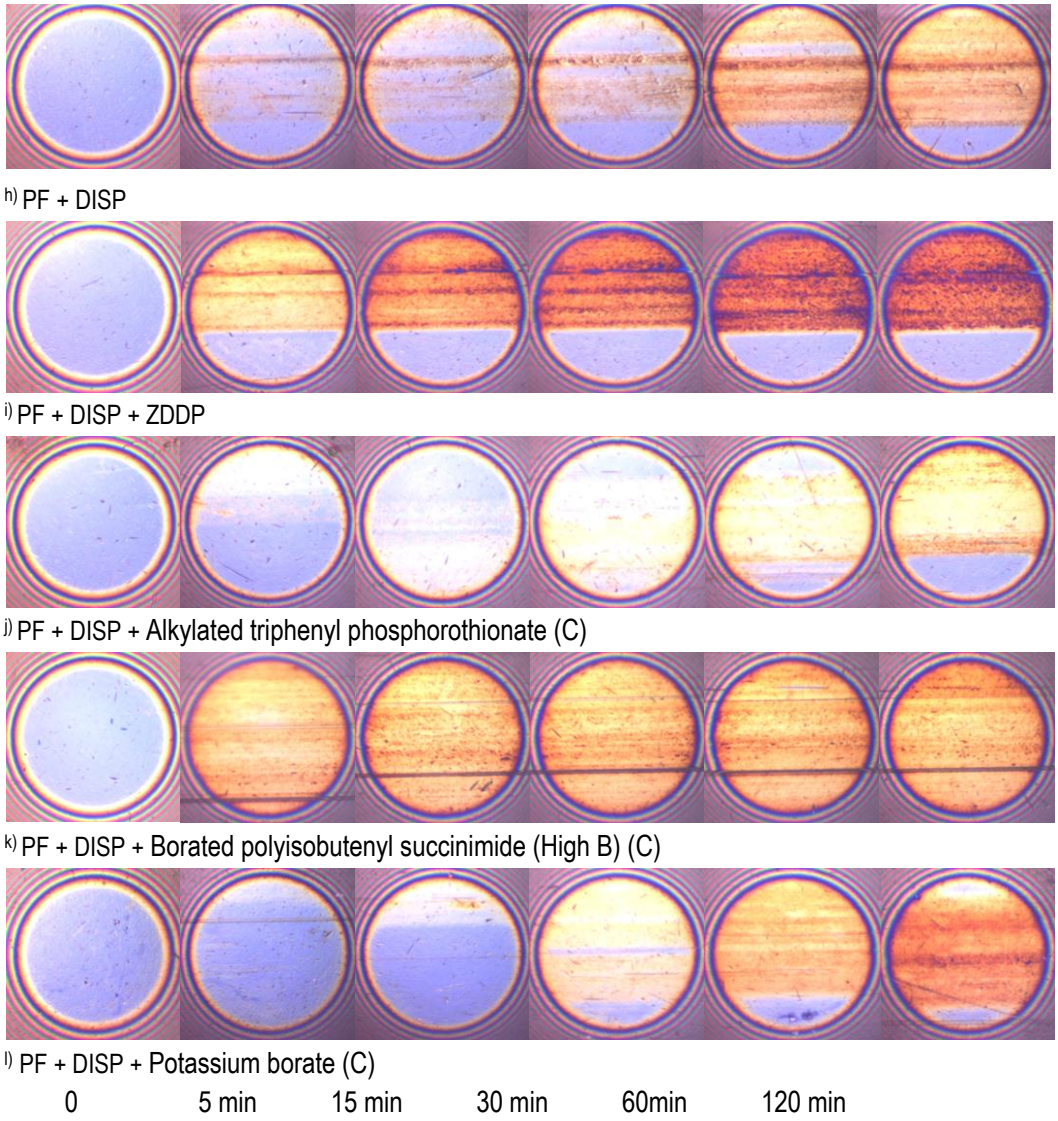


Figure 14.1 (continued): MTM-SLIM images showing: h) to l) the growth of tribofilm on the ball with increasing rubbing time (*i.e.* zero, 5, 15, 30, 60, 120 minutes).

Figures 14.2 and 14.3 present the development of mean film thickness with rubbing time for blends with and without dispersant. It is noteworthy that the tribofilms formed by Akylated triphenyl phosphorothionate (C) and Potassium borate (C) after 2 hours of rubbing without dispersant, *i.e.* PF + ATPPT: 149 nm and PF + KB: 110 nm, are much thicker than when dispersant is present, *i.e.* PF + DISP + ATPPT: 23 nm and PF + DISP + KB: 50 nm. This confirms the antagonistic effect of the dispersant on the film-forming properties of these additives in partially formulated oils.

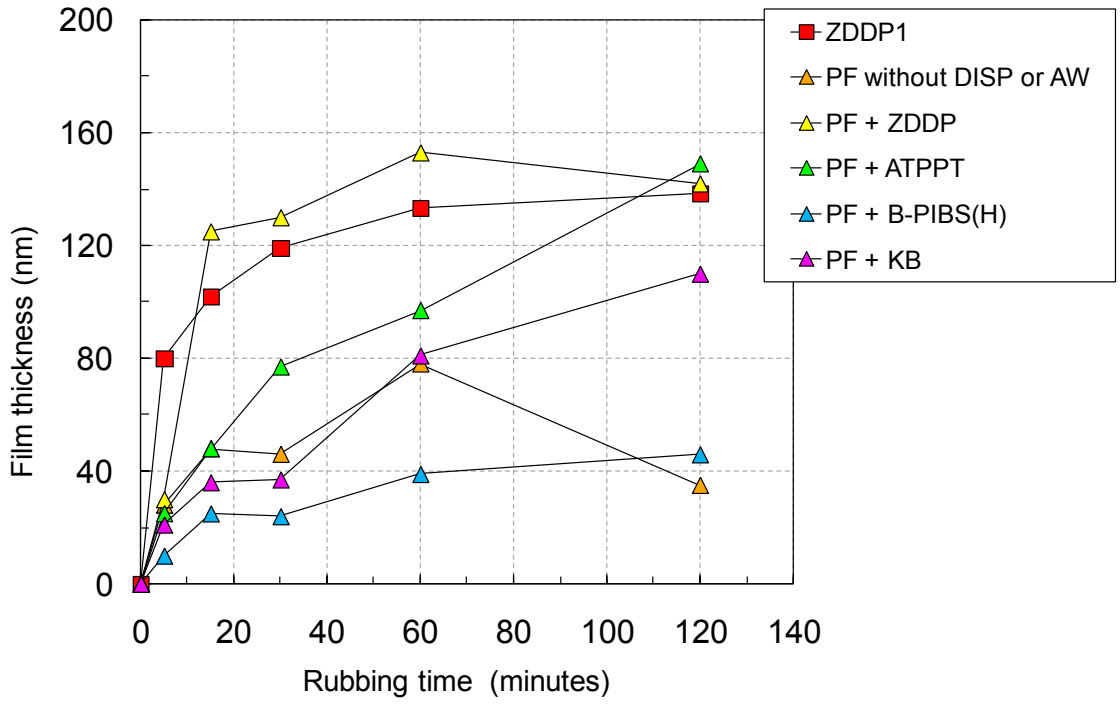


Figure 14.2: Mean film thickness with rubbing time for low and zero SAPS antiwear additives in partially formulated oils without dispersant.

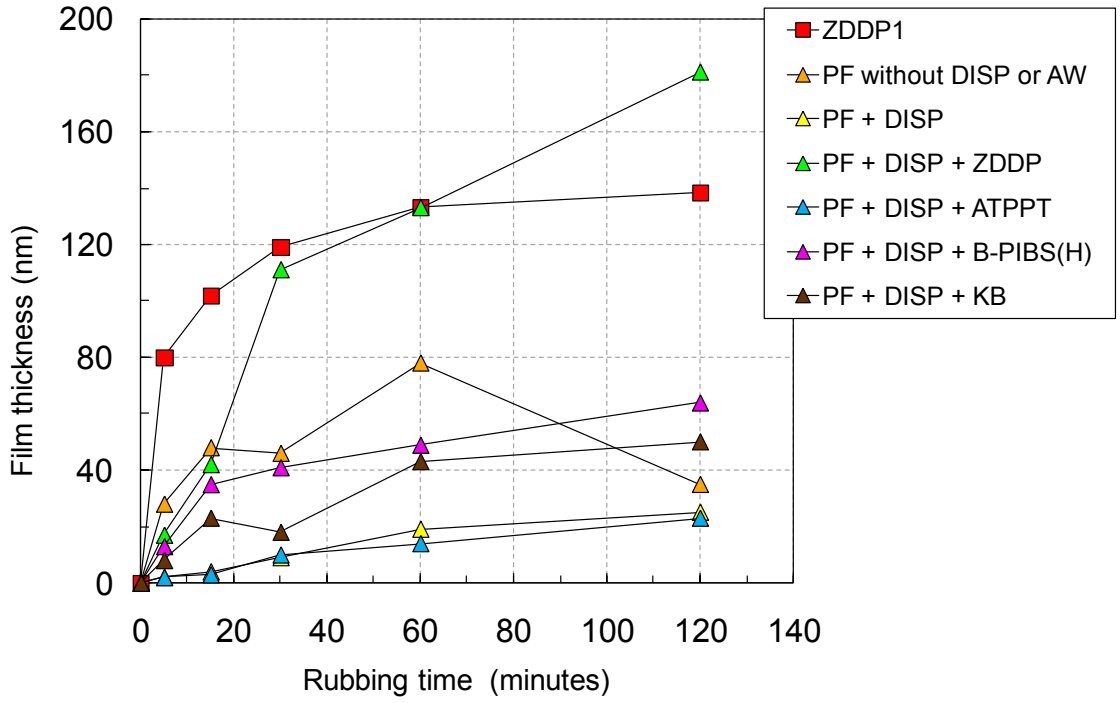


Figure 14.3: Mean film thickness with rubbing time for low and zero SAPS antiwear additives in partially formulated oils with dispersant.

14.2 Results: Friction Properties of Low and Zero SAPS Antiwear Additives in Partially Formulated Oils

The friction properties of low and zero SAPS antiwear additives in partially formulated oils were studied using the MTM under mixed rolling/sliding conditions, as described in chapter 4, section 4.1. The Stribeck curves (Figure 14.4) show the friction coefficient *versus* entrainment speed for these additives at the beginning and after 2 h of rubbing.

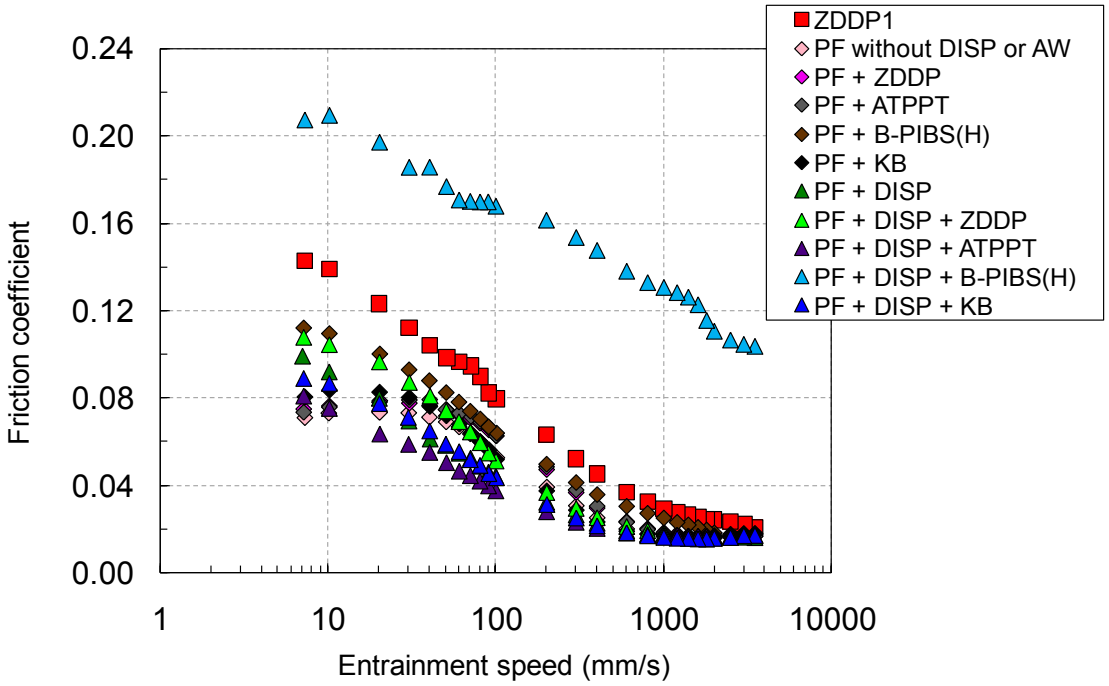
These friction curves illustrate two different types of behaviour; (i) in most cases shifting of the curves to the right and (ii) slight changes in low speed boundary friction.

There is a general increase in mixed friction for all formulations studied, which can be attributed to changes in surface texture due to the development of thick protective films on the surface, as shown in Figure 14.1.

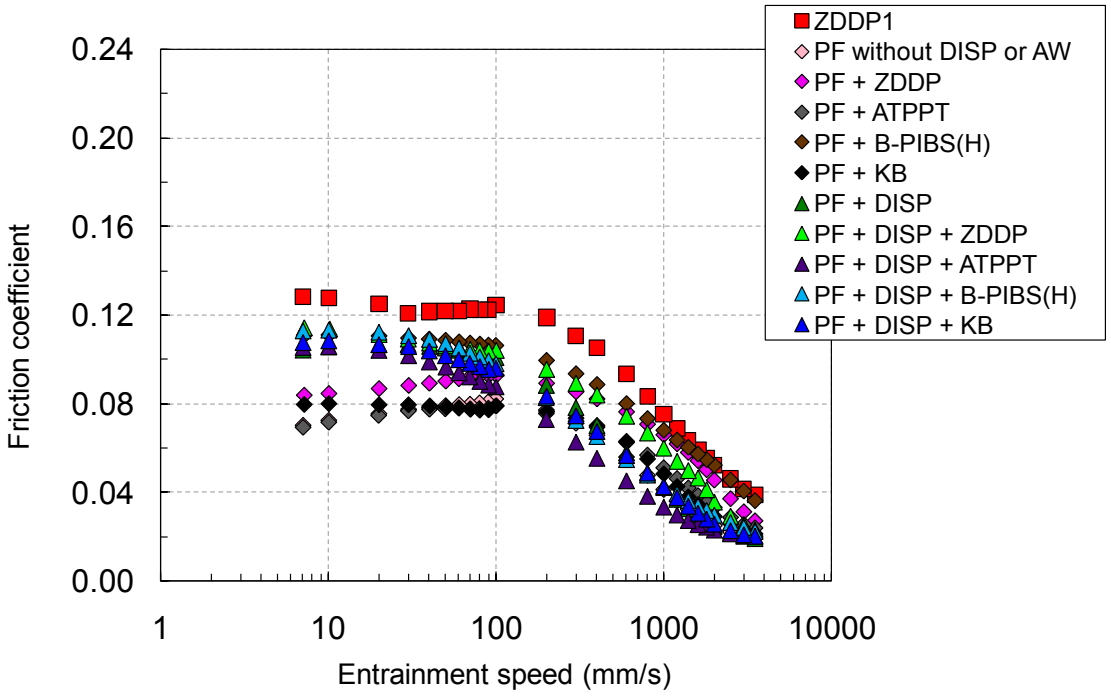
Lower boundary friction is observed for formulations without package dispersant, *i.e.* $\mu \approx 0.07\text{-}0.08$, while dispersant-containing formulations show slightly higher boundary friction, *i.e.* $\mu \approx 0.11$. Assuming that the dispersant present in formulation is a polyisobutylene succinimide type dispersant, the higher boundary friction seen for dispersant-containing formulations can be ascribed to the effect of the polyisobutylene chains, having many pendant methyl groups, attached to the surface.

The boundary friction of formulations containing Borated polyisobutenyl succinimide (High B) (C), *i.e.* PF + B-PIBS (H) and PF + DISP + B-PIBS (H), is relatively high, *i.e.* $\mu \approx 0.11$, regardless of the presence of package dispersant, probably due to the fact that this additive is actually a dispersant in nature.

The classical effect of the detergent, which is present in all partially formulated oils studied, on boundary friction behaviour is also noteworthy, particularly on dispersant-free formulations, *e.g.* PF without DISP or AW, PF + ZDDP, PF + ATPPT. This is consistent with the results shown in chapter 7, Figure 7.12 and chapter 12, Figure 12.12 and can be attributed to the contribution of the alkyl chain structure of the detergent molecule.



Initial friction, measured at the beginning of the test



Friction after 2 h of rubbing

Figure 14.4: Stribeck curve showing friction coefficient *versus* entrainment speed at the beginning and after 2 h of rubbing at 50 % SRR, 30 N and 100 ºC.

14.3 Results: Wear-reducing Properties of Low and Zero SAPS Antiwear Additives in Partially Formulated Oils

The wear-reducing properties of low and zero SAPS antiwear additives in partially formulated oils were studied using the method developed by the author, which combines the MTM-Reciprocating rig to generate the wear track on AISI 52100 steel discs with SWLI to image the track and measure wear depth, as described in chapter 4, sections 4.3 and 4.4. Results are summarised in Figures 14.5 and 14.6.

The results show that very mild levels of wear were observed for most low and zero SAPS antiwear additives in partially formulated oils, with comparable wear-reducing properties to the reference oils, *i.e.* FF 250 ppm ZDDP and FF 1200 ppm ZDDP, lower wear coefficient than the ZDDP-dispersant-containing formulation, *i.e.* PF + DISP + ZDDP, and no measurable wear after 16 hours of rubbing in some cases, *e.g.* Potassium borate (C)-containing formulations.

Interestingly, very mild levels or no measurable wear was observed for ZDDP-free formulations, *i.e.* PF without DISP or AW blend and PF + DISP blend. This might be due to the beneficial contribution of the detergent to wear, demonstrated in chapter 12, Figure 12.14.

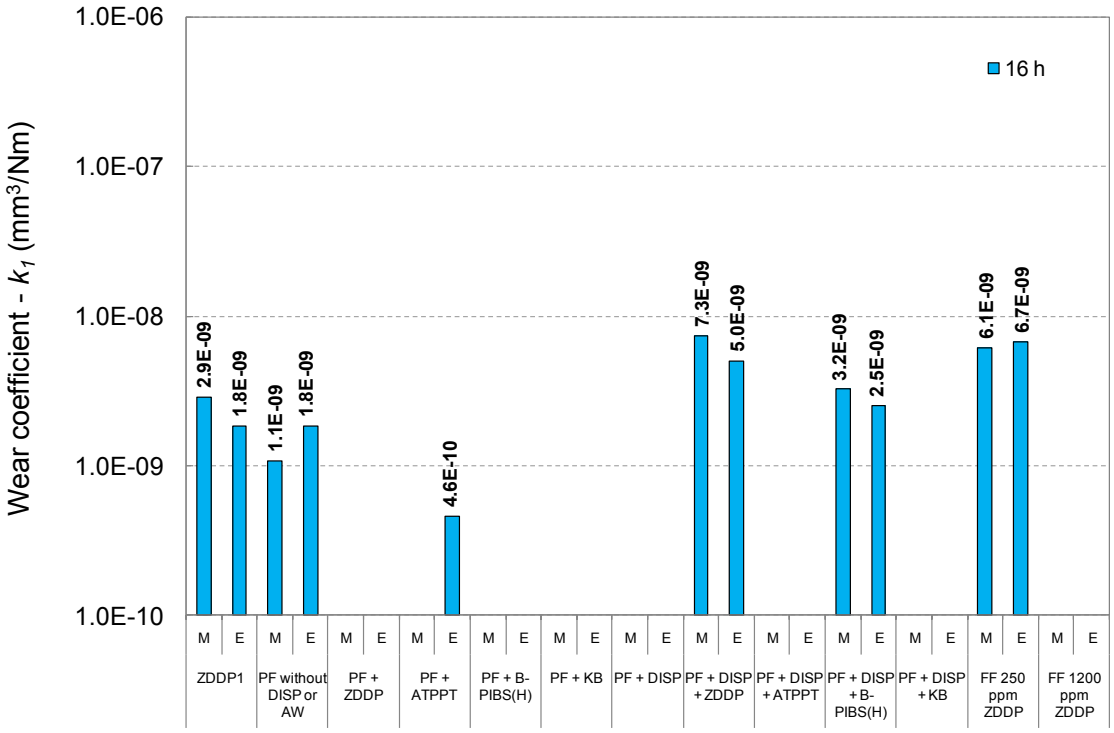


Figure 14.5: Wear coefficient (k_1) in the middle (M) and at the ends (E) of the wear track (*i.e.* average of both ends) for test lasting 16 hours.

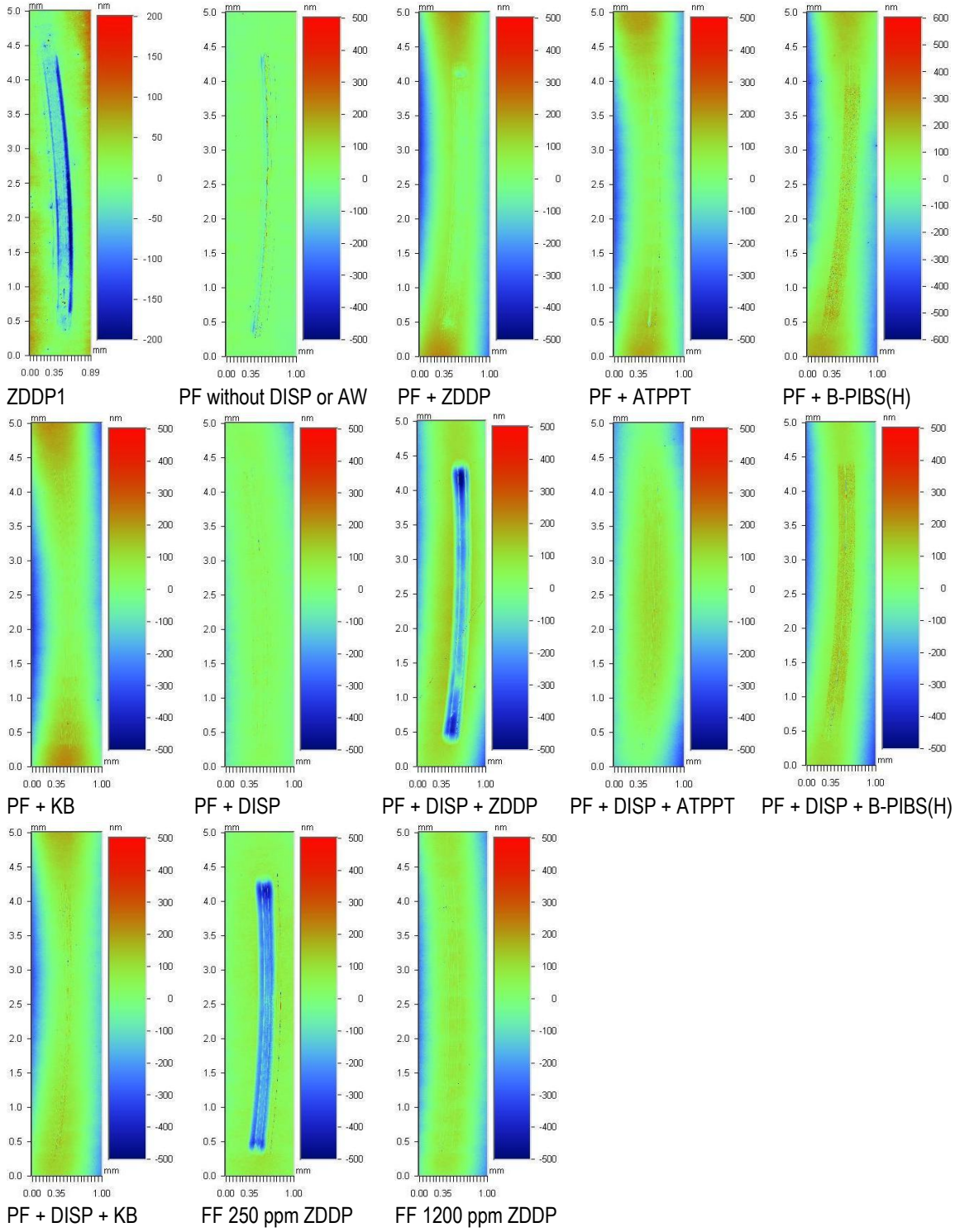


Figure 14.6: SWLI 2D topography images of the wear track on the disc after 16 h rubbing.

14.4 Discussion of Low and Zero SAPS Antiwear Additives in Partially Formulated Oils Work

A summary of the film thickness after 2 hours of rubbing, the friction coefficient at the low, intermediate and high speed regions after 2 hours of rubbing and the average of wear coefficients taken in the middle and at the edges of the wear track after 16 hours of rubbing for low and zero SAPS antiwear additives studied in partially formulated oils is given in Figures 14.7, 14.8 and 14.9, respectively.

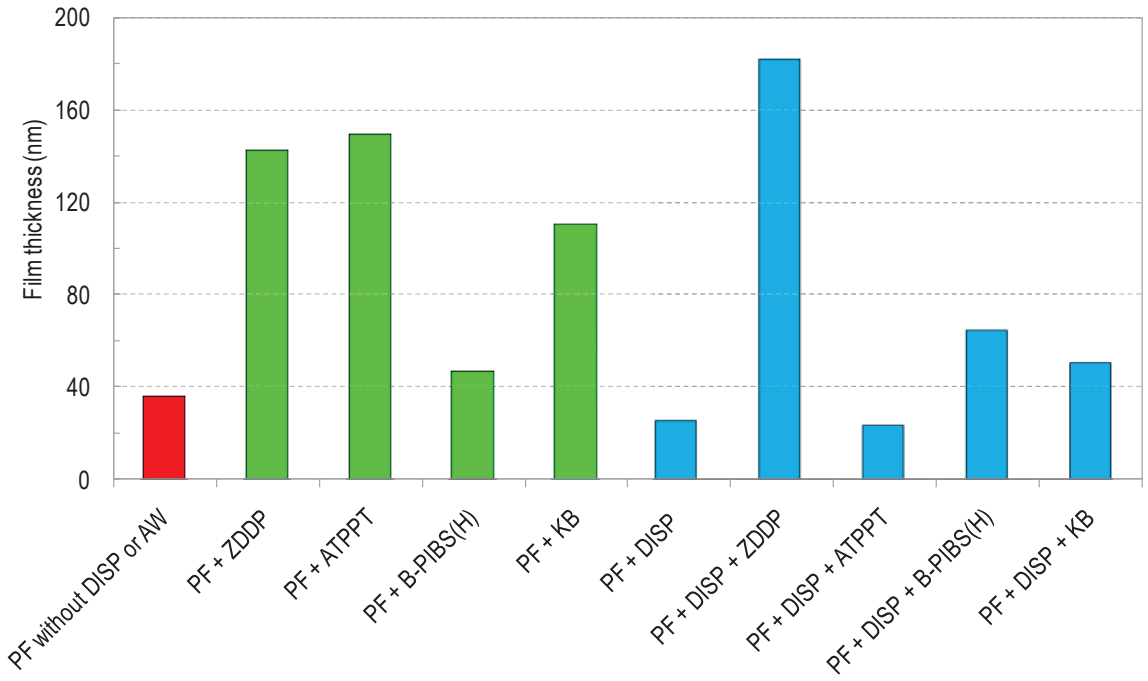


Figure 14.7: Mean film thickness after 2 hours of rubbing for low and zero SAPS antiwear additives in partially formulated oils.

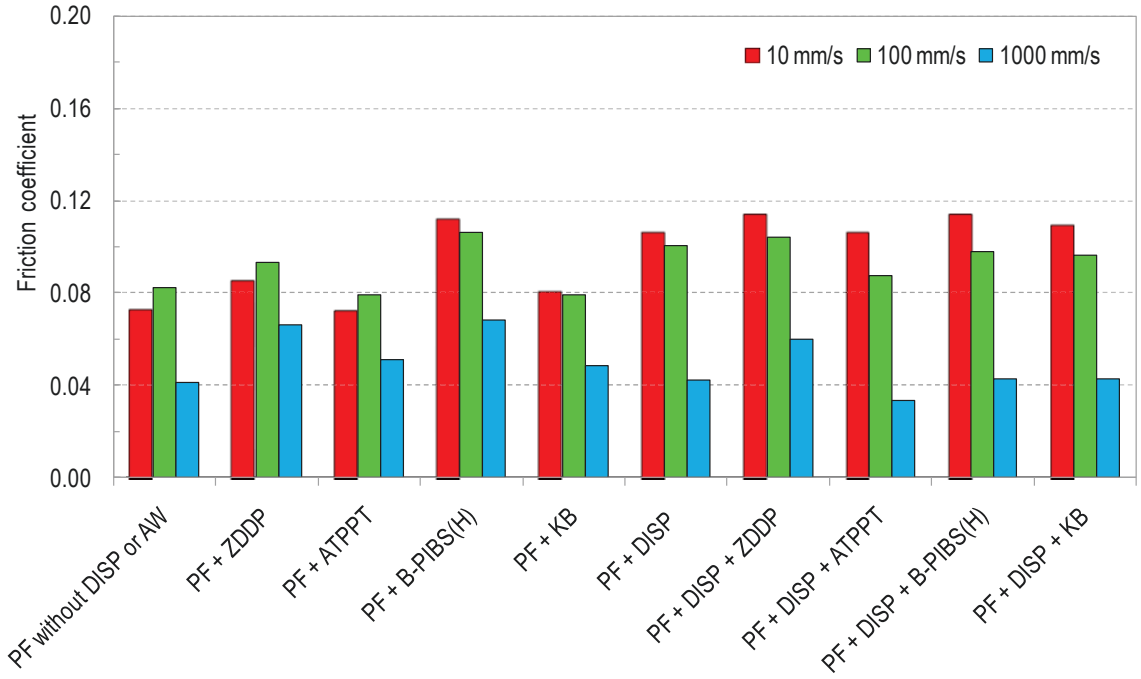


Figure 14.8: Friction coefficient after 2 hours of rubbing at the low, intermediate and high speed regions, *i.e.* 10, 100 and 1000 mm/s, for low and zero SAPS antiwear additives in partially formulated oils.

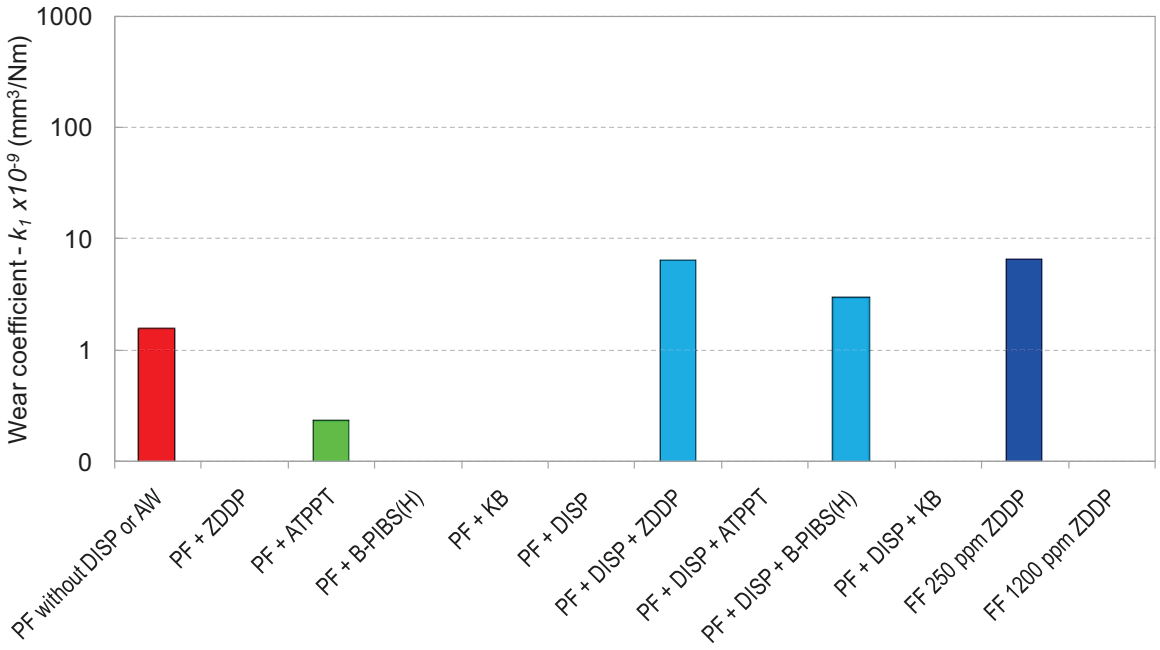


Figure 14.9: Wear coefficient[1], k_1 x 10^{-9}, after 16 hours of rubbing for low and zero SAPS antiwear additives in partially formulated oils. ([1]This corresponds to the average of wear coefficients taken in the middle and at the edges of the wear track)

The film-forming study under mixed rolling/sliding conditions using MTM-SLIM shows that there are no significant differences in the film-forming properties of ZDDP-containing formulations with and without dispersant. There is, however, a considerable increase in boundary friction after 2 hours of rubbing when dispersant is present, *i.e.* PF + DISP + ZDDP, as seen in Figure 14.8. Assuming that the package dispersant is a polyisobutylene succinimide type dispersant, the higher boundary friction seen for dispersant-containing formulations can be ascribed to the effect of the polyisobutylene chains, having many pendant methyl groups, attached to the surface. There is also an increase in wear rate in the presence of dispersant, as seen in Figure 14.9. This can be attributed to the antagonistic effect of dispersants on the wear-reducing properties of ZDDP [73, 385].

Interestingly, antiwear additive-free formulations, *i.e.* PF without DISP or AW and PF + DISP, form films on rubbing surfaces, presumably because of the presence of an overbased detergent. Such detergents are known to form thick boundary films on surfaces in rubbing contact [94]. Also noteworthy is the fact that the film formed by the dispersant-free blend, *i.e.* PF without DISP or AW is slightly thicker than when dispersant is present, *i.e.* PF + DISP, probably because of the well documented antagonistic effect of dispersants on film formation. The deleterious effects of succinimide dispersants on the film-forming properties of antiwear additives has been reported by Inoue *et al.* [386], Barcroft *et al.* [387], Barnes *et al.* [115] and Fujita *et al.* [388]. There is also an increase in boundary friction in the presence of dispersant, *i.e.* PF + DISP, probably because the polyisobutylene chains prevent the sulphonate detergent molecule from attaching/adsorbing to/onto the surface and thus reducing friction. Figure 14.9, shows that in the absence of dispersant, *i.e.* PF without DISP or AW, there is a slight increase in wear rate. This is in agreement with the results presented in chapter 12, Figure 12.14, which shows that the dispersant alone is quite effective in reducing wear, more so than overbased and neutral calcium sulphonate detergents alone. Similar interactions between polyisobutylene succinimide dispersants and detergents have been reported by Hsu *et al.* [389].

The presence of dispersant also inhibits the film-forming properties of Alkylated tryphenyl phosphorothionate (C) and Potassium borate (C) in partially formulated oils. This is probably due to an antagonistic effect of the dispersant on the film-forming properties of these additives.

It is also observed that the films formed by Alkylated triphenyl phosphorothionate (C) and Borated polyisobutenyl succinimide (High B) (C) grow much faster in partially formulated oils than in base oil alone. This indicates that these additives might have a synergistic effect with the detergent, which has been shown to have a beneficial effect on the rate at which the film grows.

There is a general increase in mixed friction, probably caused by changes in surface texture due to the development of thick protective films on the surface. The dispersant seems to have a detrimental effect on the boundary friction behaviour of the selected low and zero SAPS additives studied, probably because of the polyisobutylene branches attached to the surface. Dispersant-free formulations show much lower boundary friction behaviour overall, with the classical effect of the detergent being observed, *e.g.* PF + ATPPT, PF + KB. This effect is characterised by friction that increases with speed in the slow speed region and can be ascribed to the contribution of the long, linear chain structure of the detergent molecules.

Interestingly, the dispersant present in formulation has no detrimental effect on the film-forming and friction properties of Borated polyisobutenyl succinimide (High B) (C)-containing formulations, probably because this additive is a dispersant in nature. This indicates that the disadvantageous effects of the dispersant on the film-forming and friction properties of Alkylated triphenyl phosphorothionate (C) and Potassium borate (C)-containing formulations might be diminished by changing the type of dispersant used in formulation.

This study has also demonstrated the wear-reducing properties of low and zero SAPS antiwear additives in partially formulated oils using the reciprocating MTM, with very mild levels of wear being observed for most of the blends studied and no measurable wear after 16 hours of rubbing in some cases, *e.g.* PF + KB and PF + DISP + KB.

From comparison between the wear-reducing properties of fully formulated oils, *i.e.* FF 250 ppm ZDDP and FF 1200 ppm ZDDP, supplied by Castrol and the low and zero SAPS additives investigated in partially formulated oils, it appears that the latter have shown performance comparable to, or in some cases slightly better than the references. This indicates that these additives can prevent wear in boundary lubrication conditions.

15. GENERAL DISCUSSION

In this chapter the main findings of this thesis in terms of film-forming, friction and wear-reducing properties of the alternative low and zero SAPS antiwear additives studied are summarised and discussed. It is shown that individual members of all the families of additives studied are able to form thick films. The additives tested show a wide range of friction behaviour, especially when operating in the low speed, boundary lubrication regime. Several additives are identified which give lower wear than the Primary ZDDP (C) used as a benchmark in this study.

Correlation analysis shows that there is negligible correlation between the ability of an additive to form a thick film and its wear reducing capability. However additives that form thick films do tend to give high friction at intermediate and low entrainment speed.

15.1 Overall Comparison of Film-forming, Friction and Wear-reducing Properties of Low and Zero SAPS Antiwear Additives

The film-forming, friction and wear-reducing properties of a very wide range of antiwear additives have been studied under the same test conditions using the methods outlined in chapter 4. The film-thickness after 2 hours of rubbing, the friction coefficient at low, intermediate and high speeds, *i.e.* 10, 100 and 1000 mm/s, after 2 hours of rubbing, and the average of wear coefficients taken from the middle and at both ends of the wear track after 16 hours of rubbing, for antiwear additives in base oil alone are summarised in Table 15.1. Note that film thickness could not be measured using the MTM-SLIM for some of the nanoparticle-containing antiwear additives as discussed in chapter 12, also wear-reducing properties were evaluated for selected additives only.

Table 15.1: Summary of film thickness, friction coefficient and wear coefficient results for antiwear additives studied in base oil alone

			Friction coefficient			
Antiwear additives[1]		**Film thickness (nm)**	**10 mm/s**	**100 mm/s**	**1000 mm/s**	**Wear coefficient, k_1 x 10^{-9} (mm^3/Nm)**
Primary ZDDP (C)	ZDDP1	138	0.13	0.12	0.08	2.35
Triisopropyl phosphate	=	67	0.10	0.05	0.02	-
Triisopropyl phosphite	=	73	0.10	0.08	0.05	-
Bis(2-ethylhexyl) phosphate	=	83	0.13	0.12	0.07	-
Bis(2-ethylhexyl) phosphite	=	79	0.10	0.07	0.03	16.0
Bis(2-ethylhexyl) phosphite + 1 % nCaSu	=	77	0.11	0.10	0.04	-
Bis(2-ethylhexyl) phosphite + 1 % Ti-IPO	=	142	0.10	0.11	0.08	9.08
Triaryl phosphate (C)	TAP	26	0.06	0.06	0.03	8.11
Amine phosphate (C)	AP	33	0.11	0.10	0.04	-
Ashless dithiophosphate (C)	ADTP	51	0.11	0.07	0.03	0.80
Ashless dithiophosphate (C) + 1 % nCaSu	ADTP + 1 % nCaSu	65	0.10	0.10	0.05	5.93
Ashless dithiophosphate (C) + 1% Ti-IPO	ADTP + 1% Ti-IPO	120	0.09	0.09	0.07	294
Dialkyl dithiophosphate (C)	DADTP	25	0.13	0.07	0.03	-

Triphenyl phosphorothionate (C)	TPPT	34	0.12	0.08	0.03	1.51
Alkylated triphenyl phosphorothionate (C)	ATPPT	63	0.09	0.07	0.03	0.70
Butylated triphenyl phosphorothionate (C)	BTPPT	2	0.12	0.08	0.03	-
Amine thiophosphate (C)	ATP	19	0.10	0.08	0.04	-
Phosphorus-sulphur-nitrogen-based (C)	PSN	3	0.08	0.07	0.03	-
Phosphorus-sulphur-based (C)	PS	8	0.08	0.07	0.03	-
Di-n-hexyl disulphide	=	scuffing				
Di-n-octadecyl disulphide	=	scuffing				
Dibenzyl disulphide	=	53	0.09	0.05	0.02	-
Dialkyl pentasulphide (C)	DA5S	scuffing				
Dialkyl polysulphide (C)	DAPS	scuffing				
Sulphurised fatty acid ester (C)	SFAE	9	0.10	0.05	0.02	-
2-Isobutylthiazole	=	14	0.09	0.06	0.02	-
2,5-Dimethyl-1,3,4-thiadiazole	=	scuffing				
Dimercaptothiadiazole 1 (C)	DMTDA1	21	0.08	0.05	0.02	73.7
Dimercaptothiadiazole 2 (C)	DMTDA2	19	0.07	0.04	0.02	42.4
Mercaptobenzothiazole (C)	MBTA	41	0.08	0.05	0.02	-
Methylene-bis-dialkyl-dithiocarbamate (C)	MBDADTC	68	0.07	0.07	0.03	337
Methylene-bis-dibutyl-dithiocarbamate (C)	MBDBDTC	scuffing				
Titanium (IV) isopropoxide	Ti-IPO	scuffing				
(Methylcyclopentadienyl) manganese(I)tricarbonyl	MMT	57	0.08	0.08	0.04	18.1
Zinc alkylphosphate (C)	ZP	56	0.08	0.09	0.06	-
Zinc diamyl dithiocarbamate (C)	ZnDTC	9	0.09	0.05	0.02	218
Molybdenum dialkyldithiocarbamate (C)	MoDTC	16	0.05	0.03	0.02	4.77
Amide borate (C)	AB	10	0.08	0.04	0.03	-
Tris(2-ethylhexyl) borate (C)	TEHB	9	0.09	0.04	0.02	8.17
Hexyleneglycol biborate (C)	HGBB	43	0.18	0.14	0.06	-
Dibutyleneglycol biborate (C)	DBGBB	90	0.12	0.09	0.05	19.1
Borated polyisobutenyl succinimide (High B) (C)	B-PIBS(H)	57	0.13	0.09	0.04	not measurable
Borated polyisobutenyl succinimide (Low B) (C)	B-PIBS(L)	27	0.09	0.05	0.02	-

Potassium borate (C)	KB	46	0.10	0.09	0.03	3.47
Benzotriazole (C)	BTA	54	0.08	0.07	0.04	5.21
Hydroxyquinoline (C)	HQ	61	0.09	0.07	0.02	not measurable
Polyisobutylene succinimide dispersant 1 (C)	PIBS1	highly reflective	0.11	0.10	0.05	0.69
Titanium oxide nanoparticles (C)	TiO_2 NANO	highly reflective	0.09	0.06	0.03	12.6
Fullerene	=	highly reflective	0.09	0.07	0.03	14.8
Double walled carbon nanotubes	DWCN	highly reflective	0.11	0.10	0.05	9.8
IF-WS_2 (C)	IF-WS_2	highly reflective	0.08	0.05	0.02	3.9
p-Carborane (C)	p-CB	highly reflective	0.08	0.07	0.03	not measurable
m-Carborane (C)	m-CB	highly reflective	0.11	0.08	0.03	not measurable
Crystalline overbased calcium sulphonate (C)	cOBCaSu	42	0.09	0.09	0.03	1.7
Amorphous overbased calcium sulphonate (C)	aOBCaSu	56	0.08	0.08	0.04	47.0
Neutral calcium alkylsulphonate (C)	nCaSu	55	0.07	0.06	0.03	36.7

[1] "=" means abbreviated name is the same as full name.

Figures 15.1 to 15.5 illustrate film thickness, the friction coefficient and the average wear coefficient taken in the middle and at both ends of the wear track for ZDDP and low and zero SAPS antiwear additives studied in base oil alone.

From figure 15.1 it can be seen that some members of all additive families tested are able to form thick films. Apart from ZDDP, the P-only additives form thick films most consistently. The presence of a metal cation, *i.e.* nCaSu and Ti-IPO, has a significant synergistic effect on the film-forming properties of P- and P-S-containing antiwear additives, yielding rapid formation of relatively thick films, as demonstrated in chapter 6 and 7. This is presumably because the metal cation enables stabilisation and growth of the protective film; such glass stabilisation has been proposed to be the role of Zn in ZDPP [67].

Although it was not possible to measure the film thickness of some nanoparticle-containing antiwear additives using the MTM-SLIM, AFM study has revealed that these additives are capable of forming thick films on rubbed surfaces, particularly Fullerene, DWCN and PIBS1, the polyisobutylene succinimide dispersant used to stabilise the nanoparticle blends, as shown in chapter 12, Figure 12.13.

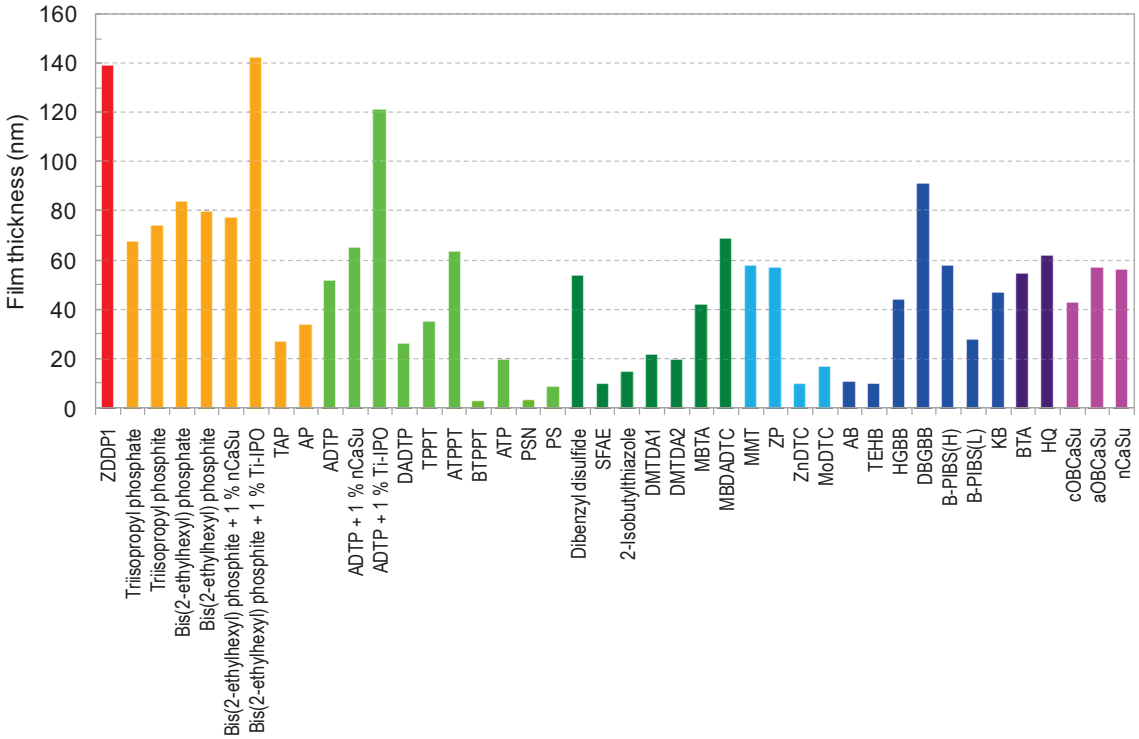


Figure 15.1: Mean film thickness after 2 hours of rubbing for ZDDP and low and zero SAPS antiwear additives in base oil alone (*i.e.* whenever possible to measure film thickness using MTM-SLIM).

In terms of friction behaviour, the ZDDP employed in this study, *i.e.* ZDDP1, has the highest friction overall. This is presumably because the thick pad-like film formed by ZDDP inhibits fluid flow through the contact and thus increases friction. Note that the anomalous high friction given by Hexyleneglycol biborate (C), *i.e.* HGBB is probably due to the presence of wear debris on the surface, as can be seen in chapter 10, Figure 10.7.

Interestingly, Triaryl phosphate (C), *i.e.* TAP, gives very low friction throughout, *i.e.* $\mu \approx 0.06$, 0.06 and 0.03 at the low, intermediate and high speed region, respectively, which might indicate that aryl groups are beneficial with respect to friction. This friction behaviour is similar to that observed for MoDTC, *i.e.* $\mu \approx 0.05$, 0.03 and 0.02 at the low, intermediate and high speed region, respectively, a widely-used friction modifier additive.

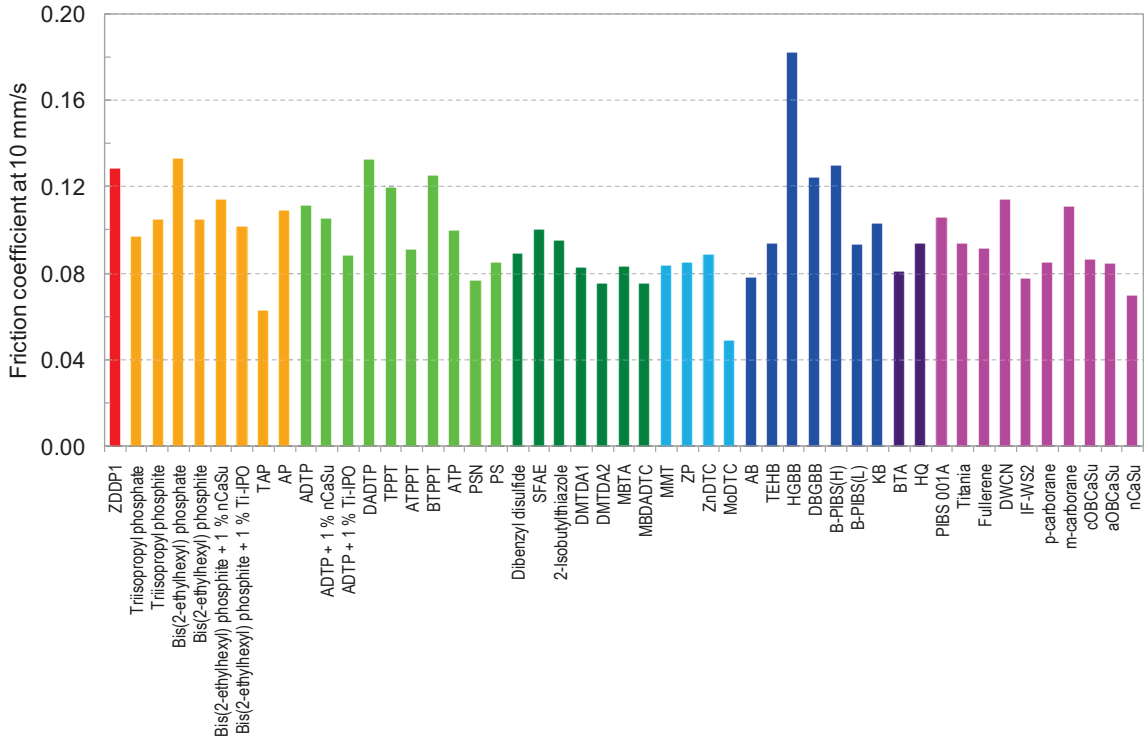


Figure 15.2: Friction coefficient after 2 hours of rubbing at the low speed region, *i.e.* 10 mm/s, for ZDDP and low and zero SAPS antiwear additives in base oil alone.

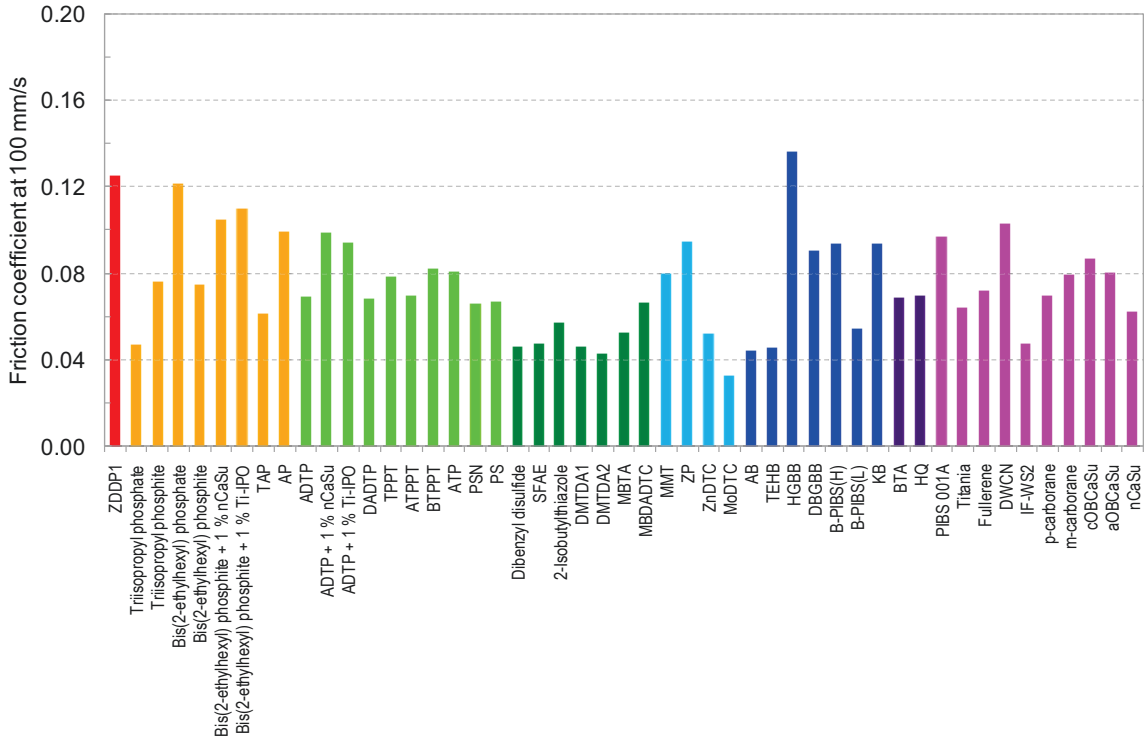


Figure 15.3: Friction coefficient after 2 hours of rubbing at the intermediate speed region, *i.e.* 100 mm/s, for ZDDP and low and zero SAPS antiwear additives in base oil alone.

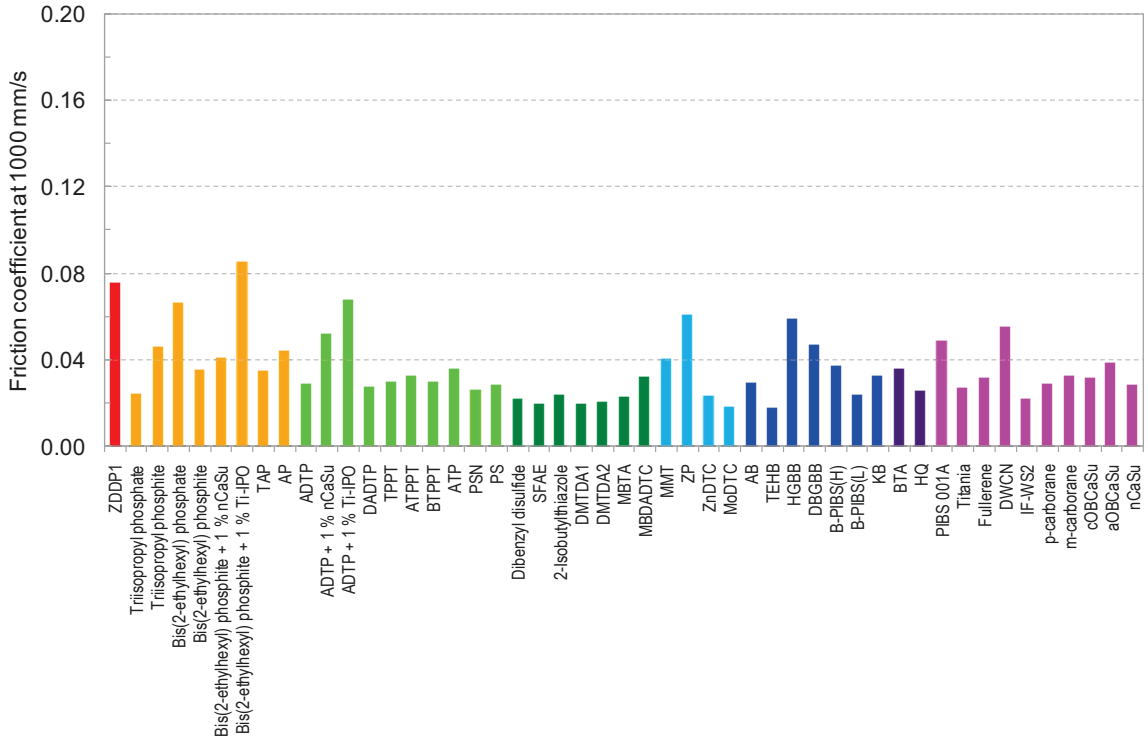


Figure 15.4: Friction coefficient after 2 hours of rubbing at the high speed region, *i.e.* 1000 mm/s, for ZDDP and low and zero SAPS antiwear additives in base oil alone.

Also noteworthy is that some of the alternative low and zero SAPS antiwear additives studied offer wear-reducing properties comparable to, or in some cases slightly better than ZDDP, in particular some of the phosphorus-sulphur-, *i.e.* ADTP, TPPT and ATPPT, boron-, *i.e.* B-PIBS(H) and KB, nitrogen-containing heterocyclic-, *i.e.* HQ and nanoparticle-additives, *i.e.* p-CB and m-CB. Interestingly, all additives that have superior wear performance form thinner or even negligible protective films on the surface, which suggests that thick boundary film formation, *i.e.* similar to ZDDP, is not required for effective wear control, at least under the wear test conditions employed in this study. Another aspect to be noted is that for some of these additives a decrease in wear rate is observed with increasing rubbing time, which is presumably due to running-in wear. In the running-in wear period, during which wear depth increases rapidly with time, the wear rate of the rubbing components is greater than during steady-state wear. This is followed by an extended steady-wear rate period during which the displacement of material from the surface is linear with rubbing time.

Most previous work on the wear-reducing properties of alternative low and zero SAPS additives employed a four-ball tester to evaluate wear. It is arguable, however, whether this type of short bench test provides a realistic measure of modern engine wear performance, *i.e.* steady-state wear. From the work carried out in this research it is clear that alternative low and zero SAPS antiwear additives do not react quite as fast as ZDDP and since short wear tests tend to favour only fast adsorbing additives, promising alternative low and zero SAPS antiwear additives, *i.e.* P-S, B, N and nanoparticle-based additives, might have been dismissed as possible supplements/replacements for ZDDP if short tests had been used.

Interestingly, the polyisobutylene succinimide dispersant, *i.e.* PIBS1, which is used to stabilise the nanoparticle blends, gives low wear in base oil alone, lower even than overbased and neutral calcium sulphonate detergent, *i.e.* cOBCaSu, aOBCaSu, nCaSu. Having said that, it is noteworthy that dispersants have a deleterious effect on wear when combined with antiwear additives, as demonstrated in chapter 14, Figure 14.5 and 14.9.

Also of importance is the overall performance of Crystalline overbased calcium sulphonate (C), *i.e.* cOBCaSu, a well known and widely used detergent, which shows comparable wear-reducing properties to ZDDP. It has been shown that this additive rapidly forms a uniform protective film on rubbed surfaces, *ca.* 40 nm after 2 hours of rubbing. The superior performance of crystalline overbased calcium sulphonate (C), *i.e.* cOBCaSu, over the Amorphous overbased calcium sulphonate (C), *i.e.* aOBCaSu, and the Neutral calcium alkylsulphonate (C), *i.e.* nCaSu, detergents might be ascribed to its higher stability under rubbing conditions. It has been suggested that crystalline calcium sulphonate detergents are more stable than amorphous calcium sulphonate detergents, because the latter forms either a calcite-deposited film or calcite-containing wear debris, which might give abrasive wear [332]. The results clearly show that cOBCaSu reacts under rubbing to form boundary films, which improve friction and wear-reducing properties and also have a synergistic effect with alternative low and zero SAPS antiwear additives, as shown in chapter 14. This is desirable, since its primary role is to influence the properties of the bulk lubricating oil.

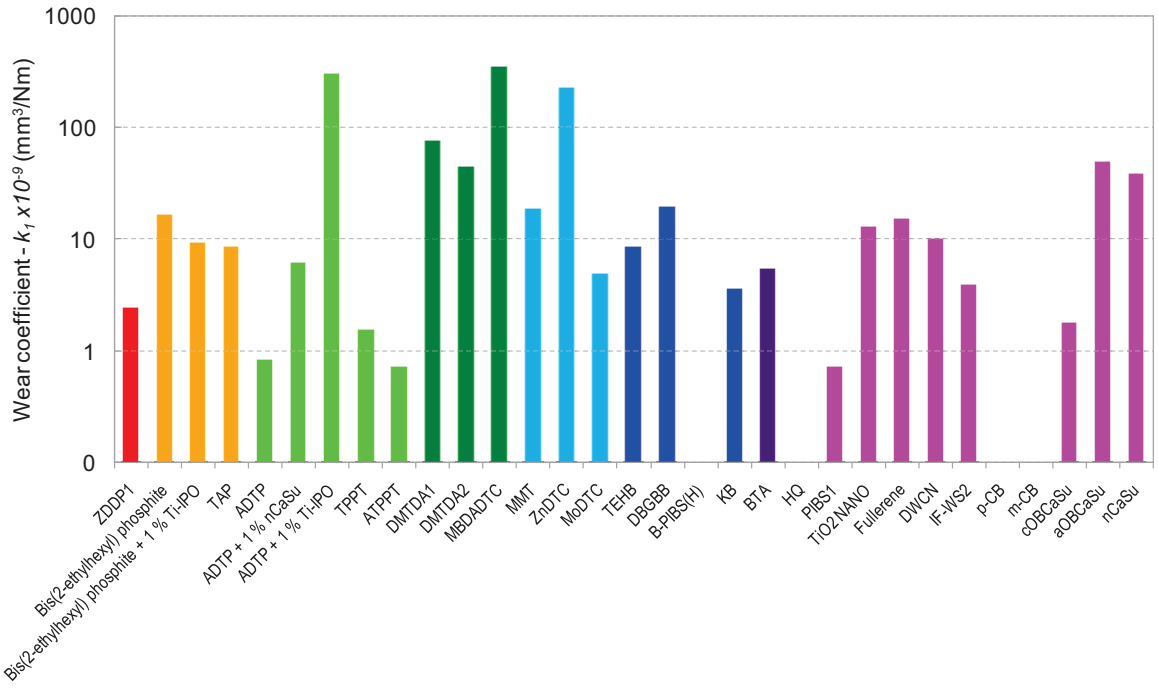


Figure 15.5: Wear coefficient[1], k_1 x 10^{-9}, after 16 hours of rubbing for ZDDP and low and zero SAPS antiwear additives in base oil alone. ([1]This corresponds to the average of wear coefficients taken in the middle and at the edges of the wear track)

15.2 Correlations

Figures 15.6 to 15.10 illustrate the correlations (or lack thereof) between film thickness and friction, film thickness and wear, and friction and wear for all antiwear additives studied in base oil alone or partially formulated oils.

As shown in Figure 15.6, there appears to be negligible correlation between film thickness and friction at the low speed region, *i.e.* boundary friction. This is not surprising, since it has long been suggested that boundary friction is controlled by the molecular structure of the protective layer attached to the surface, *i.e.* long linear alkyl chain impart lower boundary friction [198, 199]. This is clear from results shown in chapter 14, which show high boundary friction behaviour for dispersant-containing formulations, which is ascribed to the effect of the polyisobutylene chains, having many pendant methyl groups, attached to the surface.

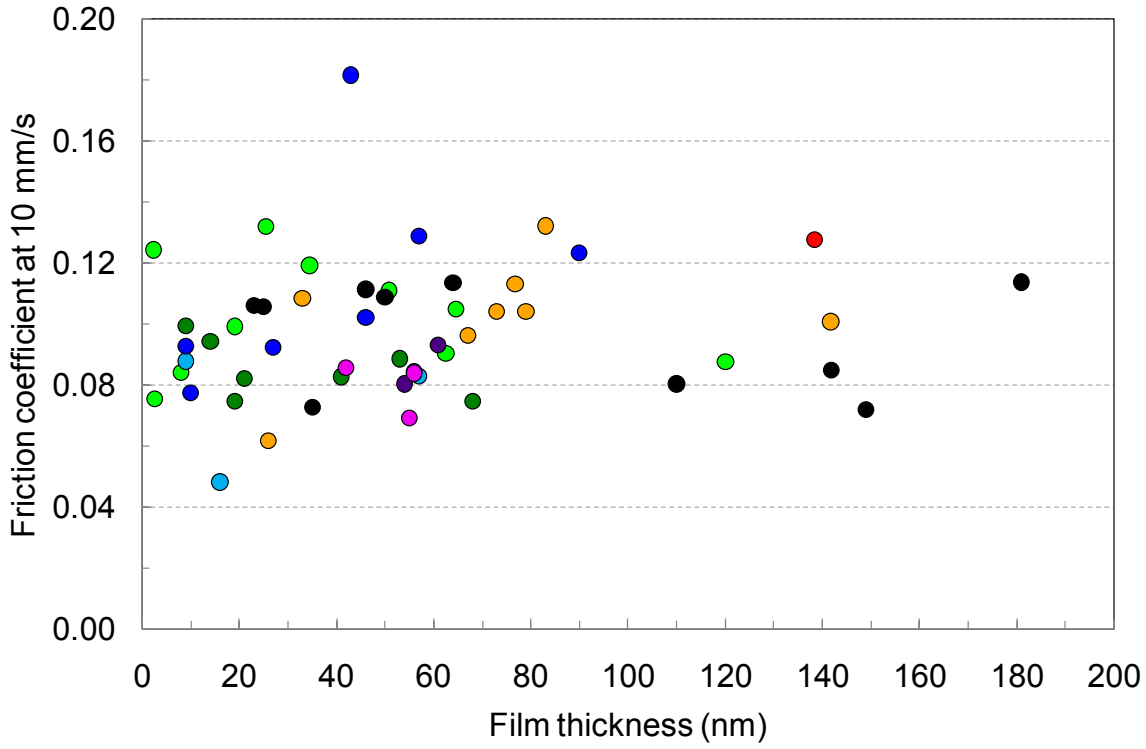


Figure 15.6: Mean film thickness *versus* friction coefficient at the low speed region, *i.e.* 10 mm/s, after 2 hours of rubbing for all additives in base oil alone, partially or fully formulated oils (*i.e.* whenever possible to measure film thickness using MTM-SLIM). Legend: red: ZDDP1, orange: phosphorus-containing compounds, light green: phosphorus-sulphur-containing compounds, dark green: sulphur-containing compounds, light blue: metal-containing compounds, dark blue: boron-containing compounds, indigo: nitrogen-containing heterocyclic compounds, magenta: nanoparticle-containing compounds, black: antiwear additives in partially formulated oils.

Figure 15.7 shows that there is a correlation between film thickness and friction at the intermediate speed region, *i.e.* mixed friction. This is in agreement with the conjecture that thicker tribofilms, *e.g.* those formed by ZDDP1 and Bis(2-ethylhexyl) phosphite + 1 % Ti-IPO, change contact surface texture and thus inhibit the entrainment of lubricant into the contact increasing friction at the intermediate speed region [390]. A similar correlation is observed at the high speed region, *i.e.* EHL, as can be seen in Figure 15.8.

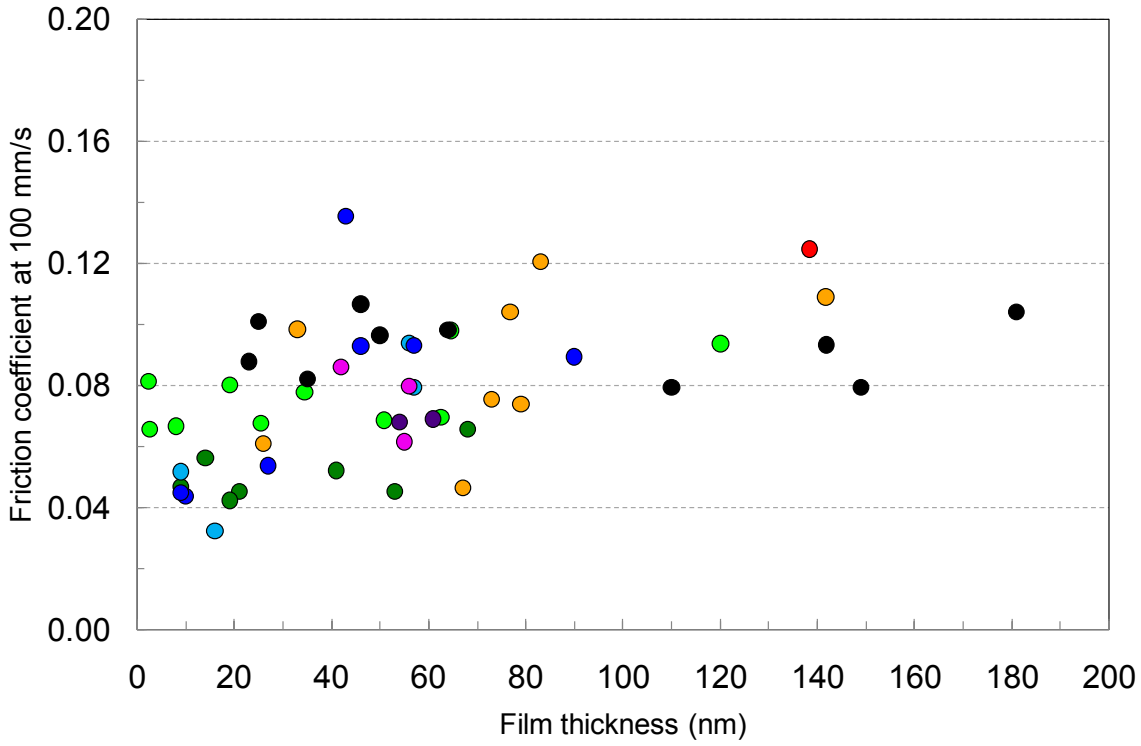


Figure 15.7: Mean film thickness *versus* friction coefficient at the intermediate speed region, *i.e.* 100 mm/s, after 2 hours of rubbing for all additives in base oil alone, partially or fully formulated oils (*i.e.* whenever possible to measure film thickness using MTM-SLIM). Legend: red: ZDDP1, orange: phosphorus-containing compounds, light green: phosphorus-sulphur-containing compounds, dark green: sulphur-containing compounds, light blue: metal-containing compounds, dark blue: boron-containing compounds, indigo: nitrogen-containing heterocyclic compounds, magenta: nanoparticle-containing compounds, black: antiwear additives in partially formulated oils.

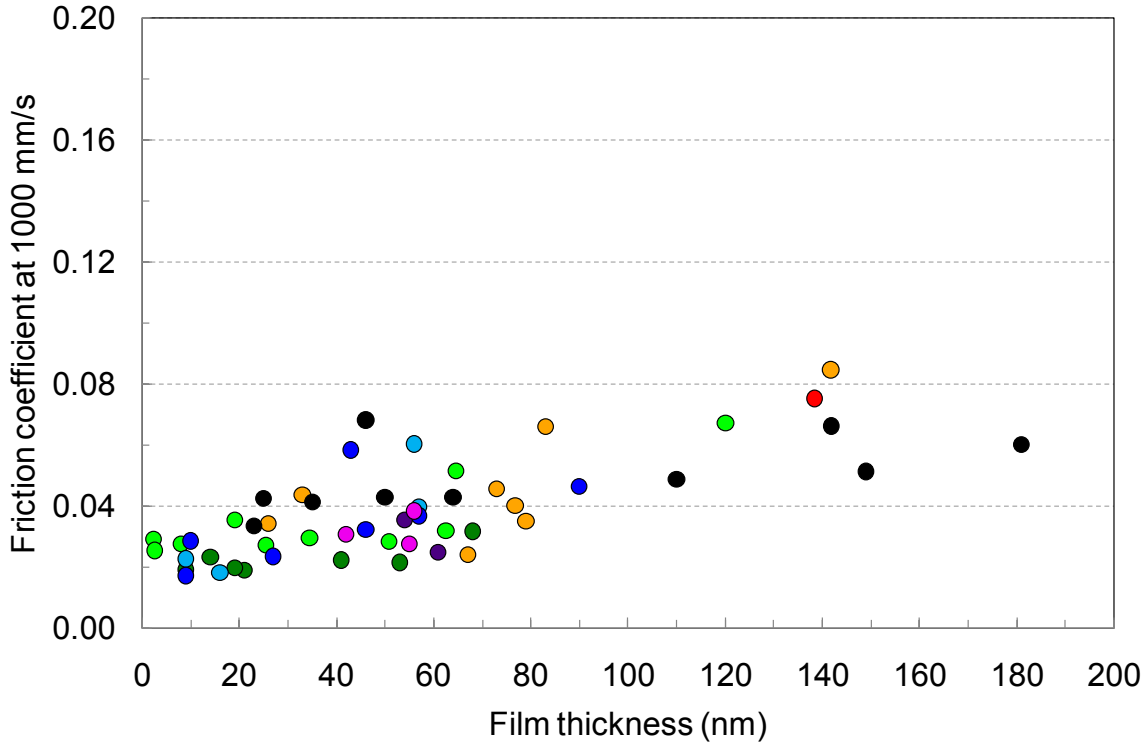


Figure 15.8: Mean film thickness *versus* friction coefficient at the high speed region, *i.e.* 1000 mm/s, after 2 hours of rubbing for all additives in base oil alone, partially or fully formulated oils (*i.e.* whenever possible to measure film thickness using MTM-SLIM). Legend: red: ZDDP1, orange: phosphorus-containing compounds, light green: phosphorus-sulphur-containing compounds, dark green: sulphur-containing compounds, light blue: metal-containing compounds, dark blue: boron-containing compounds, indigo: nitrogen-containing heterocyclic compounds, magenta: nanoparticle-containing compounds, black: antiwear additives in partially formulated oils.

Figures 15.9 and 15.10 show that there is no significant correlation between film thickness and wear and friction and wear. Thus far it had not yet been established what thickness of antiwear film is actually necessary or desirable to control wear. This research has spanned a very wide range of antiwear additive chemistries, which unambiguously shows that, contrary to popular belief, thick boundary film formation, *i.e.* similar to ZDDP, does not necessarily mean less wear. Factors that seem to influence wear control under boundary lubrication conditions include:

- Reactivity of additive or additive decomposition by-products towards the surface, *i.e.* ability to adsorb or chemisorb forming a protective layer.

- Running-in: it appears that in well lubricated systems, wear rate is controlled by the effectiveness of the interfacial layer, *i.e.* tribofilm. This means that if this film effectively adsorbs onto the surface, wear approaches a steady state, which is controlled by the removal and replenishment of this film.
- Durability of the protective layer, *i.e.* ability to withstand varying contact conditions in terms of load, temperature and speed, and prevent seizure and wear caused by direct metal-to-metal contact between moving parts operating in boundary lubrication.

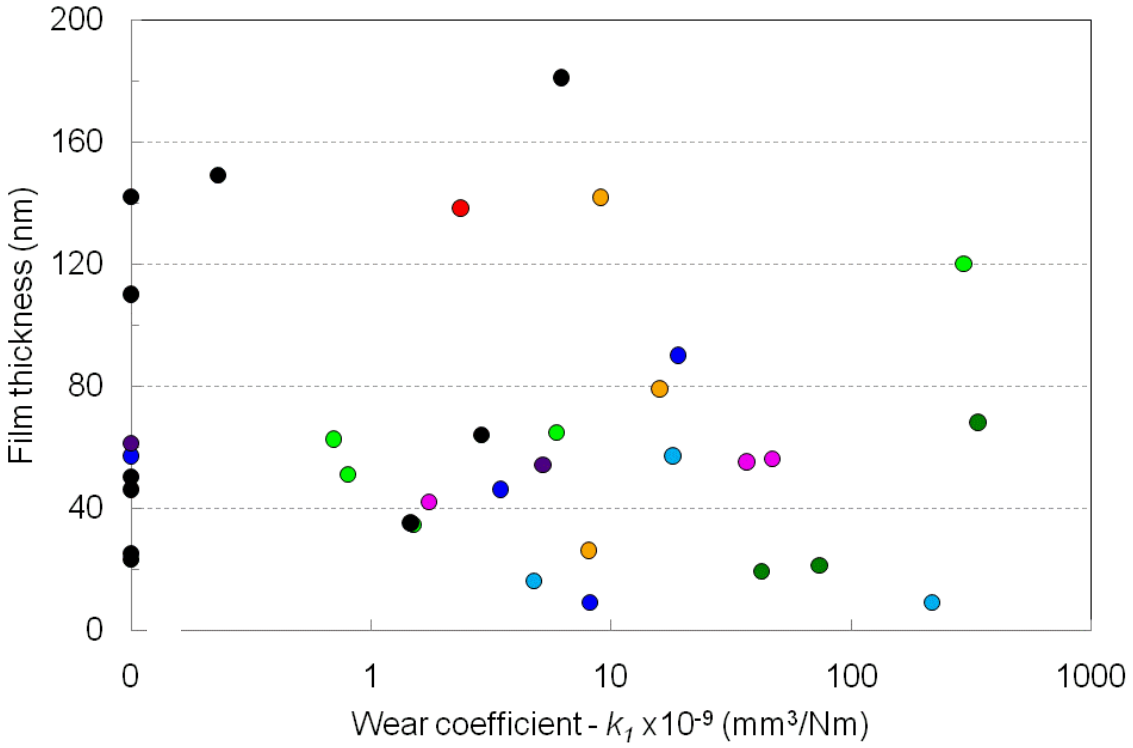


Figure 15.9: Mean film thickness after 2 hours of rubbing *versus* wear coefficient[1], k_1 x 10^{-9}, after 16 hours of rubbing for all additives in base oil alone, partially or fully formulated oils (*i.e.* whenever possible to measure film thickness using MTM-SLIM). Legend: red: ZDDP1, orange: phosphorus-containing compounds, light green: phosphorus-sulphur-containing compounds, dark green: sulphur-containing compounds, light blue: metal-containing compounds, dark blue: boron-containing compounds, indigo: nitrogen-containing heterocyclic compounds, magenta: nanoparticle-containing compounds, black: antiwear additives in partially formulated oils. ([1]This corresponds to the average of wear coefficients taken in the middle and at the edges of the wear track)

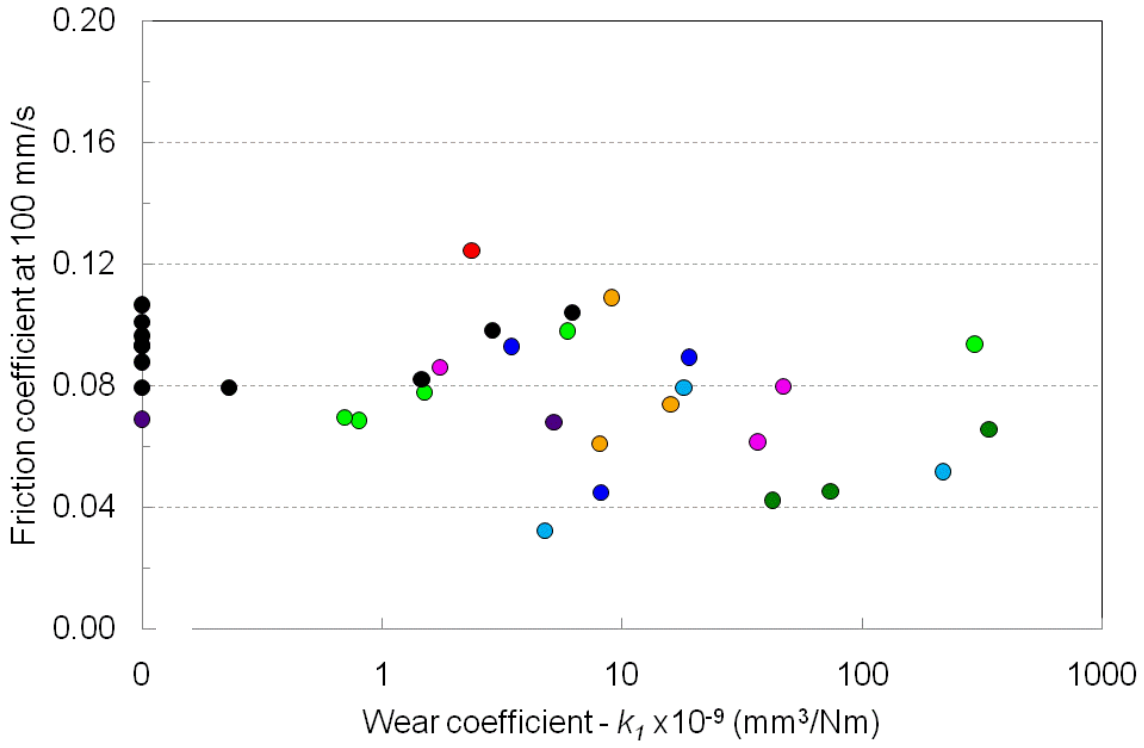


Figure 15.10: Friction coefficient at the intermediate speed region, *i.e.* 100 mm/s, after 2 hours of rubbing *versus* wear coefficient[1], k_1 x 10^{-9}, after 16 hours of rubbing for all additives in base oil alone, partially or fully formulated oils. Legend: red: ZDDP1, orange: phosphorus-containing compounds, light green: phosphorus-sulphur-containing compounds, dark green: sulphur-containing compounds, light blue: metal-containing compounds, dark blue: boron-containing compounds, indigo: nitrogen-containing heterocyclic compounds, magenta: nanoparticle-containing compounds, black: antiwear additives in partially formulated oils. ([1]This corresponds to the average of wear coefficients taken in the middle and at the edges of the wear track)

15.3 Most Promising Alternatives

The most promising alternative low and zero SAPS antiwear additives for use in the formulation of engine oils as alternatives for ZDDP are summarised in Table 15.4.

Chemical analysis of the tribofilms formed by these additives, presented in chapter 13, reveals that these films are not composed by the additives themselves, but consist of the decomposition products of these additives. More importantly, it has been shown that most commercially-available antiwear additives undergo reaction/decomposition under rubbing to form complex multilayered-type protective films. It appears that phosphorus and phosphorus-sulphur antiwear additives form analogous films to ZDDP, with Fe being the predominant cation stabilising the phosphate/polyphosphate glass instead of Zn. Boron additives form a mixture of trigonal and tetrahedral boron rich-film, which appear to be very effective in reducing wear. The nanoparticle-based additives, p-carborane and m-carborane, *i.e.* p-CB and m-CB, respectively, appear to form boron-iron rich films, with a substantial amount of Fe being incorporated into the protective layer. Unfortunately the nitrogen content in tribofilms formed by Hydroxyquinoline (C), *i.e.* HQ, was below the detection limit for the techniques employed, so the composition of these films could not be investigated.

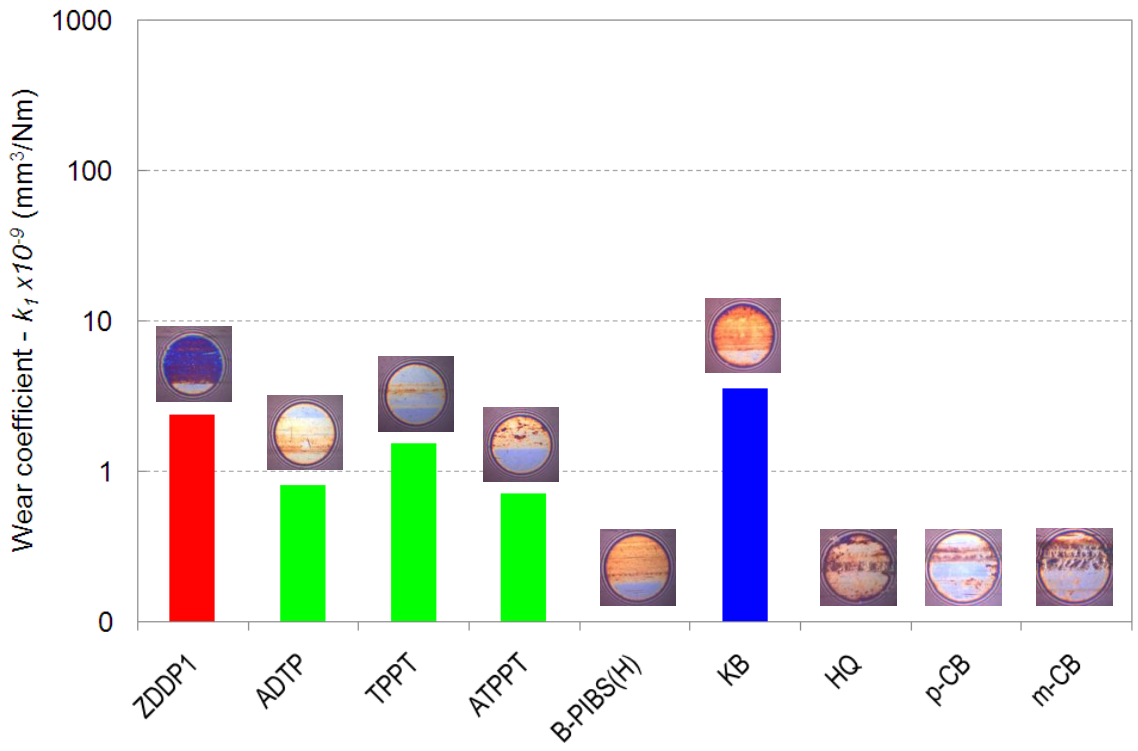


Figure 15.11: Wear coefficient[1], k_1 x 10^{-9}, after 16 hours of rubbing and MTM-SLIM images taken after 2 hours of rubbing for most promising alternative low and zero SAPS antiwear additives. ([1]This corresponds to the average of wear coefficients taken in the middle and at the edges of the wear track)

16. CONCLUSIONS AND SUGGESTIONS FOR FUTURE WORK

This chapter outlines the important findings of this work and, based on these findings, makes some suggestions for future research on this field.

16.1 Conclusions

There is a growing need to partially or fully replace ZDDP in engine oils to mitigate its deleterious effects, *i.e.* (i) contribution to SAPS, which reduce the useful life of exhaust aftertreatment systems, (ii) overall increase in engine friction, which compromises fuel economy, and (iii) corrosive-abrasive wear with soot in diesel engines.

A multi-technique approach has been systematically employed to explore, under the same test conditions, the film-forming, friction and wear-reducing properties of a very wide range of alternative low and zero SAPS antiwear additives that have been suggested as a possible replacements for ZDDP in engine oils. This study should benefit designers of the next generations of engine lubricants and also help us understand at a more fundamental level the various ways that lubricants can control wear in boundary lubrication conditions. The main findings are summarised below.

- Many low and zero SAPS antiwear additives are capable of forming thick, solid-like films similar to ZDDP, albeit more slowly.

- Additives that produce thicker tribofilms tend to give higher friction at the intermediate speed region, *i.e.* mixed friction. This is presumably because these films change the contact surface texture and thus inhibit the entrainment of lubricant into the contact increasing friction.

- Friction at the low speed region, *i.e.* boundary friction, is not dependent on the boundary film thickness, but appears to be controlled by the molecular structure of the protective layer attached to the surface, *i.e.* long linear alkyl chains, such as the ones from overbased calcium sulphonates impart lower boundary friction, whereas polyisobutylene succinimides dispersants, with many pendant methyl groups, increase boundary friction.

- Thick, transparent antiwear additive-derived tribofilms produce an apparent, optical artifact when scanning white light interferometers are employed to measure wear on rubbed surfaces, which could be incorrectly interpreted as wear. The precise origins of this effect are not clear since the optical properties of ZDDP- or low and zero SAPS antiwear additives-derived tribofilms are not well-characterised. However ZDDP-derived films have a high refractive index of *ca.* 1.6 [88], which results in a very large refractive index difference across the air/film interface. This is likely to produce internal reflection within the film which may contribute to an increase in the apparent path difference between the incident light and the instrument's reference beam, and be misinterpreted as wear. This implies that scanning white light interferometers should be used with great caution to measure small levels of wear on rubbed surface that may bear tribofilms. In order to measure wear using this technique, it is recommended that tribofilms be removed prior to wear measurement. It has been found that ZDDP tribofilms can be removed using EDTA solution, whereas the films formed by low and zero SAPS antiwear additives can be removed using a oxalic acid and EDTA in aqueous solution.

- Wear coefficient (k_1) study reveals that running-in plays a key role on the wear-reducing properties of some low and zero SAPS antiwear additives. From this work, it is clear that most of these additives do not react as fast as ZDDP to form protective films on the surface and because of this, the outcome of short wear tests, which favour fast adsorbing additives, should be interpreted with caution.

- This research has also shown unambiguously that, contrary to popular belief, thick boundary film formation, *i.e.* similar to ZDDP, is not necessary to reduce wear. Additive reactivity towards the surface, running-in and durability of the protective layer play key roles in controlling wear under boundary lubrication conditions.

- The most promising alternative low and zero SAPS antiwear additives identified for use in the formulation of engine oils were phosphorus-sulphur-, *i.e.* ADTP, TPPT and ATPPT, boron-, *i.e.* B-PIBS(H) and KB, nitrogen-containing heterocyclic-, *i.e.* HQ and nanoparticle-additives, *i.e.* p-CB and m-CB. These have shown performance comparable to, or in some cases slightly better than the Primary ZDDP (C) used as a benchmark in this study, with lower friction behaviour.

- The chemical analysis of the tribofilms formed by alternative low and zero SAPS antiwear additives reveals that these films are not composed by the additives themselves, but consist of the decomposition products of these additives. More importantly, it has been shown that these antiwear additives undergo reaction/decomposition under rubbing to form complex multilayered-type protective films. It appears that phosphorus and phosphorus-sulphur antiwear additives form analogous films to ZDDP, with Fe being the predominant cation stabilising the phosphate/polyphosphate glass instead of Zn. Boron additives form a mixture of trigonal and tetrahedral boron rich-film, which appear to be very effective in reducing wear. The nanoparticle-based additives, p-carborane and m-carborane, *i.e.* p-CB and m-CB, respectively, appear to form boron-iron rich films, with a substantial amount of Fe being incorporated into the protective layer.

- This research has also demonstrated that some of the promising alternative low and zero SAPS antiwear additives give performance comparable to the Primary ZDDP (C) in partially formulated oils, which indicates that these additives can effectively control friction and wear in boundary lubrication conditions.

16.2 Suggestions for Future Work

This study has opened up several avenues for future research. These can broadly be divided into areas of further research on the various promising additive types identified and exploration of the practical use of these additives in engine (and other) oils.

- A number of additives have been identified that show promising antiwear behaviour despite forming thin rather than thick boundary films. This raises the question of why such additives are effective. It would be of great interest to explore the features of a boundary film that enable it to control wear; in particular its durability and its physical properties. The latter is a challenge for very thin films. It is important to understand how additives can form very thin films and still prevent wear since such thin films have the benefit of not increasing friction at intermediate and high speeds.

- Some additives have been found to form thick films and control wear in an unexpected fashion; for example a nitrogen heterocyclic compound and one (but not an alternative) borated dispersant. It would be of great interest to follow-up these findings with further work to explore the nature of the films formed by these additives.

- It is clear from the results that boundary friction is strongly dependent on additive structure for the antiwear additives studied, but the origins of this are not always obvious. Thus it is clear why additives with long, saturated alkyl chains can reduce boundary friction but less obvious why aryl compounds can do so. It would be of considerable interest to explore in a systematic fashion the impact of variation of molecular structure on boundary friction for those additives identified as showing low friction as well as low wear.

- In practical applications, any antiwear additive has to be used in the presence of other additives. Further investigation is needed of promising alternative low and zero SAPS antiwear additives in partially and fully formulated oils for evaluation of the impact of other additives, such as detergent and dispersant, on wear performance and of the low and zero SAPS antiwear additives on the performance of these additives.

- For practical formulations, the use of blends low and zero SAPS antiwear additives with low concentrations of ZDDP have been suggested - to obtain a combination of rapid protective film formation and also longer term, low SAPS protection. The use of promising alternative additives in combination with low concentrations of ZDDP should be studied.

- It is important that antiwear additives remain effective during the drain interval of any lubricated system. Therefore the thermal stability and impact of ageing on the useful life of fully formulated oils containing alternative low and zero SAPS antiwear additives should be investigated. Also of interest is the volatility of the additives found to be promising, both in terms of P loss and also loss of S from blends.

- Finally, of course, it is necessary to test the most promising additives identified in realistic conditions, such as engine tests, before such additives can be considered for use in the field.

REFERENCES

1. **Twigg, M.V.,** *Twenty-five Years of Autocatalysts.* Platinum Metals Rev., 1999. 43: p. 168-171.
2. *Ground-Level Ozone*. Pollution Prevention and Abatement Handbook 1998 [cited 2009 10th January]; Available from: http://www.ifc.org.
3. *The Southland's War on Smog: Fifty Years of Progress Toward Clean Air*. 1997 [cited 2011 10th January]; Available from: http://www.aqmd.gov/news1/Archives/History/marchcov.html.
4. *50 Years of Progress Toward Clean Air: A Photographic Retrospective*. [cited 2011 10th January]; Available from: http://www.aqmd.gov/news1/Archives/History/50th_photos.htm.
5. **Kendall, T.,** *30 Years in the Development of Autocatalysts.* Platinum Today, 2004. 2009: p. 32-37.
6. **Wilkins, A.J.J.,** *The Effect of Fuel and Oil Additives on Automobile Catalysts Performance: The Suitability of Platinum Metals Confirmed.* Platinum Metals Rev., 1990. 34: p. 16-24.
7. **Koltsakis, G.C., Stamatelos, A.M.,** *Catalytic automotive exhaust aftertreatment.* Progress in Energy and Combustion Science, 1997. 23(1): p. 1-39.
8. **Moreno-Castilla, C., Perez-Cadenas, A.,** *Carbon-Based Honeycomb Monoliths for Environmental Gas-Phase Applications.* Materials, 2010. 3(2): p. 1203-1227.
9. **Alkemade, U.G., Schumann, B.,** *Engines and exhaust after treatment systems for future automotive applications.* Solid State Ionics, 2006. 177: p. 2291-2296.
10. *Schematic diagram of the three-way catalytic converter*. [cited 2009 10th January]; Available from: http://openlearn.open.ac.uk/mod/oucontent/view.php?id=398548&section=1.2.1.
11. *Rich/Lean Catalyst Conversions*. [cited 2011 10th January]; Available from: http://ect.jmcatalysts.com.
12. **Matsumoto, S.,** *Recent advances in automobile exhaust catalysts.* Catalysis Today, 2004. 90: p. 183-190.
13. *NOx adsorber catalyst - lean conditions*. [cited 2011 10th January]; Available from: http://ect.jmcatalysts.com.
14. *NOx adsorber catalyst - rich conditions*. [cited 2011 10th January]; Available from: http://ect.jmcatalysts.com.
15. **Jollie, D.,** *Palladium use in diesel oxidation catalysts.* Platinum Today, 2009: p. 39-41.
16. **Twigg, M.V.,** *Automotive exhaust emissions control.* Platinum Metals Rev., 2003. 47(4): p. 167-162.
17. *DPF, the continuously regenerating trap: taking the dirt out of diesel exhaust*. [cited 2011 10th January]; Available from: www.jmcatalysts.com.
18. **Campenon, T., Wouters, P., Blanchard, G., Macaudiere, P., Seguelong, T.,** *Improvement and simplification of DPF system using a ceria-based fuel-borne catalyst for diesel particulate filter regeneration in serial applications.* SAE Tech. Paper, 2004: p. 2004-01-0071.
19. **Bardasz, E.A., Cowling, S., Panesar, A., Tadrous, T.N.,** *Effects of lubricant derived chemistries on performance of the catalysed diesel particulate filters.* SAE Tech. Paper, 2005. 114(4): p. 1006-1021.

20. **Bardasz, E., Mackney, D., Britton, N., Kleinschek, G., Olofsson, K., Murray, I., Walker, A.P. ,** *Investigations of the Interactions between Lubricant Derived Species and Aftertreatment Systems on a State-of-the-Art Heavy-Duty Diesel Engine.* SAE Tech. Paper, 2003. 112(4): p. 1821-1839.
21. *The CRT system*. Diesel Particulate Filter [cited 2011 10th January]; Available from: http://ect.jmcatalysts.com.
22. **Wolfgang, F., Huthwohl, G., Maurer, B.,** *SCR Systems for Heavy Duty Trucks: Progress Towards Meeting Euro 4 Emission Standards in 2005*, in *9th DEER Conference*. 2003: Newport, RI.
23. **Johnson, T.,** *Diesel Engine Emissions and their Control: An Overview.* Platinum Metals Rev., 2008. 52(1): p. 23-37.
24. *Selective Catalytic Reduction: The NOx Removal Method of Choice from Passenger Cars to Power Plants*. [cited 2011 10th January]; Available from: http://www.jm-gem.com.
25. *SCRT - Selective Catalytic Reduction Technology*. Johnson Matthey Emissions Control Toolbox: A guide to emissions control after-treatment technologies [cited 2011 10th January]; Available from: http://ect.jmcatalysts.com.
26. **Wilkins, A.J.J.,** *Effects of Oil Additives on Autocatalysts.* Platinum Metals Rev., 2004. 48(1): p. 44.
27. **Nemoto, S., Kishi, Y., Matsuura, K., Miura, M., Togawa, S., Ishikawa, T.,** *Impact of oil-derived ash on continuous regeneration-type diesel particulate filter - JCAPII oil WG report.* SAE Tech. Paper, 2004(01): p. 1887.
28. **Kurihara, I., Takeshima, S., Yashima, H.,** *Development of Low-Ash Type Heavy Duty Diesel Engine Oil for After-Treatment Devices.* SAE Tech. Paper, 2004: p. 2004-01-1955.
29. **Bardasz, E.,** *Future engine fluids technologies: durable, fuel-efficient, and emissions-friendly*, in *11th Diesel Engine Emissions Reduction*. 2005: Chicago, Ill.
30. **Korcek, S., Nakada, M.,** *Engine oil performance requirements and reformulation for future gasoline engines and systems.* SAE Tech. Paper, 1996: p. 57-63.
31. **Twigg, M.V., Collins, N.R., Morris, D., O'Connell, J., Ball, I.K., Arrowsmith, S., Cassidy, L., Wrench, P.,** *The effect of phosphorus and boron lubricant additives on catalyst and engine durability.* SAE Tech. Paper, 2004: p. 2004-01-1888.
32. **Franz, J., Schmidt, J., Schoen, C., Haperscheid, M., Eckhoff, S., Roesch, M., Leyrer, J.,** *Deactivation of TWC as a function of oil ash accumulation - a parameter study.* SAE Tech. Paper, 2005(01): p. 1097.
33. **Inoue, K., Kurahashi, T., Negishi, T., Akiyama, K., Ashimura, K., Tasaka, K.,** *Effects of phosphorus and ash contents of engine oils on deactivation of monolithic three-way catalysts and oxygen sensors.* SAE Tech. Paper, 1992(06): p. 54.
34. **Kumar, S., Ferrari, V., Burk, P.L., Deeba, M., Rogalo, J.,** *Influence of phosphorus poisoning on TWC catalysts.* SAE Tech. Paper, 2003(1): p. 3735.

35. **Asanuma, T., Hirota, S., Yanaka, M., Tsukasaki, Y., Tanaka, T.,** *Effect of sulphur-free and aromatics-free diesel fuel on vehicle exhaust emissions using simultaneous PM and NOx reduction systems.* SAE Tech. Paper, 2003(1): p. 1865.
36. **Li, J., Theis, J., Chun, W., Goralski, C., Kudla, R., Ura, J., Watkins, W., Chatta, M. and Hurley, R.,** *Sulfur poisoning and desulfation of the lean NOx trap.* SAE Tech. Paper, 2001(1): p. 2503.
37. *Performance tests: TEOST 33C - ASTM D6335.* [cited 2011 20th April]; Available from: www.infineum.com.
38. **Stipanovic, A.J., Schoonmaker, J.P., Paz, E.F., Mowlem, J.K., Broas, J.E., Thiel, C.Y.,** *Base oil and additive effects in the Thermo-oxidation Engine Oil Simulation Test (TEOST).* SAE Tech. Paper, 1996: p. 111-120.
39. **Chamberlin, W.B., Kelly, J.C., Wilk, M.A.,** *The impact of passenger car motor oils on emissions performance.* SAE Tech. Paper, 2003: p. 2003-01-1988.
40. *The ILSAC GF-3 Minimum Performance Standard for Passenger Car Engine Oils*. 2000. p. 9-17.
41. *ILSAC GF-4 Standard for Passenger Car Engine Oil.* 2004 [cited 2009 10th January]; Available from: http://www.ilma.org.
42. *ILSAC GF-5 Standard for Passenger Car Engine Oil*. 2009 [cited 2009 10th December]; Available from: http://www.ilma.org.
43. **Bardasz, E.A., Schiferl, E., Nahumck, W., Kelley, J., Williams, L., Rilley, M.J., Hubbard, C.P.,** *Low volatility ZDDP technology: Part 1 - Engines and lubricant performance in field applications.* SAE Tech. Paper, 2007: p. 2007-01-1990.
44. **Bardasz, E.A., Schiferl, E., Nahumck, W., Kelley, J., Williams, L., Hubbard, C.P., Thanasiu, E., Jagner, M., O'Neil, A., Uy, D.,** *Low volatility ZDDP technology: Part 2 - Exhaust catalysts performance in field applications.* SAE Tech. Paper, 2007.
45. **Hamrock, B.J., Dowson, D.,** *Ball bearing lubrication: the elastohydrodynamics of elliptical contacts*. 1981, New York: John Wiley and Sons.
46. **Hamrock, B.J.,** *Fluid film lubrication with applications to machine elements*, Fundamentals of Tribology and Bridging the Gap Between the Macro- and Micro/Nanoscales, B. Bhusham, Editor. 2001, Springer. p. 747-765.
47. **Stribeck, R.,** *The principal properties of sliding and roller bearings.* Zeit VDI, 1902. 46: p. 1341-1348, 1432-1438, 1463-1470.
48. **Olomolehin, Y.,** *The Influence of zinc dialkyldithiophosphate and other lubricant additives on soot-induced wear*, in *Mechanical Engineering*. 2009, Imperial College: London.
49. **Hsu, S.M., Gates, R.S.,** *Boundary lubricating films: formation and lubrication mechanism.* Trib. Intern., 2005(38): p. 305-312.

50. **Hsu, S.M., Zhang, J., Yin, Z.,** *The nature and origin of tribochemistry.* Trib. Lett., 2002. 13(2): p. 131-139.
51. **Stachowiak, G.W., Batchelor, A. W.,** *Engineering Tribology*. 3rd ed. 2006: Butterworth-Heinemann.
52. **Spikes, H.A.,** *Mixed lubrication - an overview.* Lubr. Sci., 1997. 9: p. 221-253.
53. **Spikes, H.A., Olver, A.V.,** *Basics of mixed lubrication.* Lubr. Sci., 2003. 16: p. 3-28.
54. **Williams, J.A.,** *Engineering Tribology*. 1994: Oxford University Press.
55. **Cameron, A.,** *Principles of Lubrication*. 1966, London: Longmans. 591.
56. **Spikes, H.A.,** *Tribology Notes: Introduction to Tribology*. 2008, Imperial College, London.
57. **Watson, D.,** *Elastohydrodynamic lubrication*. Introduction to Lubrication [cited 2011 10th January]; Available from: www.maxxtorque.com.
58. **Henderson, H.A., Steckle, W. M., Swinney, B.,** *Higher quality base oils for tomorrow's engine oil performance categories.* SAE Tech. Paper, 1998: p. 982582.
59. *API Base oil interchangeability guidelines for passenger car motor oils and diesel engine oils*. 2008 [cited 2009 10th January]; Available from: http://www.api.org/.
60. **Sethuramiah, A.,** *Lubricated Wear: Science and Technology*. Trib. Ser., ed. D. Dowson. Vol. 42. 2003: Elsevier.
61. **Stachowiak, G.W.**, ed. *Wear - Materials, Mechanisms and Practice*. Tribology in Practice. 2005, John Wiley & Sons.
62. **Archard, J.F.,** *Contact and rubbing of flat surfaces.* J. Appl. Phys., 1953. 24: p. 981-988.
63. **Taylor, L., Glovnea, R., Ribeaud, M., Spikes, H.A.,** *The nature and properties of antiwear additive films*. International Tribology Conference. 2000. Nagasaki.
64. **Najman, M.N., Kasrai, M., Bancroft, G.M.,** *Chemistry of antiwear films from ashless thiphosphate oil additives.* Trib. Lett., 2003. 17(2): p. 217-229.
65. *Structure of $Zn(DTP)_2$.* [cited 2008 10th January]; Available from: http://en.wikipedia.org/wiki/File:Zn%28dtp%292.png.
66. **Khorramian, B.A., Iyer, G.R., Kodali, S., Natarajan, P., Tupil, R.,** *Review of antiwear additives for crankcase oils.* Wear, 1993. 169: p. 87-95.
67. **Spikes, H.A.,** *Low- and zero-sulphated ash, phosphorus and sulphur anti-wear additives for engine oils.* Lubr. Sci., 2008. 20(2): p. 103-136.
68. **Fujita, H., Spikes, H.A.,** *The formation of zinc dithiophosphate antiwear films.* Proc. Inst. Mech. Eng., Part J: Journal of Engineering Tribology, 2004(218): p. 265-277.
69. **Benedet, J., Spikes, H.A., Green, J.H., Lamb, G.D.,** *Film forming, friction and wear properties of alternative antiwear additives*, in *66th STLE Annual Meeting & Exhibition*. 2011: Atlanta, USA.
70. **Cann, P.M., Hutchinson, J., Spikes, H.A.,** *The development of spacer layer imaging method (SLIM) for mapping elastohydrodynamic contacts.* Trib. Trans., 1996. 39: p. 915-921.

71. **Spikes, H.A., Cann, P.M.,** *The development and application of the spacer layer imaging method for measuring lubricant film thickness* Lubr. Sci., 2001. 17: p. 25-43.
72. **Brow, R.K., Tallant, D.R., Myers, S.T., Phifer, C.C.,** *The short-range structure of zinc polyphosphate glass.* J. Non-Cryst. Solids, 1995. 191: p. 45-55.
73. **Fujita, H., Glovnea, R. P. and Spikes, H. A.,** *Study of zinc dialkyldithiophosphate antiwear film formation and removal processes, Part I: Experimental.* Trib. Trans., 2005. 48: p. 558-566.
74. *MTM 3D-SLIM.* [cited 2008 10th January]; Available from: http://www.pcs-instruments.com/mtm/accessories/mtm_3d_slim_option.shtml.
75. **Mate, C.M., McClelland, G.M., Erlandsson, R., Chiang, S.,** *Atomic-scale friction of a tungsten tip on a graphite surface.* Phys. Rev. Lett., 1987. 59: p. 1942–1945.
76. **Binnig, G., Quate, C.F., Gerber, Ch.,** *Atomic force microscope.* Phys. Rev. Lett., 1986. 56: p. 930-933.
77. **Pidduck, A.J., Smith, G.C.,** *Scanning probe microscopy of automotive anti-wear films.* Wear, 1997. 212: p. 254-264.
78. *Atomic Force Microscope*. 2008 [cited 2008 10th January]; Available from: http://commons.wikimedia.org/wiki/File:Atomic_force_microscope_block_diagram.svg.
79. *MTM-Reciprocating motion*. [cited 2008 10th January]; Available from: http://www.pcs-instruments.com/mtm/accessories/mtm-reciprocating-option.shtml.
80. **MacGeehan, J.A., Ryanson, P.R.,** *Preventing catastrophic camshaft lobe failures in low emission diesel engines.* SAE Tech. Paper, 2000: p. 2000-01-2949.
81. **Brown, R.D.,** *Chapter 12. Test Methods*, Boundary Lubrication: an Appraisal of World Literature, F.F. Ling, Klaus, E. E. and Fein, R.S., Editor. 1969, ASME: New York. p. 341-392.
82. **Ruff, A.W.,** *Wear Measurement*, Friction and Wear Testing Source Book of Selected References from ASTM Standards and ASM Handbooks. 1997, ASTM and ASM: West Conshohocken, PA. p. 22-29.
83. **Gahlin, R., Jacobson, S.,** *A Novel Method to Map and Quantify Wear on a Micro-Scale.* Wear, 1998(222): p. 93-102.
84. **Veeco,** *WYKO NT9100 Technical Manual*.
85. **Tasan, Y.C., De Rooij, M.B., Schipper, D.J.,** *Measurement of wear on asperity level using image-processing techniques.* Wear, 2005(258).
86. **Benedet, J., Spikes, H.A., Green, J.H., Lamb, G.D.,** *Spurious mild wear measurement using white light interference microscopy in the presence of antiwear films.* Trib. Trans., 2009(52): p. 841-846.
87. *MTM-Reciprocating: wear scar on the disc.* [cited 2008 10th January]; Available from: http://www.pcs-instruments.com/mtm/accessories/mtm-reciprocating-option.shtml.
88. **Spikes, H.A.,** *The history and mechanisms of ZDDP.* Trib. Lett., 2004. 17(3): p. 469-489.

89. **Benedet, J., Spikes, H.A., Green, J.H., Lamb, G.D.,** *Tribological characteristics of low and zero SAPS antiwear additives*, in *65th STLE Annual Meeting & Exhibition*. 2010: Las Vegas, USA.

90. **Bell, C.F.,** *Principles and applications of metal chelation*. Oxford Chemistry Series, ed. P.W. Atkins, Holker, J.S.E., Holliday, A.K. 1977, Oxford: Oxford University Press.

91. **Topolovec-Miklozic, K., Forbus, T.R., Spikes, H.A.,** *Film thickness and roughness of ZDDP antiwear films.* Trib. Lett., 2007. 26(2).

92. **ZYGO,** *NewView 200 Technical Manual*.

93. **Gao, F., Leach, R.K., Petzing, J., Coupland, J.M.,** *Surface measurement errors using commercial scanning white light interferometers.* Meas. Sci. Technol., 2008(19): p. 015303.

94. **Topolovec-Miklozic, K., Forbus, T.R., Spikes, H.A.,** *Film-forming and friction properties of overbased calcium sulphonate detergents.* Trib. Lett., 2008. 29: p. 33-44.

95. **Panias, D., Taxiarchou, M., Paspaliaris, I., Kontopoulos, A.,** *Mechanisms of dissolution of iron oxides in aqueous oxalic acid solutions.* Hydrometallurgy, 1996. 42(257-265).

96. **Vickerman, J.C., Briggs, D.,** *ToF-SIMS: Surface Analysis by Mass Spectrometry*. 2001: IM Publications and Surface Spectra Limited.

97. **Taylor, M.,** *Surface Analysis of Polymer Microarrays*. 2008, University of Nottingham: Nottingham.

98. *Principle of ToF-SIMS*. [cited 2009 10th January]; Available from: http://www.geobiologie.uni-goettingen.de/people/vthiel/tof_sims/index_e.shtml.

99. **Rossi, A., Elsener, B., Hahner, G., Textor, M., Spencer, N.D.,** *XPS, AES and TOF-SIMS investigation of surface films and the role of inclusions on pitting corrosion in austenitic stainless steels.* Surface and Interface Analysis, 2000. 29(7): p. 460-467.

100. **Najman, M.N., Kasrai, M., Bancroft, G.M.,** *Investigating binary oil additive systems containing P and S using X-ray absorption near-edge structure spectroscopy.* Wear, 2004. 257(1-2): p. 32-40.

101. **Zhang, Z., Yamaguchi, E.S., Kasrai, M., Bancroft, G.M., Liu, X., Fleet, M.E.,** *Tribofilms generated from ZDDP and DDP on steel surfaces: Part 2, chemistry* Trib. Lett., 2005. 19(3): p. 221-229.

102. **Hongling, Y.I., Xiangqiong, Z., Yan, C., Tianhui, R., Kasrai, M., Bancroft, G.M.,** *XANES analysis of tribo-chemical and thermal films generating from some organic polysulfides.* Chin. Sci. Bul., 2006. 51(22): p. 2710-2716.

103. **Yu, L.G., Yamaguchi, E.S., Kasrai, M., Bancroft, G.M.,** *The chemical characterization of tribofilms using XANES - Interaction of nanosize calcium-containing detergents with zinc dialkyldithiophosphate.* Can. J. Chem., 2007. 85(10): p. 675-684.

104. **Yong, W., Kasrai, M., Bancroft, G.M.,** *X-ray absorption study of tribofilms from ZDDP and overbased salicylate detergents.* Chin. Chem. Let., 2009. 20(1): p. 119-122.

105. **Nicholls, M., Najman, M.N., Zhang, Z., Kasrai, M., Norton, P.R., Gilbert, P.U.P.A.,** *The contribution of XANES spectroscopy to tribology.* Can. J. Chem., 2007. 85: p. 816-830.

106. **Stohr, J.,** *NEXAFS Spectroscopy*. Surface Sciences, ed. G. Ertl, Gomer, R., Mills, D.L., Lotsch, H.K.V. 1992: Springer.

107. *The photoelectric effect*. [cited 2009 10th January]; Available from: www.bessy.de/?icat=163&changelang=5.

108. **De Barros, M.I., Bouchet, J., Raoult, I., Le Mogne, T., Martin, J.M.,** *Friction reduction by metal sulfides in boundary lubrication studied by XPS and XANES analysis.* Wear, 2003. 254: p. 863-870.

109. **Najman, M.N., Kasrai, M., Bancroft, G.M., Davidson, R.,** *Combination of ashless antiwear additives with metallic detergents: interactions with neutral and overbased calcium sulfonates.* Trib. Intern., 2006. 39: p. 342-355.

110. **Yamaguchi, E.S., Wilson, D.M., Kasrai, M., Bancroft, G.M.,** *XANES analysis of used engine oils and relationship to wear.* Trib. Trans., 2002. 45(4): p. 437-443.

111. **Assef, P.A.,** *US Patent 2261047: Lubricant*. 1941, The Lubrizol Corp.: USA.

112. **Cook, E.W., Thomas Jr., W.D.,** *US Patent 2344392: Crankcase lubricant and chemical compound therefore*. 1944, American Cyanamid Company: USA.

113. **Freuler, H.C.,** *US Patent 2364283: Modified lubricating oil*. 1944, Union Oil Company: USA.

114. **Freuler, H.C.,** *US Patent 2364284: Modified lubricating oil*. 1944, Union Oil Company: USA.

115. **Barnes, A.M., Bartle, K.D., Thibon, V.R.A.,** *A review of zinc dialkyldithiophosphates (ZDDPs): characterisation and role in the lubricating oil* Trib. Intern., 2001. 34: p. 389-395.

116. **Gellman, A.J., Spencer, N.D.,** *Surface Chemistry in Tribology.* Proc. Inst. Mech. Eng., Part J: Journal of Engineering Tribology, 2002(216): p. 443-461.

117. **Nicholls, M., Do, T., Norton, P.R., Kasrai, M., Bancroft, G.M.,** *Review of the lubrication of metallic surfaces by zinc dialkyl-dithiophosphates.* Trib. Intern., 2005. 38: p. 15-39.

118. **Dacre, B., Bovington, C.H.,** *The Adsorption and Desorption of Zinc Di-isopropyldithiophosphate on Steel.* ASLE Trans., 1982. 25(4): p. 546-554.

119. **Dacre, B., Bovington, C.H.,** *The Effect of Metal Composition on the Adsorption of Zinc Di-Isopropyldithiophosphate.* ASLE Trans., 1983. 26(3): p. 333-343.

120. **Bec, S., Tonck, A., Georges , J.M., Coy, R.C., Bell, J.C., Roper, G.W.,** *Relationship between mechanical properties and structures of zinc dithiophosphate anti–wear films.* Proc. R. Soc. Lond. A, 1999. 455(1992): p. 4181-4203.

121. **Palacios, J.M.,** *Thickness and chemical composition of films formed by antimony dithiocarbamate and zinc dithiophosphate.* Trib. Intern., 1986. 19(1): p. 35-39.

122. **Fuller, M.L.S., Fernandez, L.R., Massoumi, G.R., Lennard, W.N., Kasrai, M., Bancroft, G.M.,** *The use of X-ray absorption spectroscopy for monitoring the thickness of antiwear films from ZDDP* Trib. Lett., 2000. 8(4): p. 187-192.

123. **Taylor, L., Dratva, A., Spikes, H.A.,** *Friction and wear behaviour of zinc dialkyl dithiophosphate.* Trib. Trans., 2000. 43: p. 469-479.

124. **Aktary, M., McDermott, M.T., McAlpine, G.A.,** *Morphology and nanomechanical properties of ZDDP antiwear films as a function of tribological contact time.* Trib. Lett., 2002. 12: p. 155-162.

125. **Yin, Z., Kasrai, M., Fuller, M., Bancroft, G.M., Fyfe, K., Tan, K.H.,** *Application of soft X-ray absorption spectroscopy in chemical characterisation of antiwear films generated by ZDDP, Part I: the effects of physical parameters.* Wear, 1997. 202: p. 172-191.

126. **Martin, J.M., Grossiord, C., Le Mogne, T., Bec, S., Tonck, A.,** *The two-layer structure of Zndtp tribofilms: Part I: AES, XPS and XANES analyses.* Trib. Intern., 2001. 34(8): p. 523-530.

127. **Eglin, M., Rossi, A., Spencer, N.D.,** *X-Ray photoelectron spectroscopy analysis of tribostressed samples in the presence of ZnDTP: a combinatorial approach.* Trib. Lett., 2003. 15(3): p. 199-209.

128. **Bell, J.C., Delargy, K.M., Seeney, A.M.**, ed. *The Removal of Substrate Material through Thick Zinc Dithiophosphate Anti-Wear Films*. Trib. Ser., Wear Particles: From the Cradle to the Grave, Proceedings of the 18th Leeds-Lyon Symposium on Tribology ed. D. Dowson, et al. Vol. 21. 1992, Elsevier. 387–396.

129. **Kasrai, M., Fuller, M., Bancroft, G., Yamaguchi, E., Ryason, P.,** *X-Ray absorption study of the effect of calcium sulfonate on antiwear fim formation generated from neutral and basic ZDDPs: Part I - phosphorus species.* Trib. Trans., 2003. 46(4): p. 534-542.

130. **Topolovec-Miklozic, K.,** *Challenges and Opportunities for Wear Evaluation in Rolling Contacts*. 18th International Colloquium Tribology 2012, Industrial and Automotive Lubrication, Solving Friction and Wear Problems. 2012. Technische Akademie Esslingen, Stuttgart / Ostfildern, Germany.

131. **Kennedy, S., Moore, L.D.,** *Additive effects on lubricant fuel economy.* SAE Tech. Paper, 1987: p. 681-691.

132. **Bovington, C., Spikes, H.A.,** *Prediction of the influence of lubricant formulation on fuel economy, from laboratory bench tests*. Proc. Int. Trib. Conf. 1995. Yokohama.

133. **Tripaldi, G., Vettor, A., Spikes, H.A.,** *Friction behaviour of ZDDP film in the mixed, boundary lubrication regime.* SAE Tech. Paper, 1996: p. 962036.

134. **Taylor, L., Spikes, H.A., Camezind, H.,** *Film forming properties of zinc based and ashless antiwear additives.* SAE Tech. Paper, 2000: p. 2000-01-2030.

135. **Taylor, L., Spikes, H.A.,** *Friction-enhancing properties of ZDDP antiwear additive: Part 1 - friction and morphology of ZDDP reaction films.* Trib. Trans., 2003. 46: p. 303-309.

136. **Taylor, L., Spikes, H.A.,** *Friction-enhancing properties of ZDDP antiwear additive: Part 2 - influence of ZDDP reaction films on EHD lubrication.* Trib. Trans., 2003. 46: p. 310-314.

137. **Topolovec-Miklozic, K., Spikes, H.A.,** *Application of atomic force microscopy to the study of lubricant additive films.* J. Tribology, 2005. 127: p. 405-415.

138. **Zhu, Y., Granick, S.,** *Apparent Slip of Newtonian Fluids Past Adsorbed Polymer Layers.* Macromolecules, 2002. 35(12): p. 4658-4663.

139. **Hutchins, I.M.,** *Tribology: Friction & Wear of Engineering Materials*. 1992, London: Edward Arnold.

140. **Habeeb, J.J., Stover, W.H.,** *The Role of Hydroperoxides in Engine Wear and The Effect of Zinc Dialkyldithiophosphates.* ASLE Trans., 1987. 30(4): p. 419-426.

141. **Rounds, F.,** *Effects of Hydroperoxides on Wear as Measured in Four-Ball Wear Tests.* Trib. Trans., 1993. 36(2): p. 297-303.

142. **Martin, J.M., Belin, M., Mansot, J.L., Dexpert, H., Lagarde, P.,** *Friction-Induced Amorphization with ZDDP - An EXAFS Study.* ASLE Trans., 1986. 29(4): p. 523-531.

143. **Belin, M., Martin, J. M., Mansot, J.L.,** *Role of Iron in the Amorphization Process in Friction-Induced Phosphate Glasses.* Trib. Trans., 1989. 32(3): p. 410-413.

144. **Martin, J.M.,** *Antiwear mechanisms of zinc dithiophosphate: a chemical hardness approach.* Trib. Lett., 1999. 6(1): p. 1-8.

145. **Bancroft, G.M., Kasrai, M., Fuller, M., Yin, Z., Fyfe, K.,Tan, K.H.,** *Mechanisms of tribochemical film formation: stabilityof tribo- and thermally-generated ZDDP films* Trib. Lett., 1997. 3(1): p. 47-51.

146. **Fujita, H., Spikes, H.A.**, ed. *The influence of soot on lubricating films*. Transient processes in tribology, Proceedings of the 30th Leeds-Lyon Symposium on Tribology ed. D. Dowson, et al. Vol. 43. 2004, Elsevier: Oxford. 37-43.

147. **Campen, S.,** *Fundamentals of organic friction modifier behaviour*, in *Mechanical Engineering*. 2012, Imperial College: London.

148. **Aoki, S., Suzuki, A., Masuko, M.,** *Comparison of sliding speed dependency of friction between steel surfaces lubricated with several ZnDTPs with different hydrocarbon moieties.* Proc. Inst. Mech. Eng., Part J: Journal of Engineering Tribology, 2006. 220: p. 343-351.

149. **Sheasby, J.S., Caughlin, T.A., Blahey, A.G., Laycock, K.F.,** *A reciprocating wear test for evaluating boundary lubrication.* Trib. Intern., 1990. 23(5): p. 301-307.

150. **Zhang, J.,** *Influence of Succinimide Dispersants on Film Formation, Friction and Antiwear Properties of Zinc Dialkyl Dithiophosphate*, in *Mechanical Engineering*. 2011, Imperial College: London.

151. **Smalheer, C.V., Mastin, T.W.,** *Phosphorus in the lubricants field.* Petroleum Processing, 1952. 7: p. 1780-1784.

152. **Peale, L.F., Messina, J., Ackerman, B., Sasin, R., Swern, D.,** *Evaluation of long-chain phosphorus compounds as lubricity additives.* ASLE Trans., 1960. 3(1): p. 48-54.

153. **Xia, Y., Weimin, L., Xue, Q.,** *Tribological properties of P- and N-containing organic compounds as potential extreme-pressure and antiwear additives.* Lubr. Sci., 2003. 15(2): p. 173-183.

154. **Papay, A.G.,** *Antiwear and extreme-pressure additives in lubricants.* Lubr. Sci., 1998. 10(3): p. 209-224.

155. **Beeck, O., Givens, J.W., Williams, E.C.,** *On the Mechanism of Boundary Lubrication: II. Wear Prevention by Addition Agents* Proc. R. Soc. Lond. A, 1940. A117(968): p. 103-118.

156. **Barcroft, F.T., Daniel, S.G.,** *The action of neutral organic phosphates as EP additives.* Trans. ASME J. Basic Eng., 1965. 87(3).

157. **Godfrey, D.,** *The lubrication mechanism of tricresyl phosphate on steel.* Wear, 1965. 8(5).

158. **Faut, O.D., Wheeler, D. R.,** *On the mechanism of lubrication by tricresyl phosphate (TCP) - The coefficient of friction as a function of temperature for TCP on M-50 steel.* ASLE Trans., 1983. 26(3): p. 344-350.

159. **Wheeler, D.R., Faut, O.D.,** *The adsorption and thermal decomposition of tricresylphosphate (TCP) on iron and gold.* Applic. Surf. Sci., 1984. 18: p. 106-122.

160. **Forbes, E.S., Silver, H. B.,** *The effect of chemical structure on the load carrying properties of organo phosphorus compounds.* J. Inst. Petrol., 1970. 57: p. 90-98.

161. **Forbes, E.S., Neustadter, E.L., Silver, H.B., Upsdell, N.T.,** *The effect of chemical structure on the load-carrying properties of amine phosphates.* Wear, 1971. 18.

162. **Sakurai, T., Sato, K.,** *Chemical reactivity and load carrying capacity of lubricating oils containing organic phosphorus compounds.* ASLE Trans., 1970. 13: p. 252-261.

163. **Kawamura, M., Fugita, K.,** *Organic sulphur and phosphorus compounds as extreme-pressure additives.* Wear, 1981. 72.

164. **Minami, I., Memita, M., Hirao, K.,** *Investigation of antiwear additives for synthetic esters.* Lubr. Eng., 2002. 58: p. 18-22.

165. **Barber, R.I.,** *The preparation of some phosphorus compounds and their comparison as load-carrying additives by the four-ball machine.* ASLE Trans., 1976. 19: p. 319-328.

166. **Riga, A., Cahoon, J., Pistillo, W.R.,** *Organophosphorus chemistry structure and performance relantionships in FZG gear tests.* Trib. Lett., 2000. 9: p. 219-225.

167. **Minami, I., Hong, H.S., Mathus, N.C.,** *Effect of alkenes on the antiwear mechanism of dialkyl hydrogen phosphites.* Lubr. Sci., 2001. 13: p. 219-230.

168. **Klaus, E.E., Bieber, H.E.,** *Effect of P^{32} impurities on the behaviour of tricresylphosphate^{32} as an antiwear additive.* ASLE Trans., 1965. 8: p. 12-20.

169. **Rounds, F.G.,** *Some environmental factors affecting surface coating formation with lubricating oil additives.* ASLE Trans., 1966. 9: p. 88-100.

170. **Forbes, E.S., Battersby, J.,** *The effect of chemical structure on the load-carrying and adsorption properties of dialkyl phosphites.* ASLE Trans., 1974. 17(4): p. 263-270.

171. **Lacey, I.N., Kelsall, G.H., Spikes, H.A.,** *Thick antiwear films in elastohydrodynamic contacts. Part I: film growth in rolling/sliding EHD contacts.* ASLE Trans., 1985. 29(3): p. 299-305.

172. **Lacey, I.N.,** *The antiwear performance of organo-phosphorus (III) esters*, in *Mechanical Engineering*. 1985, Imperial College: London.

173. **Cann, P.M., Johnston, G.J., Spikes, H.A.,** *The formation of thick films by phosphorus-based anti-wear additives.* Proc. Inst. Mech. Eng., 1987. C208/87: p. 543-554.

174. **Lacey, I.N., Kelsall, G.H., Spikes, H.A.,** *Thick antiwear films in elastohydrodynamic contacts. Part II: chemical nature of the deposited films.* ASLE Trans., 1985. 29(3): p. 306-311.

175. **Zheng, M., Naeim, A.H., Walter, B., John, G.,** *Break-in linear wear and piston ring assembly friction in a spark-ignited engine.* Trib. Trans., 1998. 41(4): p. 497-504.

176. **Kumar, R., Prakash, B., Sethuramiah, A.,** *A systematic methodology to characterise the running-in and steady-state wear process.* Wear, 2002. 252: p. 445-453.

177. **Sanin, P.I., Shepeleva, E.S., Ulyanova, A.V., Kleimenov, B.V.,** *The effect of synthetic additives in lubricating oil on wear under friction.* Wear, 1960. 3: p. 200-218.

178. **Sanin, P.I., Shepeleva, E.S., Mannik, A.O., Kleimenov, B.V.,** *Chemical modification of friction surfaces.* Trans. ASME J. Basic Eng., 1965. 87: p. 771-777.

179. **Schumacher, R., Zinke, H.,** *Tribofragmentation and antiwear behaviour of isogeometric phosphorus compounds.* Trib. Intern., 1997. 30: p. 199-208.

180. **Zinke, H., Schumacher R.,** *The thermal stability and antiwear performance of some thiophosphoric acid derivatives.* Wear, 1994. 179: p. 45-48.

181. **Zaskal'ko, P.P., Parfenova, V.A., Markov, A.A., Lesninova, V.A., Belov, P.S.,** *Amidothiophosphates - effective antiwear and extreme-pressure additives for lubricating oils.* Chem. and Techn. of Fuels and Oils, 1976. 12(1): p. 58-60.

182. **Borshchevskii, S.B., Shabanova, E.V., Trofimov, G.A., Karamnova, V.P.,** *Antioxidant , antiwear and extreme-pressure properties of amides of dithio acids of phosphorus.* Chem. and Techn. of Fuels and Oils, 1981. 17(3): p. 157-160.

183. **Vipper, A.B., Belov, P.S., Lashkhi, V.L., Parfenova, V.A., Blokhina, I.V., Kulagin, V.V.,** *Amidothiophosphates as antifriction and antiwear additives for lubricating oils.* Chem. and Techn. of Fuels and Oils, 1982. 18(4): p. 174-176.

184. **Borshchevskii, S.B., Shabanova, E.V., Markov, A.A., Rebrov, I.Y.,** *Antifriction and antiwear properties of dialkyldithioaminophosphates.* Chem. and Techn. of Fuels and Oils, 1984. 20(10): p. 503-506.

185. **Sarin, R., Tuli, D.K., Martin, V., Rai, M.M., Bhatnagar, A.K.,** *Development of N, P and S-containing multifunctional additives for lubricants.* Lubr. Eng., 1997. 53: p. 21-27.

186. **Vipper, A.B., Lashkhi, V.L., Belov, P.S., Parfenova, V.A., Blokhina, I.V.,** *Antifriction and antiwear efficiency of ashless thiophosphates and dithiophosphates.* Chem. and Techn. of Fuels and Oils, 1983. 19(3): p. 136-139.

187. **Borshchevskii, S.B., Levitina, I.S., Shabanova, E.V., Kotova, G.G.,** *Additives based on dithiophosphoric acids and unsaturated compounds for lubricating oils.* Chem. and Techn. of Fuels and Oils, 1991. 27(6): p. 326-328.

188. **Sharma, M., Bansai, V., Ray, S.S., Sarin, R., Tuli, D.K., Shainagar, A.K.,** *Role of alkyl moieties in the antiwear and antioxidant performance of alkyl phosphorodithiophosphates.* Lubr. Sci., 2003. 15(321-328).

189. **McDermott, J.P., Roselle, N.J.,** *US Patent 2689258: Reaction of terpenes with thiophosphorus acid esters and products thereof*. 1954, Standard Oil Co.: USA.

190. **Le Suer, W.M.,** *US Patent 3197405: Phosphorus- and Nitrogen-containing compositions and process for preparing the same*. 1965, Lubrizol Corp.: USA.

191. **Elliot, J.S., Jayne, G.J.J., Askew, H.F.,** *US Patent 3929653: Lubricant additives*. 1975, Edwin Cooper & Company Limited: USA.

192. **Camezind, H., Dubs, P.,** *US Patent 5328621: Dithiophosphates as antiwear additives*. 1994, Ciba-Geigy Corp.: USA.

193. **Esche Jr., C.K., Dancy, J.H., Love, D.,** *US Patent 5405544: Ashless antiwear-antioxidant lubricating oil additive*. 1995, Texaco Inc.: USA.

194. **Rossi, A., Piras, F.M., Kim, D., Gellman, A.J., Spencer, N.D.,** *Surface reactivity of tributyl thiophosphate: effects of temperature and mechanical stress.* Trib. Lett., 2006. 23(3): p. 197-208.

195. **Zhang, Z., Yamaguchi, E.S., Kasrai, M., Bancroft, G.M., Liu, X., Fleet, M.E.,** *Tribofilms generated from ZDDP and DDP on steel surfaces: Part 1, growth, wear and morphology.* Trib. Lett., 2005. 19(3): p. 211-220.

196. **Kim, B., Jiang, J.C., Aswath, P.B.,** *Mechanism of wear at extreme load and boundary conditions with ashless anti-wear additives: Analysis of wear surfaces and wear debris.* Wear, 2011. 270(3-4): p. 181-194.

197. **Olomolehin, Y., Kapadia, R., Spikes, H.A.,** *Antagonistic interaction of antiwear additives and carbon black.* Trib. Lett., 2009. 37: p. 49-58.

198. **Hardy, W.B., Doubleday, I.,** *Boundary Lubrication. The paraffin series.* Proc. R. Soc. Lond. A, 1922. 100(707): p. 550-574.

199. **Jahanmir, S.,** *Chain length effects in boundary lubrication.* Wear, 1985. 102(4): p. 331-349.

200. **Spikes, H.A.,** *Boundary lubrication and boundary films.* Trib. Ser., Proceedings of the 19th Leeds-Lyon Symposium on Tribology, 1993. 25: p. 331-346.

201. **Allum, K.G., Forbes, E.S.,** *The load-carrying properties of organic sulphur compounds. Part II: The influence of chemical structure on the anti-wear properties of organic disulfides.* J. Inst. Petrol., 1967. 53: p. 173-185.

202. **Allum, K.G., Ford, J.F.,** *Influence of chemical structure on load-carrying properties of certain organo-sulphur compounds.* J. Inst. Petrol., 1965. 51: p. 145-161.

203. **Forbes, E.S., Allum, K.G., Neustadter, E.L., Reid, A.J.D.,** *The load-carrying properties of diester disulfides.* Wear, 1970. 15: p. 341-352.

204. **Belov, P.S., Trofimov, V.A., Ermolaeva, A.N., Vipper, A.B., Lashkhi, V.L., Gusev, A.A.,** *Synthesis and investigatigation of antiwear properties of higher esters of 5,5'-thiodivaleric acid.* Chem. and Techn. of Fuels and Oils, 1980. 16: p. 461-463.

205. **Katafuchi, T., Shimizu, N.,** *Evaluation of the antiwear and friction reduction characteristics of mercaptocarboxylate derivatives as novel phosphorus-free additives.* Trib. Intern., 2007. 40: p. 1017-1024.

206. **Baldwin, B.A.,** *The effect of adsorption and molecular structure of antiwear additives on wear mitigation.* ASLE Trans., 1985. 28: p. 381-388.

207. **Davis, R.H., Farng, L.O., Horodysky, A.G.,** *US Patent 4908144: Dimercaptothiadiazole-derived, organic esters, amides and amine salts as multifunctional antioxidant/antiwear additives*. 1990, Mobil Oil Corp.: USA.

208. **Farng, L.O., Horodysky, A.G., Murray, J.G.,** *US Patent 5199960: Sulfur coupled hydrocarbyl derived mercaptobenzothiazole adducts as multifunctional antiwear additives and compositions containing same*. 1993, Mobil Oil Corp.: USA.

209. **Hsu, S.Y., Horodysky, A.G.,** *US Patent 5217502: Quaternary ammonium salt derived thiadiazoles as multifunctional antioxidant and antiwear additives*. 1993, Mobil Oil Corp.: USA.

210. **Love, D., Dancy, J.H., Lucas, J.M.,** *US Patent 5414090: Lubricant ashless antiwear-antioxidant additive*. 1995, Texaco Inc.: USA.

211. **Oumar-Mahamat, H., Horodysky, A.G., Jeng, A.,** *US Patent 5514289: Dihydrobenzothiophenes as antioxidant and antiwear additives*. 1996, Mobil Oil Corp.: USA.

212. **Singh, T., Singh, R., Verma, V.K., Nakayama, K.,** *A study of N, O and S heterocyclic compounds as extreme-pressure additives.* Trib. Intern., 1990. 23: p. 41-46.

213. **Singh, T., Chandrasekharan, C.V.,** *The effect of nitrogen and sulphur compounds on extreme-pressure lubrication.* Trib. Intern., 1993. 26: p. 245-250.

214. **Wei, D.P., Cao, L., Wang, L.I.,** *An investigation into the antiwear, antioxidation, and anticorrosion behaviour of some derivatives of 2,4-dimercapto-1,3,4-thiadiazole.* Lubr. Sci., 1995. 7(365-377).

215. **Gao, Y., Wu, Z., Zhang, Z., Xue, Q.,** *Study on tribological properties of 2,5-dialkoxymethylthio-1,3,4-thiadiazoles.* Wear, 1998. 222: p. 129-134.

216. **Zhu, F., Fan, W., Wang, A., Zhu, Y.,** *Tribological study of novel S-N style 1,3,4-thiadiazole-2-thione derivatives in rapeseed oil.* Wear, 2009. 266: p. 233-238.

217. **Chen, H., Yan, J., Ren, T., Zhao, Y., Zheng, L.,** *Tribological behavior of some long-chain dimercaptothiadiazole derivatives as multifunctional lubricant additives in vegetable oil and investigation of their tribochemistry using XANES.* Trib. Lett., 2012. 45: p. 465-476.

218. **Zhang, J., Liu, W., Xue, Q.,** *The effect of molecular structure of heterocyclic compounds containing N, O, and S on their tribological performance.* Wear, 1999. 231: p. 65-70.

219. **Liang, P., Wu, H., Zuo, G., Ren, T.,** *Tribological performances of heterocyclic-containing ether and/or thioether as additives in the synthetic diester.* Lubr. Sci., 2009. 21: p. 111-121.

220. **Liang, P., Ren, T., Li, J., Ma, H., Wu, H.,** *Tribological behaviour of two ash-less and phosphorous-free anti-wear additives and their synergetic effect with zinc dialkyldithiophosphates in mineral oil* Proc. Inst. Mech. Eng., Part J: Journal of Engineering Tribology, 2010. 224: p. 65-72.

221. **Li, J., Xu, X., Wang, Y., Ren, T.,** *Tribological studies on a novel borate ester containing benzothiazol-2-yl and disulfide groups as multifunctional additive.* Trib. Intern., 2010. 43: p. 1048-1053.

222. **Ren, T., Sha, G., Zheng, L., Xia, J., Liu, W., Xue, Q.,** *The tribological study of S-(1H-benzotriazol-1-yl) methyl N, N-dialkyldithiocarbamates as additives in pentaerythritol ester.* Lubr. Eng., 1997. 53: p. 39-43.

223. **Huang, W., Dong, J., Li, F., Chen, B.,** *The performance and antiwear mechanism of (2-sulfurone-benzothiazole)-3-methyl esters as additives in synthetic lubricant.* Trib. Intern., 2000. 33: p. 553-557.

224. **Huang, W., Dong, J., Wu, G., Zhang, C.,** *A study of S-[2-(acetamido) benzothiazol-1-yl]N,N-dibutyl dithiocarbamate as an oil additive in liquid paraffin.* Trib. Intern., 2004. 37: p. 71-76.

225. **Kim, Y.W., Chung, K., Kim, N.S., Hwang, D.H., Cho, W.O.,** *Synergistic lubricating effect of several ashless dithiocarbamates with Mo-donor additives.* Trib. Intern., 2007. 40: p. 397-404.

226. **He, Y.H., Song, Y.P., Shao, H.Y., Zhan, W.Q., Ren, T.H.,** *A study of the synergistic effect of a triazine-dithiocarbamate derivative with TCP in vegetable oil.* Lubr. Sci., 2005. 21: p. 287-297.

227. **Kumar, S., Roy, N.N.,** *Studies to evaluate the extreme-pressure properties and anti-wear activity of some thiuram disulfides, xanthogens and dithiocarbamates. .* Wear, 1997. 209: p. 1-7.

228. **Xu, X., Wan, Y., Cao, L.,** *Tribological performance and action mechanism of S-alkyl and S-benzimidazole substituted dialkyldithiocarbamates.* Wear, 2000. 241: p. 41-46.

229. **Ren, T., Xue, Q., Wang, H.,** *The tribological study of S-(1H-benzotriazol-1-yl) methyl alkyl xanthates as adiitives in synthetic lubricants.* Lubr. Eng., 1995. 51: p. 847-850.

230. **Fan, K., Li, J., Ma, H., Wu, H., Ren, T., Kasrai, M., Bancroft, G.M.,** *Tribological characteristics of ashless dithiocarbamate derivatives and their combinations with ZDDP as additives in mineral oil.* Trib. Intern., 2008. 41(12): p. 1226-1231.

231. **Wu, H., Li, J., Ma, H., Ren, T.,** *The tribological behaviours of dithiocarbamate-triazine derivatives as additives in mineral oil.* Surface and Interface Analysis, 2009. 41: p. 151-156.

232. **Knipple, R., Thich, J.,** *The history of aviation turbine lubricants.* SAE Tech. Paper, 1981: p. 810851.

233. **McHugh, K.L., Smith, T.O.,** *US Patent 3242081: Lubricating compositions*. 1966, Monsanto Corp.: USA.

234. **Guevremont, J., Guinther, G., Szemenyei, D., Jao, T.C.,** *Enhancement of engine oil wear and friction control performance through titanium additive chemistry.* 62nd STLE Annual Meeting & Exhibition, 2007.

235. **Carre, D.J., Bertrand, P.A., Lince, J.R.,** *Lead naphthenate additive tribochemistry in hydrocarbon oils.* Aerospace Report No. TR-2002(8565)-2, SMC-TR-02-08, 1981.

236. **Didziulis, S.V., Fleischauer, P.D.,** *Chemistry of the extreme-pressure lubricant additive lead naphthenate on steel surfaces.* Langmuir, 1991. 7(12): p. 2981-2990.

237. **Buckley, D.H.,** *Effectiveness of various organometallics as antiwear additives in mineral oil. .* NTIS, NASA-TP-1096, 1977.

238. **Luo, X., Wang, D., Dong, J.,** *The antiwear mechanism of an organotin compound.* Proc. Eurotrib, 1993.

239. **Liu, R.D., Tao, D.H., Fu, S.F., Zhao, Y.A., Zhang, J.H.,** *A study of the tribological behaviour of an organotin compound.* Lubr. Sci., 2005. 17: p. 419-429.

240. **Lashkhi, V.L., Tsvetkov, O.N., Ermolov, F.N., Komarova, N.N., Vipper, A.B., Belov, P.S., Kaidala, E.V., Korenev, K.D., Kulagin, V.V., Markov, A.A.,** *Organotin derivatives of alkylphenols as antiwear additives for lubricating oils.* Chem. and Techn. of Fuels and Oils, 1977. 13: p. 289-292.

241. **Kadjas, C.Z., Dominiak, M., Firkowski, A., Dabrowski, J.R., Misterkiewicz, B.,** *Tribochemistry of some ferrocene derivatives.* ASLE Trans., 1983. 26: p. 11-24.

242. **Farrington, B.B., Clayton, J.O.,** *US Patent 2228658: Coumpounded mineral oil*. 1941, Standard Oil Co.: USA.

243. **Farrington, B.B., Clayton, J.O., Rutherford, J.T.,** *US Patent 2228659: Coumpounded mineral oil*. 1941, Standard Oil Co.: USA.

244. **Dorinson, A.,** *The antiwear action of zinc di-n-butyl phosphate.* ASLE Trans., 1979. 22: p. 190-192.

245. **Yagashita, K., Igarashi, J., Koizumi, T.,** *US Patent 6656887: Lubricating oil compositions*. 2003, Nippon Mitsubishi Oil Corp.: USA.

246. **Hoshino, K., Yagishita, K., Tagawa, K., and Spikes, H.,** *Tribological Properties of Sulphur-Free Antiwear Additives Zinc Dialkylphosphates (ZDPs).* SAE Tech. Paper, 2011: p. 2011-01-2132.

247. **Galloupoulos, N.E.,** *Thermal decomposition of metal dialkyl dithiophosphate oil blends.* ASLE Trans., 1964. 7: p. 55-63.

248. **Allum, K.G., Forbes, E.S.,** *The load-carrying properties of metal dialkyl dithiophosphates: the effect of chemical structure.* Proc. Inst. Mech. Eng., 1968. 183: p. 7-14.

249. **Rowe, C.N., Dickert, J.J.,** *The relation of antiwear function to thermal stability and structure for metal O,O-dialkyl phosphorodithioates.* ASLE Trans., 1967. 10(85-90).

250. **Born, M., Hipeaux, J.C., Marchand, P., Parc, G.,** *Relationship between chemical structure and effectiveness of some metallic dialkyl and diaryl dithiophosphates in different lubricated mechanisms.* Lubr. Sci., 1992. 4(93-116).

251. **Chen, B., Dong, J., Chen, G.,** *Tribochemistry of gadolinium dialkyldithiophosphate.* Wear, 1996. 196: p. 16-20.

252. **Sarin, R., Tuli, D.K., Rai, M.M., Mehta, A.K., Bhatnagar, A.K.,** *Titanium dithiophosphates: a new class of multifunctional lubricant additives.* Lubr. Eng., 1995. 51(313-320).

253. **Zhang, J., liu, W., Xue, Q., Wang, Q.,** *Investigation of the friction and wear behaviours of Cu(I) and Cu(II) dioctyldithiophosphates as additives in liquid paraffin.* Wear, 1998. 216: p. 35-40.

254. **Willermet, P.A.,** *Some engine oil additives and their effects on antiwear film formation.* Trib. Lett., 1998. 5: p. 41-47.

255. **Givens, W.A., Buck, W.H., Jackson, A., Kaldor, A., Hertzberg, A., Moehrmann, W., Mueller-Lunz, S., Petz, N., Wenninger, G.,** *Lube formulation effects on transfer of elements to exhaust after-treatment system components.* SAE Tech. Paper, 2003: p. 2003-01-3109.

256. **Verma, V.K., Singh, R., Srivastava, V., Singh, P.K.,** *EP/AW performance evaluation of zinc alkyl/dialkyl/alkylaryl-dithiocarbamates in four ball tests.* Lubr. Sci., 2004. 16: p. 195-203.

257. **Braithwaite, E.R., Green, A.B.,** *A critical analysis of the performance of molybdenum.* Wear, 1997. 46: p. 405-431.

258. **Chen, L., Dong, J., Chen, G.,** *The study of tribo-induced deposits from a copper-containing antiwear additive.* Trib. Trans., 1997. 40: p. 339-345.

259. **Chen, G., Chen, L., Dong, J.,** *Preparation and tribological behaviour of oil-soluble cerium dioctyl dithiocarbamate.* Lubr. Eng., 1997. 53: p. 24-29.

260. **Beatty, H.A.,** *Organolead compound as lubricant additives.* Chem. & Ind., 1968. 8: p. 733-736.

261. **Palacios, J.M.,** *Films formed by antiwear additives and their incidence in wear and scuffing.* Wear, 1987. 114: p. 41-49.

262. **Tuli, D.K., Sarin, R., Gupta, A.K., Kumar, A.H., Rai, M.M., Bhatnagar, A.K.,** *Synthetic metallic dialkyldithiocarbamates as antiwear and extreme-pressure additives for lubricting oils: role of metal on their effectiveness.* Lubr. Eng., 1995. 51: p. 298-303.

263. **Isoyama, H., Sakurai, T.,** *Inhibition of autooxidation by d-μ-thio-bis(dialkyldithiocarbamates) dimolybdenum.* Bulletin of the Japanese Petroleum Institute, 1974. 16: p. 112-117.

264. **Sakurai, T., Okabe, H., Isoyama, H.,** *The synthesis of di-μ-thio-bis(dialkyldithiocarbamates) dimolybdenum (V) and their effects on boundary lubrication.* Bulletin of the Japanese Petroleum Institute, 1971. 13: p. 243-249.

265. **Grossiord, C., Varlot, K., Martin, J.M., LeMogne, T.H., Esnouf, C., Inoue, K.,** *MoS_2 single sheet lubrication by molybdenum dithiocarbamate.* Trib. Intern., 1998. 31: p. 737-743.

266. **Graham, J., Korcek, S., Spikes, H.A.,** *The friction-reducing properties of molybdenum dialkyldithiocarbamate additives. Part 1. Factors influencing friction reduction.* Trib. Trans., 2001. 44: p. 626-636.

267. **Topolovec-Miklozic, K., Graham, J., Spikes, H.A.,** *Chemical and physical analysis of reaction films formed by molybdenum dialkyldithiocarbamate friction modifier additive using Raman and atomic force microscopy.* Trib. Lett., 2001. 11: p. 71-81.

268. **Yamamoto, Y., Gondo, S.,** *Friction and wear characteristics of molybdenum dithiocarbamate and molybdenum dithiophosphate.* Trib. Trans., 1989. 32: p. 251-257.

269. **Tanaka, H., Hashimoto, M., Gondo, S., Yamamoto, Y.,** *Friction and wear characteristics of molybdenum dithiocarbamate with alloy steels.* Tribology Online, 2006. 1: p. 9-13.

270. **Popovitz-Biro, R., Rosentsveig, R., Tenne, R.,** *HRTEM of Inorganic Fullerene-like nanoparticle of MoS_2.* 2011 [cited 2011 1st June]; Available from: http://www.weizmann.ac.il/Chemical_Research_Support/EM_Unit/Ronit/current-activities.

271. **Plaza, S.,** *The load carrying action of organolead dithiophosphates, dithiocarbamates and xanthates. Part I: Assessment of the lubricating properties and mechanism of lubrication.* Wear, 1983. 85: p. 193-204.

272. **Yan, L., Yue, W., Wang, C., Wei, D., Xu, B.,** *Comparing tribological behaviours of sulfur- and phosphorus-free organomolybdenum additive with ZDDP and MoDTC.* Trib. Intern., 2012. 53: p. 150-158.

273. **Shoemaker, B.H., Loane, C.M.,** *US Patent 2160917: Lubricant*. 1939, Standard Oil Co.: USA.

274. **Rogers, D.T., McNab, J.G.,** *US Patent 2526506: Hydrocarbon lubricant containing sulfurised aliphatic borates as stabilisers.* 1950, Standard Oil Co.: USA.

275. **Thomas, J.R., Harle, O.L.,** *US Patent 2795548: Lubricant compositions*. 1957, California Research Corp.: USA.

276. **Cook, J.F.,** *US Patent 2975134: Antiwear lubricants containing boron esters*. 1961, Union Oil Co.: USA.

277. **Choudhary, R.B., Pande P.P.,** *Lubrication potential of boron compounds: an overview.* Lubr. Sci., 2002. 14: p. 213-222.

278. **Mang, T., Dresel, W.**, ed. *Lubricants and lubrication*. 2007, Wiley-VCH.

279. **Kreuz, K.L., Fein, R.S.,** *EP films from borate lubricants.* ASLE Trans., 1967. 10: p. 67-76.

280. **Baldwin, B.A.,** *Relative antiwear efficiency of boron and sulphur surface species.* Wear, 1977. 45: p. 345-353.

281. **Horodysky, A.G., Kaminski, J.M.,** *US Patent 4370248: Borated hydroxyl-containing acid esters and lubricants containing same*. 1983, Mobil Oil Corp.: USA.

282. **Horodysky, A.G.,** *US Patent 4382006: Friction reduction additives and compositions thereof*. 1983, Mobil Oil Corp.: USA.

283. **Horodysky, A.G.,** *US Patent 4410438: Borated epoxides and lubricants containing same*. 1983, Mobil Oil Corp.: USA.

284. **Horodysky, A.G., Kaminski, J.M.,** *US Patent 4492640: Trihydroxyhydrocarbyl sulfides and lubricants containing same*. 1985, Mobil Oil Corp.: USA.

285. **Davis, K.E.,** *US Patent 4584115: Method of preparing boron-containing compositions useful as lubricant additives*. 1986, Lubrizol Corp.: USA.

286. **Holstedt, R.A., Baron, K., Jessup, P.J.,** *US Patent 4627930: Boron-containing heterocyclic compounds and lubricating oil containing same*. 1986, Union Oil Co.: USA.

287. **Jessup, P.J., Holstedt, R.A., Baron, K.,** *US Patent 4629579: Boron derivatives*. 1986, Union Oil Co.: USA.

288. **Braid, M.,** *US Patent 4547302: Borate esters and lubricant compositions containing such esters*. 1985, Mobil Oil Co.: USA.

289. **Small Jr., V.R., Liston, T.V., Onopchenko, A.,** *US Patent 4975211: Diethylamine complexes of borated alkyl catechol and lubricating oil compositions containing the same*. 1990, Chrevron Research Co.: USA.

290. **Liu, W., Xue, Q., Zhang, X., Wang, H., Huang, C.,** *The performance and antiwear mechanism of tridodecyl borate ester as an oil additive.* Trib. Trans., 1992. 48: p. 475-479.

291. **Liu, W., Xue, Q., Zhang, X., Wang, H.,** *Effect of molecular structure of organic borates on their friction and wear properties.* Lubr. Sci., 1993. 6: p. 41-49.

292. **Liu, W., Jin, Z., Xue, Q.,** *The performance and antiwear mechanism of S-containing organic borate as an oil additive.* Lubr. Sci., 1994. 7: p. 49-60.

293. **Yao, J., Dong, J.,** *Improvement of hydrolytic stability of borate esters used as lubricant additives.* Lubr. Eng., 1995. 51: p. 475-479.

294. **Yao, J.B., Wang, Q.L., Chen, S.Q., Sun, J.Z., Dong, J.X.,** *Borate esters used as lubricant additives.* Lubr. Sci., 2002. 14(4): p. 415-423.

295. **Yao, J.,** *Antiwear function and mechanism of borate containing nitrogen.* Trib. Intern., 1997. 30: p. 387-389.

296. **Yao, J., Dong, J., Xiong, R.,** *Antiwear synergism of borates and copper oleate.* Lubr. Eng., 1994. 50: p. 695-698.

297. **Yao, J., Dong, J.,** *Antiwear synergism of borates and dibutyl tin dilaurate.* Lubr. Eng., 1996. 52: p. 553-556.

298. **Zhang, Z., Yamaguchi, E.S., Kasrai, M., Bancroft, G.M.,** *Interaction of ZDDP with borated dispersant using XANES and XPS.* Trib. Trans., 2004. 47: p. 527-536.

299. **Kapadia, R., Glyde, R., Wu, Y.,** *In situ observation of phosphorus and non-phosphorus antiwear films using a mini traction machine with spacer layer image mapping.* Trib. Intern., 2007. 40(10-12): p. 1667–1679.

300. **Shah, F.U., Glavatskih, S., Antzutkin, O.N.,** *Synthesis, physicochemical, and tribological characterization of S-di-n-octoxyboron-O,O'-di-n-octyldithiophosphate.* ACS Appl. Mater. Interfaces, 2009. 1(12): p. 2835-2842.

301. **Shah, F.U., Glavatskih, S., Antzutkin, O.N.,** *Topography of the wear scar on the ball after rubbing with base oil alone, 1 % ZDDP and 1 % DOB-DTP.* 2009 [cited 2011 10th January]; Available from: http://pubs.acs.org/doi/abs/10.1021/am900572y.

302. **Wang, J., Wang, J., Li, C., Zhao, G., Wang, X.,** *A high-performance multifunctional lubricant additive for water-glycol hydraulic fluid.* Trib. Lett., 2011. 43: p. 235-245.

303. **Huang, W., Tan, Y., Dong, J., Chen, B.,** *Tribological properties of the film formed by borated dioctyl dithiocarbamate as an additive in liquid paraffin.* Trib. Intern., 2002. 35: p. 787-791.

304. **Shah, F.U., Glavatskih, S., Antzutkin, O.N.,** *Novel alkylborate-dithiocarbamate lubricant additives: synthesis and tribophysical characterisation.* Trib. Lett., 2012. 45: p. 67-78.

305. **Philippon, D., De Barros-Bouchet, M.I., Lerasle, O., Le Mogne, Th., Martin, J.M.,** *Experimental simulation of tribochemical reactions between borates esters and steel surface.* Trib. Lett., 2011. 41(1): p. 73-82.

306. **Harrison, J.J., Nelson, K.D., Buitrago, J.A.,** *US Patent 6737387 B2: Dispersed hydrated potassium borate compositions having improved properties in lubricating oil compositions*. 2004, Chevron Oronite Co. LLC: USA.

307. **Carron, K.T., Xue, G., Lewis, M.L.,** *A surface-enhanced Raman spectroscopy study of the corrosion-inhibiting properties of benzimidazole and benzotriazole on copper.* Langmuir, 1991. 7: p. 2-4.

308. **Waynick, J.A.,** *The development and use of metal deactivators in the petroleum industry.* Energy and Fuels, 2001. 15: p. 1325-1340.

309. **Rudston, S.G., Whitby, R.D.,** *The effect of model lubricating oil constituents on the wear of steel.* J. Inst. Petrol., 1971. 57: p. 189-203.

310. **Miller, A.H.,** *Boundary lubricity studies: structure-activity correlations in alkylpyridines.* J. Inst. Petrol., 1973. 59: p. 27-31.

311. **Ren, T., Liu, W., Xue, Q., Wang, H.,** *The effect of molecular structure of N-containing heterocyclic compounds on their wear properties.* Lubr. Sci., 1993. 5: p. 205-212.

312. **Wei, D., Han, X., Wang, R.,** *The influence of chemical structure of certain nitrogen-containing organic compounds on their antiwear effectiveness: the critical role of hydroxy group.* Lubr. Sci., 1989. 2: p. 63-87.

313. **Wei, D., Song, H.,** *The wear behaviour of steel lubricated by some oxygen-containing derivatives of heterocyclic nitrogen-containing compounds (HNCC) under boundary lubrication conditions.* Lubr. Sci., 1992. 4: p. 219-232.

314. **Cai, M., Liang, Y., Zhou, F., Liu, W.,** *Tribological properties of novel imidazolium ionic liquids bearing benzotriazole group as the antiwear/anticorrosion additive in poly(ethylene glycol) and polyurea grease for steel/steel contacts.* ACS Appl. Mater. Interfaces, 2011. 3(12): p. 4580-4592.

315. **Fodor, J.,** *EP 0420868 B1: Method for reducing wear on surfaces subjected to frictional forces*. 1993, British Technology Group Ltd.

316. **Chinas-Castillo, F.,** *The behaviour of colloids in lubricated contact*, in *Mechanical Engineering*. 2000, Imperial College: London.

317. **Bakunin, V.N., Suslov, A.Y., Kuzmina, G.N., Parenago, O.P.,** *Recent achievements in the synthesis amd application of inorganic nanoparticles as lubricant components.* Lubr. Sci., 2005. 17: p. 127-145.

318. **Zhou, J., Wu, Z., Zhang, Z., Liu, W., Xue, Q.,** *Tribological behaviour and lubricating mechanism of Cu nanoparticles in oil.* Trib. Lett., 2000. 8: p. 213-218.

319. **Qiu, S., Zhou, Z., Dong, J., Chen, G.,** *Preparation of Ni nanoparticles and evaluation of their tribological performance as potential antiwear additives in oils.* Trans. ASME, 2001. 123: p. 441-443.

320. **Chinas-Castillo, F., Spikes, H.A.,** *The behaviour of colloidal solid particles in elastohydrodynamic contacts.* Trib. Trans., 2000. 43: p. 387-394.

321. **Chinas-Castillo, F., Spikes, H.A.,** *The lubricating properties of dilute colloidal solid dispersions*. Proc. Int. Trib. Conf. 2000. Nagasaki.

322. **Li, B., Wang, X., Liu, W., Xue, Q. ,** *Tribochemistry and antiwear mechanism of organic–inorganic nanoparticles as lubricant additives.* Trib. Lett., 2006. 22: p. 79-84.

323. **Xue, Q., Liu, W., Zhang, Z., ,** *Friction and wear properties of a surface-modified TiO_2 nanoparticle as an additive in liquid paraffin.* Wear, 1997. 213: p. 29-32.

324. **Hu, Z.S., Dong, J.X.,** *Study of antiwear and reducing friction additive of nanometer titanium oxide.* Wear, 1998. 216: p. 92-96.

325. **Hu, Z.S., Dong, J.X., Chen, G.X.,** *Study of antiwear and reducing friction additive of nanometer ferric oxide.* Trib. Intern., 1998. 31: p. 355-360.

326. **Zhang, Z., Liu, W., Xue, Q.,** *Study of lubricating mechanism of $La(OH)_3$ nanocluster modified by compound containing nitrogen in liquid paraffin.* Wear, 1998. 218: p. 139-144.

327. **Battez, A.H., Rico, J.E.F., Ariasa, A.N., Rodriguez, J.L.V., Rodriguez, R.C., Fernandez, J.M.D.,** *The tribological behaviour of ZnO nanoparticles as an additive to PAO6.* Wear, 2006. 261: p. 256-263.

328. **Wu, Y.Y., Tsui, W.C., Liu, T.C.,** *Experimental analysis of tribological properties of lubricating oils with nanoparticle additives.* Wear, 2007. 262: p. 819-825.

329. **Gu, C., Zhu, G., Li, L., Tian, X., Zhu, G.,** *Tribological effects of oxide based nanoparticles in lubricating oils.* J. Marine Sci. Appl., 2009. 8: p. 71-76.

330. **Zhang, L., Chen, L., Wan, H., Chen, J., Zhou, H.,** *Synthesis and tribological properties of stearic acid-modified anatase (TiO_2) nanoparticles.* Trib. Lett., 2011. 41.

331. **Oganesova, E., Kuz'mina, G., Bordubanova, E., Khodzhaeva, V., Ezhov, A., Ivanov, V., Parenago, O.,** *Comparison of antiwear properties of titanium-containing compounds.* Petroleum Chemistry, 2012. 52: p. 204-207.

332. **Costello, M.T.,** *X-ray diffraction of amorphous and crystalline overbased sulphonates.* Tribotest, 2005. 11: p. 207-212.

333. **Cizaire, L., Martin, J.M., Le Mogne, T., Gresser, E.,** *Chemical Analysis of overbased calcium sulphonate detergents by coupling XPS, ToF-SIMS, XANES, and EFTEM.* Colloids and Surfaces A: Physicochemical and Engineering Aspects, 2004. 238: p. 151-158.

334. **Shirahama, S., Hirata, M.,** *The effects of engine oil additives on valve train wear.* Lubr. Sci., 1989. 1: p. 365-384.

335. **Mansot, J.L., Hallouis, M., Martin, J.M.,** *Colloidal antiwear additives. 2. Tribological behaviour of colloidal additives in mild wear engine.* Colloids and Surfaces A: Physicochemical and Engineering Aspects, 1993. 75: p. 25-31.

336. **Adams, J.H.,** *Borate - a new generation EP gear lubricant.* Lubr. Eng., 1977. 33: p. 241-246.

337. **Sims, M.J.,** *US Patent 3819521: Lubricant containg dispersed borate and a polyol*. 1974, Chevron Research Co.: USA.

338. **Liu, W., Xue, Q., Wang, H., Zhang, X., Huang, C.,** *The antiwear properties of sodium metaborate as an oil additive.* Lubr. Eng., 1992. 48: p. 290-293.

339. **Qiao, Y., Liu, W., Qi, S., Xue, Q., Xu, B., Ma, S.,** *The tribochemical mechanism of the borate modified by N-containing compound as oil additive.* Wear, 1998. 215: p. 165-169.

340. **Adams, J.H.,** *US Patent 3997454: Lubricant containing potassium borate*. 1976, Chevron Research Co.: USA.

341. **Liu, W., Zhang, B., Huang, C, Zhang, X., Xue, Q., Wang, H.,** *The antiwear properties of potassium borate as an oil additive.* Lubr. Eng., 1991. 47: p. 344-347.

342. **Morizur, M.F., Taysset, O.,** *Antiwear actions of additives in solid dispersion.* Lubr. Sci., 1992. 4: p. 277-299.

343. **Normand, V., Martin, J.M., Ponsonnet, L., Inoue, K.,** *Micellar calcium borate as an antiwear additive.* Trib. Lett., 1998. 5: p. 235-242.

344. **Hu, Z.S., Dong, J.X.,** *Study on antiwear and reducing friction additive of nanometer titanium borate.* Wear, 1998. 216: p. 87-91.

345. **Dong, J.X.H., Z.S.,** *A study of the anti-wear and friction-reducing properties of the lubricant additive, nanometer zinc borate.* Trib. Intern., 1998. 31: p. 219-223.

346. **Hu, Z.S., Dong, J.X., Chen, G.X., He, J.Z.,** *Preparation and tribological properties of nanoparticle lanthanum borate.* Wear, 2000. 243: p. 43-47.

347. **Hu, Z.S., Shi, Y.G., Wang, L.G., Peng, Y., Chen, G.X., Dong, J.X.,** *Study of antiwear and reducing friction additive of nanometer aluminium borate.* Lubr. Eng., 2001. 57: p. 23-27.

348. **Chen, G.X., Hu, Z.S., Nai, R., Wang, L.G., Peng, Y., Dong, J.X.,** *Preparation and tribology of ultrafine and amorphous strontium borate.* Proc. Inst. Mech. Eng., 2001. J215: p. 133-140.

349. **Hu, Z.S., Lai, R., Lou, F., Wang, L.G., Chen, Z.L., Chen, G.X., Dong, J.X.,** *Preparation and tribological properties of nanometer magnesium borate as lubricating oil additive.* Wear, 2002. 252: p. 370-374.

350. **Taniguchi, M., Tomioka, Y., Kumegava, N., Isibashi, M.,** *Japanese Patent 05-179269: Lubricants*. 1991: Japan.

351. **Shigematsu, K., Abe K.,** *Japanese Patent 05-117174: Hydrogenated closed-structure fullerene and its preparation*. 1991: Japan.

352. **Shigematsu, K., Abe K.,** *Japanese Patent 05-229966: Preparation of hydrogenated fullerene*. 1992: Japan.

353. **Patil, A.O., Schriver, G.W., Lundberg, R.D.,** *US Patent 5292444: Lube oil compositions containing fullerene-grafted polymers*. 1994, Exxon Research and Engineering Co.: USA.

354. **Patil, A.O., Schriver, G.W., Lundberg, R.D.,** *US Patent 5292813: Fullerene-grafted polymers and process for their preparation*. 1994, Exxon Research and Engineering Co.: USA.

355. **Gupta, B.K., Bushan, B.,** *Fullerene particles as an additive to liquid lubricants and greases for low friction and wear.* Lubr. Eng., 1994. 50: p. 524-528.

356. **Ginzburg, B.M., Kireenko, O.F., Shepelevskii, A.A., Shibaev, L.A., Tochilnikov, D.G., Leksovskii, A.M.,** *Thermal and Tribological Properties of Fullerene-Containing Composite Systems. Part 2. Formation of Tribo-Polymer Films during Boundary Sliding Friction in the Presence of Fullerene C60.* J. Macromolecular Science, 2005. 44: p. 93-115.

357. **Lee, J., Cho, S., Hwang, Y., Cho, H., Lee, C., Choi, Y., Ku, B., Lee, H., Lee, B., Kim, D., Kim, S.H.,** *Application of fullerene-added nano-oil for lubrication enhancement in friction surfaces.* Trib. Intern., 2009. 42: p. 440-447.

358. **Ku, B., Han, Y., Lee, J., Lee, J., Park, S., Hwang, Y.,** *Tribological effects of fullerene (C_{60}) nanoparticles added in mineral lubricants according to its viscosity.* Int. J. Prec. Eng. Man., 2010. 11: p. 607-611.

359. **Chen, C.S., Chen, X.H., Xu, L.S., Yang, Z., Li, W.H.,** *Modification of multi-walled carbon nanotubes with fatty acid and their tribological properties as lubricant additive.* Carbon, 2005. 43: p. 1660-1666.

360. **Peng, Y., Hu, Y. Wang, H.,** *Tribological behaviours of surfactant-functionalised carbon nanotube as lubricant additives in water.* Trib. Lett., 2006. 25: p. 247-253.

361. **Choo, J.W.,** *The influence of carbon nanotubes on friction reduction in elastohydrodynamic lubrication*, in *62th STLE Annual Meeting & Exhibition*. 2007: Philadelphia, USA.

362. **Gajewicz, A., Rasulev, B., Dinadayalane, T.C., Urbaszek, P., Puzyn, T., Leszczynska, D., Leszczynski, J.,** *Advancing risk assessment of engineered nanomaterials: application of computational approaches* Advanced Drug Delivery Rev., 2012. ADR-12309.

363. **Hwang, Y., Lee, C., Choi, Y., Cheong, S., Kim, D., Lee, K., Lee, J., Kim, S.H.,** *Effect of the size and morphology of particles dispersed in nano-oil on friction performance between rotating discs.* J. Mech. Sci. Tech., 2011. 25: p. 2853-2857.

364. **Cizaire, L., Vacher, B., Le Mogne, T., Martin, J.M., Rapoport, L., Margolin, A., Tenne, R.,** *Mechanism of ultra-low friction by hollow inorganic fullerene-like MoS_2 nanoparticles.* Surfaces and Coatings, 2002. 160: p. 282-287.

365. **Tenne, R.,** *Inorganic nanotubes and fullerene-like nanoparticles.* Nature Nanotechnology, 2006. 1: p. 103-111.

366. **Jolly-Pottuz, L., Dassenoy, F., Belin, M., Vacher, B., Martin, J.M., Fleischer, N.,** *Ultra-low friction and wear properties of IF-WS_2 under boundary lubrication.* Trib. Lett., 2005. 18: p. 477-485.

367. **Jolly-Pottuz, L., Martin, J.M., Dassenoy, F., Belin, M., Montagnac, G., Reynard, B., Fleischer, N.,** *Pressure-induced exfoliation of inorganic fullerene-like WS_2 particles in a Hertzian contact.* J. Appl. Phys., 2006. 99: p. 023524.

368. **Huang, H.D., Tu, J.P., Zou, T.Z., Zhang, L.L., He, D.N.,** *Friction and wear properties of IF-MoS_2 as additive in paraffin oil.* Trib. Lett., 2005. 20: p. 247-250.

369. **Wu, J.F., Zhai, W.S., Jie, G.F.,** *Preparation and tribological properties of WS_2 nanoparticles modified by trioctylamine.* Proc. Inst. Mech. Eng., J: Journal Engineering Tribology, 2009. 223: p. 695-703.

370. **Chinas-Castillo, F., Spikes, H.A.,** *Mechanism of action of colloidal solid dispersions.* Trans. ASME, 2003. 125: p. 552-557.

371. **Perfiliev, V., Moshkovith, A., Verdyan, A., Tenne, R., Rapoport, L.,** *A new way to feed nanoparticles to friction interfaces.* Trib. Lett., 2006. 21: p. 89-93.

372. **Yamaguchi, E.S., Zhang, Z., Kasrai, M., Bancroft, G.M.,** *Study of the interaction of ZDDP and dispersants using X-ray absorption near edge structure spectroscopy - part 2: tribochemical reactions* Trib. Lett., 2003. 15(4): p. 385-394.

373. **Najman, M., Kasrai, M., Bancroft, G.M.,** *XANES of thermal and antiwear films of phosphate esters*. 27 February 2009]; Available from: http://www.uwo.ca/csrf/.

374. **Najman, M.N., Kasrai, M., Bancroft, G.M., Frazer, B.H., Stasio, G.D.,** *The correlation of microchemical properties to antiwear (AW) performance in ashless thiophosphate oil additives.* Trib. Lett., 2004. 17(4): p. 811-822.

375. **Kim, B., Mourhatch, R., Aswath, P.B.,** *Properties of tribofilms formed with ashless dithiophosphate and zinc dialkyl dithiophosphate under extreme pressure conditions.* Wear, 2010. 268(3-4): p. 579–591.

376. **Li, J., Ma, H., Ren, T., Zhao, Y., Zheng, L., Ma, C., Han, Y.,** *The tribological chemistry of polysulfides in mineral oil and synthetic diester.* Appl. Surf. Sci., 2008. 254(22): p. 7232-7236.

377. **Kasrai, M., Lennard, W.M., Brunner, R.W., Bancroft, G.M., Bardwell, J.A., Tan, K.H.,** *Sampling depth of total electron and fluorescence measurements in Si L- and K-edge absorption spectroscopy.* Appl. Surf. Sci., 1996. 99(4): p. 303-312.

378. **Kasrai, M., Fleet, M.E., Muthupari, S., Li, D., Bancroft, G.M.,** *Surface modification study of borate materials from B K-edge X-ray absorption spectroscopy.* Phys. Chem. Miner., 1998. 25(4): p. 268-272.

379. **Marezio, M., Remeika, J.P., Dernier, P.D.,** *The crystal structure of the high-pressure phase CaB_2O_4(IV), and polymorphism in CaB_2O_4.* Acta Cryst., 1969. B25: p. 965-970.

380. **Varlot, K., Kasrai, M., Bancroft, G.M., Yamaguchi, E.S., Ryason, P.R., Igarashi, J.,** *X-ray absorption study of antiwear films generated from ZDDP and borate micelles.* Wear, 2001. 24(12): p. 1029-1035.

381. **Fleet, M.E., Muthupari, S.,** *Boron K-edge XANES of borate and borosilicate minerals* American Mineralogist, 2000. 85(7-8): p. 1009-1021.

382. **Zhang, Z., Najman, M., Kasrai, M., Bancroft, G.M., Yamaguchi, E.S.,** *Study of interaction of EP and AW additives with dispersants using XANES.* Trib. Lett., 2005. 18(1): p. 43-51.

383. **Kasrai, M., Fuller, M.S., Bancroft, G.M, Yamaguchi, E.S., Ryason, P.R.,** *X-ray absorption study of the effect of calcium sulfonate on antiwear film formation generated from neutral and basic ZDDPs: part 2 - sulfur species.* Trib. Trans., 2003. 46(4): p. 543-549.

384. **Costello, M.T., Kasrai, M.,** *Study of surface films of overbased sulfonates and sulfurized olefins by X-ray absorption near edge structure (XANES) spectroscopy.* Trib. Lett., 2006. 24(2): p. 163-169.

385. **Ratoi, M., Castle, R. C., Bovington, C.H., Spikes, H.A.,** *The influence of soot and dispersant on ZDDP film thickness and friction.* Lubr. Sci., 2004. 17(1): p. 25-43.

386. **Inoue, K., Watanabe, H.,** *Interactions of Engine Oil Additives.* ASLE Trans., 1983. 26(2): p. 189-199.

387. **Barcroft, F.T., Park, D.,** *Interactions on heated metal surfaces between zinc dialkyldithiophosphates and other lubricating oil additives.* Wear, 1986. 108(3): p. 213-234.

388. **Fujita, H., Spikes, H.A.,** *Study of zinc dialkyldithiophosphate antiwear film formation and removal processes, Part II: Kinetic Model.* Trib. Trans., 2005. 48: p. 567-575.

389. **Hsu, S.M., Lin, R.S.,** *Interactions of additives and lubricating base oils.* SAE Tech. Paper, 1983: p. 831683.

390. **Spikes, H.A.,** *Origins of the friction and wear properties of antiwear additives.* Lubr. Sci., 2006. 18(3): p. 223-230.

APPENDIX

Stribeck Curves

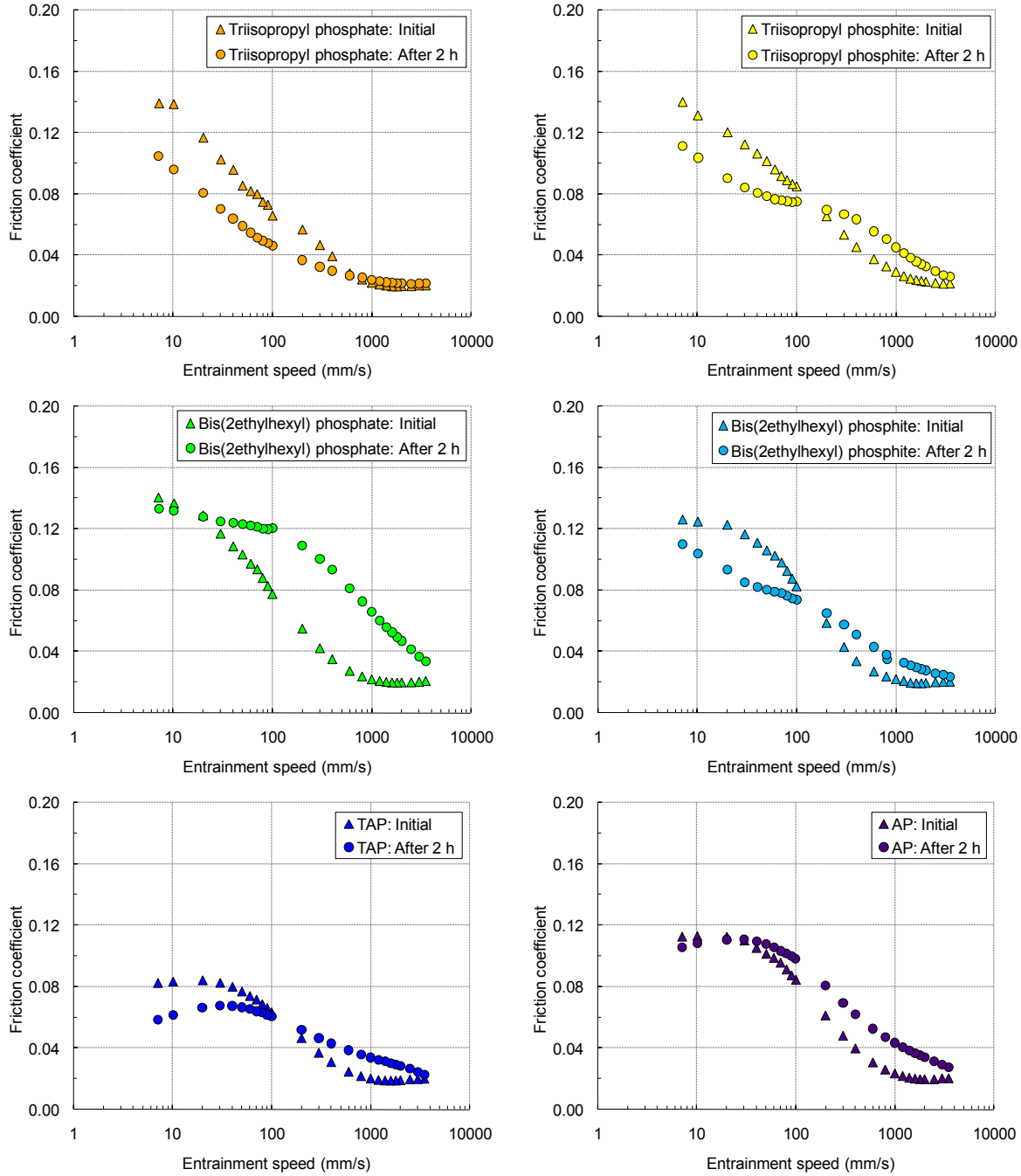


Figure A.1: Stribeck curves showing friction coefficient versus entrainment speed at the beginning and after 2 h of rubbing for P-containing antiwear additive solutions at 50% SRR, 30 N and 100 ºC.

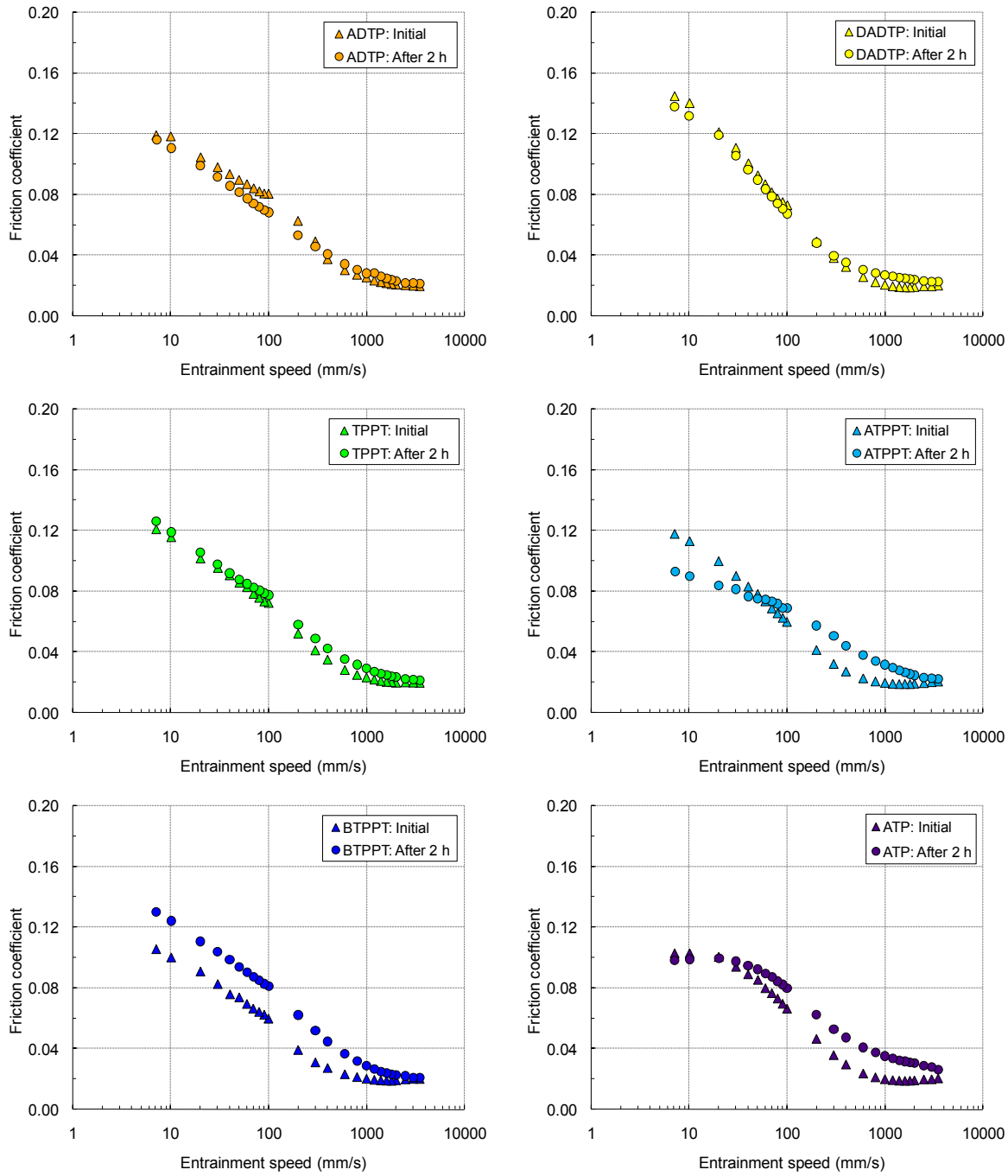


Figure A.2: Stribeck curves showing friction coefficient versus entrainment speed at the beginning and after 2 h of rubbing for P-S-containing antiwear additive solutions at 50% SRR, 30 N and 100 ºC.

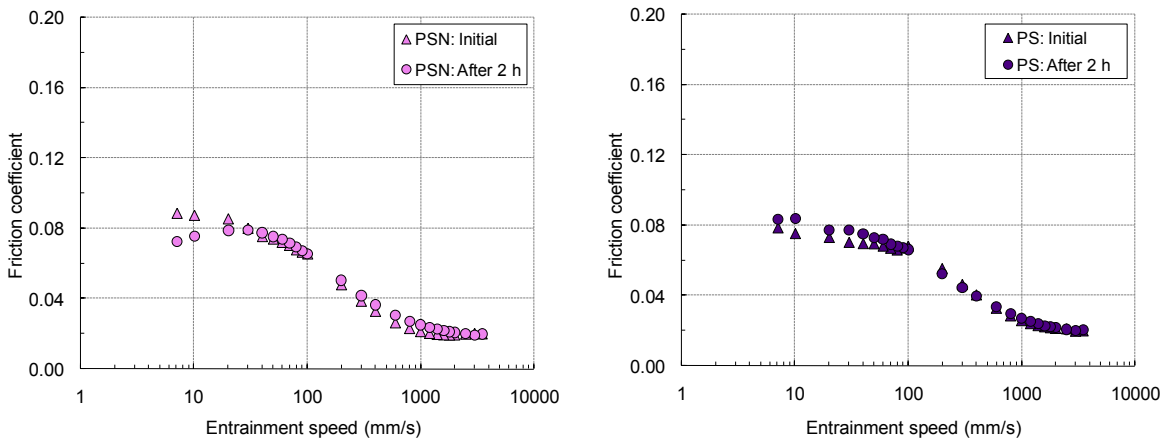


Figure A.2 (continued): Stribeck curves showing friction coefficient versus entrainment speed at the beginning and after 2 h of rubbing for P-S-containing antiwear additive solutions at 50% SRR, 30 N and 100 ºC.

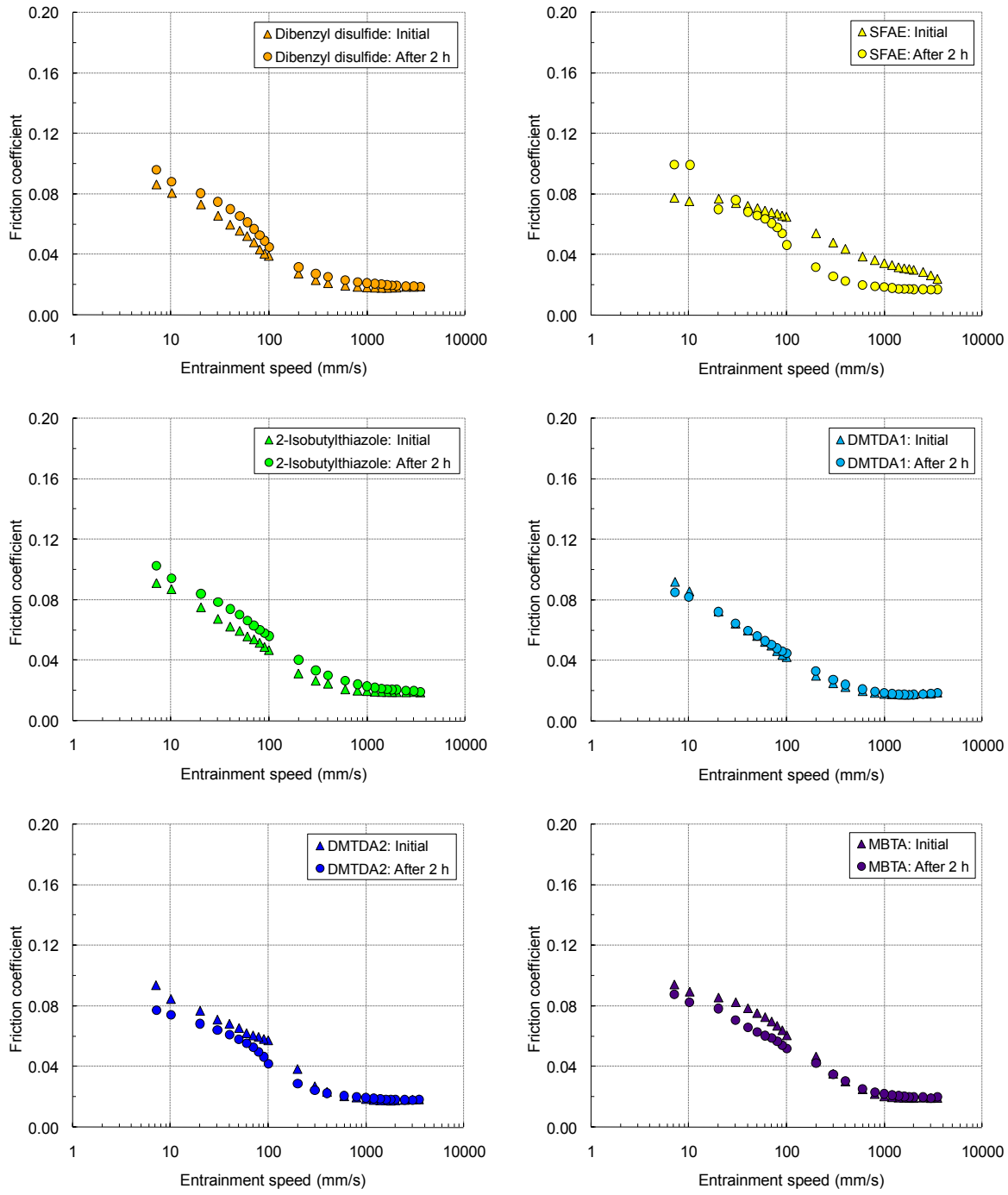


Figure A.3: Stribeck curves showing friction coefficient versus entrainment speed at the beginning and after 2 h of rubbing for S-containing antiwear additive solutions at 50% SRR, 30 N and 100 ºC.

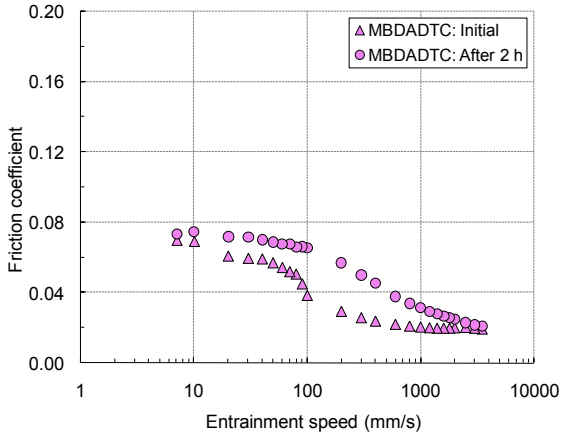


Figure A.3 (continued): Stribeck curves showing friction coefficient versus entrainment speed at the beginning and after 2 h of rubbing for S-containing antiwear additive solutions at 50% SRR, 30 N and 100 ºC.

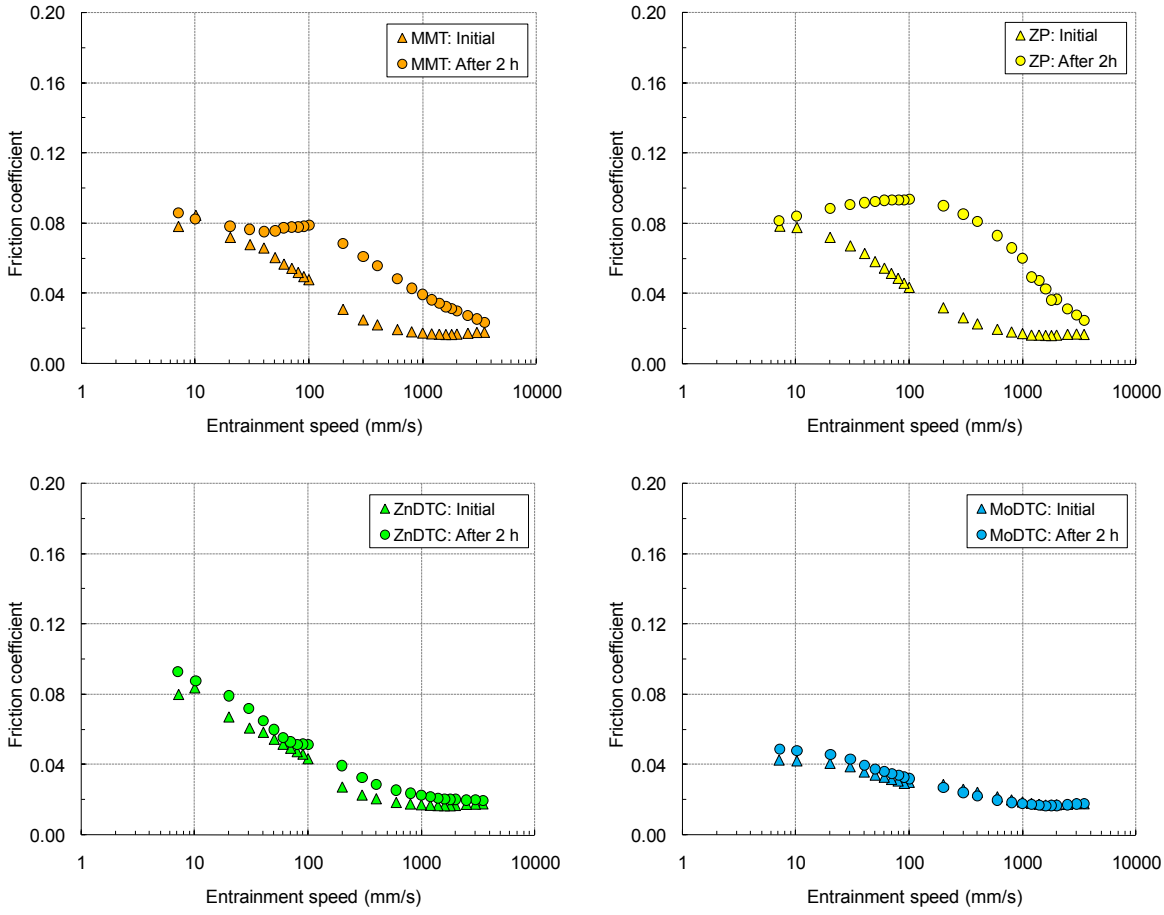


Figure A.4: Stribeck curves showing friction coefficient versus entrainment speed at the beginning and after 2 h of rubbing for M-containing antiwear additive solutions at 50% SRR, 30 N and 100 ºC.

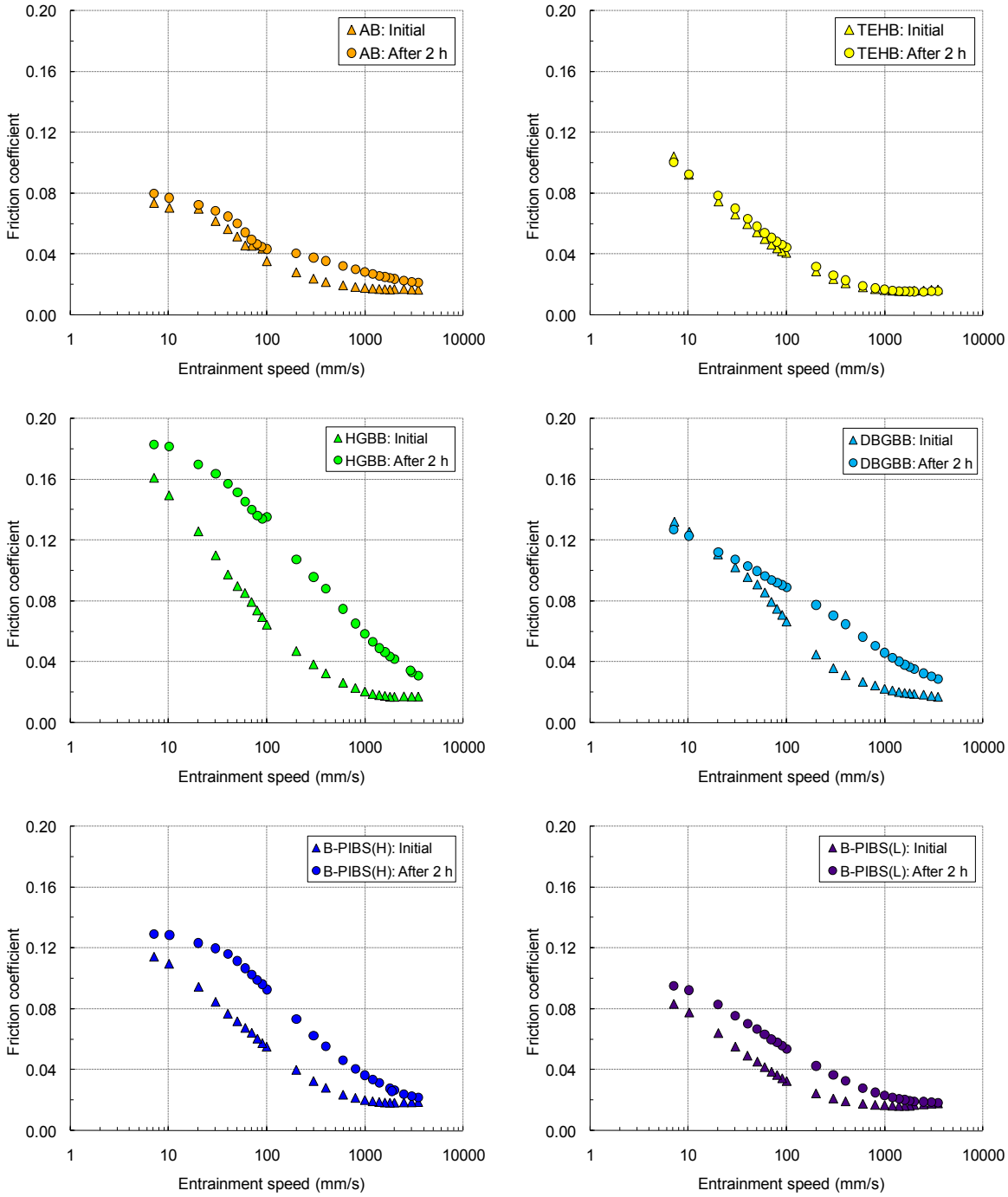


Figure A.5: Stribeck curves showing friction coefficient versus entrainment speed at the beginning and after 2 h of rubbing for B-containing antiwear additive solutions at 50% SRR, 30 N and 100 ºC.

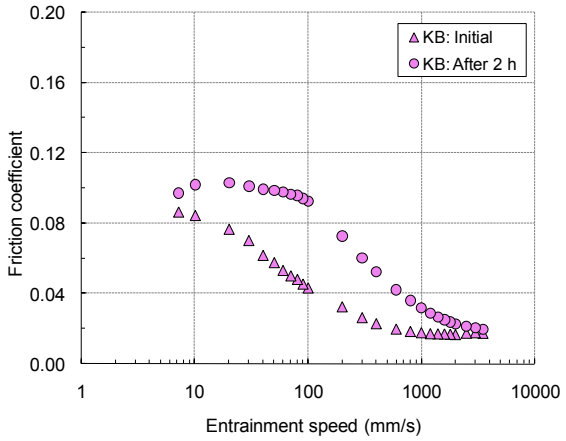


Figure A.5 (continued): Stribeck curves showing friction coefficient versus entrainment speed at the beginning and after 2 h of rubbing for B-containing antiwear additive solutions at 50% SRR, 30 N and 100 ºC.

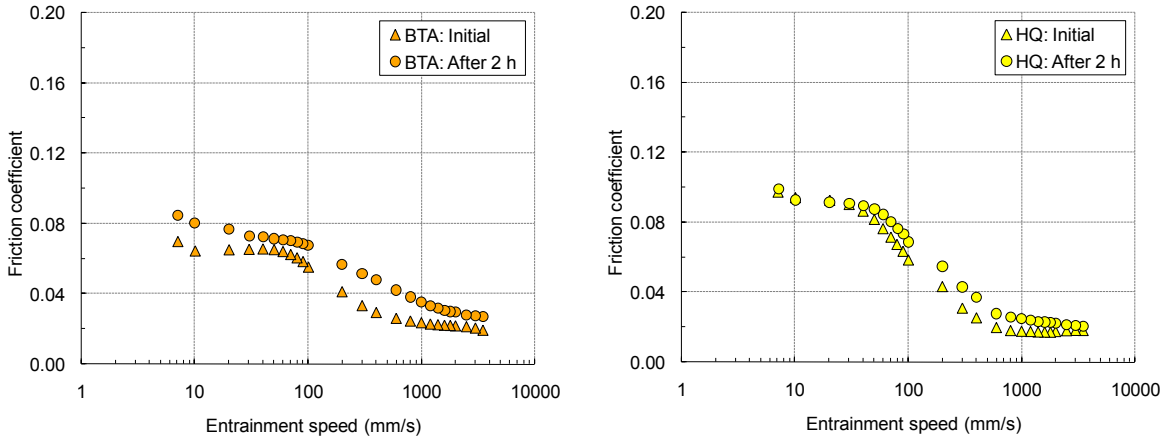


Figure A.6: Stribeck curves showing friction coefficient versus entrainment speed at the beginning and after 2 h of rubbing for N-containing heterocyclic antiwear additive solutions at 50% SRR, 30 N and 100 ºC.

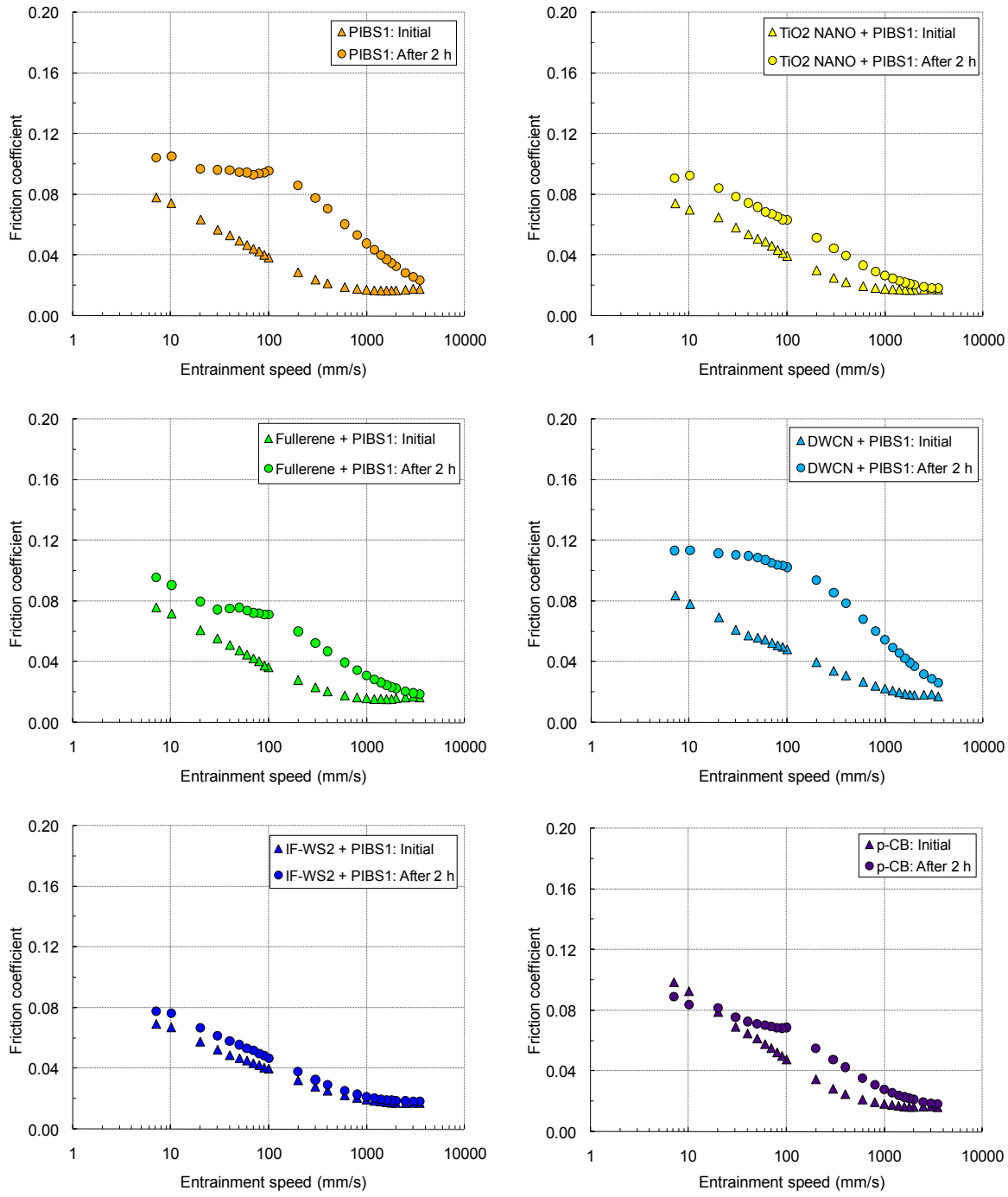


Figure A.7: Stribeck curves showing friction coefficient versus entrainment speed at the beginning and after 2 h of rubbing for Nanoparticle-containing antiwear additive solutions at 50% SRR, 30 N and 100 ºC.

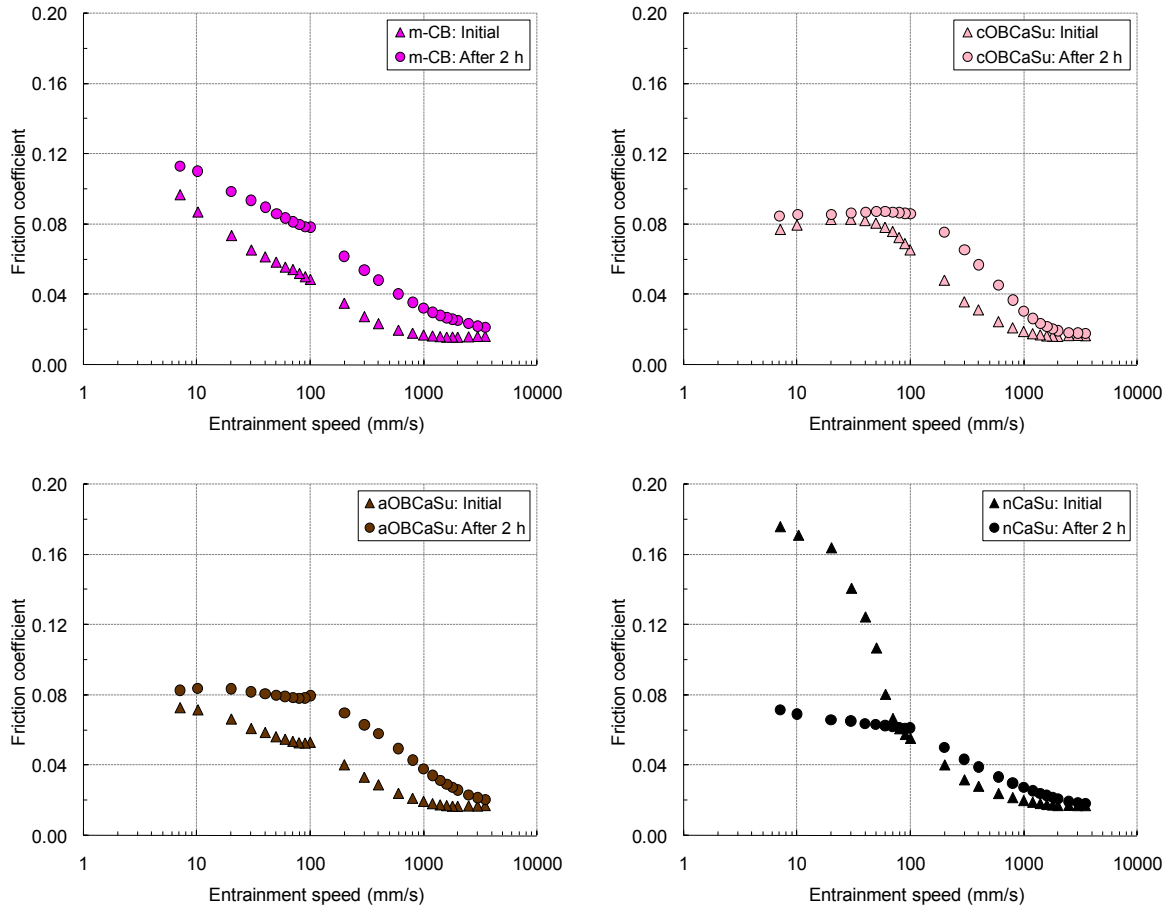


Figure A.7 (continued): Stribeck curves showing friction coefficient versus entrainment speed at the beginning and after 2 h of rubbing for Nanoparticle-containing antiwear additive solutions at 50% SRR, 30 N and 100 ºC.

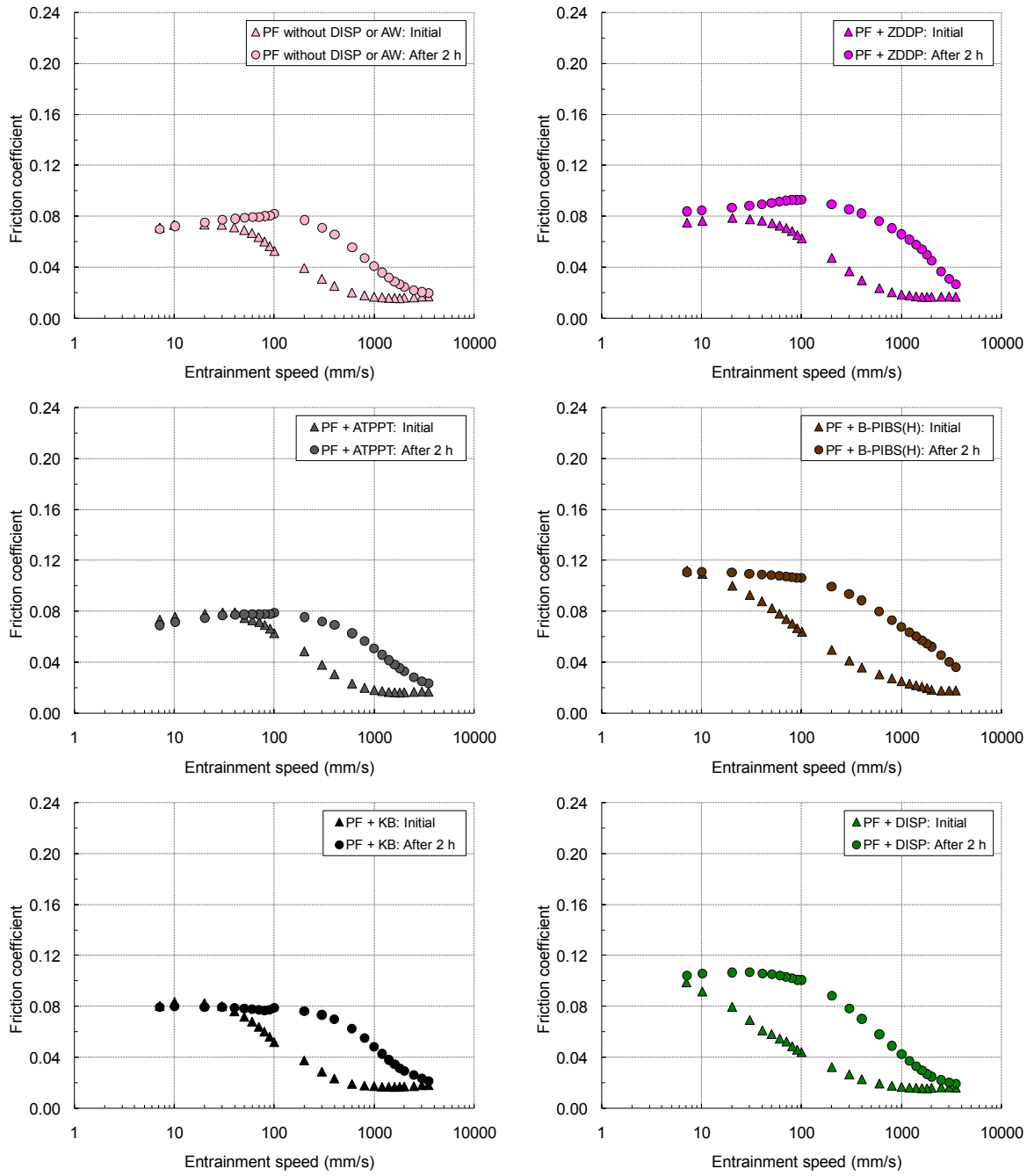


Figure A.8: Stribeck curves showing friction coefficient versus entrainment speed at the beginning and after 2 h of rubbing for low and zero SAPS antiwear additives in partially formulated oils at 50% SRR, 30 N and 100 ºC.

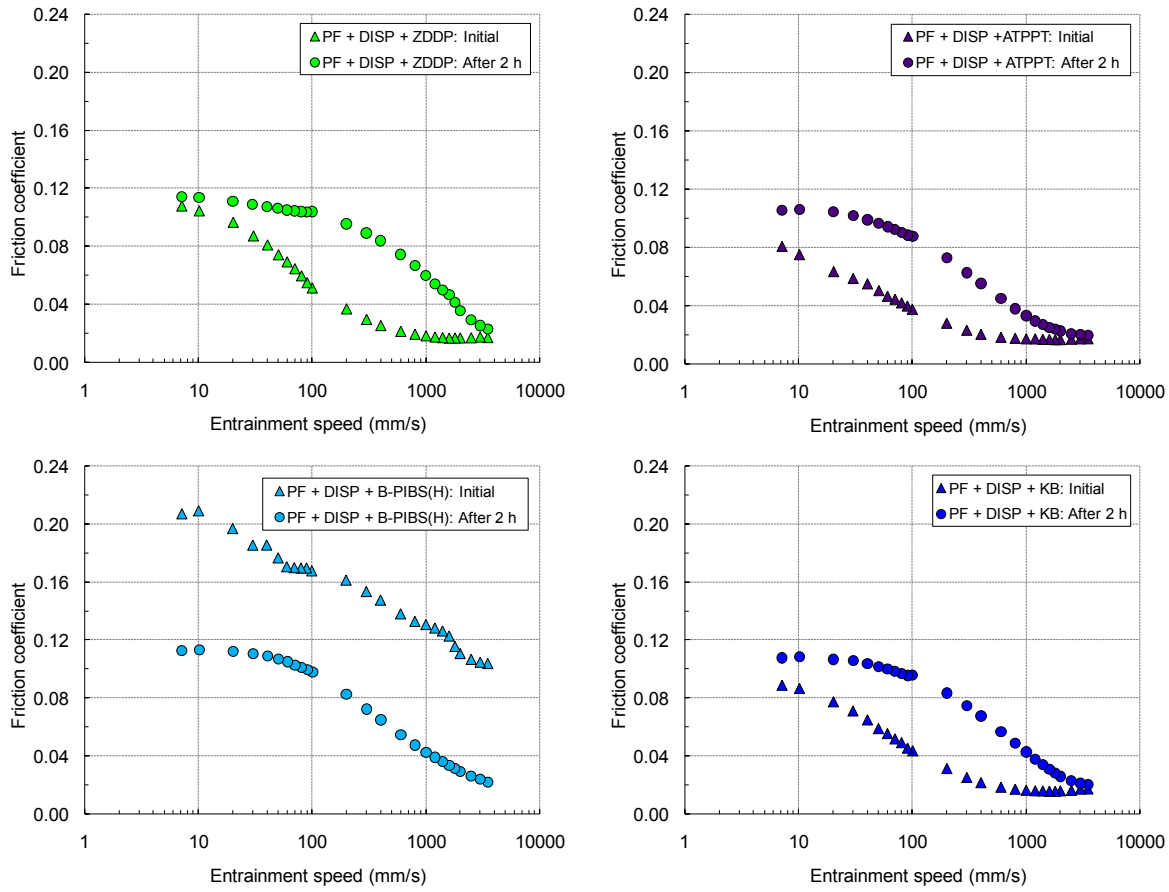


Figure A.8 (continued): Stribeck curves showing friction coefficient versus entrainment speed at the beginning and after 2 h of rubbing for low and zero SAPS antiwear additives in partially formulated oils at 50% SRR, 30 N and 100 ºC.

List of Publications

Benedet, J., Spikes, H.A., Green, J.H., Lamb, G.D., *Tribological characteristics of* Ashless Phosphorus and Phosphorus-Sulphur *based antiwear additives,* Advances in Boundary Lubrication and Boundary Surface Films*. 2009: Seville, Spain.*

Benedet, J., Spikes, H.A., Green, J.H., Lamb, G.D., *Tribological characteristics of* Ashless Phosphorus and Phosphorus-Sulphur *based antiwear additives, 64th STLE Annual Meeting & Exhibition. 2009: Orlando, USA.*

Benedet, J., Spikes, H.A., Green, J.H., Lamb, G.D., *Tribological characteristics of* Ashless Phosphorus and Phosphorus-Sulphur *based antiwear additives,* 4th World Tribology Congress*. 2009: Kyoto, Japan.*

Benedet, J., Spikes, H.A., Green, J.H., Lamb, G.D., *Tribological characteristics of* Ashless Phosphorus and Phosphorus-Sulphur *based antiwear additives,* 18th Mission of Tribology Research, IMechE*. 2009: London, UK.*

Benedet, J., Spikes, H.A., Green, J.H., Lamb, G.D., *Spurious mild wear measurement using white light interference microscopy in the presence of antiwear films.* Trib. Trans., 2009(52): p. 841-846.

Benedet, J., Spikes, H.A., Green, J.H., Lamb, G.D., *Tribological characteristics of low and zero SAPS antiwear additives*, *65th STLE Annual Meeting & Exhibition*. 2010: Las Vegas, USA.

Benedet, J., Spikes, H.A., Green, J.H., Lamb, G.D., *Film forming, friction and wear properties of alternative antiwear additives*, *66th STLE Annual Meeting & Exhibition*. 2011: Atlanta, USA.